Low-Cost, Close-Range Digital Photogrammetry for Coastal Cliff Deformation and Beach Monitoring

Mitchell Ayemere Eboigbe

THIS THESIS IS SUBMITTED IN PARTIAL FULFILMENT OF THE REQUIREMENT FOR THE DEGREE OF

DOCTOR OF PHILOSOPHY (Ph.D.)

Faculty of Computing, Engineering, and Science
University of South Wales, UK

June 2021

Abstract

Global warming, environmental change and sea-level rise are now perceived as a real threat to coastal communities across the World, including Wales, where coastal flooding and erosion have become more widespread and accepted. Existing techniques for monitoring the coastal environment are generally very expensive, in particular, remotely sensed datasets like LiDAR or satellite images. Consequently, many governments pay less attention to monitoring coastal areas and this has led to poor management programmes, resulting in the loss of lives and properties. In the United Kingdom, the Shoreline Management Plan does not necessarily encourage active intervention in protecting against coastal flooding and erosion. Photogrammetry is the most adopted technology for shoreline monitoring and management. While there are existing efforts in the application of close-range digital photogrammetry in monitoring Coastal Areas, there is no widespread adoption of a low-cost, consistent and regular monitoring methodology for data capture; processing and analysing that would accommodate the coastal cliff as well as accurately monitoring beach accretion and erosion. A cliff monitoring infrastructure is required to understand the cliff change pattern and correctly predict cliff falls. This research develops some new technologies for coastal cliff deformation and beach monitoring which are: A new pole-photogrammetry technique for regular cliff surveys; a new algorithm for coastal cliff deformation monitoring; an innovative predictive model for detecting and quantifying cliff fall and collapse; an innovative low-cost computational analysis and visualization for Beach Modelling and Monitoring. The new pole-photogrammetry technique is low-cost, accurate, rapid, and can generate high-resolution images. The methodology includes the most practicable survey distance to the cliff, vertical camera angle, and the best time Interval for executing a pole survey using the Integrated Sensor Orientation (ISO) from very cheap single frequency inbuilt GNSS. The new python algorithm for analysing the structural changes on the coastal cliff point cloud incorporates some existing libraries such as the Open3d, Numpy, and Pandas. This innovative algorithm reads every point in both point clouds and detects the changes. The algorithm creates three new point clouds for; where change has taken place, where there is no change, and the change array itself. The generated change-array point cloud was for computing the change volume and developing the coastal cliff prediction model. The new prediction model generates a probabilistic segmentation of all critical faults on the cliff and correctly predicts the date and quantity of cliff fall and collapse. The innovative low-cost computational analysis and visualization for Beach Modelling and Monitoring includes best practices; for low-cost and accurate UAV surveys, opensource and low-cost processing of digital images to acquire accurate orthomosaic and digital surface models, and for analysing digital images using open-source photogrammetric software. A three-stage monitoring procedure commencing with the small-scale photogrammetric datasets and ending in the critical evaluation of the dataset from the drone using the open-source QGIS was able to detect changes as small as 1cm to 3cm. The datasets from the drone and the pole integrate into a coastal monitoring infrastructure for monitoring the coastal area. The 1cm vertical accuracy and super-high-resolution images show an effective low-cost methodology for implementing strategic monitoring of the coastal cliff and beach. The recommendation includes a similar monitoring technique for the nearshore and coast and incorporates volume computation into the new change algorithm.

Acknowledgments

In the Name and Power of our Lord Jesus Christ, now and forevermore, Amen. To my Father His Holiness Olumba Olumba Obu. Father, I am very grateful for your unending Love towards, me. Thank You, Father.

I would commence with deep appreciation to my Director of Studies, Dr. David Kidner for all his love and for always inspiring me with practical illustrations such that coastal monitoring has become a part of me. Although I have had very tough financial difficulties, he kept encouraging me academically and morally, and that kept me focused not minding the hard times.

I also wish to thank my Supervisors Dr. Malcolm Thomas and Dr. Nathan Thomas for their encouragement and support. Malcolm was instrumental in accessing the Surveying equipment and licence to some proprietary software. Nathan was supportive in flying the drones. To my co-PhD colleague Hamzeh Aldwairy, words cannot be enough to appreciate you for participating in the drone and pole surveys. It was indeed a complete team!

Special thanks to the Vale of Glamorgan Council for giving approvals for the drone surveys. Similarly, I will not forget to thank Derek Elliott of the Aerial Photography Unit of the Wales National Assembly for graciously providing the historic photograph of the Penarth.

Others contributed one way or the other to the success of this research. Amongst those are Prof. Garry Higgs and other senior members of the USW GIS research group. I will also thank Dr. Elaine Huntley, Llinos Spargo, Sally Davies, Alison Crudgington, and Jane MacCuish in the Post Graduate Research Office. Special thanks too to Prof. Paul Roach for uncommon leadership in the Postgraduate Research Studies.

Special thanks to Edo State Polytechnic Usen and the Tertiary Education Trust Fund (TETFUND) Nigeria for providing the initial funding for this Ph.D.

To all my Ph.D. friends too numerous to mention, I remain grateful to you.

Most importantly, I will thank my wife Florence and our lovely children Henry, Omosefe, Oghogho, and Evan for being there for me. Your love and steadfastness have made this possible.

Finally, I would thank my Dad and my lovely Brothers Ken, Sly, and Dan for all their moral and spiritual support. Words are not enough to appreciate you guys.

Table of Contents

List of Figures

List of Tables

List of Abbreviations and Notations

AAT Automatic Aerial Triangulation

AGSD Average Ground Sampling Distance

AOI Area of Interest

BA Bundle Adjustment

BBA Bundle Block Adjustment

CCD Charge-coupled devices

CMOS complementary metal-oxide-semiconductor

CMS Centimeter

DEM Digital Elevation Model

EDM Electronic Distance Measurement

EO Exterior Orientation

FOV Field of View

GCP Ground Control Point

GNSS Global Navigation Satellite System

GNSS-AT GNSS-supported Aerial Triangulation

GSD Ground Sampling Distance

ICP Interactive Closest Point

IID Identical Distributed Variables

IO Interior Orientation

ISO

KNN Kd-tree nearest neighbor

LiDAR

MEMS IMU Micro-Electro-Mechanical Systems Inertial Measurement Unit

MPD Maximum Predictable Duration

NRW Natural Resources Wales

OCCUR Number of occurrence

PSPC Pole Survey Point Cloud

PSR Poisson surface reconstruction

QGIS Quantum GIS

SIFT Scale Invariant Feature Transform

SSSI Sites of Specific Scientific Interest

SUR Survey

TLS Terrestrial Laser Scanner

TLSPC Terrestrial Laser Scanner Point Cloud

UAS Unmanned Aerial System

UAV Unmanned Aerial Vehicle

FLANN Fast Library for Approximate Nearest Neighbours

SFM Structure from motion

Chapter 1

Introduction: Low-Cost Digital Photogrammetry for Coastline Monitoring

1.1 Statement of the Problem

The World's coastal zone is changing rapidly as a result of global warming and other environmental activities (King et al, 2017; Cloern et al, 2016; Paravolidakis et al, 2016; Robinet et al, 2016; Bio et al, 2015; Callaghan et al, 2015; Chikhradze et al, 2015; Smeeckaert et al, 2013; Sesli et al, 2009). There is the change in ocean currents, coupled with its associated upwelling and downwelling, thereby resulting in frequent coastal flooding and erosion (Samanta and Paul, 2016; Ringim et al, 2016; Bio et al, 2015; Chaaban et al, 2012). Sea behaviour and change may lead to the development of hurricanes, typhoons, or cyclones (Tseng et al, 2010). Changes have become so unpredictable and uncontrollable that man's quest in monitoring, managing, and predicting changes in the coastal environment is now of urgent global concern.

" *the search for more sustainable solutions has been given further impetus by the widespread public and media acceptance of climate change and recognition of the threats from rising sea levels"* (BBC, 2009) as in (Pontee and Parsons, 2012).

Shoreline monitoring and management have therefore become very crucial and inevitable (Anandabaskaran and Vijayakumar, 2017) requiring immediate, reliable, and cost-effective monitoring techniques (Ahmed et al, 2018).

This study aims to demonstrate the use of low-cost and large-scale (localised) methodologies for coastline monitoring which are practical and affordable for adopting throughout the World, especially for developing nations. Furthermore, the research will show that such large-scale monitoring approaches need to be accurate and easily and readily repeatable. The aim is to demonstrate that cheap localised monitoring approaches will allow local stakeholders with specialised knowledge of their environment the ability to undertake accurate surveys to better understand the changes in their coastal landscapes.

1.2 Case Study Area: Erosion at Penarth, South Wales, UK

The beach and cliffs of Penarth (see Figure 1.1) were chosen as the main case study site for this research, as it is an area experiencing cliff erosion; has been a cause for concern in respect of beach erosion (Phillips, 2005); is local to the University of South Wales; and the

Vale of Glamorgan Council with the Wales Coastal Monitoring Centre (WCMC) were very supportive of new and efficient monitoring approaches for Penarth. Furthermore, the Vale of Glamorgan Council organised and facilitated the necessary permissions for each occasion in which a drone was used to survey the site.

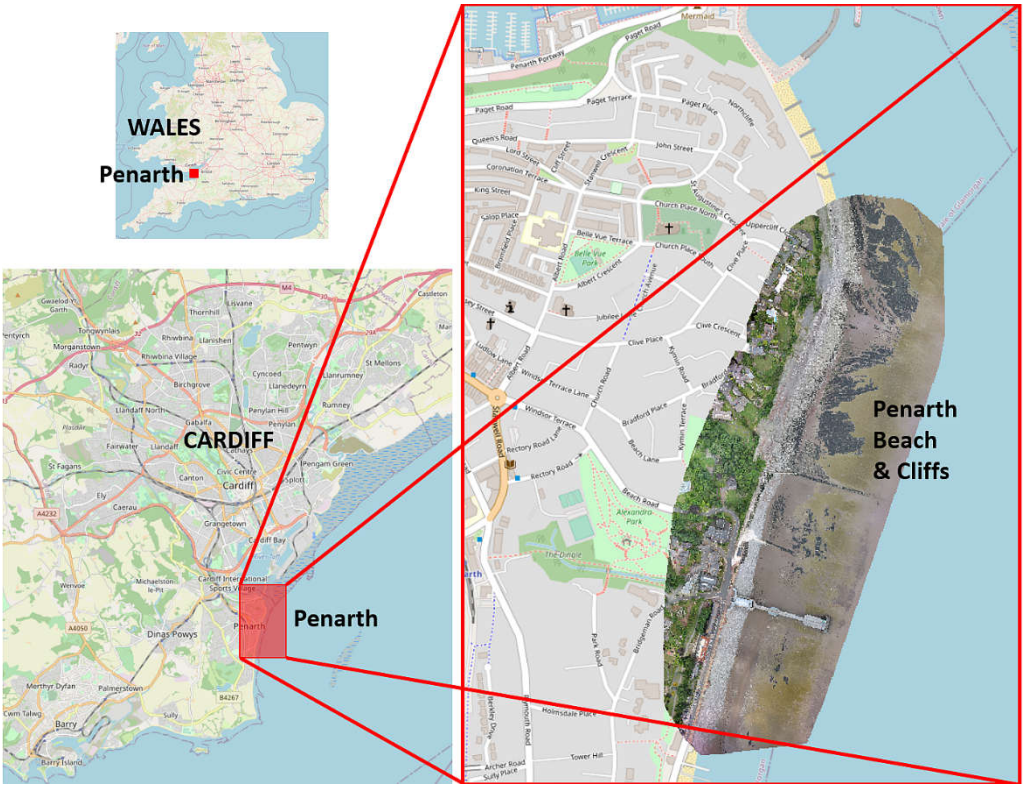

Figure 1.1 - Case Study Area of Penarth Beach and Cliffs in South Wales.

Penarth is a small town in the Vale of Glamorgan neighbouring Cardiff, South Wales on the north shore of the Severn Estuary, which has the second largest tidal range in the World. The county's coastline is approximately 45 kilometres in length (Farr et al, 2017), half of which is designated the Glamorgan Heritage Coast including Sites of Special Scientific Interest (SSSI) and is characterised by stunning limestone cliffs, which are predominant on the Penarth stretch.

The focus is on the area to the north of the pier where the lower cliffs are composed mainly of shales and thin bands of limestone of late Triassic age, while the top of the cliff exhibit layers of grey limestones and shales from the Jurassic Blue Lias. Interspersed between these periods, resistant gypsum or alabaster layers were formed within the Triassic red marls (see Figures 1.2 and 1.3).

Figure 1.2 - The cliffs at Penarth (north of the pier) illustrating the strata in the Triassic Marls. Evidence of landslips is visible, as are the resistant layers or ledges formed into the cliffs. Source: USW, August 2020.

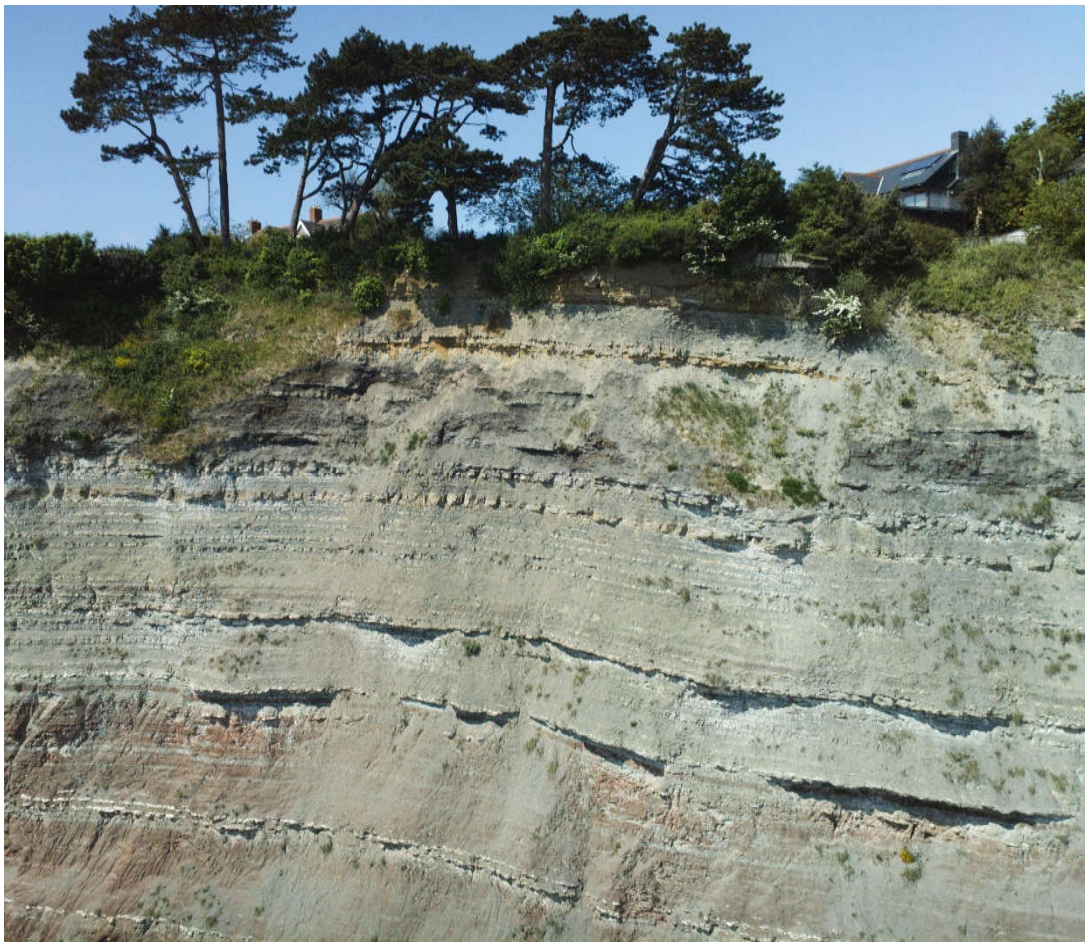

Figure - 1.3 Strata including Gypsum (alabaster) outcrops at Penarth (corresponds to the area on the right of Figure 1.2). Source: USW, May 2016.

These cliffs are constantly eroding as small quantities of shale and debris can be seen (or be heard) to fall in any site visit to the beach below. On occasion, large landslips occur resulting in tonnes of rocks falling onto the beach below (see Figures 1.4 and 1.5).

Figure 1.4 - Penarth on 2nd December, 2016. Evidence of the April 2014 landslide on the beach below. Also, the red box highlights the felling of Penarth's iconic pine trees which once overlooked the coastline (as seen in Figure 1.3). A decision was made to fell the trees in order to stabilise and protect the cliff. Source: USW, December 2016.

Figure 1.5 - Aerial Photograph of Penarth Head in 2000. Evidence of cliff failure and landslide. Source: Welsh Assembly Government.

While the effects of the sea and sea level rise may have some impact on cliff erosion, the main contributing factor is the weather - rain; temperature (sub-zero and/or heatwaves); the prevailing wind; and storm events. Extreme events (prolonged heavy rainfall; prolonged cold snap; heatwave) each can have an adverse effect on the stability of the cliffs. The sea then acts in breaking down and displacing this debris rather than being a primary force of erosion. However, that is not to say that the sea does not cause its own problems with coastal flooding at Penarth (Figure 1.6) and damage to the sea defences especially during storm surges and seasonal high tide events (Figure 1.7).

Figure 1.6 - Storm and coastal flooding at Penarth Esplanade. Source: Penarth Times, 2015.

Figure 1.7 - High tide at Penarth, January 2014. Source: Penarth Times, 2015.

It is well documented (e.g. Phillips, 2005) that Penarth has suffered from erosion for many years, partly due to weather events and in part to human activities, such as the development of the Cardiff Bay barrage and off-shore sand dredging in the Bristol Channel. Previously, the Esplanade at Penarth extended all the way down to the cliffs, culminating at a small stone-built quay and a covered (sewer) outlet (see Figures 1.8 to 1.10).

Figure 1.8 - Penarth Esplanade (walkway) in use (circa 1930). Source: Uncredited Postcard.

Figure 1.9 Penarth Quay at the end of the Esplanade (1960). Source: Uncredited Postcard.

Figure 1.10 Aerial View from left to right on Penarth beach: the Pier, the short-lived multi-storey car park, the quay and sewer casements, and the two groynes (small wall sea defences to manage erosion and sediment drifting). Source: Welsh Assembly Government / RAF, 25th April, 1975.

Since the 1970s, the Esplanade north of the pier and the quay have been left to the elements and have subsequently been eroded and destroyed (see Figure 1.11). The multi-storey car park built over the beach in 1969 was demolished in 2001 due to concerns over the columns supporting the structure and the possible impact of further erosion on the beach. It is interesting to note the two groynes in Figure 1.10 and the fact that these walls had been built up to the face of the cliff. As of 2020, the cliff face has receded by quite a few metres (see Figure 1.12).

Figure 1.11 - Erosion of the Esplanade, sea defences and quay on Penarth beach.

Figure 1.12 - Significant gaps (cliff recession) between the groynes and the face of the cliff since 1975 (Figure 1.10). Source: USW, August 2020.

There are tremendous efforts to monitor and manage the whole South Wales shoreline, including Penarth. The main challenge is obtaining and managing datasets in terms of cost; frequency of data capture; and the development of dynamic, accurate and efficient methodologies. A detailed and consistent shoreline management plan is of urgent necessity (The Vale of Glamorgan Council Scrutiny Committee "Economy and Environment": 2 February 2016). According to Phillips (2008), Penarth has experienced "extreme sea levels". It has also undergone terrible coastal erosion with massive cliff degradation (Phillips, 2005). Hence, for this research, Penarth has been chosen as the case study area for evaluating the proposed coastal monitoring strategies.

1.3 Coastal Flooding and Cliff Erosion: A Global Threat

Coastal flooding and cliff recession are not specific to the UK, but a Global threat (Cloern et al, 2016). In Nigeria (Figures 1.13 & 1.14), coastal flooding has displaced more than 25 million people (Agbonkhese et al, 2014). Yearly, there are "occurrences and reoccurrences" of coastal flooding due to global warming and other climatic changes (Nwigwe and Emberga, 2015). The lack of planning and coastal zone management has led to severe degradation of the coastlines (Ringim et al, 2016). This is a threat to the Nigerian economy as the country derives the bulk of its annual income from explorations and other mining activities along the coastlines (Ringim et al, 2016). Despite the high level of reporting and the devastating nature of coastal flooding, there is no clear definition of a strategic work plan for evaluating and monitoring coastlines in Nigeria (Ringim et al, 2016 and Nwigwe and Emberga, 2015).

Figure 1.13 - Vanishing Coastlines in Lagos (Adelaja, 2013)

Figure 1.14 - Cliff Erosion causes fears of Communities Extinction in the Niger Delta of Nigeria (Agbodion, 2016).

The aim of this research is also to demonstrate that low cost photogrammetric techniques for coastline monitoring can be applied in the developing nations. Nigeria is one such country, so was also used as a small case study area (see Appendix D). This thesis does not focus on this case study here, but the reader is advised to refer to Conference Paper for further details in the Appendix.

1.4 The Need for Low-Cost Photogrammetric Techniques for Coastline Monitoring

Coastlines are fundamentally unique features whose behavioral patterns are the subjects of numerous environmental and engineering studies (Papakonstantinou et al, 2016):

i. Determining the effects of coastal flooding and erosion (Brunier et al, 2016; Paravolidakis et al, 2016; Van and Binh, 2009)
ii. Delineating of tidal surfaces (Liu et al, 2011; Li et al, 2012)
iii. Evaluation of coastal cliff recession by the frequent crashing of the sea waves (Hapke et al, 2009 and Lee, 2008).
iv. Ascertaining the Earth's gravitational displacement for any given locality as variations in tidal heights is due to the Earth's rotation (Austermann and Mitrovica, 2015).

One major challenge to coastline monitoring is the high cost of acquiring accurate data, such as LiDAR, aerial images, and other high and very-high-resolution images (Banks et al, 2017; Khalid et al, 2016; Casella et al, 2014 and Braga et al, 2013). Shoreline changes are

unpredictable and unstable (Samanta and Paul, 2016). It is also economically unrealistic to survey specific segments of the cliff surface using LiDAR or aerial photogrammetry at very regular intervals (Dewez et al, 2016). Effective monitoring will, demand, therefore, techniques of low cost for continuous; consistent and effective approaches (Artigas and Pechmann, 2010). According to Klein et al (2001), the concern now is for "technological options" in the total management of shorelines. Techniques that are frequent enough with adaptability to climatic changes will provide the most needed technological options (Clark, 2017; Results from ResMar Project, 2013 and Smeeckaert et al, 2013). There is a need for an innovative regular methodology to monitor features such as cliff surfaces (Clark, 2017; Dewez et al, 2016 and Earlie et al, 2014). Essentially, to be applicable to developing nations, then methodologies need to be affordable and regularly undertaken. Figure 1.15 presents an overview of the methods which have and can be used for coastline monitoring, which will be discussed in detail later in the thesis. Most of the traditional techniques (e.g. satellite imaging, aerial photography, LiDAR, terrestrial laser scanning, etc.) are very expensive to source data or to purchase the necessary hardware to undertake such surveys. In most cases, these are beyond the means of many coastal monitoring programmes, especially those on limited budgets or in developing nations.

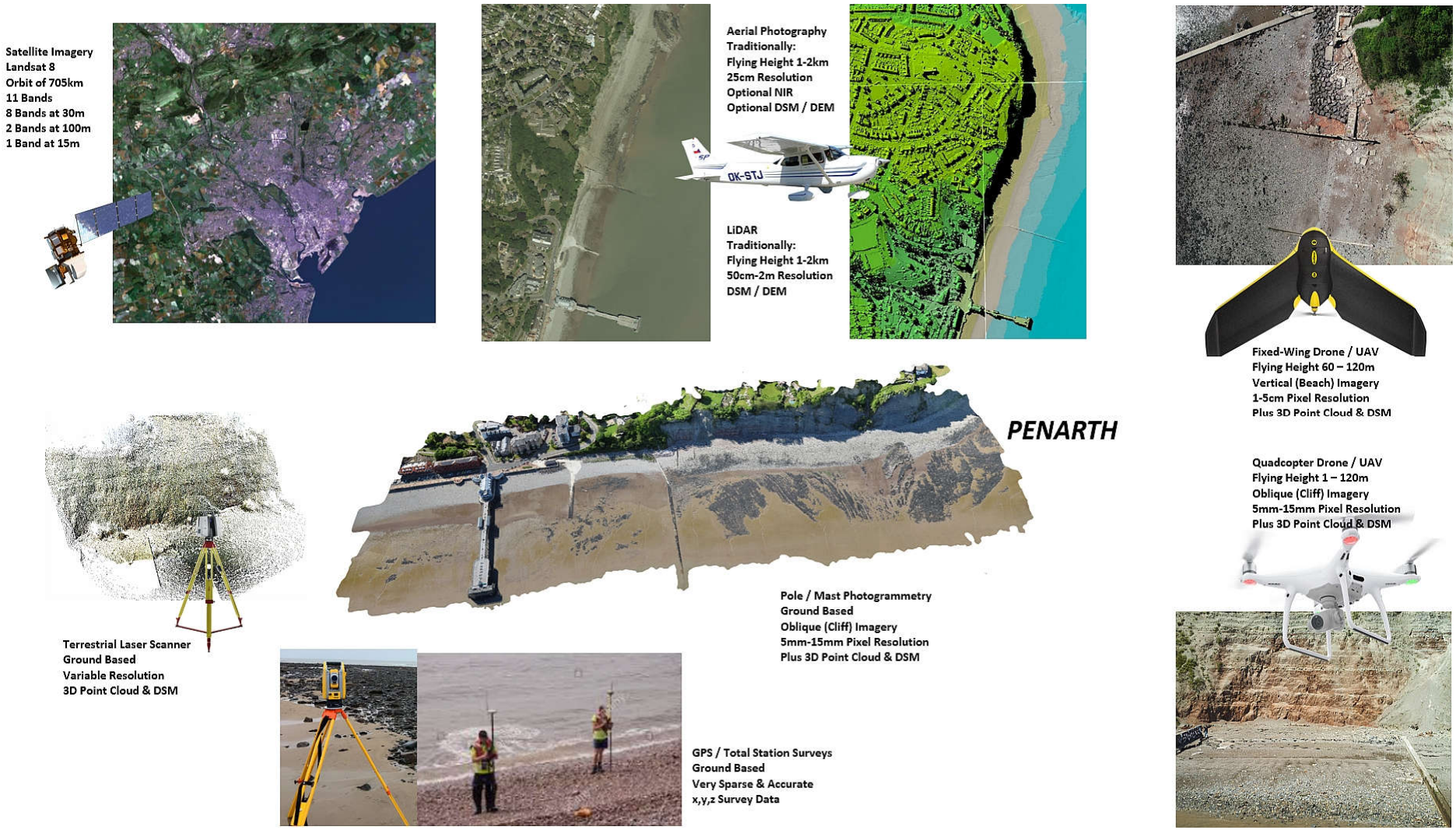

Figure 1.15 Survey Techniques for Coastal Monitoring – A Brief Overview

1.5 Research Aim

This research aims to develop new low-cost close-range digital photogrammetry techniques and practices for coastal cliff and beach monitoring with optimal frequencies of surveys, resolution, localization, precision, and accuracies.

1.6 Research Objectives

1. To implement an excellent low-cost practice in close-range digital photogrammetry comparable to LiDAR and the Terrestrial Laser Scanners for obtaining 1cm to 3cm change detection on the coastal area.

2. To develop a low-cost, simple, pole photogrammetry technique for acquiring digital images for cliff monitoring.

3. To develop change detection and prediction model algorithms for coastal cliff monitoring using images obtained from close-range digital photogrammetry.

4. To implement low-cost best practices for spatial analyses to obtain micro-level change detection and classification of features on the beach.

5. To develop a coastal area information monitoring infrastructure for beach and coastal cliff management.

1.7 Research Questions

1. Are the UAV's outputs comparable with Airborne LiDAR and the Terrestrial Laser Scanners for coastal area monitoring?

2. What are the most economically viable photogrammetry sensors and platforms to obtain 1cm to 3cm accuracies and high-resolution images for regular coastline cliff monitoring?

3. Can an algorithm from the UAV point cloud be applicable for change detection on the coastal cliff and develop a coastal cliff prediction model?

4. Can low-cost UAV outputs achieve micro-level change detection and classification of features (as small as 1 cm) along the coastal area and other geomorphological studies?

5. Can coastal area information monitoring infrastructure for beach and cliff management be developed with low-cost digital photogrammetry techniques?

1.8 Outline of Thesis

Chapter 2 is in two sections. The first section provides a historical outline of traditional surveying equipment in providing topographical information about the coastline. The second part is a contemporary review of the application of remote sensing and digital photogrammetry techniques in monitoring the shoreline and its cliffs.

Chapter 3 provides detailed background studies on the methodologies adopted in this thesis. These illustrate the author's understanding of the Automatic Aerial Triangulation (AAT) and the bundle adjustment (BA) and on how these conceptualise the theoretical framework and the design of the adopted close-range digital photogrammetry techniques.

Chapter 4 is the actual reconstruction process of a new close-range digital photogrammetry technique for monitoring the coastal cliff. This chapter develops an innovative low-cost and simple field survey method of digital photogrammetry using the pole as a platform and a mobile phone as a sensor. The chapter objectives provide the most practical vertical camera angle, survey distance to the cliff, practical overlaps, and realistic time range duration for executing these surveys are determined from the basic surveying principles.

Chapter 4 also develops another innovative theoretical and digital computational framework for determining areas of change and volume of change between two-point clouds. A straightforward and flexible python algorithm can determine change using the Kd-tree nearest neighbor (KNN) search on pre-aligned points clouds. This algorithm also extracts the change array for visualization and volumetric change computation.

Chapter 5 evaluates the accuracies of the pole photogrammetry and the newly developed point cloud change-detection algorithm for cliff deformation monitoring. This chapter also designs and develops a new prediction model to monitor the cliff collapse/fall. This prediction model helps to forecast when and where the next cliff fall would likely occur.

Chapter 6 evaluates the best drone photogrammetry practices for acquiring 1cm resolution and 1cm vertical accuracy digital outputs for monitoring the beach. This chapter research the best low-cost practices for Global Navigation Satellite System (GNSS) Ground Control Points (GCP); low-cost strategies for processing digital images; an open-source solution for detecting and analysing 1cm changes on the beach. This chapter introduces a new three-tier analysis technique from the small-scale LiDAR datasets to the large-scale drone dataset.

Chapter 7 is a beach monitoring infrastructure developed from the accurate and low-cost strategies in chapter 6. Small changes (1cm-3cm) are visible on the digital models for scientific and visualization purposes.

Chapter 8 is the general discussion of results, conclusion, research limitation and recommendation for future research.

Chapter 2

Literature Review (Section A)

This chapter is presented in two Sections. The first part presents the literature review with respect to the main approaches to surveying techniques which have been used for modelling and managing the coastal environment. The second part then focuses on the use of digital photogrammetry, or the use of imagery for capturing measurements from objects in the photographs.

2.1 Historical Evaluation of Traditional Land Surveying Methods in Coastal Area Monitoring (Shoreline, Beach and Cliff)

Historically, shorelines were monitored using conventional land surveying equipment like the plane table, alidade, levelling instrument, and theodolite (Braga et al, 2013; Zhou and Xie, 2009 and Fairley et al, 2016). In contemporary times, modern surveying equipment like digital theodolites, total stations, differential Global Navigation Satellite System (GNSS) and terrestrial laser scanners are still of relevance in shoreline monitoring (Chen et al, 2018; Elaksher, 2017; Labuz, 2016; Allan and Stimely, 2013; Zhou and Xie, 2009). Tidal lines derived from theodolites and total stations are more accurate and precise (Zhou and Xie, 2009) compared to those from satellite imagery (Krueger and Souza, 2014; Mason et al, 2000). Similarly, the automatic levelling technique can attain a vertical accuracy of ± 10mm, which still makes it one of the most accurate methods of determining volume change along the beach (Fairley et al, 2016). Monitoring of beach erosion using Electronic Distance Measurement (EDM) like the total station is also accurate with high temporal resolution (Cheng et al, 2016 and Fairley et al, 2016). However, the use of traditional land surveying equipment is tedious; difficult to survey certain seascapes or beaches with limited access; has very low spatial density of measurement; and often both labour-intensive and time-consuming (Brunier et al, 2016; Giannini and Parente, 2015; Cheng et al, 2016; Braga et al, 2013). A historical evaluation of the application of traditional land surveying methods is necessary to understand the advantages and disadvantages of large/medium scale surveys in coastline monitoring (Westoby et al, 2018 and Mason et al, 2000). This will help to justify the need for alternative low-cost coastal surveying with centimetre accuracies (Goncalves et al, 2018 and Turner et al, 2016) and lastly, it elucidates the efficiencies of large/medium scale

very high-resolution mapping for generating time-series data for monitoring the coastal environment (Mahabot et al, 2017 and Papakonstantinou et al, 2016).

2.1.1 Theodolites

A theodolite is a precision optical instrument for measuring angles between designated visible points in the horizontal and vertical planes. The use of theodolites in monitoring shorelines dates to the 1970s (Loureiro et al, 2014; Overduin and Couture, 2006). Theodolites are simple to use land survey equipment which can be used repeatedly and reliably to capture data – for example, as in the extent of change along the Barrow Strait beach between 1970 and 1980 (Overduin and Couture, 2006). Theodolites can derive both primary and secondary geospatial data with derived accuracies in centimetres (Overduin and Couture, 2006).

Loureiro et al (2014) successfully used theodolite surveying to develop beach monitoring programmes at localized mapping scales. This includes a detailed topographical survey showing the extent of accretion and erosion between the El-Bar and Damietta Harbour coastlines in Egypt (El-Asmar et al, 2016). Horizontal and vertical angles measured between successive transects on sections of the coastline will precisely define the geolocation and describe the surface configurations of points measured (Bailey and Lusseau, 2004; Mason et al, 2000). Theodolite surveying can be used to accurately determine the extent of cliff retreat and sea erosion (Anfuso et al, 2007).

Despite the high accuracies of results and the ease of surveys using the theodolite in the aforementioned shoreline management projects, photogrammetry, and remote sensing techniques will improve on the temporal, spatial and spectral resolutions especially in difficult coastline terrains (El-Asmar et al, 2016; Anfusoet al, 2007 and Wangensteen et al, 2007). Furthermore, automated techniques will not only improve the volume of data collected, but using less labour; possibly less cost; and possibly less (human) errors or mistakes.

2.1.2 Total Stations

A total station is an electronic/optical surveying instrument comprising an electronic transit theodolite integrated with electronic distance measurement (EDM) to measure both vertical and horizontal angles and the slope distance from the instrument to a particular point, and uses an on-board computer to collect data and perform triangulation calculations. Motorised

versions allow the operator to control the instrument from a distance via remote control or mobile device, thereby eliminating the need for an extra surveyor.

The application of the total station theodolite in coastline monitoring and management began to gain popularity in the 2000s (Labuz, 2016). Detailed usage of the total station in coastline monitoring from the 2000s is described by Cheng et al, 2016; Gutierrez et al, 2001 and Schwimmer, 2001. It can generate precise and accurate data for coordinating and quantifying beach morphology (Cheng et al, 2016; Bio et al, 2015; Allan and Stimely, 2013; Vila-Concejo, 2010).

The study by Cheng et al, (2016) analyzes the practicability of the electronic total-station surveying in measuring beach accretion and erosion and compares the results with LiDAR and UAV photogrammetry. The several beach profiles along the Microtidal Coast of west-central Florida were accurately coordinated and delineated using the total station. The flexibility of usage enhances the temporal resolution. The usage of the total station is therefore limited by low spatial resolution and likely not feasible to survey shorelines with high wave-energy patterns (Cheng et al, 2016).

To validate slope estimated on the shorelines of Kerteh Bay, Terenggau, Malaysia from Landsat imagery, comparisons have also be made on the total station readings (Tunji et al, 2014). Periodic total-station readings along the Port Stephens of Sydney in New South Wales were used to generate precise DTMs to determine the actual angular deflections in the beach slope and quantify volumetric changes (Vila-Concejo et al, 2010). This research by Vila-Concejo et al. (2010) recommends the need for similar surveys at other survey sites to be able to simulate correctly on erosion and sediment pattern. Such intermediary surveys on smaller scales with high temporal resolution are often rarely practicable with the total station (Bio et al, 2015; Brunier et al, 2016).

Liu et al, 2017 monitored changes in tidal lines using the total-station surveying equipment. This study evaluates changes from a fixed tidal surface as caused by high-energy waves and other manufactured defense measures. Whereas the use of the total station and the RTK-DGPS will successfully map out the tidal surfaces over time, the researchers swiftly admit the uncertainties with this methodology especially for shorelines with abrupt changes. Tidal surfaces are also spontaneous with varying spatial resolutions (Samanta and Paul, 2016; Tseng et al, 2010 and Murray et al, 2009).

Although ground-surveying methods can attain vertical height accuracies of 1cm along transects of tidal heights (Mason et al, 2000), there is no defined methodology of monitoring coastal cliffs using the total station. The morphological structure of coastal cliffs is very unstable due to constant land-sea interference (Matano et al, 2016 and Lee, 2008). Landslides on the cliff surface are therefore unpredictable (Brun et al, 2016 and Moore et al, 2010). Effective management of the coastal cliff surface should involve methodologies that are safe enough, with excellent temporal, spatial, and spectral resolutions (Westoby et al, 2018 and Brun et al, 2016). Due to the structural deformation pattern, surveying coastal cliff surfaces in segments might not produce the correct insight on the cliff geo-mechanical formations (Dewez et al, 2013). Janerals et al, (2015) in their proposed monitoring plan for the Montserrat Mountain in Catalonia, North-East Spain, had included the total-station as one of the four techniques. The total-station in most cases is to provide precise and accurate reference station(s) for coastal cliff monitoring (Janeras et al, 2015 and Matano et al, 2015). Effective coastal cliff monitoring should include techniques with varying spatial and increased temporal resolutions (Janerals et al, 2015).

2.1.3 Conclusion on Land Surveying Methods

Ground surveying methods in coastal monitoring and management are time demanding (Kim and Lee, 2017; Bio et al, 2015; Allan and Stimely, 2013; Zhou and Xie, 2009). These techniques are also labour intensive (Kim and Lee, 2017; Cheng et al, 2016; Bio et al, 2015; Zhou and Xie, 2009). Ground surveys are easier and accurate on favorable atmospheric conditions (Westoby et al, 2018and King et al, 2017). Acquisition of data using the theodolite and total station is often at intervals and this could lead to systematic errors (Loureiro et al, 2014). Conventional land surveying equipment is very difficult to survey complex and dangerous topographies (King et al, 2017). The high spatial density of surface points cannot be achieved from the use of only the conventional land surveying techniques (Brunier et al, 2016 and Cheng et al, 2016) whereas such clusters of surface points are required to generate DEM (James and Quinton, 2013). Total stations and electronic theodolite for coastal monitoring are therefore preferred to validate results obtained from other methodologies (Anandabaskaran and Vijayakumar, 2017; Cheng et al, 2016; Janeras et al, 2015 and Tunji et al, 2014).

2.2 Airborne LiDAR

LiDAR (Light Detection and Ranging) is an optical remote sensing technology that measures properties of scattered light to identify the distance and/or other information of a remote target (Doyle and Woodroffe, 2018; Irwin et al, 2017 and Martins et al, 2016). LiDAR is an active sensor that uses a pulsed laser (Light Amplification by Stimulated Emission of Radiators) to measure between distances (Bater and Coops, 2009). A laser scanner uses the laser beam of intense coherent electromagnetic radiation to digitally recreate the physical properties of an object, building or the terrain from dense point clouds created by stimulated emission on the object, building or terrain surface (Kromer et al, 2017; Barrand et al, 2009; Bater and Coops, 2009 and Eitel et al, 2009). The laser beam recorded by a sensor produces the 3D dense point cloud (Eitel et al, 2016). 3D scanning equipment first came into the limelight in the early 1960s and at present, the laser scanners could use other wavelengths apart from the visible light (Doneus et al, 2013 and Jha et al, 2008).

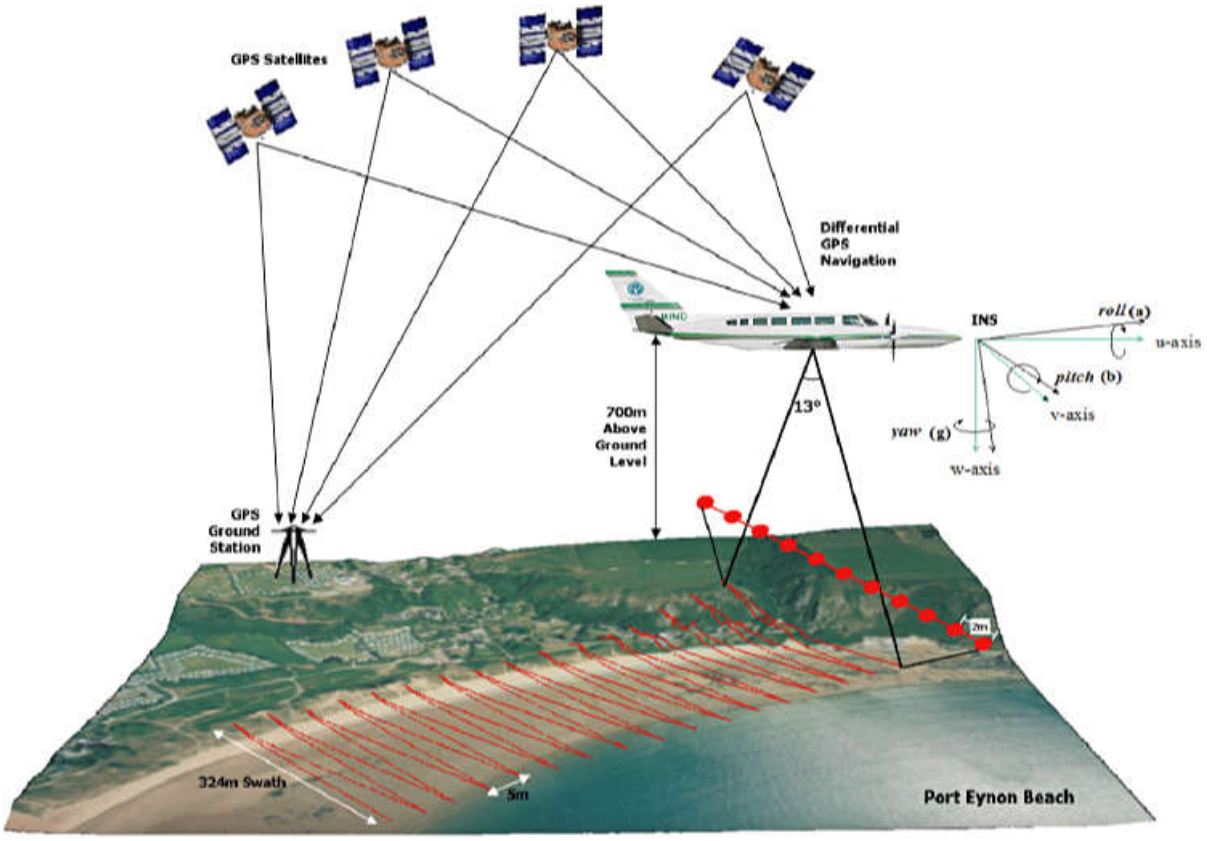

Figure 2.1 - A typical LiDAR system that produces a swath of finely sampled x,y,z surface points across a beach environment (Reproduced by kind permission of Leigh et al. 2009).

As Leigh et al. (2009) illustrates, a LiDAR system comprises three data collection tools mounted on an aircraft: a laser scanner, a Global Positioning System (GPS) receiver and an Inertial Navigation System (INS). The GPS accurately measures the position of the aircraft and the INS measures the roll, pitch and yaw of the aircraft. The laser is emitted and the elapsed time from when the laser is reflected from an object or the ground is measured, and knowing the speed of light, the distance can be easily determined (see Figure 2.1).

Researchers and professionals are using the airborne LiDAR to obtain reliable information about the shoreline (Lee et al, 2011b; Liu et al, 2011; Xharde et al, 2006) and applicable to several shoreline classification or composition (Andersen et al, 2017; Doyle and Woodroffe, 2018; Martins et al, 2016 and Schmid et al, 2011). LiDAR has a broader tide window for data acquisition (Li et al, 2012 and Lee et al, 2011b) and very high frequency for data capture which is relevant for the survey of an expansive area (Nijland et al, 2016; Lee et al, 2011b). Spectral variations and shadows from land cover would often not affect the efficiencies of the Laser beams (Andersen et al, 2017; Eitel et al, 2016 and Liu et al, 2011). It is also efficient in extracting the shoreline irrespective of the water level, the extent of the shoreline, or even the geography (Andersen et al, 2017 and Li et al, 2012). Digital Elevation Models obtained from airborne LIDAR has excellent categorization and "detailed delineation" as compared with elevation models from aerial and satellite imagery (Li et al, 2012 and Gesch, 2009). The key element of LIDAR DEM is the contouring network capable of delineating between the grid pixels with an elevation below or above tidal datum and each representing "water" and "land" respectively (Liu et al, 2011 and Lee et al, 2011b). At larger scales, LiDAR DEMs will quantify volumetric changes on mountainous glaciers (Barrand et al, 2009). Previous attempts to monitor the cliff surface using airborne LiDAR are often limited by scale, verticality, and a flying height of the platform and make it difficult to generate a coherent light beam on the sea-caves and wave-cut notches (Young et al 2010; Xharde et al, 2006). Leigh (2008) documents a study to measure the volumetric changes of the beaches of the Gower Peninsular in South Wales using annual LiDAR surveys.

The Laser beams from several Laser returns produce the elevation grid and tidal heights (Yousef and Iftekharuddin, 2014; Schmid et al, 2011). The reliability and effectiveness of this elevation grid network is dependent on the accuracy of point registration and interpolation (Yousef and Iftekharuddin, 2014; Barrand et al, 2009). The quality of the ground controls and how sparsely distributed will greatly influence the accuracies of the LiDAR DEM (Liu et al,

2011 and Aguilar et al, 2010). To minimize errors from point registration and interpolation, Gesch et al (2016) and Li et al (2012) both suggest the inclusion of the vertical datum transformation in the processing routine. The vertical datum transformation model automatically converts the derived LiDAR data from the ellipsoidal datum to any desired local tidal datum (Gesch et al, 2016; Cooper et al, 2013 and Li et al, 2012).

Airborne LiDAR is used to monitor coastal morphology and landforms (Doyle and Woodroffe, 2018; Andersen et al, 2017; Martins et al, 2016; Nijland et al, 2016; Pye and Blott, 2016; Li et al, 2012; Lee et al, 2011b; Aguilar et al, 2010 and Zhou and Xie, 2009). Doyle and Woodroffe (2018) used the LiDAR datasets to differentiate between the several layers of vegetation and the other components of the bare earth. This study also examined the vertical canopy of the sea vegetation, characterization, and layering of other components of the bare earth along the foredune using the LiDAR datasets. The processing of the LiDAR LAS files was cumbersome with several stages of file conversion. In a similar study, sediment computation using LiDAR datasets is to primarily evaluate and access the effects of coastal erosion and accretion along the dune and beach of several coast locations in the United Kingdom (Pye and Blott, 2016). The study identifies the potential classification errors between the bare earth and vegetated ground as causes of errors in the LiDAR's DEM. Although some filtering algorithms are effective on the LiDAR, this study does not provide clear evidence of whether the tidal contour of the respective morphological features was inherently not influenced by unfiltered LiDAR data.

Zhou and Xie (2009) performed a time series 3-D morphological change study to be able to establish the influence of weather variation on the volumetric change pattern of the typical beach and dunes. This study evaluates the consistencies of the spatial data pattern of the LiDAR's dataset in modelling the Assateague Island National Seashore in the United States. The gridded LiDAR DEMs are used to calculate the accretion and erosion. The vertical levels of the beach and dunes are similarly marked out on the gridded LiDAR DEMs to understand the beach change pattern. The tidal crest derived from the delineated beach and dunes did not tally with the 3D morphological change pattern due to minimal temporal resolution and the changeable climatic conditions. Incoherence in several data sources, unfiltered LiDAR data, and variability in the processing routine for LiDAR are potential sources of errors on the gridded LiDAR's elevation (Amante, 2018).

LiDAR is also used to determine tidal heights and vertical surfaces along the shorelines (Obu et al, 2016; Cooper et al, 2013; Li et al, 2012; Gesch, 2009; Lee et al, 2011b; Liu et al, 2011; Zhou and Xie, 2009; Liu et al, 2007). A special quality with the LiDAR is the DEM contouring network that can delineate easily between the grid pixels whose elevation is below or above a tidal datum representing water and land (Obu et al, 2016; Liu et al, 2011 and Lee et al, 2011b). The study by Obu et al (2016) used the LiDAR datasets to evaluate tidal lines elevations along the Yukon Coastal Plain and the Herschel Island in Canada. This study establishes the impact of short-term tidal lines changes on other coastal processes. Though the LiDAR DTM depicts a 3-D breaking for the respective surveys, this study, however, did not outline a clear methodology for obtaining shorelines from LiDAR. According to Cooper et al (2013), a standard and well-outlined methodology would assist to reduce associated errors in the LiDAR datasets. Unresolved errors in the LiDAR datasets also amount to an inconsistent DEM with wrong interpolations on the respective vertical surfaces (Cooper et al, 2013). LiDAR-based elevation of the shoreline could be difficult to resolve in coastlines characterized by seaweeds or dunes (Nijland et al, 2016). Although the LiDAR can incorporate additional sensors, there is still the limitation of matching the flying height of the digital camera with the LiDAR relative to the vertical accuracy requirement of the digital camera (Mitishita et al, 2016). Nijland et al (2016) had used therefore the threshold elevation derived from other erosion classifiers to generate a shore-perpendicular bisector that marked the shoreline on a LiDAR DTM. The confusion matrix and cohen's statistical models compute the threshold elevations.

Other limitations and bias of LiDAR-derived DEM in delineating tidal surfaces are encapsulated in Cooper et al (2013) and Liu et al (2007). Cooper et al (2013) and Nijland et al (2016) also identify areas vulnerable to sea-rise as difficult to map accurately. The difficulty with the LiDAR DEM in categorizing between coastal marshes and the bare earth could be a challenge in identifying the thin line between land and sea (Hladik and Alber, 2012 and Schmid et al, 2011). Shorelines cannot be mathematically or visually extracted from LiDAR raw dataset (Liu et al, 2011 and Lee et al, 2009) but from LiDAR DTM correctly referenced to a tidal datum (Nijland et al, 2016; Yousef and Iftekharuddin, 2014; Li et al, 2012 and Liu et al, 2011). Liu et al (2011) and Lee et al (2009) both emphasized that shorelines from LiDAR elevations are best extracted by creating a center of mass about the regions immediately above and below the tidal datum surface. The conversion of LiDAR raw

points into defined tidal datum can also displace the tide-coordinated shorelines (Liu et al, 2011). LiDAR raw data are heavy files and rigorous to process (Du and Lee, 2012).

Coastal cliff erosion is monitored from derived airborne LiDAR DEMs (Young, 2018; Palaseanu-Lovejoy et al 2016; Earlie et al, 2014; Earlie et al, 2013; De Rose and Basher, 2011; Bowles and Cowgill, 2012; Young et al, 2011 and Young et al, 2010). Cliff surfaces monitored by airborne LiDAR are mainly on the large and medium-scale (Young, 2018; Palaseanu-Lovejoy et al, 2016 and Earlie et al, 2014). For precise digital spatial analysis, the cliff surface surveyed from airborne LiDAR often requires auxiliary datasets from other photogrammetric sources (Young, 2018 and Young et al, 2010). It is difficult to survey the cliff surface with the airborne LiDAR without the LiDARs erroneous data (Michoud et al, 2014 and Young et al, 2009). According to Michoud et al (2014), airborne LiDAR cannot generate accurate DTM for cliff monitoring. Erroneous data are caused by the cliffs' surface unstable slope (Earlie et al, 2014), poor textural surface, and other illuminations as caused by vegetation (De Rose and Basher, 2011; Young et al, 2009). To survey the cliff surface with reduced LiDARs erroneous data, Young (2018), Palaseanu-Lovejoy et al, (2016), and Young et al, (2010) suggest the need to segment the grid cells on the cliff surface. Cliff surface change from inferences on the cliff-top and cliff-toe lines is recommended by (Palaseanu-Lovejoy et al, 2016); inferences from the cliff edge (Young et al, 2011); using deposited materials on the cliff toe (Earlie et al, 2014) and by the differencing of successive DEMs (Young et al, 2009). The preciseness of these methodologies is still in doubt due to the rapid geomorphologic changes and extreme weathering processes present at the cliffs' top, toe and sides (Matano et al, 2016; Barton and Pearce, 2015; Somma et al, 2015 and Fanti et al, 2013).

Presently, there is no specific methodology for monitoring the cliff surface (De Rose and Basher, 2011 and Young et al, 2011). Airborne LiDAR is best suited for long-term monitoring (Earlie et al, 2014). Monitoring of the cliff surface would require DEMs created in series (De Rose and Basher, 2011 and Young et al, 2010). Close range laser scanning generates more details about the cliff surface than airborne laser scanning (Young et al, 2010). It also produces higher vertical accuracies than the LiDAR (Chen et al, 2018). Recent research recommends the close-range laser scanning for precise and continuous deformation monitoring of the cliff surface (Earlie et al, 2017; Matano et al, 2016; Smith, 2015; Young et al, 2010; Abellan et al, 2010).

It should be noted that in Wales, the Natural Resources Wales (NRW) is currently allowing LiDAR datasets to be downloaded for use under an Open Government Licence. However, the data is typically at least five years old. LiDAR datasets are available at resolutions of 1 or 2 metres, with some limited areas available at 50cms or 25cms (see Figure 2.2 for an example of the data available for Penarth).

Figure 2.2 LiDAR Datasets available for Penarth, South Wales through LLE, the Natural Resources Wales (NRW) Geo-Portal website funded by the Welsh Assembly Government at: http://lle.gov.wales/catalogue/item/lidarcompositedataset?lang=en

2.3 Terrestrial Laser Scanners (TLS)

The terrestrial laser scanner (TLS) is LiDAR mounted on a tripod on the ground (Abella et al, 2010; Kuhn and Prufer, 2014; Abella et al, 2010). By 1999, there were attempts to monitor the cliff and coastlines using the TLS (Huber and Hebert, 1999). TLS is typically on tripods like other conventional land surveying equipment with its principles like the Airborne Laser Scanners (ALS). Points are measured 360^0 in the horizontal and 100^0 vertical directions (Letortu et al, 2018). The laser beam can capture discrete parts of the object, building, or terrain precisely as point measurements are at multiple angles and close range (Caputo et al, 2018 and Letortu et al, 2018).

The application of the TLS to monitor slope deviations and instability in the Pozzuoli bay coastal cliff of Posillipohill, Napales, mainly used inferences from discontinuities on the spatial correlation of parts of the modeled cliff surface (Somma et al, 2015). The dimension of the cliff monitored is 140m high by 250m wide. This study relied on the magnitude of submerged point clouds as generated from the intensities of the Laser beams to create a 3D model of the cliff surface. The entire process relied on the magnitude of the submerged point clouds generated from the intensity of the Laser beams (Somma et al, 2015). TLS is usually with erroneous data (Smith et al, 2015). This is likely as in the case with this study that used the time-of-flight TLS technique to acquire the 3D model of the cliff surface. In the time-of-flight, the TLS technique, the speed of the emitted pulse of light can be influenced by the surrounding illumination not traveling in the same wavelength as the laser beam (Kromer et al, 2017 and Olsen et al, 2009). Irregular surface edges with varying spectral reflectance characterize the coastal cliff surfaces (Galea et al, 2014 and Lague et al, 2013). Erosion and other natural sedimentation processes frequently alter and disintegrate analogous components causing varying spectral intensities on the cliff surface (Brodu and Lague, 2013). The Homogenous surface nature of most cliff surfaces would often lead to a change in the temperature of the emitted laser beams, which alters the time of the returned beams (Letortu et al, 2018). Un-edited flaws cause wrong intensities of spatial variations, which could lead to anomalies in the digital surface model (Kromer et al, 2017; Young et al, 2009). The study by Calligaro et al (2013), confirms the availability of flaws in scanned laser beams, as caused by the complexities in the surface morphology of the cliff.

Other studies by (Matano et al, 2016 and Calligaro et al, 2013) on the application of the TLS in coastal cliff monitoring only aimed at assessing the spatial correlation and angular

orientation of the cliff surface components. Both studies did not outline methodologies for regular monitoring of the cliff surface and quantifying the amount of change over time. Lague et al (2013) developed an algorithm that would compare 3D point cloud produced by the TLS using the direct distance technique. Their study aimed at removing extraneous point clouds generated from incident beams at varying intensities but did not outline a methodology for improving the temporal resolution with the application of the TLS 3D point cloud. Kuhn and Prufer (2014), expounds on the relevance of developing high spatial and multi-temporal resolution monitoring framework with the TLS.

Holland et al. (2008) also demonstrates the potential use of TLS for mapping the beach and sea defences at Penarth (see Figures 2.3 & 2.4) and comparing the data with traditional airborne LiDAR. The method has potential, but one drawback of the approach is the variable density of laser returns as the angle of the laser scanner rises. Ideally, the TLS needs to be mounted at an elevated position in order to maximise the data volume and minimise the divergence of data returns.

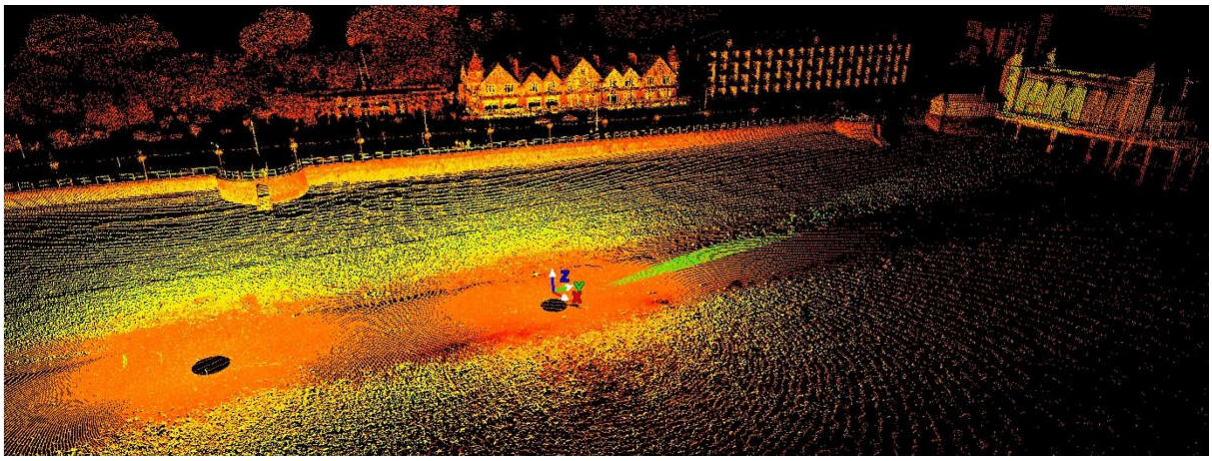

Figure 2.3 Terrestrial Laser Scanner 3D Point Cloud for the beach, sea defences, esplanade and pier at Penarth. Source: University of South Wales, 2008.

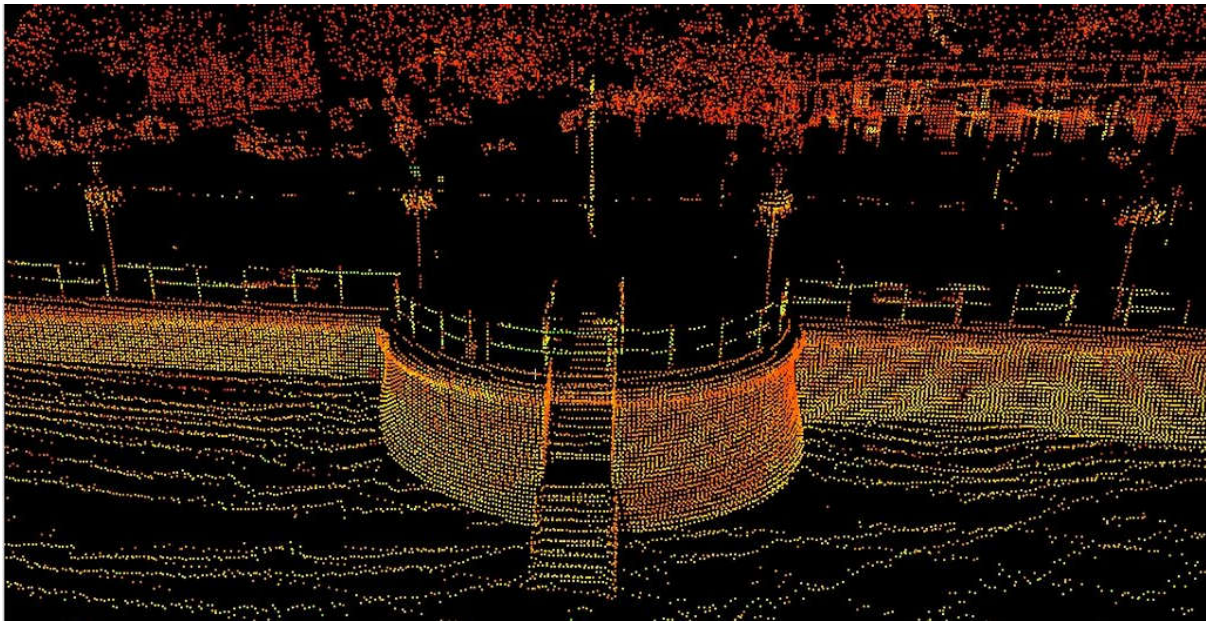

Figure 2.4 Terrestrial Laser Scanner 3D Point Cloud for the beach, Esplanade sea wall and steps at Penarth beach. Source: University of South Wales, 2008.

A long-term coastal cliff-monitoring plan could be inadequate to understand the several deformation processes (Kuhn and Prufer, 2014). A fully developed precise and short-term monitoring infrastructure will enhance the understanding of long-term coastal cliff monitoring (Westoby et al, 2018; Moore and Griggs, 2002). It is also required to develop strategic management plans (Moore and Griggs, 2002) and implement scientific hazard control/prevention on the coastal cliff area (Fraser et al, 2017). In the study by Letortu et al (2015), weekly surveys were to fully understand the several dynamics of the coastal cliff and further hypothesize a strategic work plan. In this context, the bi-annual monitoring technique as employed by Kuhn and Prufer (2014) will not conform to the definition of multi-temporal resolution.

TLS also has wide applications in managing the coastlines (Fabbri et al, 2017; Vos et al, 2017; Fairley et al, 2016; Schubert et al, 2015 and Julge et al, 2014). Application is in the monitoring of tidal heights (Bitenc et al, 2011 and Julge et al, 2014), quantifying beach erosion and accretion (Vos et al, 2017 and Julge et al, 2014) and coastal zone morphology (Fabbri et al, 2017 and Vos et al, 2017). Coastlines require surveys at very regular intervals to predict coastal flooding/erosion and devise the appropriate shoreline management techniques (Fabbri et al, 2017; Vos et al, 2017; Results from Resmar Project, 2013, and Bitenc et al, 2011). Not all coastal cliffs are easily accessible for surveys (Bitenc et al, 2011). The

flexibility of the TLS to be able to survey shorelines immediately after the storm and during other environmentally challenging situations with necessary accuracies is still debated (Vos et al, 2017; Labuz, 2016).

Coastal cliff monitoring would require frequent surveys to be able to understand change effects and patterns (Letortu et al, 2018; Kromer et al, 2017; Letortu et al, 2015; Brodu and Lague, 2012; Abellan et al, 2010). Regular surveys are also required to overcome the effects of shadow cast and unwanted beams (Brodu and Lague, 2012).

TLS unarguably produces high spatial resolution data to help understand the structural framework of the coastal cliff (Letortu et al, 2015; Kuhn and Prufer, 2014; Somma et al, 2015; Abellan et al, 2010 and Abellan et al, 2010). There are, however, uncertainties about the ability to regularly survey sites (temporal resolution) due to the high cost of purchase (Kromer et al, 2017; Cheng et al, 2016 and Gomez-Gutierrez et al, 2014) and the high level of expertise required to process the data (Westoby et al, 2018; Kromer et al, 2017 and James et al, 2013). Regular surveys are also limited by convenience and timing (Westoby et al, 2018; Brodu et al, 2012). TLS would hardly scan the "sink and shielded" sections of undulating surfaces (Chen et al, 2018). The overall accuracies of the use of the TLS depend on the regular power supply and favourable atmospheric and weather condition(s). Similarly, the fixed height of surveying on the beach might limit the density of data capturing the cliff surface.

The monitoring of the cliff surface with TLS would require a high volume of scanned points taken over an appreciable time range (Somma et al, 2015; Caputo et al, 2018 and Olsen et al, 2009). Kromer et al (2017) had therefore developed the "automatic terrestrial laser scanner with near-real-time change" intending to provide high temporal resolution. Influence on the results obtained by Kromer et al (2017) is mainly by atmospheric conditions and the entire system depends on the power supply, which could make the methodology very difficult to use such as in an emergency survey like immediately after a storm. According to Chandler and Buckley (2016), the average cost of a terrestrial laser scanner is between US$30,000-$80,000 (£25K to £55K). It would be difficult therefore to achieve time-series surveys with the TLS as cost would be a limiting factor.

2.4 Aerial Photography

Aerial photographs have been used to monitor the shorelines due to its high spectral and spatial resolution (Braga et al, 2013; Li et al, 2012; Webb and Kench, 2010; Sesli et al, 2009). The use of aerial images for coastal monitoring is also coupled with the availability of very old time series aerial photos (see Figure 2.5 below) for comparative evaluations (Redweik et al, 2016; Braga et al, 2013; Sesli et al, 2010; Slonecker et al, 2010; Webb and Kench, 2010; Sesli et al, 2009; Addo et al, 2008). The older aerial photographs could suffer from shrinkage and poor resolution (Redweik et al, 2016 and Webb and Kench, 2010) while cost and time of executing aerial surveys further limit their use for coastal monitoring (Braga et al, 2013).

The wet/dry land indicator visible on aerial images are useful for visual delineation of the several tidal heights on the coastlines (Braga et al, 2013; Slonexker et al, 2010) but the visual interpretation of the thin line between the sea and land is more achievable on higher-resolution images (Callaghan et al, 2015). Paravolidakis et al (2016) explain the procedure to eliminate noise and techniques to modify the threshold in land and sea segmentation.

Hamylton (2017) suggests that geomorphologic processes on the coastlines are discernible through visualizations on aerial images. Multi-band aerial photographs can be on several ground elevations networks (Li et al, 2012 and Lipakis et al, 2007). This, however, depends on the wet/dry land indicator mainly deduced from the high-water line (Su and Gibeaut, 2017; Hoang et al, 2017; Braga et al, 2013 and Chaaban et al, 2012). The wet/dry land indicators sometimes differ from the actual mathematical tidal surfaces HWL or MHWL (Pardo-Pascual et al, 2018 and Pussella et al, 2015). Aerial images should be rectified and of high resolution to achieve correct assertions on the physical morphology of the coastlines (Braga et al, 2013; Bheeroo et al, 2016). The temporal resolution of the aerial images is often not consistent due to variability in flying height, tilt, haze, and shadow (Morgan et al, 2010). In general, the capturing of aerial images is constrained by weather conditions (Paravolidakis et al, 2016 and Morgan et al, 2010). Ford (2013) explains other sources of possible errors in evaluating tidal lines and coastal morphology from aerial images.

Aerial images can give a historic transition of the cliff's surface (Warrick et al, 2017; Earlie, 2014; Stuiver, 2013; Montreuil and Bullard, 2012; Zviely and Klein, 2004). Existing studies on the application of aerial images in monitoring the cliff do not provide detailed analytical descriptions and geometric measurements about the cliff (Addo et al, 2008; Zviely and Klein, 2004; Moore and Griggs, 2002). The research by Stuiver (2013) further explains the

possibilities of wrong interpretation of the cliff surface such as from plotting, interpretative, and distortion errors. Aerial images cannot capture the cliff surface in detail (Earlie et al, 2014) but according to Warrick et al (2017), detailed topographical data are crucial in determining the continuous failure and recession pattern on the cliff surface.

Figure 2.5 RAF / Welsh Government Aerial Photograph of Penarth in June, 1942.

2.5 Satellite Imagery

Satellite remote sensing can provide high-resolution multi-spectral digital imageries for shoreline monitoring and coastline management (Maglione et al, 2014; Maglione et al, 2015; Braga et al, 2013 and Lipakis et al, 2007). The World-view, GeoEye, and the Pleiades are among the world's highest spatial resolution optical satellite imagery that can create DEMs (Barbarella et al, 2017; Ali et al, 2016; Mutluoglu et al, 2016 and Madden et al, 2015). For now, none of this satellite imagery has a spatial resolution higher than 31cm in the panchromatic channel (Barbarella et al, 2017 and Madden et al, 2015). Meanwhile, digital photogrammetry can achieve a spatial accuracy of 2cm (Woodget et al, 2017; Papakonstantinou et al, 2016 and Benassi et al, 2017). The ordering and purchasing of high-resolution satellite imagery are difficult and expensive (Lerodiaconou et al, 2016; Madden et al, 2015; Turner et al, 2015). The temporal resolution of digital satellite imageries varies from 1 to 16 days depending on the satellite (Pardo-Pascual et al, 2018; Maglione et al, 2017; Raspini et al, 2014 and Braga et al, 2013). Shorelines and coastlines morphology, however, will be required at hourly, daily, or weekly intervals (Pardo-Pascual et al, 2018; Xu, 2018, Pruszak et al, 2011 and Kim et al, 2013).

Monitoring and detection of shoreline change from satellite imageries are well utilized and documented (Ali et al, 2017; Hagenaars et al, 2017; Aedla et al, 2015; Maglione et al, 2015; Barik et al, 2014; Maglione et al, 2014; Yu et al, 2013; Azaz, 2012; Chand and Archarya, 2010). Despite the availability of very high-resolution optical imagery, recent research findings are that the excellent spectral resolution of these optical satellite imageries is not the only requisite to ascertain the correct delineation of shorelines and effective coastal monitoring (Ali et al, 2017; Bruno et al, 2016). There are a variety of checks to correct for compilation errors (Ali et al, 2017; Bruno et al, 2016 and Braga et al, 2013). There is also pan-sharpening to reduce spectral distortion (Choi et al, 2017; Demir et al, 2017 and Maglione et al, 2015) and data check for extreme weather conditions/unpredictable water levels (Ali et al, 2017; Palezzo et al, 2017; Bruno et al, 2016).

The IKONOS has an orbital altitude of 681km (Yu et al, 2013) and a revisit time of 1 to 3 days (Lipakis et al, 2007; Di et al, 2003). IKONOS is high-resolution satellite imagery with a multispectral range of four bands (Belfiore and Parente, 2014; Braga et al, 2013; Lipakis et al, 2007). Coastal monitoring and shoreline extraction have been successful using the IKONOS (Giannini et al, 2011; Maglione et al, 2014; Lipakis et al, 2007). Accurate geometric processing of the IKONOS is usually by the rational function coefficients (Di et al, 2003). The improvement of the IKONOS image geometry uses photogrammetric models like the collinearity conditions (Elaksher, 2008) and the line-based transformation model (Hu and Shi, 2016). These models require an adequate number of GNSS ground control to improve on the stereo image geo-positional accuracies (Belfiore and Parente, 2014). Similarly, the remote sensing image-to-image matching technique would require expensive third-party commercial software for rectification (Liu and Chen, 2009; Gianinetto and Scaioni, 2008).

Very high resolution multispectral optical satellite imageries (VHR) like the World-view, GeoEye, COSMO-SkyMedcan provide accurate and high-resolution datasets for shoreline monitoring (Hisabayashi et al, 2017; Lee et al, 2016; Maglione et al, 2015; Maglione et al, 2014; Braga et al, 2013; Ford et al, 2013 and Aguilar et al, 2011). Due to smaller pixel dimensions and the increased number of bands, the VHR satellite imageries can generate better radiometric and geometric accuracies for coastal monitoring as compared with the IKONOS, Quickbird and other high-resolution satellite imageries (Lee et al, 2016; Maglione et al, 2014 and Aguilar et al, 2011). Due to their smaller ground sampling distance (GSD), the VHR optical satellite imageries have a higher spatial resolution that enhances scientific

analysis of geomorphological processes on the coastlines (Aguilar et al, 2014; Barbarella et al, 2017; Maglione et al, 2015; Maglione et al, 2014 and Ford, 2013).

Lee et al (2016) in their studies used the WorldView-2 satellite imagery for automatic extraction of the shoreline. This study develops a new technique to improve the spectral propensity of the WorldView-2 by converting shadows into digital signals which are segmented as an elevation value. This makes the shoreline more visible for delineation. Although the research used the shadow, NDVI, and spectrum analysis to incorporate other features along the shoreline, there is no clarity on how the "elevation information" will improve on the overall spectral resolution of the imagery. The research methodology did not also specify a balanced ratio for existing bands as a further improvement on the multispectrum of the WorldView-2 is necessary considering the frequent changes of the water surface intensity across the electromagnetic spectrum (Lee et al, 2016). According to Aguilar et al (2011), the additional bands in the VHR satellite imageries enhance the interpretation and classifications of shorelines and coastal geomorphology.

Maglione et al (2014) used the WorldView-2 to interpret shorelines from interspersed coastlines of reefs and sandy beaches. The interpretations of the results obtained are relative to both the spectral and spatial resolution of the WorldView-2 imagery. Pansharpening is, therefore, applied to the coarser 2.0 m multispectral imagery to achieve pixel dimensions not more than 0.50cm as with the WorldView-2 panchromatic imagery. As with the high-resolution satellite imagery, the multispectral VHR satellite imageries will require pan-sharpening to enhance spatial enhancement for coastline monitoring (Giannini and Parente, 2015; Maglione et al, 2014 and Aguilar et al, 2011).

Satellite altitude and their orbital positions are limiting factors in the acquisition of time-series VHR imageries due to the lack of a synoptic view of coastlines with rugged terrains (Hisabayashi et al, 2017). Maglione, (2016) explains the geostationary and sun-synchronous orbits of optical satellites. The maximum adjoining area in a unit pass of the WorldView satellite is normally off-nadir inclined between 1.37 to 25.64 degrees (Hisabayashi et al, 2017). At this angle, there are possibilities of geometric errors, which could influence the coverage between contiguous passes (Crisp et al, 2018) and the accuracies in their DEMs (Hu et al, 2016). Palazzo et al (2017) on a coastal monitoring program used the Synthetic Active Radar (SAR) COSMO-Sky constellation. This study highlights the best satellite acquisition geometry to overcome the effects of shadow and other cover-ups. Aguilar et al (2012) also

recommend very accurate geometric transformation to correct for such topographical relief displacement. However, it is very difficult to obtain time series VHR satellite imageries with the same satellite sensor (Solano-Correa et al, 2018).

The applications of VHR satellite imageries for precise shoreline and coastal monitoring are a function of how and when such imageries are derived and processed (Barbarella et al, 2017 and Palazzo et al, 2017).

Literature Review (Section B)

Contemporary Digital Photogrammetry

2.6 Digital Photogrammetry Introduction

The principle of optical perspectivity as demonstrated by Leonardo da Vinci in 1492 is the concept of photogrammetry (Baqersad et al, 2017). Photogrammetry has been defined as the science of creating the accurate 3D structural geometry of physical objects and the environment by recovering their exact X, Y, and Z coordinate positions from photographs (Baqersad et al, 2017; Granshaw, 2017). This is illustrated by the collinearity constraint derived from the principle of the pin-hole-camera which states that an object point, the camera projection centre, and the image point all align in a straight line (Khoramshahi and Honkavaara, 2018; Zhang et al, 2014 and Bechle et al, 2010). In digital photogrammetry, these basic photogrammetric principles are photogrammetric algorithms for executing the stages of photogrammetry from image acquisition to image processing. (Murtiyoso et al, 2018; Damon, 2016; Hastedt and Luhmann, 2015; Micheletti et al, 2015 and Visockiene et al, 2014). There are robust photogrammetric software compacted into digital sensors for the rapid and automatic acquisition of geometrically related digital images (Logie and Coburn, 2018; Hastedt and Luhmann, 2015; Strecha et al, 2015; Colomina and Molina, 2014; Visockiene et al, 2014; Gini et al, 2013; Harwin and Lucieer, 2012; Vallet et al, 2011). Similarly, the derived 3D information is automatically extracted from the digital images and converted into 2D and/or 3D point clouds and digital models (Bemis et al, 2014; Gini et al, 2013; Koutsoudis et al, 2013; Harwin and Lucieer, 2012). The expected accuracies and precisions of terrain topography with their specific scientific application would determine the choice of every photogrammetric technique (Meng et al, 2017 and Westoby et al, 2012). This chapter section highlights the existing digital photogrammetry techniques for the continuous evaluating of several geographies in the coastal environments and identifies gaps that negate the implementation of a systematic low-cost and functional coastal management program.

2.7 The Importance of Digital Photogrammetry in Coastline Monitoring

Coastal flooding and erosion are now global threats (Spencer et al, 2016; Van and Binh, 2009; Klein et al, 2001). In recent times, climatic changes have led to spontaneous and continuous changes in the ocean currents (Spencer et al, 2016). The coastal environment is a dynamic geography with complex land and sea processes resulting in multi-landscapes and

geological structures (Robinet et al, 2016; Cloern et al, 2016; Cazenave and Cozannet, 2013). The management of the coastline, therefore, requires hands-on solutions (Alizad et al, 2016 and Turner et al, 2016) from regular monitoring techniques that can easily identify, confirm and quantify changes with accuracies and precisions (Cook, 2017; Papakonstantinou et al, 2016; Turner et al, 2016; Goncalves and Henriques, 2015). This helps to calculate the area of the sections under threats and compute the volume of materials deposited or eroded (Marzolff and Poesen, 2009; Yakar and Yilmaz, 2008). Long-term monitoring programs will help understand the overall impacts of climate change on the coastal zone to design the most appropriate engineering interventions (Masria et al, 2014) that will help to protect and maintain the coastlines (Chen et al, 2018 and Masria et al, 2014).

In recent times, the application of digital cameras as sensors mounted on close-range platforms for coastal monitoring has been successful (Damon, 2016; Goncalves and Henriques, 2015; Eulie et al, 2013; Kim et al, 2013 and Westoby et al, 2012). Digital sensors allow wavelengths across the electromagnetic spectrum to be captured and recorded accurately as high-resolution digital images (Pamart et al, 2017; Pepe, 2017; Damon, 2016 and Honkavaara et al, 2009). Images obtained in most instances are clear and sharp (if stabilization measures are undertaken) and allow for the identification of the lines (e.g. high and low watermarks) that differentiate land from water (Damon, 2016; Goncalves and Henriques, 2015; Eulie et al, 2013). They also have the spectral capabilities to differentiate between the geomorphological features on the shoreline (Brunier et al, 2016) and the evaluation of coastal cliff recession (Letortu et al, 2018; Westoby et al, 2012; Hapke et al, 2009; Lee, 2008).

Digital images are used to produce point clouds with sub-pixel accuracies and excellent radiometric image texture (Brunier et al, 2016; Bartos et al, 2014; Landes et al, 2013 and Leberl et al, 2010). Processing of geometrically related digital images is enhanced by a variety of choices of photogrammetric software (Pix4D Manual 2.0, 2016; Bartos et al, 2014; Colomina and Molina, 2014; Koutsoudis et al, 2013). Photogrammetry triangulation is used to recover the metric and non-metric characteristics of all photographic features (Barazzetti, 2017; Ai et al, 2015; Bemis et al, 2014). With this, it is possible to produce an accurate Digital Surface Model (DSM) and Digital Elevation Model (DEM) required for computational analysis (Barazzetti et al, 2017; James and Robson, 2012). High-resolution

multispectral imagery will improve the visualization and understanding of the coastal environment (Westoby et al, 2018; James and Robson, 2012; Leberl et al, 2010).

Remote sensing and photogrammetry have traditionally been very expensive but the cost has fallen significantly with the development of automated techniques for data capture and data processing (Cimoli et al, 2017; Logie and Coburn, 2018; Brunier et al, 2016). Set-up and field survey costs have also been very expensive due to the difficulties in mobilizing very heavy and expensive equipment with well-trained personnel to operate the aircraft and other equipment (Moloney et al, 2018; Cunningham et al, 2011 and Westoby et al, 2012). Cost-effectiveness and ease of executing photogrammetry will determine the frequencies of such surveys (Molony et al, 2018; Cimoli et al, 2017 and Casella et al, 2014). Effective coastal zone monitoring requires data at regular and repeatable intervals (Westoby et al, 2018; Casella et al, 2014; Kim et al, 2013) for continuous assessment of changes (Westoby et al, 2018; Bio et al, 2015) that will develop into a coastal zone information-monitoring infrastructure (Brown et al, 2016; Goncalves and Henriques, 2015).

2.8 Coastal Zone Information Monitoring Infrastructure

In present-day global warming situations, long-term monitoring programmes are required in the management of the coastal zones (Behling et al, 2018; Sagar et al, 2017; Turner et al, 2016b and Goncalves and Henriques, 2015). A long-term coastal zone information-monitoring infrastructure is to develop a coastal zone management plan (Chang et al, 2018 and Turner et al, 2016b). A thorough monitoring programme would integrate surveys at several temporal and spatial scales (Papakonstantinou et al, 2016; Temiz and Durduran, 2016 and Mills et al, 2005). Several methodologies have been developed using close-range digital photogrammetry for the continuous assessment of beach morphology (Long et al, 2016; Papakonstantinou et al, 2016; Yoo and Oh, 2016 and Chikhradze et al, 2015), coastal cliff recession and the shorelines (Obanawa and Hayakawa, 2018; Templin et al, 2018; Cermakova et al, 2016; Westoby et al, 2012). None of these existing methodologies has developed an integrated approach of several datasets at different scales for coastal zone management. The small-scale (high altitude) datasets allow for better visual inspection and identifying critical areas of concerns (Topouzelis et al, 2017 and Papakonstantinou et al, 2016). Such scales, however, might not be too accurate for qualitative and quantitative analysis (Topouzelis et al, 2017). The large scale (low/close altitude) surveys will generate very high-resolution orthomosaics and digital models in centimetres of accuracies needed for

both qualitative and quantitative evaluation of change (Benassi et al, 2017; Long et al, 2016; Papakonstantinou et al, 2016, Harwin and Lucieer, 2012). An integrated approach from the different spatial and temporal scales is required to understand and simulate the different dissipating factors and their patterns on the coastlines (Goncalves and Henriques, 2015; Mills et al, 2005 and Ai et al, 2015).

A holistic scientific framework of the coastal area will incorporate the monitoring of the cliff, the beach, and the shorelines (Burningham and French, 2017; Richter et al, 2013; Addo et al, 2008 and Hapke et al, 2009). It is required to sustain all intervention mechanisms considering the resourcefulness of the datasets (Turner et al, 2016; Hapke et al, 2009 and Mills et al, 2005). Lastly, the integrated topographical datasets will enable the scientific actualization of a sustainable coastal zone management plan(s) (Pikelj et al, 2018; Turner et al, 2016b; Famuditi et al, 2014; Mills et al, 2005) considering also the economic viability of the datasets (Pikelj et al, 2018 and Klemas, 2015). According to the Vale of Glamorgan Council report on the coastline monitoring update, the emphasis is now on carrying out surveys at larger scales for specific areas of the coastal zone (The Vale of Glamorgan Council Report, 2016).

According to Sesli (2010), photogrammetry and digital Photogrammetry are active and efficient technologies for "planning activities". Specific management of the coastlines would require a well-developed monitoring strategy (Famuditi et al, 2014) as the coastal environment is a component of complex terrains formations (Sacchi et al, 2016; Turner et al, 2016; Bio et al, 2015; Sesli et al, 2010). Close range digital photogrammetry provides flexible surveys that can capture the complex geographies present in the coastal zone (Gray et al, 2018; Bio et al, 2015; Goncalves and Henriques, 2015). Such surveys carried out regularly will generate detailed topographical data required to produce both qualitative and quantitative coastal zone indicators (Pikelj et al, 2018 and Casella et al, 2014).

Coastal zone monitoring infrastructure is enabled by accurate regular surveys (Pikelj et al, 2018; Sturdivant et al,2017; Long et al, 2016; Bio et al, 2015; Goncalves and Henriques, 2015; Caselle et al, 2014 and Klemas et al, 2011b). The beach and dune systems have recently been mapped using digital photogrammetry techniques (Pikelj et al, 2018 and Goncalves and Henriques, 2015). Coastal vulnerability and phenomenon from UAS-SFM photogrammetry are easily comprehensible (Gray et al, 2018 and Sturdivant et al, 2017). The geographic object-based image analysis classification-model developed by Papakonstantinou et al (2016) from imageries obtained by digital photogrammetry is a physical object

identification routine for coastal monitoring. A coastal zone information plan should include processes that integrate datasets of different remote sensing and photogrammetric sources (Turner et al, 2016b; Bio et al, 2015 and Hapke et al, 2009).

Bio et al (2015) developed a robust coastal zone monitoring technique but using terrestrial videogrammetric mobile mapping, aerial mapping with other bathymetric and ground-based observations. The process of the videogrammetric would require a rugged mobile vehicle and dedicated 3D software for conversion from video into 3D images (Julzarika, 2017). Ahn et al (2017) have used the indirect time-lapse DSLR imaging system to develop robust quantitative data sourcing along the coastline. This technique is photogrammetrically stable, low-cost with the ability to generate real-time data. The indirect time-lapse DSLR imaging system would capture digital images however at slope angles that would require further geometric corrections making the direct imaging systems a more reliable technique (Ahn et al, 2017). Scarelli et al (2017) had used the Fledermaus-v7 software as a tool for seasonal beach/dune changes. This software can detect changes between successive digital models using the threshold filtering or other change analysis parameters. Differentiation was only by the digital surface models while parameterization did not include vertical surfaces like the cliff.

The workflow developed by Casella et al (2014) by digital photogrammetry incorporates bathymetric datasets and does not include the topography of the cliff surface. Existing coastal zone monitoring program by close-range digital photogrammetry does not include the geospatial-monitoring infrastructure (Chen et al, 2018; King et al, 2017; Brunier et al, 2016; Cermakova et al, 2016; Long et al, 2016; Turner et al, 2016; Yoo and Oh, 2016; Chikhradze et al 2015; Guillot and Pouget, 2015; Casella et al, 2014 and Darwin et al, 2014). Existing literature on coastal monitoring whose techniques incorporates datasets from the other remote sensing platforms and at varying mapping scales does not incorporate the geospatial infrastructure as an update service (Ahmed et al, 2018; Al-Zubieri et al, 2018; Kaliraj et al, 2017; Temiz and Durduran, 2016; Klemas, 2011; Norman et al, 2012 and Meiner, 2010). Sagar et al (2017) developed an automated geospatial framework from Landsat imagery that could monitor the intertidal zone but at a spatial scale of 25m. Water-Land Monitor technique by Behling et al (2018) can estimate accretion and erosion but continuous capture of the cliff face with the wave-cut notch will be difficult due to the Spatio-temporal scale and the angle of data acquisition. Li et al (2006) developed a comprehensive coastal zone

monitoring/management infrastructure from several high-resolution datasets including a web-based coastal data update, which again, does not include the coastal cliff.

Methodologies for coastal zone management survey would include and depict the spatial relationship between the several coastal processes, complex coastal elements and simulate their physical interactions (Casella et al, 2014; Ostrowski and Pruszak, 2011 and Lee et al, 2008). Topographical surveys will clearly define the extent and elevations of all sections of the backshore within centimeters of horizontal and vertical accuracies (Clark, 2017; Zhou et al, 2017; Longhitano, 2015 and Casella et al, 2014) for the coastal engineers to accurately and precisely decide on coastal structures (Mancini et al, 2013 and Melby et al, 2012). A more realistic coastal geospatial framework would require regular surveys for continuous updates of vulnerable sections (Nayak, 2017; Turner et al, 2016; Goncalves and Henriques, 2015). UAVs and other close-range platforms are progressively utilized to generate low-cost "spatially extensive" high-resolution aerial imageries with such required temporal frequencies (Long et al, 2016; Goncalves and Henriques, 2015 and Shin and Kim, 2015) as their usage is not limited to particular sections of the beach, cliff and nearshore (Goncalves and Henriques, 2015; Westoby et al, 2012). Such spatial frameworks are geographically accurate and enhance a consistent, jointless, and flawless transition from the backshore into the offshore with visible delineation of the respective tidal height indicators (Werff, 2019). This research, therefore, develops a geospatial infrastructure for coastal monitoring update from several remote sensing datasets with an emphasis on very high-resolution imagery (where possible and cost-effective) obtained by close-range platforms, which includes sections of the foreshore, the beach, and the coastal cliff. However, there may sometimes be a trade-off between the camera resolution and the distance to the cliff or surface. As this research aims to develop low-cost solutions, it may well be possible to use lower resolution cameras (i.e. very low-cost) but use more images to undertake the photogrammetric process.

2.9 Digital Photogrammetry in Coastal Cliff Deformation and Beach Monitoring

2.9.1 Digital Photogrammetry Techniques for Coastal Cliff Deformation Studies

Several close-range digital photogrammetry techniques are presently in use for monitoring the coastal cliff (Sacchi et al, 2016). The limitations on the use of the TLS that include cost and irregular deflection of beams incident on the cliff surface are highlighted in section 2.3.

According to Obanawa and Hayakawa (2018) and Dewez et al (2016), the UAS can assess such inaccessible segments of the cliff surface that is difficult with the TLS. It is also a "promising competitor" (Genchi et al, 2015). An accurate geotechnical assessment on critical structural discontinuities on the cliff surface would require methodologies with close distance range advantages, easy to use, all-encompassing, and cost-effectiveness (Sacchi et al, 2016 and Ruzic et al, 2014). There is no existing literature on close-range digital photogrammetry by the structure-from-motion approach using the drones, poles, kites, or camera locations on the ground that has developed a systematic cost-effective, accurate and easy to use field procedure for the regular monitoring of the coastal cliff.

This may be due to the belief that other approaches might be quicker or more efficient for such a small area survey. However, just as a Terrestrial Laser Scanner (TLS) might be utilised for surveying a cliff (and widely documented in the literature), it is reasonable to assume that a close-range platform (e.g. a camera system on a pole) might perform equally as well (or possibly better due to the surveying elevation advantage) and generate a richer variety of data (i.e. good imagery as well as the photogrammetrically-derived point cloud).

2.9.2 Coastal Cliff Monitoring by Drones

2.9.2.1 Methods by Varying Distances and Positions of the Drone to the Cliff Surface

Irvine et al (2018) used a quadcopter to capture the cliff surface in a manual mode, which is subjective to irregular overlap especially on complex and irregular shaped cliff surfaces. Obanawa and Hayakawa (2018) carried out their UAV survey from above the cliff. The super-spectral resolution will depend on the quality of the digital camera with possibilities of obscuring hidden sections of the cliff. The study by Barlow et al (2017) is by the automated UAV image capture across a steep slope cliff surface on a relative distance of 50 metres between the octocopter and the cliff surface. The distance of 50 metres from the cliff surface will not capture very high-resolution images with the use of a 10 or 12- megapixel digital camera. Clark (2017) positioned the drone to specifically delineate the cliff top and toe without emphasis on the cliff surface.

2.9.2.2 Methods by Varying Angles and Multiple Systematic Flights Coverage

The deliberate acquisition of oblique images by UAVs in mapping vertical or near-vertical surfaces could lead to a reduction in systematic errors, particularly with enhanced overlap. (Dewez et al, 2016; Harwin et al, 2015; James and Robson, 2014). Mancini et al (2017);

James and Robson (2014) both suggest some alternative flight plan approach such as the combination of oblique and near-vertical images to reduce doming effects when using the drone to capture the cliff. It is difficult to automate a flight plan with the drone at very close range to the cliff surface at such angles that could capture irregular sections due to irregular protruding and instability of the coastal cliff (De Vilderet al, 2017; Mancini et al, 2017 and Rosser et al, 2013).

Dewez et al (2016) carried out three different UAV surveys at three different photographic angles to achieve complete overlap and stereoscopic coverage of the cliff surface. Digital photographs acquired were with a 24-megapixel Sony Nex digital camera at vertical, horizontal, and oblique angles. This technique is time-consuming and expensive. Genchi et al (2015) developed a methodology using a consumer-grade camera attached to a hexacopter. The speed of the drone was 1m/s to achieve complete stereoscopic coverage. The cost of the digital camera and the hexacopter is approximately US$1250. Letortu et al (2018) flew the electric hexacopter manually in their study with repetitive captures to ensure complete stereoscopic coverage but no defined methodology using the drone. In Carter et al (2018), a multi-rotor quadcopter with a 24-megapixel camera was flown in "multiple downwind traverse" to avert the influences of both wind and sea turbulence. This study, however, did not outline any specific flight plan and direction. This is similar in other recent studies by Caprioli et al (2016), Drummond et al (2016), Perez-Alberti, and Trenhaile (2014) as no specific field procedural technique/flight plan is mention on the use of the drones to map the cliff surface.

2.9.3 Coastal Cliff Monitoring by Kites/Balloon Photogrammetry

Kite photogrammetry has been in use for more than a century (Aber and Babb, 2018; Ulvi et al, 2017; Lorenz and Scheidt, 2014). Balloon aerial photography is reckoned however to be the oldest (Colomina and Molina, 2014). Kites have better stability than the balloons during windy conditions (Currier, 2015) although a combination of the kite and balloon (helikite) has proved to be more stable in the air (Campana, 2017; Mozas-Calvache et al, 2012; Verhoeven et al, 2009) – see Figure 2.6. Kites are in use for monitoring dune and general geomorphology of the coastline (Duffy et al, 2018; Currier, 2015; Lorenz and Scheidt, 2014), archaeological/cultural studies (Ulvi et al, 2017 and Rinaudo et al, 2012), and for other environmental monitoring (Feurer et al, 2018; Fonstad et al, 2013; Yakar et al, 2010; Gimenez et al, 2009 and Smith et al, 2009). Kite photogrammetry may be an alternative to

drones for rugged coastlines with sediments and during light winds and rains (Duffy et al, 2018; Smith et al, 2009). There is no scientific evidence on the application of kite photogrammetry in cliff monitoring. Kites and balloons are heavier than the pole and mast with the minor payloads such as the helium gas (Campana, 2017). The system could have distortions in the geometry adjacent to digital images (Aber and Babb, 2018) due to regular translational and rotational displacements from weight and aerodynamic forces (Campana, 2017; Mozas-Calvache et al, 2012). Such displacements apply to the helikites (Mozas-Calvache et al, 2012). Despite the advantage of a higher-flying height (Aber and Babb, 2018 and Currier, 2015), it is practically difficult to design a pre-flight plan due to the kite's instability and presence of the payloads (Feurer et al, 2018). A pre-flight plan is required for a systematic survey with a degree of precision (Aber and Babb, 2018; James and Robson, 2014; Mozas-Calvache et al, 2012).

Figure 2.6 Desert Star Helikite (Hybrid Kite and Helium Balloon) used for surveying. This helikite is rugged and can withstand sand-blown weather conditions. It was initially meant for the UK and US Army.

2.9.4 Coastal Cliff Monitoring by Terrestrial Photogrammetry

Terrestrial/ground station photogrammetry is flexible, fast, and does not require expensive and cumbersome hardware that limits photogrammetry in bad weather conditions (Medjkane

et al, 2018). Terrestrial photogrammetry would, however, require careful planning and systematic field procedure to achieve accurate and precise digital models (James and Robson, 2012) as a regular change in the focal length and camera position would result in misalignment, barrel and pincushion errors (Murtiyoso et al, 2018 and Neale et al, 2011). Some tedious photogrammetric transformation would be required to correct such errors (Westoby et al, 2012).

In the study by Ruzic et al (2014), digital images taken by the single digital camera at different horizontal and vertical angles were by the operator, on foot. The several point clouds obtained were mosaic by some series of point registration with accurately pre-determined controls. For an easy survey with complete coverage, the cliff and rock sections were in segments.

In Westoby et al (2012), digital photographs were acquired discretionally from different ground locations and camera orientations with the digital camera mounted on a tripod. The coastal cliff monitored is 80 meters average height and has some horizontal segments that allowed the laying of some carpet tiles as GCPs whose coordinates thereafter used to transform the digital images from the image space to the object space.

Letortu et al (2018) carried out terrestrial photogrammetry to map the coastal cliff using a Nikon D800 36-megapixel camera. The camera position was approximately 20 meters from the cliff. Images acquired were from different angular positions and at a horizontal spacing of 2 to 3 meters to ensure maximum overlap and cliff surface coverage. The study did not specify whether the Nikon D800 camera was on the tripod during all photography and no systematic mapping procedure developed for terrestrial photogrammetry.

Medjkane et al (2018) and Westoby et al (2018) both explain the difficulties of obtaining correlated digital images that can generate a homologous point matching while mapping the cliff surface from ground stations. Medjkane et al (2018) recommend a sequence of a few regular baselines from the cliff surface while maintaining a fixed camera orientation. Westoby et al (2018) reiterate a systematic acquisition of digital photos from ground stations with the maximum possible overlap. The sequence of such field methodologies adopted by Medjkane et al (2018) and Westoby et al (2018) are not specific.

For correct image matching and bundle adjustment, existing coastal cliff monitoring methodologies by terrestrial photogrammetry relied on accurately predetermined control points with expensive high-resolution digital cameras. These methodologies might not apply to other vertical or near-vertical coastal cliffs where it is difficult or impossible to establish control points due to the verticality of the cliff (De Vilder et al, 2017 and Rosser et al, 2013) and regular cliff face falls (Letortu et al, 2018). It is also difficult to develop a systematic methodology by foot or the camera on a tripod due to irregularity in the orientation angles (Letortu et al, 2018).

2.9.5 Coastal Cliff Monitoring by Pole Photogrammetry

Elevated viewpoints like the poles will enhance terrestrial photogrammetry with broader options for camera positions and orientations (Pierzchala et al, 2016). Such enhanced viewpoints will improve image overlap, alignment, and advance the image matching process (Smith et al, 2016). Pole photogrammetry is prominently used to monitor archaeological sites (Thomas and Williams, 2019; Holata et al, 2018; Girelli et al, 2017; Willis et al, 2016; Fallavollita et al, 2013 and Verhoeven et al, 2009). There is the recent application of pole photogrammetry in beach monitoring (Conlin et al, 2018; Pikelj et al, 2018) and for other large-scale mappings (Carrivick and Smith, 2018; Goncalves et al, 2016).

Poles surveys are convenient and easy to use in such areas there are restrictions to the use of UAV's (Thomas and Williams, 2019; Goncalves et al, 2016; Verhoeven et al, 2009) and also in areas with environmental constraints (Conlin et al, 2018 and Goncalves et al, 2016).

2.9.6 Contemporary Models for Analysing Change Detection in 3D Point Clouds

Point clouds are the first and direct outputs from the bundle adjustment computation with every point an X, Y, and Z representation of the terrain (Wang et al, 2019; Leberl et al, 2010). 3D point cloud analysis provides a range of photogrammetric and geodesic options for accurate structural deformation studies (Mukupa et al, 2017; Bureick et al, 2016 and Aryal et al, 2012). This includes the monitoring of rock slopes (Kromer et al, 2015) and coastal cliff (Espositi et al, 2017) with sub-millimetres accuracies (Kromer et al, 2015). Point clouds for structural deformation monitoring are from LiDAR, TLS, and the SFM (Esposito et al, 2017 and Kromer et al, 2015). Change detection by comparing two point clouds are in both the horizontal and vertical axes (Esposito et al, 2017 and Shen et al, 2017). The Alignment and geo-registration of the point clouds will first be determined before been used for the change analysis (Lague et al, 2013; Harwin and Lucieer, 2012)

Change detection between two point clouds is by the direct distance computations between a reference and a compared point cloud (Catalucci et al, 2018 and Esposito et al, 2017). Existing distance computation algorithms on point clouds include the direct cloud-to-cloud (C2C), the cloud-to-mesh (C2M), and the multiscale model-to-model (M3C2) (Ahmad et al, 2018 and Esposito et al, 2017).

The mainstream point cloud analyzing software with the basic geometric triangulation network does not necessarily include the distance-to-distance change computation (Vercator, 2020; Catalucci et al, 2018; and Lopez-Fernandez et al, 2017). Recent scientific research confirms the accuracies of the cloud2cloud C2C, the cloud2mesh C2M, and the multiscale model-to-model (M3C2) distance computation in the open-source CloudCompare software (Esposito et al, 2017). These computations however do not include the segmenting of the point clouds and the visualization of output segments on their actual change array.

The C2C and C2M distance computation are tolerable on regular surface correlation (Ahmad et al, 2018 and Lague et al, 2013). Recent studies show that the M3C2 will be more effective for comparing irregular surfaces like the cliff (Lague et al, 2013). This is because the algorithm distance computation is not dependent on the spatial correlation and the dimensional orientation between the surfaces (Esposito et al, 2017). However, to meet the required accuracy level of the K nearest neighbor (KNN) classification, there is a need to introduce more than one search_radius_vector_3d to increase the cell categories of clusters and reach to every point in the search cluster (Open3d, 2020).

2.10 Digital Photogrammetry in Monitoring the Beach and the Dunes

The beach or shore stretches from the low-tide shoreline to the coastline and includes the foreshore and the backshore (Scarelli et al, 2017 and Longhitano, 2015). The beach consists of silt, sand, pebbles, shells, gravel, rocks, and cobbles (Kwarteng et al, 2016).

Periodic changes in the low tide and high tide shorelines will help understand the sea wave pattern for resource planning and emergency (Caudle et al, 2019; Rouse et al, 2019; Scarelli et al, 2017; Robinet et al, 2016; Lentz and Hapke, 2011). The movement of sediment and deposits on the berm and dunes are key factors to understand the several geomorphological processes (Naylor et al, 2017; Goncalves and Henriques, 2015; Lentz and Hapke, 2011). The tidal wave will result in sediments and/or wash-over (Mulhern et al, 2017). An effective Coastal zone management infrastructure will include therefore the spatial relationship and

variability between the nearshore, the shore, and the coast (Joevivek et al, 2018 and Papakonstantinou et al, 2016). Beach transects are periodically represented relative to distances from assigned tidal heights at very accurate and precise x. y, z coordinates (Casella et al, 2016; Theuerkauf and Rodriguez, 2012).

The 3-dimensional reconstruction of photogrammetric points should incorporate the smallest fractions of coastal features on recognizable segmentation indicators for each ground feature layer (Woodget et al, 2017) with accurate planimetric and vertical geo-positioning to produce very accurate topographical maps with contours (Fonstadet al, 2013). Horizontal and vertical accuracies between 1cm to 6cm are using surveying grade equipment such as the GPS in RTK mode (Yoo and Oh, 2016; Goncalves and Henriques, 2015; Perez-Alberti, and Trenhaile 2014). The inbuilt GPS in the consumer-grade digital cameras could be inaccurate by 2.5m in the X and Y-axes (Carbonneau and Dietrich, 2017; Clapuyt et al, 2016). Their precision, however, is usually with the excellent approximation that can optimize drone positions and image geo-tagging provided enough images have been acquired with very good overlap (Muji and Tahar, 2017; Huang et al, 2015). By optimizing image geotagging, the precision of the scale-invariant feature transform (SIFT) is significantly improved and generates fine-scale and 3D orientations of the digital models (Carbonneau and Dietrich, 2017; Muji and Tahar, 2017; Clapuyt et al, 2016 and Huang et al, 2015).

Despite such precision in the 3-d orientations, the vertical of the consumer-grade GNSS equipment is very problematic and inaccurate and could be inaccurate by 5 to 10 meters (Varela et al, 2019 and Zhao et al, 2017). Such inaccuracies in the inbuilt GPS-derived heights are influences from variations between the ellipsoidal and the geoid (Odera et al, 2014 and Mukherjee et al, 2013). These errors are reduced in the RTK GNSS measurements with some calibrated signals received from a designated online server or base station for real-time processing or post-processing kinematic (PPK) (Gervaix and Voorhees, 2017) measurements. Accuracies in the RTK observations are an average of 1cm+1ppm in horizontal and 2cm+1ppm in vertical (Aykut et al, 2015; Hwang et al, 2012; Feng and Wang, 2008).

Drone surveys can achieve vertical accuracy of 1cm to 6cm in mapping sections of the coastline by coordinating some sparsely distributed ground control points through separate, tedious and time-consuming RTK-GNSS surveys (Chen et al, 2018; Jeong et al, 2018; Long et al, 2016; Papakonstantinou et al, 2016; Goncalves and Henriques, 2015). The use of the

GNSS equipment for every drone survey is stressful and also constrained by cost (Long et al, 2016) and/or accessibility to GNSS network correction servers for RTK surveys (Bae and Kim, 2018 and Clark, 2017). The cost of survey-grade receivers is an average of $10,000 (Varela et al, 2019 and Weaver et al, 2015).

The availability of survey-grade mapping drones with inbuilt RTK-GNSS antenna can now provide an easier, faster, and accurate topographical mapping of the coastal region thereby eliminate the separate time-consuming RTK-GNSS surveys (Drummond et al, 2016; Turner et al, 2016). Onboard RTK-GNSS will provide accurate navigation with accurate geo-tagging for each digital image (Drummond et al, 2016). Such inbuilt RTK-drones are been sold for more than £10,000 (Carbonneau and Dietrich, 2017).

None of the existing digital photogrammetry methods with a high temporary resolution for coastal monitoring has attained such vertical delineation accuracy of 1cm to 6cm without the use of the RTK-GNSS for each specified survey (Conlin et al, 2018 and Casella et al, 2016). The physical orthometric heights may be more realistic for obtaining precise heights for relatively smaller areas (Odera et al, 2017) and precise verticals in orthomosaic, especially in large-scale digital surveys. There is, therefore, the need for a cost-effective, easy, and flexible method that would include the very high spatial density of survey points with centimetre accuracies in both vertical and horizontal axis. This is important in coastal areas where it is difficult to establish permanent GCP and such situations; cost limits the frequencies on the use of RTK-GNSS equipment or the onboard Survey grade RTK drone.

2.11 Chapter Summary and Conclusion

Sections A and B in the literature review are clear evidence of the advantages and disadvantages of the traditional land surveying equipment, remote sensing, and photogrammetric techniques for coastal area monitoring (coastal cliff and beach precisely). The literature review is an indication that the use of two or more of these techniques will provide accuracy and completeness in the coastal zone information-monitoring infrastructure. Table 2.1 below is a summary of the literature review showing the weaknesses, capability, and cost implications for all the land surveying, remote sensing, and photogrammetry techniques for beach and coastal cliff monitoring.

Table 2.1 Orders of Emergence, Weaknesses, and Capabilities of Individual Methodology for coastal Area (beach and cliff) Monitoring.

Order of Evolution ⟶	**Plane Table/Total Station/GNSS**	**Aerial Photography**	**Satellite Remote Sensing**	**LiDAR /TLS**	**UAV and Close-range Photogrammetry**
Cost-Effective-ness	Thousands of dollars for survey-grade GNSS equipment (Odolinski et al, 2020)	US$35 per scanned aerial image; US$6300 to generate DSM from aerial image (Ishiguro et al, 2016).	US$10 to US$60 per km^2 (Witjes and Olbrich, 2017).	US$30,000-$80,000 (Chandler and Buckley, 2016)	UAS set-up ±$ 500 (Cimoli et al, 2017) Any elongated pole with any camera or smart phone
Sub- Pixel Accuracies	1-2 cm horizontal and 3 cm vertical accuracy(Aykut et al, 2015)	20cm Spatial Resolution (Ishiguro et al, 2016).	31cm Spatial Resolution (Barbarella et al, 2017 and Madden et al, 2015)	3cm Spatial Resolution (Xiong et al, 2017)	2cm Spatial resolution (Woodget et al, 2017 and Benassi et al, 2017)
Flexibility/ Ease of data collection	Time and labour intensive (Kim and Lee, 2017; Cheng et al, 2016)	Executing aerial surveys constrained by weather (Braga et al, 2013; Morgan et al, 2010)	Orbital Positions could limit coastlines and cliffs coverage (Hisabayashi et al, 2017)	Scanning every part of the cliff can be difficult. (Chen et al, 2018)	Flexible and fast (Medjkane et al, 2018)
Generate DEM from Imageries	Difficult to generate point cloud from only point-based surveys (Cheng et al, 2016)	Could generate DEM (Ishiguro et al, 2016).	Could generate DEM (Hu et al, 2016)	Generates DEM (Young, 2018; Earlie etal, 2013 and Vos et al, 2017)	Generates DEM (Irvine et al, 2018 and Long et al, 2016)

Influence by Weather	Ionosphere and Troposphere Bias (Aykut et al, 2015)	Influenced by weather (Paravolidakis et al, 2016 and Morgan et al, 2010)	Influenced by weather (Zulkifle et al, 2017)	Influenced by weather (Kromer et al, 2017)	Light and rugged (Medjkane et al, 2018)
Contains Pictorial information	Nil (Ahn et al, 2017 and Brunier et al, 2016)	Geomorphologic processes are discernable (Hamylton, 2017)	Geomorpholo - gic processes are discernible (Braga et al, 2013)	Geomorpholo - gic processes are discernible (Mitasova et al, 2009)	Geomorpholo - gic processes are discernible (Templin et al, 2018)
Wide Area Coverage	Lacks spatial coverage (Cheng et al, 2016)	Wide area coverage (Redweik et al, 2016)	Wide area coverage (Braga et al, 2013)	Wide area coverage (Mitasova et al, 2009)	Wide area coverage (Templin et al, 2018)
Surveying at different electromagnet ic bands spectrum	Lack of photographic imaging (Jalloh et al, 2017)	High spectral multiband imagery (Braga et al, 2013)	High spectral multiband imagery (Maglione et al, 2014)	High spectral multiband imagery (Andersen et al, 2017)	High spectral multiband imagery (Damon et al, 2016)
Data processing	Mathematical computations with software applications (Jalloh et al, 2017)	Processing and scanning of aerial photos are by proprietary photogrammetry workstations (Fernandez et al, 2017)	Remote sensing software applications (Dominici et al, 2019)	Specialized proprietary LiDAR processing software (Doyle and Woodroffe, 2016)	SFM + MVS Proprietary and open source software (Forsmoo et al, 2019)
Data collection in rapid succession	Point coordinates are manually observed but automatically stored (Cheng et al, 2016)	Rapid data collection with digital aerial cameras (Morgan et al, 2010)	Regular revisiting time with digital sensors (Morgan et al, 2010)	Rapid data collection (scanning) (Doyle and Woodroffe, 2016)	Rapid data collection with digital cameras (Kromer et al, 2015)

The close-range digital photogrammetry techniques such as drones have the best resolution accuracies. Digital photogrammetry techniques are also the cheapest and have better user flexibility, especially for large-scale surveys. The following chapters in this thesis will be researching the best practices for using more than one of these options for low-cost and accurate monitoring of the beach and coastal cliff. It will also develop low-cost strategies as the option to the use of the drone due to civil aviation restrictions. Alternative close-range platforms will be useful to survey the cliff at different distances and angles. This is necessary as what is required is not a one–time survey of the beach and coastal cliff but the continuous monitoring that can develop management information infrastructure.

Chapter 3

Digital Photogrammetry

3.0 Chapter Aim

This chapter explains the mathematical principles involved in implementing the processes of digital photogrammetry for coastal monitoring, i.e. using overlapping raw images to generate highly accurate three-dimensional measurements of real-World features. What was once a highly sophisticated and mechanical task using expensive hardware has now become a low-cost computational (i.e. mathematical) process to calculate the 3D position of the camera based on unconnected elements in the images, which are identified in multiple views. This is all underpinned by a series of mathematical equations for digital image capture, processing, and analysing. These solutions are now readily available as free, open-source and licensed automated software. There is a common belief that open-source solutions are not well supported and error-prone, but during this research study, the algorithms have become more widely accepted and supported by the photogrammetry community to such an extent that their robustness is no longer an issue. Meanwhile, commercial digital photogrammetric solutions have had to evolve into offering a much wider range of functionality alongside the production of 3D models and orthomosaics; such as application-based solutions (e.g. agriculture, BIM – Building Information Modelling, road traffic forensics, etc.) and cloud-based network solutions.

This chapter explains the procedures for all field measurements and processing of the data. It explains the basic principles of photogrammetry vis-à-vis digital photogrammetry and the rationale behind the adopted technology relative to emerging trends in photogrammetric surveying (Templin et al, 2018; Sturdivant et al, 2017; Bernis et al, 2014 and Dai et al, 2014). This project is very specific to the pattern of data capture with multiple digital images captured at several locations with small ground sampling distance on surfaces that are often mainly homogenous in texture (e.g. rocks, cliffs, beaches, etc.). The aim is to develop a simple straightforward field procedure applicable to several coastal geographies using digital photogrammetry techniques.

3.1 Basic Principles of Digital Photogrammetry

Existing research on digital photogrammetry and other geosciences focus on the capability of the combination of the close-range platforms and the several non-metric digital cameras to produce accurate and precise orthomosaics with digital models relative to some high order geodetic network (Shahbazi et al, 2015 and Poser, 2012). The last decade has seen the development of robust photogrammetric processing and image acquisition software (Ai et al, 2015; Bernis et al, 2014). These advanced algorithms employ the basic photogrammetry principles (Bernis et al, 2014 and Poser, 2012) of the pinhole camera (Hastedt and Luhmann, 2015) to aerial triangulation (Benassi et al, 2017 and Gini et al, 2013). These now provide a major advance in digital photogrammetry with improvements in digital image acquisition, mosaicking, reconstructing of tie-points and a dense point cloud from matched digital images and processing into orthomosaics and 3D digital surface models (Juad et al, 2016; James and Robson, 2014 and Remondino et al, 2011).

Photogrammetric processing software solutions include the likes of VisualSFM, Photosynth, Pix4D, Python Photogrammetry, Bundler Photogrammetry, Arc3D, and many others (Granshaw, 2016; Ai et al, 2015; Bernis et al, 2014 and Gini et al, 2013). All photogrammetric algorithms integrate the general photogrammetric theories of aerial triangulation, camera calibration parameters, and bundle block adjustment (Ai et al, 2015; Lee and Rhee, 2013). Triangulation is possible from the relationship between the object and image space as represented by the photographic scale **(S) = f/H' or d/D in figure 3.1 below.** The shorter the Focal Length then the wider the Field of View (FOV) becomes, which mean more details will be captured.

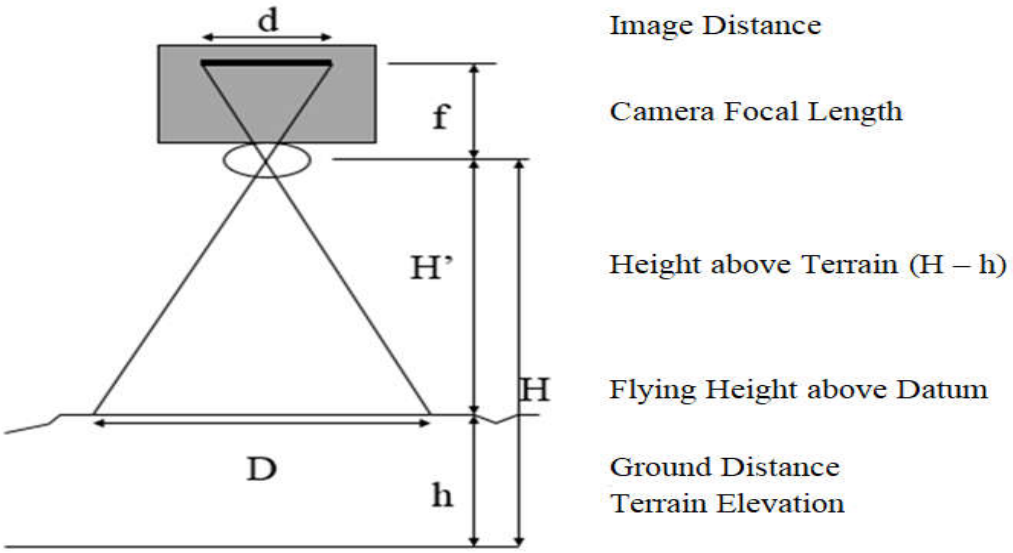

Figure 3.1 - The Scale of Photography is the Relationship between the Camera Focal Length and the Height of the Measuring Platform (Drone, Pole, etc.) above the Ground (Pix4D Mapper 2.0, 2016; Wolf and Dewitt, 2000).

Rays emanating from the object space (X, Y, Z) coordinate system, are formed as an image in (X^o, Y^o, Z^o) coordinate system (Poser, 2012) produced as digital images in the camera lens (Pritt, 2014 and Gini et al, 2013). These rays conjugate in conformity with the object's spatial and spectral attributes depicted by some mathematical representation (Krtalic et al, 2019). For digital photogrammetry to be possible there must be considerable overlap between the digital images (Ai et al, 2015; Shahbazi et al, 2015; Barry and Coakley, 2013). The geometric relationship as at the time of exposure will reconstruct onto the image space as shown in figure 3.2 below:

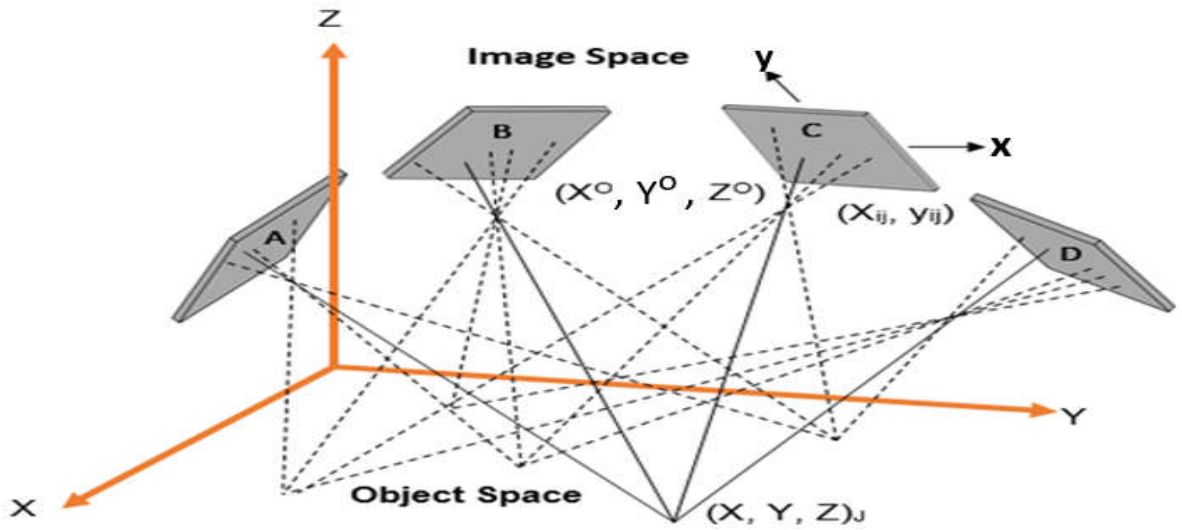

Figure 3.2 Geometric Relationships between Object and Image Space. The Mathematics of the Automatic Aerial Triangulation (AAT) Replicates all the Physical Features and Positional information of the Object on the Ground as a 3D Image on Space (Fraser et al, 2014).

Processing of images obtained by photogrammetry is by the reconstruction of bundles of light rays from the object space unto the image space to exactly recover the X, Y, and Z coordinates of ground points (Massad and Omer, 2014; Neale et al, 2011). Photogrammetric procedures have to deal with the high-level matching of points from coordinates of some pre-designed matrices prepared as algorithms that can compute points by triangulation (Neale et al, 2011). Photogrammetry is therefore governed by the geometric relationship of light rays (Oniga and Cardei, 2015).

3.2 Automatic Aerial Triangulation (AAT)

The AAT is a point-based mathematical process to extract, align, match, and re-optimize key points using a precise and accurately defined origin (Ackermann and Krzystek, 1997). The optimization of the internal and external camera parameters is iterative and geometrically enhanced by the AAT using the Bundle Block Adjustment (BBA). The entire computational process in digital photogrammetry on a regular block network involves the 3-D positions of points delivered by aerial triangulation (Benassi et al, 2017 and Colomina and Molina, 2014). Fig 3.3 illustrates a typical BBA in an Integrated Sensor Orientation (ISO) using the camera's approximate position and altitude (Gneeniss et al, 2015; Choi and Lee, 2013; Westoby et al, 2012).

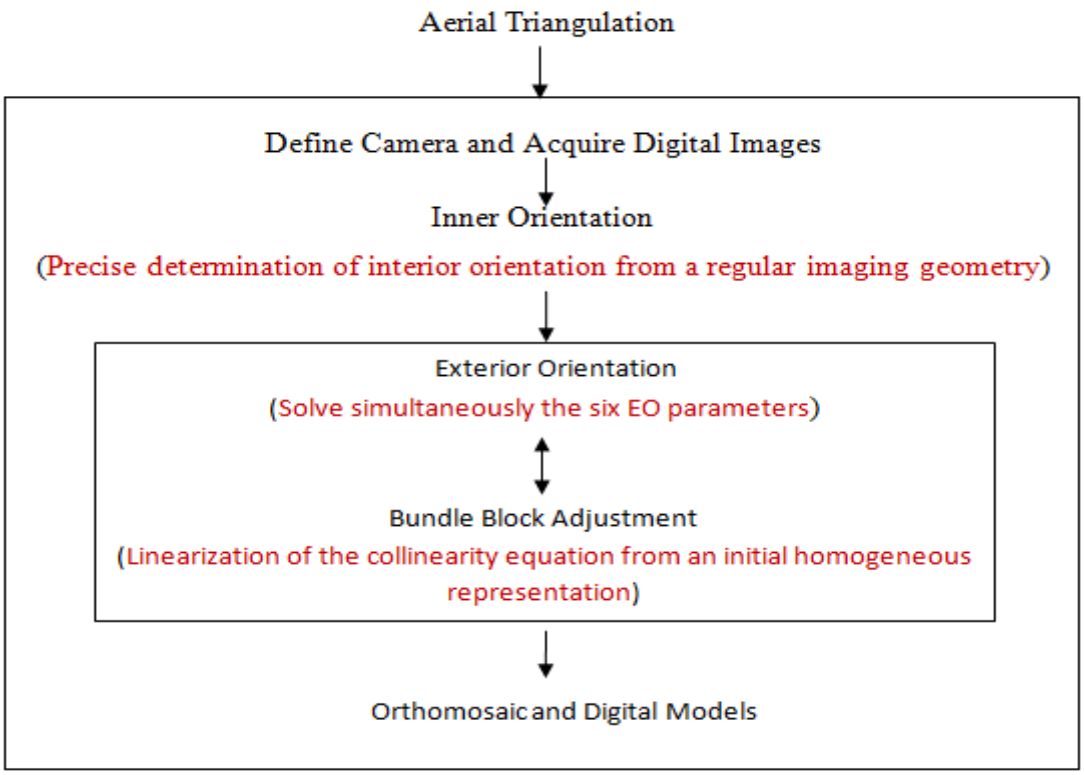

Figure 3.3 Conceptual Design of Close-Range Digital Photogrammetry. This explains the Procedures in Executing the Methodologies in this Thesis.

AAT also has the capability of real-time digital photogrammetry over a large area with desired accuracies and precisions (Choi and Lee, 2013; Sesli et al, 2010).

3.3 Automatic Calibration of Digital Cameras

According to Poser (2012, p. 1) "Advancements in camera technology and the reduction in camera costs have made it possible to obtain low-cost ultrahigh-resolution spatially accurate imagery in a static environment". Although not primarily designed for photogrammetric purposes (Yuan et al, 2014 and Wackrow et al, 2007), digital cameras have become relevant in close-range remote sensing and photogrammetry (Goncalves and Henriques, 2015; Hastedt and Luhmann, 2015; Strecha et al, 2015). The concern now is how to attain the standard photogrammetric positional accuracies with higher resolutions (Benassi et al, 2017 and Balletti et al, 2014). The metric capabilities of compact digital cameras are currently evaluated for precise close-range photogrammetric purposes (Balletti et al, 2014; Sanz-Ablanedo et al, 2009; Remondino and Fraser, 2006). Compact metric and non-metric digital cameras are small, portable, and cheap (Sanz-Ablanedo et al, 2009 and Wackrow et al, 2007).

They are easily attached to different platforms (Campana, 2017) with image capture at multiple and rapid successions (Fyffe et al, 2016). Some metric digital cameras have provisions to exchange lenses (Sanz-Ablanedo et al, 2009). Despite these advantages, precise and accurate photogrammetric surveys with compact digital cameras would require accurate calibration as they could be influenced by atmospheric and environmental conditions (Oniga and Cardei, 2015; Yuan et al, 2014).

Orientation and calibration of camera sensors are achieved by bundle adjustment (Colomina and Molina, 2014; Kim et al, 2013). The AAT facilitates the digital camera self-calibration and resection to generate a geometrically accurate image from the object (Damon, 2016; Pix4D Manual, 2016; Colomina and Molina 2014 and Vallet et al, 2011). The qualities of the images then formed are a function of the interior and exterior parameters of the digital camera (Pix4D Manual, 2016 and Kim et al, 2013). These parameters constitute the mathematical relationship of points in the 3-D coordinates between the object and the image space (Strecha et al, 2015 and Kim et al, 2013). The camera in-built model defines its interior parameters (Vallet et al, 2011). Interior parameters are a function of the lens type, lens distortion, transformation propensities that generates pixel coordinates from the camera frame, and the focal length (Damon, 2016 and Pix4D Manual, 2016). The exterior parameters are determined by the bundle block adjustment from the exact camera location and orientation (PP_x, PP_y, PP_z) to the exposure points (SP_x, SP_ySP_z) (Vallet et al, 2016) where PP and SP are the pixel projection and space projection respectively. Within software such as Pix4D, there are options to further calibrate the camera's external parameters to boost image quality (Pix4D Manual, 2016).

3.4 Interior Orientation in Digital Cameras

The mathematical outline for executing digital photogrammetry is the same as with analytical photogrammetry (Konecny, 2014). The 3-D similarity or affine transformation synchronizes the camera coordinate space with the image coordinate space (Chiabrando et al, 2015 and Westoby et al, 2012). In a digital photogrammetric mission, image acquisition commences with Interior orientation (Chiabrando et al, 2015) while the principles of the pinhole camera (Figure 3.4) remain the process of reconstruction of bundles of light rays (Hastedt et al, 2016; Hastedt and Luhmann, 2015; Balletti et al, 2014).

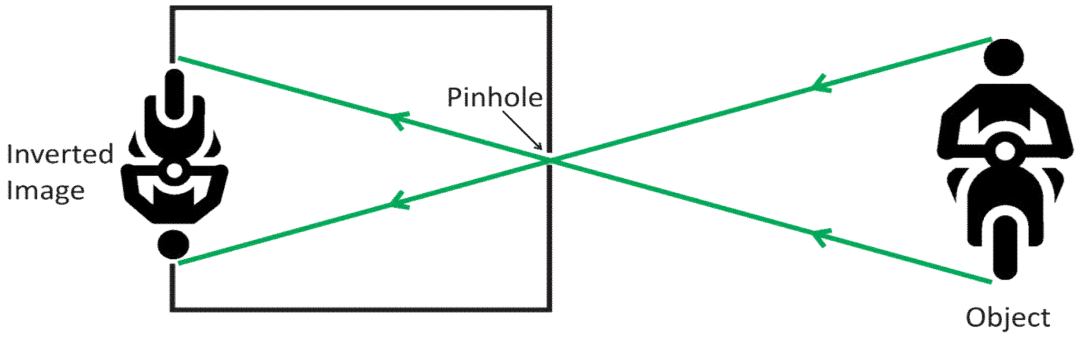

Figure 3.4 Principles of the Pinhole Camera, i.e. the Basic Mathematical Concept for Projecting the Object onto the Image Space (Wolf and Dewitt, 2000).

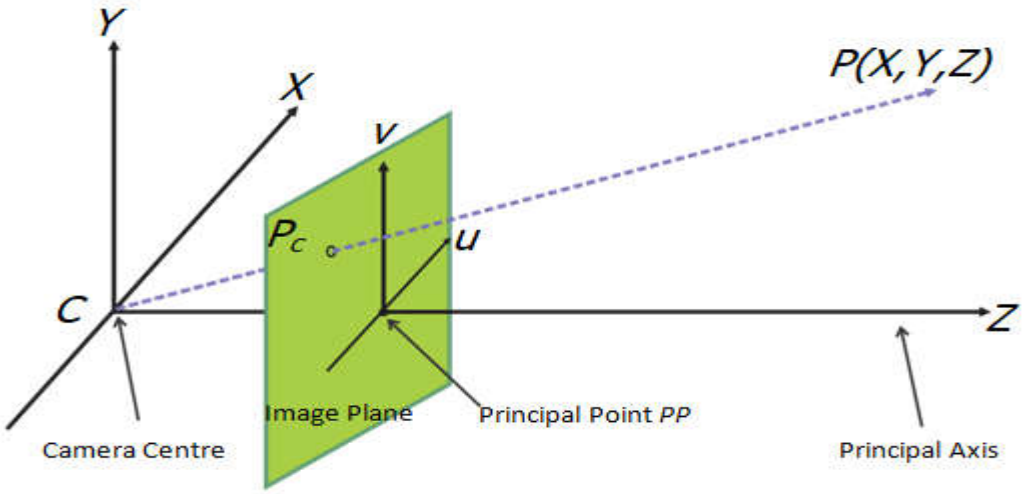

Figure 3.5 The Camera Centre and the Principal Point are Collinear. The Pinhole Camera Model also describes the Mathematical Relationship between the Coordinates of Points in the Image Space and the Object Space (Huang et al, 2015).

All the points in space as projected from the perspective centre (Figure 3.5) unto the image plane will have coordinates.

$P1 = (x,y,z)^T$

$(f*x/z, f*y/z)^T$

Interior Orientation is, therefore, the reconstruction of the bundle of rays from the object through the principal point to create an image (Habib et al, 2014). Interior orientation is the reconstruction of the metric features of the object at the time of exposure to coincide with the internal geometry of the camera sensor (Yuan et al, 2014). The degree of precision of the metric qualities is a function of the stability of the digital camera internal geometry (Habib et al, 2014 and Fraser, 2013). Parameters needed to fulfil interior orientation are:

a. The digital camera focal length

b. The optical distortion describes the extent of deviation of the image location(s) from its true location relative to the fiducial marks. These deviations are relative to how the camera lenses are assemblage in the factory and are in two facets.

i. Radial distortion

ii. Eccentric distortion

c. The origin of the fiducial marks and the distances between them

d. The array of the pixel frame which denotes the resolution of the image

e. Position of the perspective centre and the principal point as measured from the fiducial marks

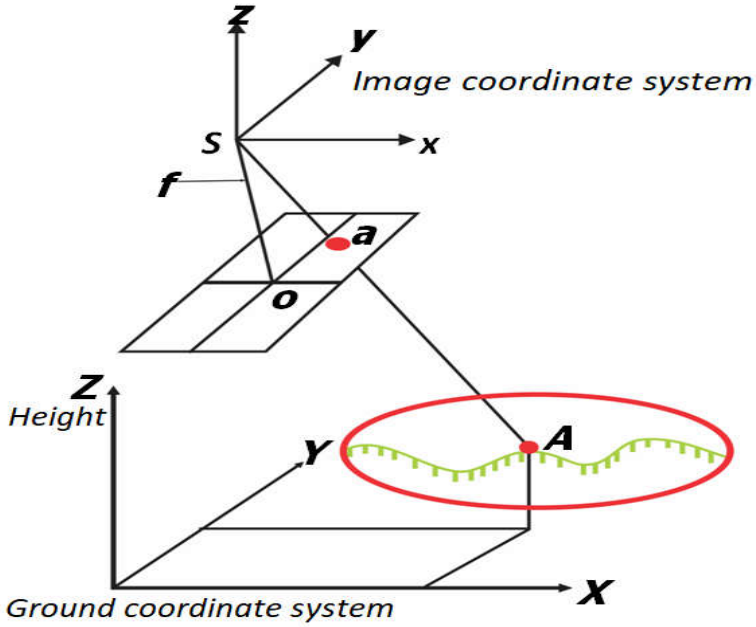

Figure 3.6

a = Image Vector

F = Focal length

O = Perspective centre

Figure 3.6 Image Coordinate Relative to the Ground Coordinate System. The co-ordinates transformation from the object to the image space enhances the positioning of the points for precise photogrammetry (Nishiyama et al, 2015).

3.5 Exterior Orientation in Digital Cameras

Exterior orientation is the transformation of the ground space to the image space (Xiuxiao et al, 2010). By this, the camera's exact position and orientation at the time of exposure will coincide with that of the object making the image coordinates to be the same as the ground coordinate (figure 3.6). The computation of exterior orientation depends on the interior orientation parameters (Elnima, 2015). GNSS and INS-enabled cameras will facilitate the computation of exterior orientation by geotagging (Mitishita et al, 2016; Colomina and Molina, 2014 and Verhoeven et al, 2013). On-board GNSS enables the camera position and orientation relative to the camera's perspective centre and altitude (Verhoeven et al, 2013). The perspective centre coordinates (X0, Y0, Z0) define the camera position and camera location defined by the three angular motions Omega, Phi, and Kappa (ω, φ, κ). These parameters X_0, Y_0, Z_0, ω, φ, and κ are the EO parameters. For digital photogrammetry, the GNSS/INS or IMU onboard the digital cameras automate the photogrammetric process of obtaining the EO parameters from the automatic aerial triangulation AAT (Goncalves and Henriques, 2015; Barazzetti et al, 2010).

The automatic multi-image matching improves the overall accuracy of the EO computation (Dominici et al, 2017; Barazzetti et al, 2010). Fig. **3.3** illustrates the bundle adjustment vis-à-vis the EO as an interactive computational routine for maximization in the accuracies of the EOs and tie-points creation (Alsubaie et al, 2017 and Khoshelham, 2009).

The fundamental conditions to determine the EO parameters are the coplanarity, collinearity, and coangularity conditions (El-Ashmawy, 2015 and Elnima, 2015). The collinearity equation is now preferred for computing the bundle adjustment (He et al, 2018) due to the computational speed and automation in relating the object space with the image space (Murtiyoso et al, 2018; Dominici et al, 2017 and El-Ashmawy, 2015). The modelling of software applications to ease multiple camera stations is another advantage (Schneider et al, 2012).

Dominici et al (2017); Oda et al (2015) and Strecha et al (2015) explain the modern bundle adjustment algorithms. Bundle adjustment is "stable" and "scalable" (Dominici et al, 2017 and Strecha et al, 2015). BA is executable with approximate GCPs and tie points (He et al, 2018; Oniga et al, 2018). It is also able to improve on the IO parameters and refine the scene geometry (Dominici et al, 2017). This functionality enables the model in processing large

numbers of digital images, unlike space resection that requires ground control points that are identifiable on the images (Easa, 2013; Xu et al, 2016).

EO parameters are relative to the self-calibration of the digital cameras and subject to systematic errors from aerial triangulation (Luhmann et al, 2016; Remondino and Fraser, 2006). Synchronization errors caused by responses between the digital camera hardware and the programmed time-series digital sensors orientation and navigation also influence the automaticity of the EO in digital photogrammetry (Rieke et al, 2011). In general, the overall success of automatic EO in digital photogrammetry is determined by the stability of the platform sensor's orientation and navigation (Rau et al, 2011; Colomina and Molina, 2014; Rehak et al, 2013; Blazquez and Colomina, 2012). The optimization of orientation parameters is from the further processing of the digital images using the respective photogrammetric software (Liu et al, 2018; Papakonstantinuo et al, 2016; Goncalves and Henriques, 2015; Bartos et al, 2014). For precise scientific purposes such as coastline monitoring, an almost constant internal geometry for digital cameras is required (Wackrow et al, 2007). The digital camera's internal geometry is always influenced by environmental or other systematic errors on the autopilot's aircraft position, velocity, and altitude 'tPVA' (Colomina and Molina, 2014; Blazquez and Colomina, 2012). It is imperative, therefore, to evaluate periodically the core metric values of non-digital cameras for stabilities and consistencies in the self-calibration leading to improved EO parameters (Benassi et al, 2017; Balletti et al, 2014). Manufacturers may provide approximate EO parameters and procedures for digital camera re-calibration and orientation.

3.6 The Collinearity Equation:

The principle that the object point *P* location, the perspective centre of the camera *O,* and the corresponding image point on the photograph are on a straight line formulates the collinearity equation (Liang et al, 2017; Elnima, 2015). This is demonstrated in figure 3.7 below.

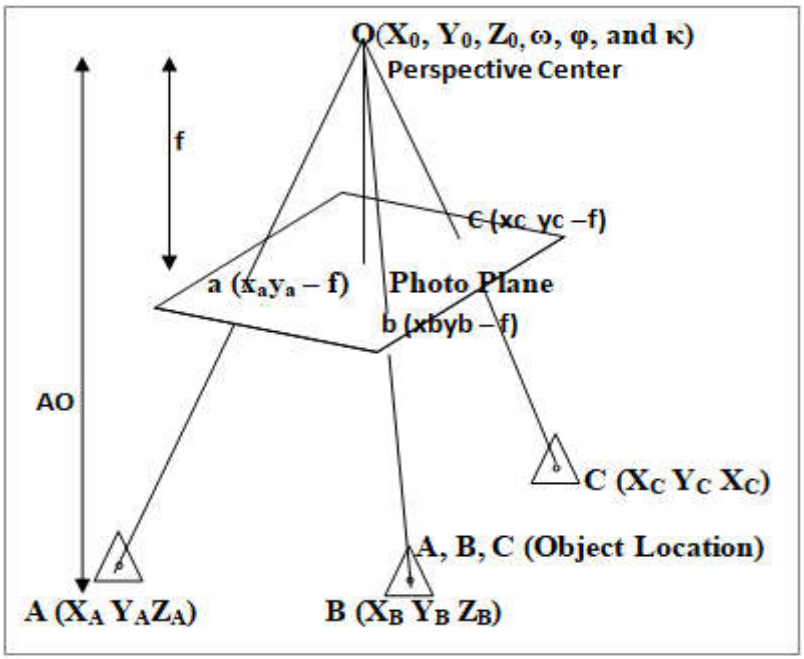

Figure 3.7 Principle of the Collinearity Equation. The Image Coordinates (Angular Orientation and Perspective Origin) can be derived from the Ground Coordinates).

AaO, BbO, and CcO are all on straight lines from exposure station O. *R* at the perspective centre O is presented as **(ω, φ, and κ).** If ABC is three object locations with coordinates X,Y,Z, the corresponding coordinates on the exposure station O, would then be X_0, Y_0, Z_0. Linearizing the vector AO, relative to their inner orientation parameters oa, will become,

$$Oa = \begin{pmatrix} Xa - X_0 \\ Ya - Y_0 \\ -f \end{pmatrix} \text{ and } AO = \begin{pmatrix} X_A - X_0 \\ Y_A - Y_0 \\ Z_A - Z_0 \end{pmatrix}$$

$$\begin{pmatrix} Xa - X_0 \\ Ya - Y_0 \\ -f \end{pmatrix} = \lambda R \begin{pmatrix} X_A - X_0 \\ Y_A - Y_0 \\ Z_A - Z_0 \end{pmatrix} \quad \text{.....(1)}$$

λ Is the scale factor and R is the (3 x 3) rotation matrix $\begin{pmatrix} R_{11} & R_{12} & R_{13} \\ R_{21} & R_{22} & R_{23} \\ R_{31} & R_{32} & R_{33} \end{pmatrix}$ .....(2)

Expanding (1) into (2) will derive,

$$\begin{pmatrix} Xa - X_0 \\ Ya - Y_0 \\ -f \end{pmatrix} = \lambda \begin{pmatrix} R_{11} & R_{12} & R_{13} \\ R_{21} & R_{22} & R_{23} \\ R_{31} & R_{32} & R_{33} \end{pmatrix} \begin{pmatrix} X_A - X_0 \\ Y_A - Y_0 \\ Z_A - Z_0 \end{pmatrix} = \lambda \begin{pmatrix} R_{11}(X_A - X_0) + R_{12}(Y_A - Y_0) + R_{13}(Z_A - Z_0) \\ R_{21}(X_A - X_0) + R_{22}(Y_A - Y_0) + R_{23}(Z_A - Z_0) \\ R_{31}(X_A - X_0) + R_{32}(Y_A - Y_0) + R_{33}(Z_A - Z_0) \end{pmatrix} \quad ...(3)$$

Rearranging and dividing equation (3), the orthogonal matrix will become;

$$X_a - X_0 = -f \frac{R_{11}(X_A - X_0) + R_{12}(Y_A - Y_0) + R_{13}(Z_A - Z_0)}{R_{31}(X_A - X_0) + R_{32}(Y_A - Y_0) + R_{33}(Z_A - Z_0)}$$

$$Y_a - Y_0 = -f \frac{R_{21}(X_A - X_0) + R_{22}(Y_A - Y_0) + R_{23}(Z_A - Z_0)}{R_{31}(X_A - X_0) + R_{32}(Y_A - Y_0) + R_{33}(Z_A - Z_0)} \quad .....(4)$$

Equ (4) is used for the self-calibration of digital cameras (Li and Liu, 2018; Pritt, 2014 and Sampath et al, 2012)

The collinearity equation is the fundamental equation used in digital photogrammetric bundle adjustment (He et al, 2018; Wang et al, 2017; Shahbazi et al, 2011) as it is easier to model the image coordinates, ground coordinates, EO and IO parameters even on low-cost digital cameras (Khalil, 2011). Collinearity adjustments accommodate multiple camera locations in a simultaneous least square estimation of coordinates of the several 3D point locations (Murtiyoso et al, 2018) as the bundle adjustment itself relies on the triangulation of points in 3D axes (Pan et al, 2016; Luhmann et al, 2016; Remondino and Fraser, 2006; Triggs, 2000). Applications are in the calibration of digital cameras by manual computations or using the respective photogrammetric software (Luhmann et al, 2016; Fraser, 2013; Previtali et al, 2013 and Remondino and Fraser, 2006). A dense image matching with minimum error is then created (Pan et al, 2016) with radiometric and geometric correlation with every point surveyed on the tidal lines, on the beach, and the cliff. The two major implications for coastal area monitoring would be;

a) Flexibility and ease of acquiring cheap survey-grade information on both the instantaneous and tide coordinated Shorelines required to implement a functional time-series beach monitoring program
b) Flexibility and ease of developing a consistent geomatic methodology for coastal cliff monitoring with time-series thematic maps.

Barazzetti et al, (2017) explain the relevance of a functional mathematical model for accurate image orientation. A well-defined collinearity model will accurately project the three-dimensional axis of the object into its corresponding points in the image plane without distortions in the object's geometry (Fraser, 2013). This is further justified by the fact that the model retains both the interior and the exterior parameters of images (Elnima, 2015). Equation (1) above explains this symmetry $X_{A,}$ $Y_{A,}$ $Z_{A,}$ and $X_{O,}$ $Y_{O,}$ coordinates of a single point in the object location and the perspective centre. This straight-line extends unto the image space as shown: (see the collinearity equation and fig 3.7).

The designs of the off-the-shelf non-metric digital cameras are such that the accuracies of their IO parameters improve on the principle of the collinearity equation (Wang et al, 2017; Ruzgiene, 2005). This is relevant in the design of the flight plan(s) or the gridding of survey routes (e.g. camera positions along flight lines covering the survey area) in terrestrial photogrammetry (Barazzetti, 2017 and Barazzetti et al, 2010).

This will help to minimize errors from the instability of the digital camera's internal parameters during photography (Abdullah et al, 2019) and to precisely relate the camera coordinate frame with the real world 'object coordinates' (Ahn et al, 2017; Taborda and Silva, 2012) and to minimize digital image curvature and distortion (Abdullah et al, 2019).

Accurate tide coordinated shorelines are only achievable when the grid pixels depicting several tidal heights are correctly transformed into an assigned coordinate system (Wu et al, 2019; Sagar et al, 2017; Ojiako et al, 2015). Similarly, the several spatial variations between adjoining pixel discontinuities on the cliff surface must transform correctly from digital numbers into appropriate geometrical values (Lim et al, 2005). Overlapping digital images should stitch and register without distortions in their perpendicularity, parallelism, and co-planarity (Elnima, 2015).

The transformation model from the 3D object coordinate to the 2D image object must ensure variation in the irregular surface topography does not lead to the loss of depth information. The collinearity equation models all camera positions and aiming angles as existed at the exact time of photography (Lee and Yu, 2009).

3.7 The Bundle Block Adjustment

The bundle block adjustment in photogrammetry is a mathematical process to extract, optimize, and re-project and match points of similar intrinsic/internal parameters between overlapping images to create a dense geometric 3D structure of the scene (Triggs et al, 2000). This 3D transformation aligns and improves the geometric accuracies between tie points and control points of adjacent digital images (Murtiyoso et al, 2018). Bundle adjustment is a phase in solving the Automatic Aerial Triangulation AAT problem (Gneeniss et al, 2015). The AAT (Rothermel et al, 2012) minimizes errors from misalignment and transformation between multiple images.

In digital photogrammetry, an independent 3D reconstruction mathematical algorithm performs the block bundle adjustment BBA (Murtiyoso et al, 2018; Jaud et al, 2016; Hastedt and Luhmann, 2015 and Rumpler et al, 2014) using the image tie points, the EXIF data of the camera image and GCPs (Vallet et al, 2011 and Strecha et al, 2015). The tie points minimize errors from misalignments while the GCPs reduce errors from transformation and helps to georeference the 3D model (Goncalves et al, 2018 and Strecha et al, 2015). The EXIF data optimizes the interior orientation (Murtiyoso et al, 2018 and Strecha et al, 2015). Unlike the analogue and analytical photogrammetry, the BBA performs the relative, absolute and exterior orientations as a simultaneous least-squares computation by multi-view reconstruction process (Remondino and Fraser, 2006) which makes the entire process cheap, quick and reliable for deriving DEM/DSM of beaches and cliffs (Goncalves and Henriques, 2015). Apart from providing the exterior orientation parameters, BBA also computes the GCP of tie points and with additional optimization algorithms reduces the projection errors between points (Zhao et al, 2018). The general methodology for automatic BBA is the structure from motion (SFM) algorithms using the non-linear regression algorithms (Juad et al, 2016; Hansch et al, 2016; Mancini et al, 2013; Remondino and Fraser, 2006). The entire process of SFM commences with the Scale Invariant Feature Transform (SIFT) that detects and computes the image features (Madden et al, 2019 and Qu et al, 2018). The general nonlinear least-square formulae for refining the structure for motion in digital photogrammetry is;

$$\sum_{i=1}^{m}\sum_{j=1}^{n} d\left(\tilde{u}_{ij}, P_i \tilde{X}_j\right)$$

The transformation precision between GCPs and tie points on the digital images and the positional accuracies of the bundle adjustment is a function of the reliability and robustness of the error propagation mathematical model (Yan et al, 2016, and Triggs et al, 2000). Either of the two commonly adopted error propagation, the mathematical algorithm will solve and propagate errors using the non-linear regression solutions. These are the Levenberg-Marquardt algorithm and the Gauss-Newton algorithms (Mendikute et al, 2017; Deseilligny and Clery, 2011; Remondinot al, 2017). Rothermel et al (2012), Lee and Yu (2009); Remondino and Fraser (2006) explain the advantages of the non-linear regression over the linear regression for multiple digital images. BBA mathematical solutions will be different for all photogrammetry software (Remondino et al, 2011).

Solutions with the open-source photogrammetry software are usually in the public domain that offers alternative processing tools and plugins to suit specific scientific needs (Champion and Rahaman, 2019; Rupnik et al, 2017). For instance, MicMac uses the Levenberg-Marquardt least square solution (Murtiyoso et al, 2018) whereas proprietary software such as Pix4D and Agisoft do not make their solutions public (Murtiyoso et al, 2018; James et al, 2016 and Juad et al, 2016). Goncalves et al (201; Fernandez-Hernandez et al (2015); Colomina and Molina (2014) and Rothermel et al (2012) recommend digital photo overlap of above 60% forward and 30% sideward for an effective and accurate bundle adjustment process.

3.8 Chapter Summary

In simplistic terms, while photography converts the 3D real world into a series of 2D images, photogrammetry converts these 2D images back into a 3D model. The early photogrammetric solutions using mechanical hardware were cumbersome and required technical skills. Photogrammetric algorithms and digital cameras now make the entire photogrammetry process easier and faster. Photogrammetric algorithms are developed by integrating the general photogrammetry theories of aerial triangulation, camera calibration parameters, and bundle block adjustment (Ai et al, 2015; Lee and Rhee, 2013). Image stitching, point clouds, mesh, and orthomosaic are deduced from the digital photogrammetry workflow.

In processing the digital images, there are many (free) open-source solutions (e.g. VisualSFM, OpenDroneMap & WebODM, Precision Mapper, Python Photogrammetry Toolbox, etc.); free but restricted solutions (e.g. RAPID by DroneMapper) which may be

limited to processing a maximum number of images (e.g. 150 for RAPID); the entry-level solutions (such as the cheap Agisoft Metadata); and the high-end/professional approach (e.g. Pix4D which costs about £200 per month as of 2021). In essence, all of these solutions undertake the same mathematical procedures as outlined in this chapter. While the commercial solutions do offer additional functionality, such as in editing capabilities, post-processing, visualisation, and cloud processing and sharing, the fundamental outputs of 3D point clouds, orthomosaics, and digital surface models are common to all. In terms of "low-cost" solutions, the open source solutions are now more than capable of handling a few hundred source images (of cliffs or beaches) to generate the necessary outputs for coastal mapping and monitoring. The various stages of digital photogrammetry as described in this chapter will be illustrated in the cliff and beach examples in the later chapters.

Provided these mathematical digital photogrammetry principles are obeyed, this chapter also demonstrates the practicability of digital photogrammetry open-source and low-cost solutions in providing accurate digital models such as for coastal cliff and beach monitoring. This is well demonstrated in the new digital photogrammetry technique for coastal cliff monitoring in chapter 4 and the low-cost computational analysis and visualization for coastal morphology and volumetric changes in chapter six.

Chapter 4

Development of a Low-Cost Digital Photogrammetry for Coastal Cliff Monitoring

Chapter Aim

New trends in close-range digital photogrammetry have seen the use of different measuring platforms such as drones, the use of poles/masts, balloons, tripods, and other approaches. Often cheap (or high-resolution expensive) cameras are mounted on these platforms to obtain images of the terrain, surface or object. While this technique has been successful in photo interpretation in other sciences such as the monitoring of cultural heritage and forensics, this chapter develops new pole photogrammetry, documents and suggests best practice guidelines for coastal cliff monitoring using the pole or mast as a photogrammetry platform. The methodology developed is easy to use, very low-cost, and can be executed by one person. It answers the big question on the availability of an accurate, localized, cheap, and ready–to–go methodology for coastal cliff monitoring if the cliff requires very regular monitoring.

The first Section (A) presents this methodology, while Section B develops a new algorithm that can detect changes on the point cloud derived from using this pole photogrammetry. The algorithm, developed in Python, is straightforward to use and automatically saves the area(s) of change for further spatial analysis. This chapter also answers the question of how to locally and accurately determine the areas of change on the coastal cliff using pole photogrammetry without resorting to the use of commercial software.

Section A

4.0 Low-Cost Digital Photogrammetry Survey Methodology for Coastal Cliff Monitoring

4.0.1 Section Aim:

Due to health, safety, environmental, Civil Aviation Authority (CAA) and military constraints, more regulations and restrictions are being placed on the use of drones all over the world. For example, CAA drone safety rules suggest a 50m exclusion zone around people, buildings, roads and railways; and 150m from crowds and built-up areas. Failure to comply can lead to criminal prosecution. These negate the application of Unmanned Aerial

Vehicle (UAV) in some coastal cliff monitoring environments, and certainly many beach and foreshore locations. Permissions to fly an area such as Penarth require the approval of a number of different local authority departments, landowners, and operators of Penarth Pier and Pavilion. Coordinating and synchronizing these permissions well in advance of the proposed survey with low tide, good weather and personnel availability constraints has been a significant restriction on the use of drones within this research project. On a number of occasions, drone surveys at Penarth were postponed or cancelled on site due to detrimental weather, such as rain or very localised wind gusts. Postponing for 24 hours is not always possible due to the permissions (and tides). An alternative to the use of drones was sought, and a method which demonstrated the use of low-cost technologies. Some drones which have been trialled at Penarth (and illustrated in later chapters) cost in excess of £20K, which defeats the underlying philosophy of this research project, i.e. low-cost solutions.

This chapter is an innovative rapid, low-cost, and precise digital photogrammetry methodology for the continuous monitoring of the cliff surface by using a pole or mast as the platform and cheap digital sensors (e.g. cameras and mobile phones).

4.0.2 Section A Objectives:

1. This chapter determines how the camera faces the cliff surface during image capture. The quality of the digital images is determined by how the camera mounted on the pole with the pole itself held on the ground are positioned and directed towards the cliff.

2. Another factor that determines the quality of the digital images is the distance of the measuring device (digital camera and pole) to the object measured (cliff). The best distance that will apply to other cliff surfaces will be determined in this chapter.

3. This chapter will also determine the forward and side distance(s) overlap between adjacent images for the best illusion of depth (picture clarity and sharpness). Successful photogrammetry must be detailed, clear, and sharp enough for both visualization and photo interpretations.

4. Finally, this chapter will determine the best duration for executing a pole survey that will generate excellent photogrammetric products such as 3D orthomosaic and digital surface models from using cheap small phones and digital cameras.

4.0.3 Section Overview:

Coastal cliffs are mostly vertical or near-vertical elongated structures with a wave-cut notch and a landslip. With drones, the pre-programmed flight routes are automatically set at the best angle that captures images on a regular grid pattern and flight speed (Varela et al, 2019; Colomina and Molina, 2014; Perez-Alberti and Trenhaile, 2014). To survey the cliff surface on a manual flight mission with the drone requires great experience to obtain an optimal flight mission and generate orthometric and digital models required for mapping purposes (Mancini et al, 2017). Digital images acquired arbitrarily from the ground stations to survey the cliff would be difficult to generate a complete overlapping stereo oriented model for consistent and precise 3D models and 3D maps except as a rare 'accidental success'.

The use of poles or masts as platforms would require ground-based camera locations. The distance between these ground-based stations and the cliff surface is the equivalent of the height above the ground in aerial surveys. Like traditional aerial surveys, camera-based stations on the ground also require very careful and systematic planning to achieve the best Ground Sampling Distance (GSD) (Huang et al, 2015), sensor stability (Roncella et al, 2014), overlap and reduce the effects of random errors and accumulation of systematic errors (Aber and Babb, 2018; James and Robson, 2014). The length between the baseline and cliff (L), the linear dimension of the pixel (px), and the camera lens' focal length (f) will determine GSD accuracies as camera pixels will be mapped to the cliff surface. This chapter develops the most realistic GSD when mapping the cliff surface by pole photogrammetry.

Geological formations of limestone, sandstone, chalk, rock shelters and granite characterize the cliff surface (Terefenko et al, 2018). Several crests of waves on the cliff surface depend on the formation of the sections on the cliff and such irregular spectral frequencies cause both low and high contrast across the electromagnetic spectrum (Young et al, 2016). Digital photogrammetry is more challenging when using low-quality complementary metal-oxide-semiconductor CMOS or the Charge-coupled devices CCD image sensors (Dai et al, 2014) as with this research. The best pattern of forward and side overlap and the distance between camera stations to the cliff surface is determined to generate the best spatial and spectral resolutions for deformation analysis.

Due to the height of the coastal cliff and considering the very short distance between the camera location and the cliff surface, there must be careful considerations on the angle of the camera, camera calibration, stabilization, and sensor orientation to overcome yaw variation,

roll variation, altitude variation, perspective variation, barrel, and pincushion. The accuracies on the computation of the exterior orientation parameters by the BBA using the Integrated Sensor Orientation (ISO) is usually affected by both the GNSS satellite geometry and the lock on the available GNSS constellation (Rau et al, 2011). GNSS radio signals delays are mainly by the free electrons in the ionosphere and by other atmospheric conditions in the troposphere (Zhang et al, 2019). The Earth rotation induces charged particles into the magnetic field line in the ionosphere and capable of distorting the propagation of radio waves signal (Constable, 2016). Ionospheric propagation delays are of higher magnitude than the tropospheric delays and largely degrade the accuracies in single-frequency GNSS receivers' especially inbuilt GNSS sensors on Smartphones and other inexpensive digital cameras (Karaim et al, 2018). Considerations are in place also to obtain the best time-lapse for satellite geometry when mapping the cliff surface using the pole photogrammetry due to drift in the GPS/INS low-quality digital camera/GPS sensor (Masiero et al, 2017).

The coastal cliff undergoes regular physical and chemical weathering processes (Earlie et al, 2017 and Sciarra et al, 2014) as well as seawater crashing against the surface (Earlie et al, 2017). Cliff surface weathering causes an almost unpredictable and unstoppable detachment between formations and eventual collapse (Singh et al, 2016). The coastal cliffs are therefore asymmetrical with complex surface discontinuities (Letortu et al, 2018; Westoby et al, 2018; Ruzic et al, 2015; Galea et al, 2014; Somma et al, 2015 and Sciarra et al, 2014). It is difficult therefore to establish temporary/permanent control points on the cliff surface. The establishment of GNSS points close to the cliff at either the top or toe in some coastal areas is practically difficult due to such high-volume sea wave and cliff surface erosion (Earlie et al, 2017). This is the situation in Penarth (study location) and specifically this stretch of the Bristol Channel coastline, with almost constant cliff face weathering and sometimes collapse. GNSS equipment is expensive to buy or hire and may not be available in most situations. It is imperative to develop a cost-effective and precise methodology using the Structure from Motion (SFM) derived point cloud for coastal cliff geotechnical and structural change detection analysis. For existing close-range digital photogrammetry techniques, consistent and accurate time-series orthomosaics and digital models for environmental monitoring are feasible on the availability of GNSS points (Ruzgiene et al, 2015 and Turner et al, 2015). The method developed is a simple and straightforward photogrammetry technique for consistent and precise evaluation of the cliff surface with or without the GNSS controls.

4.0.4 The Ground Sampling Distance (GSD), Pixel and Field of View (FOV)

The three main terms: GSD, Pixel and FOV are defined below as follows:

1. The Ground Sampling Distance GSD relates to the size of pixel represented on the actual ground surface. It is the ground equivalent of how much detail is visualized in the pixel of an image (Pix4D, 2016 and Fernandez-Hernandez et al, 2015).

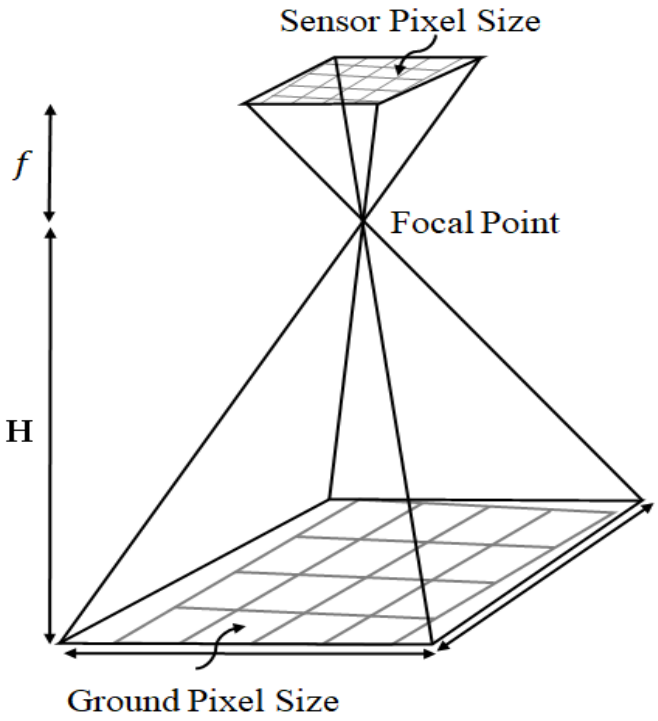

Figure 4.1 – The Ground Sampling Distance. The smaller the GSD, the more details that can be viewed on the image. GSD, therefore, determines the image resolution.

$$GSD = \frac{f}{H} = \text{Photographic Scale} = \frac{Sensor\ Pixel\ Size}{Ground\ Pixel\ Size}$$

f is the camera's focal length and H is the flying height above a given datum. The application of the GSD in section 4.1.3 gives further explanation on its relevance in determining quality images.

2. Pixel

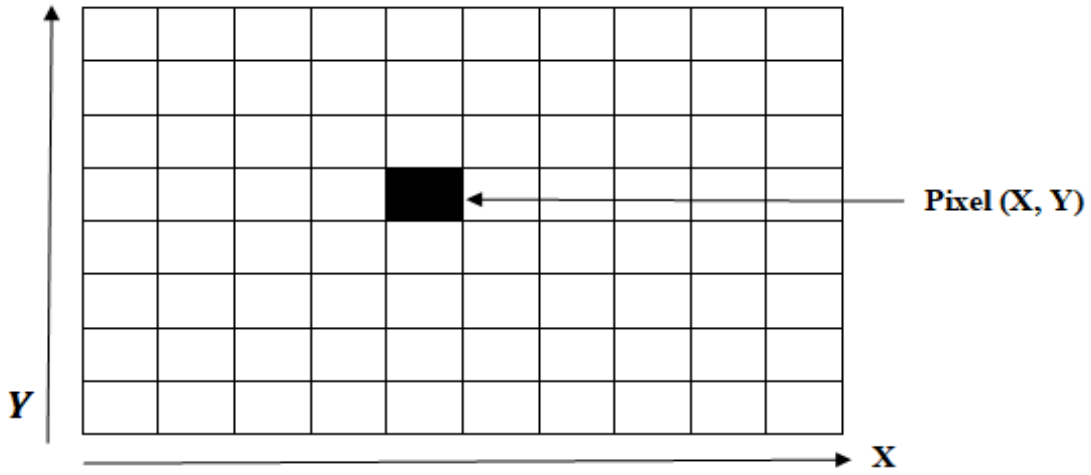

Figure 4.2 – The Pixel. Every digital image is a 2D array of pixels. The image resolution (how clear the image is) is defined by the size of the pixel in the X, Y units (Fernandez-Hernandez et al, 2015 and Ruzgiene et al, 2015). This is illustrated in figure 4.2.

3. Field of View (FOV)

Figure 4.3 – The Field of View (FOV). This is how much details can be captured by the camera lens at a time. This is how many details can be captured by the camera lens at a time. The larger the field of view Θ^{O} the more details that are captured. The higher the FOV, the likely a lesser resolution. However, there could be a trade-off between the FOV with using a higher megapixel digital camera.

4.1 New Survey Methodology for Coastal Cliff Monitoring

4.1.1 Possible Sources of Errors in Precise Close-Range Digital Photogrammetry

1. The internal and external working mechanism of the digital camera: These errors are lens distortion, approximation in the principal distance, and digital camera sensor resolution (Dai et al, 2014). These are systematic errors, reduced by calibrating the digital camera (Dai et al, 2014).
2. Errors and Blunders such as skipping ground stations or not saving digital images during photography.
3. Digital image photogrammetry software: The image-stitching and bundle adjustment algorithms of the respective software differ in functionalities (Murtiyoso et al, 2018; Juad et al, 2016 and Elnima et al, 2015).
4. Field Measurements Procedure determines the degree of overlap, angle(s) of image capture, convergent images, and the degree of perspective (Barazzetti et al, 2010).

Table. 4.1

Sources of Distortions	**Manifestation**	**Type of Error**	**Effects**
Irregular focal length	Change in the FOV during the survey.	Systematic	Can cause a change in image pixel coordinates and pixel size (Cantreul et al, 2018; Dai et al, 2014) Can lead to scale error in the object scale (Luhmann et al, 2016)
Camera stations not properly gridded	Not maintaining a defined baseline An irregular grid pattern causes changes in the FOV.	Systematic	Pair matching is easier on a regular image scale (Zhang et al, 2011).
Multiple angles of incidence on a single survey	The camera's angle of tilt determines image acquisition accuracies and precision.	Systematic	The accuracies of digital camera self-calibration are influenced by the sensor's geometry (Nesbit and Huhenholtz, 2019; Jaud et al, 2016).
Percentage of Photo Overlap	Effective overlap improves the accuracy of tie-points and points cloud.	Systematic	Image network geometry improves significantly with effective overlap (Jaud et al, 2019; Hartmann et al, 2016).

4.1.2 Determine an Appropriate Vertical Camera Angle to the Cliff

The basic transformational matrixes of each grid cell relate every pixel location in the image relative to the cliff surface elevation. The digital camera self-calibration solution includes the direct computation for the interior and exterior parameters, which allows the transformation from 3D coordinate (X, Y, Z) of the ground point to a 2D coordinate (u, v) of the image in pixels. The basic perspective projection centre of the perspective lens cameras relates the scene properties as pixels where the origin is the camera centre defined by its position and orientation.

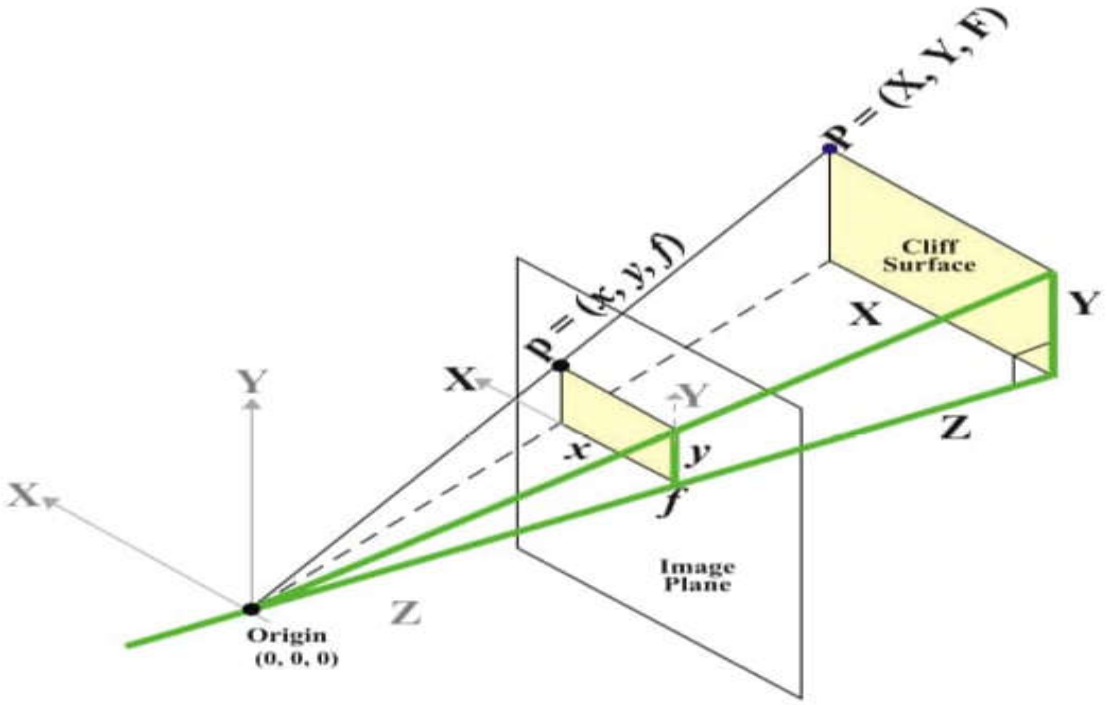

Figure 4.4 Perspective projection enables the camera location, the centre of the camera lens, and the cliff surface monitored to be viewed together as 3D. It gives a better visual of the entire photographic process (Liang et al, 2017).

The origin and geometrical sequence between each grid cell determine the transformation matrix of orientation parameters that form the image of the object by relating the scene properties as pixels (Liu et al, 2016). The origin is the camera centre defined by its position and orientation (Xu et al, 2017) illustrated in figure 4.5.

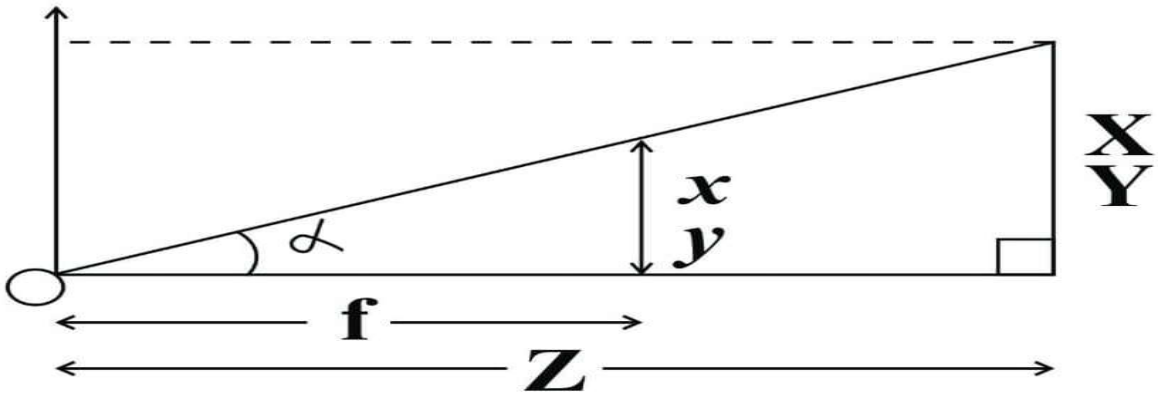

Figure 4.5 Central Projection is the origin of the survey that relates the camera coordinates system with the pixel coordinate system.

$x = f\frac{X}{Z}$, $y = f\frac{Y}{Z}$ ……..equ (1)

A homogenous coordinate system introduces the matrix equation by including a fictitious third coordinate. The 2D point (x, y) will then be

$x = \frac{X^1}{Z^1}$, $y = \frac{Y^1}{Z^1}$ …….equ (2)

$(X, Y, Z)^T = (f\frac{X}{Z} + P_x, f\frac{Y}{Z} + P_y)^T$ …… ….....equ (3)

$(P\varkappa, Py)^T$ is the image coordinates of the principal point. The homogenous coordinates of a perspective lens camera for undistorted images is given therefore as;

$$\begin{bmatrix} x^1 \\ y^1 \\ z^1 \end{bmatrix} \longleftrightarrow \begin{bmatrix} fX + Zpx \\ \\ fY + Zpy \end{bmatrix} = \begin{bmatrix} f & 0 & 0 & 0 \\ 0 & f & 0 & 0 \\ 0 & 0 & 1 & 0 \end{bmatrix} \begin{bmatrix} X \\ Y \\ Z \\ 1 \end{bmatrix} \quad \text{……equ(4)}$$

Consistent orthogonal vector geometry is required to provide stable least-squares estimation (Ai et al, 2015) from 3D transformations and parameterization as provided by the BBA (Ai et al, 2015 and Triggs et al, 2000). The accuracies of the BBA also rely on the orientations and regularity of each pixel grid cell (James and Robson, 2012).

A trade-off between the focal length, incidence angle, and distance from the cliff surface is necessary to generate the maximum number of tie-points. There is practically no

mathematical relationship for the different variables due to the different digital camera resolutions, focal length, the height of the cliff, pattern of the cliff verticality, and the chemical composition of the cliff.

Digital photos acquired from off-nadir angle geometry will generate denser tie-points and create a better model for the cliff surface compared with photos acquired from the nadir positions (Nesbit and Hugenholtz, 2019; Juad et al, 2016; Mancini et al, 2017). The reduction of systematic errors is from the reduction of gaps between adjoining digital images on the cliff surface geometry that is vertically irregular (Nesbit and Hugenholtz, 2019). This section experiments on an appropriate vertical camera angle that would be suitable to;

a) High overlapping images that can generate a dense point cloud

b) Obtain pixel texture accuracies for cliff surfaces

c) Survey the entire height of the cliff with acceptable geometric accuracy.

This practical solution is reliant on the cliff surface characteristics, the resolution of the digital camera, and the pole as a platform using the perpendicular orientation geometry as shown in figure 4.3 below.

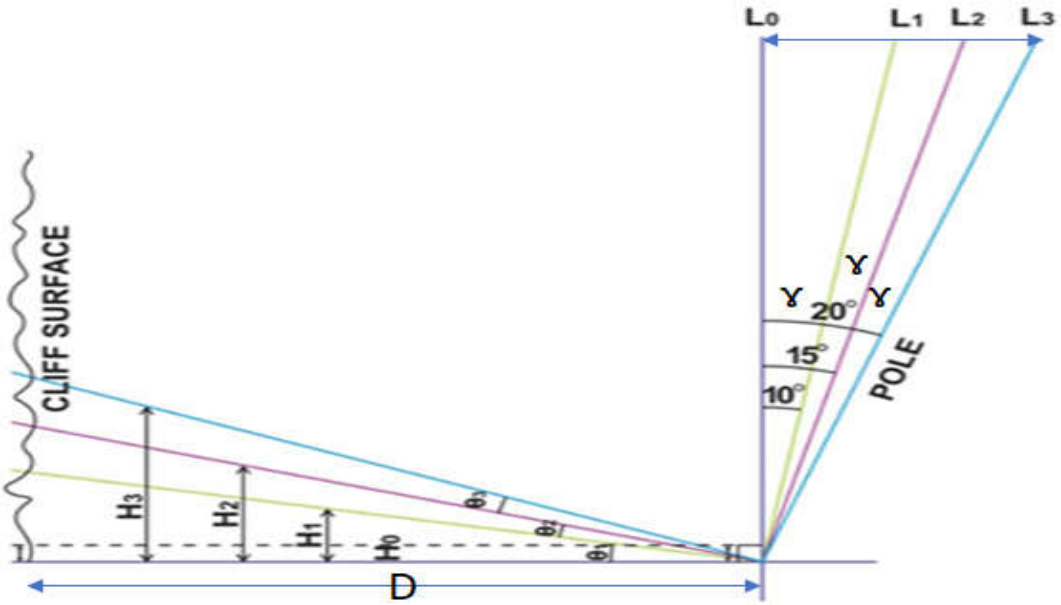

Figure. 4.6 Viewing and Orientation Geometry to the Cliff

Θ = Observing angle
ɤ= Vertical camera angle
H = Height of the section on the cliff
D = Ground distance
Pɤ = Pixel size perpendicular to the vertical camera angle

PΘ = Angular segment on the cliff surface. $\tan \Theta = \frac{H}{D} =$

At L, the height of the cliff will be H while Pɤ is smaller provided every other photogrammetric constraint such as clouds, haze, and poor image overlap are minimal. This research experiments on the perpendicular orientation geometry using four different surveys at four different vertical cameras angle to the cliff section measuring 27 metres in length. The outcome is figure 4.7 below.

The Cell sizes (X, Y) for the 0^0, 5^0, 10^0, and 15^0 vertical inclinations are 0.00799/0.00799, 0.01142/0.01142, 0.00771/0.00771 and 0.008/0.008. The geometrical pattern for all four-point clouds is the same. The 10^0 vertical tilt had a little more overlapping than the 15^0. The 15^0, however, can capture the top of the cliff with the use of the eleven metre (11m) pole / mast used in this survey.

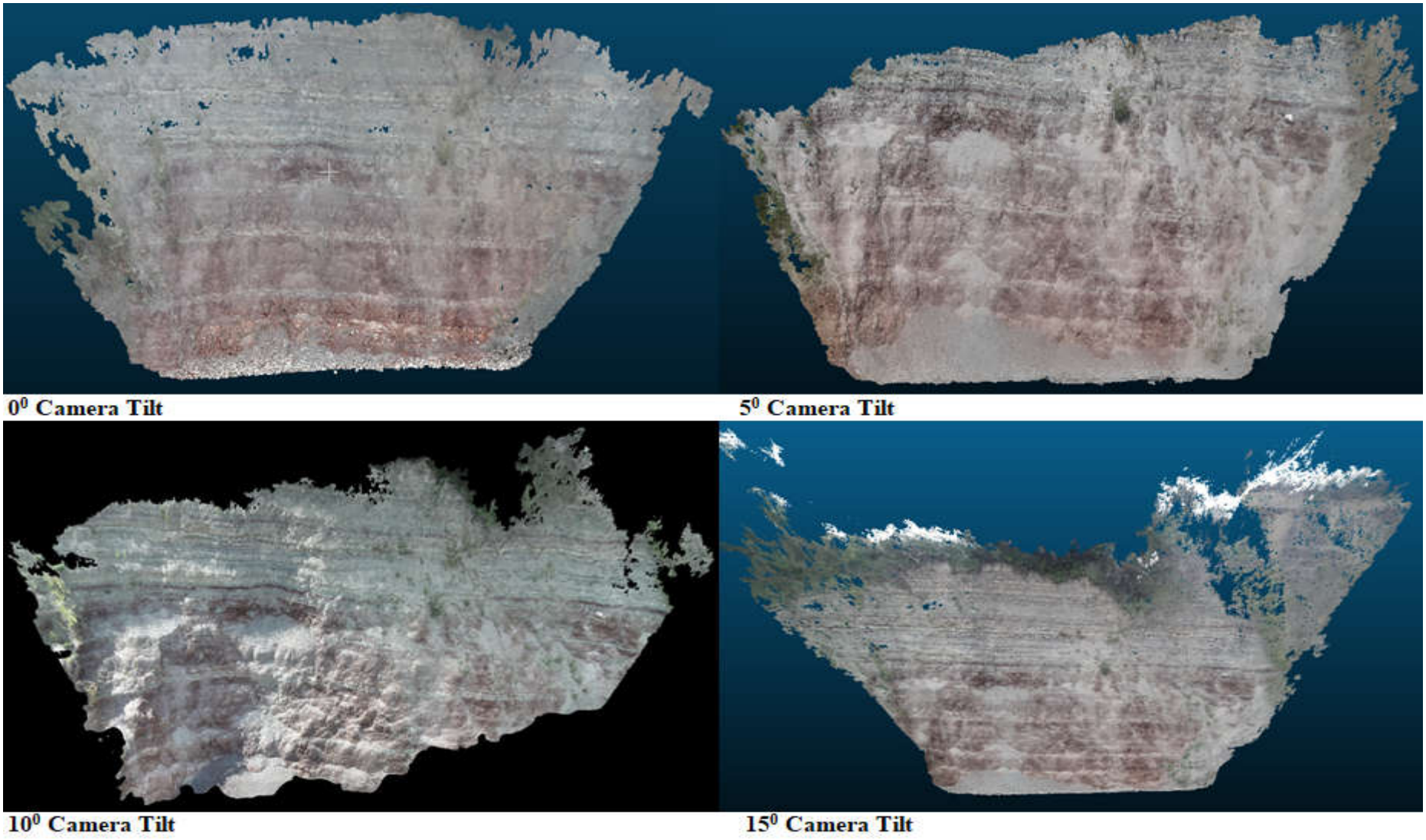

Figure 4.7 Dense Point Cloud obtained from Four Vertical Camera Angles to Determine the Pattern of Overlap and Image Quality. The Location is the Cliff Stretch Monitored at Penarth on the 16th and 17th July 2019.

4.1.3 Determining the Best Distance between the Cliff Surface and the Base Line

In close-range photogrammetry, the digital camera could be as close as a few centimetres to the object being monitored which favourably improves image resolution (Westoby et al, 2015). However, when monitoring an unstable cliff like in Penarth, even a couple of metres could be dangerous and also unfavourable to the field of view (FOV) with constraints on the orientation angle of the digital camera. The best practice would be a trade-off between the distance to the cliff surface, the FOV, and the cliff height. The camera distance to the cliff surface determines the GSD. Shorter distances between the camera and the cliff will produce a smaller GSD provided every other photogrammetric constraint is minimised, while larger distances could amount to greater GSD especially with the use of low/medium resolution digital cameras.

Smaller GSD will have a higher spatial resolution. The GSD should be at least half of the smallest object on the ground for measurement (Tziavou et al, 2018).

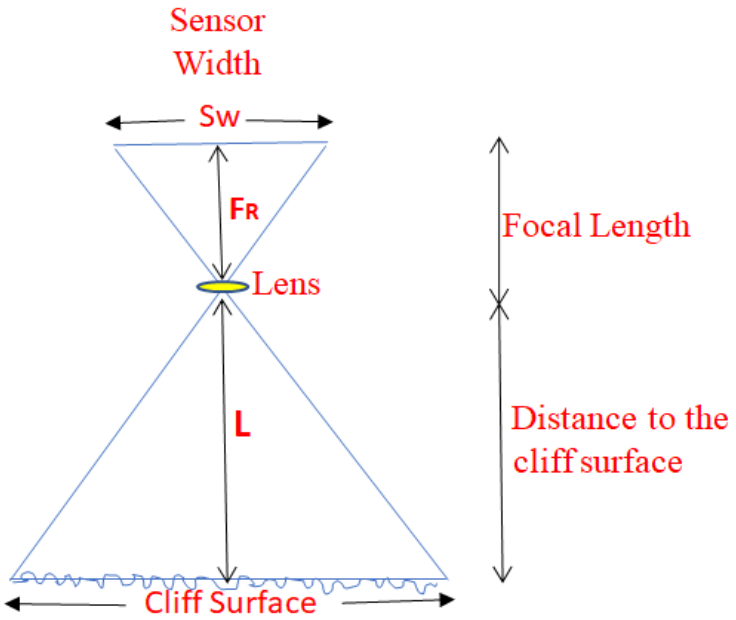

Figure 4.8 Sensor Width Relative to the FOV

$$GSD = \frac{\mathbf{L} * px}{f}$$

$$\mathrm{L}= \frac{\mathbf{GSD} * \boldsymbol{F}}{\boldsymbol{PX}}$$

Most times the pixels, when projected onto the ground, will not be squared perfectly. The GSD would then be computed in terms of sensor width and sensor height.

$$\text{GSD (height)} = \frac{L * \text{Sensor height}}{f * \text{Image height}}$$

$$\text{GSD (width)} = \frac{L * \text{Sensor width}}{f * \text{Image width}}$$

GSD = Ground Sampling Distance
L = the length between the baseline and cliff
f= the focal length of the digital camera
px = the pixel linear dimension

To determine approximately the GSD For a distance of 3 metres between the baseline and the cliff, using the Samsung (SM-G850F Camera);

The focal length of the Samsung SM-G850F camera = 1.2 mm
Pixel height = 1920
Pixel width = 1080
Approximate sensor width = 9.61923 mm
Approximate sensor height = 5.410082 mm

$$\text{Width} = \frac{3 * 5.410821}{1.2 * 1080} = \mathbf{1.25cm/px} \qquad \text{Height} = \frac{3*9.619238}{1.2*1920} = \mathbf{1.25cm/px.}$$

To derive a baseline that is photogrammetric stable between the camera position and the cliff, the cliff was surveyed three different times at three different baselines. The section of the cliff monitored is 27 metres in length. The Samsung Alpha phone SM-G850F Front Camera of 2.1 megapixels was on an 11 metre pole for these surveys. The outcome of each survey is table 4.2 below.

Table 4.2 Outcome of three Different Surveys to determine a Practical Base Line to the Cliff

L (m)	No. of Photos	Average GSD (cm)	2D Key points extracted for BBA	3D Key points for BBA	Mean projection errors in pixel
3	169	1.68	3782815	1303566	0.254
5	169	0.73	3174090	786342	0.268
10	169	2.05	3958836	838557	0.309

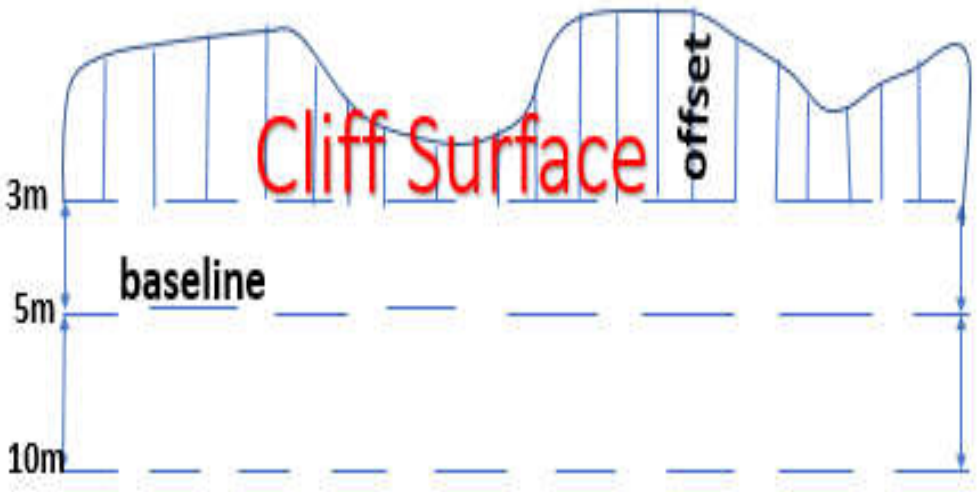

Figure 4.9 The Three Different Baseline Distances from the Cliff will Determine the best Distance(s) between the Camera Position to the Cliff.

This is a practical application of the FOV, Pixel, and GSD in close-range digital photogrammetry. This innovation on the best survey practice for the pole/masts as platforms for cliff monitoring will be suitable for other monitoring/deformation surveys.

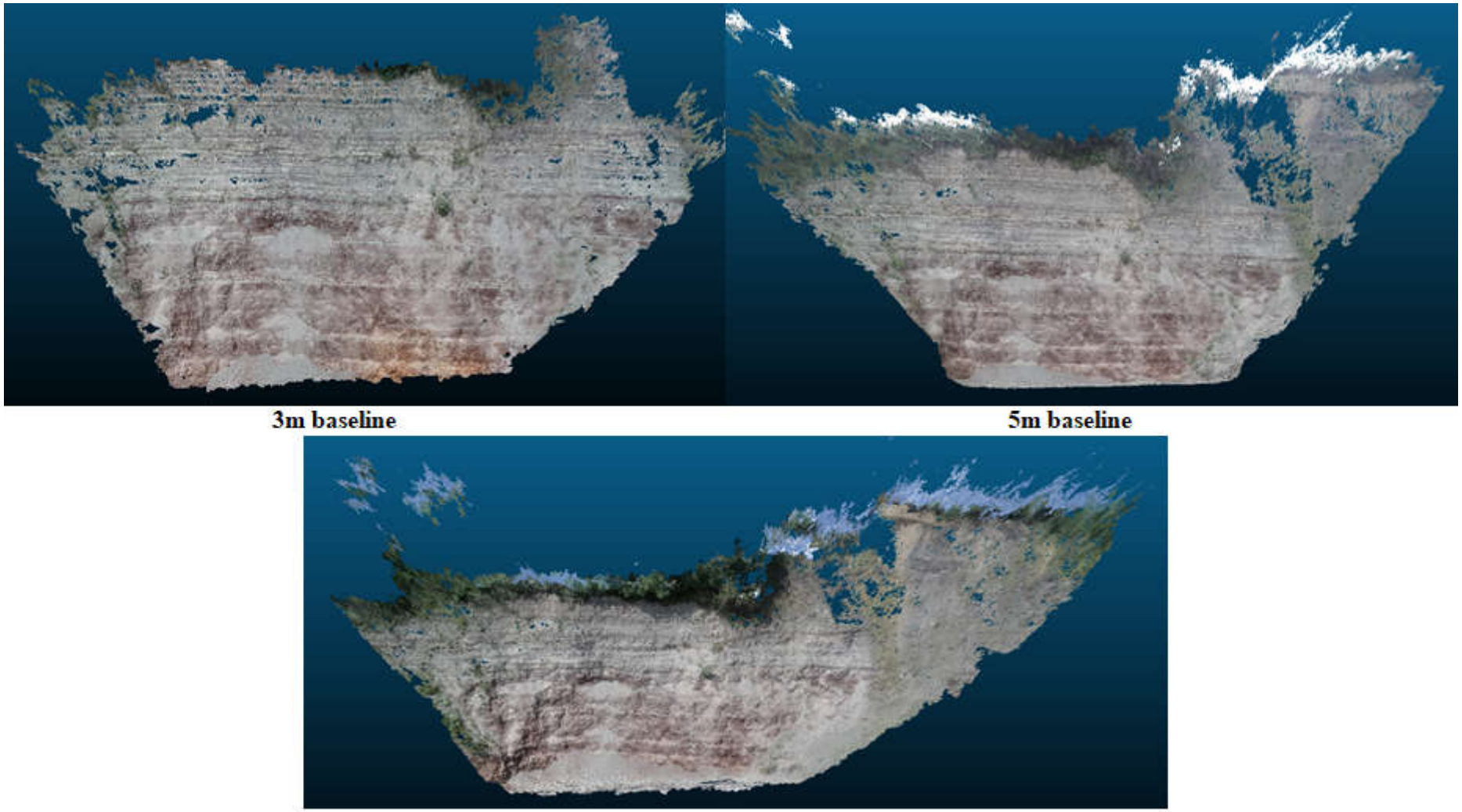

Figure 4.10 Showing the Point Clouds Outputs Obtained using the Different Experimented Baselines between Camera Stations and the Cliff Section at Penarth. Survey was done on the 18th of May 2019.

It was difficult and dangerous surveying from the 3-metre baseline due to regular cliff falls and the irregular protruding of the cliff face. In some sections, the offset distances were less than 1-metre as illustrated in figure 4.9 (above) causing a very small FOV and limiting the camera from capturing the cliff top. According to Cwiakala et al (2018), irregular distances between the camera location and the object could negatively influence the accuracy of the Average Ground Sampling Distance (AGSD).

Irregular FOV changes the depth of the field and the visual content on the pixel grids (Dansereau et al, 2017). Contemporary processing digital photogrammetric software such as the Scale Invariant Feature Transform (SIFT) matching techniques relies on corresponding pixel neighbourhoods for feature point matching (Qu et al, 2018).

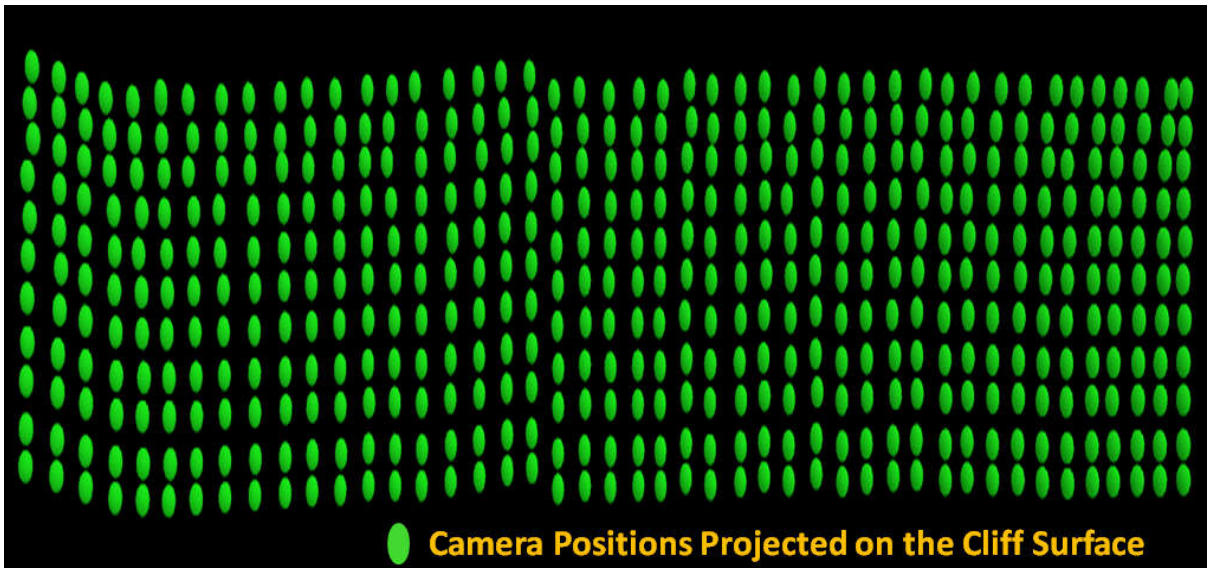

Figure 4.11 Showing Camera Positions with the Pole Survey at Penarth. Each camera position indicates a change in the camera location as seen in figure 4.12 below.

Each ground (pole) station along the baseline would have eleven camera vertical positions ideally (with the possibility of some extra images due to weather conditions such as wind gusts or insurance in case of perceived image confidence). Eleven camera vertical positions at each of the fifteen ground stations for this survey with some extras resulted in 169 images in this instance.

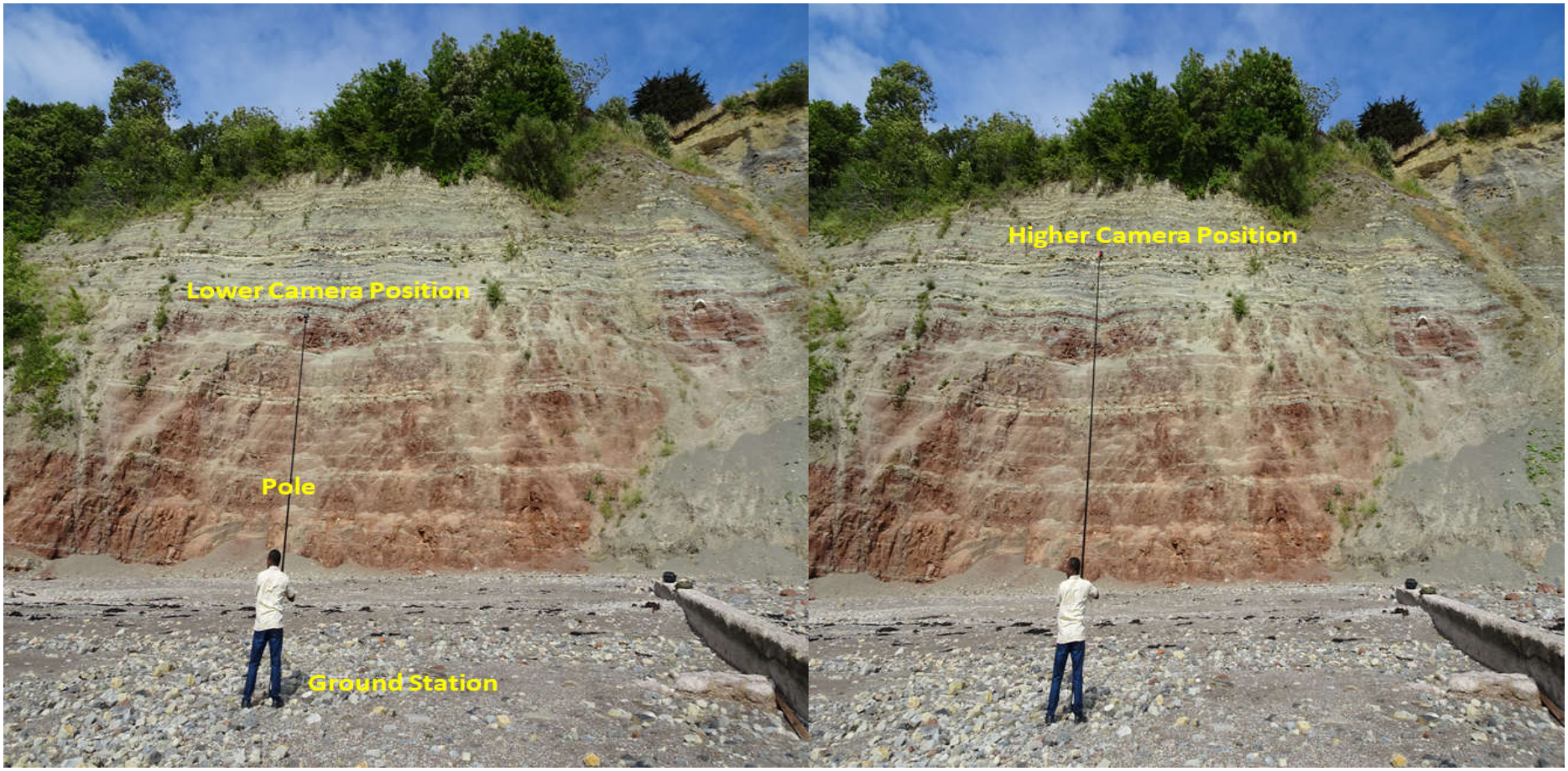

Figure 4.12 shows the camera position is changed by altering the height of the pole (lower camera position and higher camera position) and by the actual change of the pole ground Station - The pole is 7 metres on the LHS and 9 metres on the RHS. The light telescopic pole is 12 metres in length.

The average distance of 5-metres from the toe of the cliff is, therefore, most appropriate to survey the section of the Penarth cliff monitored using the pole.

1. This distance is with lesser risk and hazard. This distance enhances a more consistent block symmetry due to safer camera stations.
2. It enhances overlap and boosts the visual content (the provided survey is under friendly environmental conditions).
3. With this distance, there is the certainty of an increased spatial and spectral resolution irrespective of the quality of the camera sensor used.
4. It ensures the more regular offsets, as most cliffs are irregular in shape.

4.1.4 Determine a Practicable forward and side overlap

The terrain topography and purpose of the photogrammetric project determine the choice and percentage of overlap (Pepe et al, 2018). Recommendations, however, are for a regular grid pattern (Carter et al, 2019) of 60% side overlap and 80% forward overlap (Cwiakala et al, 2018; Turner et al, 2015; Colomina and Molina, 2014). To generate tie-points with maximum density, every point in the object space should be in a minimum of 4-5 images (Ruzgiene et al, 2015).

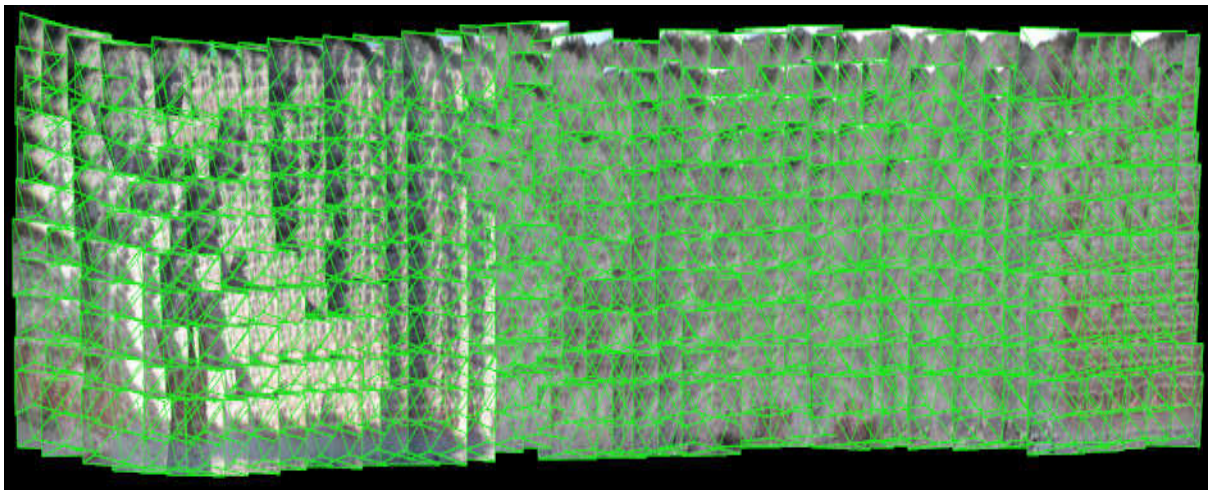

Figure 4.13 Degree of Overlap from Marked Points on the Ground – This overlap is relative to the change on the cliff height (figure 4.12 above) and the ground stations (figure. 4.14 below). Each green box represents one pole photograph at Penarth cliff face (at 1m vertical steps and 1.65m horizontal intervals).

Figure 4.14 shows the pole stations marked at 1.65m horizontal intervals (by white locations markers on the beach at Penarth).

Poles stations were defined at every 1.65m interval, marked on the ground with a white paper as shown in figure 4.14. The average percentage of overlap is 55% horizontal and 58% vertical. Figure 4.15 below illustrates the survey Area of Interest (AOI) and the number of overlapping images which capture this area. An accurate photogrammetric model requires plenty of overlap. Areas of low overlap are expected on the boundary, but interior fallout is usually a sign of poor roll, pitch and yaw in the camera orientation.

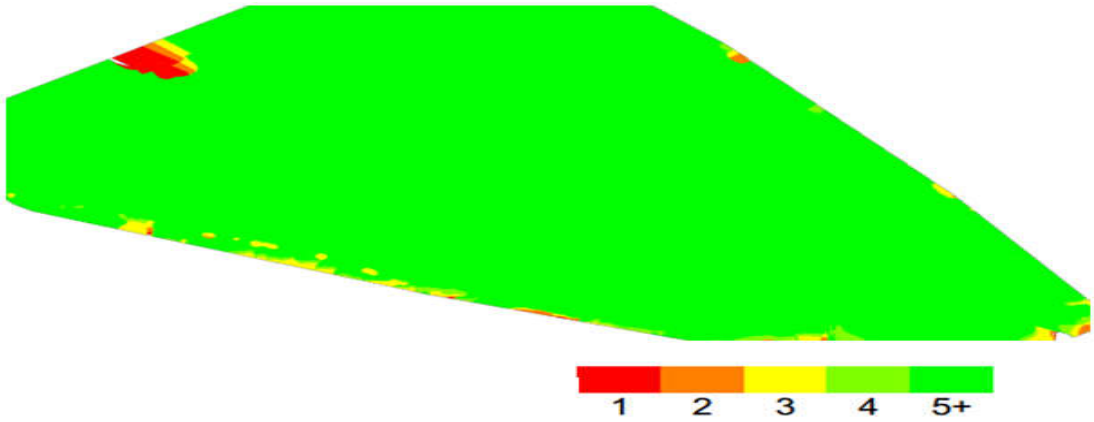

Figure 4.15 Number of Overlapping Images on Penarth cliff face surface.

4.1.5 Determine an Appropriate Time-Lapse for Surveying the Cliff with the Pole Using the Integrated Sensor Orientation (ISO)

In the ISO, the computation of the Bundle Block Adjustment BBA is through the use of the inbuilt GNSS sensors and the compact Micro-Electro-Mechanical Systems Inertial Measurement Unit (MEMS IMU) without GNSS controls and pre-defined tie points (Pepe et al, 2018 and Benassi et al, 2017). Although the ISO is straightforward to use, the cheap miniature sensors with inbuilt GPS are downgraded easily especially in very dynamic environments (Benassi et al, 2017). The accelerometer and gyros of the MEMS-IMU are also flexible and can easily drift during use due to their microstructure compartments.

The tropospheric signal delays characterized by pressure, temperature, and water vapour are relative to geographical elevation (Yu et al, 2018 and Zhu et al, 2017) with water vapour predominant in the coastal areas. The accuracies of close-range photogrammetric surveys will improve on favourable atmospheric conditions (Pepe et al, 2018) likely on lesser time durations.

Inexpensive GNSS sensors would be difficult to generate consistent and reliable dense point clouds due to inherent anomalies in the Scale Invariant Feature Transformations (SIFT) (Qu et al, 2018) which detects and extracts the local features in the corresponding digital images. It would be difficult then to minimize errors from transformation and misalignments which ideally are reduced by the GNSS controls and tie points as with the Integrated Sensor Orientation (ISO) and GNSS-supported Aerial Triangulation (GNSS-AT) in digital photogrammetry (Benassi et al, 2017).

To balance the systematic and random errors from the ionospheric and tropospheric delays, drifting, and downgrading of the inbuilt GPS, this research relies on the systematic field procedure(s) developed in the foregoing sections. The aim is to obtain the maximum number of images that would be calibrated for SIFT. The cliff surface was surveyed at different time-ranges to establish the level-of-tolerance of the inexpensive Samsung SM-G850F MEMS-IMU/inbuilt GNSS sensors on favourable atmospheric and illumination (shadow cast) conditions.

Table 4.3 Time Range to Determine the Level-of Tolerance of the Miniature Sensors

	Time Range (Hours:Mins: Seconds)	No. of images acquired	% of calibrated images	Using the developed systematic survey procedure	Point cloud Generated
a	00:30:03	86	100	yes	Single block mosaic
b	00:59:28	187	100	yes	Single block mosaic
c	01: 28:20	198	100	yes	Single block mosaic
d	02:16:31	490	98	80%	Multiple block mosaic
e	02:52:50	377	100	yes	Single block mosaic
f	03:05:36	517	99	yes	Single block mosaic

While surveys executed more quickly can still easily overcome systematic and random errors; good overlap, and a regular survey grid pattern can compensate for errors. The pattern for capturing images in **d** on table 4.3 was a horizontal survey grid with more images taken after the main survey to verify the effect of drifting. The dense point cloud from survey **d** on table 4.3 is downgraded into multiple block point cloud as shown in figure 4.16 below.

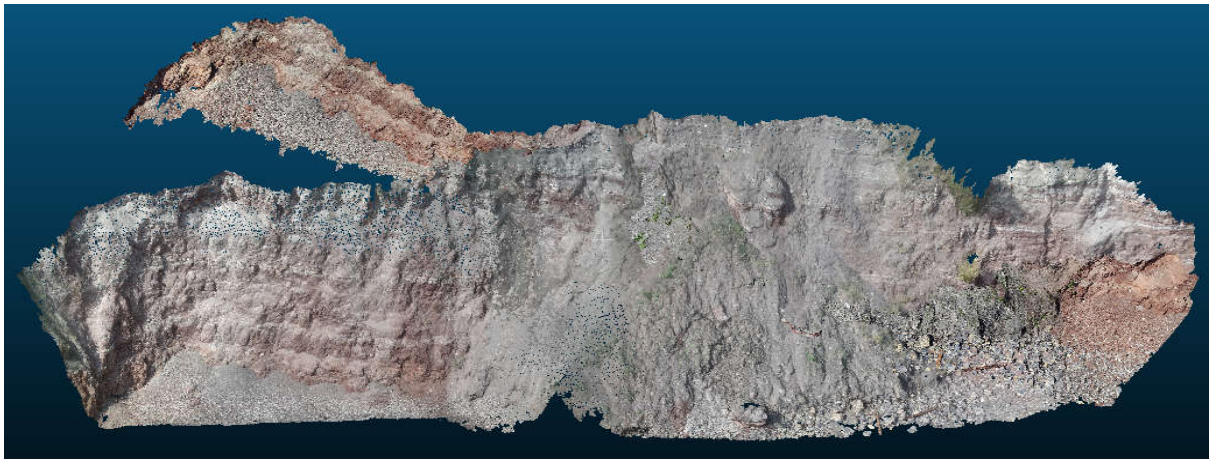

Figure 4.16 Multiple Block Point Cloud Showing the Effect of Drifting on the Inexpensive GNSS Sensors.

It will be difficult to generate accurate Orthomosaics and the other digital models from the multiple block point cloud. Aside from the multiple block point cloud; there is also the tendency not to capture every part of the cliff. Despite 80% compliance with the systematic procedure of capturing the images, the survey at **d** took 136 minutes. This shows the systematic survey procedure will reduce the time of capturing the digital images. Accurate digital outputs are unlikely derived from terrestrial photogrammetry executed in different atmospheric conditions (Wolf and Dewitt, 2000) even as the multiple block point cloud is likely generated from surveys without flight planning and camera orientation (Chiabrando et al, 2017).

Section B

4.2 Development of an Algorithm for Analysing Structural Change(s) on the Coastal Cliff Point Cloud

4.2.1 Aim:

This section of the chapter develops a straightforward, flexible, and generalized algorithm for detecting changes between two-point clouds. It precisely computes the volume change using the arrays of the change segment and determines the volume of change from the segmented change array. The new change detection algorithm is developed in python using the existing libraries in Open3d, Numpy, and Pandas.

Objectives:

1. Perform the Kd-tree nearest neighbor (KNN) search on pre-aligned points clouds for unfixed but balanced spatial streaming for every closest point in search relative to a search query for nearest neighbour matching.
2. Generate a change-array point cloud from the change segments for visualization of change segments and accurate determination of volume change.
3. Determine change analysis for specific segments on the point cloud on a predefined radius search on the change detection algorithm.
4. Generate the x, y, z coordinates of the change array on an excel spreadsheet.

4.2.2 Section Overview:

Existing algorithms for change detection on point clouds do not include an inclusive workflow to determine change segment(s) with precise volume computation for the change segment. There is therefore no existing functional spatial database for change detection in coastal cliff monitoring. Existing applications for the Nearest Neighbours algorithm in change detection do not integrate a loop for the sequential creation of change arrays. In this algorithm, a structured loop range can assign change arrays using distance and colour range variables with the KDTree concurrently as it searches for the nearest neighbour.

The Numpy array provides a short, simple and effective coding irrespective of the size of the point cloud (Johansson, 2019 and Zhou et al, 2018) while the Open3d library provides the implementation of the geometry manipulation including better rendering for point cloud visualization (Zhou et al, 2018). The Pandas data frame can provide a segmentation utility

with its data structure and manipulation capability (Hoyer and Hamman, 2017; Sandeep et al, 2017). The different Python libraries are compatible with data mining and manipulation (Sandeep et al, 2017).

This algorithm structures for intermittent visualization of outputs useful for change detection of several coastal components as well as for the coastal cliff. For better computational accuracy, the algorithm incorporates the output of the ICP transformation matrix into a KNN computational loop sequence.

4.3 Methodology Workflow:

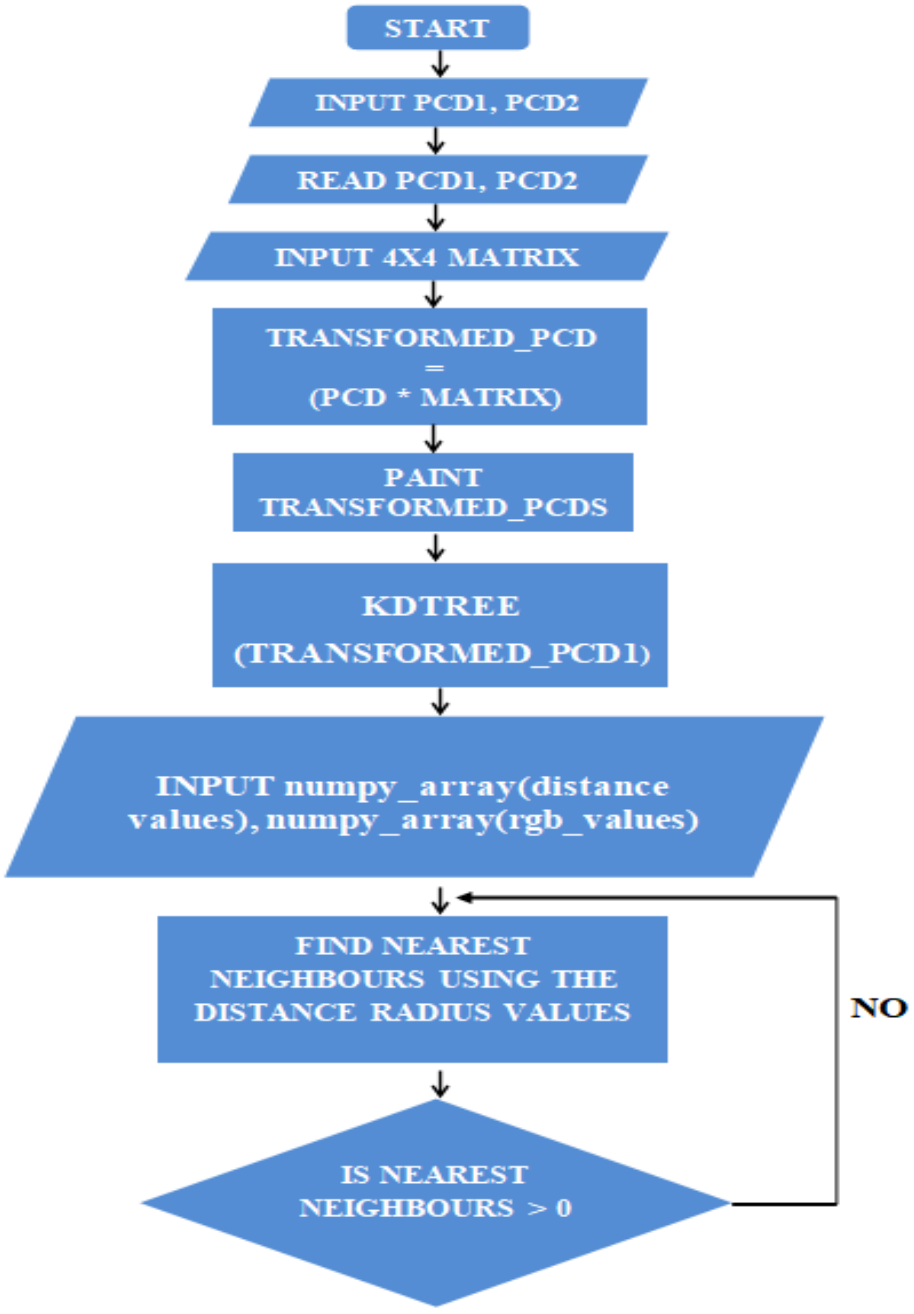

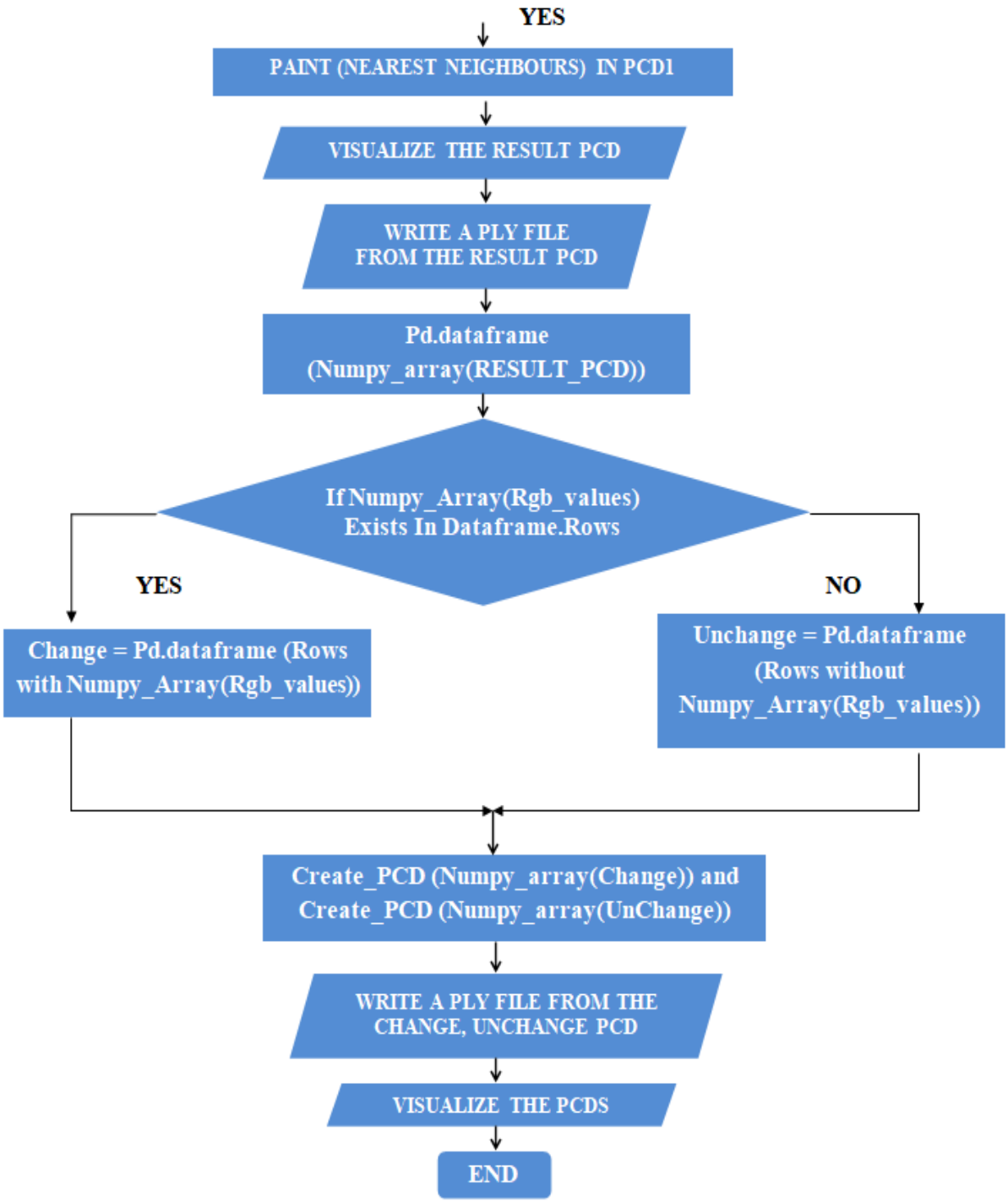

Figure 4.17 The New Point Cloud Change Detection Algorithm Workflow. This computational routine explains the importance of every step in developing the algorithm.

4.3.1 Open3d to Read Point Cloud:

Open3D supports point cloud data structures and reads data as pointcloud.points, pointcloud.normals, and pointcloud.colours (Zhou et al, 2018). The filename extension identifies the file types. Open3d supports the XYZ, PLY, PCD, XYZRGB, PTS, and XYZN file formats with Numpy compatibility (Open3d, 2020). In this algorithm, the function

03d.io.read_point_cloud() reads the point cloud data file, while the Numpy function np.asarray() converts the derived points from the point clouds into an array.

```
def read_point_cloud(pcd_file):

    return o3d.io.read_point_cloud(pcd_file)

pcd1 = read_point_cloud(pcd1_file)
pcd2 = read_point_cloud(pcd2_file)
```

4.3.2 The Loop Range Variable

The variable **loop_range** holds an array value for a defined loop range. This can be set to none for the default loop range.

```
loop_range = None
#loop_range = [10406, 20000]
```

4.3.3 Numpy Array Transformation of Point Cloud

a. The transformation parameters were generated by using the "align two clouds by picking (at least 4) equivalent point pairs" in CloudCompare (CloudCompare, 2020 and Panagiotidis et al, 2016). The point pairs picking tool in CloudCompare is more accurate than the ICP registration for aligning two-point clouds by picking at least four identical points on both point clouds (CloudCompare, 2020). The 4 x 4 transformation matrix parameters are generated from the aligned point clouds and are a combination of the rotational axis, the rotational angle, and the translational 3Dvector (CloudCompare, 2020 and Horn, 1987).

```
transform_matrix = [[0.828376293182, -0.084649063647, -
0.553739368916, 1.914794921875],
                    [0.140533283353, 0.988307297230, 0.059152640402, -0.511735439301],
                    [0.542257428169, -0.126819446683, 0.830586373806, 2.317070960999],
                    [0.000000000000, 0.000000000000, 0.000000000000, 1.000000000000]]
```

The variable **transform_matrix** holds a 4 x 4-transformation matrix as its value while the function **pcd.transform (transform_matrix)** transforms a point cloud using the matrix passed to it as a parameter. This is after the point cloud has been transformed, thereafter converted into a **Numpy** array. The total number of rows and columns in the transformed point clouds are stored in variables. The new point cloud with the number of rows of the point cloud is returned in the function **transforming_point_cloud().**

```
#function 2
def transforming_point_cloud(pcd):

    transformed_pcd = pcd.transform(transform_matrix)
    transformed_pcd_arr_rows, _ = np.asarray(transformed_pcd.points).shape

    return transformed_pcd, transformed_pcd_arr_rows

#usage

transformed_pcd1 = transforming_point_cloud(pcd1)
transformed_pcd2 = transforming_point_cloud(pcd2)
```

4.3.4 Paint_Uniform_Colour()

This function paints all the points in the transformed point clouds to specific colours using

```
#recoloring point cloud
transformed_pcd1[0].paint_uniform_color([0.5, 0.5, 0.5])
transformed_pcd2[0].paint_uniform_color([0, 0, 1])
```

4.3.5 Open3d Geometry KD TreeFLANN for Nearest Neighbour Search

The KD tree organises the point clouds in a range of assigned dimensional spatial scales. It uses the data structure that organises the point clouds as a tree-like data structure and the nearest neighbour of any desired point of interest is found by navigating down the tree to the region, which will likely have the most of the nearest neighbour for the desired point. The KdTreeFLANN is a generic type of 3D spatial locator using the KD Tree structure. KD Tree works by repeatedly finding the median of the random dimension and splitting the data class as shown below.

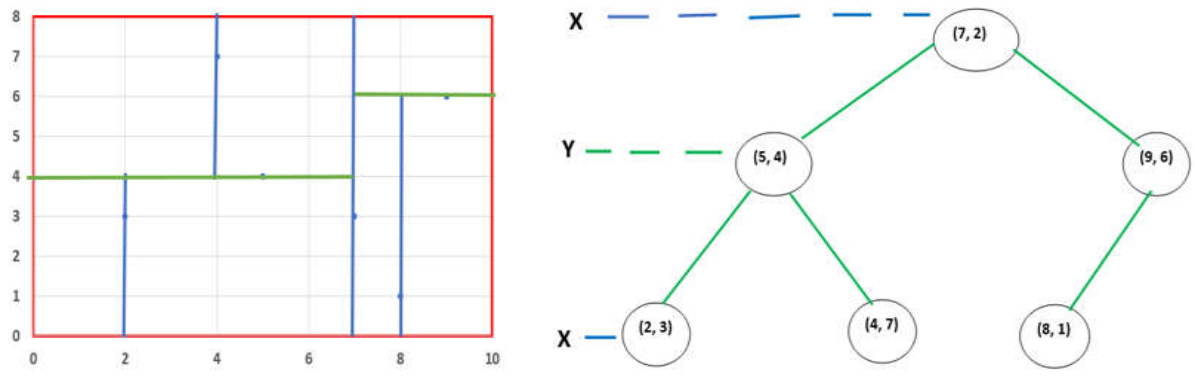

Figure 4.18 Example of a KD Tree Partitioning

If X points are assigned as X1, X2, X3, X4……, Xn in the X metric space, the quarrel, q ∈ X, that will locate the nearest point X to Y will be repeatedly partitioned to locate the Y as quickly as possible (Open3d, 2020) from the base point cloud. Open3d uses the Fast Library for Approximate Nearest Neighbours (FLANN) digital library for very fast determination of the nearest neighbour search of X to Y.

4.3.5.1 *pcd_tree = o3d.geometry.KDTreeFlann (transformed_pcd1)* builds a KDTree from

```
#building a kdtree flan from poin cloud 1
pcd_kdtree = o3d.geometry.KDTreeFlann(transformed_pcd1[0])
```

4.3.6 Initiate Variables used for the Change Detection Algorithm

a) count is the overall count for the loop performing the change detection.

b) **dist** holds a NumPy array of distance radius values.

c) **colordist** holds a NumPy array of RGB values to be allocated with the distance radius values respectively. Each distance radius has an allocated colour.

```
count = 0
dist = np.array([0.02, 0.03, 0.04, 0.05, 0.1, 0.2])
colordist = np.array([[1, 0, 0],[1, 0.2, 0],[1, 0.4, 0],[1, 0.6, 0],[1, 0.8, 0],[1, 1, 0.3]])
```

4.3.7 Loop_range is none

The condition ***if loop_range is None*** checks if the loop_range variable as earlier declared was set to ***None*** or an array value. ***Loop_range is none*** creates a new array ***loop_r*** with the value set to the number of rows in the **transformed point cloud2**. Otherwise, if the ***loop_range*** is set to an array value and not ***None,*** a new array is created also but set to the ***loop_range*** value instead.

```
if loop_range is None:
    loop_r = [0, transformed_pcd2[1]]
else:
    loop_r = loop_range
```

This loop iterates with a range based on the value of the new array **loop_r** generated from the conditional statement above.

4.3.8 *for i in range*

The variable ***i*** increase by 1 for each time the loop iterates

```
for i in range(loop_r[0], loop_r[1]):
```

4.3.9 The Function searc_radius_vector3d performs a Search on the KDTree Built from the Transformed *pcd_1*

a. The ***pcd_kdtree.search_radius_vector_3d*** queries by using the indices of neighbours in a specified radius. This algorithm functions to disintegrate the points queried into a new batch of the array.

b. transformed_pcd2[0].points [i] denotes the commence point from the transformed point cloud two on loop iterates point after point. ***For i in range (0, nth….nth+ 1):*** and checks for the nearest neighbour while comparing each point to the entire KDTree built from the point cloud one using the specified radius.

c. ***np.asarray (transformed_pcd1.colors)[idx[1:], :] = [0.5, 0.5, 0.5]*** paints any nearest neighbour point cloud found in the base transformed point cloud one.

d. ***matched_points = np.asarray (transformed_pcd1[0].points)[idm[1:], :]***

This stores the nearest neighbours points as found in the **KDTree** and in the variable matched_points.

```
for v in range(0, len(dist)):
        #print(v)
        [m, idm, n] = pcd_kdtree.search_radius_vector_3d(transformed_pcd2[0].points[i], dist[v
])
        if m == 0:
            transformed_pcd2[0].points[i]
            continue
        else:
            np.asarray(transformed_pcd1[0].colors)[idm[1:], :] = colordist[v]
            matched_points = np.asarray(transformed_pcd1[0].points)[idm[1:], :]
            break
```

4.3.10 o3d.visualization.draw_geometries()

The ***o3d.visualization.draw_geometries()*** function in Open3d draws the geometries by using PointCloud.points geometries as inputs (Zhou et al, 2018) and provides an effective visualization function that will determine the accuracy of the aligned colour coded point

clouds (Open3d, 2020). The result from the loop is visualized and a new pcd file is created using the open3d function **o3d.io.write_point_cloud()**

```
o3d.visualization.draw_geometries([transformed_pcd1[0]])

# #CREATING A NEW POINT CLOUD DATA FILE USING THE CHANGE/DIFFERENCE ARRAY
output_file_name = pcd1_file.split(".")[0] + '_' + pcd2_file.split(".")[0] + 'output.ply'
o3d.io.write_point_cloud(output_file_name, transformed_pcd1[0])
```

4.3.11 Read_point_cloud(output_file_name)

The derived point cloud data read off while the colour from the point cloud converted to NumPy arrays.

```
pcd1 = read_point_cloud(output_file_name)

points = np.asarray(pcd1.points)
colors = np.asarray(pcd1.colors)
```

4.3.12 Pandas Data Frame

Pandas data frame is created from the numpy arrays and then stored in a new variable called **dataframe.**

```
d = {'x': points[:,0], 'y': points[:,1], 'z': points[:,2], 'r': colors[:,0], 'g': colors[:,1], 'b': colors[:,2]
}

dataframe = pd.DataFrame(data = d)
```

4.3.13 Data Frame to Create Similarities and Change Arrays

The R column in the data frame is queried to check where values are greater than 1. All rows found with R column value >1 create a new data frame. This new data frame is then stored in a variable ***change*** which are the points for the change array. Similarly, all rows that do not have their R column value > 1 are stored in another separate data frame with a variable name ***sim*** which are the points for the unchanged array.

```
change = dataframe[dataframe.r < 1]

sim = dataframe[dataframe.r == 1]
```

4.3.14 Convert the Data Frame to a Numpy Arrays

The Pandas function **df.to_numpy()** converts the generated data frames to a Numpy array.

```
#funtion to convert from pandas dataframe to numpy array
def pandas_to_numpy(df):
    points_array = df[['x', 'y', 'z']].to_numpy()
    rgb_array = df[['r', 'g', 'b']].to_numpy()

    return points_array, rgb_array

#usage

change_array = pandas_to_numpy(change)
sim_array = pandas_to_numpy(sim)
```

4.3.15 Creates New Point Cloud

The Numpy arrays **change_array, sim_array** creates new point clouds using the open3d function **o3d.geometry.pointcloud()** and retains the metadata field of the point clouds (Johansson, 2019).

```
def creating_point_cloud(array_data):

    pcd = o3d.geometry.PointCloud()
    pcd.points = o3d.utility.Vector3dVector(array_data[0])
    pcd.colors = o3d.utility.Vector3dVector(array_data[1])

    return pcd

#usage

change_pcd = creating_point_cloud(change_array)
sim_pcd = creating_point_cloud(sim_array)
```

4.3.16 Save Point Clouds to .ply Files

```
simcloud_file_name = pcd1_file.split(".")[0] + '_' + pcd2_file.split(".")[0] + 'sim.ply'
o3d.io.write_point_cloud(simcloud_file_name, sim_pcd)

changecloud_file_name = pcd1_file.split(".")[0] + '_' + pcd2_file.split(".")[0] + 'ch.ply'
o3d.io.write_point_cloud(changecloud_file_name, change_pcd)
```

4.3.17 Visualize Both Clouds

```
o3d.visualization.draw_geometries([sim_pcd])
o3d.visualization.draw_geometries([change_pcd])
o3d.visualization.draw_geometries([change_pcd, sim_pcd])
```

Open3D displays the point clouds for visualization. All points' clouds created (change array, unchanged array and both the changed and unchanged area together are saved automatically as .ply files. Figure 4.19 shows an example of the time series changes along the cliff face at Pearth between various survey dates.

The algorithm cuts out and separates the point clouds of the change areas from the areas that have no change for the correct determination of the volume of both areas (change and no change).

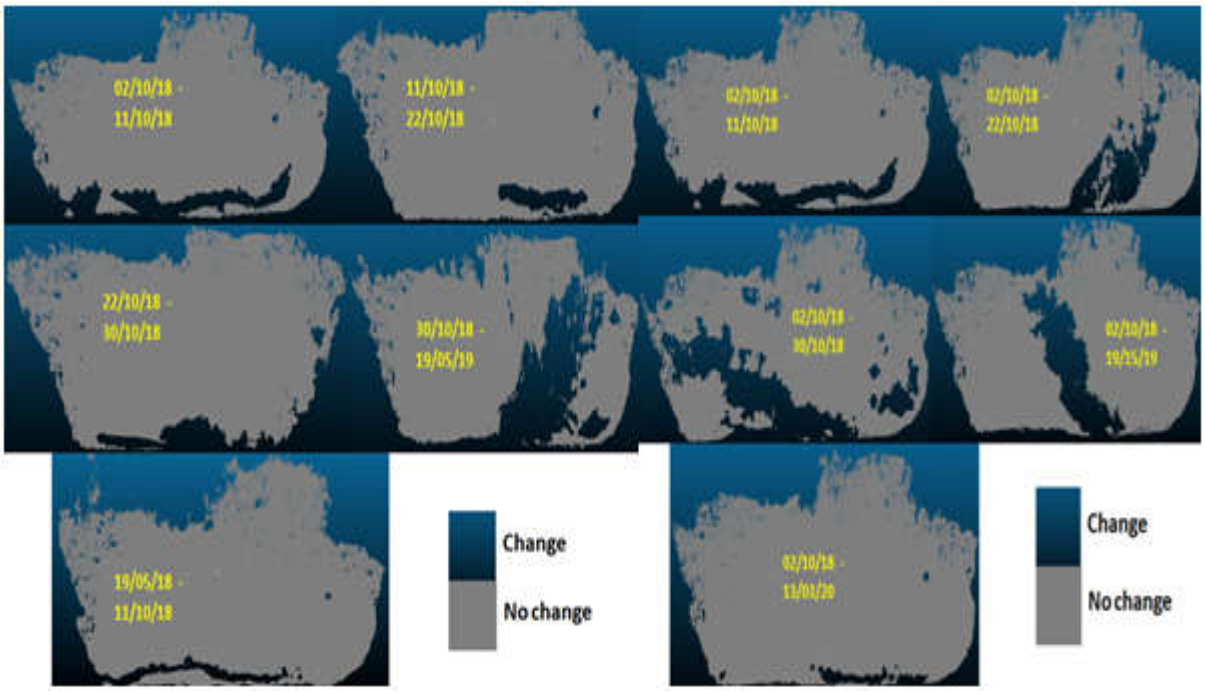

Figure 4.19 Shows the Areas of Major Change by Applying the New Algorithm to Penarth Cliff Segment between every two surveys.

4.4 Volume Computation

This section determines the volume from the change array ***change.ply*** point clouds.

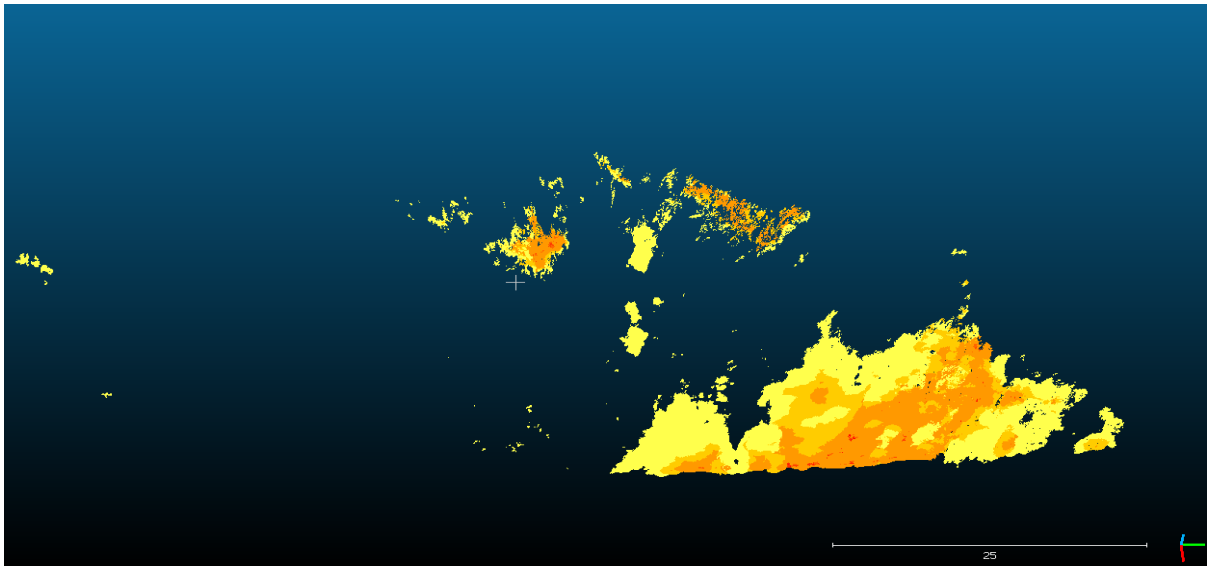

Figure 4.20 An Example of a Change Array obtained from the Change Detection from 30/10/18 to 17/05/19 – Change has occurred at the different highlighted areas between the two compared survey point clouds.

4.4.1 Compute Volume in CloudCompare

Small Segments of the change arrays scattered at the different parts of the cliff with noise might result in errors in the computation of volume. For accurate volume computation, the point cloud is reconstructed to a Poisson surface reconstruction using a plugin (CloudCompare, 2020) in the CloudCompare open-source software. The Poisson surface reconstruction (PSR) generates a triangular mesh from the 3D oriented point cloud arrays, which are in millions of points into a finely coherent registered mesh ***figure 4.21***.

In CloudCompare, the normals are first created using the edit > normals > compute > plane before applying the PSR plugin. The Plane local surface model is preferred as it is robust to noise. The volume of the mesh is then derived from the edit > mesh > and measure volume. The volume computed is therefore accurate as all the points are within the closed mesh.

The PSR scans, aligns, converge the outlines, smooths, estimates and reconstructs the input data into a surface triangular mesh (Estellers et al, 2015 and Li et al, 2010). It is also able to close gaps inherent in the point clouds (Estellers et al, 2015). The implemented PSR by Kazhdan et al (2006) has been improved to overcome over-smoothing which leads to the

omission of vital points by introducing positional constraints (Kazhdan and Hoppe, 2013) and an envelope constraint (Kazhdan et al, 2020). Another advantage of using the PSR plugin in CloudCompare is that all the points inside the polygon border are considered in the computation of the mesh volume as shown in the figure 4.22.

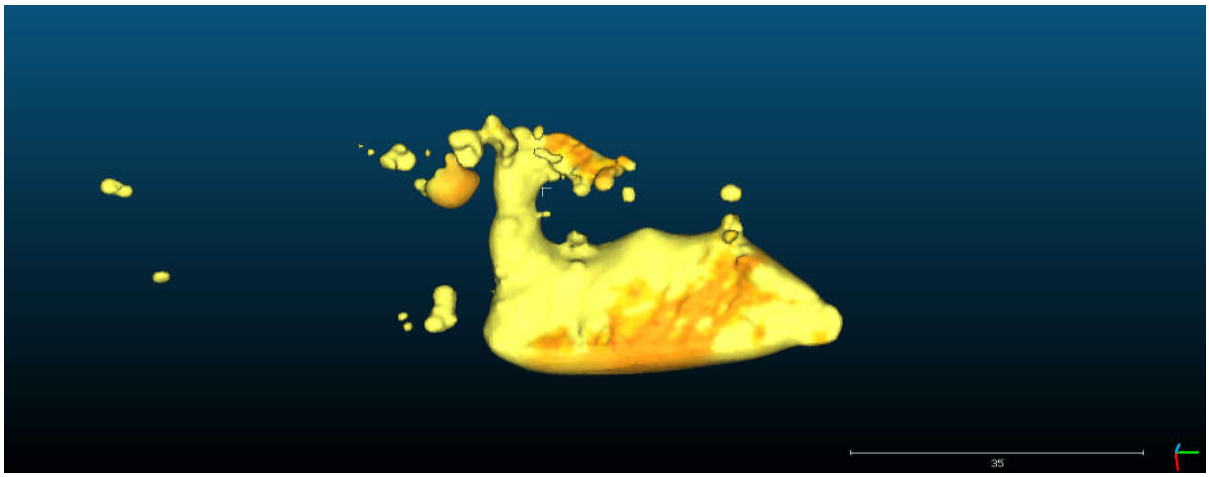

Figure 4.21 The Change Array Point Cloud from 30/10/18 to 17/05/19 now Converted into a Triangular Mesh in CloudCompare –

All the points are locally fitted (Kazhdan et al, 2020) and are all defined within the triangular mesh without noise or undefined outlines. This ensures the accurate computation of volume especially for the cliff surface that has uneven and unpredictable tendencies for cliff erosion and disintegrating.

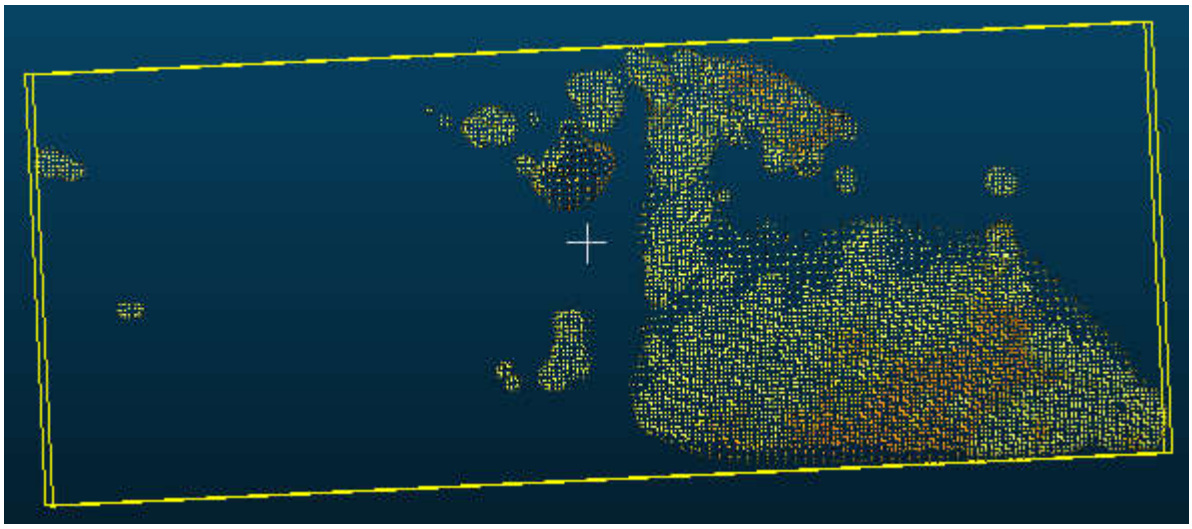

Figure 4.22 All the Points with the Polygon Border have been summed in Determining the Volume.

4.5 Chapter Summary and Conclusion

This chapter has shown that it is possible to determine the:

1. Appropriate Vertical Camera Angle to the Cliff;
2. The most favourable survey distance to the cliff surface when carrying out a close-range pole survey;
3. A practicable forward and side overlap between images;
4. The best time Interval for executing a pole survey using the Integrated Sensor Orientation (ISO) from very cheap single frequency inbuilt GNSS sensors;
5. Using the pole/mast with a cheap camera to accurately survey the cliff surface

The chapter demonstrates a new pole digital photogrammetry methodology for coastal cliff monitoring. **Section A** utilizes the very basic principles of photogrammetry in developing a systematic image capture plan and camera orientation to be able to generate precise and accurate 3D reconstructed point clouds by terrestrial pole survey for coastal cliff monitoring. The methodology developed is simple, straightforward with a regular grid network for complete stereoscopic coverage. The verification of results obtained has been by third-party software and an alternative remote sensing survey.

This methodology generates precise geometrical related point clouds with or most importantly, without precise GNSS controls. For use in the photogrammetry community, the most appropriate vertical camera inclination and distance to the cliff surface have been practically demonstrated and theoretically documented. Depending on the area been mapped, surveys can be from 10 minutes to 2 hours. It is possible to attach the different digital cameras on the pole with the higher resolution cameras resulting in higher spectral accuracies. The limitation is to perform a survey in an almost equal atmospheric condition to avoid the drifting of the MEMS-IMU during the survey.

To illustrate the effectiveness and accurateness of this methodology, a cheap 2.1 megapixel camera on a mobile phone was used to perform all the surveys. Any camera can be used which can be operated from the ground remotely, or on a time series lapse to capture images at the different heights. Most mobile phones have this capability and certainly capture photographs at much higher resolutions than 2.1 megapixels. In practice, these higher resolutions will generate much richer 3D point clouds and therefore superior digital surface models, orthomosaics and volumetric analysis. This is illustrated below in Figure 4.23 to 4.25

for a very small subset of the Penarth cliff captured at the same time as one of the 2.1MP surveys, but instead using a higher resolution Sony Cybershot 18MP camera (originally £250, but now circa £170). As of 2021, alternative Sony digital cameras at 20MP are available for under £100; alternative digital cameras in the 18MP to 21MP range are available for under £40; very low-cost cameras in the 12MP to 16MP range are available for under £20; while smartphones with 48MP cameras are available for £200 (or £300 in ruggedised or more shockproof formats). Cost is no longer a constraining factor in undertaking a close-range digital photogrammetric survey.

Aside from the cost, this new pole photogrammetry for cliff monitoring offers flexibility for the survey of sections or the entire stretch of the different cliff morphologies from close range. Figures 4.23 to 4. 26 explain a typical high-resolution pole survey for precise differential surveys on the coastal cliff. The change array in the new change detection algorithm keeps track of the change motion/deflection pattern present on the cliff surface. This innovation will help to determine the wave action and other weathering patterns of the cliff profile.

Figure 4.23 Pole Surface 3D Model – BEFORE. Penarth 3D Point Cloud generated from a Sony Cybershot 18 MP Camera. Compare with the image below …

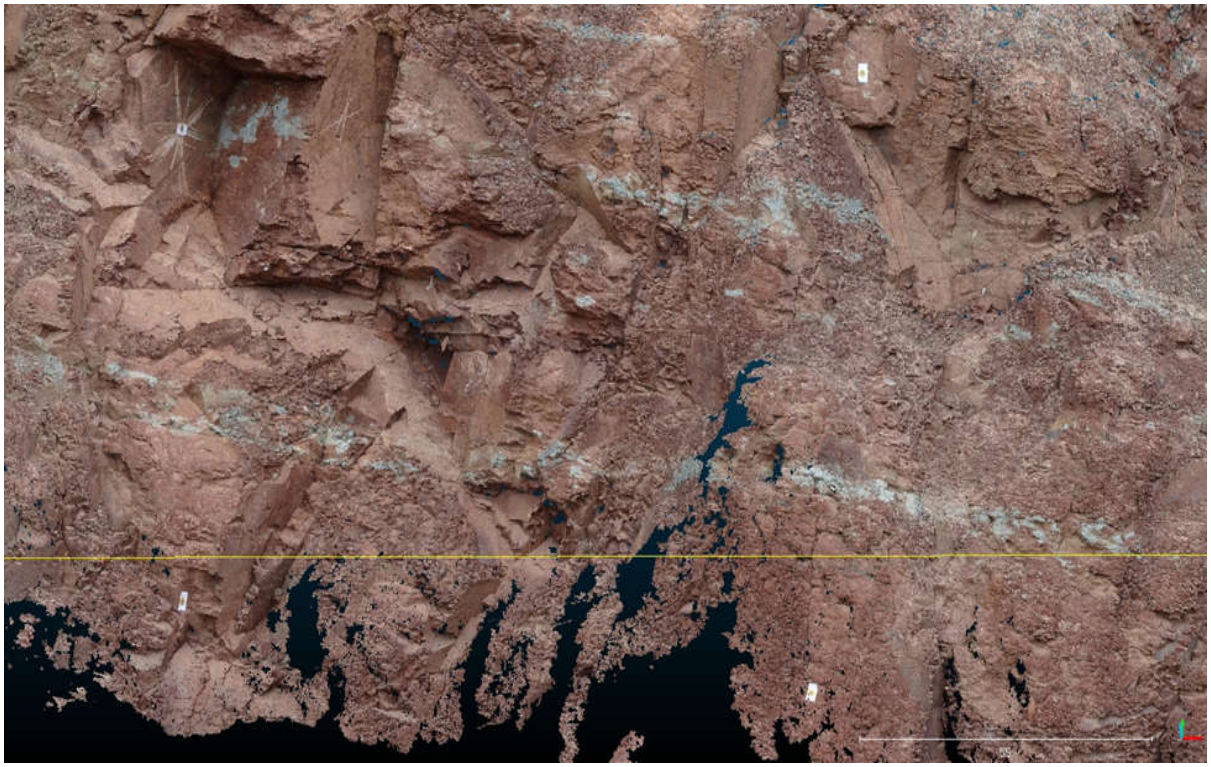

Figure 4.24 Pole Surface 3D Model – AFTER. Penarth 3D Point Cloud generated after a small cliff fall. (Spot the Difference? Or use Volumetric Differences of Figure 4.25 to inspect the Before & After areas of change).

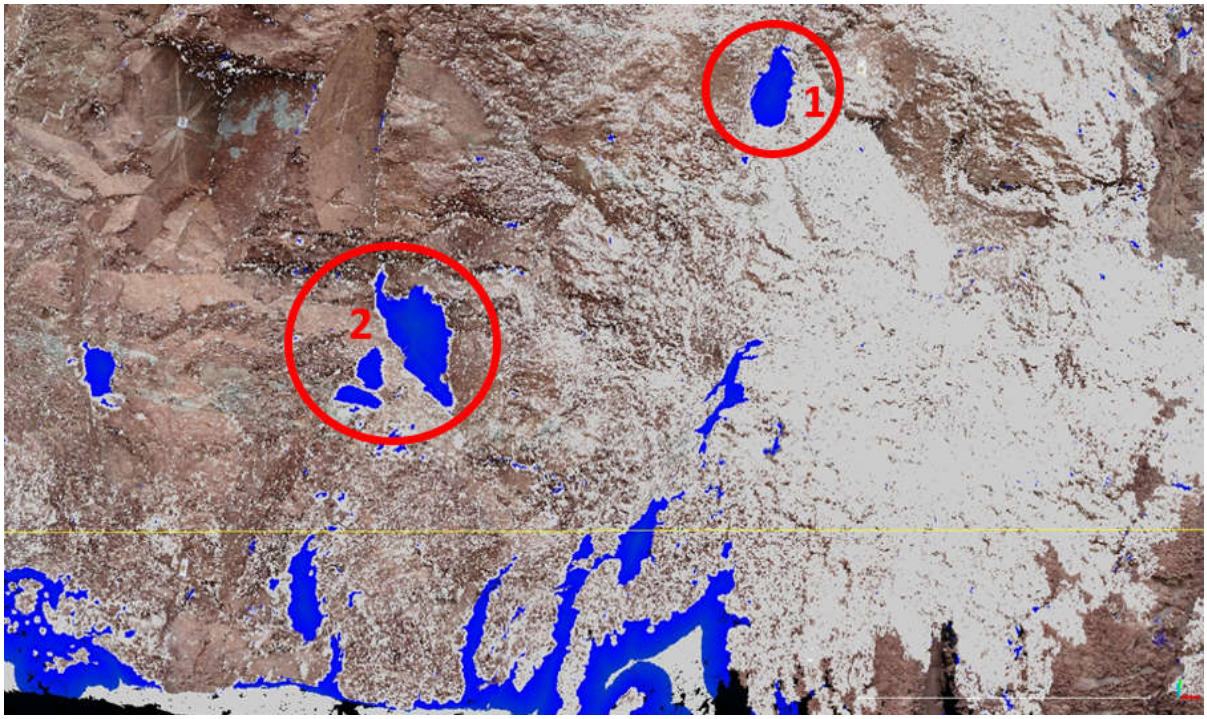

Figure 4.25 Pole Surface 3D Model – VOLUMETRIC DIFFERENCE between surveys of Figure 4.23 and 4,24. The blue areas indicate the areas of change. Note areas 1 and 2 in Figure 4.23 and 4.24 above, and in close-up detail in Figure 4.26 below. Areas in grey are within a 1mm difference level. The areas in blue in the lower part of the Figure are not an indication of volumetric change, but the lack of data (NO Data transparent values at the bottom of Figure 4.24). In a full survey, the complete cliff would have been captured with sufficient overlap to minimise the No Data coverage.

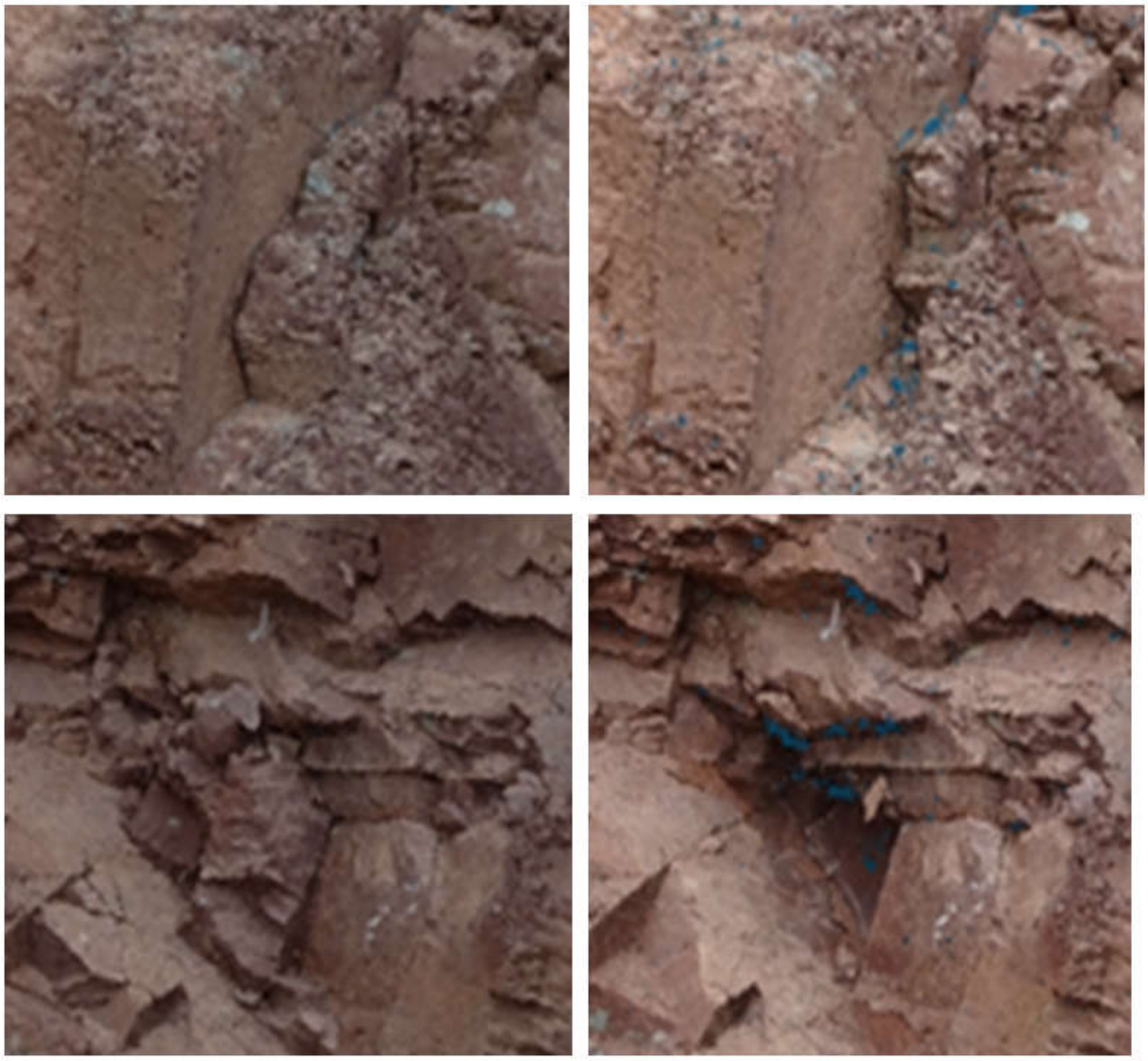

Figure 4.26 Pole Surface 3D Point Clouds BEFORE & AFTER for Regions 1 and 2 as highlighted in Figure 4.25 above. Small chunks of the cliff face have fallen away and volumetrically calculated using the approach presented in this chapter. It should be noted that these differences are relatively small (i.e. a few cubic cms) as the pixel resolution (GSD) is approximately 3mm.

Further analysis and results on the cliff change detection are presented in Chapter 5. Surveys performed at close range (and/or high resolution) can detect hidden sections/cracks on the cliff as in Figure 4.25 above, but care must be taken not to change the viewing angles of the digital camera during use.

Surveys are not restricted in the same way that drone surveys have to be undertaken,, but care (risk assessments and Health & Safety guidelines, e.g. hard hat, protective boots, etc) must be

taken when working close to an eroding cliff face. The lightweight pole that is used in these surveys only requires a single operator. At full extension, care must also be taken to ensure the stability of the camera and pole, particularly in windy or gusty conditions. Too much displacement may result in poorer overlap regions and hence a sparser point cloud.

This survey technique improves on existing close-range digital photogrammetry and can be replicated in developing countries in the monitoring of cliffs. Field data generated over time from the regular surveys can be modelled into a time series monitoring framework as discussed in the next chapter.

Section B develops algorithms for determining the change detection and extracting the change array of the change segments for visualization and precise volume computation. The change detection algorithm can be run in the open cmd python folder or by downloading the open-source pyzo or any free python package. This algorithm is used to detect changes on all the pole surveys in Chapter five. This is an entry-level that is free to use.

The volume computation is by applying the PSR algorithm inside the CloudCompare software. Unlike the volume computation by DSM, the change arrays that determine the volume are the actual change at the different parts of the cliff. The open-source CloudCompare runs on Windows, MacOS, and Linux. More importantly, change detection or relative change and volumetric differences between surveys is suitable for identifying areas of concern on the cliff face. An absolute referencing system (e.g. using precise and accurate Ground Control Points or GCPs) is ideal, but the margin of error in using even real-time kinematic GPS GCPs still requires an approach which ensures that differences in cliff surfaces are actual differences are not due to the survey margin of error.

Chapter 5

5.0 Evaluation of Results of Low-Cost Digital Photogrammetry for Coastal Cliff Monitoring

Chapter four presented a low-cost digital photogrammetry technique for regular coastal cliff monitoring. This chapter will evaluate the outputs from the pole surveys for scientific applications such as coastal cliff monitoring. It answers the question of the viability of close-range digital photogrammetry in coastal cliff monitoring.

Also presented in chapter four is an algorithm that can detect changes on the coastal cliff point cloud. How effective is this algorithm? What are the scientific attributes in terms of being able to model the coastal cliff change? This chapter provides scientific evidence to the need for the new point cloud algorithm. It, therefore, validates this contribution to knowledge.

5.0.1 Aim

This chapter discusses the geometric accuracies of the pole photogrammetry and the new change detection algorithm for cliff surface deformation surveys by evaluating the data of the periodic surveys and the change detection algorithm

5.0.2 Objectives

1. Evaluate the geometric precision and accuracy of the pole survey for cliff surface deformation study. This will determine if the pole photogrammetry is accurate and precise enough for scientific evaluations.

2. Determine the Periodic Changes on the Coastal Cliff. Scientific evaluations will determine how effective are the pole photogrammetry and the new point cloud change detection algorithms can periodically evaluate the changes on the coastal cliff.

3. Evaluate the change array and determine the periodic volume change. The exact quantity of eroded materials will be computed at every segment on the cliff surface. This quantitative data is further modelled statistically as in ‘4’ below.

4. Develop a new cliff monitoring statistical prediction routine using the mean forecast model. This quantitative forecasting model is satisfied by the availability of numerical information on the cliff change pattern and the availability of the physical and chemical constraining components present on the cliff.

5.1 Evaluating the Geometric Precisions of the Pole Survey for Cliff Surface Deformation Studies

The different point clouds generated should be geometrically precise for evaluative purposes (Kromer et al, 2015). Among other conditions, the accuracies of photogrammetric "range measurements" are also the functions on the consistencies of the point cloud scene geometry, orientation, and reflectivity (Weinmann and Jutzi, 2015). This chapter uses the interior and exterior orientation reconstruction consistencies determined by alternative photogrammetric measurement techniques and software for further evaluation. Comparisons were on four different point clouds obtained from weekly surveys to determine the consistencies and reliability of the new pole mapping field sequence.

To overcome possible errors from the routine computation by the KDtree (Otair, 2003), the subtraction between two different survey point clouds is also in two phases. This chapter also uses the change arrays generated by the new change detection algorithm to develop a new and simple prediction model called the Change Array Prediction Model 'CAPM' for monitoring the cliff fall and possible collapse. CAPM is an innovation that gives empirical and pictorial evidence of the frequencies of the changes in arrays of millimetres in exact coordinates and helps determine the critical sections on the cliff.

The coastal zone management strategies should include established physical evidence for risk assessment (Philips et al 2018).

Figure 5.1 is the Georectified dense point clouds from four different weekly surveys of the section of the Penarth cliff monitored. These four weekly surveys will be used to analyse the geometric accuracy of the point clouds. The aim is to determine how accurate and reliable the new pole methodology is.

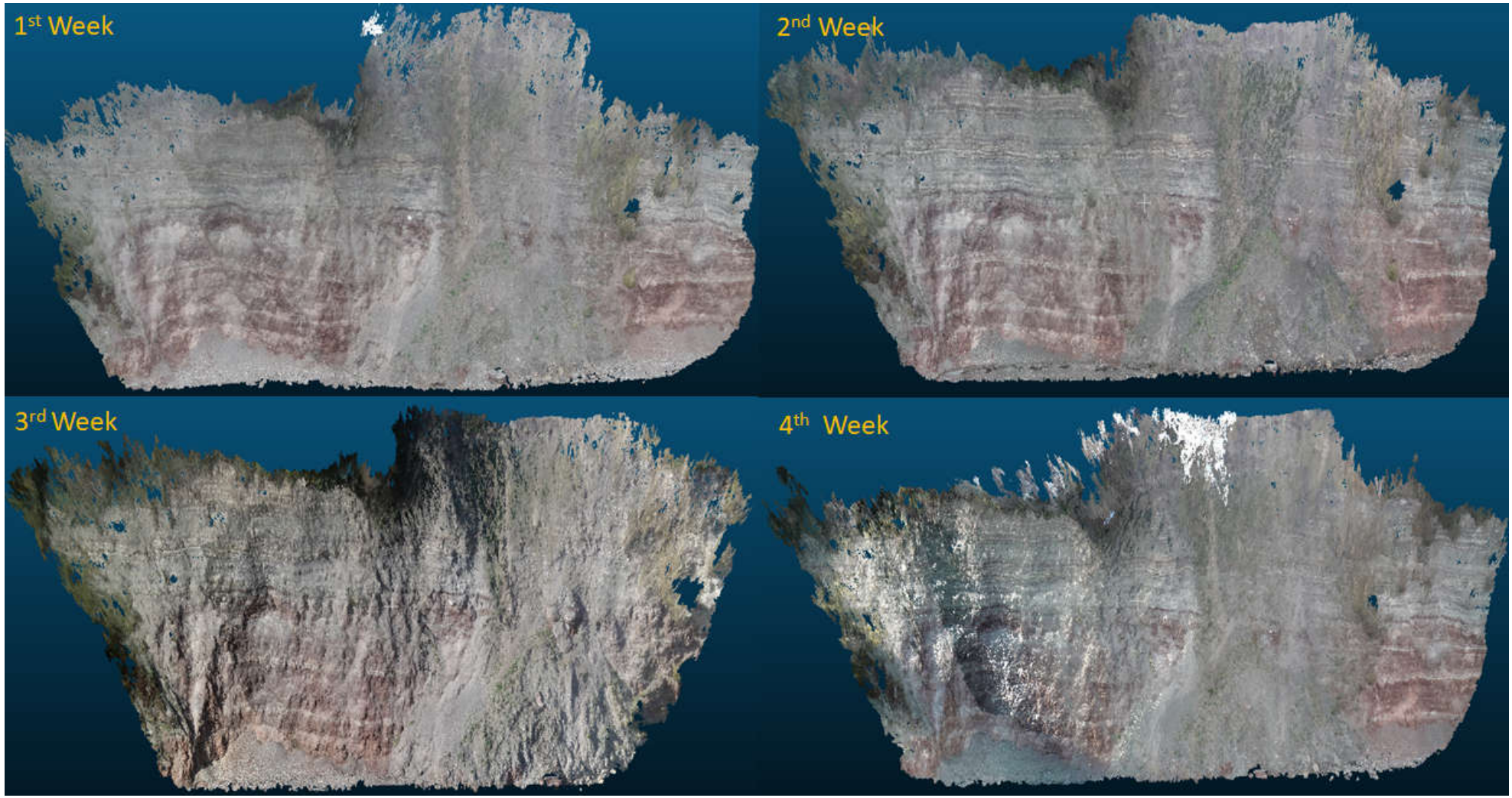

Figure 5.1 Dense Point Clouds from four Weekly Surveys of Penarth Cliff - These point clouds were aligned in CloudCompare and the coordinates of five control points visible in all four-point clouds were compared as shown in the table and figure below.

Table 5.1 Procedure for the four Weekly Surveys - This gives further details for the four-weekly surveys.

	1st Survey	2nd Survey	3rd Survey	4th Survey
Date of survey	02-10-18	11-10-18	22-10-18	30-10-18
N0. of images	409	461	377	496
Area covered	0.0033km^2	0.0029km^2	0.0018km^2	0.0035km^2
Average density (m^3)	12646	21118.3	25141.3	14089.7

The number of images and area covered in table 5.1 above explains the consistency of the surveys. The average density determines the reliability of the processing photogrammetric software relative to the number of images.

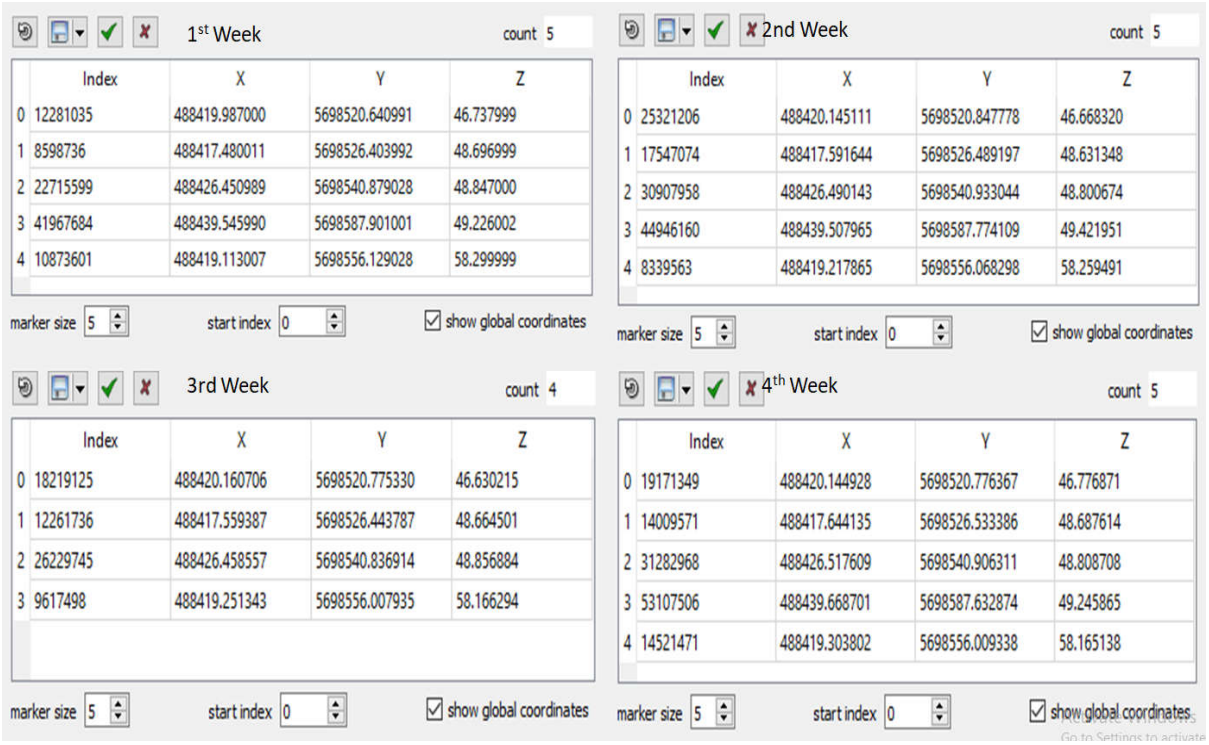

Figure 5.2 Geographical Coordinates of all four Weekly Surveys in CloudCompare

With reference to figure 5.1, all four-point clouds are georectified. Coordinate system could be local or national depending on the availability of GNSS equipment. In both instances, figure 5.2 shows the reliability of the methodology. For surveys done within a period, the control points can therefore be virtual

Table 5.2 Accuracies of all four Weekly Surveys

	Wk 1 –week 2		Wk 1 –week 3		Wk 1 –week 4	
	ΔN	**ΔE**	**ΔN**	**ΔE**	**ΔN**	**ΔE**
Point1	-0.158111	-0.206787	-0.173706	-0.134339	-0.157928	-0.135376
Point 2	-0.111633	-0.085205	-0.079376	-0.039795	-0.164124	-0.129394
Point 3	-0.039154	-0.054016	-0.007568	0.042114	-0.06662	-0.027283
Point 4	0,038025	0.126892	-0.138336	0.121093	-0.122711	0.208127
Point 5	-0.104858	0.06073			-0.190795	0.11969

The standard deviation for "alignment and surface deviation" (Westoby et al, 2018) at every point on each point cloud is ± 0.05m in the Northing and ± 0.12m on the Easting's for the self-calibrated digital camera and without the use of GNSS control points. This shows that each of the point cloud models geometrically fits into the other for a second-order cliff monitoring deformation study (Westoby et al, 2018 and Ruzic et al, 2015).

5.1.1 Verifying the Correctness of the CloudCompare Global Coordinates

To verify the correctness of the CloudCompare coordinates, the DSM of one of the PSPC was imported into ArcMap and the coordinates of the control points in CloudCompare as in Figure 5.2 are found to be the same as in ArcMap. It is imperative to determine if the global shifts and scaling by the CloudCompare does affect the geodetic precision of the point clouds.

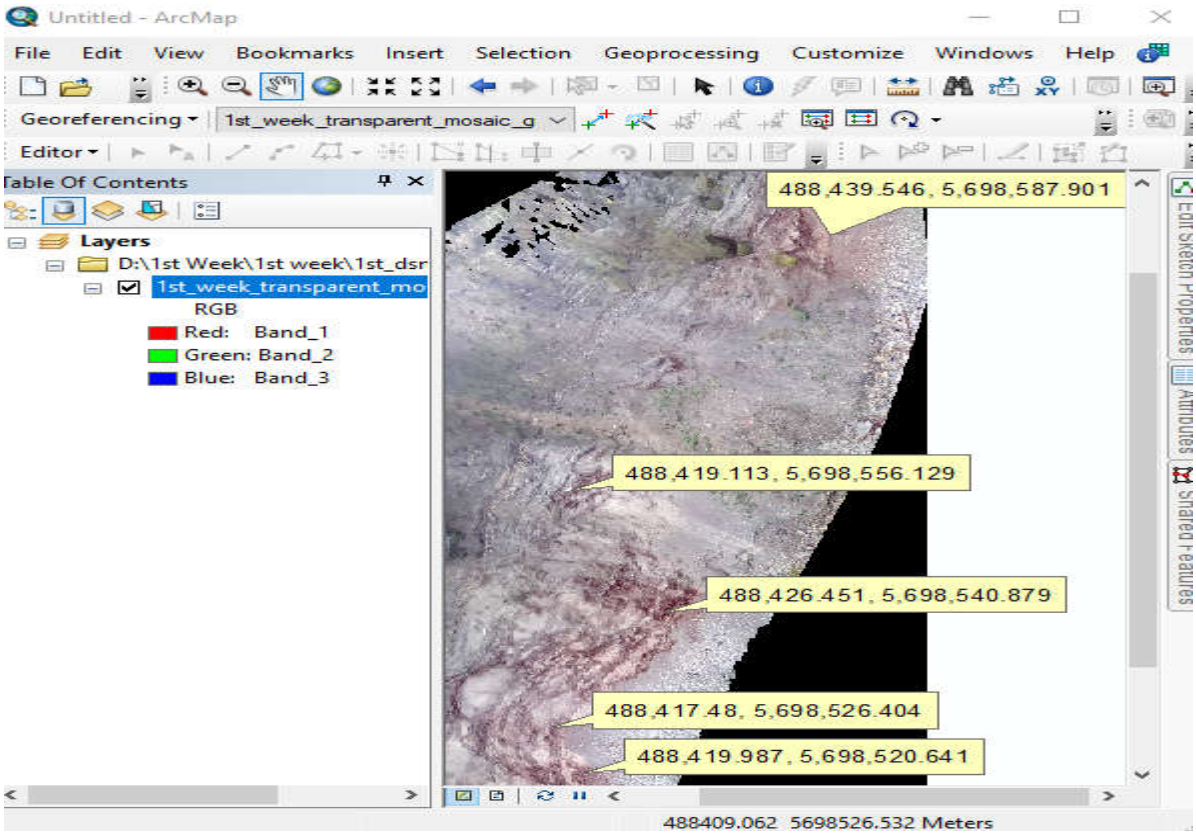

Figure 5.3 Verification of the CloudCompare Global Coordinates in ArcMap – Since the coordinates of the DSM in ArcMap are the same as the global coordinates of the points in the Open source CloudCompare, it, therefore, implies that the CloudCompare retains the original coordinates of the point clouds.

5.1.2 The Geometric and Absolute Accuracies and of the Pole Survey Point Clouds

The geometric accuracy defines the comparative evaluation with datasets obtained from other reliable photogrammetric techniques while the absolute accuracy is the difference of the x, y, and z coordinates of every point on the point cloud to their true geographical position on the ground (Harwin and Lucieer, 2012). The 3D reconstruction process in the bundle adjustment may distort the original shape of the cliff surface alignment.

The TLS and the Pole survey were both used to survey the same stretch of the cliff surface on the 13th of March 2020. This is to be able to determine the global correctness of the digital image EXIF and structure from motion computation for bundle adjustment that optimizes the 3D location between the tie-points and the camera internal parameters (Turner et al, 2012).

The TLS survey used the Topcon Laser scanner GLS-2000M series (figure 5.4 below). This TLS uses the 8.9-degree telephoto camera to scan the cliff surface and obtain images at

standard speed. This function provided complete stereoscopic coverage of the cliff surface at pre-set intervals of 10m scans at 6.3 mm resolution. Two different prism scan locations provided the precise and accurate modelling of the cliff section monitored. The fixed pole at (window scanning) enhances accuracies although it takes longer to scan but reduces the registration of the point cloud in the Topcon ScanMaster software. The height of the pole for this survey was 2 m and the prisms are 125 mm. Georeferencing was by the GEOMAX Zenith 35 series on Real-Time Kinematic (RTK) mode.

Figure 5.4 Topcon Laser Scanner GLS-2000M Series at Penarth on 13th March, 2020.

5.1.3 Control Points for Georeferencing the Pole Survey

Four markers at the bottom of the cliff with other visible points on both surveys at the middle of the inaccessible cliff top were used as manual tie-points for geolocating the pole survey in Pix4D on OSGB 1936 coordinate system as shown in Fig.5.5. Some visible points appearing on multiple surveys could be virtual controls control for further change detection and research. An example of the importance of virtual control and the uniqueness of this research methodology is figure 5.14.

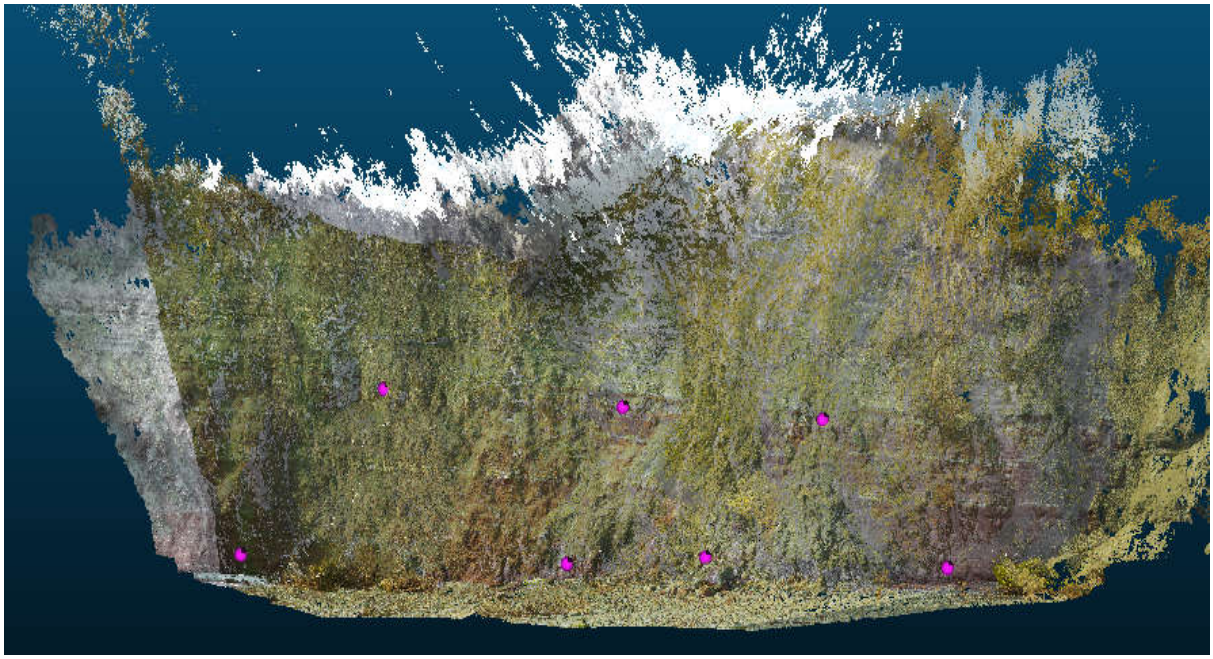

Figure 5.5 Control Points for Geolocating the Pole Survey

Figure 5.5 above superimpose the TLSPC and the PSPC. The purple dots are the control points identified on the cliff during both surveys. Figures 5.6 and 5.7 below are the individual point clouds of the TLS and the pole survey. Both figures further show the survey was at the same time.

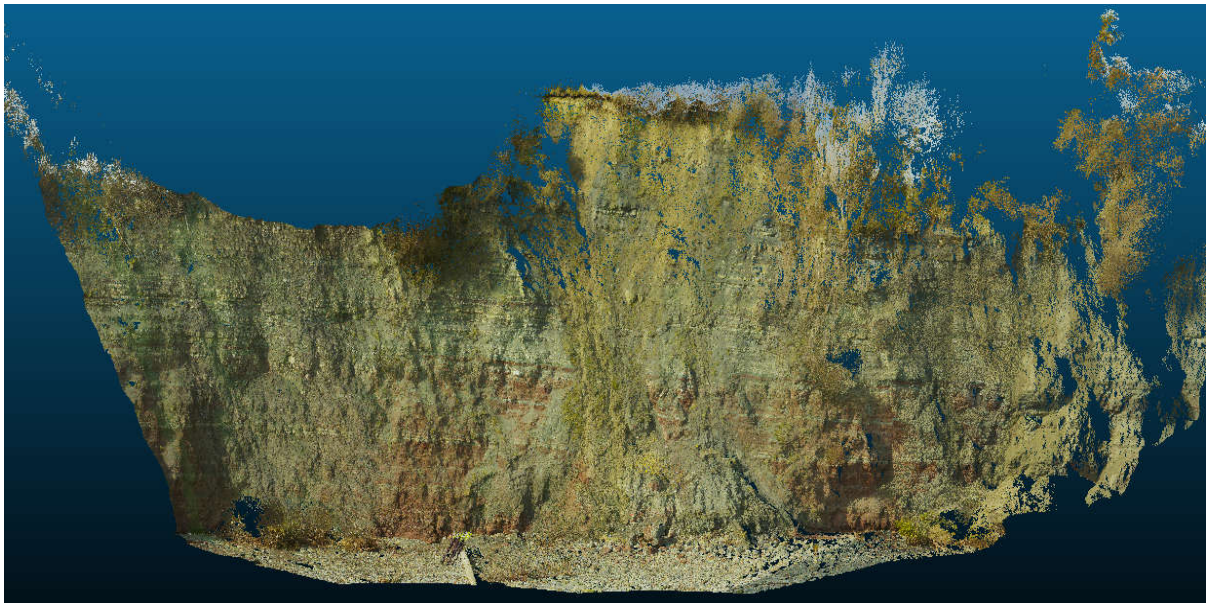

Figure 5.6 TLS Point Cloud

Figure 5.7 Pole Survey Point Cloud

The X, Y, and Z coordinates of some points at the top, sides, and at the bottom of the pole and TLS point clouds, were examined and compared in CloudCompare as shown in the Table 5.3 and Figure 5.8 below.

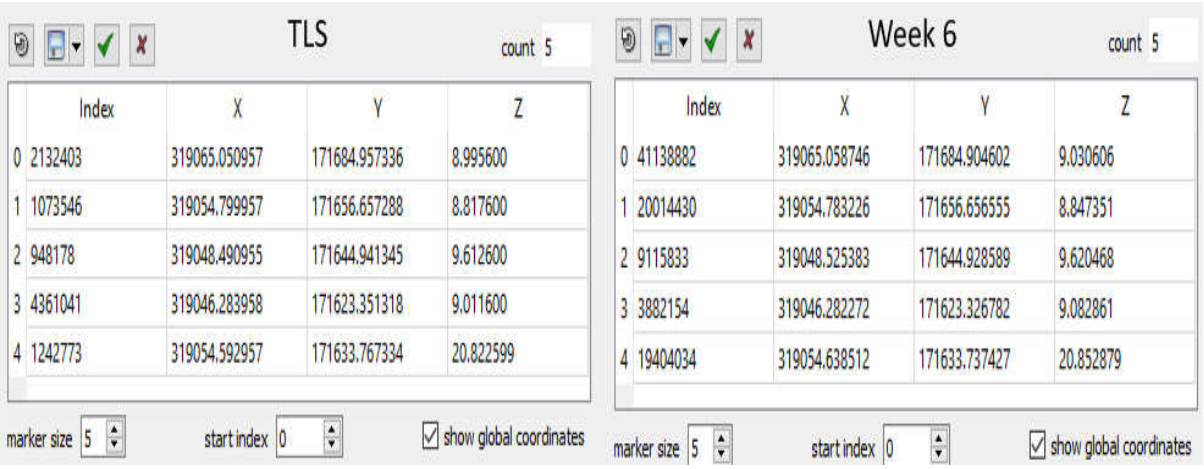

TLS

count 5

	Index	X	Y	Z
0	2132403	319065.050957	171684.957336	8.995600
1	1073546	319054.799957	171656.657288	8.817600
2	948178	319048.490955	171644.941345	9.612600
3	4361041	319046.283958	171623.351318	9.011600
4	1242773	319054.592957	171633.767334	20.822599

marker size 5 start index 0 show global coordinates

Week 6

count 5

	Index	X	Y	Z
0	41138882	319065.058746	171684.904602	9.030606
1	20014430	319054.783226	171656.656555	8.847351
2	9115833	319048.525383	171644.928589	9.620468
3	3882154	319046.282272	171623.326782	9.082861
4	19404034	319054.638512	171633.737427	20.852879

marker size 5 start index 0 show global coordinates

Figure 5.8 Examples of Coordinates of TLS and Pole Survey in CloudCompare -

Table 5.3 Differences in the Coordinates of some Points in the TLS and Pole Surveys

	TLS – Week 6		
	ΔN	**ΔE**	**ΔZ**
Point1	-0.008	0.053	-0.035
Point 2	0.017	0.001	-0.030
Point 3	-0.034	0.013	-0.008
Point 4	0.002	0.024	-0.071
Point 5	-0.045	0.030	-0.030

The maximum deviation in the XYZ coordinates of the PSPC at every point as compared with the TLSPC is less than 5 cm. This may seem relatively high, but these are generally at the extremes of the survey area of interest (e.g. in areas of vegetation).

The accuracies of the geometry of the PSPC and the TLSPC are subject to further scrutiny by creating their contours using the triangulation and the linear interpolation gridding method in the Surfer Golden Software (Sufer, 2018). The triangulation with linear interpolation uses the anisotropy to determine its contour (Bayazit, 2019). Anisotropy is dependent on the direction irrespective of the properties of the surface materials will generate an unbiased contour interpretation (Bayazit, 2019). The choice to use the multiple refractive indexes is due to the irregular surface nature of the cliff that has the capabilities for change in direction within the shortest possible period resulting from falls and collapse. This is illustrated in figures 5.13 to 5.16 below.

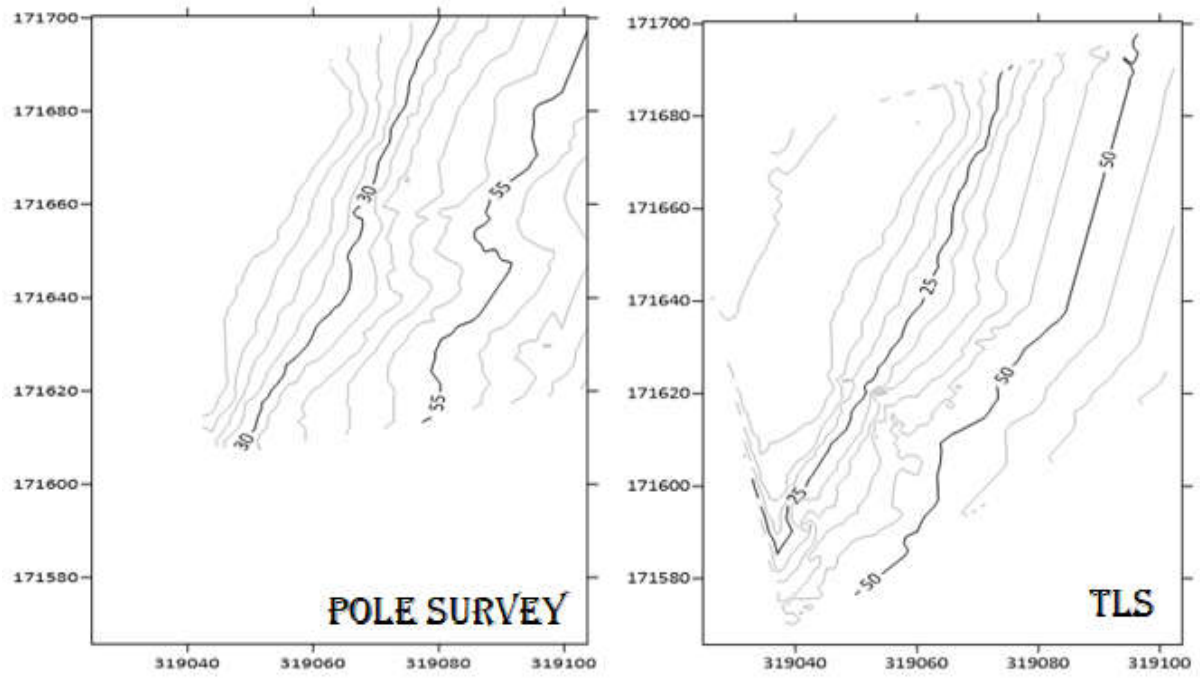

Figure 5.9 PSPC and TLSPC Contours generated in Suffer Golden Software – The X, Y coordinates at every point has the same elevation (the contour shapes are similar at every projected point from both axes on the pole and the TLS survey).

5.1.4 Visual Comparison with the Exact Height and Length with an Equivalent Drone Survey

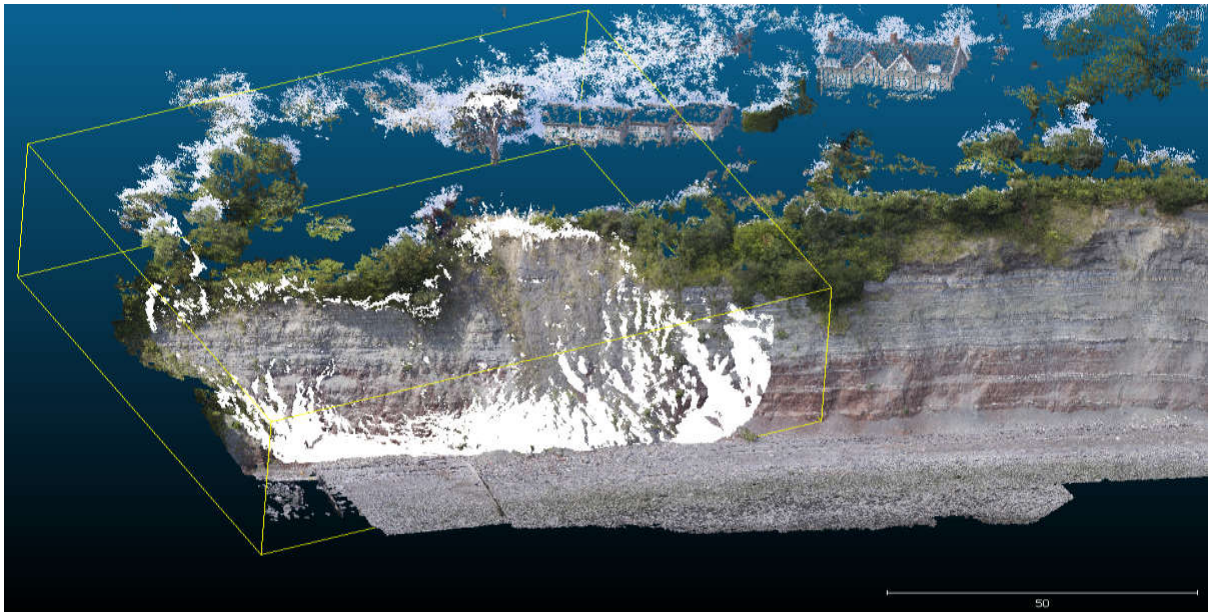

Figure 5.10 Pole Survey (on white) Superimposed on an Equivalent Drone Survey in CloudCompare – the drone survey was on the 23rd of July 2019 using the DJI Mavic Pro while the pole survey was on the 18th of July 2019.

5.1.5 Visual Comparison with Other Datasets

Figure 5.11 Like-to-like Alignment (Pole Survey up and Drone Survey down). The Drone survey was on the 18th of May 2019, while the drone survey was on the 23rd of July 2019

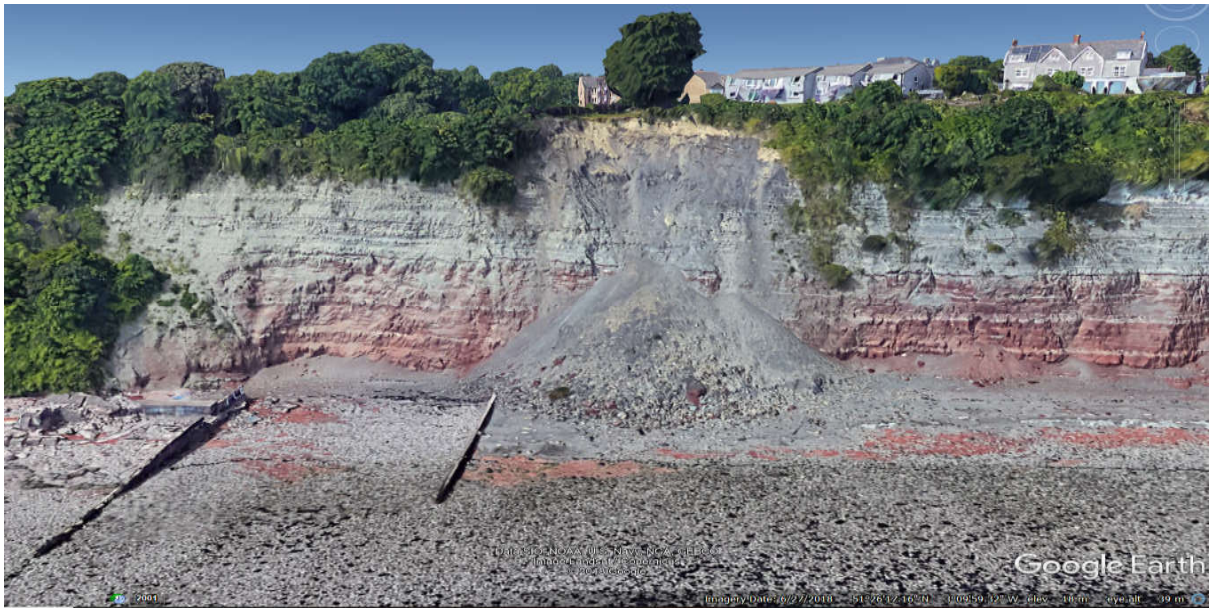

Figure 5.12 2018 Google Earth Imagery of the Study Area – The average update period for Google Earth is typically every five years. At the moment, point clouds generated from Google Earth imagery use expensive third-party software. The point clouds generated by Google Earth are not georeferenced. They also have scaling instabilities. There could be

multiple surveys every day with the pole. The point clouds are accurate, high resolution, and surveys can be undertaken by one person at minimal cost.

5.2 Periodic Changes on the Penarth Coastal Cliff

5.2.1 Pattern and Evidence of the Cliff Erosion

The pole photogrammetry and the change detection algorithm give an accurate delineation of the areas of change and the quantity of the cliff face material eroded. For a better understanding of the wave-cut pattern and the wave-cut notch on the cliff surface and at the base of the cliff, there were two other pole surveys one each in 2019 and 2020 in addition to the initial four weekly surveys in 2018.

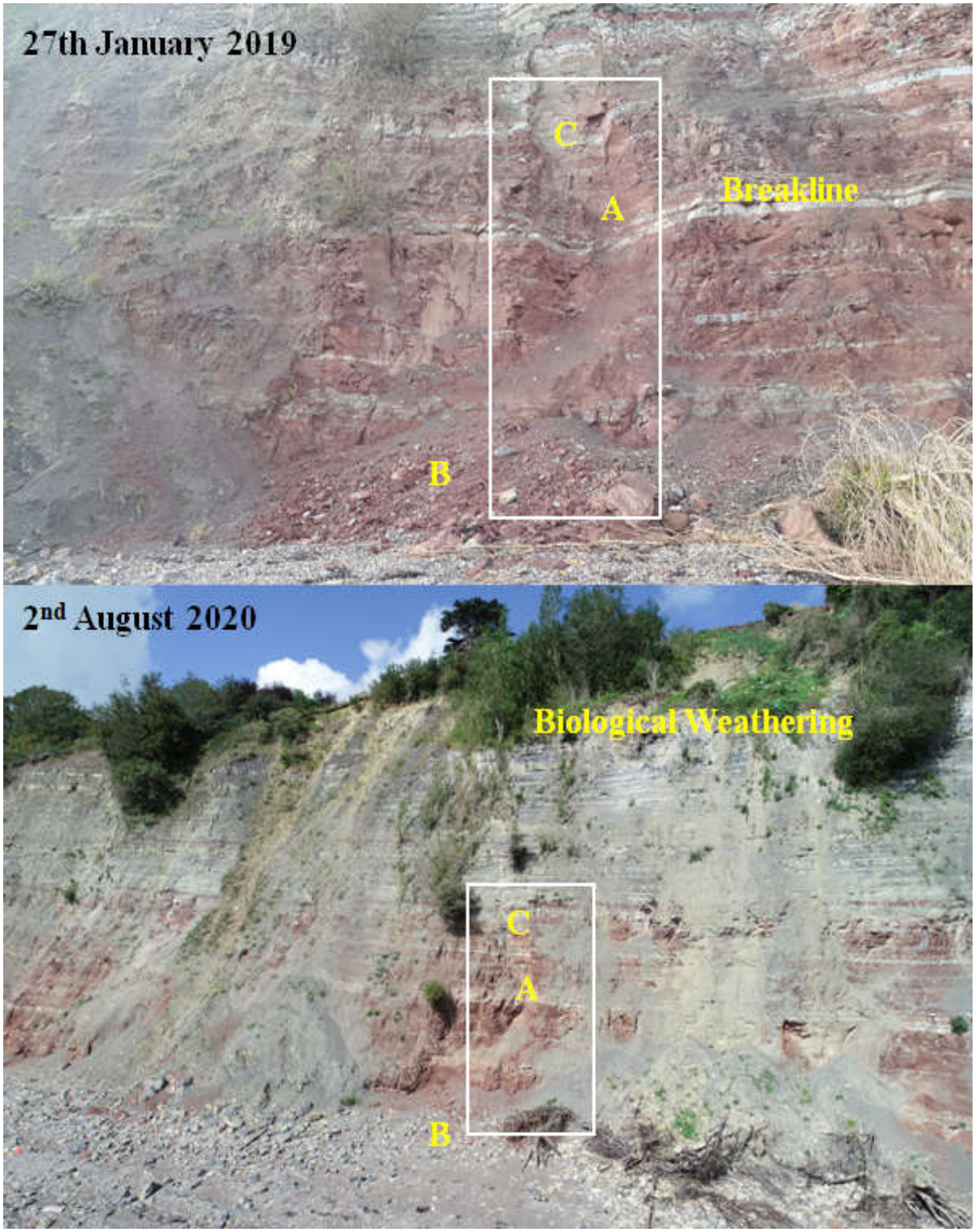

Figure 5.13 Demonstrate some Natural Eroding Processes such as the Breaklines, Weak Stacks, and Stumps at the Stretch of the Penarth Cliff Understudy - At **A** and **C** there are cracks on the Breaklines with an eventual collapse of some rock strata such as in 2019 with evident debris fell and rock particles at **B.**

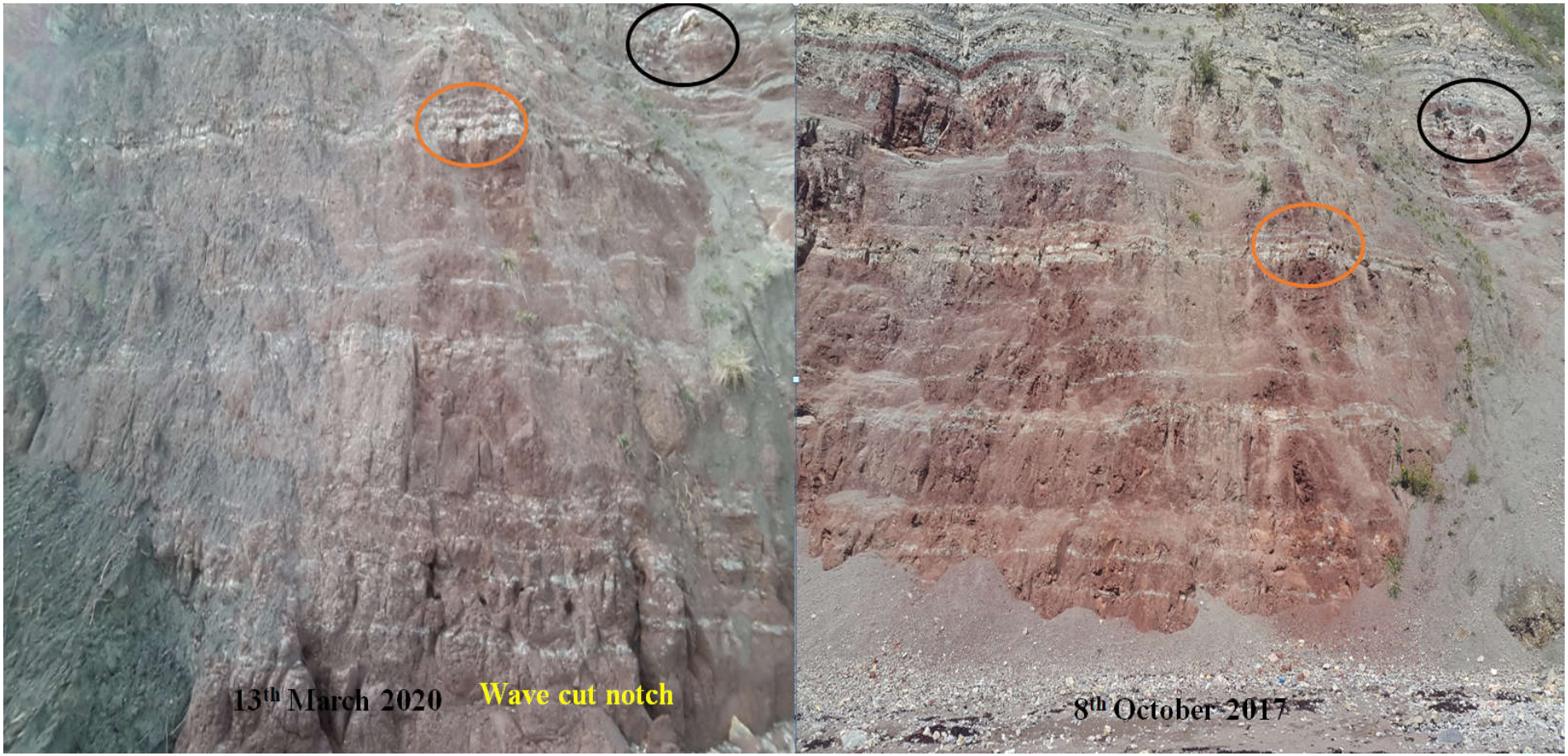

Figure 5.14 Shows the presence of Wave-Cut Notch on the Penarth Coastal Cliff – The black and orange circles are common points on both digital photos. By March 2020, the bottom of the cliff has suffered from the severe wave-cut notch. The wave-cut gradually disintegrates the cliff with change mostly scientifically determined.

Figure 5.15 Explains the Penarth Cliff Undergoes Differential Erosion and a Gradual Cliff Retreat -The softer and weaker rock fragments disintegrate easily by the further backwash from the sea. Another advantage of close-range photogrammetry is being able to capture every detail on the cliff irrespective of the quality of the digital camera used. In this survey, a 2.1-megapixel camera has been used to survey the cliff.

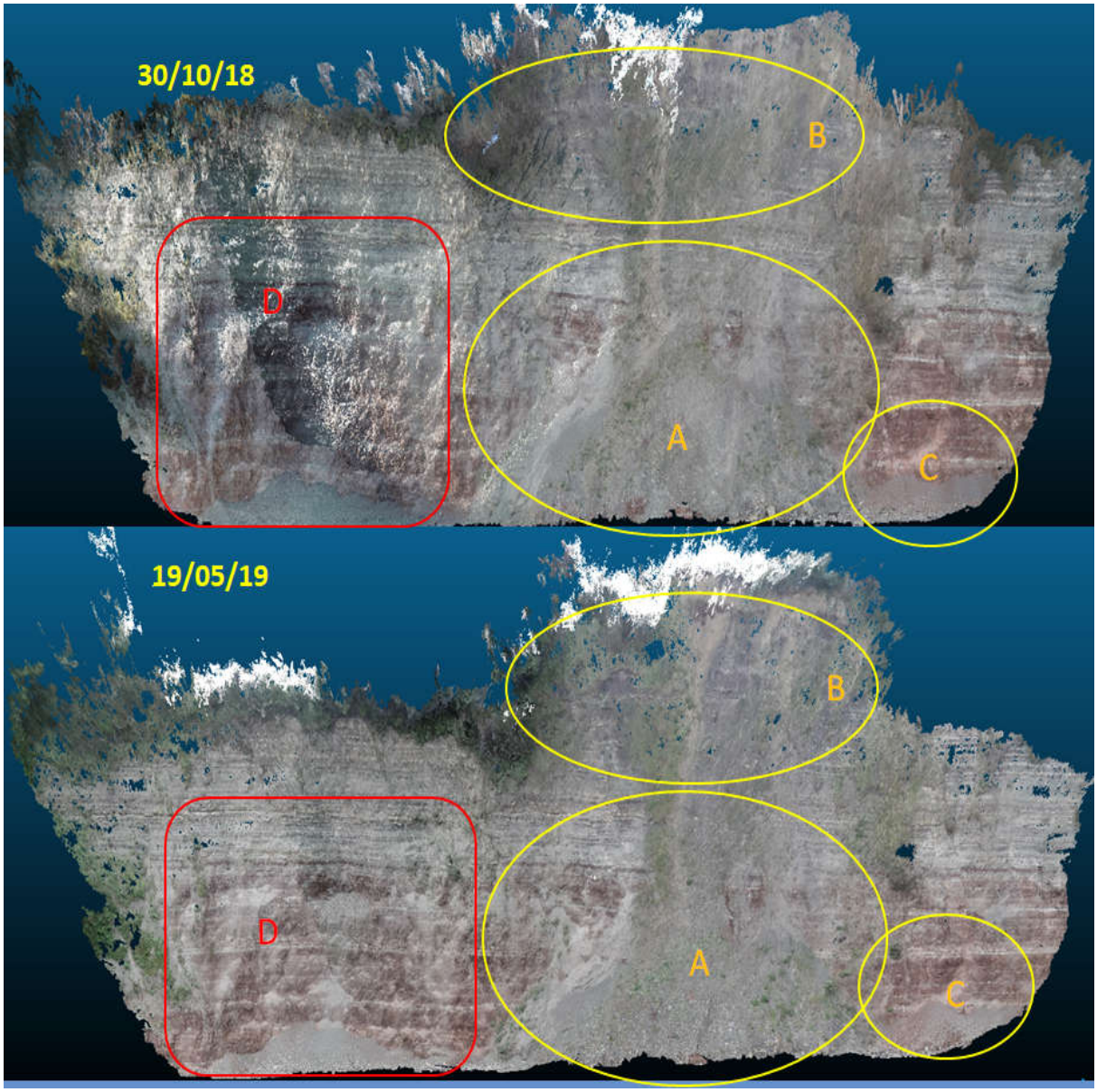

Figure 5.16 is a detailed comparison between two weekly surveys. At A on the 30/10/18 is an evident heap of cliff collapse eventually reduced at **A** as at the 19/05/19. At **B** are weeds hanging on the cliff but reduced by the 19/05/19. There is no significant evidence of change occurred on location **D** in both instances. C elucidates the possibility of rock strata collapse.

5.2.2 Periodic Change Detection Using the New Algorithm

While the cliff erosion is constant and gradual, their change areas in some instances are not physically inferred except for very careful examinations or by scientific evaluation. The range search result by the KD-tree partitions the exact distance radius values as dimensional radius scales on a very conspicuous colour ramp (reference can be made to section **4.3.5**)

Each of the Point cloud datasets which have been evaluated has more than 50 million points. The aligned point clouds using the Numpy array transformation parameters ensure that the outputs from the newly developed change detection algorithm show the areas of significant changes. There are, however, concerns on the clustering performance with the implementation of the KDTree for millions of points that will amount to multiples of the data tree structure (Otair, 2013). To solve this problem of each data array not being within a particular query, the algorithm structure accommodates a regular symmetry that automatically assigns a colour for each hierarchical colour-ramp tree structure within a distance class node. This sequence also helps to save memory and quickens the implementation duration of the algorithm (Choi and Oh, 2012).

For I in range (loop_r [0], loop_r [1]) where r is the search radius,

$$r(0,1) = r(1, 0); \quad \ldots\ldots\ldots\ldots\ldots\ldots\ldots\ldots\ldots \quad \text{Equ (5.1)}$$

$$r(0,1) \leq r(0, 0+1) + r(1, 0+2) \ldots\ldots\ldots\ldots r(1, 0+n) \ldots\ldots\ldots \quad \text{Equ(5.2)}$$

An example of the change detection output between week 4 and 5 is figure 5.17 below:

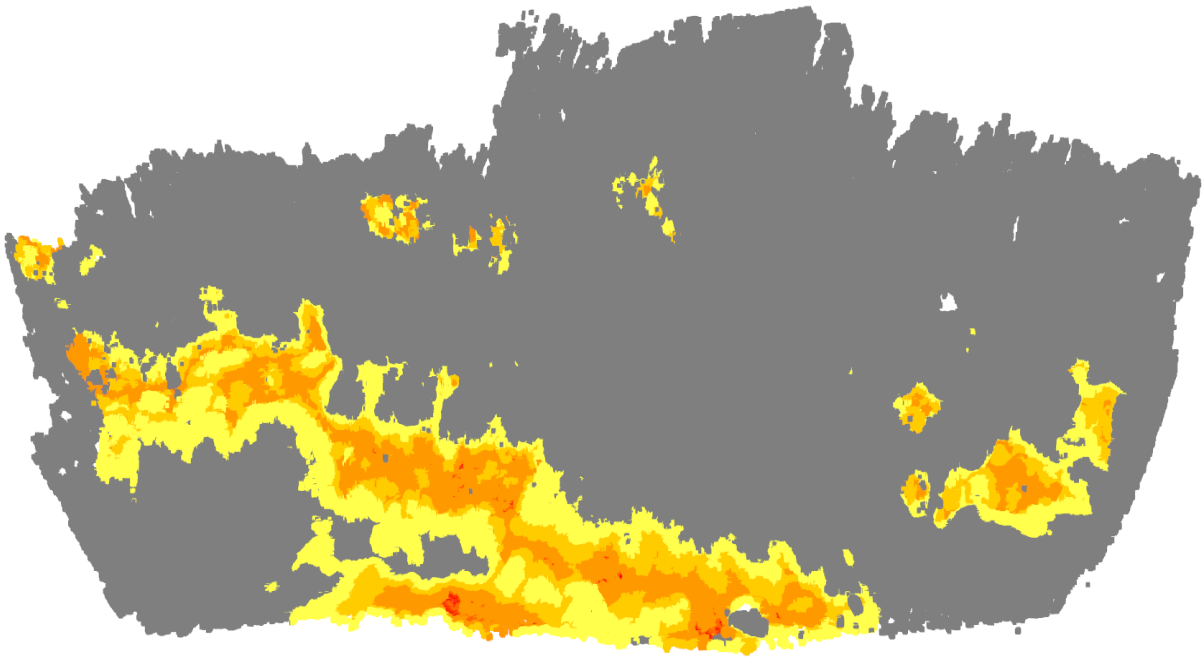

Figure 5.17 Output of the find Nearest Neighbour using the Distance Radius Value from 02nd October 2018 – 30th October 2018.

The colour distance '***colordist***' RGB Numpy array on range '0 – 1'on a gradient change starting from 0.2 depicts a colour range from red to yellow. At the start-count of zero, the algorithm assigns the specific colour that matches every single point on the Point cloud for the loop sequence using a distance change radius of 0.02, 0.03, 0.04, 0.05, and 0.1. Figure

5.17 indicates a major change has occurred both at the bottom of the cliff and on the cliff surface. It also indicates weathering at the top extreme left and the middle of the cliff.

Another advantage with this algorithm is being able to generate the change array for the different weeks automatically on the same coordinate system. Visualizations of these arrays on the open-source CloudCompare provide better understanding and analytical evidence(s) about their change patterns. This gives an insight to both researchers and policymakers the degree to the extent of the cliff falls during future storm upsurge and by other sub-aerial processes. This is illustrated in figure 5.18 below.

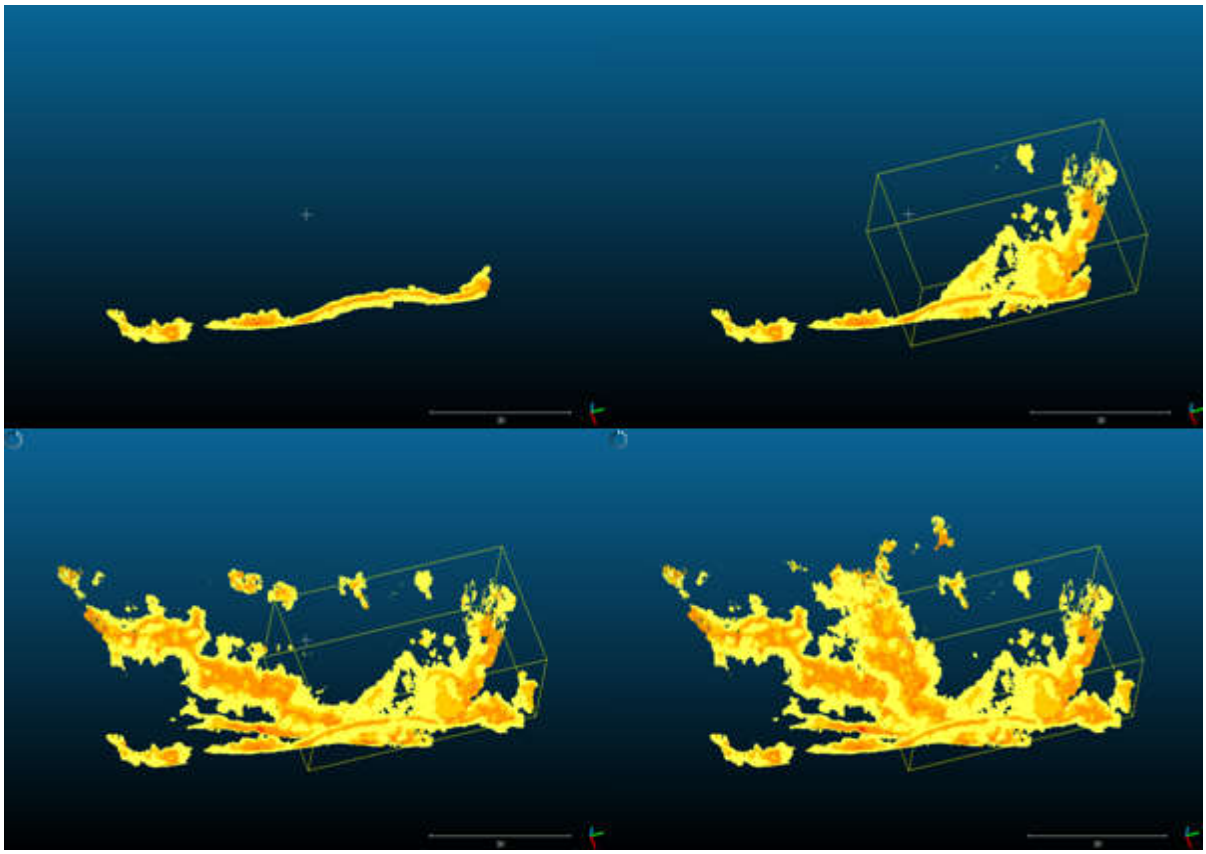

Figure 5.18 – A Change Flyby Created in CloudCompare Provides a Dimensional Data Pattern Identification of the weekly Change Segments.

The change-array also serves as a probabilistic segmentation model for the effective theoretical time-series classification for the Penarth cliff. It also functions to determine the percentage of the areas of critical crack and to identify those areas of imminent collapse or falls. To reveal correctly all the areas of critical change, evaluate, and segment the region(s) of imminent fall, the change analysis is as follows -

a. From the first survey (02/10/18) to the other surveys – figure 5.19
b. From each survey to the succeeding surveys – figure 5.20

This evaluation approach using two different sequences on the subtraction will help to overcome possible errors arising during the classification of points in the algorithm steps that determine the distances between the points of corresponding matrices in the KD Flann radius search.

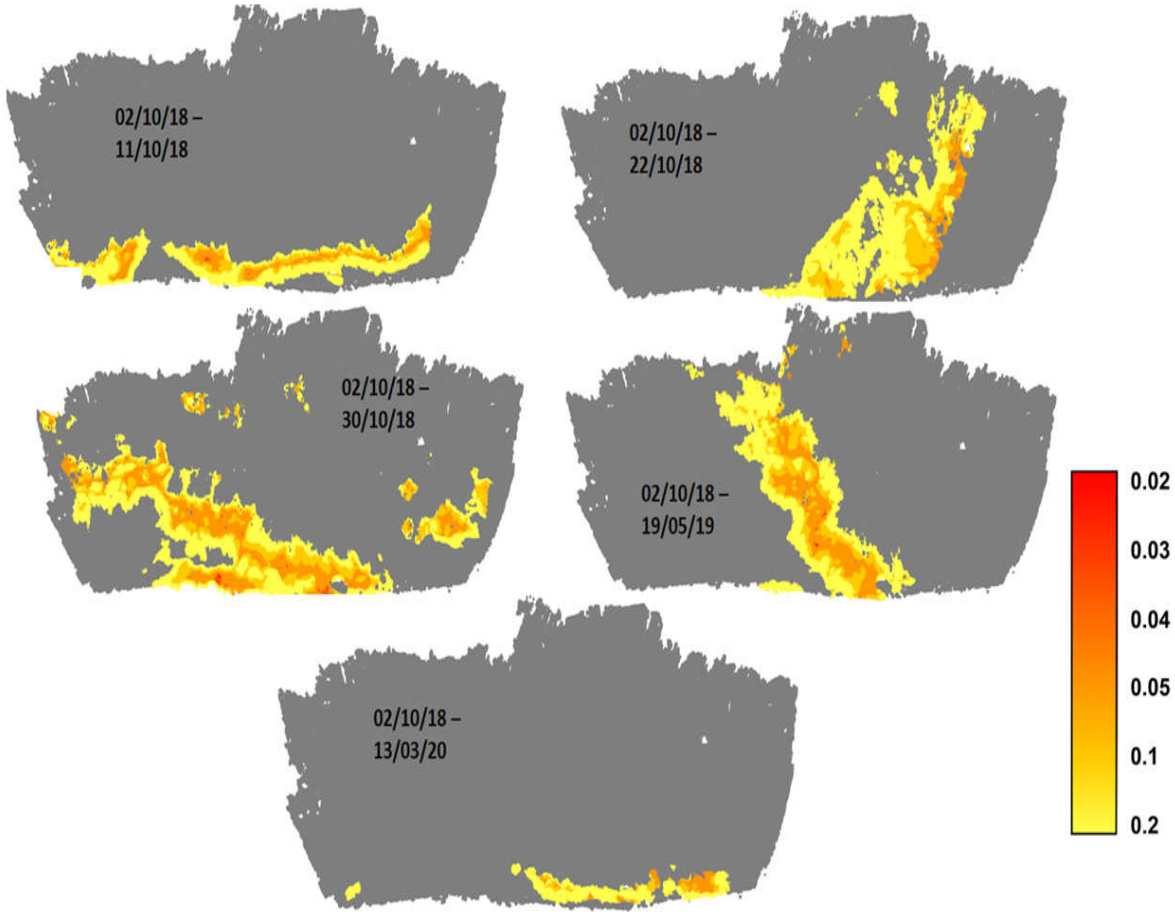

Figure 5.19 Periodic Changes between Successive Point Clouds from a Particular Start Date of 2nd October 2018.

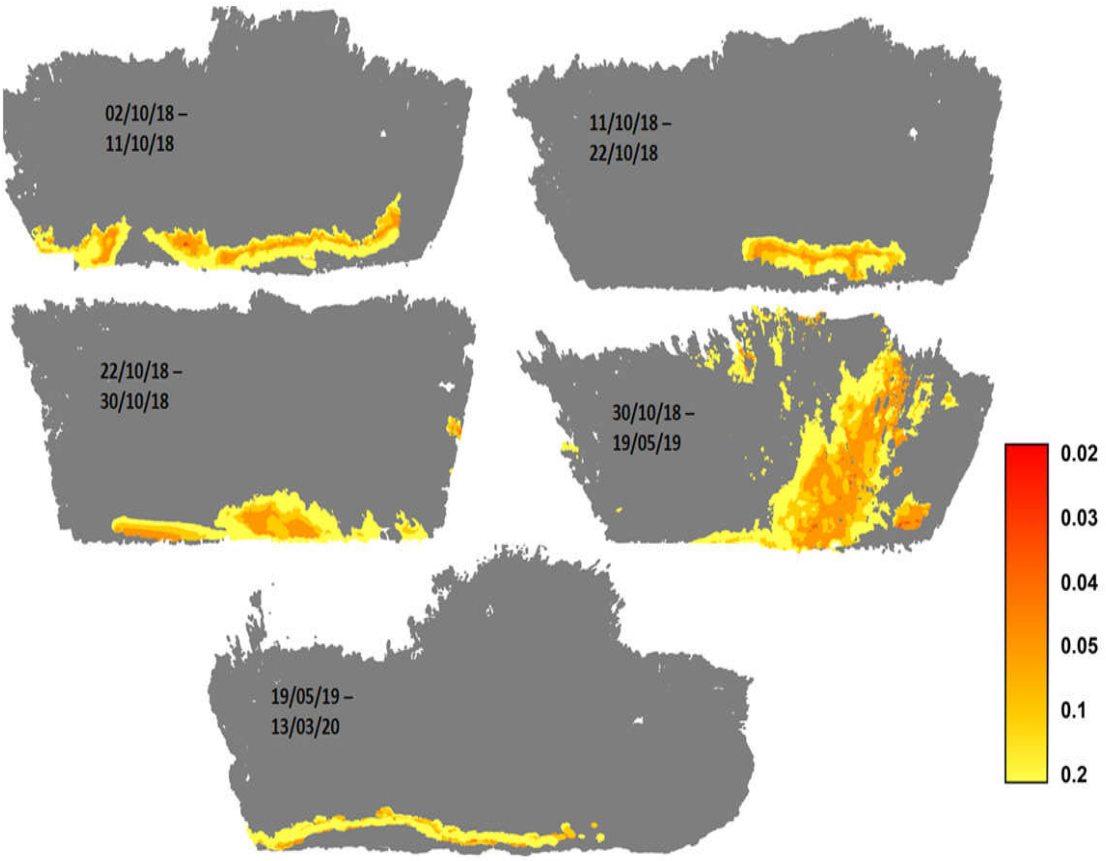

Figure 5.20 Periodic Changes between Successive Point Clouds from Individual Surveys to the Succeeding Surveys.

5.2.2.1 Identifying the Degree of Areas under Significant Change

The RGB indicator identified by the distance change radius of 0.02, 0.03, 0.04, 0.05, and 0.1, symbolises the depth of the Wave-Cut Notch, depth of fall, and crack on the cliff. The smallest distances in the KNN query search and the cached node represent the tree depth (Choi and Oh, 2012). This research evaluation of the degree of the area change uses the smallest distance indicator of 0.02 meters to outline the segment of 'most significant change'. This evaluation is useful for predicting future cliff fall(s). A distance change ratio piechart drawn using the Python Matplotlib and Numpy, depicts the percentage of change for each change distance ratio 'Appendix A'.

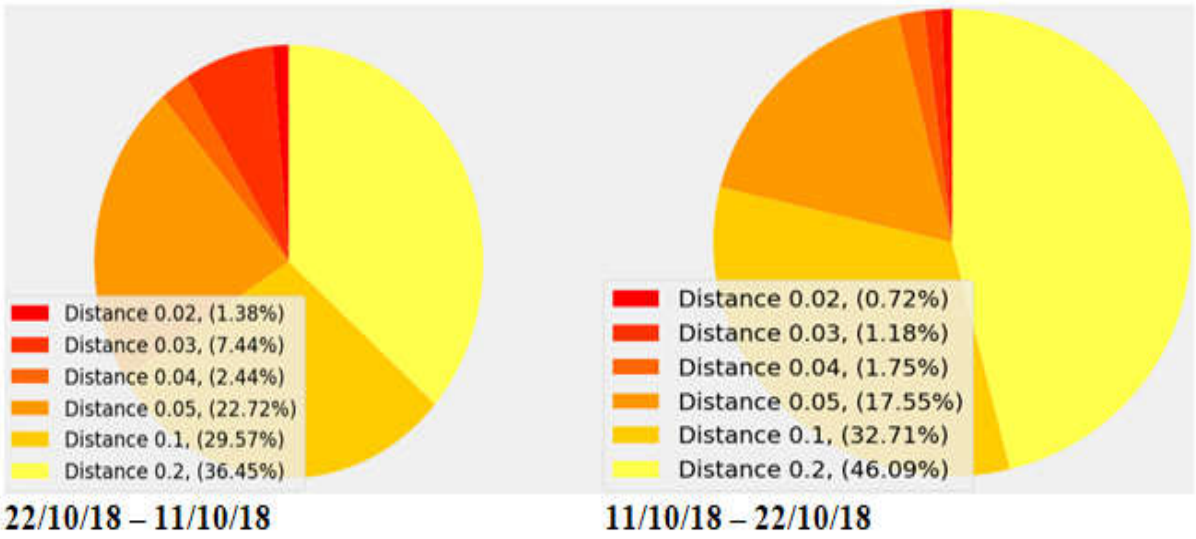

Figure 5.21 – An Example of the Distance Change Ratio Represented as Pie Chart for each of the Change Array. The percentages are the total area covered by the specific distance change between the Change Difference of two Different surveys.

Table 5.4 – The Summation of the Total Area Covered by Each of the Change Distance Radii for all the Change Differences Performed between the 2nd of October 2018 – 13th of March 2020.

	dist_0.02	dist_0.03	dist_0.04	dist_0.05	dist_0.1	dist_0.2
Suv_1-2	1.38%	7.44%	2.44%	22.72%	29.57%	36.45%
Suv_1-3	0.72%	1.18%	1.75%	17.55%	32.71%	46.09%
Suv_1-4	7.12%	11.36%	13.52%	19.77%	22.81%	25.42%
Suv_1-5	4.51%	7.85%	9.95%	18.76%	24.77%	34.15%
Suv_1-6	0.01%	0.11%	0.97%	18.49%	22.15%	58.27%
Suv_ 2-3	0.000%	0.000%	0.000%	19.28%	35.2%	45.52%
Suv_ 3-4	0.000%	1.18%	4.6%	15.73%	29.53%	48.97%
Suv_ 4-5	1.46%	3.66%	4.59%	15.75%	29.79%	44.76%
Suv_ 5-6	0.000%	0.0041%	0.4984%	17.2432%	35.6208%	46.6336%
Total_%	15.2%	32.7841%	38.3184%	165.2932%	262.1508%	386.2636%

The total coverage (**Total_%)** is used to plot a pie chart for each change distance region. This pie chart represents the statistical reality of all the nine times each survey was subtracted from one from the other.

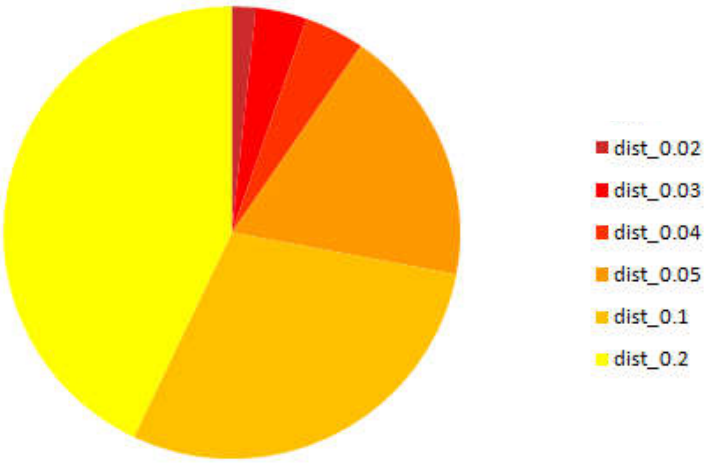

Figure 5.22 – Pie chart Draw from the Total_% (Tab 5.4) Summation of all Change Arrays Radii in the Different Change Detection that Identifies the Extent of Areas under Significant Change using Distance 0.02 as Major to Distance 0.2 as Minor Change Radius.

This represents the amount of fall or collapse that is of imminent collapse on the cliff surface within the period under review. In the following section, this will be helpful to determine the volume of change in each of the change regions.

5.2.2.2 Risk Assessment and Coastal Cliff Prediction Model

This section evaluates the extent of areas under significant change. An image grid draw using the python matplotlib (Appendix B) helps to sectionalize the change arrays into regions with the region(s) with the highest occurrences indicating the exact area on the cliff that is undergoing cliff fall or already undergone changes. Figures 5.23 – 5.25 illustrate the procedures and outline the outcomes.

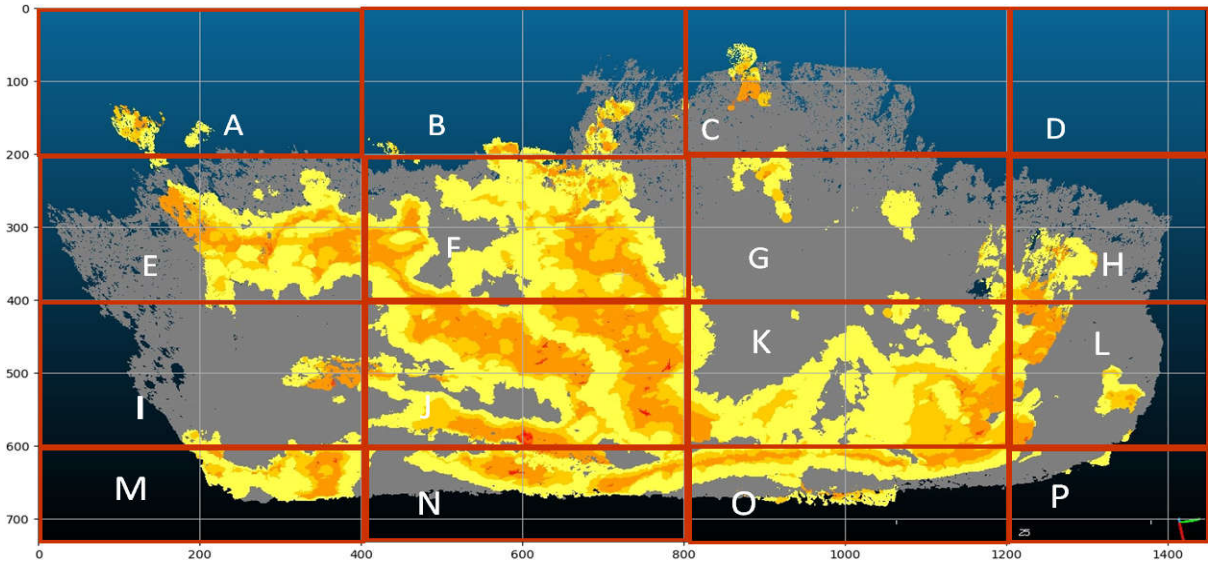

Figure 5.23 - Five Different Change Arrays from the 2nd October 2018 Start Date Superimposed on a Single Point Cloud in CloudCompare i.e. 02/10/18 – 11/10/18; 02/10/18 – 22/10/18; 02/10/18 – 30/10/18; 02/10/18 – 19/05/19; 02/10/18 – 13/03/20.

All Change arrays and point clouds are on the same scale and orientation before the gridding in Python.

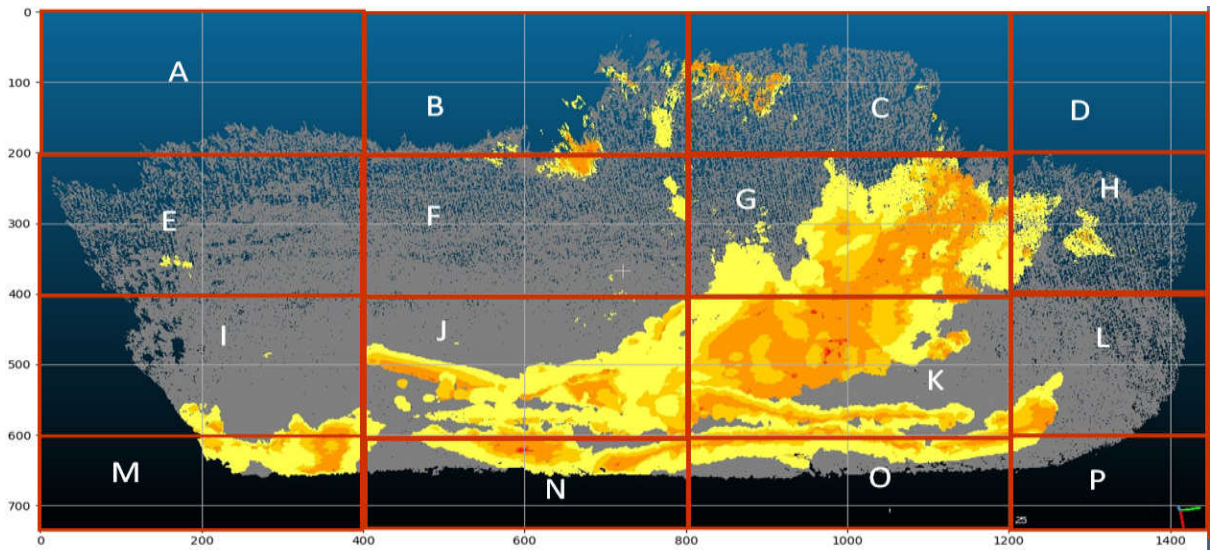

Figure 5.24 - Five Different Change Arrays from Individual Surveys to the Succeeding Surveys Superimposed on one of the Point Cloud in CloudCompare i.e. 02/10/18 – 11/10/18; 11/10/18 – 22/10/18; 22/10/18 – 30/10/18; 30/10/18 – 19/05/19; 19/15/19 – 13/03/20.

All Change arrays and point clouds are also on the same scale and orientation before the gridding in Python.

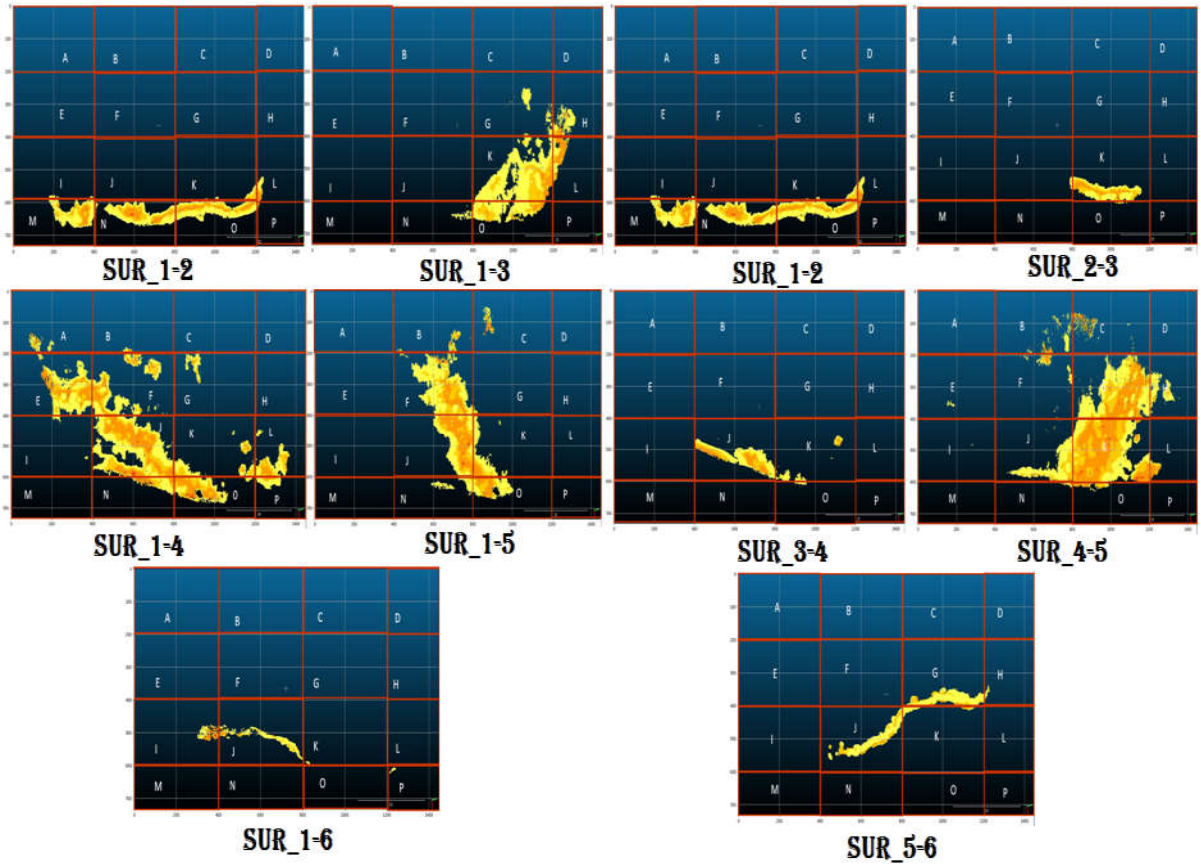

Figure 5.25 – The individual Change Array Exported from CloudCompare and Gridded in Python using Matplotlib - The different regions help to generate statistical data on the change location and the frequencies of occurrences. These frequencies help to formulate a prediction model monitoring the coastal cliff.

Table 5.5 – Shows the Frequencies of the Change Array Per Region. Unlike existing probabilistic model, this prediction model uses the actual change ratio fig 5.20, which is the actual quantity of the cliff fall for the different level of cliff wears, breaks and collapse at their exact geographical locations figures 5.25.

Table 5.5 – Shows the Frequencies of the Change Array Per Region.

Area	A	B	C	D	E	F	G	H	I	J	K	L	M	N	O	P
Suv_1-2									I		K	L	M	N	O	P
Suv_1-3							G	H			K	L		N	O	
Suv_1-4	A	B			E	F	G		I	J	K	L		N	O	P
Suv_1-5		B	C			F	G			J	K			N	O	
Suv_1-6									I	J	K					P
Suv_ 2-3										J	K				O	
Suv_ 3-4										J	K				O	
Suv_ 4-5		B	C		E	F	G	H	I	J	K	L		N	O	
Suv_ 5-6							G	H		J	K					
Occur_	**1**	**3**	**2**		**2**	**3**	**5**	**3**	**4**	**7**	**9**	**4**	**1**	**5**	**7**	**3**

A gradient of the change frequency density is generated from table 5.5. The gradient frequency table evaluates the severity of the change occurrence per region with an eventual cliff falls prediction graph. The practicability of this prediction model is the applicability of the three constant variables exact location, time, and frequency.

Table 5.6 – Shows the Severity of the change from the Sum of the Smallest ‘0.02meters’ to the Largest ‘0.2meters’ Distance Ratio – The clustering of these change arrays are from the different physical, biological and chemical constraints that lead to the cliff loss and eventual cliff collapse makes this model also quantitative.

Table 5.6 – Shows the Severity of the change from the Sum of the Smallest '0.02meters' to the Largest '0.2meters' Distance Ratio

Area	A	B	C	D	E	F	G	H	I	J	K	L	M	N	O	P
Suv_1-2									I		K	L	M	N	O	P
Suv_1-3							G	H			K	L		N	O	
Suv_1-4	A	B			E	F	G		I	J	K	L		N	O	P
Suv_1-5		B	C			F	G			J	K			N	O	
Suv_1-6									I	J	K					P
Suv_ 2-3										J	K				O	
Suv_ 3-4										J	K				O	
Suv_ 4-5		B	C		E	F	G	H	I	J	K	L		N	O	
Suv_ 5-6							G	H		J	K					
Occur_	**1**	**3**	**2**		**2**	**3**	**4**	**2**	**3**	**3**	**5**	**4**	**1**	**5**	**5**	**2**

Sur_1-6, Sur_ 2-3, Sur_ 3-4, and Sur_ 5-6 are not included in the severity zone as their search percentage in the critical search region (0.02 search_radius) are 0.01, 0.00, 0.00, and 0.00 respectively (Table 5.4).

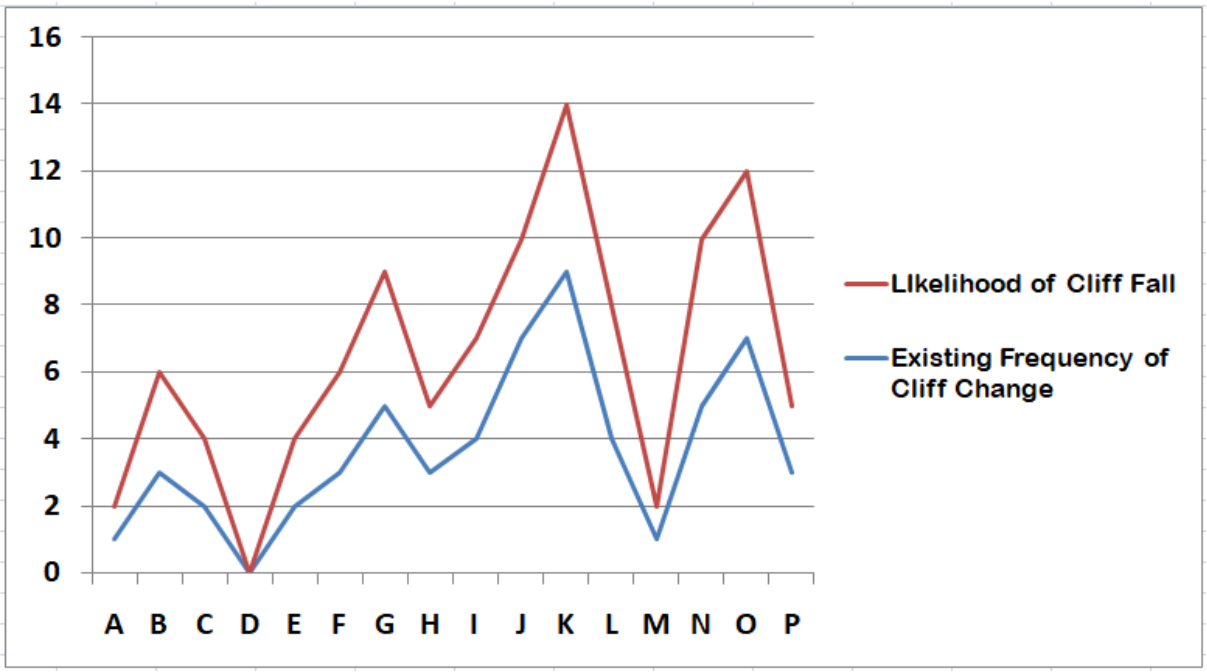

Figure 5.26 – Cliff Fall Prediction Graph – At K where there is the highest number of change occurrence with an 80% chance of the cliff fall or collapse with a projected minimum of eroding materials as shown below in figure 5.27.

5.3 Evaluate the Change Array and Determine the Weekly Volume Change – Change radius volumes in all change detections computed using the PSR in CloudCompare (Section 4.4.1).

Table 5.7 – Periodic Change Array and Weekly Volume. This automatically and periodically updates the volume as programmed.

	dist_0.02	dist_0.03	dist_0.04	dist_0.05	dist_0.1	dist_0.2	**Wk_sum**
Suv_1-2	19.4398	39.5215	55.1231	846.836	1327.98	2045.04	4333.9404
Suv_1-3	0.33922	0.728443	1.18098	358.06	984.04	3471.87	4816.2186
Suv_1-4	136.097	357.765	608.652	4587.44	6823.06	12690.7	25203.714
Suv_1-5	6.56196	16.6234	59.0122	1302.71	2329.8	2459.72	6174.4276
Suv_1-6	0.035041	0.130098	0.565455	59.5885	80.7963	392.267	533.3824
Suv_ 2-3	0.0003	0.0024	0.0054	41.416	140.983	198.605	381.0121
Suv_ 3-4	0.0005	7.44725	14.3338	135.013	265.64	658.488	1080.923
Suv_ 4-5	12.3117	12.3116	44.508	820.587	1564.92	5511.23	7965.8683
Suv_ 5-6	0.0005	0.735606	2.55989	150.99	471.866	733.922	1360.0735
dist_sum	174.786	435.265	785.941	8302.6405	13,989.085	28,161.842	**51,849.560**

0.33922 And **136.097** are the smallest and highest Percentage of change in the 0.02 search_radius (Table 5.4).

Depending on the stretch of the cliff been monitored and the frequency of the surveys, this approach will provide both short-term and long-term predictions. The position and the shape of the change array in their respective region (Table. 5.6) are useful for determining the hazard zoning (Castedo et al, 2017) figure 5.27 below.

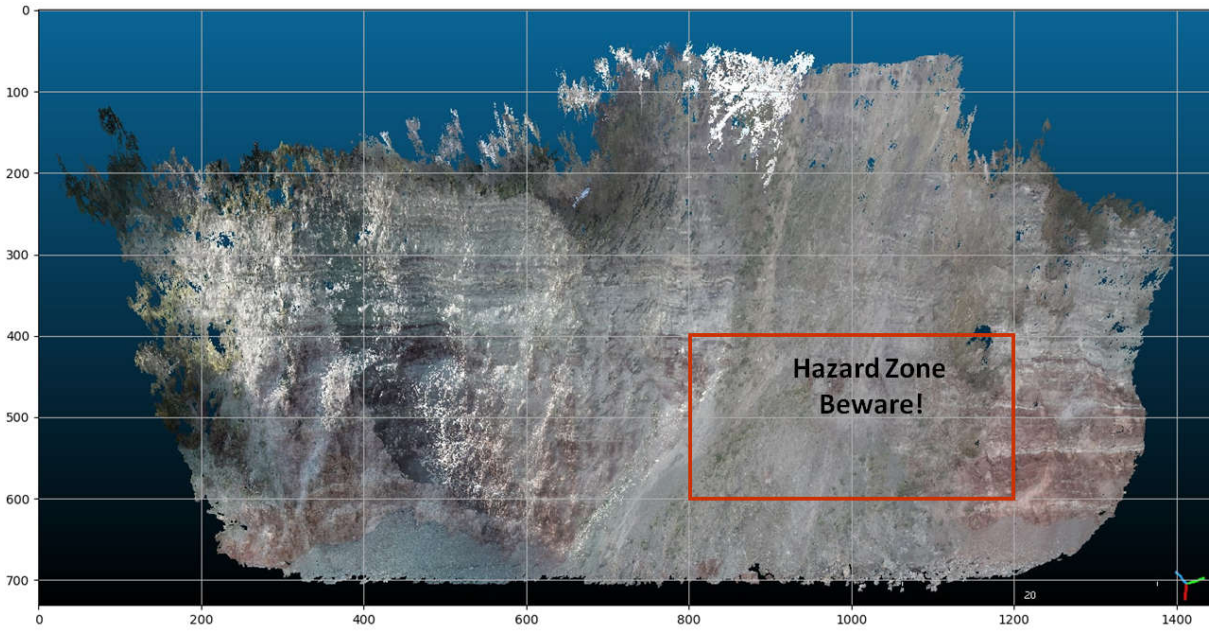

Figure 5.27 – Hazard Zone Warning Projected until the September of 2020

A projected minimum volume expected to erode from the hazard zone would be useful in developing Health and Safety precautions. From tab. 5.7 (the computed volume for each distance radius for all the nine-change detection performed). The computation of volume per distance radius for each change array also enhances the accuracies of the volume computation.

The mean model with the change array provides a 'true population variable' for forecasting future cliff fall and collapse. The average of all the change arrays throughout evaluation is such that,

$\mu = \sum_{i}^{N} = 1^{x} i/N$……..…….equ. 5.1

X = the change array variable

N = the entire size of X population

By applying the mean forecast model with independent and identical distributed variables on the cliff surface where;

O = total duration for observation of the change detection

hca = highest change array

sca = smallest change array

α = proportional

The total duration for observation of the change detection (O) / 2 = maximum predictable duration (mpd). Similarly, the minimum and maximum volume computed for the smallest

and highest change array, which falls within the K zone (Hazard zone), are 0.33922cm^3 and 135.75778cm^3 respectively.
mpd = 17 months (from 2nd of October 2018 – 13th of March 2020).
mpd α 1 / (hca – sca) = 8.5 months α 1/ 135.75778

For example, in the next 8.5 months (from the 13th of March 2020), it is predicted that a minimum of 135.75778cm^3 of materials would erode from region K. Another advantage of using this change array prediction model is that the predictions can be determined for each region on the cliff surface.

5.4 Chapter Summary and Conclusion

This chapter has shown that we can determine the;

1. Precise and accurate photogrammetric datasets using the pole surveys. While the precision is dependent on the systematic field procedure developed in chapter 4, the accuracy is a function on the GNSS.
2. Every point on the cliff surface that change has occurred can be detected.
3. The exact amount of change material(s) can be computed for.
4. Knowing the exact locations of change with the quantity of change creates a forecasting model for future change(s) on the cliff.

The contributions to knowledge in evaluating the changes on the coastal cliff and in the accurate computation of volume are;
The outputs from the pole survey when evaluated with the outputs from the other digital photogrammetry techniques are geometrically and radiometrically accurate for scientific evaluations. With evidence of cliff falls and collapse due to both weathering and the sea in different rock strata on the cliff, the scientific evaluations performed using the algorithm can detect complex and minor changes.

In this chapter, a change detection pattern-series using the different pole surveys ensures there is completeness in the change detection process. This can apply to any change detection algorithm in ensuring every change point is captured within the period of evaluation. Every change point is a 3-dimensional change array point cloud. The change-array which is automatically saved for each of the change detection performed helps to accurately determine both the volume change and a prediction model for future cliff fall and collapse. This chapter

also developed a cliff-fall prediction graph that shows the likelihood of the cliff fall with the existing frequency of the change-pattern. Whilst it is acknowledged that past erosion events on the cliff surface are not necessarily precise indicators of future erosion, the method does help identify those areas of the cliff which may require closer monitoring.

The volume computed using the PSR algorithm in the CloudCompare software, ensures that every change point is included in the computation. The PSR algorithm minimizes the possibility of including open spaces between disjointed meshes. Improved accuracy in the computation of the volume is achieved by computing the individual change distance array.

The least change radius distance of 0.02 indicates the radius closest to the middle of the change-area and is used therefore to determine the segment of significant change. With the help of a change ratio pie chart, the percentage of each change distance provides an analytical classification of the change-pattern. The statistical reality is a risk assessment and a cliff prediction model. The level of certainty of the risk assessment is a function of the exact change location, the frequency of change(s), and the time the change occurs. Provided these three variables have been correctly recorded, the evaluations performed in this chapter are accurate and can be applied to other coastal cliffs. The availability of a hazard zone correctly delineated makes the work of the policymakers and coastal cliff monitoring agencies becomes much easier.

Chapter 6

Low-Cost Computational Analysis & Visualization on Digital Surface Models Obtained by Drone Photogrammetry for Coastal Morphological and Volumetric Changes

This chapter answers such questions on a low-cost photogrammetry technique capable of acquiring high resolution digital surface models (e.g. 1-5cm resolution) for coastline monitoring. It discusses the best practices for acquiring digital images using drones for coastal monitoring. The emphasis is also on the most applicable open-source, low-cost, and high-level photogrammetry software for processing digital images. Is there also zero cost or low-cost GIS software for analysing the digital products (orthomosaic and Digital Surface Model) derived after processing the digital images? Lastly, is there an improvement to the existing methodologies of analysing the beach and foreshore to detect changes and change patterns at very precise levels (e.g. 1 cm)?

6.1 Chapter Aim:

This chapter aims to develop large-scale (small area at high resolution) cost-efficient solutions for monitoring coastal environments (i.e. Penarth as a case study; and others) by executing low-cost field procedures, data processing, computation, and analysis.

6.2 Chapter Objectives:

1. Develop low-cost, large-scale (small area), and regular (and repeatable) techniques for shoreline monitoring by:

a) Images obtained from UAVs
b) Determine the number of ground control points required to generate accurate digital models for shoreline monitoring
c) Processing of images using a variety of commercial and open-source software
d) Generating a set of output products (orthomosaics, DSMs, visualizations, etc.) relatively and accurately evaluated with or without the GPS ground control points.
e) Evaluate the performance against traditional shoreline monitoring techniques such as laser scanning or LiDAR.

2. Develop a shoreline information-monitoring infrastructure from DSM and DEM to identify changes, evaluate, and record shoreline behaviour.

3. Develop a shoreline classification model for delineating key features (e.g. high and low watermarks; and shoreline objects such as rocks, pebbles, sand, silt, seaweed, and other vegetation, etc.).

6.3 Chapter Overview:

None of the existing literature on low-cost digital photogrammetry for coastal monitoring and Geomorphology studies addresses a complete geospatial sequence for implementing low-cost UAV surveys, photogrammetry processing software for generating digital models, and GIS software for data computation and data analysis (Laporte-Fauret et al, 2019; Conlin et al, 2018; Goncalves et al, 2018; Molony et al, 2018; Templin et al, 2018; Cook, 2017; Masiero et al, 2017; Casella et al, 2016; Cermakova et al, 2016; Famuditi et al, 2014 and Westoby et al, 2012). This chapter elucidates and improves on existing methodologies for a low-cost centimetre-level accuracy-grade photogrammetry procedure using cheap and open-source solutions for coastal monitoring.

Shorelines are predominantly homogenous (Sander et al, 2015 and Averbukh et al, 2014). Application of SFM-MVS software to process imageries of featureless surfaces like the shoreline may lead to misalignment in image matching with prevalent noise (Koutsoudis et al, 2013; Skarlatos and Kiparissi, 2012). Flight planning and ground control points would improve the quality of the generated point clouds and the accuracies of the digital surface models (Unger et al, 2014).

Existing literature in the monitoring of coastlines with UAV photogrammetry has been on a planned flight pattern with pre-determined flying heights (Goncalves et al, 2018; Goncalves and Henriques, 2015). A flight plan of 85% forward overlap and 50% side overlap is used to acquire the required overlapping photographs that would produce high contrast and textured orthomosaics for beach morphodynamics (Brunier et al, 2016). How effective therefore are the several digital outputs from a well-designed UAV flight mission able to monitor the coastline in cms of spectral and spatial resolution?

In photogrammetry, the BBA refines the scene geometry and visual composition using 3D coordinates transformation (Murtiyoso et al, 2018; Qu et al, 2018; Molg and Bolch, 2017; Wang et al, 2017; Triggs et al, 2000). Section 3.7 explains the 3D transformation process that improves the geometric accuracies between adjoining aerial photos by the BBA. This section

explores the different Georeferencing options and best practices for low-cost and accurate 3D models from a series of overlapping 2D digital images.

The different photogrammetry software has different output radiometric and geometric accuracies in both the planimetric and on the vertical (Eboigbe et al, 2019 and Unger et al, 2014) despite the general principle is the AAT (Forlani et al, 2018 and Chesley et al, 2017). Unlike the analog and analytical photogrammetry, the different digital photogrammetric (computer vision) software are developed specifically for some photogrammetric functions (Grussenmeyer and Khalil, 2008) with different output accuracies (Murtiyoso et al, 2018; Smith et al, 2016; Micheletti et al, 2015 and Unger et al, 2014). What therefore are the image stitching patterns for these SFM-MVs? The chapter also evaluates the robustness and the analytical functionalities of the respective bundle adjustment computation in processing digital images for an accurate and functional coastline monitoring infrastructure.

6.4 Develop Low-cost, Large-scale (small area), and Regular (and repeatable) Techniques for Shoreline Monitoring by:

This research focuses on the suitability for survey-grade data capture (e.g. centimetre or sub-centimetre accuracy) to be able to model and analyse small changes in coastal environments (e.g. beach volumetric change or cliff erosion) (Eboigbe and Kidner, 2020). The mapping of the Penarth coastline stretches from the south end of the pier towards the northern side capturing the cliff embankments (see Figure 6.4). For each of the surveys, the average stretch of the coastline surveyed is an average of 80 acres. Four surveys one in 2015 and 2016 (see Figure 6.1) and two in 2020 help to accurately determine the rate of accretion and erosion on the stretch of the coastline been monitored.

Figure 6.1 – University of South Wales UAV shoreline survey on Penarth Beach (with the candidate) and the SenseFly eXom UAV drone.

6.5 Evaluation of Study Area

With thanks to Derek Elliott of the Aerial Photography Unit of the National Assembly of Wales, an archive of historic photography of the Penarth area (e.g. see Figures 6.2 and 6.3) has been supplied and analysed concerning changes of the shoreline through time (i.e. since WWII). It is evident that coastal processes have had an effect on this shoreline and that erosion has occurred. The photographs have been digitised, and subsequently geo-referenced to Ordnance Survey mapping to be able to represent these datasets in a Geographical Information System (GIS) for comparisons with other aerial surveys. The small-scale (high altitude) nature of many of these images allows for a visual comparison, but not for an accurate qualitative and quantitative analysis.

Figure 6.2 - Oblique aerial photograph of Penarth shoreline (Summer 1960).

Figure 6.3 – Vertical Aerial Photograph of Penarth shoreline (10th June 1960) (with thanks to the National Assembly of Wales).

6.6 Images obtained from UAVs

High-resolution digital images are from a fully autonomous UAV flight mission using vertical take-off and landing (Papakonstantinou et al, 2016). Photogrammetrically, automatic flight control is essential for radiometrically and geometrically precise orthomosaics (Hernandez-Lopez et al, 2013). It also helps to optimize the flight duration (Chiabrando et al, 2017). Due to the topographical nature of the coastlines, the automatic flight mission from a pre-planned flight plan is required to achieve a higher degree of overlap between images (Chiabrando et al, 2017; Harwin and Lucieer, 2012). It also helps to overcome influences from the external coastal environment such as wind, humidity, sea spray, and other coastal area conditions that could affect UAV performance (Villa et al, 2016).

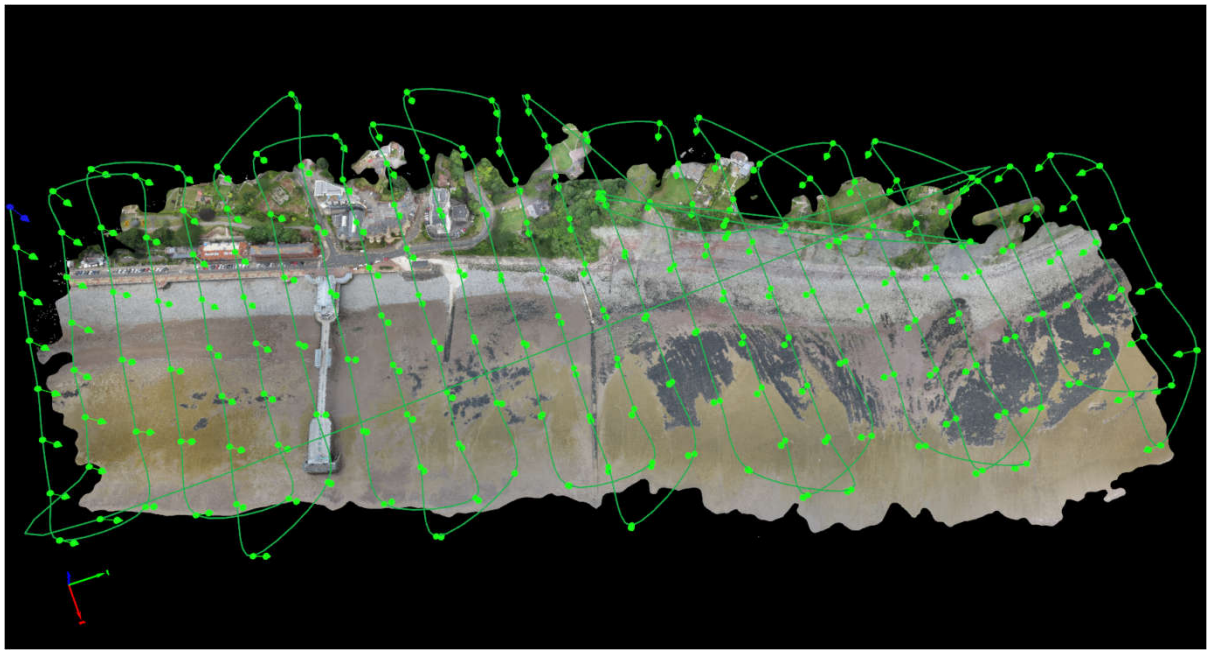

Figure 6.4 – Trajectory Showing the Flight Path Pattern of the Penarth Survey in 2015 together with the corresponding Orthomosaic.

6.7 Determine the Number of Ground Control Points required to generate accurate Digital Models for Shoreline Monitoring

The consumer-grade-GPS onboard a drone is often not very accurate and could cause further errors in the 3D position, scale, and orientation (Pix4D Mapper, 2016 and Wing, 2011). GNSS surveys will determine the precise and accurate positional accuracies of the drone surveys (Draeyer and Strecha, 2014).

The 2015 drone survey demonstrates that if just the onboard GPS of the drone is used to generate the 3D point cloud and digital surface model, then very large elevation errors (z) are typical. For example, for this survey, the onboard drone's uncorrected elevations are 52.02m above the true location (i.e. very dangerous or not practicable if taken at face value if used for coastal erosion modelling). The error is random based on the drone onboard GPS used and the actual satellite constellation at the time of the survey as discussed in chapter 4 section 4.1.5. For example, for the 2016 survey, the elevation error was +1.106m as shown below. Figures 6.5 to 6.9 illustrate the BBA process of generating the orthorectified orthomosaic and digital surface model from the raw drone images.

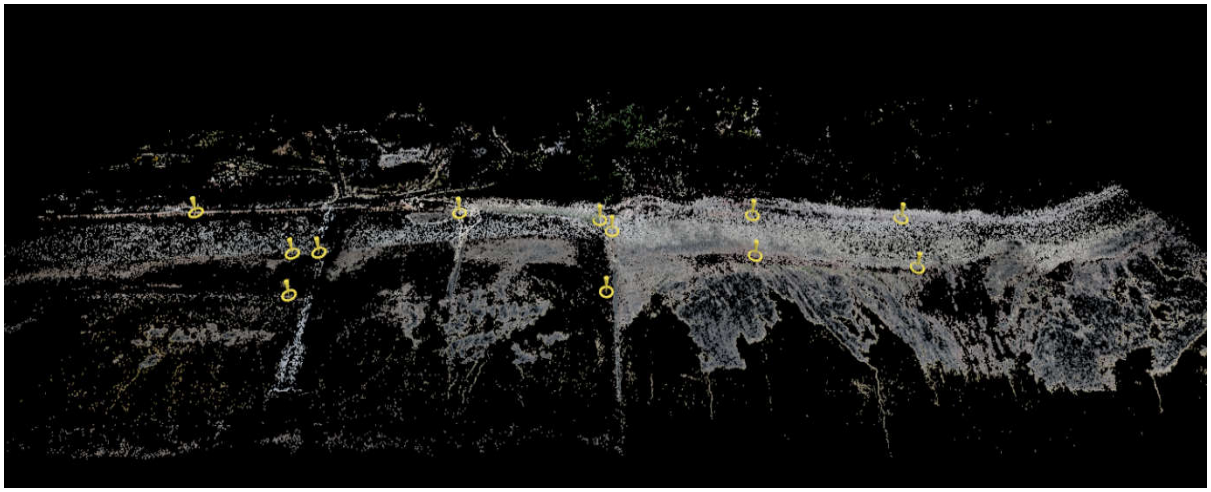

Figure 6.5 - 2020 Initial Sparse Point Cloud (using onboard Drone GPS) and Blue Circle Markers Indicate Actual GPS Locations

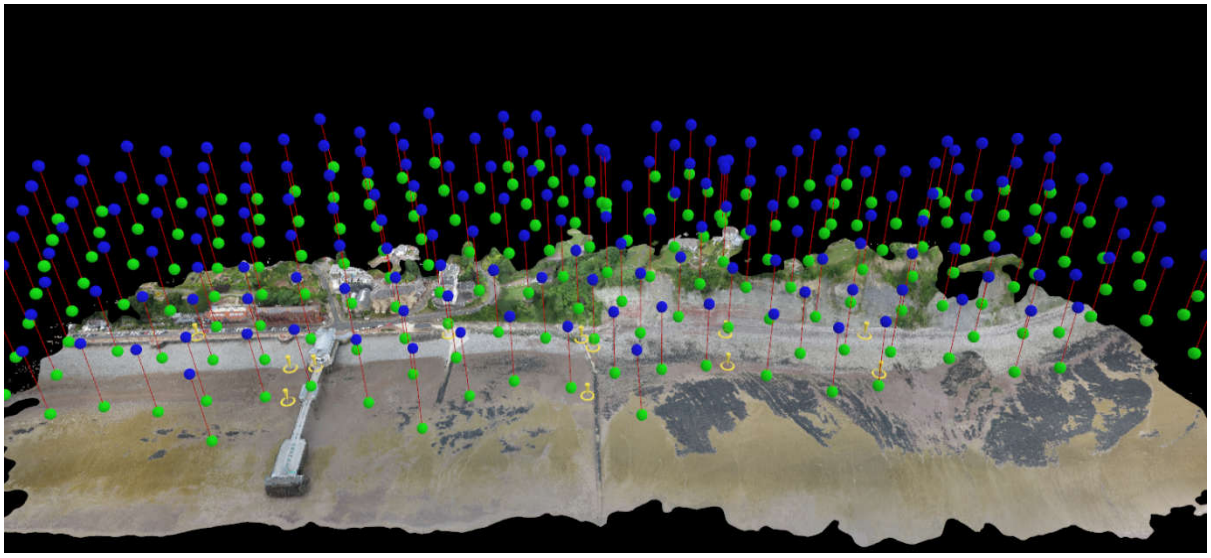

Figure 6.6 – 2015 Drone Survey Dense Point Cloud. BLUE Initial Camera Positions (using onboard Drone GPS) and GREEN Corrected Actual Camera Positions. Red Lines Indicate the Positional Error between onboard GPS and survey-quality GPS Ground Control Points while the YELLOW is the actual GNSS control points.

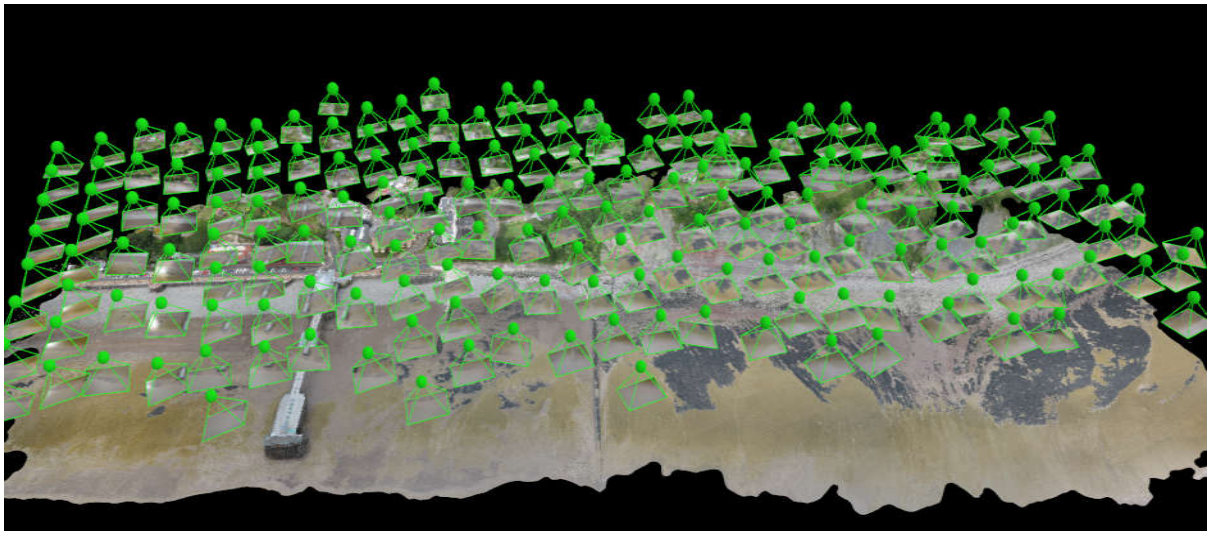

Figure 6.7 - 2015 GREEN Corrected Actual Camera Positions and Projected Drone Imagery Thumbnails

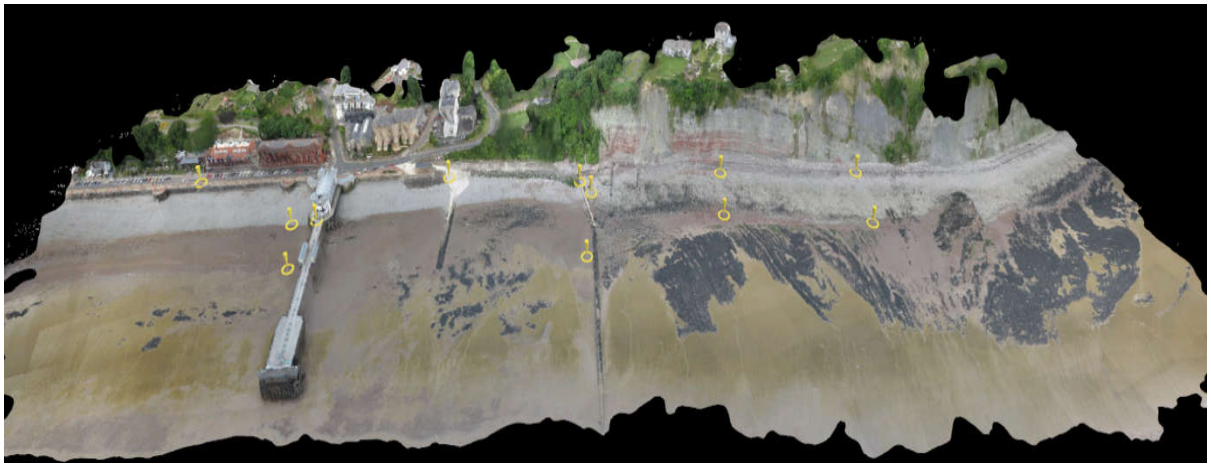

Figure 6.8 - 2015 Digital Surface Model and yellow GNSS Ground Control Points.

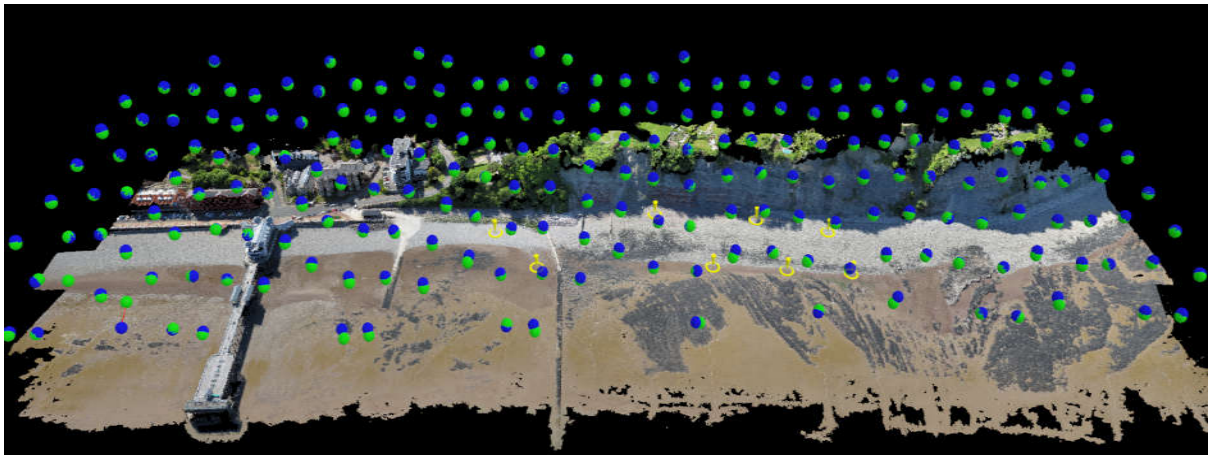

Figure 6.9 – 2016 Drone Survey Dense Point Cloud. BLUE Initial Camera Positions (using onboard Drone GPS) close to the GREEN Corrected Actual Camera Positions. Red Lines (Positional Error between onboard GPS and survey-quality GPS Ground Control Points) not visible as the distance difference is 1.1m. The YELLOW is the actual GNSS control points.

For each of the surveys undertaken, 3D point clouds and digital surface models were generated with and without GPS ground control (typically 6 to 8 points covering the area of interest) to understand the magnitude of the error; and also with additional GCPs to determine whether extra survey control influenced the quality of the overall model, i.e. "Do additional survey points improve the accuracy of the data outputs?". The results show that while the use of GCPs is essential (as can be shown in the figures above), extending the number of GPS GCPs to 12 or more points had no real improvement on the models' accuracies. This is

probably due to the additional GCPs extending beyond the area of interest (AOI), so not necessarily having an impact on the quality of the data inside the AOI. For this reason, the results discussed in the foregoing sections/chapters focus on using the best available dataset (i.e. with 4, 6, or 8 GCPs on the beach itself).

Some GCPs were established permanently on visible points which will appear on the images for subsequent drone surveys (Figure 6.10). The other drone surveys may not require GNSS surveys for as long as these points are static and visible. However, it is appreciated that in some coastal environments, without the manmade features visible at Penarth, it might not be possible to use a fixed set of visible GCPs.

On the unavailability of a GNSS survey, a local origin can be established by any of the traditional land surveying equipment (section 2.1). By implication, a local origin will keep the established GCPs fixed for every other survey and attaining a precision of possibly up to 1cm in the elevations.

Figure 6.10 - Permanent GCPs at the Penarth will help to avoid frequent GNSS Surveys. This would reduce the project cost and the duration of drone surveys.

6.8 Processing of Images using a variety of Commercial and Open-source Software

The drone mapping process can capture the 3D position of all ground features "X, Y, Z" (Vautherin et al, 2016 and Strecha et al, 2015). With the reconstruction of bundles of rays (Pix4D Mapper, 2016 and Bemis et al, 2014), derived from the basic photogrammetric principles of dense matching and bundle adjustments the respective software can generate 3D stereoscopic models showing the ground features (Strecha et al, 2015). However, not all computer vision and photogrammetric algorithms work in exactly the same way for precise

mapping purposes as the bundle adjustment routines and optimization differs from one software to the other (Eboigbe et al, 2019 and Murtiyoso et al, 2018). An example of this is the reconstruction of bundles of rays from the Penarth data constructed using Pix4D, Agisoft Photoscan and VisualSFM are figures 6.11 to 6.16 below.

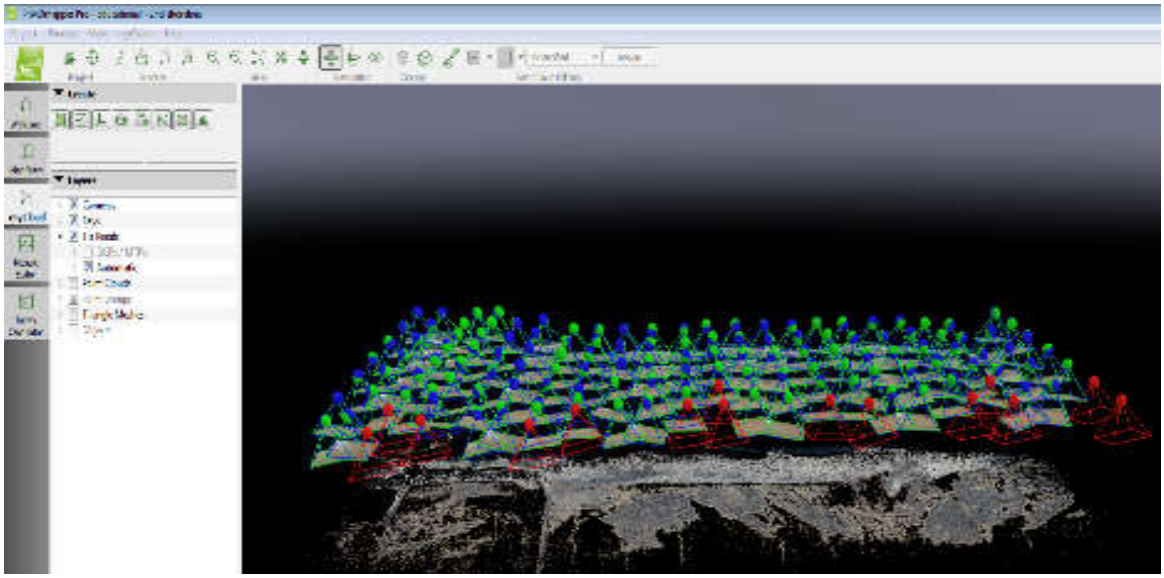

Figure 6.11 – Pix4D Photogrammetric Processing of Penarth Coastline Drone Survey.

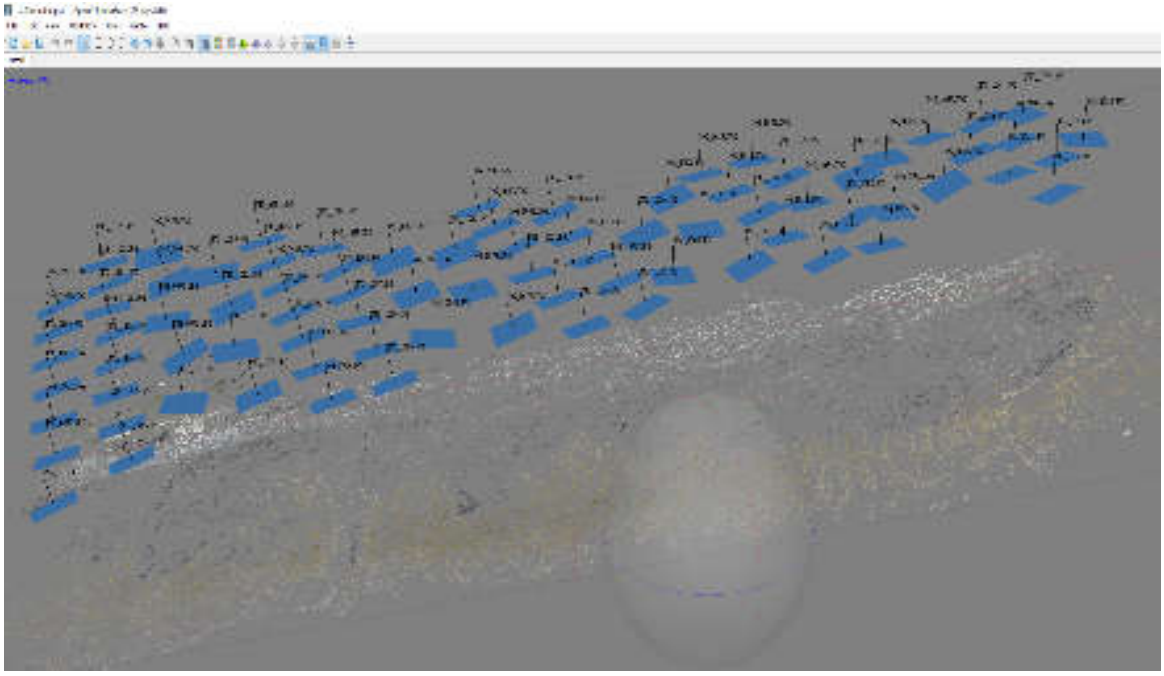

Figure 6.12 - Agisoft Metashape Photogrammetric Processing of Penarth Coastline Drone Survey.

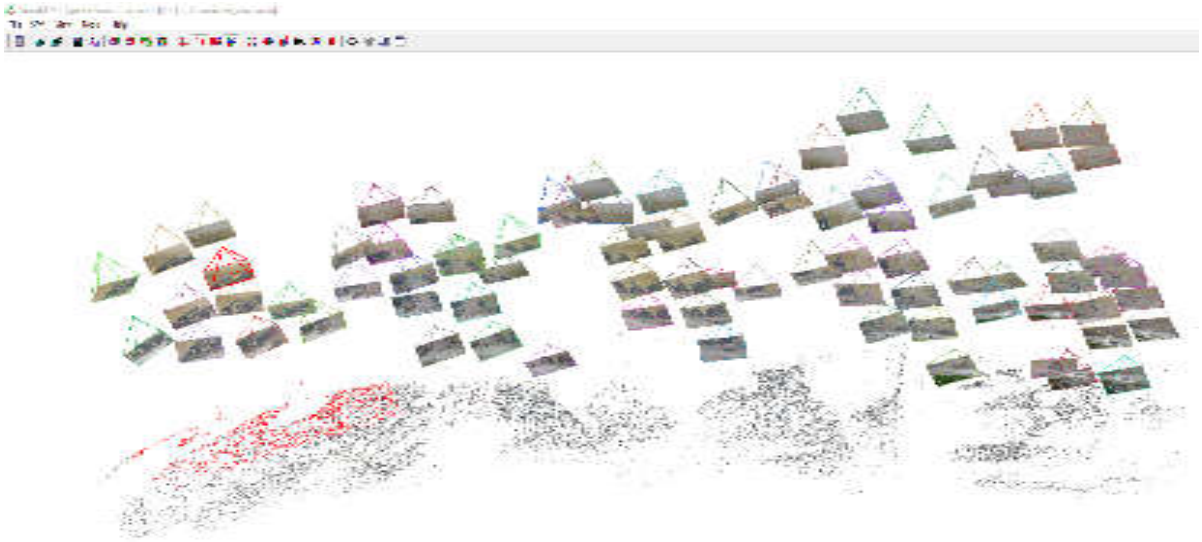

Figure 6.13 - VisualSFM Photogrammetric Processing of Penarth Coastline Drone Survey.

The VisualSFM will also generate finely registered point clouds on very close-range photogrammetry with more than 50% forward and side overlaps. With the VisualSFM, it is also possible to specify the GCPs to improve the scaling and orientation of the point clouds.

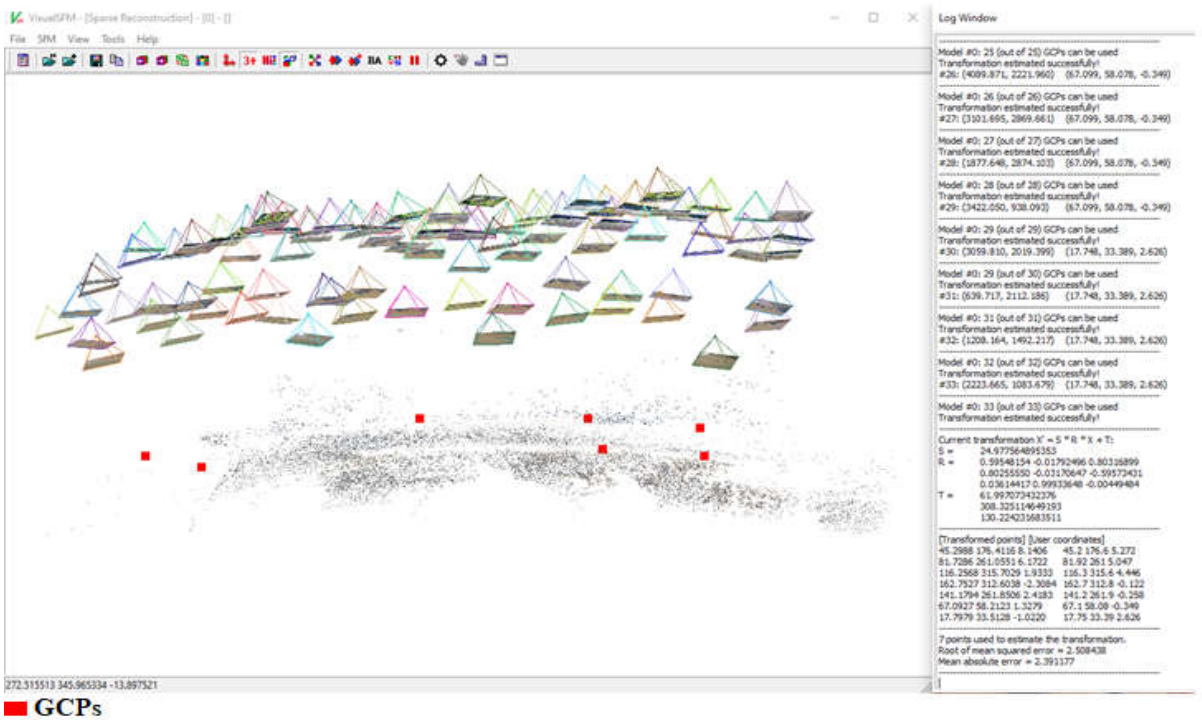

Figure 6.14 – The Seven GCPs Optimizes the Camera Orientations and Positions of the Penarth Coastline Drone Survey in VisualSFM. Optimization will reduce possible projection errors and improve the accuracy of the point cloud.

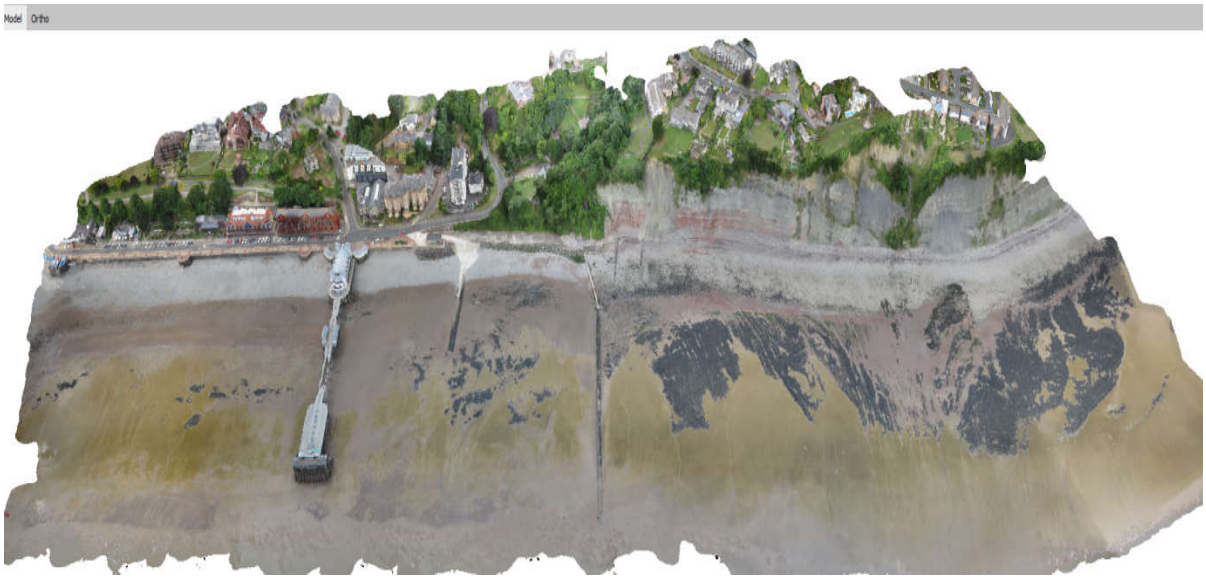

Figure 6.15 - 2015 3D_Model of Penarth Processed using the Agisoft Metashape

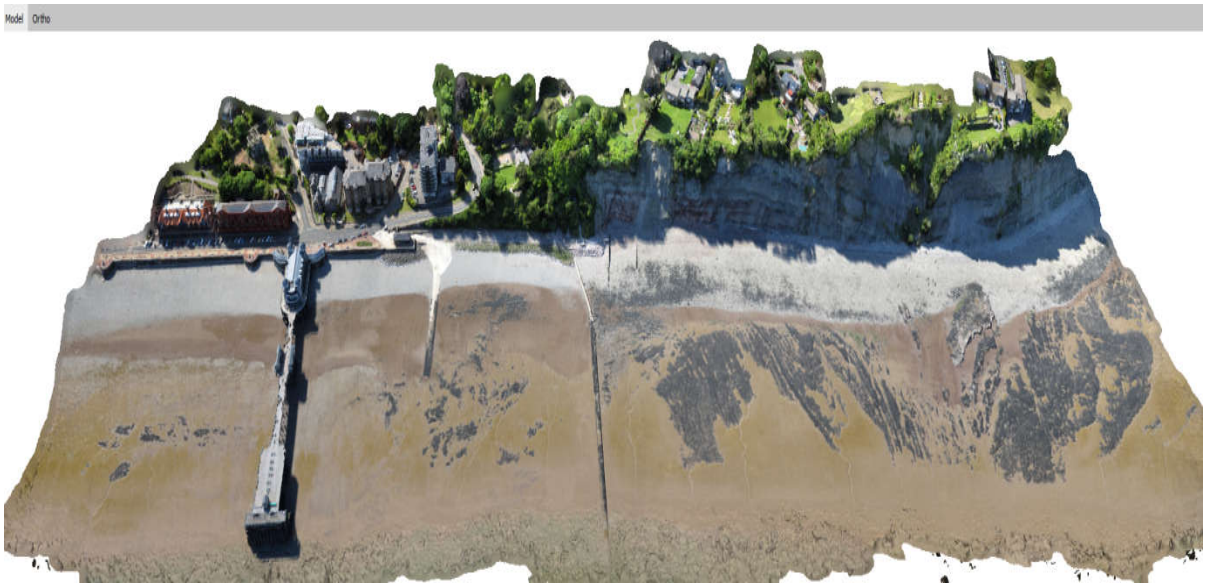

Figure 6.16 - 2016 3D_Model of Penarth Processed using the Agisoft Metashape

However, while each software package has its own unique features, each of them largely adheres to the same methodological approach as presented in Chapter 3. **Figures 6.16 – 6.22** illustrate the complete photogrammetric processing workflow for the Penarth Beach dataset using the Pix4D photogrammetric software.

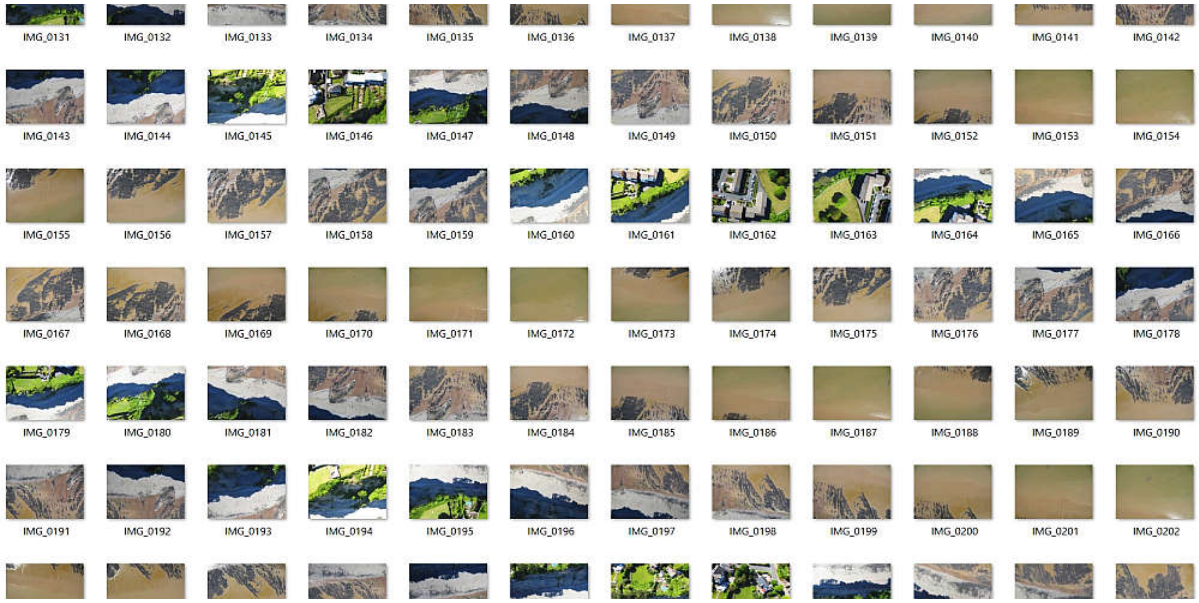

Figure 6.17 – University of South Wales sample of the hundreds of individual Geotagged UAV drone images of Penarth shoreline before processing (vertical/overhead photography).

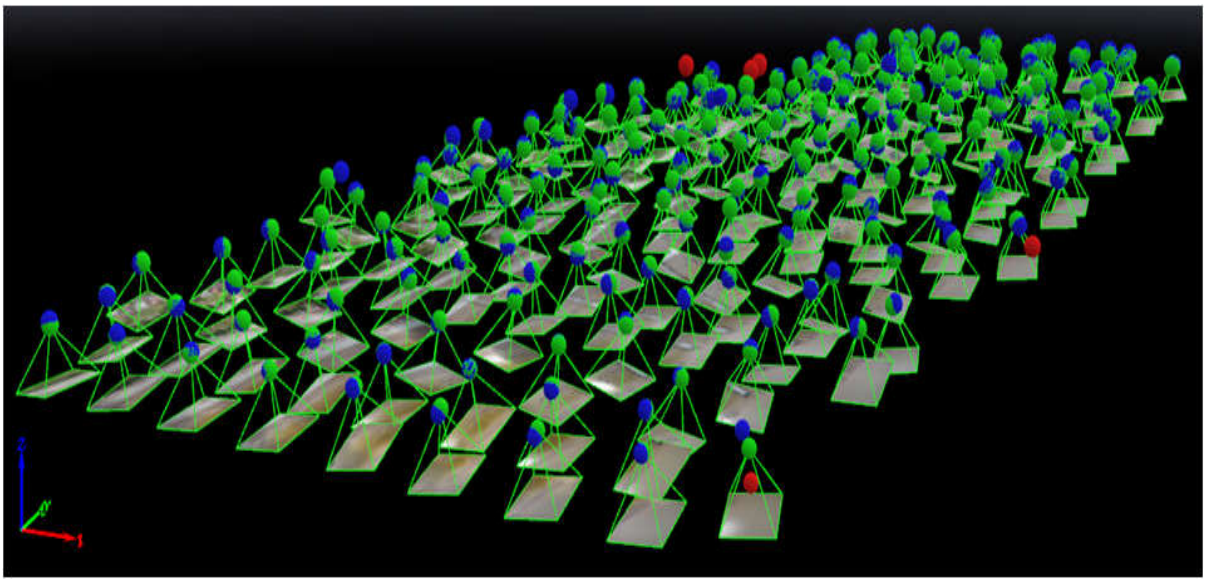

Figure 6.18 – Individual Geotagged position (and projected image) of each beach survey photograph of Figure 6.16 in 3D map space.

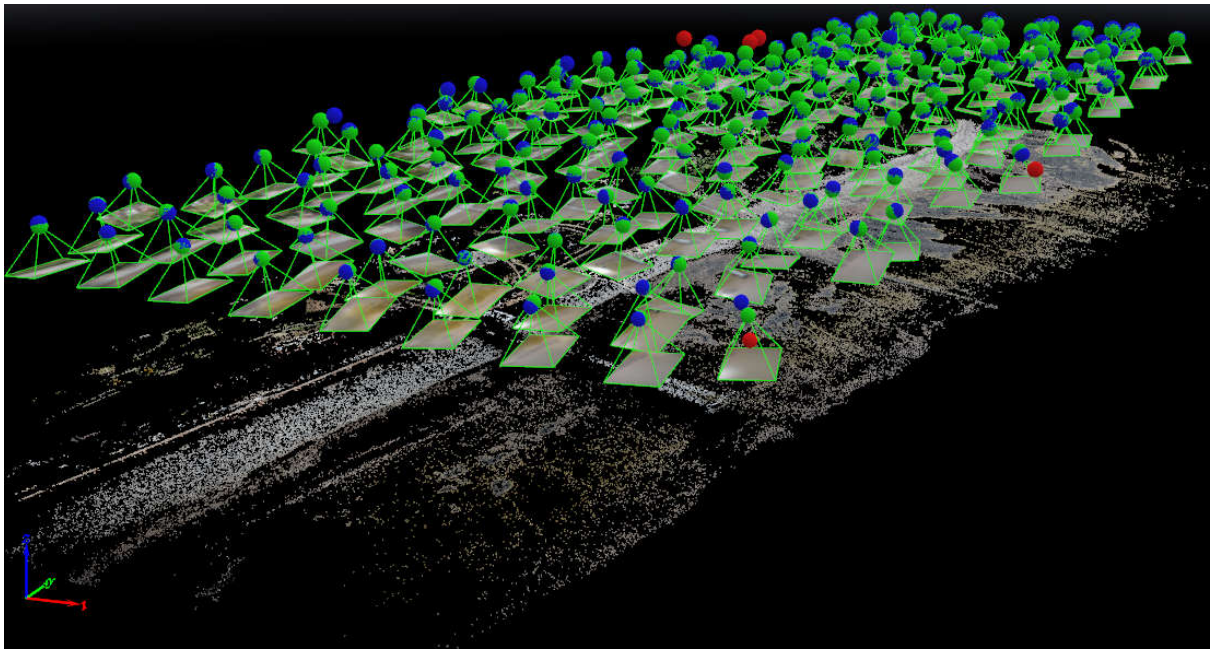

Figure 6.19 – Sparse 3D Point Cloud of Penarth shoreline with the Geotagged image position of Figure 6.17

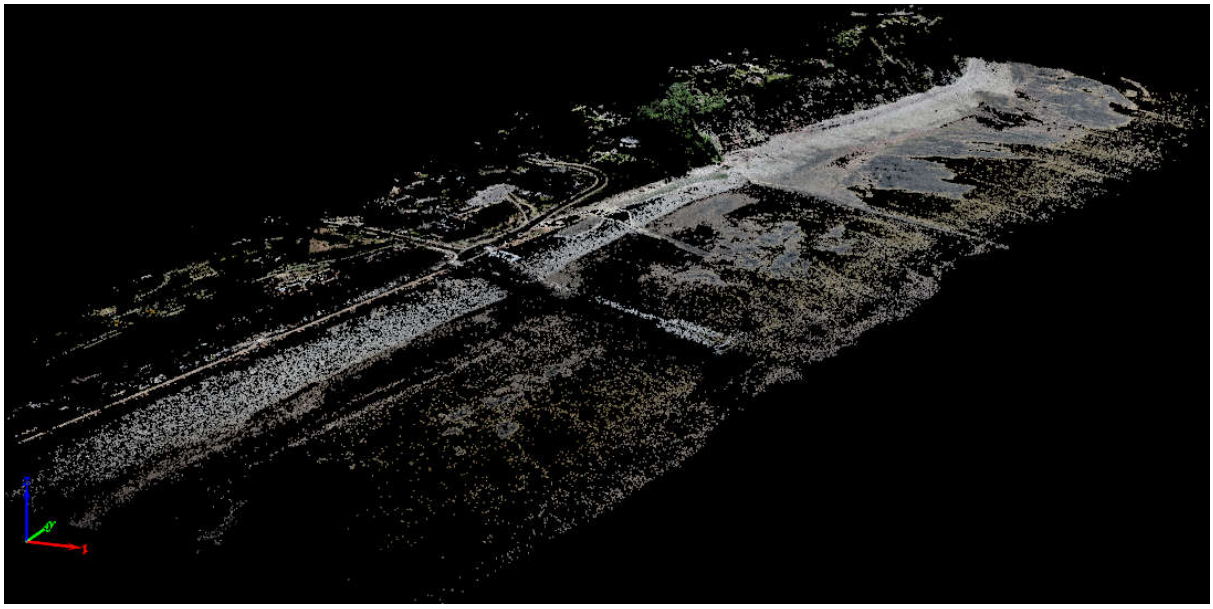

Figure 6.20 – Sparse 3D Point Cloud of Penarth shoreline (as in Figure 6.18 without the highlighted Geotagged image positions).

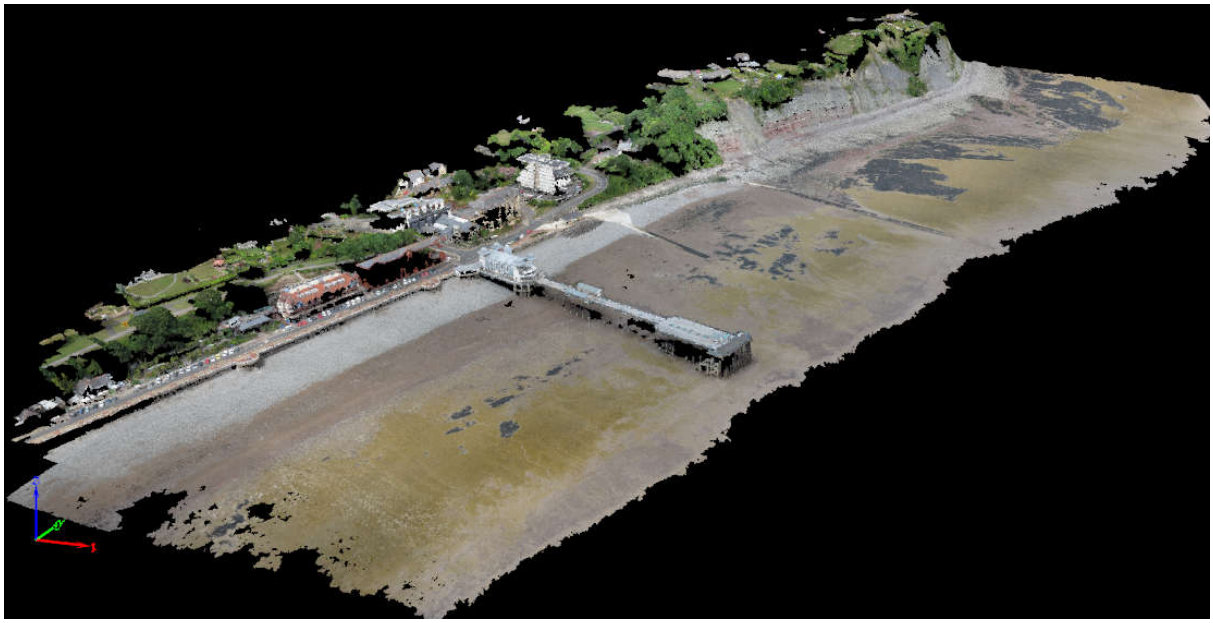

Figure 6.21 – Densified 3D Point Cloud of Penarth shoreline.

Figure 6.22 – DSM or Digital Surface Model (as a Triangulated Irregular Network) of Penarth shoreline.

6.9 Generating a set of Digital output products (Orthomosaics, DSMs, visualizations, etc.) Required for Change Analytics.

As all digital images are on the same coordinate systems, spatial manipulations are possible in the open-source Quantum GIS (QGIS) and the proprietary ArcGIS.

The very high-resolution digital model as derived from the UAVs surveys enhances the computation of volume by determining the areas of cuts and fill as explained in figures 6.22 and 6.23 below.

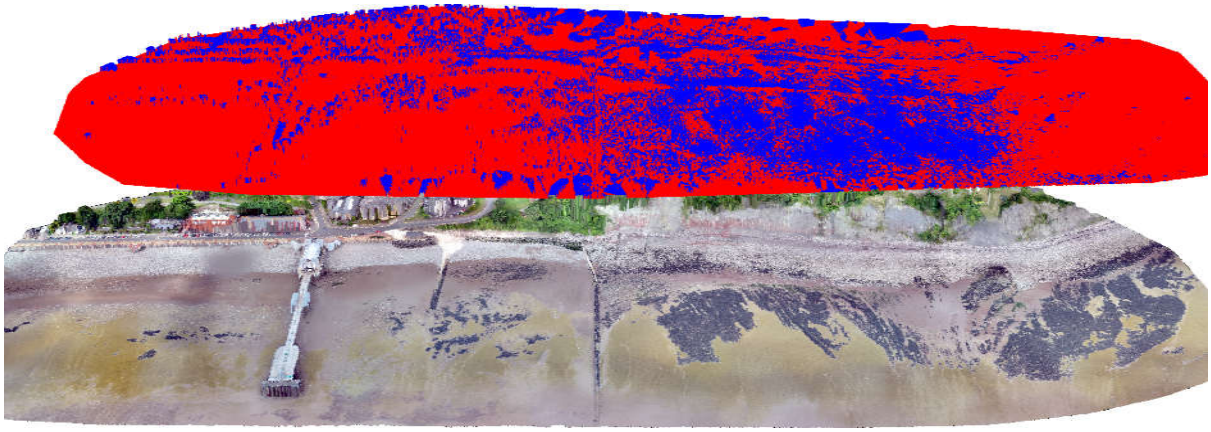

Figure 6.23 – 2015 DSM with 2016 Orthomasaic. On top is the 2015 DSM showing the areas of cut and fill and the 2016 Orthomosaic below. The red segments on the DSM are the areas of materials loss and the blue segment are the areas of material gains.

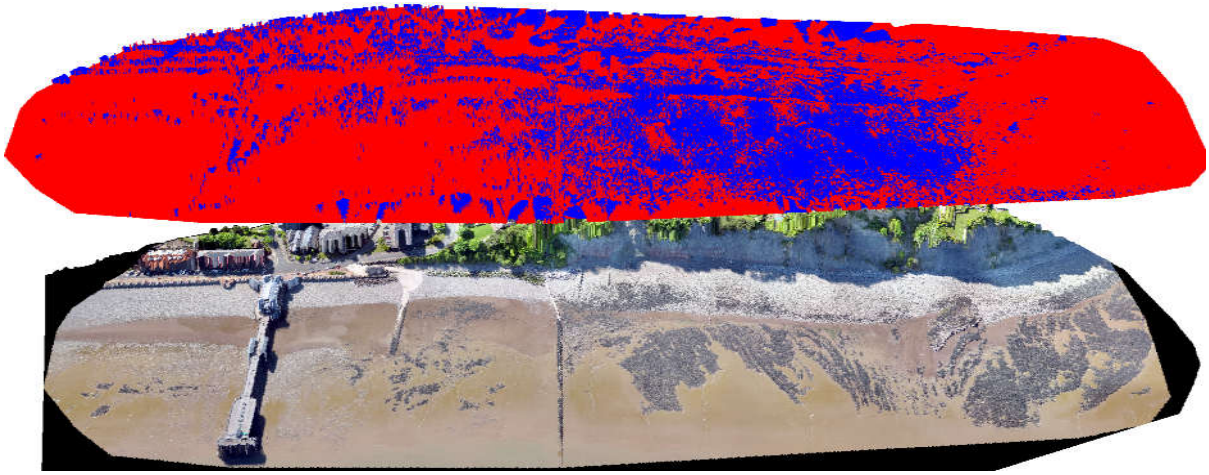

Figure 6.24 – 2016 DSM with 2015 Orthomasaic. On top is the 2016 DSM showing the areas of cut and fill and the 2015 Orthomosaic below. The red segments on the DSM are the areas of materials loss and the blue segment are the areas of material gains.

The drone survey generated high-resolution and accurate orthomosaic and digital models. These digital outputs are then analysed for change analytics. The actual area(s) of change detected between the different years are presented in detail in chapter seven.

6.10 Change Analytics

This section compares the computation of the change areas using the proprietary ArcGIS and the open-source QGIS. The results obtained validate the reliability of the QGIS in determining the areas of cut and fill, volume computation, computation of spot heights and contouring, hill-shading, and cross-sectioning.

6.10.1 Determining Areas of Change (Cut and Fill)

The aim is to create a multi-temporal transformation through image subtraction which would highlight the areas of cut and fill between two DSMs. The QGIS uses the **raster calculator** to subtract the smallest difference between the elevations of points in the DSM while the ArcMap uses the minus 3D analyst to subtract the digital values between two input rasters by cell-to-cell. Simple arithmetic operators like the addition and subtraction are with minimal uncertainties (Yamamoto et al, 2018).

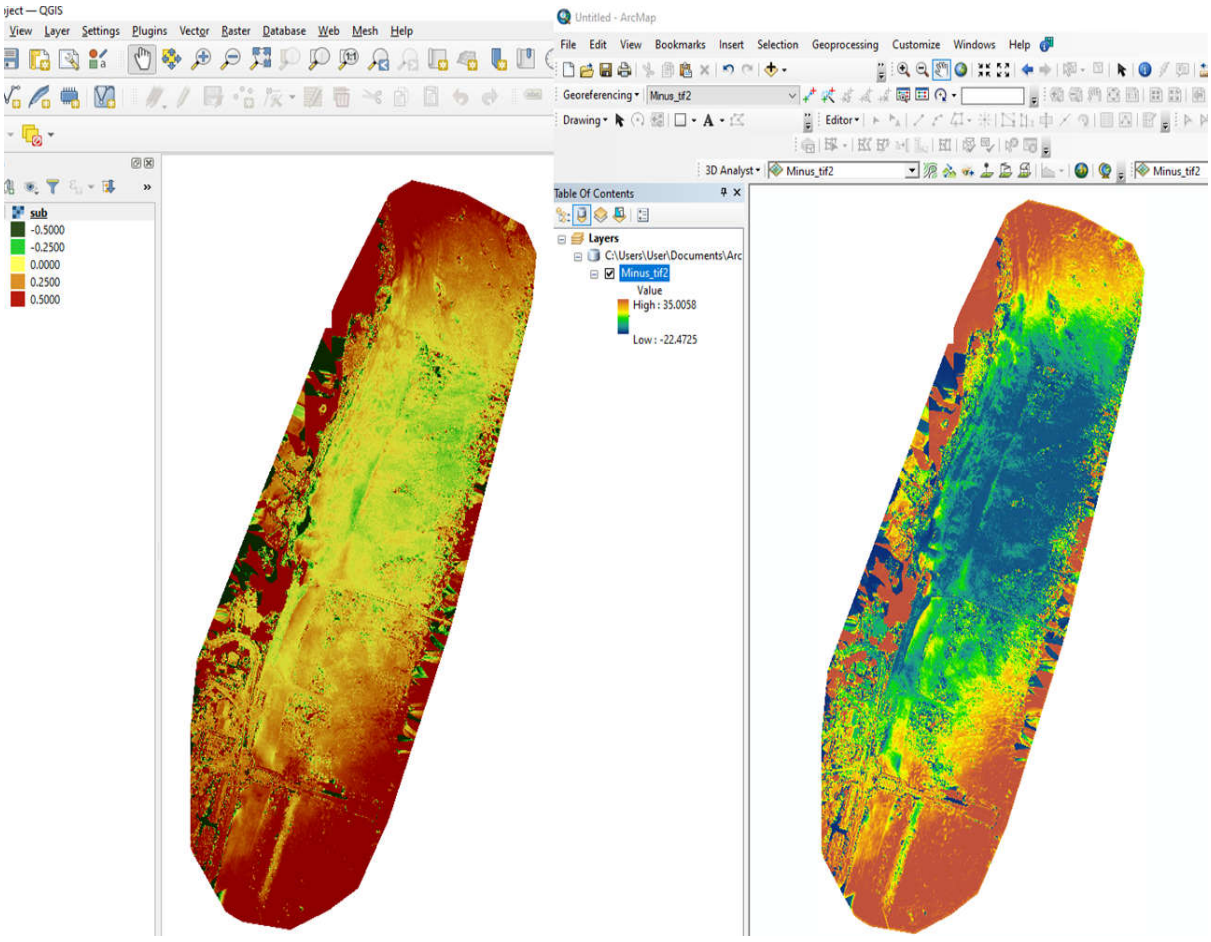

Figure 6.25 - An Example of the Subtraction and Minus Spatial Analysis Performed in QGIS (Left) and in ArcGIS (Right). This Outcome Validates the Results Obtained using the Open-Source QGIS. Further Analyses on this are in Chapter Seven.

6.10.2 A Three (3) Stage Analyses

An improvement to existing monitoring techniques is the establishment of a three-stage monitoring technique. The aim is to be able to detect a change to up to 1cm.

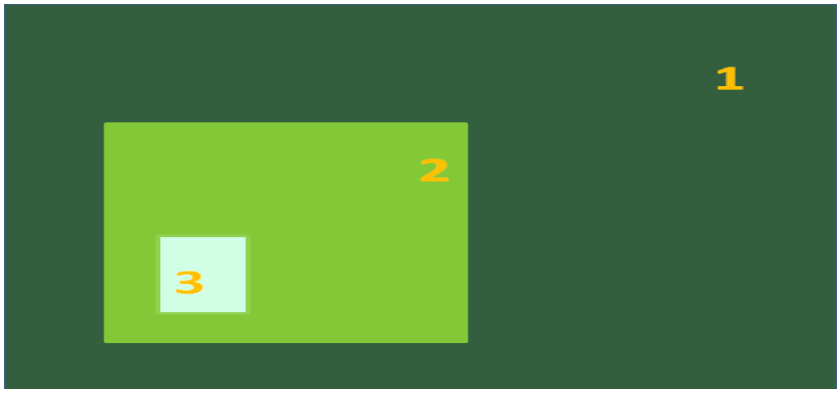

Figure 6.26 – A Three_Stage Analysis.

Stage 1 is on a small scale. It gives an overview of the coastline in detail with the help of accurate and high-resolution orthomosaics and digital models. Stage 2 in medium-scale focus on the areas where changes have occurred. Stage three is the large scale which can detect change up to 1 cm.

The extract by mask algorithm available in both the ArcMap and the open-source QGIS extract the entire cells (including the Z dimension) of the input raster as outline by the defining mask (Pathan and Agnihotri, 2019; Chamat and Anupriya, 2018). In QGIS, this facility extracts the area of interest in stage 2.

Figure 6.27 –2015 Penarth Orthomasaic below with Cropped Area on top. The crop area will be further analysed to determine the area for stage 3.

For stage 3, the digital images will be re-processed for up to 1cm accuracy or by using the extract by polygon tool depending on the accuracy of the initial digital model.

6.10.3 Volume Computation

The very high-resolution digital model as derived from the UAVs surveys enhances the computation of volume by determining the areas of cuts and fill. Our methodology improves on existing methodologies by first extracting the areas of interest between successive digital models for comparative and accurate volume computation.

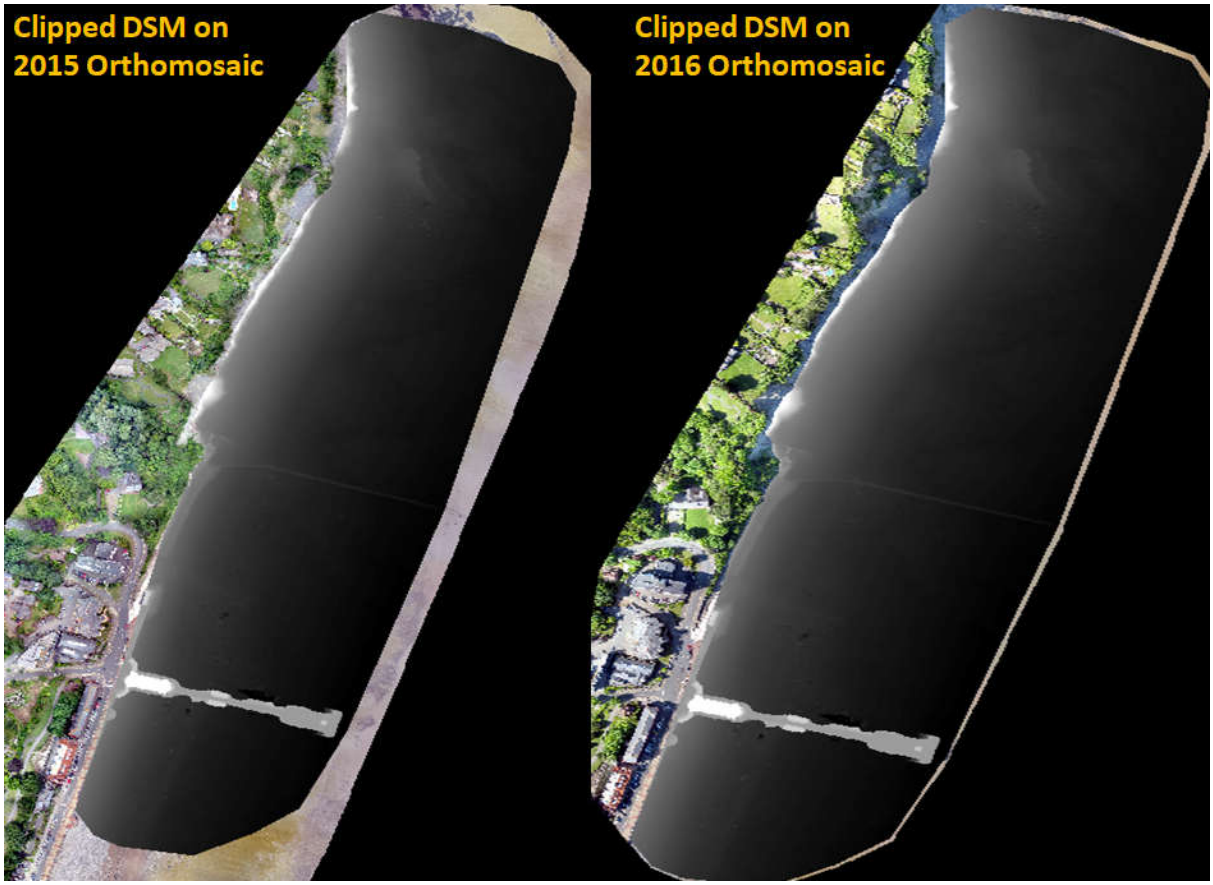

Figure 6.28 –2015 Orthomasaic below with Cropped Area on top.

The volumetric computation in both the QGIS and the ArcMap is by comparing the digital model with a base elevation. The extraction by a clipped polygon will ensure the evaluation of the same surface areas in the respective digital models. This section also compares the DEM of the area of interest with an accurate base elevation. The results using the ArcMap and the QGIS is illustrated in table 6.1 below

Table 6.1 – Results of Volume Computation using the QGIS and ArcMap. The area 1 is stage 1 while the area 2 is stage 2.

	QGIS		ArcMap	
	2015	**2016**	**2015**	**2016**
Area 1	18665.0712450m^3	18348.828167 m^3	18732.058963 m^3	18480.4875 m^3
Area 2	1263660.7675 m^3	2285252.3996 m^3	1338031.4779 m^3	2404840.3784 m^3

These results indicate the reliability of the open-source QGIS for volume computation.

6.11 Chapter Summary

This chapter crucially appraised and improved the existing methodologies for monitoring the coastline using digital photogrammetry techniques. An important feature is being able to acquire high-resolution and precise digital images with low-cost drones. The best practices of acquiring the digital images with or without the GCPs have shown the importance of this research. The results obtained also show the reliability of some low-cost and open source photogrammetry software for processing digital images.

An important coastline feature is the surface reflectance caused by water particles. The results in this chapter also show that only low altitude photogrammetry can robustly map out a dune area due to its unique spectral resolution capabilities. The drone photogrammetry also provides an absolute geometry between the control points and the spatial coverage. This implies that the permanent GCPs using ground features are realistic and precise.

This chapter improves on the existing methodologies of analyzing the coastline by introducing a three-stage analysis technique. The outcomes from analysing with the forgoing techniques are such that objects as small as 1cm can be detected, matched with other points, and analysed for change detection. The classification model developed will be used for further analyses in chapter seven.

Chapter 7

Analysis of Low-Cost UAV Photogrammetry Solutions for Beach Modelling and Monitoring

7.0 Chapter Aim

The aim of this chapter is to document the performance of the Digital Surface Models (DSMs) and orthomosaics produced from the methodology presented in Chapter Six for Penarth beach. In all cases, there is a requirement to use free and open-source software for analysing these models and visualising the outputs (e.g. erosion / accretion maps; volumetric analysis; contouring; profile cross-sections, etc.). The chapter will demonstrate that change detection can be undertaken between drone-based surveys to better understand the coastal processes which might be undergoing at Penarth, whilst also being able to compare these datasets with more traditional survey products such as LiDAR DSMs. Analytical comparisons with the LiDAR DSMs are also in terms of spatial and spectral accuracies. Finally, the chapter needs to demonstrate that the proposed UAV models have a role in future coastal mapping, monitoring and management – and are low-cost or cost-effective compared to the more traditional surveying techniques.

7.1 Chapter Objectives

1. Demonstrate the UAV (Drone) based DSMs and orthomosaics produced using the methodology presented in Chapter 6.
2. Compare the performance of the UAV outputs against more traditional and well-established coastal survey products such as LiDAR.
3. Demonstrate the analytical capabilities of UAV-based outputs for understanding the coastal morphological changes to Penarth beach over the survey period.
4. Demonstrate the analytical capabilities of large-scale UAV-based outputs for microscale analysis (i.e. sites of less than 1 square kilometre) to understand (and visualise) very small changes on the beach (e.g. sediment movement; erosion/accretion of individual features).
5. Determine an acceptable method or approach to registering UAV-based outputs to accurate and precise Ground Control Points (GCPs), say in OSGB Coordinate System.

7.2 LiDAR Digital Models for Penarth

As documented in Chapter 2, Natural Resources Wales (NRW) with support from the Welsh Assembly supports a publicly available portal of spatial datasets including LiDAR digital surface models. These datasets have become widely accepted as the preferred dataset of choice for large-scale surface analysis such as flood-risk analysis, runoff modelling, landslip/landslide analysis, and coastal monitoring (Leigh, 2008). Most of Wales has now been captured with LiDAR and the datasets are free to download for non-commercial applications under licence. The focus on the data acquisition plans for NRW is on the rivers and coast. For example, Figure 7.1 below illustrates the LiDAR data available for South Wales and the Penarth area.

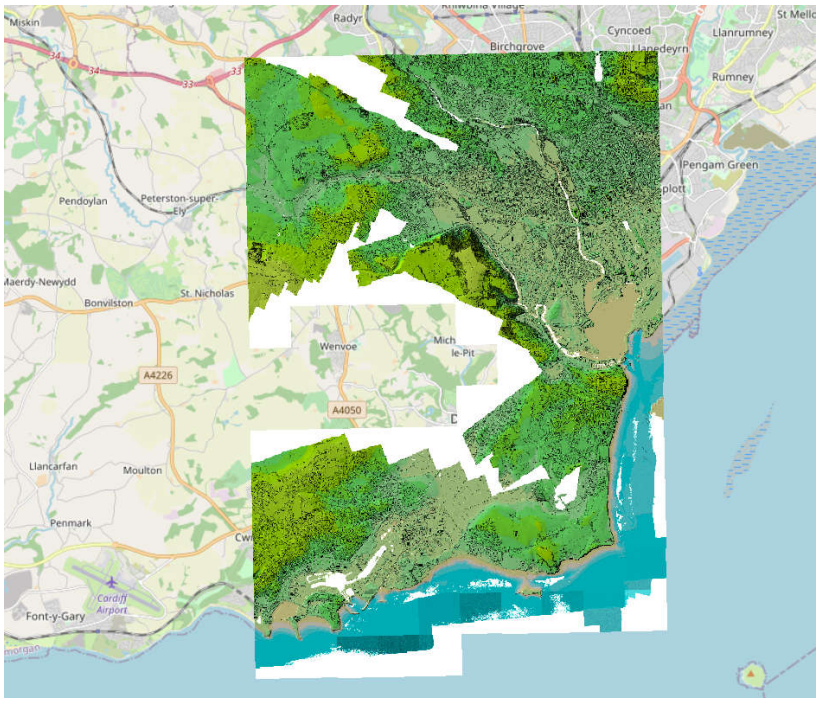

Figure 7.1 LiDAR Coverage for Penarth, Cardiff and South Wales.

The cost of LiDAR data acquisition is very expensive. Typical LiDAR surveys as documented by Leigh (13 years ago in 2008) would cost in the region of £10K for the Gower Peninsular including post-processing of the data. Repetitive surveys of a coastal area of interest are therefore not practicable. Penarth has been captured with LiDAR four times since 1998 using public money (Figure 7.2). A more realistic alternative is to hire a drone-based LiDAR survey company to capture areas such as Penarth at a cost of a few thousand pounds per day. A LiDAR based drone would cost in excess of £120,000 to buy and operate, so again is not viable for most stakeholders responsible for monitoring the coastal zone.

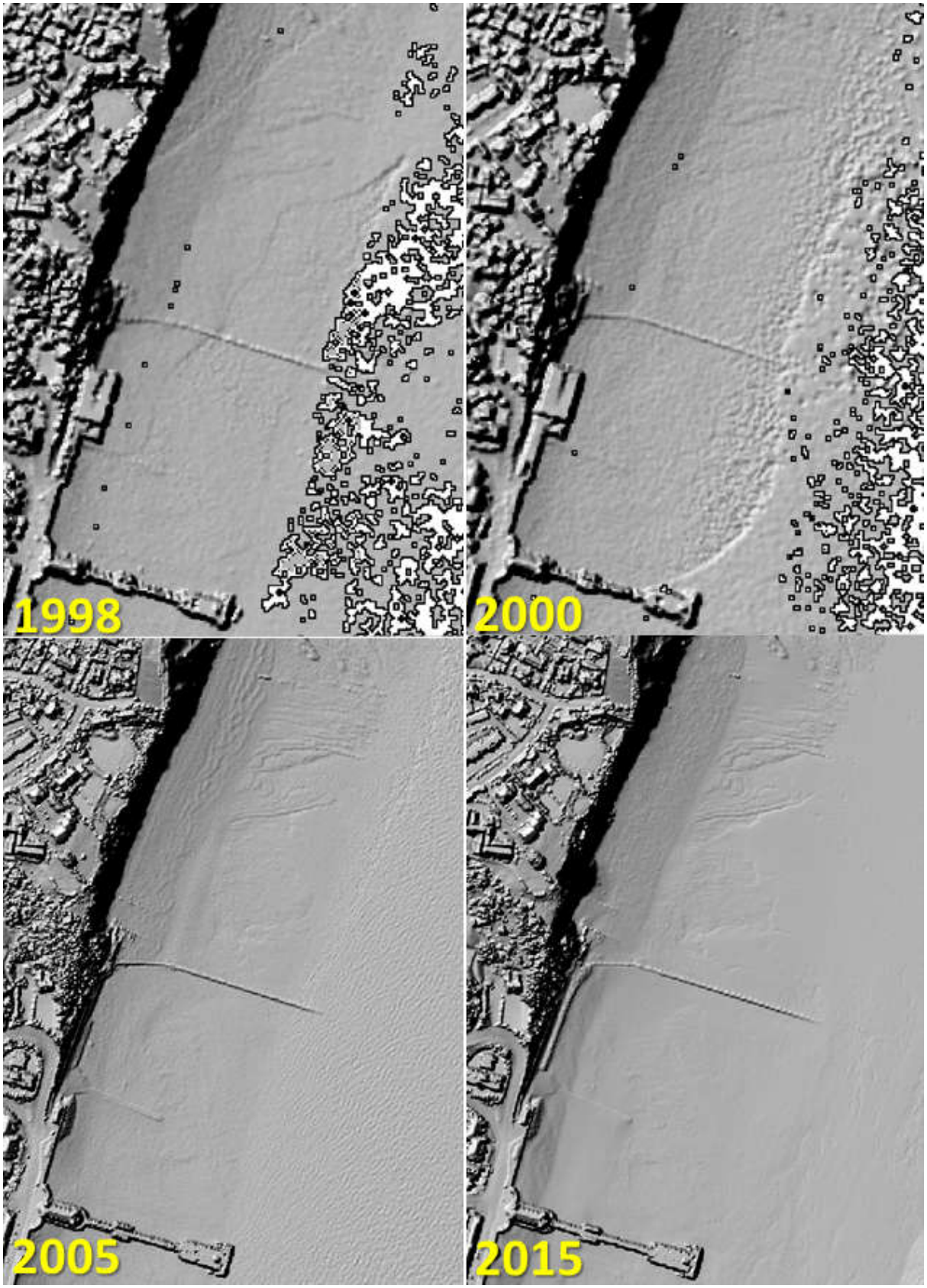

Figure 7.2 LiDAR Data for Penarth Beach (1998 and 2000 at 2m Pixel Resolution; 2005 and 2015 at 1m Resolution) Visualised as a Shaded Relief Map. Note the old multi-storey car park visible in the 1998 and 2000 surveys.

To demonstrate the use of LiDAR data for coastal analysis, consider a subset of the beach data for Penarth, whereby the datasets of Figure 7.2 are clipped to a common area, as in Figure 7.3.

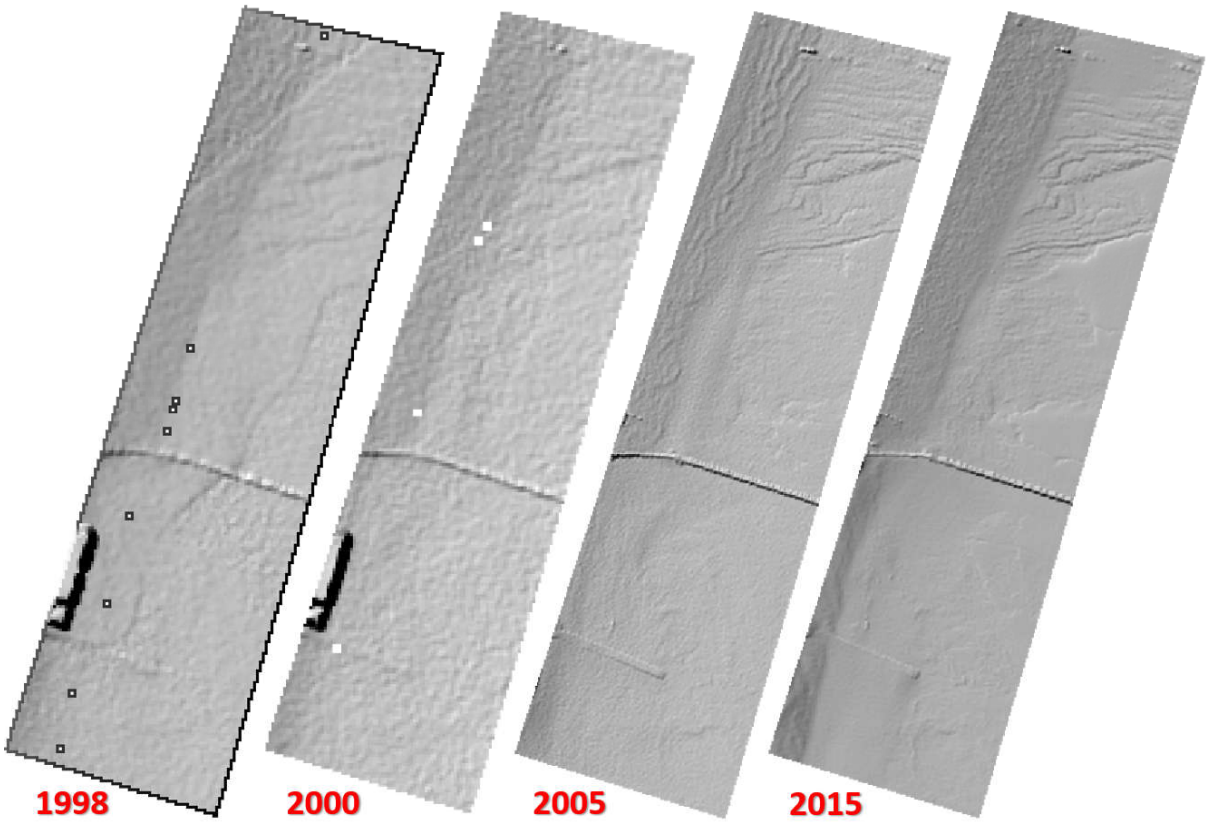

Figure 7.3 Penarth Beach LiDAR Datasets of Figure 7.2 Clipped to a Common Analysis Area.

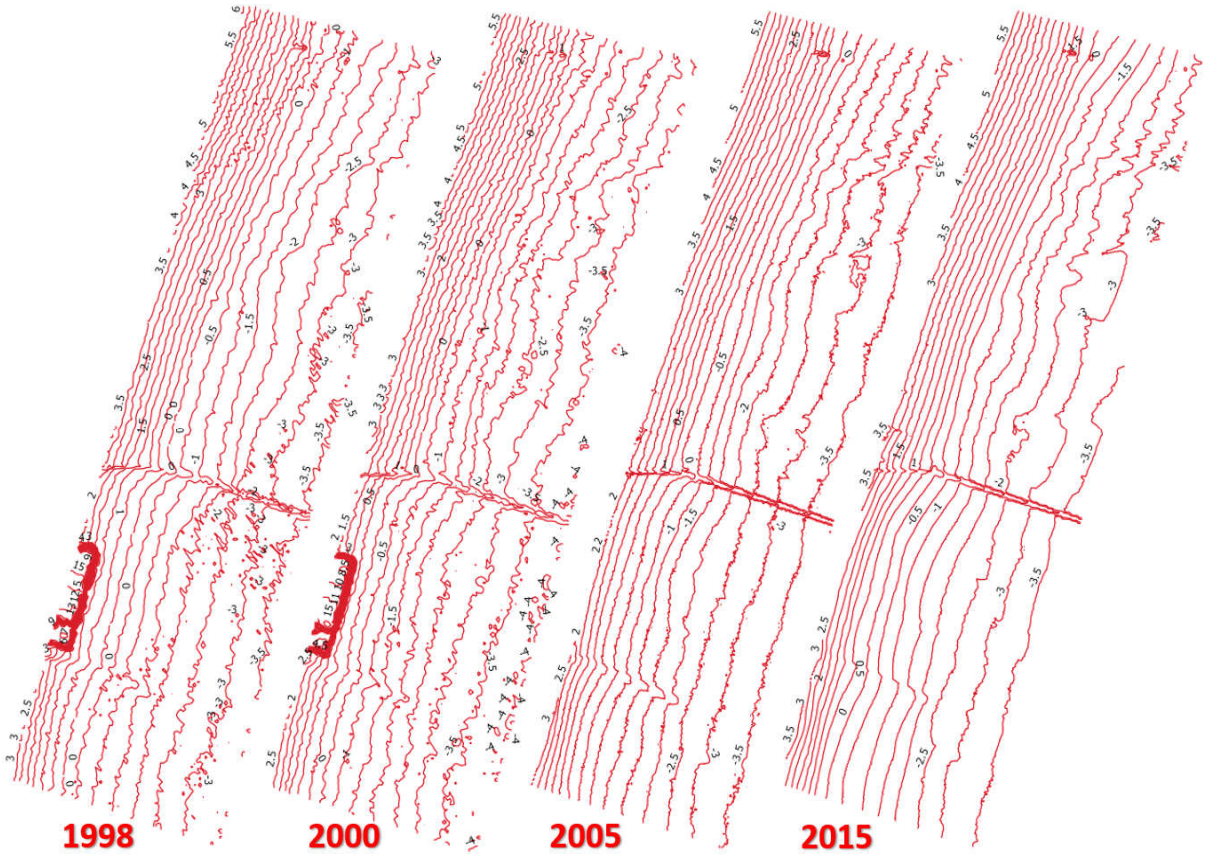

Figure 7.4 Contour Maps of Penarth Beach LiDAR Datasets of Figure 7.3.

The hill-shaded LiDAR DSMs and corresponding contour maps of Figures 7.3 and 7.4 are difficult to discern any noticeable changes. In coastal analysis it is more usual to present differences as erosion / accretion maps (Figure 7.5).

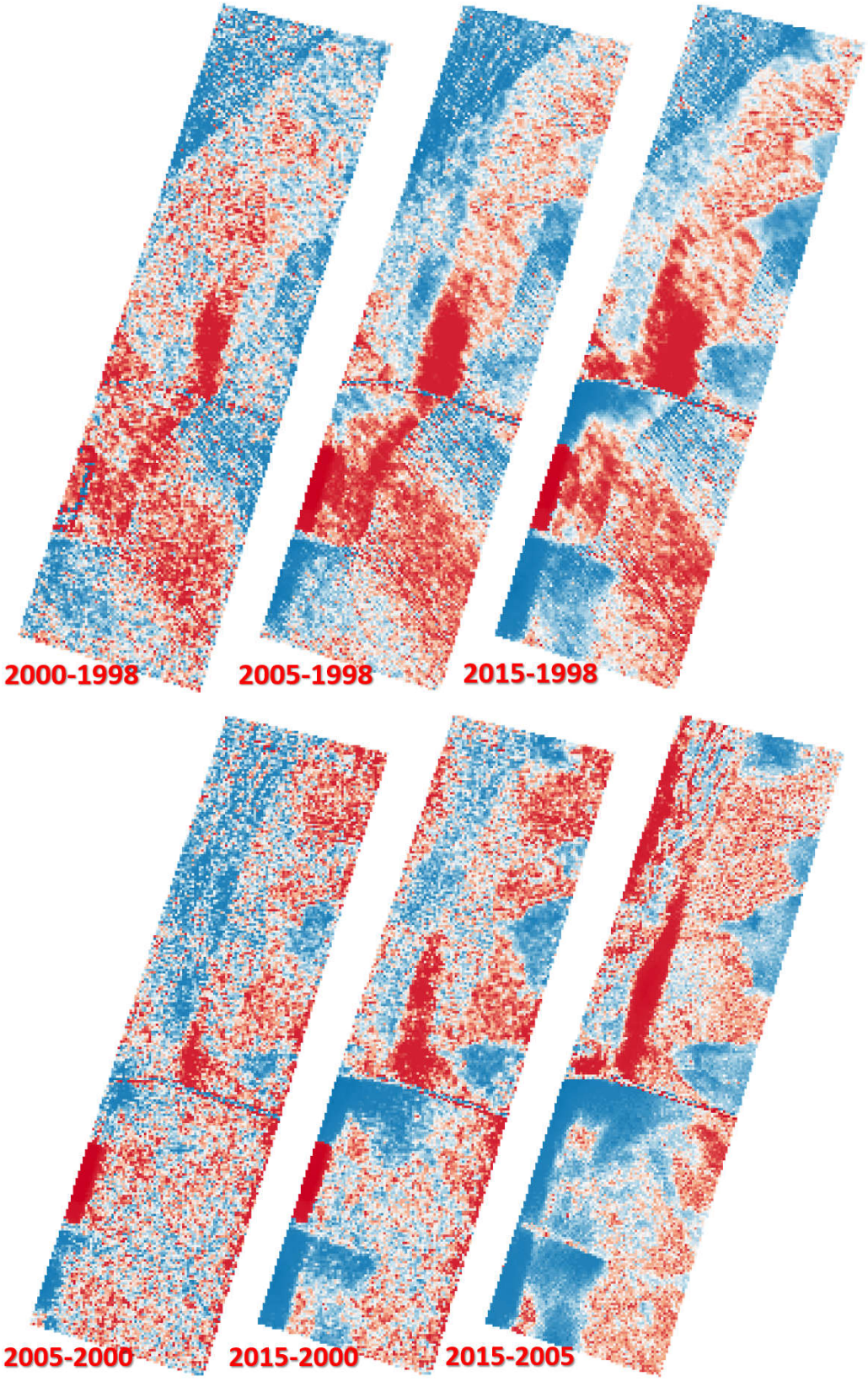

Figure 7.5. Erosion (Red) / Accretion (Blue) LiDAR Maps between the Different Surveys.

In summary, the earlier LiDAR datasets demonstrated a loss of sand, sediment and pebbles on the foreshore in front of the multistorey car park, as reported and documented by Phillips (2005). Later LiDAR surveys highlight a loss of material north of the groynes/outlet (i.e. longshore drift), but a build up of material behind these sea defences. The LiDAR datasets were deemed high resolution models (2m or 1m GSD) at the time – when digital terrain modellers were used to working with Ordnance Survey DEMs at 10m or 50m resolution. Coastal applications were crying out for such ubiquitous datasets at such resolutions. In 2021, it can be argued that such LiDAR datasets need to be further improved and developed at higher resolutions, such as the 50cm and 25cm resolution DSMs which the Environment Agency have rolled out in high flood risk areas. LiDAR serves a purpose in understanding the dynamics of coastal environments such as Penarth and seeing the trends that are occurring. There is a need though, for microscale analysis to understand not just what is happening on the beach, but what is happening in very specific areas of a beach. In the meantime, LiDAR is a great resource for understanding coastal processes at the regional level. However, the lack of regular surveys means that LiDAR is not a tool that those responsible for managing the coastal environment can rely upon. The following sections address the question of whether UAV photogrammetry is a low-cost viable alternative to LiDAR.

7.3 UAV (Drone) Models for Penarth

As outlined in Chapter 6, a number of UAV photogrammetric models have been developed for Penarth using USW drone surveys between 2015 & 2020. Not all are documented here, as the discussion will focus on three surveys of 2015, 2016, and 2020 (Fig 7.6a, Fig 7.6b & Fig 7.6d). A further 2020 survey (Fig7.6c) will be discussed later in the context of comparing two very high resolution surveys within 48 hours with the aim of identifying very small changes in the foreshore environment. For each dataset, raw UAV images are processed to produce a variety of output products, including a DSM; an orthomosaic; point clouds; animated flybys; and for sharing visualizations – Google Earth KML mosaics, and a 3D PDF for interactive exploration of the 3D models. Point cloud management and visualization software is now more widely available which use optimized data engines for handling millions of data points or rendered triangulated irregular networks or TINs (see Figure 7.7). The range of output products depends upon the software environment used to photogrammetrically process the images. In general, the open source solutions produce a

basic set of data outputs which can then be visualised and analysed in other open source software. For these datasets, most of the analysis is undertaken in Quantum GIS– a free and open-source Geographical Information System.

Figure 7.6a Penarth UAV 3D Photogrammetric Model 16th July, 2015.

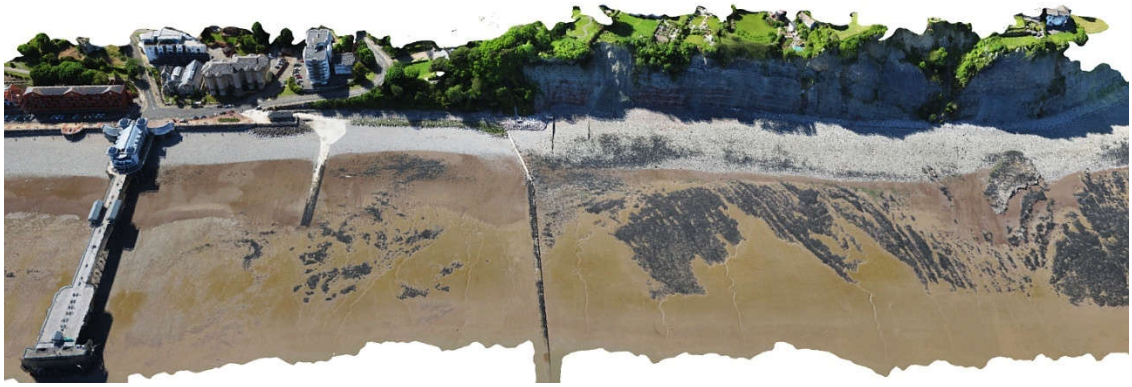

Figure 7.6b Penarth UAV 3D Photogrammetric Model 27th May, 2016.

Figure 7.6c Penarth UAV 3D Photogrammetric Model 31stJuly, 2020.

Figure 7.6d Penarth UAV 3D Photogrammetric Model 2nd August, 2020.

Figure 7.7 Rendered Triangulated Irregular Network (TIN) of 3D Point Cloud (Penarth 2020) Which Allows for Real-time Exploration of the Landscape.

As in Section 7.2, subsets of the models are clipped to a common area of the beach for more detailed analysis (Figure 7.8). Unlike LiDAR, the UAV models generate very high-resolution RGB imagery or point clouds for visual inspection of the surfaces to help understand the differences between surveys.

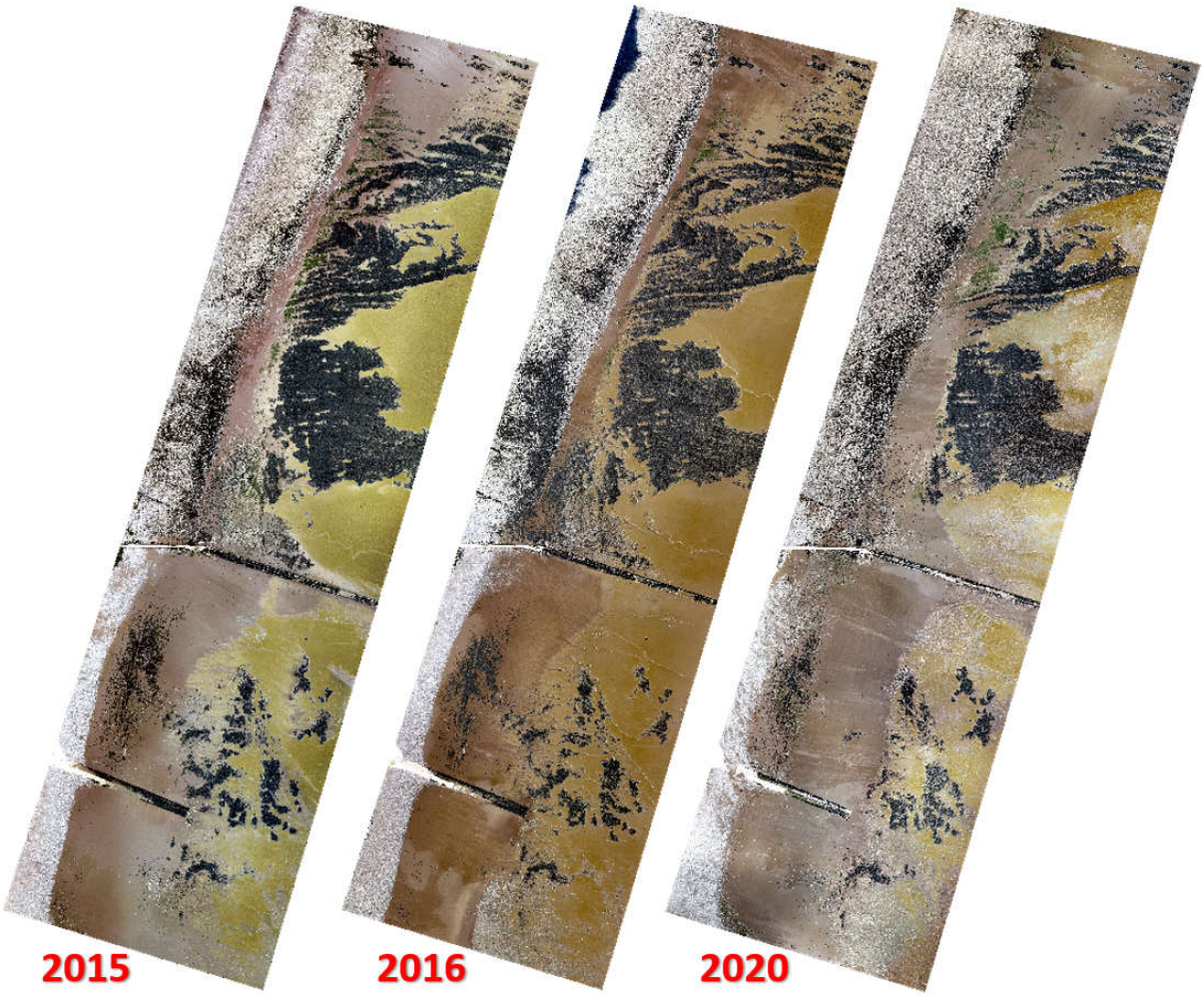

Figure 7.8 – UAV Orthomosaics of the 2015, 2016 and 2020 Clipped Datasets.

This is stage 2 of the three-stage analysis in chapter 6 (figures 6.26 and 6.27).

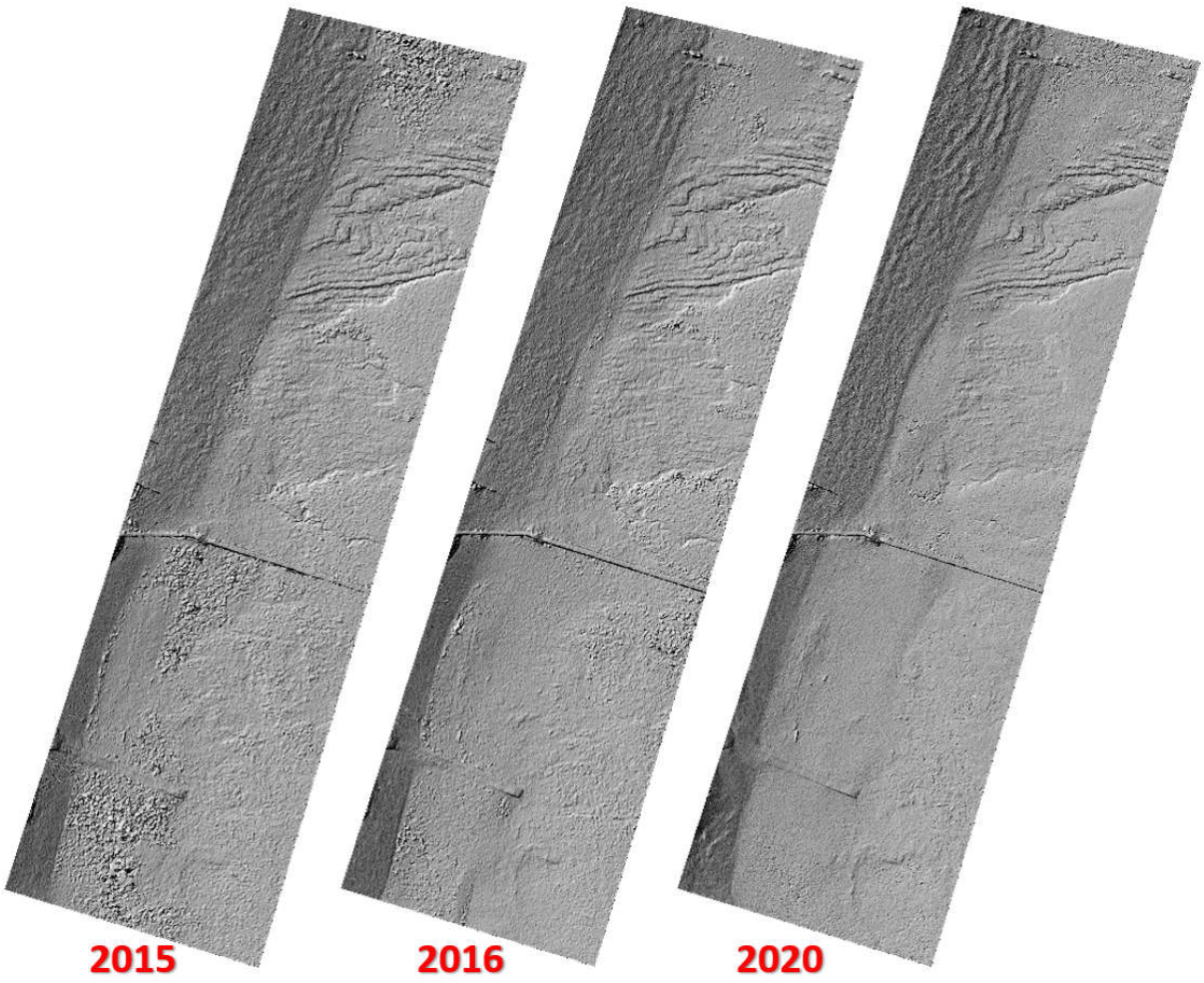

Figure 7.9 – UAV Hill-Shaded Relief Models of the 2015, 2016 and 2020 Clipped Datasets.

As in Section 7.2, the erosion and accretion maps can be generated for the differences between 2020 and 2016 (Figure 7.10), 2020 and 2015 (Figure 7.11) and 2016 and 2015 (Figure 7.11). A better understanding of the results can be accompanied with a visual presentation of the orthomosaics.

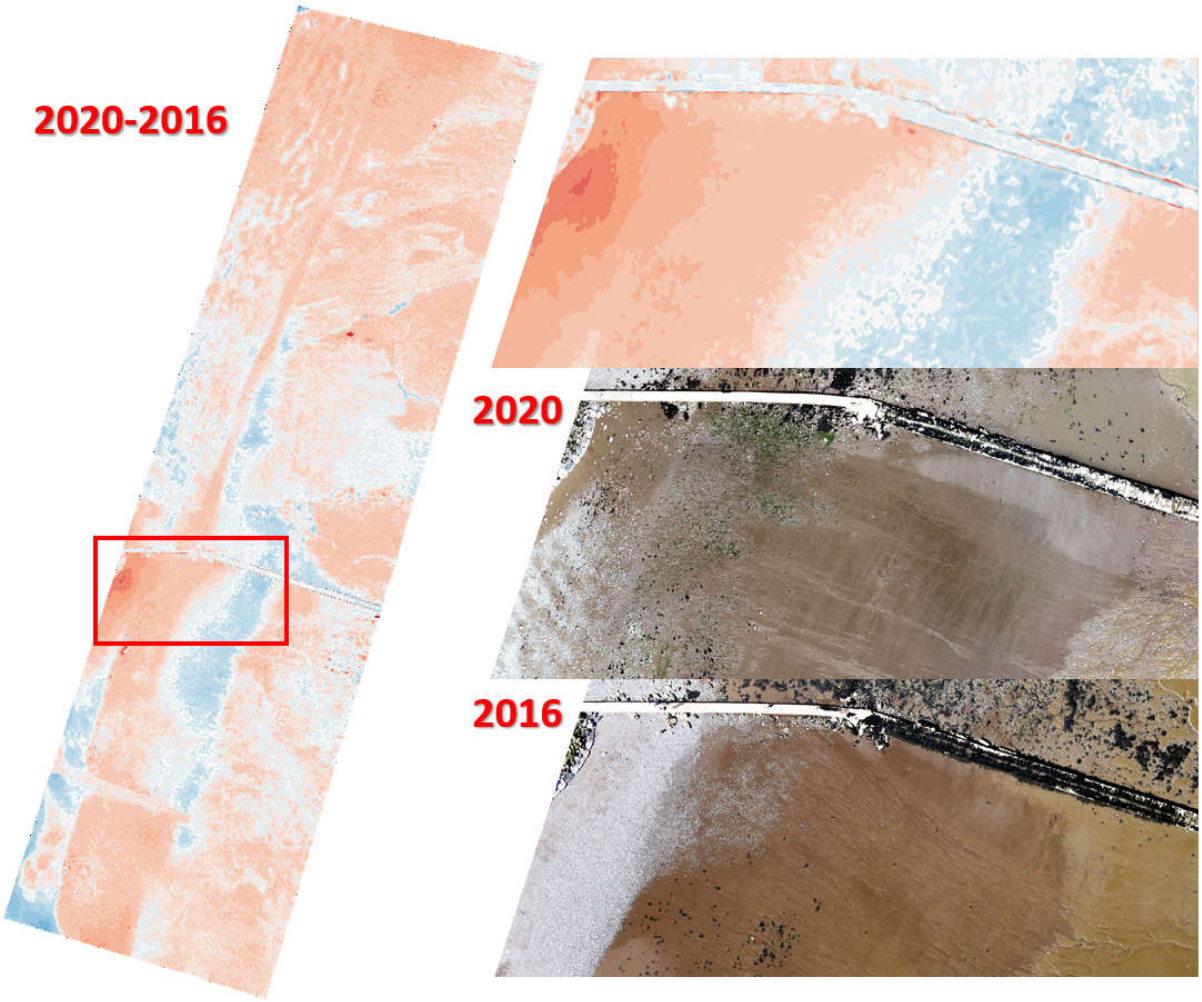

Figure 7.10 Erosion & Accretion Map for the UAV Photogrammetrically Derived Models Between 2020 and 2016. Overall, the map suggests that there is a net loss between the two surveys, but the average loss across the whole of the AOI is about 2cms (as the colour scale is quite small, i.e. any loss is recorded in pink). The Inset maps illustrate a close up view of the area of greatest loss. As can be seen from the orthomosaic, a large amount of pebbles/shingle has been lost since 2016.

(Stage 3 of the three-stage analysis).

Additional uniqueness is the digital models figure 7.6a, 7.6b, 7.6c, and 7.6d provide further visual inference on the insert maps attached to the erosion and accretion maps in figure 7.10 above and 7.11 and 7.12 below. The all-inclusive transition does not only provide cost-effectiveness but improves the overall geometric accuracies.

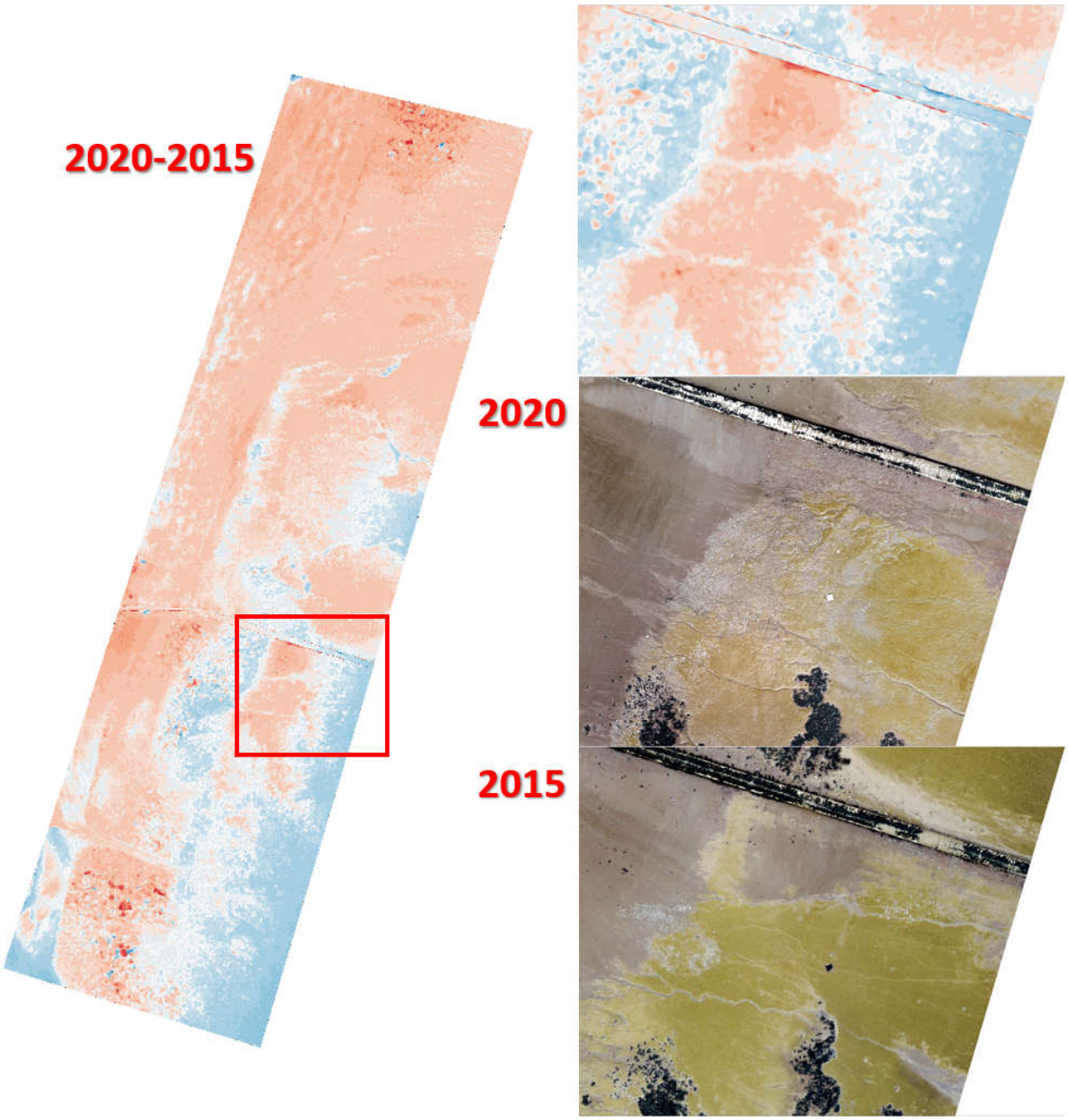

Figure 7.11 Erosion & Accretion Map for the UAV Photogrammetrically Derived Models Between 2020 and 2015. Overall, the map suggests that there is a net loss between the two surveys, but the average loss across the whole of the AOI is about 8cms (as the colour scale is quite small, i.e. any loss is recorded in pink). The Inset maps illustrate a close up view of the area south of one of the outlet casings (cf. groyne) which illustrates intermittent gains and losses in sediment. In general, areas north of this casing have experienced the greatest losses, whilst areas south of this have recorded sediment gains.

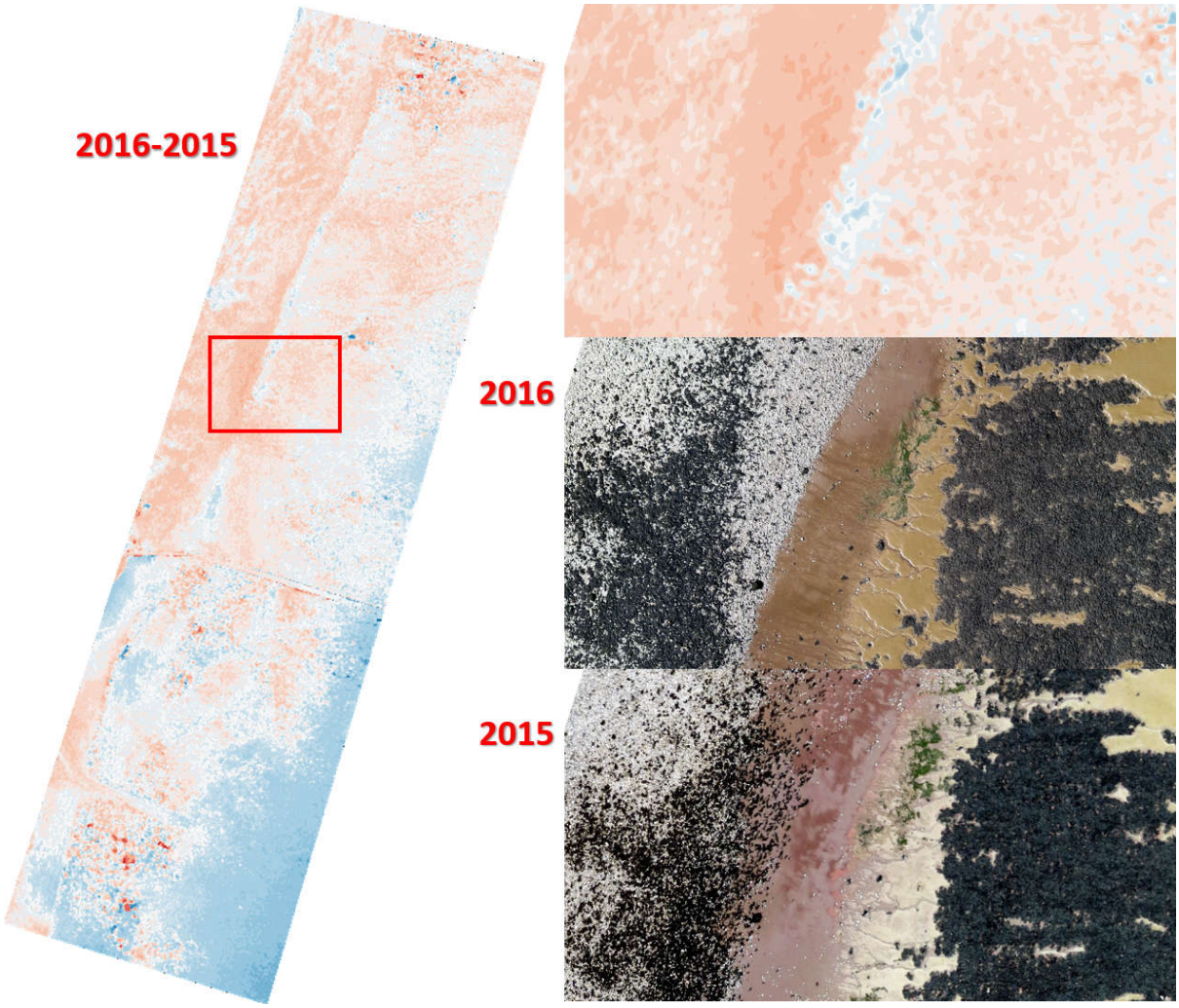

Figure 7.12 Erosion and Accretion Map for the UAV photogrammetrically Derived Models Between 2016 and 2015. Again, the map demonstrates a net loss of sediment north of the outlet casing and a net loss south of this. The inset map illustrates an area of net loss, but the orthomosaic shows an increase in shingle and stone. However, whilst that may be the case, the underlying sand levels are significantly lower than in 2015.

The analysis of Penarth beach using these datasets shows some interesting trends and morphological changes on the foreshore. This section has demonstrated that analyses can be undertaken at much finer scales than LiDAR data. As one further exercise, the LiDAR data is also compared against the UAV-derived DSM in Figure 7.13. However, the LiDAR data is taken at face value in this experiment, as no validation of the quality or accuracy of the LiDAR data has been performed. The following section will consider much finer analysis of the UAV datasets.

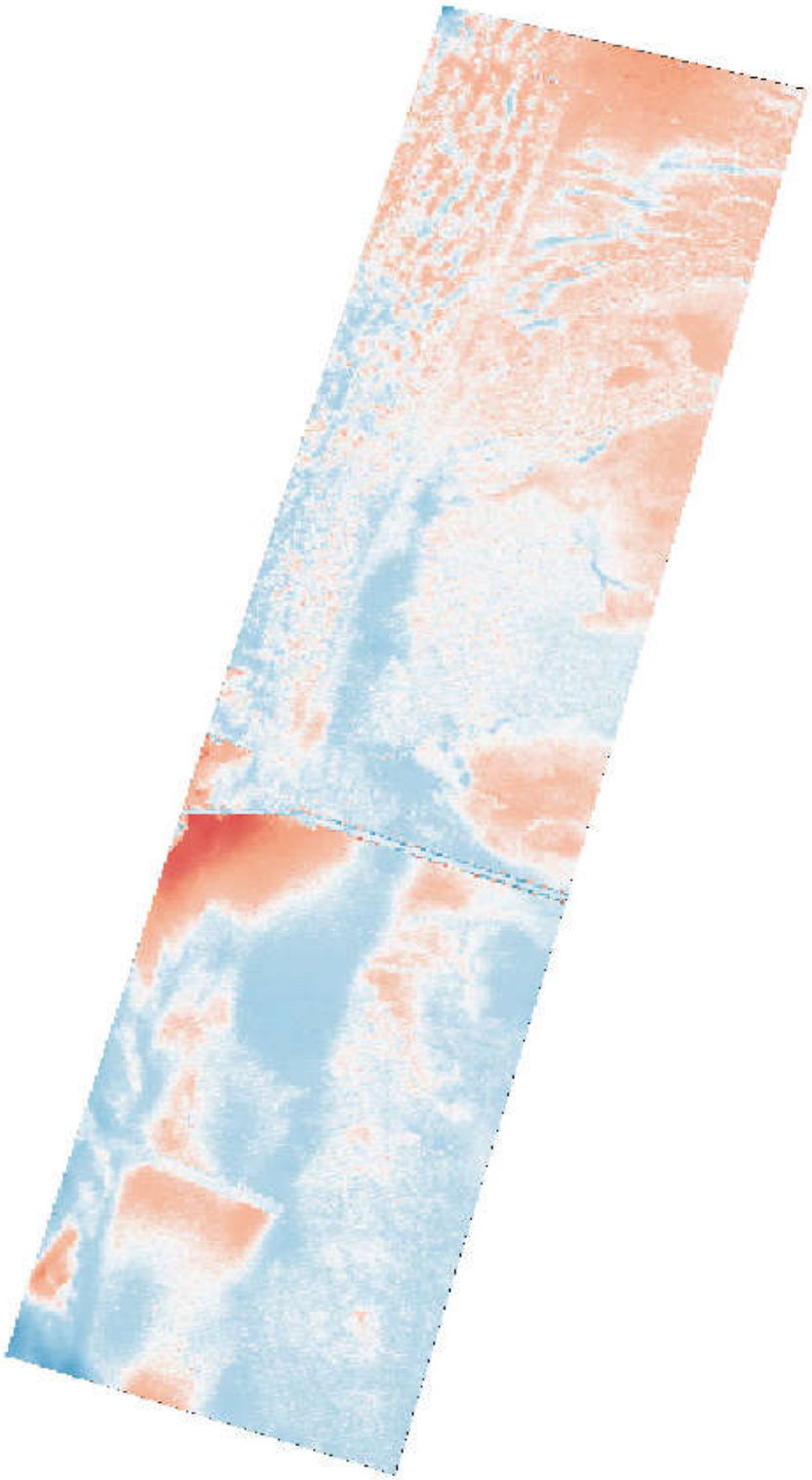

Figure 7.13 Erosion and Accretion Map for the UAV Photogrammetrically Derived Model of 2020 in Comparison to the 2015 LiDAR Dataset. Disclaimer: No validation of the accuracy of the LiDAR dataset has been undertaken. However, there are clearly some trends in relation to the groynes that suggest such analysis is valid.

7.4 Large Scale Analysis of UAV Datasets for Penarth

Consider the two UAV orthomosaics (Fig. 7.14) captured 48 hours apart. What's changed?

Figure 7.14 UAV Orthomosaic for Penarth - Top: 31st July 2020 Bottom: 2nd August 2020.

Figure 7.14 above illustrates two UAV orthomosaics captured on Friday July 31st 2020 and Sunday August 2nd 2020 (48 hours apart). These solely focus on a zoomed in section of the datasets of Figure 7.6c and 7.6d above respectively. The high tide prior to the first survey was at 10.08m, with subsequent tides at 10.24m, 10.45m, 10.82m, and 10.93m before the second survey. Weather over the 48 hours was very calm, light southerly winds of less than 10mph, and generally warm (maximum of 30 degrees Centigrade on July 31st).

The answer to the above question "what's changed?" is presented below in Figure 7.15 as an erosion / accretion map. A visual inspection of Figure 7.14 above might have noticed that the tree trunk close to the cliff face north of the groyne had moved in a southerly direction (and somebody had placed some UAV surveying equipment on the beach!). Otherwise, it is difficult to ascertain much in the way of physical changes. However, Figure 7.15 suggests that some other changes have occurred. Hopefully, it is noticeable that the movement of the tree trunk is recorded as a red blob in its previous location (i.e. a loss) and a blue blob (i.e. a gain) in its new position.

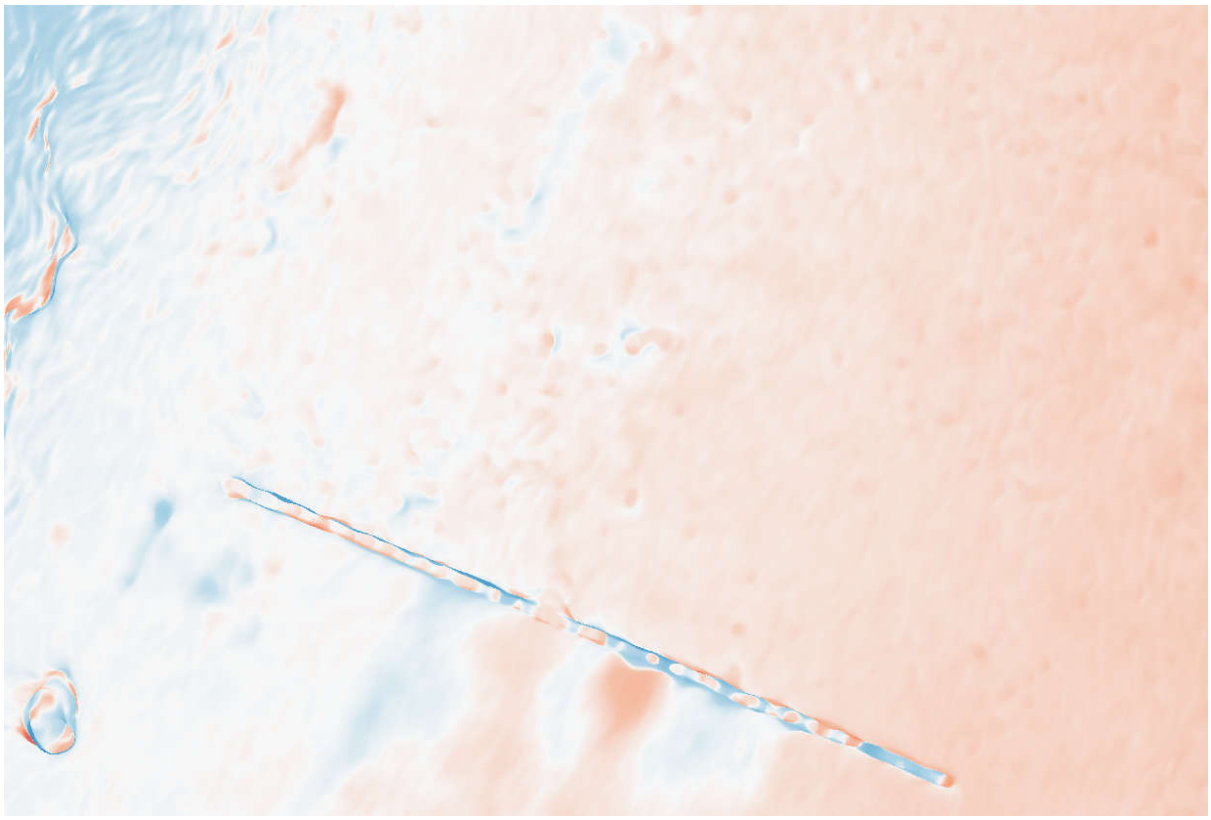

Figure 7.15 – Erosion / Accretion Map for the two Surveys of Figure 7.14 (48 hours apart).

The cliff face is represented in blue (a gain), but should not be taken as accurate, since surveying a near vertical structure from a sensor being flown 120 metres above the beach and parallel to it, will only capture a small proportion of points on the cliff surface. Similarly, the large bush in the bottom left of the maps/images appears both blue and red as some points will be captured differently in the two surveys, i.e. it's not a well-defined object for photogrammetry – nor is any vegetation for that matter. The features close to the cliff face including the tree trunk are illustrated below in Figures 7.16 and 7.17.

However, the foreshore should be captured accurately in both surveys, so the predominant pinks and reds suggest that there has been a small loss in sediment over the 48-hour period. The colour scale is defined in centimetres, but nonetheless, the easterly area of this map space suggests that there is a loss in the foreshore of up to 5 cms. Similarly, the area of greatest change in Figure 7.15 is the red patch just below the groyne. This is worthy of greater examination in Figures 7.18 and 7.19. Essentially, the difference map (erosion/accretion) calculation is suggesting that there has been a significant change in sediment in this vicinity, but not immediately clear from the orthomosaics themselves.

On closer inspection, it is worth examining the concrete support (or step) perpendicular to the groyne. In the second figure of 7.18 the corresponding step on the south side of the groyne is partly exposed (as proven by the red patch in the difference map at this location). Sediment has been moved to expose this step. Of more interest is the larger red blob. From the orthomosaics in Figure 7.18, it is not instantly clear what has changed or to what extent. By looking at the shaded relief map for the corresponding UAV DSMs (see Figure 7.19) it is easier to see the volume of sediment on this part of the foreshore. In the top figure, the sediment appears as a slight mound, which in the second survey has disappeared (or been dispersed).

The amount of sediment loss can be examined further using other traditional analytical tools such as digital contouring and profiling (Figures 7.20 and 7.21). Both datasets are contoured in Figure 7.20, so the differences can be examined more easily than using the erosion/accretion (difference) map. In the location of the larger red blob, there is a three-contour difference (of 5 cms each = 15 cms difference) while northwards of the groyne there is evidence of a longshore drift of 5cms of sediment. These are further visualised as cross-sections either side of the groyne in Figure 7.21.

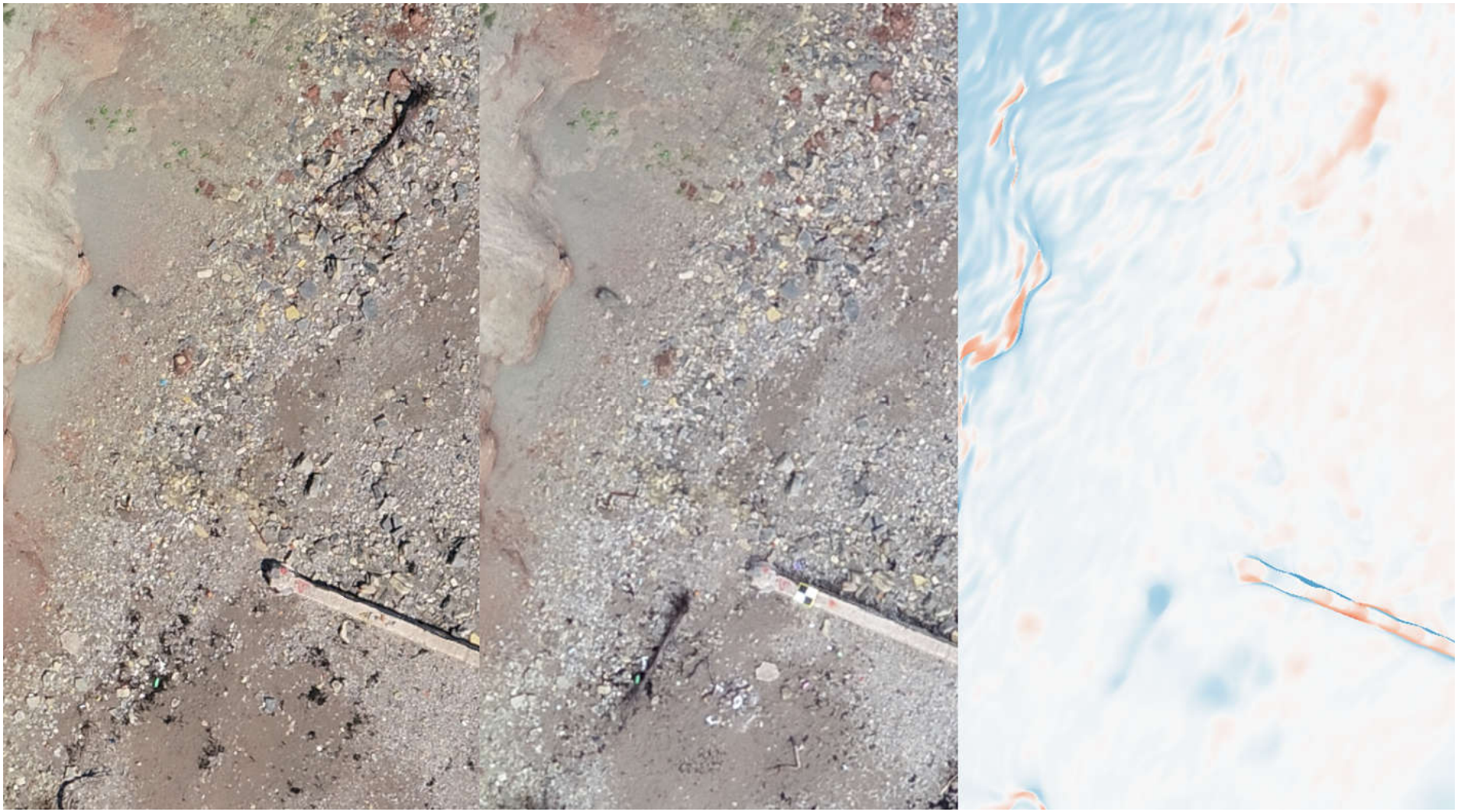

Figure 7.16 Zoomed section of the beach near to the cliff face highlighting the movement of the tree trunk and the corresponding erosion/accretion map. (Left: Survey 1; Middle: Survey 2: Right: Difference Map).

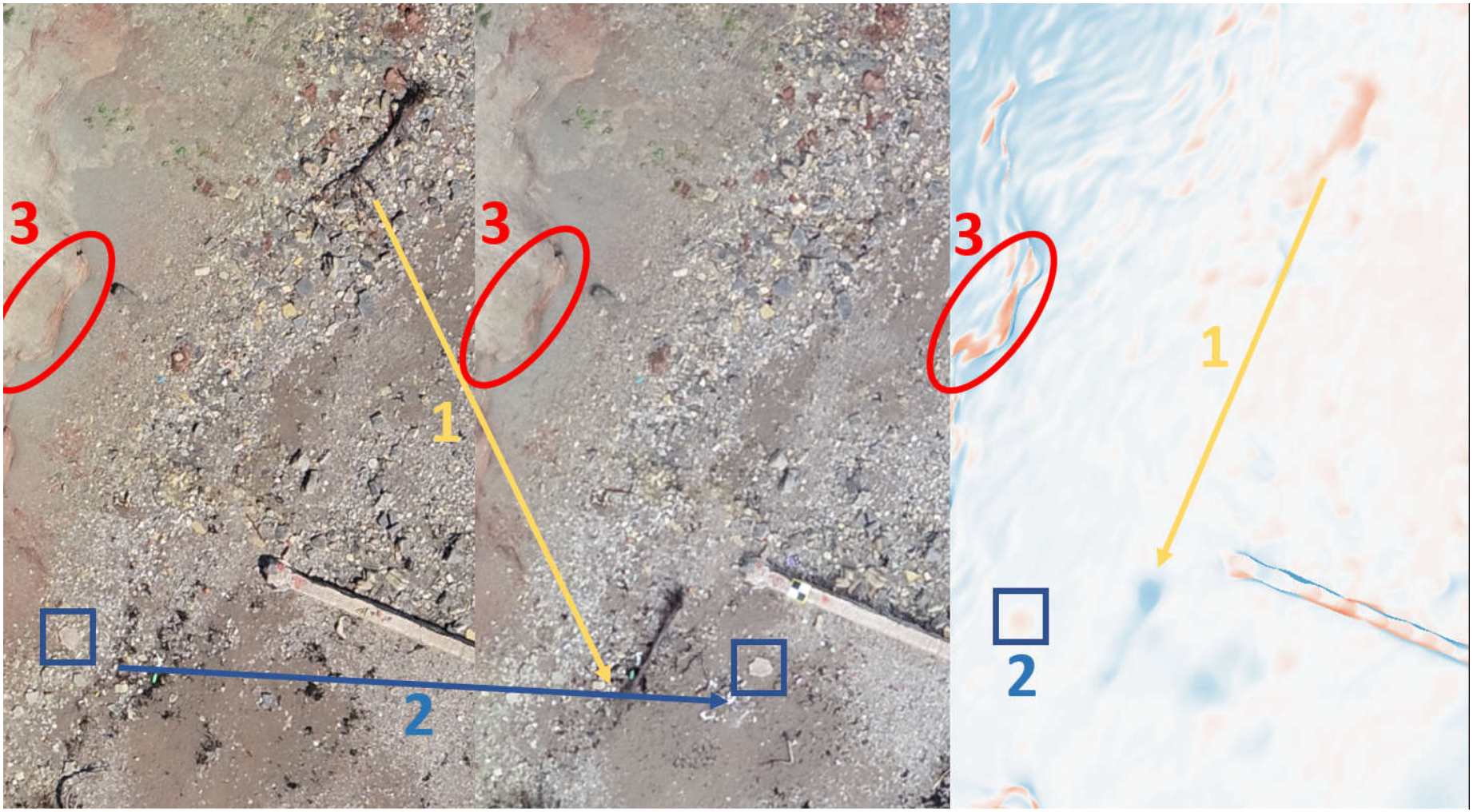

Figure 7.17 Zoomed Section of the Beach Near to the Cliff Face Highlighting the Movement of the Tree Trunk (1); the movement of a slab of rock (2) which is identified as a loss (slight pink) in the difference map; and some displacement of the very fine stones/scree at the base of the cliff (3). (Left: Survey 1; Middle: Survey 2: Right: Difference Map).

Figure 7.18 Close-up View of the Area around the Groyne. (Survey 1, 2 and Difference Map respectively).

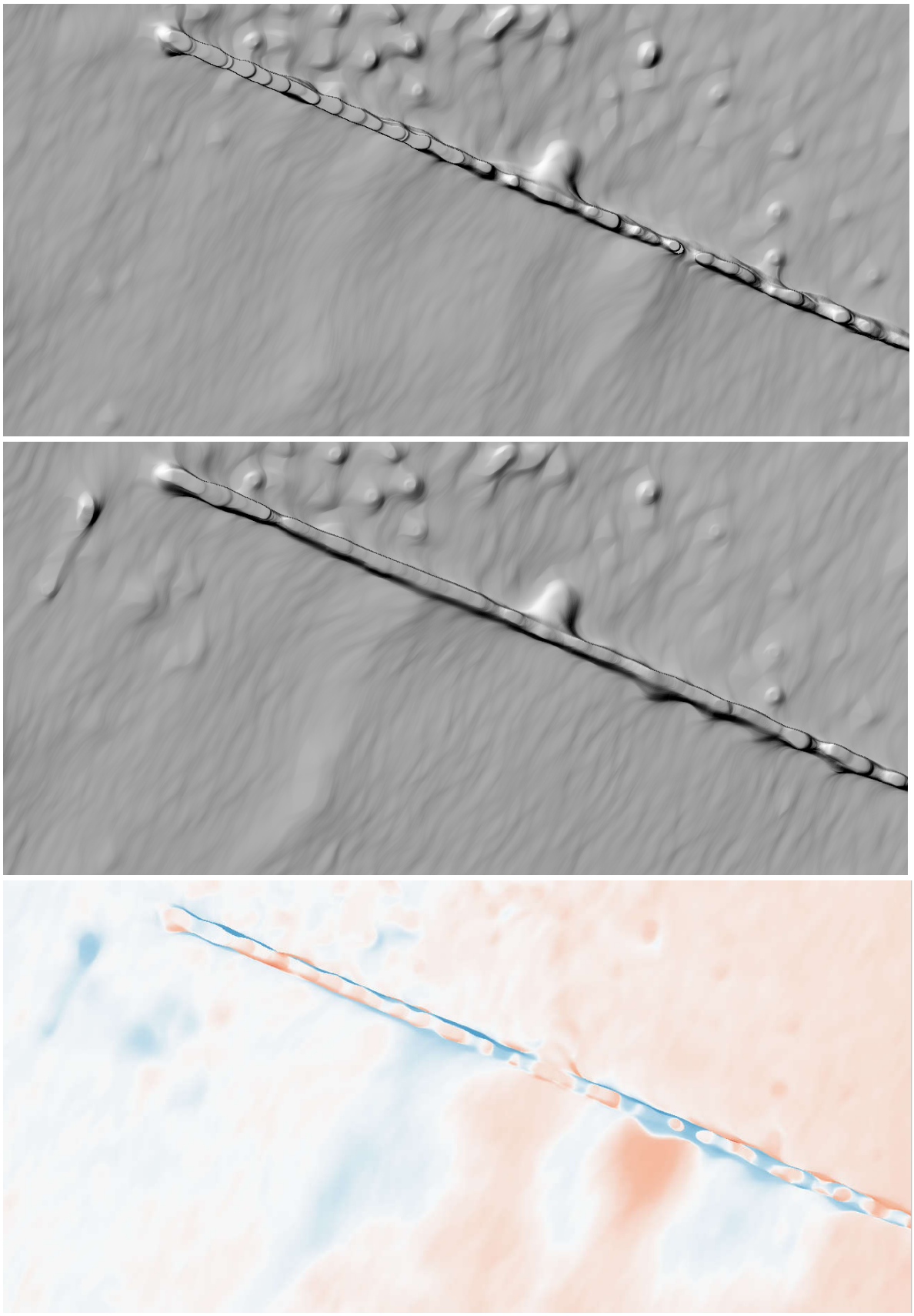

Figure 7.19 TOP: Hillshade of DSM 31st July 2020, MIDDLE: Hillshade of DSM 2nd August 2020, BOTTOM: Erosion (Red) / Accretion (Blue) Over the 48-Hour Period.

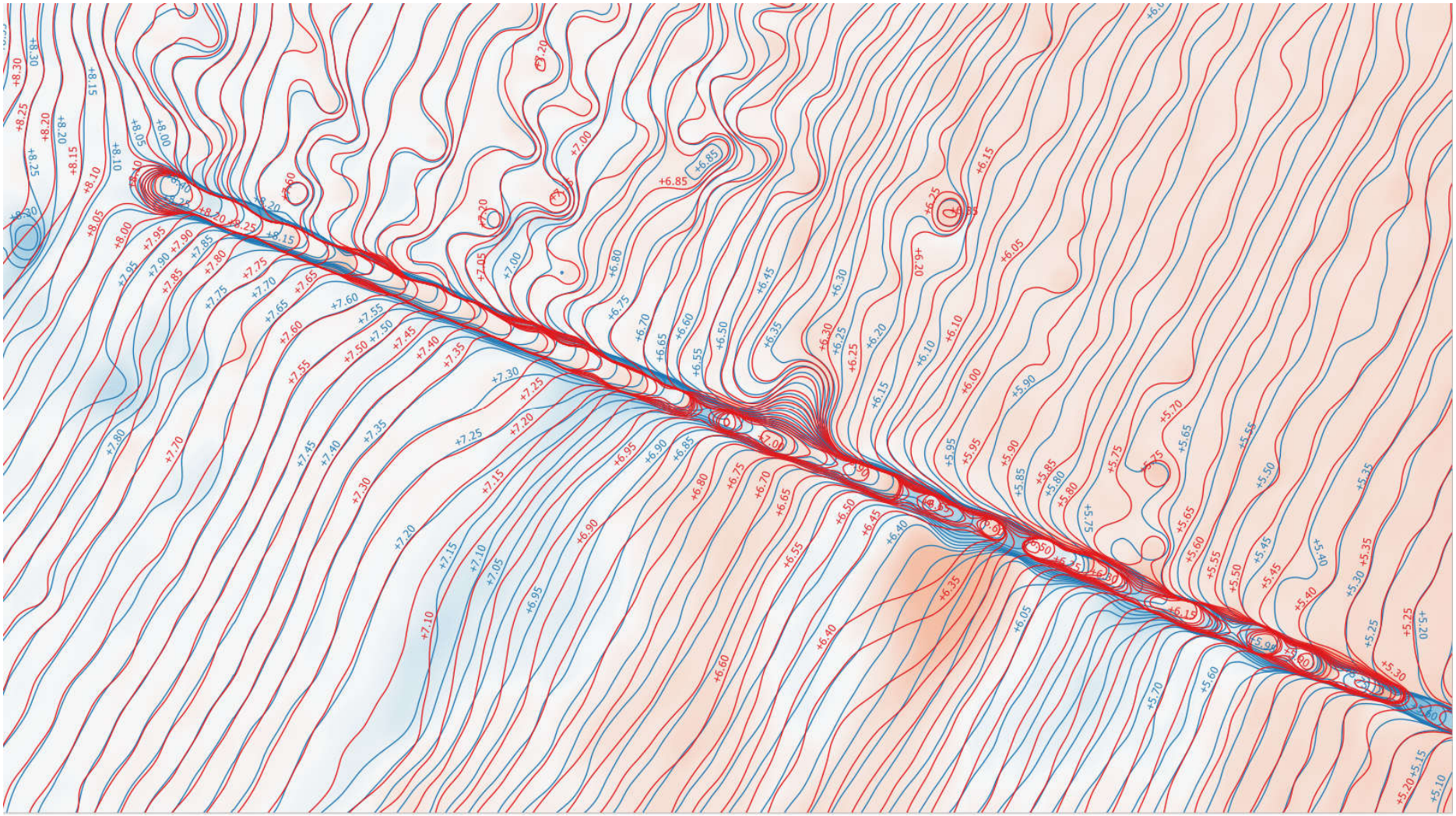

Figure 7.20 Erosion (Red Areas) / Accretion (Blue Areas) over the 48-Hour Period between 31/07/2020 and 02/08/2020. The Red Contours denote the first survey and the blue contours denote the second survey (contours are at 5cm intervals). Northeast of the groyne, the pink area denotes a typical sediment loss of 5cms, probably due to longshore drift; while south of the groyne there are bands of erosion and accretion, i.e. the groyne has disrupted the prevailing longshore drift. The area of most erosion (red patch) exhibits a 3-contour interval or 15cms loss of sediment and pebbles.

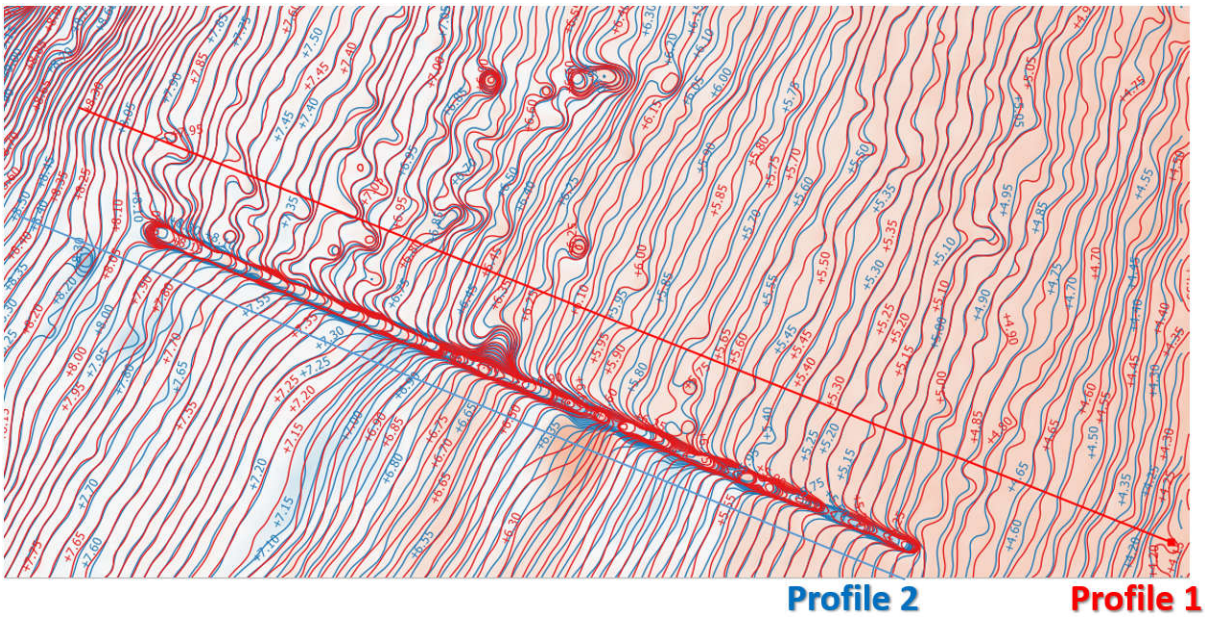

Figure 7.21a Location of Two Profile Cross Sections (Profile 1 and Profile 2: North and South of the Groyne).

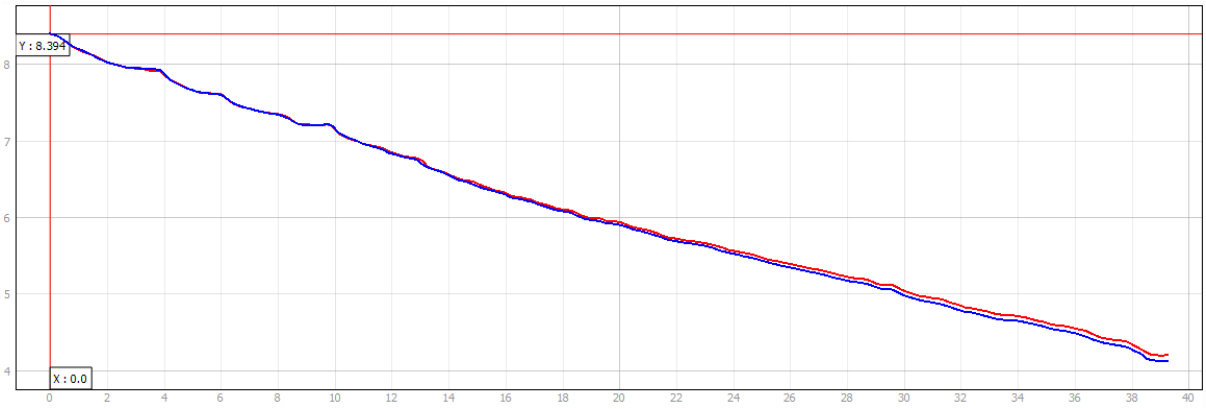

Figure 7.21b Profile 1 Cross Section illustrates the red line (1st survey) is approximately 5cms above the blue line (2nd survey 48 hours later) after 20 metres.

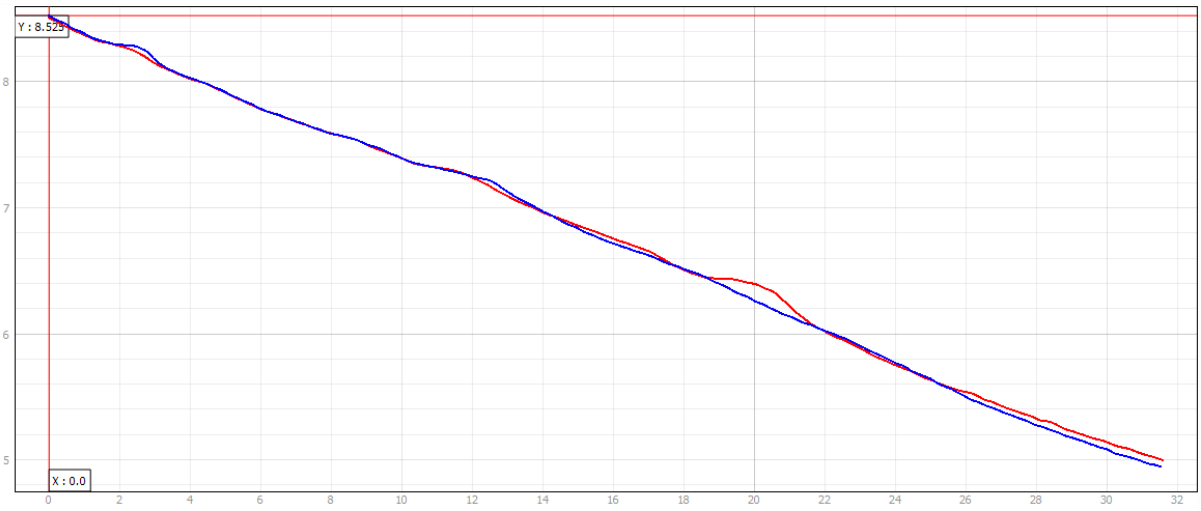

Figure 7.21c Profile 2 Cross Section illustrates the intermittent crossing of the red line (1st survey) and blue line (2nd survey 48 hours later) indicating areas of both erosion and accretion. The big difference at 20m indicates a loss in elevation (erosion) between 15 and 20cms.

These analyses show that even though the two surveys were undertaken just 48 hours apart on a very calm weekend of warm, sunny weather with very light winds, the effect of the tides on Penarth beach have had a significant volumetric change of sediment on the beach. This analysis has also demonstrated that UAV photogrammetric models can clearly map, model and identify these changes on the foreshore. All of this modelling was undertaken using free and open-source software.

One other area of further mention is the issue of modelling changes in the cliff face from aerial (vertical) imagery from drones. In Figure 7.16 and 7.17 it was suggested that some changes in the cliff face had been identified in the volumetric analysis. Vertical photography will identify the outlier points (or protruding features) of the cliff face, but clearly not the recesses of the cliffs. However, these outliers may have some value in identifying changes to the cliff face, as there will be far fewer points captured in these 3D models, but are clear indicators of change (erosion). Figure 7.22 explores this further by considering the contours of the cliff face between the two surveys, rather than just the erosion/accretion map. The original orthomosaics of the two surveys are presented alongside their corresponding contour maps at 5cm intervals. The dense packing of the contours reveals the shape of the cliff surface, in much the same way as the hillshaded maps revealed the sediment displacement on

the beach itself. By comparing these contour maps, more definition is given to the shape of the cliff which is not easily discernible from the orthophotos themselves. The difference map supports these areas of change on the cliff surface. This result is an interesting by-product of such a microscale analysis of very high-resolution data.

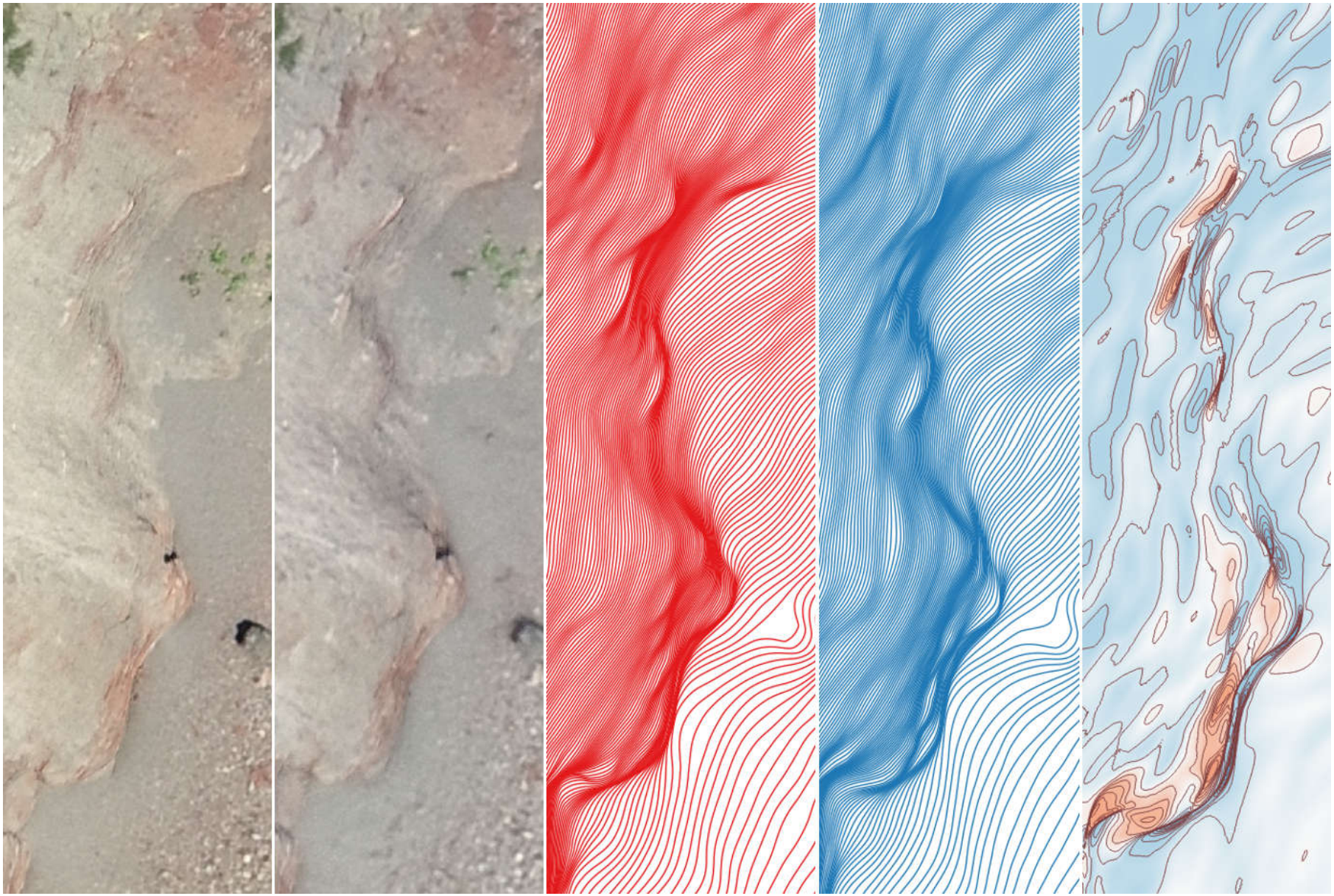

Figure 7.22 3D Digital Orthomosaic for Cliff Analysis. From left to right: 3D Orthomosaic of 31/07/2020; 3D Orthomosaic of 02/08/2010; 5cm Cliff Contours of 31/07/2020; 5cm Cliff Contours of 02/08/2020; Difference Map between 31/07/2020 and 02/08/2020 where the dark pink/orange colours indicate areas of cliff / scree losswhich appears to correspond with the difference in shape of the red and blue contours.

Chapter Summary

The results obtained in this chapter show the close-range UAV photogrammetry and the three-stage analysis procedure can detect 1cm change on the beach using the free and open-source software. The cost implication would be less than £350 at the first instance of purchasing the drone and less than £50 (transportation to the site) for other surveys. This procedure has not dismissed the use of the traditional LiDAR for beach modelling and monitoring but rather improved on the use of LiDAR together with the close-range digital photogrammetry for higher resolution images and accurate spatial and spectral resolution.

The spatial analyses of the zoomed area of Figures 7.15 -7.19 at the different viewpoints and scales improve the confidence level of the hillshading and conour of that particular section. Spatial analysis of the beach at different scales provides a repetitive beach topography measurement quality (Casella et al, 2020). On its own, it is not possible to obtain the LiDAR datasets at such different scales and with such spectral accuracy.

All analyses performed were using the open-source QGIS shows the reliability of the free-to-use GIS software. Figures 7.4, 7.5, 7.8 - 7.13, 7.15 – 7.22 shows that QGIS is excellent in creating accurate 3D models and maps for coastal morphology and visualization. For more interactive and advanced spatial analysis, 3D maps can be created from python based plugins (Eboigbe, 2017). The procedure enumerated in carrying out the spatial analysis in the QGIS, therefore, becomes a standard for beach monitoring. The contribution to knowledge, therefore, is that technically there is the LiDAR at the regional scale with improved methodology ‘the three-stage analysis’ for accurate spatial analysis and low-cost viability for coastal monitoring

Chapter 8

Discussion of Results and Conclusion

8.1 Discussion of Results

This project aims to investigate the possibility of accurate and precise coastal monitoring using very low-cost photogrammetry techniques. With the summary at the end of each chapter, the evaluation of the research methodologies in chapters 5 and 7, this section will discuss the results as relates to the main research objectives presented in chapter one.

The new field observation methodology developed in chapter four is similar in principle to the TLS. Both methods are ground-based and have the advantages of close-range photogrammetry. The measuring sensor for the pole platform is closer to the coastal cliff and can capture all segments of the cliff surface. The TLS was effective in capturing the 3D point cloud of the cliff surface. A direct comparison between the TLS and the pole survey point clouds in this research shows that the pole survey captured every point on the cliff (figures 5.5, 5.6, and 5.7). This is due to difficulties of the TLS extracting the edges of some hidden points due to ambient light interferences. Also, the pole survey has the added advantage of height (e.g. 11m above the ground), therefore narrowing the acuteness of the angle to the top of the cliff and allowing more points to be captured.

The pole photogrammetry methodology had an automatic positional and rotational calibration that displaced the systematic errors even with the low-cost miniature sensors in the phone. The accuracies of the pole photogrammetry point cloud were scrutinized relative to the point clouds from the TLS and a drone survey using third-party software such as Surfer Golden and CloudCompare (section 5.1.2, 5.1.3, 5.1.4, and 5.1.5). The 2.1-megapixel phone camera without the GNSS GCPs produced point clouds with positional precisions between 5cm to 12cm (table 5.2). The 2.1-megapixel phone camera with the GNSS GCPs generated a positional accuracy of 1cm to 5cm (table 5.3). In both instances of with or without the GNSS GCPs, the resolution of the digital model was 1cm. There was also visual inspection for the vertical and horizontal extent with an equivalent drone survey and Google Earth images (figure 5.10, 5.11, and 5.12). Depending on the budget, the new photogrammetry survey practice can monitor the cliff surface with or without the GNSS control points. The methodology also demonstrated higher resolutions with the higher grade digital cameras

(figures 4.23, 4.24 and 4.25). The lightweight pole survey was simple to use and can be undertaken by one person. The digital images were fast to acquire and the digital cameras attached to the pole can be interchanged right in the field for multispectral imaging (e.g. near infrared camera). The high photo overlap provided stable image geometry for the point clouds, in the same way the registration of the 3D scans can provide an accurate geometry for the TLS point clouds. Two different point clouds from two surveys were then analysed using the newly developed algorithm for the purpose of detecting changes (section 5.2.2).

Chapter six gives an overview of obtaining accurate, low-cost, and very high-resolution digital models from UAVs for micro change detection on the beach. The two 2020 models evaluated in Chapter seven were generated at a spatial resolution of 1cm, allowing for individual features on the beach to be captured. Meanwhile, LiDAR surveys can extend to tens of miles at a resolution of only 1m (or 50cms in focused surveys, e.g. Aberystwyth seafront) with typical vertical accuracies of 5-10cm. In the same way the LiDAR swath angle determines point density and the resolution of the Digital Surface Models, the 85% forward and 50% side overlap of the drone increased the point density with an excellent spectral and spatial orthomosaic and DSM resolution (figures 6.20 and 6.21). The low-cost, large-scale and regular drone generated very high spatial resolutions of 1cm and vertical accuracies of 1cm with the GNSS GCPs (figure 6.8 and 6.9).

Although the GNSS GCPs are important in improving the overall accuracy of the digital model, the results show that some permanent controls in the Area of Interest (AOI) will improve the vertical accuracy to 1-2cms. The traditional land surveying techniques can also be used to extend/re-establish GCPs in the AOI.

At this juncture, it is essential to discuss the possibilities available for drone surveys in coastal environments – with an emphasis on low-cost approaches. The whole philosophy of this research has been in developing, implementing and evaluating low-cost techniques. It is self-defeating if an entry-level drone (e.g. circa £300 DJI Phantom 3 to £1400 DJI Phantom 4 Professional) is recommended, but is then reliant on a relatively costly GNSS survey before every drone survey. For example, suitable GNSS survey equipment starts at a cost of £5K and upwards, while kit hire is typically in excess of £300 per day. Trained personnel are also required, while surveying accurate GCPs requires setting up on a tripod over the locations for a minimum of 10 minutes per point. Capturing the GCPs will usually take a lot longer than

the drone survey itself. This is a big issue and a constraint, especially if the approach is to be adopted in developing nations. For a drone survey, there are a number of options:

(1) UAV Survey without any GCPs;
(2) UAV Survey with a PPK / RTK GNSS enabled drone;
(3) UAV Survey with a pre-flight GNSS survey of 4 to 8 GCPs;
(4) UAV Survey with fixed visible GCP features which will be in all surveys (e.g. years).
(5) Combination of (3) and (4).

In this research, all of these approaches were evaluated. It should be noted that the area around the seafront in Penarth did not have very good mobile phone network coverage during the survey periods of 2015-2020. As a result, RTK GNSS surveys were problematical due to signal fallout. Some GCP locations required longer than expected to survey. Similarly, for one of the RTK GNSS enabled drones, the risk of flying in RTK mode and the signal dropping out, thereby rendering the locational data unusable was felt to be too much of a risk, so was used in PPK mode with a base station set-up on the seafront. PPK/RTK enabled UAVs, such as the DJI Phantom start at a price of £5K, so are not within the realms of "low-cost". For the 2015 and 2016 surveys, visible GCPs were set up and surveyed on the beach before flying (Figure 8.1).

Figure 8.1 Location of Eight GNSS-surveyed GCPs at Penarth (2015 Survey).

In these surveys, 1-metre square carpet tiles (with a big white cross) were placed on the foreshore and then surveyed accurately (Figure 8.2). These points are then manually identified in 3 or more images during the photogrammetric modelling process to snap the model to these precise locations.

Figure 8.2 Location of the GCP near Penarth Pavilion (bottom left GCP in Figure 8.1) visible in the UAV imagery for 2015 survey.

The eight GCPs took a two-person team about 2 hours to lay out and survey. For one of the 2020 surveys, a series of 8 mobile visible GCPs were used with in-built GPS receivers which record their position for a minimum of 40 minutes and are then post-processed to generate highly accurate locations (Figure 8.3).

Figure 8.3 Mobile GCP Target (Black & White quadrant mat next to the beer handle) while the red circle identifies the location of a virtual GCP.

The advantage of using this approach is that the mats are simply placed around the survey site, switched on, and then collected an hour later after the UAV survey has been completed. There is no need to GNSS survey any locations on the day of the survey. Whilst extremely convenient, simple to use, and highly accurate, these specific targets cost nearly £450 each, so not within the realms of "low-cost".

An alternative approach is to use "virtual" GCPs as illustrated next to the GCP target in Figure 8.3. The points are not surveyed on the day, but are surveyed once and then used for subsequent UAV surveys. For Penarth, there are many features in the landscape which are easily recognizable from the aerial photographs which can be used as GCPs – mostly man-made structures, such as the pier, esplanade, walkways, slipways, walls, groynes, outlet casings, etc. (see Figure 8.4) as well as natural features, such as specific rocks (Figure 8.5 and 8.6). Not all these Virtual GCPs will be used for all UAV surveys, whilst it is good practice to have plenty in reserve in case of difficulty in identifying the locations, or changes in the real world.

Figure 8.4 Some examples of the Virtual GCPs surveyed accurately using GNSS which are clearly visible in the UAV imagery.

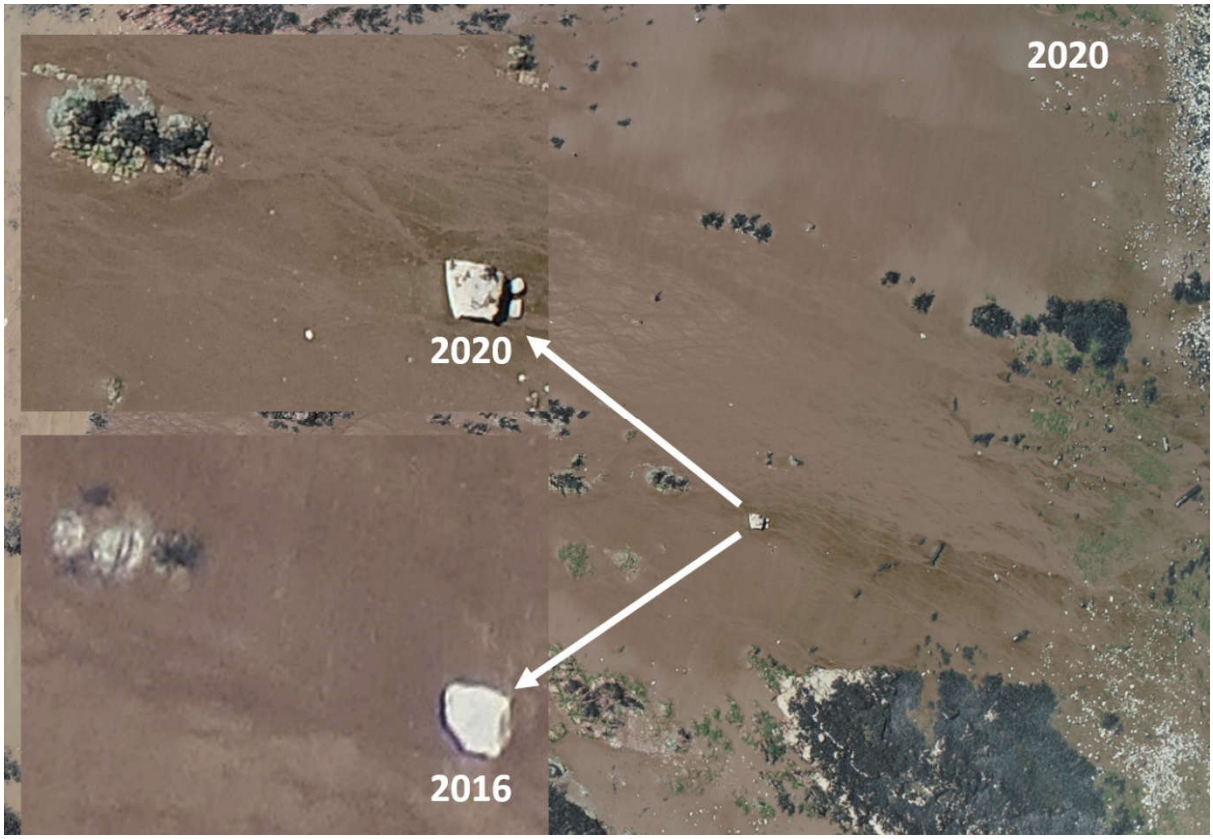

Figure 8.5 Virtual GCP (big heavy rock) on the Beach Clearly Visible in Imagery. Note the inset 2016 image with a much higher level of sand on the beach. Need to ensure chosen locations will be visible, static, and not buried.

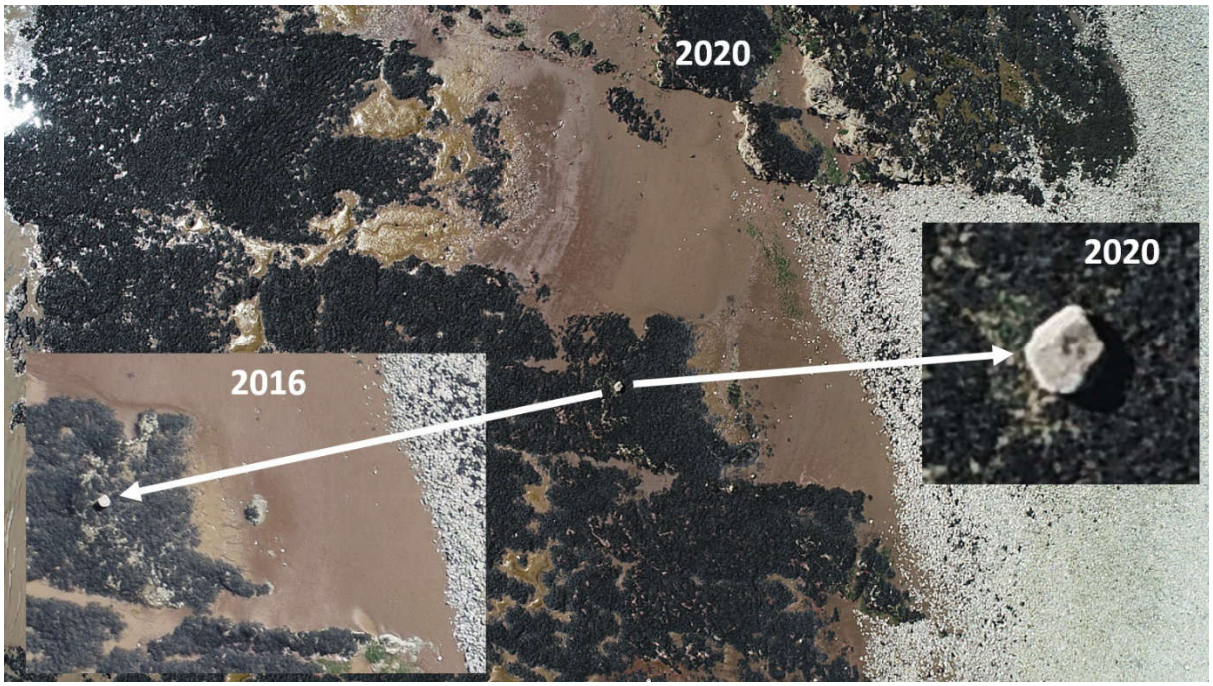

Figure 8.6 Virtual GCP (big heavy rock) on the Beach Clearly Visible in Imagery.

Essentially, even in the case of flying a UAV survey with no visible GCPs, then the Virtual GCPs can be used to attribute the precise locations to the photogrammetric outputs. Even if the UAV surveys were undertaken before the Virtual GCPs were captured, as long as they are visible in the imagery, then they can be accurately geo-referenced and orthomosaicked. During this research, some of the UAV surveys were evaluated without using the target GCPs, but just using the onboard-GPS of the drone. Whilst data in the X-Y plane is generally quite accurate, the elevation data can be out by as much as 100m in OSGB elevation depending on the satellite constellation. Using a good distribution of between 4 and 6 Virtual GCPs, then the output products were on a par with the target GCP models. Similarly, additional experiments were undertaken on the target GCP models to be supplemented with additional Virtual GCPs, but no real improvements were found. This research indicates that as long as the GCPs are accurate, then extending the number of GCPs used has no real benefit to the model. An accurate arrangement of say 6 GCPs (or a minimum of 4) is sufficient. In terms of meeting the criteria "low-cost", one feasible solution may be to "ground survey once, fly many times", in that a set of highly visible features, such as those in Figure 8.4 to 8.6 are accurately surveyed once (using a day's hire of a GNSS solution) and then used during the lifetime of the UAV surveys. This minimises both the financial cost and the time and manpower costs of each GNSS survey. Chapters 4 and 5 outlined an approach which matches point clouds from close-range photogrammetric solutions. It should also be remembered that the same approach could also be used for UAV-derived aerial point clouds, provided the density of points is big enough to snap features. Again, these Virtual GCPs may be used if easily identified in the point clouds.

It is worth noting that the photogrammetric modelling uses the on-board (consumer-grade) GPS geotags of each image as a starting point for the 3D-point matching process. As the model evolves, then these less-accurate GPS geotags move to their correct geometrical location based on the relative position of objects in other images. The more accurate the GPS geotags are, then the more efficient the process becomes. However, the photogrammetric software is not dependent upon receiving the geotags of each image, as not all photogrammetry is related to geographic modelling. If images are used without geotags, then the starting assumption is that the origin of evey photograph is at 0, 0, 0. As the process evolves, then the location of each photograph actually moves away from this origin until the final model is achieved. This can then be georectified to the Virtual or target GCPs. The reason why this is important is that there are a plethora of cheap drones now on the market

which uses much of the same technology as say the DJI Phantom drones, but at a fraction of the price, e.g. £75 - £200, whilst still offering HD-quality images. Whilst the camera is not stabilized and the images are not geotagged, this is no longer a drawback for many of the photogrammetric modelling software packages. Based on the experiments undertaken on the UAV datasets (and the cliff modelling with a 2.1MP camera), it would be feasible to generate orthomosaics and DSMs of the beach using a very cheap drone and Virtual GCPs. The use of hobby drones under a CAA-licence and local authority authorisation and permissions may be another matter though. In other countries, it could very well be feasible and worth exploring further.

In the meantime, the analysis documented in Chapter Seven demonstrates the viability and accuracy of using CAA-licenced and approved UAVs within the framework of local authority and stakeholder permissions for generating highly accurate datasets. Very small changes in beach morphology can be detected between surveys, e.g. 48 hours or possibly before and after a storm event. The results are far superior to LiDAR at this scale (e.g. 1cm vs. 1m for Penarth, i.e. 10,000 times the resolution of LiDAR). However, LiDAR results were comparable at the whole beach level; and LiDAR still has the ability to fly a whole stretch of coastline of 20 or 30 miles – which is beyond the scope of UAVs without weeks of effort. LiDAR will always be of great benefit for regional analysis, but could then be combined as part of a regional management programme to identify coastlines of concern for higher resolution UAV surveys.

Change detection on the point cloud is more accurate as point clouds are the actual 3D positions of points on the surface. For instance, the accuracy of the other digital products such as the orthomosaic and the DSM/DEM depend on the point cloud's resolution. The results obtained in this research have overcome some challenges in evaluating point clouds for change detection, such as classification, structure, and segmentation. The algorithm was able to perfectly align two different point clouds by using their transformation parameters as a Numpy array that retains their exact number of rows and columns. For classification, the new algorithm created multiple search radiuses on the point cloud 'search_radius_vector_3d' that increased the cell categories of clusters reaching every point on both point clouds (sections 4.3.6, 4.3.7, and 4.3.8). For structure, three new Numpy arrays (point clouds) were created: the area that is similar without change shown on the reference point cloud; the area of change shown on the reference point cloud; and the last is the change segmented from the

reference point cloud (section 4.3.13, 4.3.14, 4.3.15 and 4.3.16). The results show all the three new point clouds displayed for visualization (section 4.3.17).

The new Change Array Prediction Model 'CAPM' detected changes on the point clouds for up to 1 cm (section 5.2.2). The results also include a change flyby that shows the amount of changes for the different weeks under review (figure 5.18). The interpretation of the different search radius was on their change detection distance radius of 0.02, 0.03, 0.04, 0.05, and 0.1. Each of these radii was allocated a different colour (section 5.2.2, figures 5.19, 5.20). The different colours are the depth (severity) of the cliff surface change pattern (wave-cut notch, crack, depth of fall, etc.).

This research is also unique because the results obtained from the significant change areas have been modelled into a prediction algorithm for the coastal cliff (section 5.2.2.1). The algorithm categorized all the change distance radii by their areas under the severe change in percentage (Table 5.4).

The new risk assessment and coastal cliff prediction model shows the severity of the changes for the different areas (region-by-region) on the cliff surface (figure 5.25). This research also presents the frequencies of these changes region-by-region as a frequency table for the different weeks under review (tables 5.5 and 5.6). The outcome is a cliff prediction graph (figure 5.26) and the most severe region (hazard zone). The experimental mean prediction model determines when the next cliff fall may occur and the minimum to the maximum amount of cliff fall (section 5.3). The predicted minimum and maximum cliff fall were calculated as $0.33922cm^3$ and $135.75778cm^3$. The results also include the periodic volume change between the successive weeks under review (table 5.7).

The risk assessment has subsequently been proven to work accurately as explained in figures 8.1 and 8.2 below.

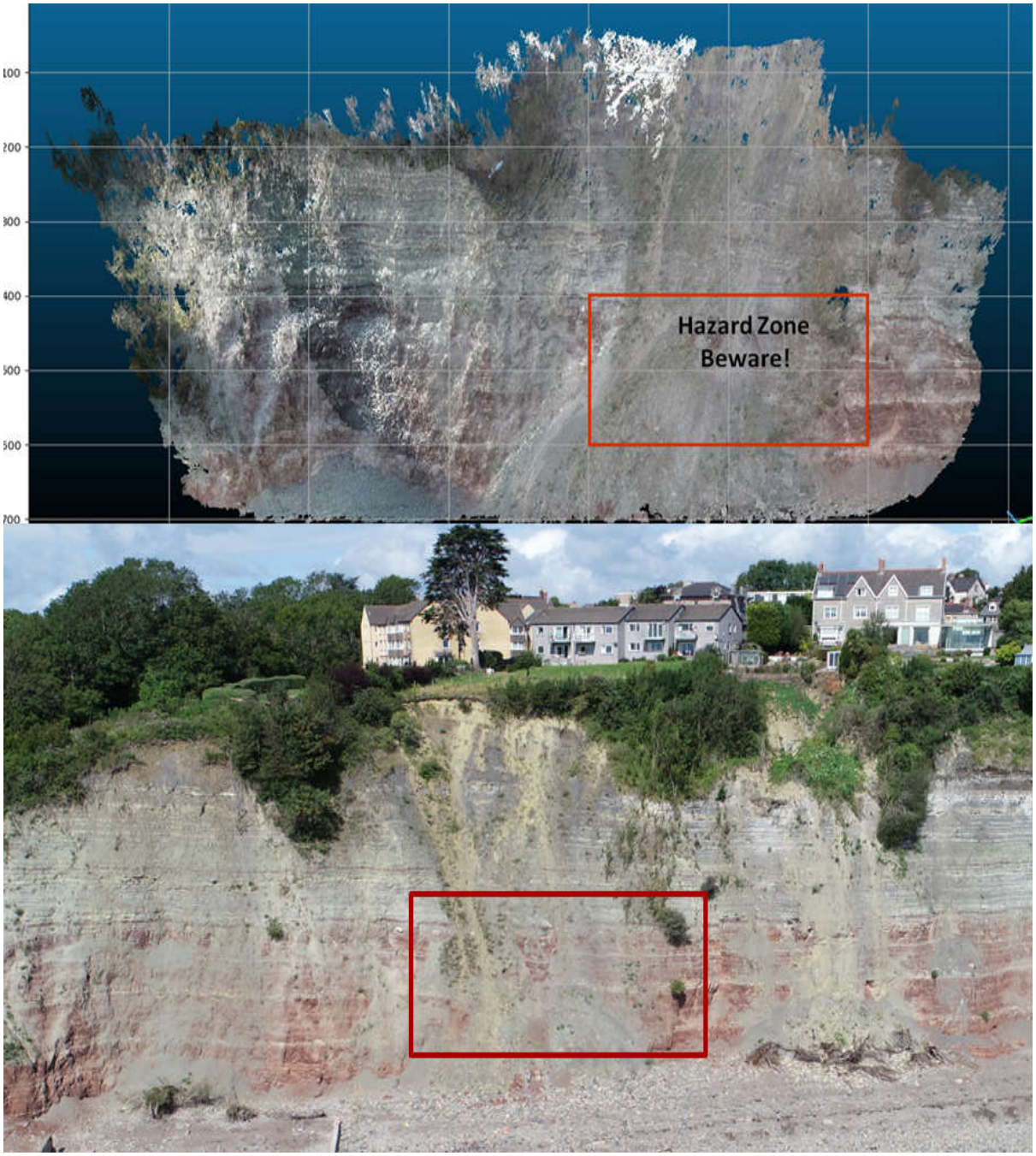

Figure 8.1 – A Photo Below was taken on the 2nd of August 2020 to Verify to Correctness of the Prediction Model. The hazard zone warning area on the model above corresponds to the same in the photo below. As predicted, a significant portion of the cliff in the predicted zone, did collapse. Figure 8.2 below explains further where the collapsed cliff is visible on the ground.

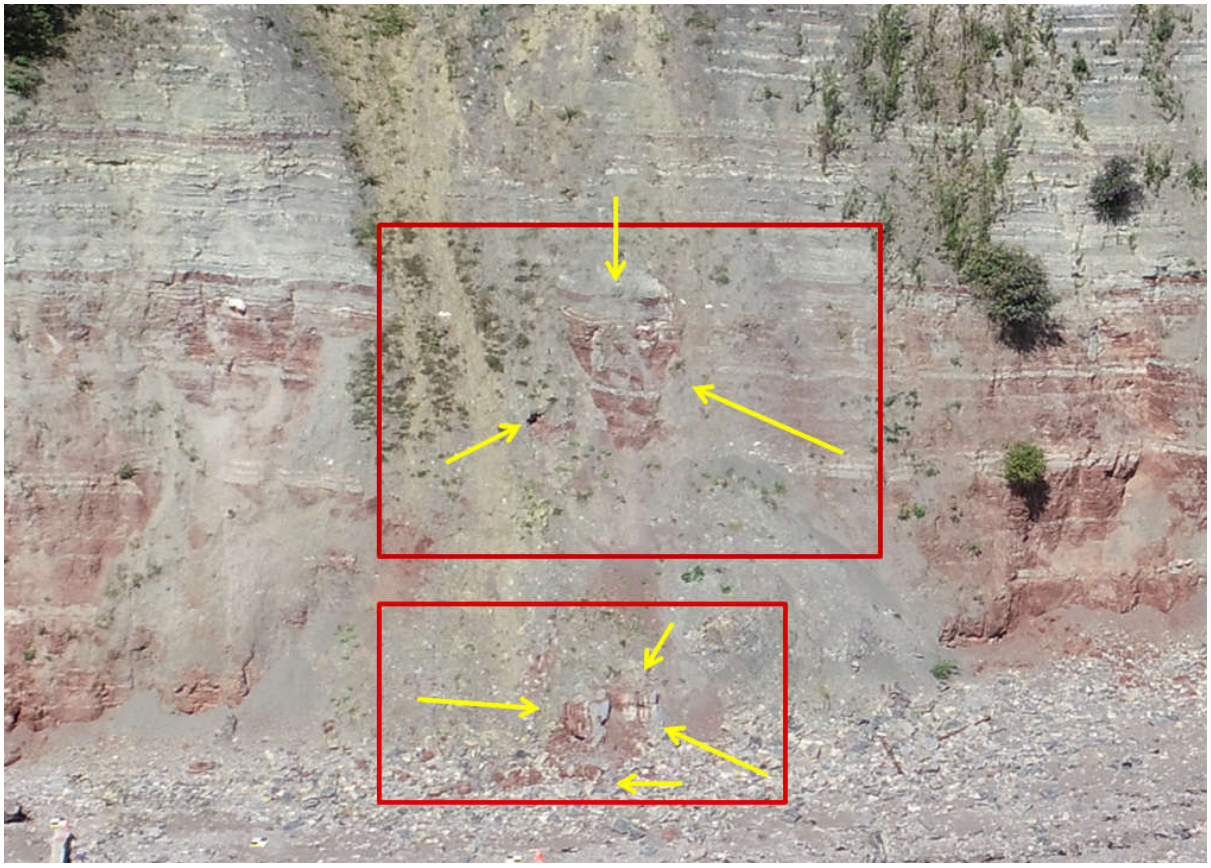

Figure 8.2 – Shows the Exact Spot the Cliff Collapsed Inside the Hazard Zone Warning and the Cliff Debris on the Ground.

Another advantage of this prediction model is that it helps to explain the chemical, biological or physical factors leading to the collapse. In this regard, the action is hydraulic (hard rock, soft rock and undercutting) leading to an eventual cliff wave-cut and collapse. The volume of the cliff chunks on the ground (figure 8.2) is also within the predicted 0.33922cm^3 - 135.75778cm^3.

In Table 5.6, aside from the severe region that is no. 5 (regions K, M, N) on the scale, the other scale grouping such as no. 4 (regions L. G), no. 3 (regions B, F, I and J), gives an insight on the prevailing erosion cause and type. In no. 3 (regions B, F, I, and J) are regions closely joined and likely to be influenced by similar weathering conditions. Similarly, the prediction model will also give an insight into when the cliff erosion could become severe. This information is important to geologists and other environmentalists.

Chapter seven shows an original application in applying open-source GIS solutions for detecting 1cm to 3cm changes on the beach. The three-stage analysis procedure detects

change as little as 1cm using the open-source QGIS. The three-stage analysis is also a typical example of maximizing LiDAR usage. Hillshades were created for change maps while the choices of the colour ramp, the number of classes, and the colour ramp values, clearly identify the beach pebbles, stones, rocks, beach weeds, erosion, and other man-made features. The erosion maps depict the pattern of the pull-in sand around the cliff and from offshore to the beach itself. The accretion highlights sediment relative to the direction of the accumulation agents. This is very useful to morphologists while monitoring the development of the impact of the resulting wave pattern on the beach (figures 7.20 and 7.21a-c). With the very low financial implication of executing and analysing these surveys, this technique becomes feasible to generate time-series maps of the beach for the evaluation of the volume of sediments. The elevation changes and profile (figure 7.21a-c), are the absolute spatial changes of the beach for the period under review. This frequency distribution from 1 cm to 5 cm reflects a low-energy level. Regular drone surveys with subsequent modelling will develop a risk assessment for the Penarth beach.

8.2 Conclusion

A £20,000-£60,000 estimated cost will be too expensive for weekly surveys with LiDAR. LiDAR is not able to achieve an accuracy of 1cm-2cm considering the distance from the cliff. Due to the inclination angle of the sensors, the LiDAR will not be the best option to capture hidden sections of the cliff. However, LiDAR remains the best option to survey the 14 miles of Glamorgan Heritage Coast and provide details of areas that require regular monitoring (by other techniques such as TLS, UAV or digital photogrammetry). The initial cost of the TLS is over £20,000. Daily hiring is over £500. TLS cannot generate a 1cm resolution model, while the cost is not feasible in developing countries. While the new pole methodology for coastal cliff monitoring is also possible using drones, a drone will require a licence and formal approval for every survey. Considering the resolution and the accuracies derived from this research, pole photogrammetry is then an excellent option for regular cliff monitoring here in the UK and the developing countries. The methodology illustrated in Chapter 5 used a 2.1MP camera on a pole using an off-the-shelf £5 attachment. It is probably not possible to buy such a low resolution camera these days, while 12MP cameras can be bought for less than £40 including the capability to automatically capture at set intervals, e.g. 1s, 2s, 5s, 10s, etc. Moreover, most mobile phones are now both GPS-enabled and have cameras of 8MP or more). The 11m lightweight telescopic and extendable pole used in these surveys are widely

available (for estate agents aerial views of properties) at a cost of about £200. Cheaper alternatives are available (i.e. initial surveys were undertaken using a carbon-fibre fishing rod and a 6m painters pole!). However, the flexibility of being to easily adjust the camera height at 1m intervals allowed for consistent imagery overlap. This research has demonstrated that for an outlay of approximately £250, a 1-person pole-based photogrammetric survey tool can be realised which consistently accurately modelled the cliff at Penarth to identify changes and areas of concern.

Even with LiDAR and aerial mapping, the image overlap, flying height, and the angle of inclination of the camera define the image quality, vis-à-vis their digital outputs. Having reliability and repeatability by maintaining the reconstruction of the metric features of the cliff for every other survey is a breakthrough for coastal cliff monitoring. An example is a coastal cliff (close to Cardiff Airport) where drones cannot fly and where a cliff survey needs to be undertaken to monitor change. This methodology will be useful immediately after a cliff fall to determine the quantity of the eroded material and designate a hazard zone for health and safety (alert the public for any future occurrence). The surveys will repeatedly be for the area of cliff fall (AOI) to develop a monitoring infrastructure for that segment of the cliff. The pole survey, therefore, becomes an economically viable digital photogrammetry technique for regular cliff monitoring.

Pole surveys do not require a licence or permission from the local authorities. Execution of surveys can be just before or after the cliff falls. The pole is lightweight and with no setup. Pole photogrammetry does not require expert knowledge in the fieldwork, processing of the data, and data analyses. With a budget of £250 (or significantly less if a painters pole or bamboo is used), the surveyor can repeat surveys on maximum precision and accuracy. For coastal cliffs that are very high, there are also telescopic poles which extend as high as 30 metres, but these often require anchoring at the base for stability. Another advantage of pole photogrammetry is the ability to access dangerous and inaccessible coastal cliffs which ordinarily would be very difficult using the TLS. For use in the photogrammetry community, the results obtained demonstrate the practical use of the pole for close-range digital photogrammetry. It is also useful for further research and by the local authorities.

Similarly, it will be too expensive to survey the beach regularly with LiDAR. Just as with the coastal cliff, an advantage of the close-range photogrammetry is the closeness to the terrain which amounts to a higher resolution. Just as with the coastal cliff, an advantage of the close-

range photogrammetry is the proximity to the terrain providing higher image resolutions (e.g. typically 1cm DSMs at a flying height of 100m). The drone also has the flexibility of flying height and the choice of the degree of image overlap. This flexibility with the drone provides options for spatial analysis for the beach. A drone of £300 to £1500 (DJI Phantom 3 to DJI Phantom 4 Professional) can precisely and accurately survey the beach using the best practices as shown in this research. The outputs from the beach monitoring are the information monitoring infrastructure for policymaking, especially with the beach evolution. The change detection on the beach to up to 1 cm is useful for general engineering purposes and beach simulation. Hobby drones in the region of £75 to £200 have the potential to offer comparable HD solutions, but are subject to restrictions and CAA regulations in the UK. This is certainly well worth exploring further.

This research shows the low-cost UAV outputs with the open-source GIS solutions can achieve 1 cm change detection and classification of beach features. The results obtained do not require expertise in remote-sensing to identify the areas of change (cut, fill, erosion) on the beach.

8.3 Research Limitation

1. Pole surveys with inexpensive digital cameras must be performed in an almost equal atmospheric condition to avoid the drifting of the MEMS-IMU during the survey.

2. Securing approval for a drone survey involves a protocol that usually takes some time. This protocol did not encourage quick surveys before and after a storm.

3. Acquiring LiDAR that corresponds to the period under review was difficult due to the high cost of LiDAR. Publicly available datasets are very limited.

8.4 Recommendation for Future Work

1. Enhancing the Performance of the Inbuilt GPS (Use wifi) - Develop an algorithm on raspberry pi GPS-loggers that will improve the accuracy of the pole photogrammetry. This self GNSS tracker will be able to adjust the EO parameters from coordinated point(s). This way, surveys for a long stretch of the cliff (500 -1000 meters) can take hours without the fear of losing accuracies.

2. Incorporate a Volume Computation into the CAPM - Develop an algorithm for the computation of volume in the CAPM will facilitate the determination of the amount of cliff collapse on the ground.

3. Survey the beach at different flying heights and using sensors on different wavelengths to determine the change pattern variation.

4. Undertake a beach survey using a low-cost hobby drone (e.g. less than £100) with the permissions of the relevant authorities.

5. Undertake a beach survey for small subsets of the beach (as illustrated for the 2020 surveys in Chapter 7) using pole photogrammetry (i.e. the camera attachment is rotated through 90 to face the ground). Similar approaches are used in archaeological digs, where high resolution cameras are mounted on a pole system to 3D survey the ground below.

REFERENCES

Abdullah, S., Tahar, K. N., Rashid, M. F. and Osoman, M. A. (2019) 'Camera Calibration Performance on Different Non-Metric Cameras', *Pertanika Journal Science and Technology* 27(3) pp. 1397-1406. *Pertanika* [Online]. Available at: http://www.pertanika.upm.edu.my/ (Accessed: 13 January 2020).

Abellan, A., Calvet, J., Vilaplana, J. M. and Blanchard, J. (2010) 'Detection and Spatial Prediction of Rockfalls by Means of Terrestrial Laser Scanner Monitoring', *Geomorphology* 119(3-4) pp. 162-171. *ScienceDirect* [Online]. Available at: https://www.sciencedirect.com/science/article/pii/S0169555X10001224 (Accessed: 01 March 2018).

Aber, J. W. and Babb, T. A. (2018) 'The Challenges of Processing Kite Aerial Photography Imagery with Modern Photogrammetry Techniques', *International Journal of Aviation, Aeronautics, and Aerospace* 5(2) pp. 1-30. *IJAAA* [Online]. Available at: https://commons.erau.edu/ijaaa/vol5/iss2/2/ (Accessed: 25 March 2019).

Ackermann, F. and Krzystek, P. (1997) 'Complete Automation of Digital Triangulation', *The Photogrammetric Record* 15(89) pp. 645-656. *Wiley Online*. Available at: https://onlinelibrary.wiley.com/doi/abs/10.1111/0031-868X.00074 (Accessed: 22 November 2019).

Addo, K. A., Walkden,M. and Mills, J. P. (2008) 'Detection, Measurement and Prediction of Shoreline Recession in Accra, Ghana', *ISPRS Journal of Photogrammetry and Remote Sensing* 63(5) +pp. 543-558. *ScienceDirect* [Online]. Available at: https://www.sciencedirect.com/science/article/pii/S0924271608000282 (Accessed: 23 December 2018).

Adelaja, A. (2013) 'Vanishing Coastlines in Lagos', Premium Times, 23 November [Online]. Available at: http://www.premiumtimesng.com/news/150064-vanishing-coastlines-lagos.html (Accessed: 11 May 2017).

Agbodion, J. (2016) 'Niger Delta Communities Face Extinction over Coastal Erosion – Environmentalist', TODAY, 02 July [Online]. Available at: https://www.today.ng/news/nigeria/146756/ndelta-communities-face-extinction-coastal-erosion-environmentalist (Accessed: 11 May, 2017).

Agbonkhese, O., Agbonkhese, E. G., Aka, E. O., Joe-Abaya, J., Ocholi, M. and Adekunle, A. (2014) 'Flood Menace in Nigeria: Impacts, Remedial and Management Strategies', *Civil and Environmental Research* 6(4) pp. 32-40. *CAB Direct* [Online]. Available at: https://www.cabdirect.org/cabdirect/abstract/20143248685 (Accessed: 11 March 2017).

Aguilar, F. J., Mills, J. P., Delgado, J., Aguilar, M. A., Negreiros, J. G. and Perez, J. L. (2010) 'Modelling Vertical Error in LiDAR-Derived Digital Elevation Models', *ISPRS Journal of Photogrammetry and Remote Sensing* 65 pp. 103-110. *ScienceDirect*[Online]. Available at: https://www.sciencedirect.com/science/article/pii/S0924271609001178 (Accessed: 30 August 2018).

Aguilar, M. A., Aguilar, F. J., Fernandez, A., Fernandez, I., Saldana, M. D. M., Lorca, A. M. G., Negreiros, J. G., Viciana, A. and Gonzalez, E. (2011) 'Geometric Processing of GeoEye-1 Satellite Imagery for Coastal Mapping Applications', *Proceedings of the IMProVe International Conference on Innovative Methods in Product Design*, Venice, Italy, 15-17 June. *Academia* [Online]. Available at: https://www.academia.edu/40701612/Geometric_processing_of_GeoEye-1_satellite_imagery_for_coastal_mapping_applications (Accessed: 15 May 2018).

Aguilar, M. A., Aguilar, F. J., Saldana, M. D. M. and Fernandez, I. (2012) 'Geopositioning Accuracy Assessment of GeoEye-1 Panchromatic and Multispectral Imagery', *Photogrammetric Engineering and Remote Sensing* 78(3) pp. 247-257. *Ingenta Connect* [Online]. Available at: https://www.ingentaconnect.com/content/asprs/pers/2012/00000078/00000003/art00004 (Accessed: 02 August 2018).

Aguilar, M. A., Saldana, M. D. M., Aguilar, F. J. and Lorca, A. G. (2014) 'Comparing Geometric and Radiometric Information from GeoEye-1 and WorldView-2 Multispectral Imagery', *European Journal of Remote Sensing* 47(1) pp. 717-738. *Taylor and Francis* [online]. Available at: https://www.tandfonline.com/doi/abs/10.5721/EuJRS20144741 (Accessed: 15 May 2018).

Ahmad, F. N., Yusoff, A. R. Ismail, Z. and Majid, Z. (2018) 'Comparing the Performance of Point Cloud Registration Methods for Landslide Monitoring using Mobile Laser Scanning Data', *International Conference on Geomatics and Geospatial Technology (GGT 2018),* Kuala Lumpur, Malaysia, 3-5 September. *The International Archives of the Photogrammetry, Remote Sensing and Spatial Information Sciences*, Volume XL11-4/W9 [Online]. Available at: https://www.int-arch-photogramm-remote-sens-spatial-inf-sci.net/XLII-4-W9/11/2018/ (Accessed: 11 July 2020).

Ahmed, A., Drake, F., Nawaz, R. and Woulds, C. (2018) 'Where is the Coast? Monitoring Coastal Land Dynamics in Bangladesh: An Integrated Management Approach Using GIS and Remote Sensing Techniques', *Ocean and Coastal Management* 151 pp. 10-24. *Science Direct* [Online]. Available at: https://www.sciencedirect.com/science/article/pii/S0964569117306397 (Accessed: 20th November 2018).

Ahn , Y., Shin, B. and Kim, K. (2017) 'Shoreline Change Monitoring Using HighResolution Digital Photogrammetric Technique', *Journal of Coastal Research*SI(79) pp. 204-208. *JCR* [Online]. Available at:http://www.jcronline.org/doi/abs/10.2112/SI79-042.1 (Accessed: 16th November 2018).

Ai, M., Hu, Q., Li, J., Wang, M., Yuan, H. and Wang, S. (2015) 'A Robust Photogrammetric Processing Method of Low-Altitude UAV Images', *Remote Sensing,*7(3) pp. 2302-2333 *MDPI* [Online]. Available at: http://www.mdpi.com/2072-4292/7/3/2302/htm(Accessed: 29 June 2016).

Ali, T. A., Atabay, S., Mortula, M. and Ma, R. (2015) 'Semiautomatic Extraction of the shoreline from High-Resolution Satellite Imagery and Coastal Terrain Model', *Surveying and Land Information Science* 74(1) pp. 14-20(7). *Ingenta Connect* [Online]. Available at: https://www.ingentaconnect.com/content/aags/salis/2015/00000074/00000001/art00003 (Accessed: 01 April 2018).

Alizad, K., Hagen, S. C., Morris, J. T., Medeiros, S. C., Bilskie, M. V. and Weishampel, J. F. (2016) 'Coastal Wetland Response to Sea-Level Rise in a Fluvial Estuarine System', *Earth's Future* 4 pp. 483-497. *AGU Publications* [Online]. Available at: https://agupubs.onlinelibrary.wiley.com/doi/pdf/10.1002/2016EF000385 (Accessed: 15th October 2018).

Allan, J. C. and Stimely, L. L. (2013) 'Oregon Beach Shoreline Mapping and Analysis Program: Quantifying Short-to-Long Term Beach and Shoreline Changes in the Gold Beach, Nesika Beach, and Netarts Littoral Cells, Curry and Tillmook Counties, Oregon', *Technical Report to the Oregon Department of Land Conservation and Development*, *Oregon Department of Geology and Mineral Industries Open-File Report* 0-13-07. *State Library of Oregon Digital Collections* [Online]. Available at: https://digital.osl.state.or.us/islandora/object/osl%3A26657 (Accessed: 29 September 2017).

Alsubaie, N. M., Youssef, A. A. and El-Sheimy, N. E. (2017) 'Improving the Accuracy of Direct Geo-Referencing of Smartphone-Based Mobile Mapping Systems Using Relative Orientation and Scene Geometric Constraints', *Sensors* 17(10) pp. 1-21. *NCBI* [Online]. Available at: https://www.ncbi.nlm.nih.gov/pmc/articles/PMC5677268/ (Accessed: 09 November 2017)

Al-Zubieri, A. G., Bantan, R. A., Abdalla, R., Antoni, S., Al-Dubai, T. A. and Majeed, J. (2018) 'Application of GIS and Remote Sensing to Monitor the Impact of Development Activities on theCoastal Zone of Jazan City on the Red Sea, Saudi Arabia', *Geoinformation for Disaster Management(Gi4DM),* Istanbul, Turkey, 18-21 March. International Archives of the Photogrammetry, Remote Sensing and Spatial Information Sciences [Online]. Available at: http://www.isprs.org/publications/archives.aspx (Accessed: 11 August 2018).

Amante, C. J. (2018) 'Estimating Coastal Digital Elevation Model Uncertainty', *Journal of Coastal Research* 34(6) pp. 1382-1397. *JCR* [Online]. Available at: https://www.jcronline.org/doi/pdf/10.2112/JCOASTRES-D-17-00211.1 (Accessed: 10 March 2018).

Anandabaskaran, V. and Vijayakumar, G. (2017) 'Monitoring Shoreline Changes of the Puducherry Coast, Souh India: A Review and a Case Study', *International Journal for Research in Applied Science and Engineering Technology (IJRASET)* 5(XI) pp. 2470-2477. *IJRASET* [Online]. Available at: https://www.ijraset.com/fileserve.php?FID=11658 (Accessed: 01 April 2018).

Andersen, M. S., Gergely, A., Al-Hamdani, Z., Steinbacher, F., Larsen, L. R. and Ernsten, V. B. (2017) 'Processing and Performance of Topobathymetric LiDAR Data for Geomorphometric and Morphological Classification in a High-EnergyTidal Environment', *Hydrology and Earth System Sciences* 21 pp. 43-63. *Hess* [Online]. Available at: https://www.hydrol-earth-syst-sci.net/21/43/2017/hess-21-43-2017.pdf (Accessed: 29 August 2018).

Anfuso, G., Dominguez, L. and Gracia, F. J. (2007) 'Short and Medium-Term Evolution of a Coastal Sector in Cadiz, SW Spain', *Catena* 70(2) pp. 229-242. *ScienceDirect* [Online]. Available at: https://www.sciencedirect.com/science/article/pii/S0341816206001688 (Accessed: 20 August 2018).

Artigas, F. and Pechmann, I. C. (2010) 'Balloon Imagery Verification of Remotely Sensed Phragmites Australis Expansion in an Urban Estuary of New Jersey, USA', *Landscape and Urban Planning* 95(3) pp. 105-112. *ScienceDirect* [Online]. Available at: https://www.sciencedirect.com/science/article/pii/S0169204609002424 (Accessed: 10 April 2018).

Aryal, A., Brooks, B. A., Bawden, G. W. and Pawlak, G. R. (2012) 'Displacement Fields from Point Cloud Data: Application of Particle Imaging Velocimetry to Landslide Geodesy', *Journal of Geophysical Research Earth Surface* 117(F1) pp. 1-15. *AGU* [Online]. Available at: https://agupubs.onlinelibrary.wiley.com/doi/full/10.1029/2011JF002161 (Accessed: 05 July 2020).

Austermann, J. and Mitrovica, J. (2015) 'Calculating Gravitationally Self-Consistent Sea Level Changes Driven by Dynamic Topography', *Geophysical Journal International* 203(3). pp. 1909-1922. *Gji Oxford Journal* [Online]. Available at: http://gji.oxfordjournals.org/content/203/3/1909.full.pdf+html (Accessed: 14 July 2016).

Averbukh, E., Kurkina, O., Kurkin, A. and Soomere, T. (2014) 'Edge-Wave-Driven Durable Variations in the Thickness of the Surface Film and Concentration of Surface Floats', *Physics Letters* A 378(1-3) pp. 53-58. *ScienceDirect* [Online]. Available at: https://www.sciencedirect.com/science/article/pii/S0375960113009511 (Accessed: 01 November 2017).

Aykut, N. O., Gulal, E. and Akpinar, B. (2015) 'Performance of Single Base RTK GNSS Method versus Network RTK', *Earth Sciences Research Journal* 19(2) pp. 135-139. *RevistasUnal* [Online]. Available at: https://revistas.unal.edu.co/index.php/esrj/article/view/51218/54911 (Accessed: 18 April 2019).

Bae, T. and Kim, M. (2018) 'Performance Analysis of Network-RTK Techniques for Drone Navigation Considering Ionospheric Conditions', *Journal of Sensors* ID 5154697 pp. 1-8. *Hindawi*[Online]. Available at: https://www.hindawi.com/journals/js/2018/5154697/ (Accessed: 17 April 2019).

Bailey, H. andLusseau, D. (2004) 'Increasing the Precision of Theodolite Tracking: Modified Technique to Calculate the Altitude of Land-Based Observations Sites', *Marine Mammal Science* 20(4) pp. 880-885 [Online]. Available at:https://www.abdn.ac.uk/lighthouse/documents/pdf/Baileylusseau2004.pdf (Accessed: 20 August 2018).

Balletti, C., Guerra, F., Tsioukas, V. and Vernier, P. (2014) 'Calibration of Action Cameras for Photogrammetric Purposes', *Sensors* 14(9) pp. 17471-17490. *NCPI* [Online]. Available at: https://www.ncbi.nlm.nih.gov/pmc/articles/PMC4208234/ (Accessed: 27 September 2018).

Banks, S., Millard, K., Behnamian, A., White, L., Ullmann, T., Charbonneau, F., Chen, Z., Wang, H., Pasher, J. and Duffe, J. (2017) 'Contributions of Actual and Simulated Satellite SAR Data for Substrate Type Differentiation and Shoreline Mapping in the Canadian Arctic', *Remote Sensing* 9(12) pp. 2-27. *MDPI* [Online]. Available at: https://www.mdpi.com/2072-4292/9/12/1206 (Accessed: 05 November 2019).

Baptista, P., Cunha, T., Bernardes, C., Gama, C., Ferreira, O. and Dias, A. (2011) 'A precise and Efficient Methodology to Analyse the Shoreline Displacement Rate', *Journal of Coastal Research*27(2) pp. 223-232. *JCR* [Online]. Available at: http://www.jcronline.org/toc/coas/336 (Accessed: 20 August 2018).

Baqersad, J., Poozesh, P., Niezrecki, C. and Avitabile, P. (2017) 'Photogrammetry and Optical Methods in Structural Dynamics – A Review', *Mechanical Systems and Signal Processing* 86(B) pp. 17-34. *ScienceDirect* [Online]. Available at: https://www.sciencedirect.com/science/article/pii/S0888327016000388 (Accessed: 10th October 2018).

Barazzetti, L. (2017) 'Network Design in Close-Range Photogrammetry with Short Baseline Images', *26th International CIPA Symposium*, Ottawa, Canada, 28 August-01 September. ISPRS Annals of the Photogrammetry, Remote Sensing and Spatial Information Sciences, Volume IV-2/W2 [Online]. Available at: https://re.public.polimi.it/handle/11311/1035370#.XB7Aclz7S70 (Accessed: 21 December 2018).

Barazzetti, L., Remondino, F., Scaioni, M. and Brumana, R. (2010) 'Fully Automatic UAV Image-Based Sensor Orientation ', *The 2010 Canadian Geomatics Conference and Symposium of Commission I, ISPRS Convergence in Geomatics-Shaping Canada's Competitive Landscape*, Calgary, Alberta, Canada, 15-18 June. *ISPRS Archives, Volume XXXVIII-Part 1*, [Online]. Available at: https://www.isprs.org/proceedings/XXXVIII/part1/ (Accessed: 30 November 2019).

Barazzetti, L., Scaioni and Remondino, F. (2010) 'Orientation and 3D Modelling from Marketless Terrestrial Images: Combining Accuracy with Automation', *The Photogrammetric Records* 25(132) pp. 356-381. *Wiley Library* [Online]. Available at: https://onlinelibrary.wiley.com/doi/abs/10.1111/j.1477-9730.2010.00599.x (Accessed: 17 June 2020).

Barbarella, M., Fiani, M. and Zollo, C. (2017) 'Assessment of DEM Derived from very High-Resolution Satellite Imagery for Geomorphometric analysis', *European Journal of Remote Sensing* 50(1) pp. 534-549. *Taylor and Francis* [Online]. Available at: https://www.tandfonline.com/doi/full/10.1080/22797254.2017.1372084 (Accessed: 04 August 2018).

Barlow, J., Gilham, J. and Cofra, I. I. (2017) 'Kinematic Analysis of Sea Cliff Stability Using UAV Photogrammetry', *International Journal of Remote Sensing* 38(8-10) pp. 2464-2479. *Taylor and Francis* [Online]. Available at: https://www.tandfonline.com/doi/abs/10.1080/01431161.2016.1275061 (Accessed: 22 January 2019).

Barrand, N.E., Murray, T., James, T. D., Barr, S. L. and Mills, J. P. (2009) 'Instruments and Methods: Optimizing Photogrammetric DEM's for Glacier Volume Change Assessment Using Laser-Scanning Derived Ground-Control Points', *Journal of Glaciology* 55(189) pp. 106-116. *Citeseer* [Online]. Available at: http://citeseerx.ist.psu.edu/viewdoc/download?doi=10.1.1.430.6921&rep=rep1&type=pdf (Accessed: 05 January 2018).

Barry, P. and Coakley, R. (2013) 'Field Accuracy Test of RPAS Photogrammetry', *UAV-g2013*, Rostock, Germany. 4-6 September. *International Archives of the Photogrammetry, Remote Sensing and Spatial Information Sciences, Volume XL-1/W2* [Online]. Available at: https://www.int-arch-photogramm-remote-sens-spatial-inf-sci.net/XL-1-W2/27/2013/isprsarchives-XL-1-W2-27-2013.pdf (Accessed: 21 November 2019).

Barton, M. and Pearce, R. B. (2015) 'Landslides and Stratigraphy in the Coastal Outcrop of the Barton Clay', *Proceedings of the Geologists Association* 126(6) pp. 731-741. *Science Direct* [Online]. Available at: https://www.sciencedirect.com/science/article/abs/pii/S0016787815001170 (Accessed: 09 October 2017).

Bartos, K., Pukanska, K. and Sabova, J. (2014) 'The Application of Open-Source and Free Photogrammetric Software for the Purposes of Cultural Heritage Documentation', *GeoScience Engineering* 60(2) pp. 17-24. *De Gruyter* [Online]. Available at: https://content.sciendo.com/view/journals/gse/60/2/article-p17.xml (Accessed: 16th October 2018).

Bater, C. W and Coops, N. C. (2009) 'Evaluating Error Associated with Lidar-Derived DEM Interpolation', *Computers and Geosciences* 35(2) pp. 289-300. *ScienceDirect* [Online]. Available at: https://www.sciencedirect.com/science/article/pii/S0098300408002537 (Accessed: 30 August 2018).

Bayazit, U. (2019) 'A Greedy Region Growing Algorithm for Anisotropic Stretch Adaptive Triangulation of Geometry Images', *Graphical Models* 106(101045) pp. 1524-0703. *ScienceDirect* [Online]. Available at: https://www.sciencedirect.com/science/article/pii/S1524070319300360 (Accessed: 13 June 2020).

Bechle, A. J. and Wu, C. H. (2010) 'Virtual Wave Gauges Based Upon Stereo Imaging for Measuring Surface Wave Characteristics', *Coastal Engineering* 58(4) pp. 305-316. *ScienceDirect* [Online]. Available at: https://www.sciencedirect.com/science/article/pii/S0378383910001614 (Accessed: 10 October 2018).

Behling, R., Milewski, R. and Chabrillat, S. (2018) 'Spatiotemporal Shoreline Dynamics of Namibian Coastal Lagoons Derived by a Dense Remote Sensing Time Series Approach', *International Journal of Applied Earth Observation and Geoinformation* 68 pp. 262-271. *ScienceDirect* [Online]. Available at: https://www.sciencedirect.com/science/article/pii/S0303243418300564 (Accessed: 28 November 2018).

Belfiore, O. R. and Parente, C. (2014) 'Comparison of Different Methods to Rectify IKONOS Imagery without use of Sensor Viewing Geometry', *American Journal of Remote Sensing* 2(3) pp. 15-19. *Semantic Scholar* [Online]. Available at: https://pdfs.semanticscholar.org/b81a/6f5ff9534e6fec63bcdf738895b97a9f5e92.pdf (Accessed: 23 April 2018).

Benassi, F., Dall'Asta, E., Diotri, F., Forlani, G., Morra di Cella, U., Roncella, R. and Santise, M. (2017) 'Testing Accuracy and Repeatability of UAV Blocks Oriented with GNSS-Supported Aerial Triangulation', *Remote Sensing* 9(2) pp. 2-23. *MDPI* [Online]. Available at: https://www.mdpi.com/2072-4292/9/2/172 (Accessed: 11 December 2017).

Bemis, S. P., Micklethwaite, S., Turner, D., James, M. R., Akciz, S., Thiele, S. T. and Bangash, H. A. (2014) 'Ground-Based and UAV-Based Photogrammetry: A Multi-Scale, High-Resolution Mapping Tool for Structural Geology and Paleoseismology', *Journal of Structural Geology* 69 (A) pp. 163-178. *ScienceDirect* [Online]. Available at: https://www.sciencedirect.com/science/article/pii/S0191814114002429 (Accessed: 16 June 2016).

Bheeroo, R. A., Chandrasekar, N., Kaliraj, S. and Magesh, N. S. (2016) 'Shoreline Change Rate and Erosion Risk Assessment Along the Trou Aux Biches-Mont Choisy Beach on the Northwest Coast of Mauritius using GIS-DSAS Technique', *Environment Earth Science* 75(444) pp. 1-13. *Springer* [Online]. Available at: https://link.springer.com/article/10.1007/s12665-016-5311-4 (Accessed: 03 September 2018).

Bio, A., Bastos, L., Granja, H, M., Pinho, J. L. S., Goncalves, J. A., Henriques, R. F, Madeira, S., Magalhaes, A. and Rodrigues, D. (2015) 'Methods for Coastal Monitoring and Erosion Risk Assessment: Two Portugueses Case Studies', *Journal of Integrated Coastal Zone Management* 15(1) pp. 47-63. *Repositorium*[Online]. Available at:https://repositorium.sdum.uminho.pt/handle/1822/43284 (Accessed: 23 October 2018).

Bitenc, M., Lindenbergh, R., Khoushelham, K. and Waarden, A. P. (2011) 'Evaluation of a LiDAR Land-Based Mobile Mapping System for Monitoring Sandy Coasts', *Remote Sensing* 3pp. 1472-1491. *Semantic Scholar* [Online]. Available at: https://www.semanticscholar.org/paper/Evaluation-of-a-LIDAR-Land-Based-Mobile-Mapping-for-Bitenc-Lindenbergh/c46581d4105dfeb960057a9b71d0a4f7d75b013e (Accessed: 28 November 2011).

Blazquez, M. and Colomina, I. (2012) 'On INS/GNSS-Based Time Synchronization in Photogrammetric and Remote Sensing Multi-SensorSystems', *PFG* 2012(2) pp. 91-104. *Ingentaconnect*[Online]. Available at: https://www.ingentaconnect.com/content/schweiz/pfg/2012/00002012/00000002/art00002 (Accessed: 20 July 2017).

Bowles, C. J. and Cowgill, E. (2012) 'Discovering Marine Terraces Using Airborne LiDAR Along the Mendocino-Sonoma Coast, Northern California', *Geosphere* 8(2) pp. 386-402. *GeoScienceWorld* [Online]. Available at: https://pubs.geoscienceworld.org/gsa/geosphere/article/8/2/386/132538/discovering-marine-terraces-using-airborne-lidar (Accessed: 09 February 2018).

Braga, F., Tosi, L., Prati, C. and Alberotanza, L. (2013) 'Shoreline Detection: Capability of COSMO-SkyMed and High-Resolution Multispectral Images', *European Journal of Remote Sensing* 46(1) pp. 837-853. *Taylor and Francis* [Online]. Available at: https://www.tandfonline.com/doi/abs/10.5721/EuJRS20134650 (Accessed: 02 August 2018).

Brodu, N. and Lague, D. (2012) '3D Terrestrial LiDAR Data Classification of Complex Natural Scenes Using a Multi-Scale Dimensionality Criterion: Applications in Geomorphology', *ISPRS Journal of Photogrammetry and Remote Sensing* 68 pp. 121-134. *Science Direct* [Online]. Available at: https://www.sciencedirect.com/science/article/abs/pii/S0924271612000330 (Accessed: 06 January 2018).

Brown, J. M., Ciavola, P., Masselink, R., McCall, R. and Plater, A. J. (2016) 'Preface: Monitoring and modelling to Guide Coastal Adaptation to Extreme Storm Events in a Changing Climate', *Natural Hazards and Earth Systems Science* 16 pp. 463-467. *NERC* [Online]. Available at: http://nora.nerc.ac.uk/id/eprint/512728/ (Accessed: 24th October 2018).

Bruno, M. F., Molfetta, M. G., Mossa, M., Nutricato, R., Morea, A. and Chiaradia, M. T. (2016) 'Coastal Observation through Cosmo-SkyMed High-Resolution SAR Images', Journal of Coastal Research (SI) 75- *Proceedings of the 14th International Coastal Symposium* Sydney, 6-11 March. pp. 795-799. *JCR* [Online]. Available at: https://www.jcronline.org/doi/abs/10.2112/SI75-160.1 (Accessed: 04 July 2018).

Brun, F., Buri, P., Miles, E. S., Wagnon, P., Steiner, J., Berthier, E., Ragettli, S., Kraaijenbrink, P., Immerzeel, W. W. and Pellicciotti, F. (2016) 'Quantifying Volume Loss from Ice Cliffs on Debris-Covered Glaciers using High-Resolution Terrestrial and Aerial Photogrammetry', *Journal of Glaciology* 62(234) pp. 684-695. *White Rose Research* [Online]. Available at: http://eprints.whiterose.ac.uk/113670/ (Accessed: 07 March 2018).

Brunier, G., Fleury, J., Anthony, E. J., Gardel, A. and Dussouillez, P. (2016) 'Close Range Airborne Structure-from-Motion Photogrammetry for High-Resolution Beach Morphometric Surveys: Examples from an Embayed Rotating Beach', *Geomorphology* 261 pp. 76-88. *ScienceDirect* [Online]. Available at: https://www.sciencedirect.com/science/article/pii/S0169555X16300617# (Accessed: 18 December 2017).

Bureick, J., Alkhatib, H. and Neumann, I. (2016) 'Robust Spatial Approximation of Laser Scanner Point Clouds by Means of Free-form Curve Approaches in Deformation Analysis', *Journal of Applied Geodesy* 10(1) pp. 27-35. *De Grutyer* [Online]. Available at: https://www.degruyter.com/view/journals/jag/10/1/article-p27.xml (Accessed: 05 June 2020).

Burningham, H. and French, J. (2017) 'Understanding Coastal Change Using Shoreline Trend Analysis Supported by Cluster-Based Segmentation', *Geomorphology* 282 pp. 131-149. *ScienceDirect* [Online]. Available at: https://www.sciencedirect.com/science/article/pii/S0169555X16309503 (Accessed: 23 December 2018).

Callaghan, K., Engelbrecht, J. and Kemp, J. (2015) 'The Use of Landsat and Aerial Photography for the Assessment of Coastal Erosion Susceptibility in False Bay, South Africa', *South African Journal of Geomatics* 4(2) pp. 65-79. *SAJG* [Online]. Available at: http://www.sajg.org.za/index.php/sajg/article/view/233/166 (Accessed: 26 February 2019).

Calligaro, S., Sofia, G., Prosdocimi, M., Fontana, D. G. and Tarolli, P. (2013) 'Terrestrial Laser Scanner Data to Support Coastal Erosion Analysis: The Conero Case Study', *The Role of Geomatics in Hydrogeological Risk*, 27-28 February, Padua, Italy. *The International Archives of the Photogrammetry, Remote Sensing and Spatial Information Sciences, Volume XL-5/W3* [Online]. Available at: https://www.int-arch-photogramm-remote-sens-spatial-inf-sci.net/XL-5-W3/125/2013/isprsarchives-XL-5-W3-125-2013.pdf (Accessed: 26 November 2018).

Campana, S. (2017) 'Drones in Archaeology. State-of-the-Art and Future Perspectives', *Archaeological Prospection* 24(4) pp. 275-296. *Wiley Library* [Online]. Available at: https://onlinelibrary.wiley.com/doi/full/10.1002/arp.1569 (Accessed: 08 May 2019).

Cantreul, V., Bielders, C., Calsamiglia, A. and Degre, A. (2018) 'How Pixel Size Affects a Sediment Connectivity index in Central Belgium', *Earth Surface Processes and Landforms* 43(4) pp. 884-893. *Wiley Library* [Online]. Available at: https://onlinelibrary.wiley.com/doi/abs/10.1002/esp.4295 (Accessed: 17 July 2019).

Caprioli, M., Trizzino, R., Mazzone, F. and Scarano, M. (2016) 'Experiences of UAV Surveys Applied to Environmental Risk Management', *XXIII ISPRS Congress*, Prague, Czech Republic, 12-19 July. *The International Archives of the Photogrammetry, Remote Sensing and Spatial Information Sciences*, *Volume XLI-B1* [Online]. Available at: https://www.int-arch-photogramm-remote-sens-spatial-inf-sci.net/XLI-B1/797/2016/isprs-archives-XLI-B1-797-2016.pdf (Accessed: 25 January 2019).

Caputo, T., Marino, E., Matano, F., Somma, R. Troise, C. and Natale, G. D. (2018) 'Terrestrial Laser Scanning (TLS) Data for the Analysis of Coastal Tuff Cliff Retreat: Application to Coroglio Cliff, Naples, Italy', *Annals of Geophysics* 61(1) pp. 110-118. *Annals of geophysics* [Online]. Available at: https://www.annalsofgeophysics.eu/index.php/annals/article/view/7494?acceptCookies=1 (Accessed: 31 August 2018).

Carbonneau, P. E. and Dietrich, J. T. (2017) 'Cost-Effective Non –Metric Photogrammetry from Consumer Grade sUAS: Implications for Direct Georeferencing of Structure from Motion Photogrammetry', *Earth Surface Processes and Landforms* 42(3) pp. 473-486. *Wiley Library* [Online]. Available at: https://onlinelibrary.wiley.com/doi/abs/10.1002/esp.4012 (Accessed: 16th April 2019).

Carrivick, J. L. and Smith, M. W. (2018) 'Fluvial and Aquatic Applications of Structure from Motion Photogrammetry and Unmanned Aerial Vehicle/Drone Technology', *WIREs Water* 6(1) pp. 1-17. *Wiley Library* [Online]. Available at: https://onlinelibrary.wiley.com/doi/10.1002/wat2.1328 (Accessed: 11 January 2019).

Carter, T. G., Begin, A., Dittrich, P., Evans, C., Byron, J., Rico, P., Carvalho, J. L., Solis, N., Gillinder, R., Brewster, L. F., Arthur, R., Williamson, D. and Murdock, R. (2018) 'Innovative Use of GIS and Drone Photogrammetry for Cliff Stability Modelling', *Proceedings of the Institute of Civil Engineers – Maritime Engineering* 171 (3) pp. 89-97. *ICE Virtual Library* [Online]. Available at: https://www.icevirtuallibrary.com/doi/abs/10.1680/jmaen.2018.17 (Accessed: 12 February 2019).

Carter, N., Hashemian, A., Mckelvey, N. (2019) 'An Optimization of Small Unmanned Aerial System (sUAS) Image Based Scanning Techniques for Mapping Accident Sites', *SAE Technical Paper 2019-01-0427.SAE Mobilus* [Online]. Available at: https://saemobilus.sae.org/content/2019-01-0427/ (Accessed: 11 September 2019).

Casella, E., Drechsel, J., Winter, C., Benninghoff, M. and Rovere, A. (2020) 'Accuracy of Sand Beach Topography Surveying by Drones and Photogrammetry', *Geo-Marine Letters* 40 pp. 255-268. *Springer* [Online]. Available at: https://link.springer.com/article/10.1007/s00367-020-00638-8 (Accessed: 11 November 2021).

Casella, E., Rovere, A., Pedroncini, A., Mucerino, L., Casella, M., Cusati, L. A., Vacchi, M., Ferrari, M. and Firpo, M. (2014) 'Study of Wave Runup Using Numerical Models and Low-Altitude Aerial Photogrammetry: A Tool for Coastal Management', *Estuarine, Coastal and Shelf Science* 149(5) pp. 160-167. *ScienceDirect* [Online]. Available at: https://www.sciencedirect.com/science/article/pii/S0272771414002273 (Accessed: 24th October 2018).

Casella, E., Rovere, A., Pedroncini, A.,Stark, C. P., Casella, M., Ferrari, M. and Firpo, M. (2016) 'Drones as Tools for Monitoring Beach Topography Changes in the Ligurian Sea (NW Mediterranean)', *Geo-Marine Letters* 36(2) pp. 151-163. *Springer* [Online]. Available at: https://link.springer.com/article/10.1007/s00367-016-0435-9 (Accessed: 03 April 2019).

Castedo, R., Paredes, C., Vega-Panizo, R. D. and Santos, A. (2017) 'The Modelling of Coastal Cliffs and Future Trends', in Shukla, D. P. *Hydro-Geomorphology, Models and Trends*, Croatia: InTech, pp. 53-78.

Catalucci, S., Marsili, R., Moretti, M. and Rossi, G. (2018) 'Comparison between Point Cloud Processing Techniques', *Measurement* 127 pp. 221-226. *ScienceDirect* [Online]. Available at: https://www.sciencedirect.com/science/article/pii/S0263224118305116 (Accessed: 14 May 2020).

Caudle, T. L., Paine, J. G., Andrews, J. R. and Saylam, K. (2019) 'Beach, Dune, and Nearshore Analysis of Sourthern Texas Gulf Coast Using Chiroptera LIDAR and Imaging System', *Journal of Coastal Research* 35(2) pp. 251-268. *JCR* [Online]. Available at: https://www.jcronline.org/doi/full/10.2112/JCOASTRES-D-18-00069.1 (Accessed: 04 April 2019).

Cazenave, A. and Cozannet, G. L. (2013) 'Sea Level Rise and its Coastal Impacts', *Earth's Future* 2 pp. 15-34. *AGU Publications* [Online]. Available at: https://agupubs.onlinelibrary.wiley.com/doi/pdf/10.1002/2013EF000188 (Accessed: 15th October 2018).

Cermakova, I., Komarkova, J. and Sedlak, P. (2016) 'Using UAV to Detect Shoreline Changes: Case Study-Pohranov Pond, Czech Republic', *XXIII ISPRS Congress, Prague, Czech Republic*, 12-19 July. The International Archives of the Photogrammetry, Remote Sensing and Spatial Information Sciences [Online]. Available at: https://www.int-arch-photogramm-remote-sens-spatial-inf-sci.net/XLI-B1/ (Accessed: 25 November 2018).

Chaaban, F., Darwishe, H., Battiau-Queney, Y., Louche, B., Masson, E., El Khattabi, J. and Carlier, E. (2012) 'Using ArcGIS Modelbuider and Aerial Photographs to Measure Coastline Retreat and Advance: North of France', *Journal of Coastal Research* 28(6) pp. 1567-1579. *JCR* [Online]. Available at: https://www.jcronline.org/doi/abs/10.2112/JCOASTRES-D-11-00054.1 (Accessed: 27 March 2018).

Chamat, L. R. and Anupriya (2018) 'Calculation of Cut and Fill of Earthworks with Quantum-GIS', *International Journal for Scientific Research and Development (IJSRD)* 6(3) pp. 2000-2004. *IJSRD* [Online]. Available at: http://ijsrd.com/index.php (Accessed: 03 January 2021).

Champion, E. and Rahaman, H. (2019) '3D Digital Heritage Models as Sustainable Scholarly Resources', *Sustainability* 11(8) pp. 1-8. *MDPI* [Online]. Available at: https://www.mdpi.com/2071-1050/11/8/2425 (Accessed: 11 January 2019).

Chandler, J. H. and Buckley, S. (2016) 'Structure from Motion (SFM) Photogrammetry vs Terrestrial Laser Scanning', *Geoscience Handbook: AGI Data Sheets, 5th ed, Alexandria, VA: American Geosciences Institute*, Section 20.1. *Loughborough University* [Online]. Available at: https://repository.lboro.ac.uk/articles/Structure_from_motion_SFM_photogrammetry_vs_terrestrial_laser_scanning/9457565# (Accessed: 21 November 2017).

Chang, Y., Chu, K., Chuang, L. Z. (2018) 'Sustainable Coastal Zone Planning Based on Historical Coastline Changes: A Model from Case Study in Tainan, Taiwan', *Landscape and Urban Planning*174 pp. 24-32. *ScienceDirect* [Online]. Available at: https://www.sciencedirect.com/science/article/pii/S0169204618300689 (Accessed 26 December 2018).

Chen, B., Yang , Y., Wen, H., Ruan, H., Zhou, Z., Luo, K. and Zhong, G. (2018) 'High-Resolution Monitoring of Beach Topography and its Change Using Unmanned Aerial Vehicle Imagery', *Ocean and Coastal Management* 160 pp. 103-116. *ScienceDirect* [Online]. Available at: https://www.sciencedirect.com/science/article/pii/S0964569117310013 (Accessed: 06 January 2020).

Chen, C., Liu, F., Li, Y., Yan, C. and Liu, G. (2016) 'A Robust Interpolation Method for Constructing Digital Elevation Models from Remote Sensing Data', *Geomorphology* 268 pp. 275-287. *Science Direct* [Online]. Available at: http://www.sciencedirect.com/science/journal/0169555X (Accessed: 16 December 2016).

Chesley, J. T., Leier, A. L., White, S. and Torres, R. (2017) 'Using Unmanned Aerial Vehicles and Structure-from-Motion Photogrammetry to Characterize Sedimentary Outcrops: An Example from the Morrison Formation, Utah, USA', *Sedimentary Geology* 354 pp. 1-7. *ScienceDirect* [Online]. Available at: https://www.sciencedirect.com/science/article/pii/S0037073817300817 (Accessed: 21 September 2018).

Cheng, J., Wang, P. and Guo, Q. (2016) 'Measuring Beach Profiles Along a Low-Wave Energy Microtidal Coast, West-Central Florida, USA', *Geosciences* 6(4) Art 44 pp. 2-12. *ScholarCommons* [Online]. Available at: https://scholarcommons.usf.edu/geo_facpub/1080/ (Accessed: 10 April 2016).

Chiabrando, F., Donadio, E. and Rinaudo, F. (2015) 'SFM Orthophoto Generation: A Winning Approach for Cultural Heritage Knowledge', 25th *International CIPA Symposium*, Taipei, Taiwan. 31 August – 04 September. *The International Archives of the Photogrammetry, Remote Sensing and Spatial Information Sciences, Volume XL-5/W7 ISPRS* [Online]. Available at: http://www.close-range.com/docs/SfM_for_orthophoto_to_Generation_isprsarchives-XL-5-W7-91-2015.pdf (Accessed: 25 November 2019).

Chiabrando, F., Lingua, A., Maschio, P and Lose, T. (2017) 'The Influence of Flight Planning and Camera Orientation in UAVs Photogrammetry, A Test in the Area of Rocca San Silvestro (LI), Tuscany', *3D Virtual Reconstruction and Visualization of Complex Architectures*, Nafplio, Greece. 1-3 March. *The International Archives of the Photogrammetry, Remote Sensing and Spatial Information Sciences, Volume XLII-2/W3, ISPRS* [Online]. Available at: https://www.int-arch-photogramm-remote-sens-spatial-inf-sci.net/XLII-2-W3/163/2017/isprs-archives-XLII-2-W3-163-2017.pdf (Accessed: 25 November 2019).

Chikhradze, N., Henriques, R., Elashvili, M., Kirkitadze, G., Janelidze, Z., Bolashvili, N. and Lominadze, G. (2015) 'Close Range Photogrammetry in the Survey of the Coastal Area Geoecological Conditions (on the Example of Potugal)', *Earth Ecience* 4(5-1) pp. 35-40. *SciencePG*[Online]. Available at: http://www.sciencepublishinggroup.com/journal/paperinfo.aspx?journalid=161&doi=10.11648/j.earth.s.2015040501.17 (Accessed: 04 November 2019).

Choi, J., Kim, G., Park, N., Park, H. and Choi, S. (2017) 'A Hybrid Pansharpening Algorithm of VHR Satellite Images that Employs Injection Gains Based on NDVI to Reduce Computational Coasts', *Remote Sensing* 9(10) pp. 2-21. *MDPI* [Online]. Available at: https://www.mdpi.com/2072-4292/9/10/976 (Accessed: 10 April 2018).

Choi, K. and Lee, I. (2013) 'A Sequential Aerial Triangulation Algorithm for Real Time Georeferencing of Images Sequences Acquired by an Airborne Multi-Sensor System', *Remote Sensing* 5(1) pp. 57-82. *MDPI* [Online]. Available at: https://www.mdpi.com/2072-4292/5/1/57 (Accessed: 22 November 2019).

Choi, W. and Oh, S. (2012) 'Fast Nearest Neighbor Search using Approximate Cached K-d Tree', *IEEE/RSJ International Conference on Intelligent Robots and Systems*, Vilamoura-Algarve, Portugal, 7-12 October, pp. 4524-4529. *IEEE Explore* [Online]. Available at: https://ieeexplore.ieee.org/abstract/document/6385837/authors (Accessed: 01 March 2021).

Cimoli, E., Marcer, M., Vandecrux, B., Boggild, C. E., Williams, G. and Simonsen, S. B. (2017) 'Application of Low-Cost UAS's and Digital Photogrammetry for High-Resolution Snow Depth Mapping in the Arctic', *Remote Sensing* 9(11) pp. 1-29. *MDPI* [Online]. Available at: https://www.mdpi.com/2072-4292/9/11/1144 (Accessed: 18th October 2018).

Clapuyt, F., Vanacker, V. and Oost, K. V. (2016) 'Reproducibility of UAV-Based Earth Topography Reconstructions Based on Structure-from-Motion Algorithms', *Geomorphology* 260 pp. 4-15. *ScienceDirect* [Online]. Available at: https://www.sciencedirect.com/science/article/pii/S0169555X15002652(Accessed: 12 April 2019).

Clark, A. (2017) 'Small Unmanned Aerial Systems Comparative Analysis for the Application to Coastal Erosion Monitoring',*GeoResJ* 13 pp. 175-185. *ScienceDirect* [Online]. Available at: https://www.sciencedirect.com/science/article/pii/S2214242816300729 (Accessed: 19 January 2019).

Cloern, J. E., Abreu, P.C., Carstensen, J., Chauvaud, L., Elmgren, R., Grall, J., Greening, H., Johansson, J.O., Kahru, M., Sherwood, E. T., Xu, J. and Yin, K. (2016) 'Human Activities and Climate Variability Drive Fast-Paced Change Across the World's Estuarine–Coastal Ecosystems', *Global Change Biology* 22 pp. 513-529. *John Wiley and sons* [Online]. Available at: http://onlinelibrary.wiley.com/doi/10.1111/gcb.13059/full (Accessed: 10th December 2016).

CloudCompare (2020) *3D Point Cloud and Mesh Processing Software*. Available at: https://cloudcompare.org/ (Accessed: 23 June 2020).

Colomina, I. and Molina, P. (2014) 'Unmanned aerial systems for photogrammetry and remote sensing: A review', *ISPRS Journal of Photogrammetry and Remote Sensing* 92, pp. 79-97. *Science Direct* [Online]. Available at: http://www.sciencedirect.com/science/article/pii/S0924271614000501(Accessed: 25 May 2016)

Conlin, M., Cohn, N. and Ruggiero, P. (2018) 'A Quantitative Comparison of Low-Cost Structure from Motion (SFM) Data Collection Platforms on Beach and Dunes', *Journal of Coastal Research* 34(6) pp. 1341-1357. *JCR* [Online]. Available at: https://www.jcronline.org/doi/full/10.2112/JCOASTRES-D-17-00160.1 (Accessed: 03 April 2019).

Constable, C. (2016) 'Earth's Electromagnetic Environment', *Surveys in Geophysics* 37(1) pp. 27-45. *Springer* [Online]. Available at: https://link.springer.com/article/10.1007/s10712-015-9351-1 (Accessed: 03 October 2019).

Cook, K. L. (2017) 'An Evaluation of the Effectiveness of Low-Cost UAVs and Structure from Motion for Geomorphic Change Detection', *Geomorphology* 278 pp.195-208. *ScienceDirect* [Online]. Available at: https://www.sciencedirect.com/science/article/pii/S0169555X16310686 (Accessed: 09 August 2018).

Cooper, H. M., Fletcher, C. H., Chen, Q. and Barbee, M. M. (2013) 'Sea-Level Rise Vulnerability Mapping for Adaptation Decisions Using LiDAR DEMs', *Progress in Physical Geography: Earth and Environment* 37(6) pp. 745-766. *Sage Journals* [Online]. Available at: https://journals.sagepub.com/doi/abs/10.1177/0309133313496835 (Accessed: 09 July 2019).

Crisp, N. H., Livadiotti, S. and Roberts, P. C. E. (2018) 'A Semi-Analytical Method for Calculating Revisit Time for Satellite Constellations with Discontinuous Coverage', *ArXiv e-prints*. *The University of Manchester* [Online]. Available at: https://www.manchester.ac.uk/ (Accessed: 07 August 2018).

Cunningham, K., Walker, G., Stahlke, E. and Wilson, R. (2011) 'Cadastral Audit and Assessments Using Unmanned Aerial System', *UAV-g (Unmanned Aerial Vehicle in Geomatics) Conference*, Zurich, Switzerland 14-16 September. *International Archives of the Photogrammetry, Remote Sensing and Spatial Information Sciences* [Online]. Available at: http://www.teamconsulting.cc/images/uav-geomatics.pdf (Accessed: 19th October 2016).

Currier, K. (2015) 'Mapping with Strings Attached: Kite Aerial Photography of Durai Island, Anambas Islands, Indonesia', *Journal of Maps* 11(4) pp. 589-597. *Taylor and Francis* [Online]. Available at: https://www.tandfonline.com/doi/abs/10.1080/17445647.2014.925839 (Accessed: 24 March 2019).

Cwiakala, P., Kocierz, R., Puniach, E., Nedzka, M., Mamczarz, K., Niewiem, W. and Wiacek, P. (2018) 'Assessment of the Possibility of Using Unmanned Aerial Vehicles (UAVs) for the Documentation of Hiking Trails in Alpine Areas', *Sensors* 18(1) pp. 2-28. *NCBI* [Online]. Available at: https://www.ncbi.nlm.nih.gov/pmc/articles/PMC5795845/ (Accessed: 02 July 2019).

Dada, O. A., Li, G., Qiao, L., Ding, D., Ma, Y. and Xu, Jishang (2016) 'Seasonal Shoreline Behaviours along the Arcuate Niger Delta Coast: Complex Interaction Fluvial and Marine Processes', *Continental Shelf Research* 122(1) pp. 51-67. *ScienceDirect* [Online]. Available at: https://www.sciencedirect.com/science/article/pii/S027843431630098X (Accessed: 11 April 2019).

Dai, F., Feng, Y. and Hough, R. (2014) 'Photogrammetric Error Sources and Impacts on Modelling and Surveying in Construction Engineering Applications', *Visualization in Engineering* 2(2) pp. 2-14. *Springer* [Online]. Available at: https://link.springer.com/content/pdf/10.1186%2F2213-7459-2-2.pdf (Accessed: 17 December 2018).

Damon, C. (2016) 'Small Unmanned Aircraft (SUA) Pilot Project. The USAID/Ghana Sustainable Fisheries Management Project (SFMP)', *Narragansett, RI: Coastal Resources Center, Graduate School of Oceanography, University of Rhode Island and Environmental Data Center. GH2014_SCI019_EDC. 29* pp. 1-29. [Online]. Available at: http://www.crc.uri.edu/download/GH2014_SCI019_EDC_FIN508.pdf (Accessed: 25 July 2016).

Dansereau, D. G., Schuster, G., Ford, J. and Wetztein, G. (2017) 'A Wide-Field-of-View Monocentric Light Field Camera',*The IEEE Conference on Computer Vision and Pattern Recognition,CVPR*Honglulu, Hawai, 21-26 July, pp. 5048-5057. *CVPR* [Online]. Available at: http://openaccess.thecvf.com/content_cvpr_2017/html/Dansereau_A_Wide-Field-Of-View_Monocentric_CVPR_2017_paper.html (Accessed: 10 April 2019).

Darwin, N., Ahmad, A. and Zainon, O. (2014) 'The Potential of Unmanned Aerial Vehicle for Large Scale Mapping of Coastal Area', *IOP Conference Series: Earth and Environmental Science* 38(1) pp. 1-6. *IOPScience* [Online]. Available at: http://iopscience.iop.org/article/10.1088/1755-1315/18/1/012031/meta (Accessed: 07 November 2018).

Demir, N., Oy, S., Erdem, F., Seker, D. Z. and Bayram, B. (2017) 'Integrated Shoreline Extraction Approach with use of Rasat MS and Sentinel-1A SARImages',*ISPRS Annals of the Photogrammetry, Remote Sensing and Spatial Information Sciences, ISPRS Geospatial Week* Wuhan, China, 18-22 September. *ISPRS* [Online]. Available at: https://www.isprs-ann-photogramm-remote-sens-spatial-inf-sci.net/IV-2-W4/445/2017/ (Accessed: 04 November 2019).

De Rose, R. C. and Basher, L. R. (2011) 'Measurement of River Bank and Cliff Erosion from Sequential LiDAR and Historical Aerial Photography', *Geomorphology* 126 (1-2) pp. 132-147. *ScienceDirect* [Online]. Available at: https://www.sciencedirect.com/science/article/pii/S0169555X10004861 (Accessed: 13 February 2018).

Deseilligny, M. P. and Clery, I. (2011) 'Apero, an Open Source Bundle Adjustment Software for Automatic Calibration and Orientation of Set of Images', *ISPRS Trento 2011 Workshop* , Trento, Italy, 2-4 March. *International Archives of the Photogrammetry, Remote Sensing and Spatial Information Sciences, Volume XXXVIII-5/W16. ISPRS* [Online]. Available at: https://www.int-arch-photogramm-remote-sens-spatial-inf-sci.net/XXXVIII-5-W16/ (Accessed: 28 April 2018).

Desert Star Helikite. *Allsopp Helikites Limited* [Online]. http://www.allsopp.co.uk/index.php?mod=page&id_pag=63 (Accessed 01 July 2021).

De Vilder, S. J., Rosser, N. J., Brain, M. J. and Vann, J. (2017) 'Forensic Rockfall Scar Analysis: Development of a Mechanically Correct Model of Rockfall Failure', *3rd North American Symposium on Landslides*, Roanoke, Virginia, USA, 2-8 June. *Durham Research* [Online]. Available at: http://dro.dur.ac.uk/22116/ (Accessed: 19 April 2019).

Dewez, T. J. B., Rohmer, J., Regard, V. and Cnudde, C. (2013) 'Probabilistic Coastal Cliff Collapse Hazard from Repeated Terrestrial Laser Surveys: Case Study from Mesnil Val (Normandy, Northern France)', *Journal of Coastal Research, Special Issue* 65(1) pp. 702-707. *JCR* [Online]. Available at: https://www.jcronline.org/doi/abs/10.2112/SI65-119.1 (Accessed: 25 August 2019).

Dewez, T. J. B., Leroux, J. and Morelli, S. (2016) 'Cliff Collapse Hazard from Repeated Multicopter UAV Acquisitions: Return on Experience', *XXIII ISPRS Congress*, Prague, Czech Republic, 12-19 July. *The International Archives of the Photogrammetry, Remote Sensing and Spatial Information Sciences, Volume XLI-B5. ISPRS* [Online]. Available at: https://www.int-arch-photogramm-remote-sens-spatial-inf-sci.net/XLI-B5/805/2016/isprs-archives-XLI-B5-805-2016.pdf (Accessed 02 May 2019).

Di, K., Wang, J., Ma, R. and Li, R. (2003) 'Automatic Shoreline Extraction from High-Resolution IKONOS Satellite Imagery', *ASPRS Annual Conference Proceedings Anchorage*, Alaska held in May [online]. Available at: http://shoreline.ceegs.ohio-state.edu/publications/di_asprs03.pdf (Accessed: 03 January 2013).

Dominici, D., Alicandro, M. and Massimi, V. (2017) 'UAV Photogrammetry in the Post-Earthquake Scenario: Case Studies in L'Aquila', *Geomatics, Natural Hazards and Risk* 8(1) pp. 87-103. *Taylor and Francis* [Online]. Available at: https://www.tandfonline.com/doi/full/10.1080/19475705.2016.1176605 (Accessed: 01 March 2018).

Dominici, D., Zollini, S., Alicandro, M., Torre, F. D., Buscema, P. M. and Baiocchi, V. (2019) 'High Resolution Satellite Images for Instantaneous Shoreline Extraction using New Enhancement Algorithms', *Geosciences* 9(3) pp. 1-20. *MDPI* [Online]. Available at: https://www.mdpi.com/2076-3263/9/3/123/htm (Accessed: 07 July 2020).

Doneus, M., Doneus, N., Briese, C., Pregesbauer, M., Mandlburger, G. and Verhoeven, M. (2013) 'Airborne Laser Bathymetry – Detecting and Recording Submerge Archaeological Sites from the Air', *Journal of Archealogical Science* 40(4) pp. 2136-2151. *ScienceDirect* [Online]. Available at: https://www.sciencedirect.com/science/article/pii/S0305440312005420 (Accessed: 27 August 2018).

Doyle, T. B. and Woodroffe, C. D. (2018) 'The Application of LiDAR to Investigate Foredune Morphology and Vegetation', *Geomorphology*303 pp. 106-121. *Science Direct* [Online]. Available at: https://www.sciencedirect.com/science/article/pii/S0169555X17304683 (Accessed: 22 January 2018).

Draeyer, B. and Strecha, C. (2014) 'Pix4D White Paper: How Accurate are UAV Surveying Methods?', *Pix4D* [Online]. Available at: https://pix4d.com/wp-content/uploads/2016/11/Pix4D-White-paper_How-accurate-are-UAV-surveying-methods.pdf (Accessed: 06 July 2018).

Drummond, C., Dam, T. and McDonald, G. (2016) 'Use of Drone Surveying to Quantify Risks to Coastal Assets for the Wyong Coastline', *IPWEA NSW State Conference*, Hunter, Valleys, 27-28 October. *UNSW Library* [Online]. Available at: http://unsworks.unsw.edu.au/fapi/datastream/unsworks:44242/bin0959001c-6de6-4ca7-811b-acb85ce7bd4b?view=true (Accessed: 28 January 2019).

Duffy, J. P., Shutler, J. D., Witt, M. J., DeBell, L. and Anderson, K. (2018) 'Tracking Fine-Scale Structural Changes in Coastal Dune Morphology Using Kite Aerial Photography and Uncertainty-Assessed Structure-from-Motion Photogrammetry', *Remote Sensing* 10(9) pp. 2-21. *MDPI* [Online]. Available at: https://www.mdpi.com/2072-4292/10/9/1494 (Accessed: 25 March 2019).

Du, R. and Lee, H. J. (2012) 'A Novel Compression Algorithm for LiDAR Data', *5th International Congress on Image and Signal Processing, Chongqing, China*, 16-18 October. *IEEE Xplore* [Online]. Available at: https://ieeexplore.ieee.org/abstract/document/6469993/ (Accessed: 30 August 2018).

Earlie, C., Masselink, G., Russell, P. and Shail, R. (2014) 'Application of Airborne LiDAR to Investigate Rates of Recession in Rocky Coast Environments', *Journal of Coastal Conservation* 19(6) pp. 831-845. pp. 831-845. *Springer* [Online]. Available at: https://link.springer.com/article/10.1007/s11852-014-0340-1 (Accessed: 09 March 2014).

Earlie, C., Masselink, G., Russell, P. and Shail, R. (2013) 'Sensitivity Analysis of the Methodology for Quantifying Cliff Erosion Using Airborn LiDAR-Examples from Cornwall, UK', *Journal of Coastal Research*, SI(63) pp. 470-475. *JCR* [Online]. Available at: https://www.jcronline.org/doi/full/10.2112/SI76-014 (Accessed: 07 February 2018).

Earlie, C., Masselink, G. and Russel, P. (2017) 'The Role of Beach Morphology on Coastal Cliff Erosion Under Extreme Waves', *Earth Surface Processes and Landforms* 43(6) pp. 1213-1228. *Wiley Library* [Online]. Available at: https://onlinelibrary.wiley.com/doi/full/10.1002/esp.4308 (Accessed: 15 February 2018).

Easa, S. M. (2013) 'Space Resection in Photogrammetry Using Collinearity Condition Without Linearization', *Survey Review* 42(315) pp. 40-49. *Taylor and Francis* [Online]. Available at: https://www.tandfonline.com/doi/abs/10.1179/003962609X451681 (Accessed: 30 November 2019).

Eboigbe, M. A. and Kidner, D. B. (2020) 'Assessment of the Precision of a Smart-Phone Pole Photogrammetry for a Second-Order Cliff Surface Deformation Studies' *ASPRS 2020 Annual Conference Virtual Technical Program,* 22-26 June. *The International Archives of Photogrammetry, Remote Sensing and Spatial Information Sciences*, *XLIV-M-2-2020, 44*, pp.15-24. ISPRS [Online]. Available at: https://www.int-arch-photogramm-remote-sens-spatial-inf-sci.net/XLIV-M-2-2020/15/2020/ (Accessed 08 November 2021).

Eboigbe, M. A. (2017) 'Exploring the Cartographic and Analytical Functionalities of Quantum GIS: A Comparative Evaluation with MapInfo', *International Journal for Research and Development in Technology* 8(3) pp. 217-225. *IJRDT* [Online]. Available at: https://www.ijrdt.org/see_album_all_paper/3057/Issue-3-Sept-2017 (Accessed 11 November 2021).

Eboigbe, M. A., Kidner, D. B. and Sam, A. A. (2019) 'Assessing the Respective Photogrammetric Bundle Adjustment Algorithms from Unordered Digital Images for Shoreline Monitoring' *ICCEIR 2019: 13 International Conference on Civil Engineering Informatics and Research* 05-06 August, Montreal, Canada.

Eitel, J. U. H., Hofle, B., Vierling, L. A., Abellan, A., Asner, G. P., Deems, J. S., Glennie, C. L., Joerg, P. C., LeWinter, A. L., Magney, T. S.,Mandlburger, G., Morton, D. C., Muller, J. and Vierling, K. T. (2016) 'Beyond 3-D: The New Spectrum of LiDAR Applications for Earth and Ecological Sciences', *Remote Sensing of Environment* 186 pp. 372-392. *ScienceDirect* [Online]. Available at: https://www.sciencedirect.com/science/article/abs/pii/S0034425716303212 (Accessed: 21 December 2017).

Elaksher, A. (2008) 'Fusion of Hyperspectral Images and LiDAR-Based DEMs for Coastal Mapping', *Optics and Lasers in Engineering* 46(7) pp. 493-498. *Science Direct* [Online].Available at: https://www.sciencedirect.com/science/article/pii/S0143816608000201 (Accessed: 08 January 2016).

Elaksher, A. F. (2017) 'Shorelines Extraction and Generalization Using Spatiotemporal Datasets'*Geosciences Research* 2(3) pp. 161-171. *Isaac Scientific Publishing* [Online]. Available at: http://www.isaacpub.org/9/1335/2/3/08/2017/GR.html (Accessed: 14 September 2017).

El-Ashmawy, K. L. A. (2015) 'A Comparison Study between Collinearity Condition, Coplanarity Condition, and Direct Linear Transformation (DLT) Method for Camera Exterior Orientation Parameters Determination', *Geodesy and Cartography* 41(2) pp. 66-73. *TandF* [Online]. Available at: https://www.tandfonline.com/doi/abs/10.3846/20296991.2015.1051335 (Accessed: 04 January 2020).

El-Asmar, E., Taha, M. M. N. and El-Sorogy, A. (2016) 'Morphodynamic Changes as an impact of Human Intervention at the Ras El-Damietta Harbor Coast, NW Damietta Promontory, Nile Delta, Egypt', *Journal of African Earth Sciences* 124 pp. 323-339. *ScienceDirect* [Online]. Available at: https://www.sciencedirect.com/science/article/pii/S1464343X16303296 (Accessed: 28 September 2016).

Elnima, E. E. (2015) 'A Solution for Exterior and Relative Orientation in Photogrammetry, a Genetic Evolution Approach', *Journal of King Saud University – Engineering Sciences* 27 pp. 108-113. *ScienceDirect* [Online]. Available at: https://www.sciencedirect.com/science/article/pii/S1018363913000196 (Accessed: 10 April 2018).

Esposito, G., Salvini, R., Matano, F., Sacchi, M., Danzi, M., Somma, R. and Troise, C. (2017) 'Multitemporal Monitoring of a Coastal Landslide through SFM-Derieved Point Cloud Comparison', *The Photogrammetric Record* 32(160) pp. 459-479. *Ingenta Connect* [Pnline]. Available at: https://www.ingentaconnect.com/content/asprs/pers/2010/00000076/00000010/art00001;jsessionid=2b0icttstd7nn.x-ic-live-02# (Accessed 11 July 2020).

Estellers, V., Scott, M., Tew, K. and Soatto, S. (2015) 'Robust Poisson Surface Reconstruction', *International Conference on Scale Space and Variational Methods in Computer Vision*, Lege-Cap Ferret, France, 31 May – 4 April. *Springer* [Online]. Available at: https://link.springer.com/book/10.1007/978-3-319-18461-6 (Accessed: 28 February 2021).

Eulie, D. O., Walsh, J. P. and Corbett, D. R. (2013) 'High-resolution Analysis of Shoreline Change and Application of Balloon-Based Aerial Photography, Albemarle-Pamlico Estuarine System, North Carolina, USA', *America Society of Limnology and Oceanography, Inc*.11, pp. 151-160. *Wiley Library* [Online]. Available at: http://onlinelibrary.wiley.com/doi/10.4319/lom.2013.11.151/abstract (Accessed: 24 August 2016)

Fabbri, S., Giambastiani, B. M. S., Sistilli, F. Scarelli, F., Scarelli, F. and Gabbianelli, G. (2017) 'Geomorphological Analysis and Classification of Foredune Ridges Based on Terrestrial Laser Scanning (TLS) Technology', *Geomorphology* 295 pp. 436-451. *Science Direct* [Online]. Available at: https://www.sciencedirect.com/science/article/abs/pii/S0169555X16307322 (Accessed: 28 November 2017).

Fairley, I., Thomas, T., Philips, M. R. and Reeve, D. (2016) 'Terrestrial Laser Scanner Techniques for Enhancement in Understanding of Coastal Environment', *Seafloor Mapping Along Continental Shelves*, *Coastal Research Library* 13 pp. 1-24. *Springer* [Online]. Available at: https://link.springer.com/chapter/10.1007/978-3-319-25121-9_11 (Accessed: 02 August 2018).

Fallavollita, P., Balsi, M., Esposito, S., Melis, M. G., Milanese,M. and Zappino (2013) 'UAS for Archaeology. New Perspectives on Aerial Documentation', *UAV-g2013*, Rostock, Germany, 4-6 September. *International Archives of the Photogrammetry, Remote Sensing and Spatial Information Sciences*, Volume *XL-1/W2ISPRS* [Online]. Available at: https://www.int-arch-photogramm-remote-sens-spatial-inf-sci.net/XL-1-W2/131/2013/isprsarchives-XL-1-W2-131-2013.pdf (Accessed: 11 January 2019).

Famuditi, T. O., Potts, J. and Bray, M. (2014) 'Towards Effective Public Consultation and Participation in Nigeria: Lessons from Shoreline Management Plans (SMPs) Activities in England', *International Letters of Natural Scienc*e 15(1) pp. 65-77. *AGRO* [Online]. Available at: http://agro.icm.edu.pl/agro/element/bwmeta1.element.agro-b2a10fdc-b84b-4035-be95-2ed0e26d3d45 (Accessed: 25th October 2018).

Farr, G., Jones, P. S., Pearce, H. and Woodman, J. (2017) 'Adiantum Capillus-Veneris (Maidebhair Fern) along the Vale of Glamorgan Coastline, South Wales, UK: A Comparison of Surveys over 30 years', *NERC Open Research Archive* 135 pp. 29-33. *NERC* [Online]. Available at: http://nora.nerc.ac.uk/id/eprint/517493/ (Accessed: 05 May 2020).

Feng, Y. and Wang, J. (2008) 'GPS RTK Performance Characteristics and Analysis', *Journal of Global Positioning Systems* 7(1) pp. 1-8. *Scientific Research* [Online]. Available at: https://www.scirp.org/journal/PaperInformation.aspx?paperID=376& (Accessed: 12 April 2019).

Fernandez-Hernandez, J., Gonzalez-Aguilera, D., Rodriguez-Gonzalvez, P. and Mancera-Taboada, J. (2015) 'Image-Based Modelling from Unmanned Aerial Vehicle (UAV) Photogrammetry: An Effective, Low-Cost Tool for Archaeological Applications', *Archaeometry* 57(1) pp. 128-145. *Wiley* [Online]. Available at: https://onlinelibrary.wiley.com/doi/pdf/10.1111/arcm.12078 (Accessed: 11 October 2018).

Fernandez, T., Perez, J. L., Colomo, C., Cardenal, J., Delgado, J., Palenzuela, J. A., Irigaray, C. and Chacon, J. (2017) 'Assessment of the Evolution of a Landslide using Digital Photogrammetry and LiDAR Techniques in the Alpujarras Region (Granada, Southeastern Spain)', *Geosciences* 7(32) pp. 1-23. *Digibug* [Online]. Available at: https://digibug.ugr.es/handle/10481/49122 (Accessed: 07 July 2020).

Feurer, D., Planchon, O., El Maaoui, M. A., Slimane, A. B., Boussema, M. R., Pierrot-Deseilligny, M. and Raclot, D. (2018) 'Using Kites for 3-D Mapping of Gullies at Decimetre-Resolution Over Several Square Kilometres: A Case Study on the Kamech Catchment, Tunisia', *Natural Hazards and Earth Systems Sciences* 18 pp. 1567-1582. *Natural Hazards* [Online]. Available at: https://www.nat-hazards-earth-syst-sci.net/18/1567/2018/ (Accessed: 09 May 2019).

Fonstad, M. A., Dietrich, J. T., Courville, B. C., Jensen, J. L. and Carbonneau, P. E. (2013) 'Topographic Structure from Motion: A New Development in Photogrammetric Measurement', *Earth Surface Processes and Landforms*', 38 pp. 421-430. *Wiley Library* [Online]. Available at: https://onlinelibrary.wiley.com/doi/abs/10.1002/esp.3366 (Accessed: 20 August 2018).

Ford, M. (2013) 'Shoreline Changes Interpreted from Multi-Temporal Aerial Photographs and High-Resolution Satellite Images: Wotje Atoll, Marshall Islands', *Remote Sensing of Environment* 135 pp. 130-140. *Science Direct* [Online]. Available at: https://www.sciencedirect.com/science/article/abs/pii/S0034425713001065 (Accessed: 16 February 2018).

Forlani, G., Dall'Asta, E., Diotri, F., Morra di Cella, U., Roncella, R. and Santise, M. (2018) 'Quality Assessment of DSMs Produced from UAV Flights Georeferenced with On-Board RTK Positioning', *Remote Sensing* 10(2) pp. 1-22. *MDPI* [Online]. Available at: https://www.mdpi.com/2072-4292/10/2/311 (Accessed: 21September 2018).

Fraser, C., Bernatchez, P. and Dugas, S. (2017) 'Development of a GIS Coastal Land-Use Planning Tool for Coastal Erosion Adaptation Based on the Exposure of Buildings and Infrastructure to Coastal Erosion, Quebec, Canada', *Geomatics, Natural Hazards and Risks* 8(2) pp. 1103-1125. *Taylor and Francis* [Online]. Available at: https://www.tandfonline.com/doi/full/10.1080/19475705.2017.1294114 (Accessed: 02 August 2018).

Fraser, C., S. (2013) 'Automatic Camera Calibration in Close Range Photogrammetry', *Photogrammetric Engineering and Remote Sensing* 79(4) pp. 381-388.*Ingentaconnect* [Online]. Available at: https://www.ingentaconnect.com/contentone/asprs/pers/2013/00000079/00000004/art00005?crawler=true (Accessed: 31 August 2017).

Fraser, C. S., Shortis, M. R. and Ganci, G. (1995) 'Multisensor System Self-Calibration', *SPIE Conference 2598, Videometrics IV*, Philadelphia, USA, 25-26 October. *Proceedings of SPIE- The International Society for Optical Engineering, Volume 2598, Videometrics IV. SPIE Digital Library* [Online]. Available at: https://doi.org/10.1117/12.220890 (Accessed: 11 June 2018).

Fyffe, G., Graham, P., Tunwattanapong, B. and Debevec, P. (2016) 'Near-Instant Capture of High-Resolution Facial Geometry and Reflectance', *Computer Graphics Forum* 35(2) pp. 353-363. *Wiley Library* [Online]. Available at: https://onlinelibrary.wiley.com/doi/abs/10.1111/cgf.12837 (Accessed: 28 December 2019).

Galea, P., Amico, S. D. and Farrugia, D. (2014) 'Dynamic Characteristics of an Active Coastal Spreading Area Using Ambient Noise Measurements – Anchor Bay, Malta', *Geophysical Journal International* 199(2) pp. 1166-1175. *IEEE Xplore* [Online]. Available at: https://ieeexplore.ieee.org/document/8205841 (Accessed: 17 November 2017).

Garouani, A., Alobeid, A. and Garouani, S. (2014) 'Digital Surface Model Based on Aerial Image Stereo Pairs for 3D Building', *International Journal of Sustainable Built Environment* 3(1) pp. 119-126. *Science Direct* [Online]. Available at: http://www.sciencedirect.com/science/article/pii/S2212609014000363 (Accessed: 16th December 2016).

Genchi, S. A., Vitale, A. J., Perillo, G. M. E. and Delrieux, C. A. (2015) 'Structure-from-Motion Approach for Characterization of Bioerosion Patterns Using UAV Imagery', *Sensors* 15(2) pp. 3593-3609. *MDPI* [Online]. Available at: https://www.mdpi.com/1424-8220/15/2/3593/htm (Accessed: 18 January 2019).

Gervaix, F. and Voorhees, B. (2017) 'High-Precision Assessment at the Aletsch Glacier by Remote Sensing', *Imaging and Geospatial Technology Forum, ASPRS Annual Conference*, Baltimore, Maryland, 11-17 March. *SenseFly Whitepapers* [Online]. Available at: https://www.sensefly.com/education/whitepapers/ (Accessed: 01 April 2019).

Gesch, D. B. (2009) 'Analysis of LiDAR Elevation Data for Improved Identification and Delineation of Lands Vulnerable to Sea-Level Rise', *Journal of Coastal Research* SI 53 pp. 49-58. *JCR* [Online]. https://www.jcronline.org/doi/full/10.2112/SI53-006.1 (Accessed: 19 January 2009).

Gesch, D. B., Brock, J. C., Parrish, C. E., Rogers, J. N. and Wright, C. W. (2016) 'Introduction: Special Issue on Advances in Topobathymetric Mapping, Models, and Applications', *Journal of Coastal Research* 76(SI76) pp. 1-3. *JCR* [Online]. Available at: https://www.jcronline.org/doi/full/10.2112/SI76-001 (Accessed: 05 January 2018).

Gianinetto, M. and Scaioni, M. Satellite DataSatellite Data', (2008) 'Automated Geometric Correction of High-Resolution Pushbroom satellite Data', *Photogrammetric Engineering and Remote Sensing* 74(1) pp. 107-116. *Ingenta*[Online]. Available at: https://www.ingentaconnect.com/content/asprs/pers/2008/00000074/00000001/art00008# (Accessed: 01 May 2018).

Giannini, M. B., Maglione, P., Parente, C. and Santamaria, R. (2011) 'Cartography and Remote sensing for Coastal Erosion Analysis', *WIT Transactions on Ecology and the Environment* 149 pp. 65-76. *WITpress* [Online]. Available at: https://www.witpress.com/elibrary/wit-transactions-on-ecology-and-the-environment/149/21974 (Accessed: 22 April 2018).

Giannini, M. B. and Parente, C. (2015) 'An Object Based Approach for Coastline Extraction from Quickbird Multispectral Images', *International Journal of Engineering and Technology (IJET)* 6(6) pp. 2698-2704. *Semantics Scholar* [Online]. Available at: https://pdfs.semanticscholar.org/8f07/46570468449614dc1a56919831ccf488e93f.pdf (Accessed: 02 July 2018).

Gimenez, R., Marzolff, I., Campo, M. A., Seeger, M., Ries, J. B., Casali, J. and Alvarez-Mozos, J. (2009) 'Accuracy of High-Resolution Photogrammetric Measurements of Gullies with Contrasting Morphology', *Earth Surface Processes and Landforms* 34(14) pp. 1915-1926. *Wiley Library* [Online]. Available at: https://onlinelibrary.wiley.com/doi/abs/10.1002/esp.1868 (Accessed: 22 March 2019).

Gini, R., Pagliari, D., Passoni, D., Pinto, L., Sona, G. and Dosso, P. (2013) 'UAV Photogrammetry: Block Triangulation Comparisons', *UAV-g2013*, Rostock, Germany, 4-6 September. International Archives of the Photogrammetry, Remote Sensing and Spatial Information Sciences, Volume XL-1/W2 [Online]. Available at: https://pdfs.semanticscholar.org/89a5/0c4d6cd775c98dd3893053ad97bb5343a3fd.pdf (Accessed: 01 July 2013).

Girelli, V. A., Borgatti, L., Dellapasqua, M., Mandanici, E., Spreafico, M. C., Tini, M. A. and Bitelli, T. G. (2017) 'Integration of Geomatics Techniques for Digitizing Highly Relevant Geological and Cultural Heritage Sites: The Case of San Leo (Italy)', *26th International CIPA Symposium* 28 August-01 September. *The International Archives of the Photogrammetry, Remote Sensing and Spatial Information Sciences, Volume XLII-2/W5, ISPRS* [Online]. Available at: https://www.int-arch-photogramm-remote-sens-spatial-inf-sci.net/XLII-2-W5/281/2017/isprs-archives-XLII-2-W5-281-2017.pdf (Accessed: 20 January 2019).

Gneeniss, A. S., Mills, J. P. and Miller, P. E. (2015) 'In-Flight Photogrammetric Camera Calibration and Validation Via Complementary Lidar', *ISPRS Journal of Photogrammetry and Remote Sensing* 100 pp. 3-13. *ScienceDirect* [Online]. Available at: https://www.sciencedirect.com/science/article/pii/S0924271614001142?via%3Dihub (Accessed: 02 March 2018).

Gomez, C., Wulder, M. A., Dawson, A. G., Ritchie, W. and Green, D. R. (2014) 'Shoreline Change and Coastal Vulnerability Characterization with Landsat Imagery: A Case Study in the Outer Hebrides, Scotland', *Scottish Geographical Journal* 130(4) pp. 279-299. *Taylor and Francis* [Online]. Available at: https://www.tandfonline.com/doi/abs/10.1080/14702541.2014.923579 (Accessed: 11 October 2016).

Goncalves, G. R., Perez, J. A. and Duarte, J. (2018) 'Accuracy and Effectiveness of Low Cost UASs and Open Source Photogrammetric Software for Foredunes Mapping', *International Journal of Remote Sensing* 39(15-16) pp. 5059-5077. *Taylor and Francis* [Online]. Available at: https://www.tandfonline.com/doi/abs/10.1080/01431161.2018.1446568?journalCode=tres20 (Accessed: 18 April 2018).

Goncalves, J. A., Moutinho, O. F. and Rodrigues, A. C. (2016) 'Pole Photogrammetry with an Action Camera for Fast and Accurate Surface Mapping', *XXIII ISPRS Congress*, Prague, Czech Republic, 12-19 July. *The International Archives of the Photogrammetry, Remote Sensing and Spatial Information Sciences* [Online]. Available at: https://www.int-arch-photogramm-remote-sens-spatial-inf-sci.net/XLI-B1/571/2016/ (Accessed: 19th April 2017).

Goncalves, J. A. and Henriques, R. (2015) 'UAV Photogrammetry for Topographic Monitoring of Coastal Areas', *ISPRS Journal of Photogrammetry and Remote Sensing* 104, pp. 101-111. *ScienceDirect* [Online]. Available at: https://www.sciencedirect.com/science/article/pii/S0924271615000532 (Accessed: 11 November 2016).

Granshaw, S. I. (2017) 'Journal of Photogrammetry Including Laser Scanning', *The Photogrammetric Record* 32(157) pp. 7-11. *Wiley Library* [Online]. Available at: https://onlinelibrary.wiley.com/doi/pdf/10.1111/phor.12181 (Accessed: 10th October 2018).

Granshaw, S. I. (2016) 'Photogrammetric Terminology: Third Edition', *The Photogrammetric Record* 31(154) pp. 210-252. *Wiley Library* [Online]. Available at: https://onlinelibrary.wiley.com/doi/abs/10.1111/phor.12146 (Accessed: 10th October 2018).

Gray, P. C., Ridge, J. T., Poulin, S. K., Seymour, A. C., Schwantes, A. M., Swenson, J. J. and Johnston, D. W. (2018) 'Integrating Drone Imagery into High Resolution Satellite Remote SensingAssessments of Estuarine Environments', *Remote Sensing* 10(8) pp. 2-24. *MDPI* [Online]. Available at: https://www.mdpi.com/2072-4292/10/8/1257 (Accessed 25 December 2018).

Guillot, B. and Pouget, F. (2015) 'UAV Application in Coastal Environment, Example of the Oleron Island for Dunes and Dikes Survey', *ISPRS Geospatial Week* La Grande Motte, France, 28 September – 03 October. *The International Achieves of the Photogrammetry, Remote Sensing and Spatial Information Sciences*, Volume XL-3/W3. *Hal.Archives* [Online]. Available at: https://hal.archives-ouvertes.fr/hal-01243575/document (Accessed: 07 November 2018).

Gutierrez, R., Gibeaut, J. C., Smyth, R. C., Hepner, T. L. and Andrews, J. R. (2001) 'Precise Airborne LiDAR Surveying for Coastal Research and Geohazards Applications', *Land Surface Mapping and Characterization Using LASER Altimetry, WGIII/3-6*, Annapolis, Maryland, USA 22-24 October. ISPRS Archives – Volume XXXIV-3/W4. *ISPRS* [Online]. Available at: https://www.isprs.org/proceedings/XXXIV/3-W4/ (Accessed: 02 October 2017).

Habib, A., Detchev, I. and Kwak, E. (2014) 'Stability for a Multi-Camera Photogrammetric System', *Sensors* 14 (8) pp. 15084-15112. *NCBI* [Online]. Available at: https://www.ncbi.nlm.nih.gov/pmc/articles/PMC4178982/ (Accessed: 25 November 2019).

Hamylton, S. M. (2017) *Spatial Analysis of Coastal Environments.* Cambridge, United Kingdom, Cambridge University Press.

Hansch, R., Drude, I. and Hellwich, O. (2016) 'Modern Methods of Bundle Adjustment on the GPU', *XXII ISPRS Congress*, 12-19 July, Czech Republic. *ISPRS Annals of the Photogrammetry, Remote Sensing and Spatial Information Sciences,Volume III-3. ISPRS* [Online]. Available at: https://www.isprs-ann-photogramm-remote-sens-spatial-inf-sci.net/III-3/43/2016/isprs-annals-III-3-43-2016.pdf (Accessed: 10 May 2016).

Hapke, C., Reid, D. and Richmond, B. (2009) 'Rates and Trends of Coastal Change in California and the Regional Behaviour of the Beach and Cliff System', *Journal of Coastal Research*26(3) pp. 603-615. [Online]. Available at: http://www.calboating.ca.gov/csmw/pdf/Coastal_Changes_Beaches_and_Cliffs.pdf (Accessed: 10 November 2016).

Hartmann, W., Havlena, M. and Schindler, K. (2016) 'Recent Developments in Large-Scale Tie Point Matching', *ISPRS Journal of Photogrammetry and Remote Sensing* 115 pp. 47-62. *ScienceDirect* [Online]. Available at: https://www.sciencedirect.com/science/article/abs/pii/S0924271615002063 (Accessed: 06 September 2019).

Harwin, S., Lucieer, A. and Osborn, J. (2015) 'The Impact of the Calibration Method on the Accuracy of Point Clouds Deprived Using Unmanned Aerial Vehicle Multi-View Stereopsis', *Remote Sensing*7(9) pp. 11933-11953. *MDPI* [Online]. Available at: https://www.mdpi.com/2072-4292/7/9/11933 (Accessed: 12 February 2019).

Harwin, S. and Lucieer, A. (2012) 'Assessing the Accuracy of Georeferenced Point Clouds Produced Via Multi-View Stereopsis from Unmanned Aerial Vehicle (UAV) Imagery', *Remote Sensing* 4(6) pp. 1573-1599. *MDPI* [Online]. Available at: http://www.mdpi.com/2072-4292/4/6/1573 (Accessed: 19 October 2016).

Hastedt, H. and Luhmann, T. (2015) 'Investigations on the Quality of the Interior Orientation and its Impact in Object Space for UAV Photogrammetry', *International Conference on Unmanned Aerial Vehicles in Geomatics, 30 August-02 September*, Toronto, Canada. *International Archives on the Photogrammetry, Remote Sensing and Spatial Information Sciences*, XL-1/W4. [Online]. Available at: http://www.int-arch-photogramm-remote-sens-spatial-inf-sci.net/XL-1-W4/321/2015/isprsarchives-XL-1-W4-321-2015.pdf (Accessed: 16 June, 2016).

Hastedt, H., Ekkel, T. and Luhmann, T. (2016) 'Evaluation of the Quality of Action Cameras with Wide-Angle Lenses in UAV Photogrammetry', *XXIII ISPRS Congress*, Prague, Czech Republic, 12-19 July. *The International Archives of the Photogrammetry, Remote Sensing and Spatial Information Sciences, Volume XLI-B1* [Online]. Available at: https://www.int-arch-photogramm-remote-sens-spatial-inf-sci.net/XLI-B1/851/2016/ (Accessed: 30 August 2017).

He, F., Zhou, T., Xiong, W., Hasheminnasab, S. M. and Habib, A. (2018) 'Automated Aerial Triangulation for UAV-Based Mapping', *Remote Sensing* 10(2) pp. 1-34. *MDPI* [Online]. Available at: https://www.mdpi.com/2072-4292/10/12/1952 (Accessed: 30 November 2019).

Hernandez-Lopez, D., Felipe-Garcia, B., Gonzalez-Aguilera, D. and Arias-Perez, B. (2013) 'An Automatic Approach to UAV Flight Planning and Control for Photogrammetric Applications: A test Case in the Asturias Region (Spain)', *Photogrammetry Engineering and Remote Sensing* 79(1) pp. 87-98. *Ingentaconnec* [Online]. Available at: https://www.ingentaconnect.com/content/asprs/pers/2013/00000079/00000001/art00006?crawler=true&mimetype=application/pdf (Accessed: 06 August 2018).

Hisabayashi, M., Rogan, J. and Elmes, A. (2017) 'Quantifying Shoreline Change in Funafuti Atoll, Tuvalu using a Time Series of Quickbird, Worldview and Landsat Data', *GIScience and RemoteSensing*55(3) pp. 307-330. *Taylor and Francis* [Online]. Available at: https://www.tandfonline.com/doi/abs/10.1080/15481603.2017.1367157?journalCode=tgrs20 (Accessed: 07 August 2018).

Hladik, C. and Alber, M. (2012) 'Accuracy Assessment and Correction of a LiDAR-Derived Salt Marsh Digital Elevation Model', *Remote Sensing of Environment* 121 pp. 224-235. *ScienceDirect* [Online]. Available at: https://www.sciencedirect.com/science/article/pii/S0034425712000557 (Accessed: 30 August 2018).

Hoang, V. C., Tanaka, H. and Mitobe, Y. (2017) 'A Method for Correcting Tidal Effect on Shoreline Position Extracted from an Image with Unknown Capture Time', *Geosciences* 7(3) pp. 1-9. *MDPI* [Online]. Available at: https://www.mdpi.com/2076-3263/7/3/62 (Accessed: 25 February 2018).

Holata, L., Plzak, J., Svetlik, R. and Fonte, J. (2018) 'Integration of Low-Resolution ALS and Ground-Based SFM Photogrammetry Data. A Cost-Effective Approach Providing an Enhanced 3D Model' of the Hound Tor Archaeological Landscapes (Dartmoor, South-West England)', *Remote Sensing* 10(9) pp. 2-28. *MDPI* [Online]. Available at: https://www.mdpi.com/2072-4292/10/9/1357 (Accessed: 10 March 2019).

Holland B, Kidner D, Leigh C (2008) Integration of High Definition Surveying and Geographical Information Systems – An innovative technique for the Spatio-temporal analysis of coastal terrain 4th *International conference on Computer science and Information systems*, Athens Greece.

Honkavaara, E., Arbiol, R., Markelin, L., Martinez, L., Cramer, M., Bovet, S., Chandelier, L., Ilves, R., Klonus, S., Marshal, P., Schlapfer, D., Tabor, M., Thom, C. and Veje, N. (2009) 'Digital Airborne Photogrammetry – A New Tool for Quantitative Remote Sensing? – A State-of –the-Art Review on Radiometric Aspects of Digital Photogrammetric Images', *Remote Sensing* 1(3) pp. 577-605. *MDPI* [Online]. Available at: https://www.mdpi.com/2072-4292/1/3/577 (Accessed: 15 October 2018).

Horn, B. K. P (1987) 'Closed-Form Solution of Absolute Orientation Using Unit Quaternions', *Optical Society of America* 4(4) pp. 629-642. *OSA Publishing* [Online]. Available at: https://www.osapublishing.org/josaa/abstract.cfm?uri=josaa-4-4-629 (Accessed: 23 June 2020).

Hoyer, S. and Hamman, J. J. (2017) 'Xarray: N-D Labeled Arrays and Datasets in Python', *Journal of Open Research Software* 5(1) pp. 1-6. *Open research software* [Online]. Available at: https://openresearchsoftware.metajnl.com/articles/10.5334/jors.148/ (Accessed: 05 November 2020).

Huang, S., Zhang, Z., Ke, T., Tang, M. and Xu, X. (2015) 'Scanning Photogrammetry for Measuring Large Targets in Close Range', *Remote Sensing* 7(8) pp. 10042-10077. *MDPI* [Online]. Available at: https://www.mdpi.com/2072-4292/7/8/10042/htm (Accessed: 08 February 2019).

Huber, D. F.and Hebert, M. (1999) 'A New Approach to 3-D Terrain *Mapping' IEEE/RSJ International Conference on Intelligent Robots and Systems. Human and Environmental Friendly Robots with High Intelligent and Emotional Questions (Cat. No. 99CH36289,*Kyongju, South Korea. 17-21 October. *IEEE Explore Digital Library* [Online]. Available at: https://ieeexplore.ieee.org/abstract/document/812830/authors#authors (Accessed: 31 October 2017).

Hu, K. and Shi, W. (2016) 'Rigorous Line-Based Transformation Model using the Generalized Point Strategy for the Rectification of High-Resolution Satellite Imagery', *Remote Sensing* 8(9) pp. 1-19. *MDPI* [Online]. Available at: https://www.mdpi.com/2072-4292/8/9/743 (Accessed: 22 April 2018).

Hu, F., Gao, X. M., Li, G. Y. and Li, M. (2016) 'DEM Extraction from Worldview-3 Stereo-Images and Accuracy Evaluation', *XXIII ISPRS Congress*, Prague, Czec Republic, 12-19 July. *The International Archives of the photogrammetry, Remote Sensing and Spatial Information Sciences* [Online]. Available at: https://www.int-arch-photogramm-remote-sens-spatial-inf-sci.net/XLI-B1/327/2016/isprs-archives-XLI-B1-327-2016.pdf (Accessed: 07 August 2018).

Hussain, M., Chen, D., Cheng, A., Wei, H. and Stanley, D. (2013) 'Change Detection from Remotely Sensed Images: From Pixel-Based to Object-Based Approaches', *ISPRS Journal of Photogrammetry and Remote Sensing* 80 pp. 91-106. *SciVerse ScienceDirect* [Online]. Available at: https://www.ec.gc.ca/glaces-ice/0F9E03B9-1146-4AD4-A13B-AE9E07C9F72B/1.change%20detection.pdf (Accessed: 07 January 2017).

Hwang, J., Yun, H., Suh, Y., Cho, J. and Lee, D. (2012) 'Development of an RTK-GPS Positioning Applications with an Improved Position Error Model for Smartphone's', *Sensors* 12(10) pp. 12988-13001. *NCBI* [Online]. Available at: https://www.ncbi.nlm.nih.gov/pmc/articles/PMC3545552/ (Accessed: 18 April 2019).

Irvine, M., Roberts, G. and Oldham, L. (2018) 'Assessing the Applicability of Unmanned Aerial Vehicle (UAV) Data in Environmental Monitoring of Coastal Environments: St. David's Newfoundland', *Newfoundland and Labrador Department of Natural Resources Geological Survey, Report* 81-1 pp. 15-30. [Online]. Available at: https://www.nr.gov.nl.ca/nr/mines/geoscience/publications/currentresearch/2018/Irvine_2018.pdf (Accessed: 22 January 2019).

Irwin, K., Beaulne, D., Braun, A. and Fotopoulos, G. (2017) 'Fusion of SAR, Optical Imagery and Airborne LiDAR for Structure Water Detection', *Remote Sensing* 9(9) pp. 2-18. *MDPI* [Online]. Available at: https://www.mdpi.com/2072-4292/9/9/890 (Accessed: 19 December 2019).

Ishiguro, S., Yamano, H. and Oguma, H. (2016) 'Evaluation of DSMs Generated from Multi-Temporal Aerial Photographs using Emerging Structure from Motion-Multi-view Stereo Technology', *Geomorphology* 268(1) pp. 64-71. *ScienceDirect* [Online]. Available at: https://www.sciencedirect.com/science/article/pii/S0169555X16303798 (Accessed: 10 May 2020).

ISPRS (2019) *The Society.* Available at: https://www.isprs.org/society/Default.aspx (Accessed: 08 June 2020).

Jalloh, Y., Ahmad, A., Amin, Z. M. and Sasaki, K. (2017) 'Conventional Total Station Versus Digital Photogrammetry in Land Development Applications', *Journal of Environmental and Analytical Toxicology* 7(1) pp. 1-5. *Hilaris* [Online]. Available at: https://www.hilarispublisher.com/environmental-analytical-toxicology/archive.html (Accessed: 06 July 2020).

James, M. R., Ilic, S. andRuzic, I. (2013) 'Measuring 3D Coastal Change with a Digital Camera', *Coastal Dynamics*Arcachon, France 24-28 June. *Proceedings of Coastal Dynamics 2013.* p. 893-904 [Online]. Available at: http://www.research.lancs.ac.uk/portal/ (Accessed 02 September 2018).

James, M. R., Robson, S., Oleire-Oltmanns, S. D. and Niethammer, U. (2017) 'Optimizing UAV Topographical Surveys Processed with Structure-from-Motion: Ground Control Quality, Quantity and Bundle Adjustment', *Geomorphology* 280 pp. 51-66. *ScienceDirect* [Online]. Available at: https://www.sciencedirect.com/science/article/pii/S0169555X16311291?via%3Dihub (08 September 2018).

James, M. R. and Robson, S. (2014) 'Mitigating Systematic Error in Topographic Models Derived from UAV and Ground-Based Image Networks', *Earth Surface Processes and Landforms* 39(10) pp. 1413-1420. *Wiley Library* [Online]. Available at: https://onlinelibrary.wiley.com/doi/full/10.1002/esp.3609 (Accessed 07 February 2019).

James, M. R. and Robson, S. (2012) 'Straightforward Reconstruction of 3D Surfaces and Topography with a Camera: Accuracy and Geoscience Application', *Journal of Geophysical Research, EarthSurface*117(F3) pp. 1-17. *Wiley* [Online]. Available at: https://agupubs.onlinelibrary.wiley.com/doi/full/10.1029/2011JF002289 (Accessed: 16 October 2018).

James, M. R., Robson, S., Oleire-Oltmanns, S. D. and Niethammer, U. (2016) 'Optimizing UAV Topographical Surveys Processed with Structure-from-Motion: Ground Control Quality, Quantity and Bundle Adjustment', *Geomorphology* 280 pp. 51-66. *ScienceDirect* [Online]. Available at: https://www.sciencedirect.com/science/article/pii/S0169555X16311291?via%3Dihub (08 September 2018).

James, M. R. and Quinton J. N. (2013) 'Ultra-Rapid Topographic Surveying for Complex Environments: The Hand-Held Mobile Laser Scanner (HMLS)', *Earth Surface Process and Landforms* 39(1) pp. 138-142. *Wiley Library* [Online]. Available at: https://onlinelibrary.wiley.com/doi/full/10.1002/esp.3489 (Accessed: 09 October 2019).

Janeras, M., Jara, J. A., Lopez, F., Marturia, J., Royan, M. J., Vilaplana, J. M., Aguasca, A., Fabregas, X., Cabranes, F. and Gili, J. A. (2015) 'Using Several Monitoring Techniques to Measure the Rock Mass Deformation in the Montserrat Massif', *International Symposium on Geohazards and Geomechanics ISGG,* University of Warwick, School of Engineering, 10-11 September. *IOP Conference Series* [Online]. https://iopscience.iop.org/article/10.1088/1755-1315/26/1/012030/pdf (Accessed: 09 October 2017).

Jangir, B., Satyanarayana, A., Swati, S., Jayaram, C., Chowdary, V. and Dadhwal, V. (2016) 'Delineation of Spatio-Temporal Changes of Shoreline and Geomorphological Features of Odisha Coast of India Using Remote Sensing and GIS Techniques', *Natural Hazards* 82(3) pp. 1437-1455. *Springer* [Online]. Available at: http://rd.springer.com/article/10.1007/s11069-016-2252-x (Accessed: 13 January 2016).

Jebur, A., Abed, F. and Mohammed, M. (2018) 'Assessing the Performance of Commercial AgisoftPhotoScan Software to Deliver Reliable Data for Accurate 3D Modelling', *MATEC Web of Conferences* 162 pp. 1-11. The 3rd*International Conference on Buildings, Construction and Environmental Engineering, BCEE3* [Online]. Available at: https://www.matec-conferences.org/articles/matecconf/abs/2018/21/matecconf_bcee32018_03022/matecconf_bcee32018_03022.html (Accessed 09 July 2018).

Jeong, E., Park, J. and Hwang, C. (2018) 'Assessment of UAV Photogrammetric Mapping Accuracy in the Beach Environment', *Journal of Coastal Research*SI(85) pp. 176-180. *JCR* [Online]. Available at: https://www.jcronline.org/doi/abs/10.2112/SI85-036.1 (Accessed: 04 April 2019).

Jha, M. N., Levy, J. and Gao, Y. (2008) 'Advances in Remote Sensing for Oil Spill Disaster Management: State-of-the Art Sensors Technology for Oil Spill Surveillance', *Sensors* 8(1) pp. 236-255. *MDPI* [Online]. Available at: http://www.mdpi.com/1424-8220/8/1/236 (Accessed: 26 August 2018).

Joevivek, V., Chandrasekar, N., Saravanan, S., Anandakumar, H., Thanushkodi, K., Suguna, N. and Jaya, J. (2018) 'Spatial and Temporal Correlation Between Beach and Wave Processes: Implications for Bar-Berm Sediment Transition', *Frontiers of Earth Science* 12(2) pp. 349-360. *Springer* [Online]. Available at: https://link.springer.com/article/10.1007/s11707-017-0655-y#citeas (Accessed: 02 April 2019).

Johansson, R. (2019) *Scientific Computing and Data Science Applications with Numpy, SciPy and Matplotlib* 2nd edn. New York, Apress

Juad, M., Passot, S., Bivic, R. L., Delacourt, C., Grandjean, P. and Dantec, N. L. (2016) 'Assessing the Accuracy of High-Resolution Digital Surface Models Computed by PhotoSCan and MicMac in Sub-Optimal Survey Conditions', *Remote Sensing* 8(6), 465; pp. 2-18. *MDPI* [Online]. Available at: http://www.mdpi.com/2072-4292/8/6/465 (Accessed: 26 May 2018).

Julge, K., Eelsalu, M., Grunthal, E., Talvik, S., Ellmann, A., Soomere, T. and Tonisson, H. (2014) 'Combining Airborne and Terrestrial Laser Scanning to Monitor Coastal Processes', *IEEE/OES Baltic International Symposium (BALTIC)* Tallinn, Estonia, 27-29 May.*IEEE Explore* [Online]. Available at: https://ieeexplore.ieee.org/document/6887874 (Accessed: 28 November 2017).

Julzarika, A. (2017) 'Utilization of LAPAN Satellite (TUBSAT, A2, and A3) in Supporting Indonesia's Potential as Maritime Center of the World', *IOP Conference Series: Earth and Environmental Science* 54(1). *IOPScience* [Online]. Available at: http://iopscience.iop.org/article/10.1088/1755-1315/54/1/012097/meta (Accessed: 03 November 2018).

Kaliraj, S., Chandrasekar, N., Ramachandran, K. K., Srinivas, Y. and Saravanan, S. (2017) 'Coastal Landuse and Land Cover Change and Transformations of Kanyakumari Coast, India Using Remote Sensing and GIS', *The Egyptian Journal of Remote Sensing and Space Sciences* 20(2) pp. 169-185. *ScienceDirect* [Online]. Available at: https://www.sciencedirect.com/science/article/pii/S1110982317301394

Karaim, M., Elsheikh, M. and Noureldin, A. (2018) '*GPS* GNSS Error Sources' inRustamov, R. B. and Hashimov, A. M. (eds), *Multifunctional Operation and Application of GPS,* IntechOpen, pp. 69-85. Available at: https://www.intechopen.com/books/multifunctional-operation-and-application-of-gps/gnss-error-sources (Accessed: 03 October 2019).

Kazhdan, M. Bolitho, M. and Hoppe, H. (2006)'Poisson Surface Reconstruction', *Proceedings of the Fourth Eurographics Symposium on Geometry Processing*, Postfach 2926, Goslar, Germany, 26-28 June. *ACM Proceedings* [Online]. Available at: https://dl.acm.org/doi/10.5555/1281957.1281965 (Accessed: 01 March 2021).

Kazhdan, M., Chuang, M. Rusinkiewicz, S. and Hoppe, H. (2020) 'Poisson Surface Reconstruction with Envelope Constraints', *Computer Graphics Forum* pp. 173-182. *Wiley Library* [Online]. Available at: https://onlinelibrary.wiley.com/toc/14678659/2020/39/5 (Accessed: 28 February 2021).

Kazhdan, M. and Hoppe, H. (2013) 'Screened Poisson Surface Reconstruction', ACM *Transactions on Graphics* 32(3) pp. 61-70. *ACM Digital Library* [Online]. Available at: https://dl.acm.org/doi/pdf/10.1145/2487228.2487237 (Accessed: 28 February 2021).

Khalid, N. F., Din, A. H. M., Omar, K. M., Khanan, M. F. A., Omar, A. H., Hamid, A. I. A. and Pa'suya, M. F. (2016) 'Open-Source Digital Elevation Model (DEMs) Evaluation with GPS and LiDAR Data', *International Conference on Geomatic and Geospatial Technology* (GGT) 3-5 October, Kualar Lumpur, Malaysia. *The International Archives of the Photogrammetry, Remote Sensing and Spatial Information Sciences, Volume XLII-4/W1* [Online]. Available at: https://www.int-arch-photogramm-remote-sens-spatial-inf-sci.net/XLII-4-W1/299/2016/isprs-archives-XLII-4-W1-299-2016.pdf (Accessed: 26 November 2018).

Khattabi, J. E., Carlier, E. and Louche, B. (2018) 'The Effect of Rock Collapse on Coastal Cliff Retreat Along the Chalk Cliffs of Northern France', *Journal of Coastal Research* 34(1) pp. 136-150. *JSTOR* [Online]. Available at: https://www.jstor.org/stable/26296450?seq=1#page_scan_tab_contents (Accessed: 24 January 2019).

Khalil, A. M. (2011) 'Two-Dimensional Displacement Measurement Using Static Close Range Photogrammetry and a Single Fixed Camera', *Alexandria Engineering Journal* 50(3) pp. 219-227. *Science Direct* [Online]. Available at: https://www.sciencedirect.com/science/article/pii/S1110016811000482 (Accessed: 09 January 2020).

Khoramshahi, E. and Honkavaara, 2018 'Modelling and Automated Calibration of a General Multi-Projective Camera', *The Photogrammetric Record* 33(161) pp. 86-112. *Wiley* [Online]. Available at: https://onlinelibrary.wiley.com/doi/pdf/10.1111/phor.12230 (Accessed: 10 October 2018).

Khoshelham, K. (2009) 'Role of Tie Points in Integrated Sensor Orientation for Photogrammetric Map Compilation', *Photogrammetric Engineering and Remote Sensing* 3(7) pp. 305-311. *Ingentaconnect* [Online]. Available at: https://www.ingentaconnect.com/content/asprs/pers/2009/00000075/00000003/art00005;jsessionid=1nv8c9d9oqvu0.x-ic-live-03 (Accessed: 13 July 2019).

King, S., Javier, L., Marty, M., Langus, J. and Bobbie, C. (2017) 'Conditions Survey of Coastal Structures Using UAV and Photogrammetry', *Australasian Coasts and Ports 2017: Working with Nature* Cairns, Australia 21-23 June. *Informit* [Online]. Available at: https://search.informit.com.au/documentSummary;dn=930305432739345;res=IELENG (Accessed: 07 November 2018).

Kim, J., Lee, S., Ahn, H., Seo, D., Seo D., Lee, J. and Choi, C. (2013) 'Accuracy evaluation of a smartphone-based technology for coastal monitoring', *Measurement* 46, pp. 233-248 Research gate [Online]. Available at: https://www.researchgate.net/publication/257093829_Accuracy_evaluation_of_a_smartphone-based_technology_for_coastal_monitoring (Accessed: 25 July 2016).

Kim, J. O. and Lee, J. K. (2017) 'UAV Applications for Process Controls of the Reclamation Project', *2nd International Water Safety Symposium, IWSS*, Inchon, Korea, 22-24 June. *Journal of Coastal Research Special* Issue 79 pp. 309-313 [Online]. Available at: https://www.jcronline.org/doi/abs/10.2112/1551-5036-79.sp1.i (Accessed: 15 September 2017).

Klein, R. J., Nicholls, R. J., Ragoonaden, S., Capobianco, M., Aston, J. and Buckley, E. N. (2001) 'Technological Options for Adaptation to Climate Change in Coastal Zones', *Journal of Coastal Research* 17(3) pp. 531-543. *JSTOR* [Online]. Available at: http://www.jstor.org/stable/4300206?seq=1#page_scan_tab_contents (Accessed: 19 May 2016).

Klemas, V. V. (2015) 'Coastal and Environmental Remote Sensing from Unmanned Aerial Vehicles: An Overview', *Journal of Coastal Research* 31(5) pp. 1260-1267. *JCR* [Online]. Available at: http://www.jcronline.org/doi/full/10.2112/JCOASTRES-D-15-00005.1 (Accessed: 07 November 2018).

Klemas, V. (2011) 'Beach Profiling and LiDAR Bathymetry: An Overview with Case Studies', *Journal of Coastal Research* 27(6) pp. 1019-1028. *JCR* [Online]. Available at: http://www.jcronline.org/doi/abs/10.2112/JCOASTRES-D-11-00017.1?journalCode=coas (Accessed: 10 April 2018).

Klemas, V. (2011b) 'Remote Sensing Techniques for Studying Coastal Ecosystems: An Overview', *Journal of Coastal Research* 27(1) pp. 2-17. *JCR* [Online]. Available at: http://www.jcronline.org/doi/abs/10.2112/JCOASTRES-D-10-00103.1 (Accessed: 01 June 2018).

Konecny, G. (2014) *Geoinformation, Remote Sensing, Photogrammetry, and Geographic Information Systems* 2nd edn. Boca Raton, CRC Press, Taylor and Francis Group.

Koutsoudis, A., Vidmar, B., Loannakis, G., Arnaoutoglou, F., Pavlidis, G. and Chamzas, C. (2013) 'Multi-Image 3D Reconstruction Data Evaluation', *Journal of Cultural Heritage* 15(1) pp. 73-79. *ScienceDirect* [Online]. Available at: https://www.sciencedirect.com/science/article/pii/S1296207412001926 (Accessed: 23 August 2016).

Kromer, R. A., Abellan, A., Hutchinson, D. J., Lato, M., Chanut, M., Dubois, L. and Jaboyedoff, M. (2017) Automated Terrestrial Laser Scanning with Near Real-Time Change Detection – Monitoring of the Sechilienne Landslide', *Earth Surf. Dynamics* 5 pp. 293-310. *Earth Surface Dynamics* [Online]. Available at: https://www.earth-surf-dynam.net/5/293/2017/ (Accessed: 31 August 2017).

Kromer, R. A., Abellan, A., Hutchinson, D. J., Lato, M., Edwards, T. and Jaboyedoff, M. (2015) A 4D Filtering and Calibration Techniques for Small-Scale Point Cloud Change Detection with a Terrestrial Laser Scanner, *Remote Sensing* 7(2) pp. 13029-13052. *MDPI* [Online]. Available at: https://www.mdpi.com/2072-4292/7/10/13029 (Accessed: 06July 2020).

Krueger, C. P. and Souza, A. V. (2014) 'The Geodesy in the Hydrology', *RevistaBrasileira de Cartografia, Rio de Janeiro, No. 66/7 International Issue*, pp. 1485-1493. *Semantic Scholar* [Online].Available at: https://pdfs.semanticscholar.org/3384/c6fd8b00489bf1d13fc1f7ba8fa7870a2b2d.pdf (Accessed: 15 September 2017).

Krtalic, A., Miljkovic, V., Gajski, D. and Racetin, I. (2019) 'Spatial Distortion Assessment of a Low-Cost Laboratory and Field Hyperspectral Imaging System', *Sensors* 19(9) pp. 1-19. *MDPI*[Online]. Available at: https://www.mdpi.com/1424-8220/19/19/4267/htm (Accessed: 16 November 2019).

Kuhn,D. and Prufer, S. (2014) 'Coastal Cliff Monitoring and Analysis of Mass Wasting Processes with the Application of Terrestrial Laser Scanning: A Case Study of Rugen, Germany', *Geomorphology* 213 pp. 153-165. *Science Direct* [Online]. Available at: https://www.sciencedirect.com/science/article/abs/pii/S0169555X14000233 (Accessed: 24 November 2017).

Kwarteng, A. Y., Al-Hatrushi, S. M., Illenberger, W. K. and McLachlan, A. (2016) 'Grain Size and Mineralogy of Al Batinah Beach Sediments, Sultanate of Oman', *Arabian Journal of Geosciences* 9(557) pp. 1-18. *Springer* [Online]. Available at: https://link.springer.com/article/10.1007/s12517-016-2583-7#citeas (Accessed: 17 April 2019).

Labuz, T. A. (2016) 'A Review of Field Methods to Survey Coastal Dunes-Experience Based on Research from South Baltic Coast', *Journal of Coastal Conservation* 20(2) pp. 175-190. *Springer* [Online]. Available at: https://link.springer.com/article/10.1007/s11852-016-0428-x (Accessed 26 July 2017).

Lague, D., Brodu, N. and Leroux, J. (2013) 'Accurate 3D Comparison of Complex Topography with Terrestrial Laser Scanner: Applications to the Rangitikei Canyon (N-Z)', *ISPRS Journal of Photogrammetry and Remote Sensing* 82 pp. 10-26. *Science Direct* [Online]. Available at: https://www.sciencedirect.com/science/article/abs/pii/S0924271613001184 (Accessed: 24 November 2017).

Landes, T., Waton, M. D., Alby, E., Gourvez, S. and Lopes, B. (2013) '3D Modelling of Headstones of the 2nd and 3rd Century ByLow Cost Photogrammetric Techniques', *International CIPA Symposium, 2 – 6 September* Strasbourg, France. International Archives of the Photogrammetry, Remote Sensing and Spatial Information Sciences, Volume XL-5/W2, 2013 XXIV [Online]. Available at: https://www.int-arch-photogramm-remote-sens-spatial-inf-sci.net/XL-5-W2/397/2013/isprsarchives-XL-5-W2-397-2013.pdf (Accessed: 16 October 2018).

Laporte-Fauret, Q., Marieu, V., Castelle, B., Michalet, R., Bujan, S. and Rosebery, D. (2019) 'Low-Cost UAV for High-Resolution and Large –Scale Coastal Dune Change Monitoring using Photogrammetry', *Journal of Marine Science and Engineering* 7(63) pp. 1-16. *MDPI* [Online]. Available at: https://www.mdpi.com/2077-1312/7/3/63 (Accessed: 12 April 2021).

Lazaridou, M. A. (2012) 'Image Interpretation of Coastal Areas', *XXIII ISPRS Congress*, Melbourne, Auatralia, 25 August – 01 Setember. *The International Archives of the photogrammetry, Remote Sensing and Spatial Information Sciences* XXXIX-B8 [Online]. Available at: https://www.int-arch-photogramm-remote-sens-spatial-inf-sci.net/XXXIX-B8/171/2012/ (Accessed: 07 August 2018).

Leberl, F., Irschara, A., Pock, T., Meixner, P., Gruber, M., Scholz, S. and Wiechert, A. (2010) 'Point Clouds: LiDAR versus 3D Vision', Photogrammetric Engineering and Remote Sensing 76(10), pp. 1123-1134 [Online]. Available at: https://www.cis.rit.edu/~cnspci/references/dip/urban_extraction/leberl2010.pdf (Accessed: 13 October 2016).

Lee, W. H. and Yu, K. (2009) 'Bundle Block Adjustment with 3D Natural Cubic Splines', *Sensors* 9(12) pp. 9629-9655. *MBPI* [Online]. Available at: https://www.mdpi.com/1424-8220/9/12/9629 (Accessed: 14 January 2020).

Lee, C. I. (2016) 'Instantaneous Shoreline Mapping from Worldview-2 Satellite Images by Using Shadow Analysis and Spectrum Matching Techniques', *Journal of Marine Science and Technology* 24(6) pp. 1204-1216. *Semantic Scholar* [Online]. Available at: https://www.semanticscholar.org/paper/INSTANTANEOUS-SHORELINE-MAPPING-FROM-WORLDVIEW-2-BY-Lee/eec9a7b4f7e56260ba2fd5799bd1a2c33b4e765a (Accessed: 15 May 2018).

Lee, E. M. (2008) 'Coastal Cliff Behaviour: Observations on the Relationship betweenBeach Levels and Recession Rates', Geomorphology 101(4), pp. 558-571. *ScienceDirect* [Online]. Available at: https://www.sciencedirect.com/science/article/pii/S0169555X08000573 (Accessed: 13 July 2016).

Lee, H. and Rhee, H. (2013) '3-D Measurement of Structural Vibration Using Digital Close-Range Photogrammetry', *Sensors and Actuators A: Physical* 196 pp. 63-69. *Science Direct* [Online]. Available at: http://www.sciencedirect.com/science/article/pii/S0924424713001258 (Accessed: 29 June 2016).

Lee, I., Wu, B. and Li, R. (2009) 'Shoreline Extraction from the Integration of LiDAR Point Cloud Data and Aerial Orthophotos Using Mean Shift Segmentation', *ASPRS Annual Conference*, Baltimore, Maryland 9-13 March. *CiteSeer* [Online]. Available at: http://citeseerx.ist.psu.edu/viewdoc/summary?doi=10.1.1.149.5791 (Accessed: 16 August 2018).

Lee, I. S., Park, H. J., Lee, J., O. and kim, Y. S. (2011b) 'Delineating the Natural Features of a Cadastral Shoreline in South Korea Using Airborne Laser Scanning', *IEEE Journal of Selected Topics in Applied Earth Observations and Remote Sensing*', 4(4) pp. 905-910. *IEEE Explore* [Online]. Available at: https://ieeexplore.ieee.org/document/5971789 (Accessed: 25 January 2018).

Lee, W. H. and Yu, K. (2009) 'Bundle Block Adjustment with 3D Natural Cubic Splines', *Sensors (Basel)* 9(12) pp. 9629-9665. *NCBI* [Online]. Available at: https://www.ncbi.nlm.nih.gov/pmc/articles/PMC3267192/ (Accessed: 17 January 2020).

Leigh, C.L., Kidner, D.B. and Thomas, M.C. (2009) 'The Use of LiDAR in Digital Surface Modelling: Issues and Errors', *Transactions in GIS* 13 (4), pp.345-361. *Wiley Library* [Online]. Available at: https://onlinelibrary.wiley.com/doi/abs/10.1111/j.1467-9671.2009.01168.x (Accessed: 30 June 2021).

Leigh, Charlotte (2008) *Coastal Monitoring using Lidar*, PhD Thesis, University of Glamorgan.

Lentz, E. E. and Hapke, C. (2011) 'Geologic Framework Influences on the Geomorphology of an Anthropogenically Modified Barrier Island: Assessment of Dune/Beach Changes at Fire Island, New York', *Geomorphology* 126(1-2) pp. 82-96. *ScienceDirect* [Online]. Available at: https://www.sciencedirect.com/science/article/pii/S0169555X10004708 (Accessed: 02 April 2019).

Lerodiaconou, D., Schimel, A. C. G. and Kennedy, D. M. (2016) 'A New Perspective of Storm Bite on Sandy Beaches using Unmanned Aerial Vehicles', *Annals of Geomorphology* 60(3) pp. 123-137. *Deakin University* [Online]. Available at: http://dro.deakin.edu.au/view/DU:30083413 (Accessed: 26 February 2018).

Letortu, P., Costa, S., Maquaire, O., Delacourt, C., Augereau, E., Davidson, R., Suanez, S. and Nabucet, J. (2015) 'Retreat Rates, Modalities and Agents Responsible for Erosion along the Coastal Chalk Cliffs of Upper Normandy: The Contribution of Terrestrial Laser Scanning', *Geomorphology* 245 pp. 3-14. *Science Direct* [Online]. Available at: https://www.sciencedirect.com/science/article/abs/pii/S0169555X15002615 (Accessed: 12 January 2015).

Letortu, P., Juad, M., Grandjean, P., Ammann, J., Costa, S., Maquaire, O., Davidson, R., Dantec, N. L. and Delacourt, C. (2018) 'Examining High-Resolution Survey Methods for Monitoring Cliff Erosion at an Operational Scale', *Behavioural Science and Public Health Titles* 55(4) pp. 457-476. *Hal. Archives* [Online]. Available at: https://hal.archives-ouvertes.fr/hal-01647588/document (Accessed: 31 August 2018).

Li, X., Wan, W., Cheng, X. and Cui, B. (2010) 'Am Improved Poisson Surface Reconstruction Algorithm', *International Conference on Audio, Language and Image Processing*, Shanghai, China, 23-25 2010. *IEEE Explore* [Online]. Available at: https://ieeexplore.ieee.org/document/5685081 (Accessed: 25 February 2021).

Liang, Y., Qu, Y. and Cui, T. (2017) 'A Three-Dimensional Simulation and Visualization System for UAV Photogrammetry', *International Conference on Unmanned Aerial Vehicles in Geomatics,* Bonn, Germany, 4-7 September. *The International Archives of the Photogrammetry, Remote Sensing and Spatial Information Sciences*, Volume XL11-2/W6, pp. 217-222. *ISPRS* [Online]. Available at: https://www.int-arch-photogramm-remote-sens-spatial-inf-sci.net/XLII-2-W6/217/2017/ (Accessed: 15 November 2017).

Li, J. and Liu, Z. (2018) 'Efficient Camera Self-Calibration Method for Remote Sensing Photogrammetry', *Optical Express* 26(11) pp. 1-19. *OSA Publishing* [Online]. Available at: https://www.osapublishing.org/oe/abstract.cfm?uri=oe-26-11-14213 (Accessed: 18th December 2019).

Lim, M., Petley, D. N., Rosser, N. J., Allison, R. J., Long, A. J. and Pybus, D. (2005) 'Combined Digital Photogrammetry and Time-of-Flight Laser Scanning for Monitoring Cliff Evolution', *The Photogrammetric Record* 20(110) pp. 109-129. *Wiley Library* [Online]. Available at: https://onlinelibrary.wiley.com/doi/abs/10.1111/j.1477-9730.2005.00315.x (Accessed: 13 January 2020).

Lipakis, M., Chrysoulakis, N. and Kamarianakis, Y. (2007) 'Shoreline Extraction Using Satellite Imagery', *Beach Erosion Monitoring, pubs* (4), pp. 81-95. *BEACHMED-e/OpTIMAL* [online]. Available at: http://www.iacm.forth.gr/_docs/pubs/4/2008_Lipakis_et_al.pdf (Accessed: 28 November 2012).

Li, R., Parrish, C. and Sukcharoenpong (2012) 'Developments in Tide-Coordinated Shoreline Mapping', *The Ohio State University* [online]. Available at: http://ccom.unh.edu/sites/default/files/publications/E07%20Li.pdf (Accessed: 05 January 2013).

Lim, M., Rosser, N. J., Allison, R. J. and Petley, D. N. (2010) 'Erosional Processes in the Hard Rock Coastal Cliff at Staithes, North Yorkshire', *Geomorphology* 111(1-2) pp. 12-21. *ScienceDirect* [Online]. Available at: https://www.sciencedirect.com/science/article/pii/S0169555X09000737 (Accessed: 12 January 2019).

Li, R., Bedford, K., Shum, C. K., Niu, X., Zhou, F., Velissariou, V., Ramirez, J. R. and Zhang, A. (2006) 'Digitalization of Coastal Management and Decision Making Supported by Multi-Dimensional Geospatial Information and Analysis', *Proceedings of the 2006 International conference on Digital Government Research,* San-Diego, California, USA, 21-24 May. ACM Digital Library [Online]. Available at: https://dl.acm.org/citation.cfm?doid=1146598.1146733 (Accessed: 08 December 2018).

Liu, C.C.and Chen, P. L. (2009) 'Automatic Extraction of Ground Control Regions and Orthorectification of Remote Sensing Imagery', *Opt Expre* 17(10) pp. 7970-7984. *NCBI* [Online]. Available at: https://www.ncbi.nlm.nih.gov/pubmed/19434129 (Accessed: 24 April 2009).

Liu, H., Sherman, D. and Gu, S. (2007) 'Automated Extraction of Shorelines from Airborne Light Detection and Ranging Data and Accuracy Assessment Based on Monte Carlo Simulation', *Journal of Coastal Research* 23(6) pp. 1359-1369. *JCR* [Online]. Available at: https://www.jcronline.org/doi/abs/10.2112/05-0580.1?journalCode=coas (Accessed: 01 February 2018).

Liu, J. H., Cai, F., Zhang, Z. W. and Li, B. (2017) 'Early Stage Evolution of Nourished Beach Under High-Energy, Macro-Tidal Environment',*IOP Conference Series: Earth and Environment Science* 57(1) pp. 1-9.*IOP Science [*Online]. Available at: https://iopscience.iop.org/article/10.1088/1755-1315/57/1/012039 (Accessed: 06 October 2017).

Liu, H., Wang, L., Sherman, D. J., Wu, Q. and Su, H. (2011) 'Algorithmic Foundation and Software Tools for Extracting Shorelines Features from Remote Sensing Imagery and LiDAR Data', *Journal of Geographic Information System* 3(2) pp. 99-119. *Scientific Research* [Online]. Available at: https://www.scirp.org/journal/PaperInformation.aspx?PaperID=4658 (Accessed: 30 August 2018).

Liu, S., Zhu, W., Zhang, C. and Sun, W. (2016) '3D Reconstruction of Indoor Scenes Using RGB-D Monocular Vision', *International Conference on Robots and Intelligent System (ICRIS),* Zhangjiajie, China, 27-28 August. *IEEE Xplore* [Online]. Available at: https://ieeexplore.ieee.org/abstract/document/7757064/authors#authors (Accessed: 10 September 2019).

Liu, Y., Zheng, X., Ai, G., Zhang, Y. and Zuo, Y. (2018) 'Generating a High-Precision True Digital Orthophoto Map Based on UAV Images', *International Journal of Geo-Information* 7(9) pp. 1-15. *MDPI* [Online]. Available at: https://www.mdpi.com/2220-9964/7/9/333 (Accessed 02 December 2019).

Logie, G. S. J. and Coburn, C. A. (2018) 'An Investigation of the Spectral and Radiometric Characteristics of Low-Cost Digital Cameras for use in UAV Remote Sensing', *International Journal of Remote Sensing* 39(15-16) pp. 4891-4909. *Taylor and Francis Online*. Available at: https://www.tandfonline.com/doi/abs/10.1080/01431161.2018.1488297?journalCode=tres20 (Accessed: 17 October 2018).

Longhitano, S. G. (2015) 'Short-Term Assessment of Retreating vs. Advancing Microtidal Beaches Based on the Backshore/Foreshore Length Ratio: Examples from the Basilicata Coasts (Sourthern Italy)', *Open Journal of Marine Science* 5(1) pp. 123-145. *Scientific Research* [Online]. Available at: https://www.scirp.org/journal/PaperInformation.aspx?paperID=53507 (Accessed: 19 January 2019).

Long, N., Millescamps, B., Guillot, B., Pouget, F. and Bertin, X. (2016) 'Monitoring the Topography of a Dynamic Tidal Inlet Using UAV Imagery', *Remote Sensing* 8(5) pp. 2-18. *MDPI* [Online]. Available at: https://www.mdpi.com/2072-4292/8/5/387/html (Accessed: 02 November 2018).

Lopez-Fernandez, L., Rodriguez-Gonzalvez., Hernandez-Lopez, D., Ortega-Terol, D. and Gonzalez-Aguilera, D. (2017) 'Comparative Analysis of Triangulation Libraries for Modeling Large Points Clouds from Land and their Infrastructures',*Infrastructure* 2(1) pp. 1-11. *MDPI* [Online]. Available at: https://www.mdpi.com/2412-3811/2/1/1/htm (Accessed: 04 July 2020).

Lorenz, R. D. and Scheidt, S. P. (2014) 'Compact and Inexpensive Kite Apparatus for Geomorphological Field Aerial Photography, with Some Remarks on Operations', *GeoResJ* 3-4 pp. 1-8. *ScienceDirect* [Online]. Available at: https://www.sciencedirect.com/science/article/pii/S2214242814000084 (Accessed: 15 March 2019).

Loureiro, C., Ferreira, O. and Cooper, A. G. (2014) 'Non-Uniformity of Storm Impacts on Three High-Energy Embayed Beaches', *Journal of Coastal Research Special Issue 70 – Proceedings of the 13th International Coastal Symposium*: pp. 326-331. *JCR* [Online]. Available at: https://www.jcronline.org/doi/abs/10.2112/SI70-055.1 (Accessed: 29 September 2017).

Luhmann, T., Fraser, C. and Maas, H. (2016) 'Sensor Modelling and Camera Calibration for Close Range Photogrammetry', *ISPRS Journal of Photogrammetry and Remote Sensing* 115 pp. 37-46. *ScienceDirect* [Online]. Available at: https://www.sciencedirect.com/science/article/abs/pii/S0924271615002361 (Accessed: 17 July 2019).

Lu, C. (2016) 'Applying UAV and photogrammetry to Monitor the Morphological Changes Along the Beach in Penghu Islands', *ISPRS 2016 - XXIII ISPRS Congress, Prague, Czech republic* 12th -19th , July. *ISPRS* [Online]. Available at: https://www.int-arch-photogramm-remote-sens-spatial-inf-sci.net/XLI-B8/1153/2016/isprs-archives-XLI-B8-1153-2016.pdf (Accessed: 17 July 2016).

Lu, D. and Weng, Q. (2007) 'A Survey of Image Classification Methods and Techniques for Improving Classification Performance', *International Journal of Remote Sensing* 28(5) pp. 823-870. *Taylor and Francis* [Online]. Available at: https://www.tandfonline.com/doi/full/10.1080/01431160600746456 (Accessed: 10 June 2020).

Madden, M., Jordan, T., Bernardes, S., Cotton, D. L., O'Hare, N. and Pasqua, A. (2015) 'Unmanned Aerial Systems and Structure from Motion Revolutionize Wetlands Mapping', in *Remote Sensing of Wetlands, Applications and Advances* (ed.) Tiner, R. W., Lang, M. W. and Klemas, V. V. Boca Raton, CRS Press, pp. 195-219.

Maglione, P., Claudio, P. and Vallario, A. (2014) 'Coastline Extraction Using High Resolution WorldView-2 Satellite Imagery', *European Journal of Remote Sensing*12(7) pp. 506-515. *Science Publications* [Online]. Available at: https://thescipub.com/abstract/10.3844/ajassp.2015.506.515(Accessed: 02August 2018).

Maglione, P., Claudio, P. and Vallario, A. (2015) 'High Resolution Satellite Images to Reconstruct Recent Evolution of Domitian Coastline', *American Journal of Applied Sciences* 47(1) pp. 685-699. *Taylor and Francis* [Online]. Available at: https://www.tandfonline.com/doi/abs/10.5721/EuJRS20144739 (Accessed: 08 December 2018).

Maglione, P. (2016) 'Very High-Resolution Optical Satellites: An Overview of the Most Commonly used', *American Journal of Applied Sciences* 13(1) pp. 91-99. *Semantics scholar* [Online]. Available at: https://www.semanticscholar.org/paper/Very-High-Resolution-Optical-Satellites%3A-An-of-the-Maglione/fa3622e1f21a36c3296772910cb37824fd1772ed#citing-papers (Accessed: 02August 2018).

Mahabot, M., Juad, M., Pennober, G., Le Dantec, N., Troadec, R., Suanez. S. and Delacourt, C. (2017) 'The Basics for a Permanent Observatory of Shoreline Evolution in Tropical Environments; Lessons from Back-Reef Beaches in La Reunion Island', *Comptes Rendus Geoscience* 349(6-7) pp. 330-340. *ScienceDirect* [Online]. Available at: https://www.sciencedirect.com/science/article/pii/S1631071317301165 (Accessed: 19 August 2017).

Mancini, F., Castagnetti, C., Rossi, P., Dubbini, M., Fazio, N, L., Perrotti, M. and Lollino, P. (2017) 'An Integrated Procedure to Assess the Stability of Coastal Rocky Cliffs: From UAV Close-Range Photogrammetry to Geomechanical Finite Element Modelling', *Remote Sensing* (9)12 pp. 2-21. *MDPI* [Online]. Available at: https://www.mdpi.com/2072-4292/9/12/1235 (Accessed: 30 January 2019).

Mancini, F., Dubbini, M., Gattelli, M., Stecchi, F., Fabbri, S. and Gabbianelli, G. (2013) 'Using Unmanned Aerial Vehicles (UAV) for High-Resolution Reconstruction of Topography: The Structure from Motion Approach on Coastal Environments', *Remote Sensing* 5(12) pp. 6880-6898. *MDPI* [Online]. Available at: http://www.mdpi.com/2072-4292/5/12/6880 (Accessed: 17December 2016).

Martins, K., Blenkinsopp, C. E. and Zang, J. (2016) 'Monitoring Individual Wave Characteristics in the Inner Surf with a 2-Dimensional Laser Scanner (LiDAR)', *Journal of Sensors* ID 7965431 pp. 1-11. *Hindawi* [Online]. Available at: https://www.hindawi.com/journals/js/2016/7965431/ (Accessed: 29 August 2018).

Marzolff, I. and Poesen, J. (2009) 'The Potential of 3D Gully Monitoring with GIS Using High-Resolution Aerial Photography and a Digital Photogrammetry', *Geomorphology* 111(1-2) pp. 48-60. *ScienceDirect* [Online]. Available at: https://www.sciencedirect.com/science/article/pii/S0169555X09001421 (Accessed: 22 December 2018).

Masiero, A., Fissore, F. and Vettore, A. (2017) 'A Low Cost UWB Based Solutions for Direct Georeferencing UAV Photogrammetry', *Remote Sensing* 9(5) pp. 2-21. *MDPI* [Online]. Available at: https://www.mdpi.com/2072-4292/9/5/414 (Accessed: 27 March 2019).

Mason, D. C., Gurney, C. and Kennett, M. (2000) 'Beach Topography Mapping – A Comparison of Techniques', *Journal of Coastal Conservation* 6(1) pp. 113-124. *Springer* [Online]. Available at: https://link.springer.com/article/10.1007/BF02730475 (Accessed: 20 August 2018).

Masria, A., Negm, A. Iskander, M. and Saavedra, O. (2014) 'Coastal Zone Issues: A Case Study (Egypt)', *12th International Conference on Computing and Control for the Water Industry, CCW12013*, Perugia, Italy 2-4 September. *ScienceDirect* [Online]. Available at: https://www.sciencedirect.com/journal/procedia-engineering/issues (Accessed: 22 December 2018).

Masaad, E. M. and Omer, A. H. (2014) 'Use of Scanned Aerial Images in Photogrammetric Resection and Intersection', *University of Khartoum Engineering Journal* 4(1), pp. 38-46. *UofKEJ* [Online]. Available at: http://onlinejournals.uofk.edu/index.php/kuej/article/view/1288/1307 (Accessed: 11 June 2016).

Matano, F., Pignalosa, A., Marino, E., Esposito, G., Caccavale, M., Caputo, T., Sacchi, M., Somma, R., Troise, C. and De Natale, G. (2015) 'Laser Scanning Application for Geostructural Analysis of Tuffaceous Coastal Cliffs: The Case of Punta Epitaffio, Pozzuoli Bay, Italy', European Journal of Remote Sensing 48(1) pp. 615-637. *Taylor and Francis* [Online]. Available at: https://www.tandfonline.com/doi/abs/10.5721/EuJRS20154834 (Accessed: 09 September 2017).

Mather, P. M. and Koch, M. (2011) *Computer Processing of Remotely-Sensed Images, An Introduction* 4th edn. Chichester, West Sussex. Wiley-Blackwell.

Metano, F., Iuliano, S., Somma, R., Marino, E., Del Vecchio, U., Esposito, G., Molisso, F., Scepi, G., Grimaldi, G. M., Pignalosa, A., Caputo, T., Troise, C., De Natale, G. and Sacchi, M. (2016) 'Geostructure of Coroglio Tuff Cliff, Naples (Italy) Derived from Terrestrial Laser Scanner Data', *Journal of Maps* 12(3) pp. 407-421. *Taylor and Francis* [Online]. Available at: https://www.tandfonline.com/doi/full/10.1080/17445647.2015.1028237 (Accessed: 20 October 2017).

Medjkane, M., Maquaire, O., Costa, S., Roulland, T., Letortu, P., Fauchard, C., Antoine, R. and Davidson, R. (2018) 'High-Resolution Monitoring of Complex Coastal Morphology Changes: Cross-Efficiency of SFM and TLS-Based Survey (Vaches-Noires Cliffs, Normandy, France)' *Landslides* 15(6) pp. 1097-1108. *Springer* [Online]. Available at: https://link.springer.com/article/10.1007/s10346-017-0942-4 (Accessed: 13 February 2019).

Meiner, A. (2010) 'Integrated Maritime Policy for the European Union-Consolidating Coastal and Maritime Information to Support Maritime Spatial Planning', *Journal of Coastal Conservation* 14(1) pp. 1-11. *Springer* [Online]. Available at: https://link.springer.com/article/10.1007/s11852-009-0077-4 (Accessed: 28 November 2018).

Mendikute, A., Yague-Fabra, J. A., Zatarain, M., Bertelsen, A. and Leizea, I. (2017) 'Self-Calibrated In-Process Photogrammetry for Large Raw Part Measurement and Alignment before Machining', *Sensors* 17(9) pp. 1-30. *MDPI* [Online]. Available at: https://www.mdpi.com/1424-8220/17/9/2066 (Accessed: 10 May 2018).

Meng, X., Shang, N., Zhang, X., Li, C., Zhao, K., Qiu, X. and Weeks, E. (2017) 'Photogrammetric UAV Mapping of Terrain under Dense Coastal Vegetation: An Object-Oriented Classification Ensemble Algorithm for Classification and Terrain Correction', *Remote Sensing* 9(11) pp. 1-23.*MDPI* [Online]. Available at: https://www.mdpi.com/2072-4292/9/11/1187 (Accessed: 15 October 2018).

Melby, J. A., Nadal-Caraballo, N. and Kobayashi, N. (2012) 'Wave Run-up Prediction for Flood Mapping', *Earth Surface Processes and Landforms* 33 pp. 1-15. *ICCE* [Online]. Available at: https://icce-ojs-tamu.tdl.org/icce/index.php/icce/article/view/6913 (Accessed: 20 January 2019).

Mills, J. P., Buckley, S. J., Mitchell, H. L., Clarke, P. J. and Edwards, S. J. (2005) 'A Geomatics Data Integration Technique for Coastal Change Monitoring', *Earth Surface Processes and Landforms* 30(6) pp. 651-664. *Wiley*[Online]. Available at: https://onlinelibrary.wiley.com/doi/abs/10.1002/esp.1165 (Accessed: 03 November 2018).

Micheletti, N., Chandler, J. H. and Lane, S., N. (2015) 'Structure from Motion (SFM) Photogrammetry', *Geomorphological Techniques* 2(2.2) pp. 1-12. *British Society of Geomorphology* [Online]. Available at: http://geomorphology.org.uk/sites/default/files/geom_tech_chapters/2.2.2_sfm.pdf (Accessed: 11 September 2017).

Michoud, C., Carrea, D., Costa, S., Derron, M., Jaboyedoff, M., Delacourt, C., Maquaire, O., Letortu, P. and Davidson, R. (2014) 'Landslide Detection and Monitoring Capability of Boat-Based Mobile Laser Scanning Along Dieppe Coastal Cliffs, Normandy', *Landslides* 12(2) pp. 403-418. *Springer* [Online]. Available at: https://link.springer.com/article/10.1007/s10346-014-0542-5 (Accessed:12 February 2014)

Mitasova, H., Overton, M. F., Recalde, J.J., Bernstein, D. J. and Freeman, C. W. (2009) 'Raster-Based Analysis of Coastal Terrain Dynamics from Multitemporal Lidar Data', *Journal of Coastal Research* 25(2) pp. 507-514. *JCR* [Online]. http://www.jcronline.org/doi/pdf/10.2112/07-0976.1 (Accessed: 16 November 2016).

Mitishita, E., Debiasi, P., Kersting, A. P., Centeno, J. A. S. and Machado, A. L. (2016) 'A Study on In Situ Calibration of an Off-the-Shelf Digital Camera Integrated to a Lidar System', *IEEE Journal of Selected Topics in Applied Earth Observations and Remote Sensing* 9(12) pp. 5513-5523. *IEEE Xplore* [Online]. Available at: https://ieeexplore.ieee.org/abstract/document/7517379 (Accessed: 07 November 2017).

Molg, N., and Bolch, T. (2017) 'Structure-from-Motion Using Historical Aerial Images to Analyse Changes in Glacier Surface Elevation', *Remote Sensing* 9(10) pp. 1-17. *MDPI* [Online]. Available at: https://www.mdpi.com/2072-4292/9/10/1021 (Accessed: 10 August 2018).

Molony, J. G., Hilton, M. J., Sirguey, P. and Simons-Smith, T. (2018) 'Coastal Dune Surveying Using a Low-Cost Remotely Piloted Aerial System', *Journal of Coastal Research* 34(5) pp. 1244-1255. *JCR* [Online]. Available at: http://www.jcronline.org/doi/abs/10.2112/JCOASTRES-D-17-00076.1 (Accessed: 18th October 2018).

Montreuil, A. L. and Bullard, J. E. (2012) 'A 150-year Record of Coastline Dynamics within a Sediment Cell: Eastern England', *Geomorphology* 179 pp. 168-185. *Loughborough University* [Online]. Available at: https://repository.lboro.ac.uk/articles/A_150-year_record_of_coastline_dynamics_within_a_sediment_cell_Eastern_England/9484472 (Accessed: 09 March 2018).

Moore, L. J. and Griggs, G. B. (2002) 'Long –Term Cliff Retreat and Erosion Hotspots along the Central Shores of the Monterey Bay National Marine Sanctuary', *Marine Geology* 181(1-3) pp. 265-283. *Science Direct* [Online]. Available at: https://www.sciencedirect.com/science/article/abs/pii/S0025322701002717 (Accessed: 09 March 2018).

Moore, R., Carey, J. M. and Mclnnes, R. G. (2010) 'Landslide Behaviour and Climate Change: Predictable Consequence for the Ventnor Undercliff, Isle of Wight', *Quarterly Journal of Engineering Geology and Hydrogeology* 43 pp. (447-460). *Lyell Collection* [Online]. Available at: https://qjegh.lyellcollection.org/content/43/4/447 (Accessed: 25 August 2018).

Morgan, J. L, Gergel, S. E. and Coops, N. C. (2010) 'Aerial Photography: A Rapidly Evolving Tool for Ecological Management', *BioScience*60 (1) pp. 47-59. *Oxford Academic* [Online]. Available at: https://academic.oup.com/bioscience/article/60/1/47/315840 (Accessed: 03 September 2018).

Mozas-Calvache, A. T., Perez-Garcia, J. L., Cardenal-Escarcena, F. J., Mata-Castro, E. and Delgado-Garcia, J. (2012) 'Method for Photogrammetric Surveying of Archaeological Sites with Light Aerial Platforms,' *Journal of Archaeological Sciences* 39 (2) pp. 521-530. *ScienceDirect* [Online]. Available at: https://www.sciencedirect.com/science/article/pii/S0305440311003669 (Accessed: 18 March 2019).

Muji, A. L. and Tahar, K. N. (2017) 'Assessment of Digital Elevation Model (DEM) Using Onboard GPS and Ground Control Points in UAV Image Processing', *Intelligent Systems Conference*, London,UK, 7-8 September. *IEEE Xplore* [Online]. Available at: https://ieeexplore.ieee.org/abstract/document/8324226/authors#authors (Accessed: 16 April 2019).

Mukherjee, S., Joshi, P. K., Mukherjee, S., Ghosh, A., Garg, R. D. and Mukhopadhyay, A. (2013) 'Evaluation of Vertical Accuracy of Open Source Digital Elevation Model (DEM)', *International Journal of Applied Earth Observation and Geoinformation* 21 pp. 205-217. *ScienceDirect* [Online]. Available at: https://www.sciencedirect.com/science/article/pii/S030324341200195X (Accessed: 16 April 2019).

Mukupa, W., Roberts, G. W., Hancock, C. M. and Al-Mansir, K. (2017) 'A Review of the use of Terrestrial Laser Scanning Applications for Change Detection and Deformation Monitoring of Structures', *Survey Review* 49(363) pp. 99-116.*Taylor and Francis* [Online]. Available at: https://www.tandfonline.com/doi/abs/10.1080/00396265.2015.1133039 (Accessed: 10 July 2020).

Mulhern, J. S., and Johnson, C. L. and Martin, J. M. 'Is Barrier Island Morphology a Function of Tidal and Wave Regime?', *Marine Geology*387(1) pp. 74-84. *ScienceDirect* [Online]. Available at: https://www.sciencedirect.com/science/article/pii/S002532271630189X (Accessed: 28 March 2019).

Murray, A. B., Lazarus, E., Ashton, A., Baas, A., Coco, G., Coulthard, T., Fonstad, M., Haff, P., McNamara, D., Paola, C., Pelletier, J. and Reinhardt, L. (2009) 'Geomorphology, Complexity, and the Emerging Science of the Earth's Surface', *Geomorphology*103(3) pp. 496-505. *ScienceDirect* [Online]. Available at: https://www.sciencedirect.com/science/article/pii/S0169555X08003826 (Accessed: 24 August 2018).

Murtiyoso, A., Grussenmeyer, P., Borlin, N., Vandermeerschen, J. and Freville, T. (2018) 'Open Source and Independent Methods for Bundle Adjustment Assessment in Close-Range UAV Photogrammetry', *Drones* 2(1) pp. 2-18. *MDPI* [Online]. Available at: https://www.mdpi.com/2504-446X/2/1/3 (Accessed: 20 September 2018).

Nayak, S. (2017) 'Coastal Zone Management in India-Present Status and Future Needs', *Geospatial Information Science* 20(2) pp. 174-183. *Taylor & Francis* [Online]. Available at: https://www.tandfonline.com/doi/full/10.1080/10095020.2017.1333715 (Accessed: 26 December 2018).

Naylor, L. A., Spencer, T., Lane, S. N., Darby, S. E., Magilligan, F. J., Macklin, M. G., and Moller, I. (2017) 'Stormy Geomorphology: Geomorphic Contributors in an Age of Climate Extremes', *Earth Surface Processes and Landforms* 42(1) pp. 166-190. *Wiley Library* [Online]. Available at: https://onlinelibrary.wiley.com/doi/full/10.1002/esp.4062 (Accessed: 28 March 2019).

Neale, W. T. C., Hessel, D. and Terpstra, T. (2011) 'Photogrammetric Measurement Error Associated with Lens Distortion', *SAE World Congress and Exhibition*, *SAE Technical Paper 2011-01-0268,* CoboCenter, Detroit, 12-14 April. *SAE International* [Online]. Available at: https://www.sae.org/publications/technical-papers/content/2011-01-0286/ (Accessed: 01 June 2016).

Nesbit, P. R. and Hugenholtz, C. H. (2019) 'Enhancing UAV-SFM 3D Model Accuracy in High-Relief Landscapes by Incorporating Oblique Images', *Remote Sensing* 11(3) pp. 2-24. *MDPI*[Online]. Available at: https://www.mdpi.com/2072-4292/11/3/239/htm (Accessed: 17th June 2019).

Nijland, W., Reshitnyk, L. Y., Starzomski, B. M., Reynolds, J. D., Darimont, C. T. and Nelson, T. A. (2016) 'Deriving Rich Coastal Morphology and Shore Zone Classification from LiDAR Terrain Models', *Journal of Coastal Research* 33(4) pp. 949-958. *JCR* [Online]. Available at: https://www.jcronline.org/doi/abs/10.2112/JCOASTRES-D-16-00109.1 (Accessed: 30 August 2018).

Nishiyama, S., Minakata, N., Kikuchi, T. and Yano, T. (2015) 'Improved Digital Photogrammetry Technique for Crack Monitoring', *Advanced Engineering Informatics* 29(4) pp. 851-858. *Science Direct* [Online]. Available at: https://www.sciencedirect.com/science/article/pii/S1474034615000592 (Accessed: 13th June 2021).

Norman, M., Ghazali, N. and Manaf, A. F. M. (2012) 'Shoreline Siltation Monitoring Using Remote Sensing Techniques', *IEEE Colloquium on Humanities, Science and Engineering Research* (*CHUSER 2012),* Kota, Kinabalu, Sabah, Malaysia, 3-4 December. IEEE Xplore [Online]. Available at: https://ieeexplore.ieee.org/document/6504283 (Accessed: 13 November 2018).

Numpy (2020) *Numpy.asarray.* Available at: https://numpy.org/doc/stable/reference/generated/numpy.asarray.html (Accessed: 23 June 2020).

Nwigwe, C. and Emberga, T. T. (2014) 'An Assessment of Causes and Effects of Flood in Nigeria', *Standard Scientific Research and Essays* 12(7) pp. 307-315. *SRJ* [Online]. Available at: https://standardresearchjournals.org/journals/SSRE/index.html (Accessed: 04 May 2017).

Obanawa, H., Hayakawa, Y. S. (2018) 'Variations in Volumetric Erosion Rates of Bedrock Cliffs on a Small Inaccessible Coastal Island Determined Using Measurements by an Unmanned Aerial Vehiclewith Structure-from-Motion and Terrestrial Laser Scanning', *Progress in Earth and Planetary Science* 5(33) pp. 1-10. *Springer* [Online]. Available at: https://progearthplanetsci.springeropen.com/articles/10.1186/s40645-018-0191-8 (Accessed: 23 December 2018).

Obu, J., Lantuit, H., Grosse, G., Gunther, F., Sachs, T., Helm, V. and Fritz, M. (2016) 'Coastal Erosion and Mass Wasting Along the Canadian Beaufort Sea Based on Annual Airborne LiDAR Elevation Data', *Geomorphology* 293(Part B) pp. 331-346. *ScienceDirect* [Online]. Available at: https://www.sciencedirect.com/science/article/pii/S0169555X16300502 (Accessed: 31 January 2018).

Oda, K., Hattori, S., Saeki, H., Takayama, T. and Honma, R. (2015) 'Qualification of Point Clouds Measured by SFM Software', *Indoor-Outdoor Seamless Modelling, Mapping and Navigation,* Tokyo, Japan, 21-22 May. *The International Archives of the Photogrammetry, Remote Sensing and Spatial Information Sciences, Volume XL-4/W5* [Online]. Available at: https://www.int-arch-photogramm-remote-sens-spatial-inf-sci.net/XL-4-W5/125/2015/isprsarchives-XL-4-W5-125-2015.pdf (Accessed: 10 November 2017).

Odera, P. A., Musyoka, S. M. and Gachari, M. K. (2014) 'Practical Application of the Geometric Geoid for Heighting Over Nairobi County and its Environs', *Journal of Agiculture, Science and Technology* 16(2) pp. 175-185. *JKUAT*[Online]. Available at: http://ir.jkuat.ac.ke/handle/123456789/2512 (Accessed: 16 April 2019).

Odolinski, R., Teunissen, P. J. G. and Zhang, B. (2020) 'Multi-GNSS Processing, Positioning and Applications', *Journal of Spatial Science* 65(1) pp. 3-5. *TandF* [Online]. Available at: https://www.tandfonline.com/doi/full/10.1080/14498596.2020.1687170 (Accessed: 07 May 2020).

Ojiako, C., Eboigbe, M. and Ajie, E. (2015) 'Tide Coordinated Shorelines in Delineating Between Legal Boundaries and Determining National Maritime Zones', *International Journal of Scientific and Engineering Research*, 6(6) pp. 753-761. *IJSER* [Online]. Available at: https://www.ijser.org/ (Accessed: 01 March 2016).

Olsen, M. J., Johnstone, E., Driscoll, N., Ashford, S. A. and Kuester, F. (2009) 'Terrestrial Laser Scanning of Extended Cliff Sections in Dynamic Environments: Parameter Analysis', *Journal of Surveying Engineering* 135(4) pp. 161-169. *ASCI Library* [Online]. Available at: https://ascelibrary.org/doi/abs/10.1061/%28ASCE%290733-9453%282009%29135%3A4%28161%29 (Accessed: 31 August 2018).

Oniga, E. V. and Cardei, M. (2015) 'A New Method for the Accuracy Evaluation of a Manufactured Piece', *IOP Conf. Series Materials Science and Engineering* 95 Conference 01. *IOP Science* [Online]. Available at: https://iopscience.iop.org/article/10.1088/1757-899X/95/1/012088/meta (Accessed: 20 August 2019).

Oniga, V., Breaban, A. and Statescu, F. (2018) 'Determining the Optimum Number of Ground Control Points for Obtaining High Precision Results Based on UAS Images', Proceedings 2(7) pp. 1-11. MDPI [Online] Available at: https://www.mdpi.com/2504-3900/2/7/352 (Accessed: 30 November 2019).

Open3d (2020) *Working with Numpy* Available at: http://www.open3d.org/docs/release/tutorial/Basic/working_with_numpy.html# (Accessed: 22 June 2020).

Ostrowski, R. and Pruszak, Z. (2011) 'Relationships Between Coastal Processes and Properties of the Nearshore Sea Bed Dynamic Layer', *Oceanologia* 53(3) pp. 861-880. *ScienceDirect* [Online]. Available at: https://www.sciencedirect.com/science/article/pii/S0078323411500284 (Accessed: 02 November 2018).

Otair, M. (2013) 'Approximate K-Nearest Neighbour Based Spatial Clustering using K-d Tree', *International Journal of Database Management Systems* (IJDMS) 5 (1) pp. 97-108. *Cornell University* [Online]. Available at: https://arxiv.org/abs/1303.1951 (Accessed: 01 December 2020).

Overduin, P. P. and Couture, N. (2006) 'Arctic Coastal Dynamics', *Report of the 6th International Workshop, Arctic Centre, University of Groningen*, Groningen, Netherlands, 22-26 October. *Arctic Coastal Dynamics* [Online]. Available at: https://arcticcoast.info/publications/workshop-reports/6th-acd-workshop (Accessed: 28th September 2017).

Palaseanu-Lovejoy, M., Danielson, J., Thatcher, C., Foxgrover, A., Barnard, P, Brock, J. and Young, A. (2016) 'Automatic Delineation of Seacliff Limits Using LiDAR-Derived High-Resolution DEMs in Southern California', *Journal of Coastal Research* SI(76) pp. 162-173. *JCR* [Online]. Available at: https://www.jcronline.org/doi/full/10.2112/SI76-014 (Accessed: 11 February 2018).

Palazzo, F., Latini, D., Baiocchi, V., Frate, F. D., Giannone, F., Dominici, D. and Remondiere, S. (2017) 'An Application of COSMO-SkyMed to Coastal Erosion Studies', *European Journal ofRemote Sensing* 45(1) pp. 361-370. *Taylor and Francis* [Online]. Available at:https://www.tandfonline.com/doi/abs/10.5721/EuJRS20124531(Accessed: 04 April 2017).

Pamart, A., Guillon, O., Faraci, S., Gattet, E., Genevois, M., Vallet, J. M. and Luca, L. D. (2017) 'Multispectral Photogrammetric Data Acquisition and Processing for Wall Paintings Studies', *3D Virtual Reconstruction and Visualization of Complex Architectures*,Nafplio, Greece1–3 March. The International Archives of the Photogrammetry, Remote Sensing and Spatial Information Sciences, Volume XLII-2/W3, *Hal Archives* [Online]. Available at:https://hal.archives-ouvertes.fr/hal-01480562/ (Accessed: 15 October 2018).

Panagiotidis, D., Surovy, P. and Kuzelka, K. (2016) 'Accuracy of Structure from Motion Models in Comparison with Terrestrial Laser Scanner for the Analysis of DBH and Height Influence on Error Behaviour', *Journal of Forest Science* 62(8) pp. 357-365. *CAAS* [Online]. Available at: https://www.agriculturejournals.cz/web/jfs.htm?type=article&id=92_2015-JFS (Accessed: 23 June 2020).

Pan, H., Guan, T., Luo, Y., Duan, L., Tian, Y., Yi, L., Zhao, Y. and Junqing, Y. (2016) 'Dense 3D Reconstruction Combining Depth and RGB Information', *Neurocomputing* 175(PartA 29) pp. 644-651. *Science Direct* [Online]. Available at: https://www.sciencedirect.com/science/article/abs/pii/S0925231215015805 (Accessed: 09 January 2020).

Papakonstantinuo, A., Topouzelis, K. and Pavlogeorgatos, G. (2016) 'Coastline Zones Identification and 3D Coastal Mapping Using UAV Spatial Data', *ISPRS Int. Journal of Geo-Information* 5(6),75; pp. 1-14. *MDPI* [Online]. Available at: http://www.mdpi.com/2220-9964/5/6/75 (Accessed: 30 March 2018).

Paravolidakis, V., Moirogiorgou, K., Ragia, L., Zervakis, M. and Synolakis, C. (2016) 'Coastal Extraction from Aerial Images Based on Edge Detection', *ISPRS Annals of the Photogrammetry, Remote Sensing and Spatial Information Sciences, Volume III-8, XXIII ISPRS Congress*, Prague, Czech Republic, 12-19 July. *ISPRS* [Online]. Available at: https://www.isprs-ann-photogramm-remote-sens-spatial-inf-sci.net/III-8/153/2016/isprs-annals-III-8-153-2016.pdf (Accessed 25 February 2018).

Pardo-Pascual, J. E., Sanchez-Garcia, E., Almonacid-Caballer, J., Palomar-Vazquez, J. M., Santos, E. P. D., Fernandez-Sarria, A. and Balaguer-Beser, A. (2018) 'Assessing the Accuracy of Automatically Extracted Shorelines on Microtidal Beaches from Landsat 7, Landsat 8 and Sentinel-2 Imagery', *Remote Sensing* 10(2) pp. 1-20. *MDPI* [Online]. Available at: http://www.mdpi.com/2072-4292/10/2/326 (Accessed: 03 September 2018).

Pathan, A. I. and Agnihotri, P. G. (2019) 'A combined Approach for I-D Hydrodynamic Flood Modeling by using Arc-GIS, Hec-Georas, Hec-Ras Interface – A Case Study on Purna River of Navsari City, Gujarat', *International Journal of Recent Technology and Engineering (IJRTE)* 8(1) pp. 1410-1417. *IJRTE* [Online]. Available at: https://www.ijrte.org/ (Accessed: 03 January 2021).

Penarth Times (2015*) Looking Back at Stories, which made the Headlines Between January and June 2014.* Available at: https://www.penarthtimes.co.uk/ (Accessed: 10 June 2016).

Pepe, M. (2017) 'Use of Digital Aerial Photogrammetry Sensors for Land Cover Classification', International *Journal of Applied Engineering Research* 12(24) pp. 15610-15620. *IJAER* [Online]. Available at: https://www.ripublication.com/ijaer17/ijaerv12n24_232.pdf (Accessed: 16 October 2018).

Pepe, M., Fregonese, L. and Scaioni, M. (2018) 'Planning Airborne Photogrammetry and Remote-Sensing Missions with Modern Platforms and Sensors', *European Journal of Remote Sensing* 51(1) pp. 412-436. *TandF* [Online]. Available at: https://www.tandfonline.com/doi/full/10.1080/22797254.2018.1444945 (Accessed: 04 October 2019).

Perez-Alberti, A. and Trenhaile, A. S. (2014) 'An Initial Evaluation of Drone-Based Monitoring of Boulder Beaches in Galicia, North-Western Spain', *Earth Surface Processes and Landforms* 40(1) pp. 105-111. *Wiley Library* [Online]. Available at: https://onlinelibrary.wiley.com/doi/full/10.1002/esp.3654 (Accessed: 27 March 2019).

Phillips, M.R. (2008) 'Consequences of short-Term Changes in Coastal Processes: A Case Study', *Earth Surface Processes and Landforms* 33(13), pp. 2094-2107. *Wiley* [Online]. Available at: http://onlinelibrary.wiley.com/doi/10.1002/esp.1677/epdf (Accessed: 13 November 2016).

Phillips, M.R. (2005) 'An Assessment of Processes and Strategies for Management of the Penarth Coast', Published PhD Thesis. *Bath Spa University Library* [Online]. Available at: http://researchspace.bathspa.ac.uk/id/eprint/1459 (Accessed: 10 November 2016).

Phillips, M. R., Jones, A. L. and Thomas, T. (2018) 'Climate Change, Coastal Management and Acceptable Risk: Consequences for Tourism', *Journal of Coastal Research* SI(85) pp. 1411-1415. *JSTOR* [Online]. Available at: https://www.jstor.org/stable/26488450 (Accessed: 17 May 2021).

Pierzchala, M., Talbot, B. and Astrup, R. (2016) 'Measuring Wheel Ruts with Close-Range Photogrammetry', *International Journal of Forest Research* 89(4) pp. 383-391. *Oxford Academic* [Online]. Available at: https://academic.oup.com/forestry/article/89/4/383/2197948 (Accessed: 01 May 2019).

Pikelj, K., Ruzic, I., Ilic, S., James, M. R. and Kordic, B. (2018) 'Implementing an Efficient Beach Erosion Monitoring System for Coastal Management in Croatia', *Ocean and Coastal management* 156 pp. 223-238. *ScienceDirect* [Online]. Available at: https://www.sciencedirect.com/science/article/pii/S0964569117301680 (Accessed: 01 November 2018).

Pix4D Mapper 2.0 (2016) [Online]. Available at: https://s3.amazonaws.com/mics.pix4d.com/manual_pdf/manual_2_0_January2016.pdf(Accessed: 01 November 2016).

Pontee, N.I and Parsons, A. P. (2012) 'Adaptation as Part of Sustainable Shoreline Management in England and Wales', *Institution of Civil Engineers, Maritime Engineering Journal* 165 (MA3) pp. 113-130. *ICE Virtual Library* [Online]. Available at: https://www.icevirtuallibrary.com/doi/10.1680/maen.2011.35 (Accessed: 11 November 2015).

Poser, J. (2012) 'Comparative Imagery Analysis of Non-Metric Cameras from Unmanned Aerial Survey Aircraft', *Resource Analysis* 14 pp. 1-20. *Saint Mary's University of Minnesota Central Services Press. Winona, MN.* [Online]. Available at: http://citeseerx.ist.psu.edu/viewdoc/download?doi=10.1.1.392.4394&rep=rep1&type=pdf (Accessed: 28 June 2016).

Previtali, M., Barazzetti, L., Redaelli, V., Scaioni, M. and Rosina, E. (2013) 'Rigorous Procedure for Mapping Thermal Infrared Images on Three-Dimensional Models of Building Facades', *Journal of Applied Remote Sensing* 7(1) pp. 1-20. *SPIE Digital Library* [Online]. Available at: https://spie.org/Publications/Journal/10.1117/1.JRS.7.073503?SSO=1 (Accessed: 26th April 2018).

Pritt, M. D. (2014) 'Fast Orthorectified Mosaics of Thousands of Aerial Photographs from Small UAVs', *IEEE Applied Imagery Pattern Recognition Workshop (AIPR)*, Washington, DC, USA, 14-16 October. *IEEE Explore* [Online]. Available at: https://ieeexplore.ieee.org/document/7041928 (Accessed: 01 July 2017).

Pruszak, Z., Ostrowski, R. and Schonhofer, J. (2011) 'Variability and Correlations of Shoreline and Dunes on the Southern Baltic Coast (CRS Lubiatowo, Poland', *Oceanology* 53(1) pp. 97-120. *Science Direct* [Online]. Available at: https://www.sciencedirect.com/science/article/pii/S0078323411500053. (Accessed: 19 March 2018).

Pussella, P., Gunathilake, J., Bandara, K., Dammalage, T. and Jayakody, J. (2015) 'Coastline Changes: Vulnerability and Predictions - A Case Study of the NorthwesternCoastalBelt of Sri Lanka', *The 7th Tourism outlook conference/ Tropical Outlook Conference* Dambulla, Kandalama, Sri Lanka 8-10 August. Tourism, Leisure, and Global Change, Volume 2 [Online]. Available at: http://www.igutourism.org/tlgc.html (Accessed: 02 August 2018).

Pye, K. and Blott, S. J. (2016) 'Assessment of Beach and Dune Erosion and Accretion Using LiDAR: Impact of the Stormy 2013-14 Winter and Longer Term Trends on the Sefton Coast, UK', *Geomorphology*266 pp. 146-167. ScienceDirect [Online]. Available at: https://www.sciencedirect.com/science/article/pii/S0169555X1630318X (Accessed: 22 January 2018).

Qu, Y., Huang, J. and Zhang, X. (2018) 'Rapid 3D Reconstruction for Image Sequence Acquired from UAV Camera', *Sensors* 18(1):225 pp. 2-20. *NCBI* [Online]. Available at: https://www.ncbi.nlm.nih.gov/pmc/articles/PMC5795716/ (Accessed: 11 May 2018).

Raspini, F., Moretti, S., Fumagalli, A., Rucci, A., Novali, F., Ferretti, A., Prati, C. and Casagli, N. (2014) 'The Cosmos-SkyMed Constellation Monitors the Costa Concordia Wreck', *Remote Sensing* 6(5) pp. 3988-4002. *MDPI* [Online]. Available at: https://www.mdpi.com/2072-4292/6/5/3988 (Accessed: 23 February 2018).

Rau, J. Y., Habib, A. F., Kersting, A. P., Chiang, K. W., Bang, K. I., Tseng, Y. H. and Li, Y. H. (2011),'Direct Sensor Orientation of a Land-Based Mobile Mapping System', *Sensors* 11(7) pp. 7243-7261. *NCBI* [Online]. Available at: https://www.ncbi.nlm.nih.gov/pmc/articles/PMC3231683/ (Accessed: 23 January 2019).

Redweik, P., Garzon, V. and Pereira, T. S. (2016) 'Recovery of Stereo Aerial Coverage from 1934 and 1938 into the Digital Era', *The Photogrammetric Record* 31(153) pp. 9-28. *Wiley Library* [Online]. Available at: https://onlinelibrary.wiley.com/doi/full/10.1111/phor.12137 (Accessed: 26 February 2018).

Rehak, M., Mabillard,R. and Skaloud, J. (2013) 'A Micro-UAV with the Capability of Direct Georeferencing', *UAV-g2013*, Rostock, Germany, 4-6 September. *International Archives of the Photogrammetry, Remote Sensing and Spatial Information Sciences, Volume XL-1/W. InfoScience*[Online]. Available at: https://infoscience.epfl.ch/record/197352?ln=en (Accessed: 06 November 2017).

Remondino, F., Barazzetti, L., Nex, F., Scaioni, M. and Sarazzi, D. (2011) 'UAV Photogrammetry for Mapping and 3D Modelling-Current Status and Future Perspectives', *ISPRS Zurich 2011 Workshop*, Zurich, Switzerland, 14-16 September. *International Archives of the Photogrammetry, Remote Sensing and Spatial Information Sciences, Volume XXXVIII-1/C22* [Online]. Available at: https://www.int-arch-photogramm-remote-sens-spatial-inf-sci.net/XXXVIII-1-C22/25/2011/isprsarchives-XXXVIII-1-C22-25-2011.pdf(Accessed: 29 November 2019).

Remondino, F., Nocerino, E., Toschi, I. and Menna, F. (2017) 'A Critical Review of Automated Photogrammetric Processing of Large Datasets', *26th International CIPA Symposium*, Ottawa, Canada, 28 August-01 September. *The International Archives of the Photogrammetry, Remote Sensing and Spatial Information Sciences*, Volume XLII-2/W5. *ISPRS* [Online]. Available at: https://www.int-arch-photogramm-remote-sens-spatial-inf-sci.net/XLII-2-W5/591/2017/ (Accessed: 24 April 2018).

Remondino, F. and Fraser, C. (2006) 'Digital Camera Calibration Methods: Considerations and Comparisons', *ISPRS Commission V Symposium 'Image Engineering and Vision Metrology'*, Dresden, 25-27 September. *IAPRS Volume XXXVI, Semantic Scholar* [Online]. Available at: https://pdfs.semanticscholar.org/b5e4/dde612294a5aa25c81761ee334753ed038dc.pdf (Accessed: 10 September 2019).

Remondino, F., Pizzo, S. D., Kersten, T. and Troisi, S. (2012) 'Low-Cost and Open-Source Solutions for automated Image Orientation – A critical Ovierview', *4thInternationalEuro-Mediterranean Conference* Limassol, Cyprus, October 29 – November 3. Progress in Cultural Heritage Preservation LNCS, 7616 pp. 40-54, Springer, Berlin, Heidelberg.[Online]. Available at: https://link.springer.com/book/10.1007/978-3-642-34234-9 (Accessed: 02 March 2018).

Results from ResMar Project (2013) 'Coastal Erosion Monitoring a network of Regional Observations', *Servizi* [Online]. Available at: http://www.regione.toscana.it/-/coastal-erosion-monitoring-a-network-of-regional-observatori-1 (Accessed: 01 November 2015).

Richter, A., Faust, D. and Maas, H. G. (2013) 'Dune Cliff Erosion and Beach Width Change at the Northern and Southern Spits of Sylt Detected with Multi-Temporal Lidar', *Catena* 103 pp. 103-111. *ScienceDirect* [Online]. https://www.sciencedirect.com/science/article/pii/S0341816211000440 (Accessed: 23 December 2013).

Rieke, M., Foerster, T., Geipel, J. and Prinz, T. (2011) 'High-Precision Positioning and Real-Time Data Processing of UAV-Systems', *ISPRS Workshop*, Zurich, Switzerland, 14-16 September. *International Archives of the Photogrammetry, Remote Sensing and Spatial Information Sciences, Volume XXXVIII-1/C22. ISPRS* [Online]. Available at: https://www.int-arch-photogramm-remote-sens-spatial-inf-sci.net/XXXVIII-1-C22/119/2011/isprsarchives-XXXVIII-1-C22-119-2011.pdf (Accessed: 01 December 2019).

Rinaudo, F., Chiabrando, F., Lingua, A. and Spano, A. (2012) 'Archaeological Site Monitoring: UAV Photogrammetry can be an Answer', *XXII ISPRS Congress*, Melbourne, Australia, 25August – 01 September. International Archives of the Photogrammetry, Remote Sensing and Spatial Information Sciences, Volume XXXIX-B5, *Semantics Scholar* [Online]. Available at: https://pdfs.semanticscholar.org/2835/3f03c0a00c97dd16acb06eb558af50e7ec57.pdf (Accessed: 11 March 2019).

Ringim, A. S., Sulaiman, I. M. and Lyakurwa, J. V. (2016) 'Implementation of Integrated Coastal Zone Management Approach in the Niger Delta, Nigeria: A Review', *International Research Journal of Environmental Sciences and Studies* 1(3) pp. 43-55. *Prudent Journals* [Online]. Available at: https://prudentjournals.com/about-us/ (Accessed: 14 May 2020).

Robinet, A., Castelle, B., Idier, D., Cozannet, G., Deque, M. and Charles, E. (2016) 'Statistical Modeling of Interannual Shoreline Change Driven by North Atlantic Climate Variability Spanning 2000–2014 in the Bay of Biscay', *Geo-Marine Letters* 36 pp. 479-490. *Springer* [Online]. Available at:http://link.springer.com/article/10.1007/s00367-016-0460-8(Accessed: 11 December 2016).

Roncella, R., Forlani, G., Fornari, M. and Diotri, F. F. (2014) 'Landslide Monitoring by Fixed-Based Terrestrial Stereo-Photogrammetry', *ISPRS Technical Commission V Symposium*, Riva Del Garda, Italy, 23-25 June. ISPRS Annals of the Photogrammetry, Remote Sensing and Spatial InformationSciences, Volume 11-15. *ISPRS* [Online]. Available at: https://www.isprs-ann-photogramm-remote-sens-spatial-inf-sci.net/II-5/297/2014/isprsannals-II-5-297-2014.pdf (Accessed: 08 February 2019).

Rosser, N. J., Brain, M., Petley, D. N., Lim, M. and Norman, E. C. (2013) 'Coastline Retreat via Progressive Failure of Rocky Coastal Cliffs', *Geology* 41(8) pp. 939-942. *GeoScience World* [Online]. Available at: https://pubs.geoscienceworld.org/gsa/geology/article-abstract/41/8/939/131374 (Accessed: 17 April 2019).

Rothermel, M., Wenzel, K., Fritsch, D. and Haala, N. (2012) 'SURE: Photogrammetric Surface Reconstruction from Imagery', *Proceedings LC3D Workshop, Berlin, 4-5 December, 1-9,* [Online]. Available at: http://www.ifp.uni-stuttgart.de/publications/2012/Rothermel_etal_lc3d.pdf (Accessed: 28 April 2018).

Rouse, H. L., Bell, R. G., Lundquist, C. J., Blackett, P. E., Hicks, D. M. and King, D. N. (2017) 'Coastal Adaptation to Climatic Change in Aotearoa New Zealand', *New Zealand Journal of Marine and Freshwater Research*51(2) pp. 183-222. *Taylor and Francis* [Online]. Available at: https://www.tandfonline.com/doi/abs/10.1080/00288330.2016.1185736 (Accessed 23 February 2019).

Rumpler, M., Daftry, S., Tscharf, A., Prettenthaler, R., Hoppe, C., Mayer, G. and Bischol, H. (2014) 'Automated End-to-End Workflow for Precise and Geo-Accurate Reconstructions Using Fiducial Markers', *ISPRS Technical Commission III Symposium*, Zurich, Switzerland, 5-7 September. *ISPRS Annals of the Photogrammetry, Remote Sensing and Spatial Information Sciences,* Vol. 11-3. *ISPRS* [Online]. Available at: https://www.isprs.org/publications/archives.aspx (Accessed: 25 April 2018).

Rupnik, E., Daakir, M. and Deseiligny, M. P. (2017) 'MIcMac – A Free, Open-Source Solution for Photogrammetry', *Open Geospatial Data, Software and Standards* 2(14) pp. 1-9. *Springer* [Online]. Available at: https://link.springer.com/article/10.1186/s40965-017-0027-2 (Accessed: 14 January 2019).

Ruzgiene, B. (2005) 'Performance Evaluation of Non-Metric Digital Camera for Photogrammetric Application', *Geodesy and Cartography* XXXI(I) pp. 22-27. *TandF* [Online]. Available at: https://www.tandfonline.com/doi/pdf/10.1080/13921541.2005.9636660 (Accessed: 17 January 2020).

Ruzgiene, B., Berteska, T., Gecyte, S., Jakubauskiene, E. and Aksamitauskas, V. (2014) 'Photogrammetric Processing of UAV Imagery: Checking DTM', *the 9th International Conference "ENVIRONMENTAL ENGINEERING*" 22–23 May Vilnius, Lithuania. *Mendeley* [Online]. Available at: https://www.mendeley.com/catalogue/73b7aed1-bd72-3c40-b090-63b62e886bc7/ (Accessed: 17th December 2016).

Ruzgiene, B., Berteska, T., Gecyte, S., Jakubauskiene, E. and Aksamitauskas, C. V. (2015) 'The Surface Modelling Based on UAV Photogrammetry and Qualitative Estimation', *Measurement* 73 pp. 619-627. *ScienceDirect* [Online]. Available at: https://www.sciencedirect.com/science/article/pii/S0263224115002316 (Accessed: 24 January 2019).

Ruzic, I., Benac, C., Marovic, I. and Ilic, S. (2015) 'A Stability Assessment of Coastal Cliffs Using Digital Imagery', *Acta GeotechnicaSlovenica* 12(2) pp. 25-35. *Digital Library of University of Maribor* [Online]. Available at: https://dk.um.si/IzpisGradiva.php?id=70850&lang=eng (Accessed: 24 January 2019).

Ruzic, I., Marovic, I. Benac, C. and Ilic, S. (2014) 'Coastal Cliff Geometry Derived from Structure-from-Motion Photogrammetry at StaraBaska, Krk Island, Croatia', *Geo-Marine Letters* 34(6) pp. 555-565. *Springer* [Online]. Available at: https://link.springer.com/article/10.1007/s00367-014-0380-4 (Accessed: 07 February 2019).

Sabins, F. F. (2007) *Remote Sensing, Principles and Interpretation* 3rd edn. Long Grove, Illonois. Waveland Press, INC.

Sacchi, M., Matano, F., Caccavale, M., Esposito, G., Caputo, T., Somma, R., Troise, C., De Natale, G., Minardo, A., Zeni, L. and Zeni, G. (2016) 'Application of an Integrated Monitoring System for Rock Failures in the Coroglio Tuff Cliff (Naples, Italy)', *12th International Symposium on Landslides, Integrated Monitoring System*. Naples, Italy 12-19 June. *Earth-Prints Repository* [Online]. Available at: https://www.earth-prints.org/handle/2122/11347 (Accessed: 18 January 2019).

Sagar, S., Roberts, D., Bala, B. and Lymburner, L. (2017) 'Extracting the Intertidal Extent and Topography of the Australian Coastline from a 28 year Time Series of Landsat Observations', *Remote Sensing of Environment* 195 pp. 153-169. *ScienceDirect* [Online]. Available at: https://www.sciencedirect.com/science/article/pii/S0034425717301591 (Accessed: 28 November 2018).

Samanta, S. and Paul, S. (2016) 'Geospatial Analysis of Shoreline and Land Use/Land Cover Changes Through Remote Sensing and GIS Techniques', *Modeling Earth System and Environment* 2(108) pp. 1-8. *Springer Link* [Online]. Available at: https://link.springer.com/article/10.1007/s40808-016-0180-0 (Accessed: 12 December 2016).

Sampath, A., Moe, D. and Christopherson, J. (2012) 'Two Methods for Self Calibration of Digital Camera', *XXII ISPRS Congress*, Melbourne, Australia, 25 August – 01 September. *International Archives of the Photogrammetry, Remote Sensing and Spatial Information Sciences, Volume XXXIX-B1* [Online]. Available at: https://www.int-arch-photogramm-remote-sens-spatial-inf-sci.net/XXXIX-B1/261/2012/isprsarchives-XXXIX-B1-261-2012.pdf (Accessed: 11 December 2019).

Sandeep, T., Laxmi, G. D. and Durga, A. K. (2015) 'Scripting Languages for Research in Data Mining', *International Journal of Engineering and Computer Science* 6(10) pp. 22823-22829. *IJECS* [Online]. Available at: http://www.ijecs.in/index.php/ijecs (Accessed: 02 November 2020).

Sander, L., Hede, M. U., Fruergaard, M., Nielsen, L., Clemmensen, L. B., Kroon, A., Johannessen, P. N., Nielsen, L. H. and Pejrup, M. (2015) 'Coastal Lagons and Beach Ridges as Complementary Sedimentary Archives for the Reconstruction of Holocene Relative Sea-Level Changes', *Terra Nova* 28(1) pp. 43-49. *Wiley* [Online]. Available at: https://onlinelibrary.wiley.com/doi/abs/10.1111/ter.12187 (Accessed: 18 October 2018).

Sanz-Ablanedo, E., Rodriguez-Perez, J. R., Arias-Sanchez, P. and Armesto, J. (2009) 'Metric Potential of a 3D Measurement System Based on Digital Compact Cameras', *Sensors (Basel)* 9(6) pp. 4178-4194. *NCBI* [Online]. Available at: https://www.ncbi.nlm.nih.gov/pmc/articles/PMC3291905/ (Accessed: 28 December 2019).

Scarelli, F. M., Sistilli, F., Fabbri, S., Cantelli, L., Barboza, E. G. and Gabbianelli, G. (2017) 'Seasonal Dune and Beach Monitoring Using Photogrammetry from UAV Surveys to Apply in the ICZM on the Ravenna Coast', *Remote Sensing Applications: Society and Environment* 7 pp. 27-39. *ScienceDirect* [Online]. Available at: https://www.sciencedirect.com/science/article/pii/S2352938517300666 (Accessed: 10 August 2018).

Schmid, K. A., Hadley, B. C. and Wijekoon, N. (2011) 'Vertical Accuracy and Use of Topographical LIDAR Data in Coastal Marshes', *Journal of Coastal Research* 27(6A) pp. 116-132. *JCR* [Online]. Available at: http://www.jcronline.org/doi/abs/10.2112/JCOASTRES-D-10-00188.1?code=cerf-site&journalCode=coas (Accessed: 29August 2018).

Schneider, J., Schindler, F., Laibe, T. and Forstner, W. (2012) 'Bundle Adjustment for Multi-Camera Systems with Points at Infinity', *XXII ISPRS Congress*, Melbourne, Australia, 25 August – 01 September. *ISPRS Annals of the Photogrammetry, Remote Sensing and Spatial Information Sciences 1-3* [Online]. Available at: https://www.isprs-ann-photogramm-remote-sens-spatial-inf-sci.net/I-3/75/2012/isprsannals-I-3-75-2012.pdf (Accessed: 23 May 2020).

Schubert, J. E., Gallien, T. W., Majd, M. S. and Sanders, B. F. (2015) 'Terrestrial Laser Scanning of Anthropogenic Beach Berm Erosion and Overtopping', *Journal of Coastal Research* 31(1) pp. 47-60. *JCR* [Online]. Available at: https://jcronline.org/doi/abs/10.2112/JCOASTRES-D-14-00037.1?journalCode=coas (Accessed: 28 November 2018).

Schwimmer, R. A. (2001) 'Rates and Processes of Marsh Shoreline Erosion in Rehoboth Bay, Delaware, U. S. A.', *Journal of Coastal Research* 17(3) pp. 672-683. *JSTOR* [Online]. Available at: https://www.jstor.org/stable/4300218?seq=1#page_scan_tab_contents (Accessed: 05 October 2017).

Sciarra, N., Marchetti, D., Avanzi, G. D. and Calista, M. (2014) 'Rock Slope Analysis on the Complex Livorno Coastal Cliff (Tuscany, Italy)', *GFDQ* 37 pp. 113-130. *GFDQ* [Online]. Available at: http://gfdq.glaciologia.it/037_2_04_2014/ (Accessed: 24 January 2019).

Sesli, F. A. (2010) 'Mapping and Monitoring Temporal Changes for Coastline and Coastal Area by Using Aerial Data Images and Digital Photogrammetry: A Case Study from Samsun, Turkey', *International Journal of the Physical Sciences* 5(10) pp. 1567-1575. *Academic Journals* [Online]. Available at: https://academicjournals.org/journal/IJPS/article-full-text-pdf/C02809A31117 (Accessed: 25 October 2018).

Sesli, F. A., Karsli, F., Colkesen, I. and Akyol, N. (2009) 'Monitoring the Changing Position of Coastlines Using Aerial and Satellite Image Data: An Example from the Eastern Coast of Trabzon, Turkey', *Environ Monit Assess* 152 (1-4) pp. 391-403. *NCBI* [Online]. Available at: https://www.ncbi.nlm.nih.gov/pubmed/18560986 (Accessed: 26 February 2018).

Shahbazi, M., Homayouni, S., Saadatseresht, M. and Sattari, M. (2011) 'Range Camera Self-Calibration Based on Integrated Bundle Adjustment via Joint Setup with a 2D Digital Camera', *Sensors* 11(9) pp. 8721-8740. *MDPI* [Online]. Available at: https://www.ncbi.nlm.nih.gov/pmc/articles/PMC3231487/#!po=3.57143 (Accessed: 05 October 2018).

Shahbazi, M., Sohn, G., Theau, J. and Menard, P. (2015) 'Development and Evaluation of a UAV-Photogrammetry System for Precise 3D Environmental Modelling', *Sensors* 15(11). pp. 27493-27524. *MDPI* [Online]. Available at: http://www.mdpi.com/1424-8220/15/11/27493/htm(Accessed: 15 December 2016).

Shean, D. E., Alexandrov, O., Moratto, Z. M., Smith, B. E., Joughin, I. R., Porter, C. and Morin, P. (2016) 'An automated, open-source pipeline for mass production of digital elevation models (DEMs) from very-high-resolution commercial stereo satellite imagery', *ISPRS Journal of Photogrammetry and Remote Sensing* 116, pp. 101-117. *Science Direct* [Online]. Available at: http://www.sciencedirect.com/science/article/pii/S0924271616300107 (Accessed: 17 November 2016).

Shen, Y., Lindenbergh, R. and Wang, J. (2017) 'Change Analysis in Structural Laser Scanning Point Clouds: The Baseline Method', *Sensors* 17(1) pp. 1-25. *MDPI* [Online]. Available at: https://www.mdpi.com/1424-8220/17/1/26 (Accessed: 11 May 2020).

Shin, B. and Kim, K. (2015) 'Estimation of Shoreline Change Using High Resolution Images', *Procedia Engineering* 116 pp. 994-1001. *ScienceDirect* [Online]. Available at: https://www.sciencedirect.com/science/article/pii/S1877705815020469 (Accessed: 26 December 2018).

Singh, P. K., Kainthola, A., Panthee, S. and Singh, T. N. (2016) 'Rockfall Analysis Along Transportation Corridors in High Hill Slopes', *Environmental Earth Sciences* 75(5) pp. 1-11. *Springer Link* [Online]. Available at: https://link.springer.com/article/10.1007/s12665-016-5489-5#citeas(Accessed: 06 September 2019).

Skarlatos, D. and Kiparissi, S. (2012) 'Comparison of Laser Scanning, Photogrammetry and SFM-MVS Pipeline Applied in Structures and Artificial Surfaces', *XXII ISPRS Congress*, Melbourne, Australia, 25 August – 01 September. ISPRS Annals of the Photogrammetry, Remote Sensing and Spatial Information Sciences, Volume 1-3 [Online]. Available at: https://pdfs.semanticscholar.org/c080/841fb480f503c22e565b2a6356db2d91beca.pdf (Accessed: 16 August 2018).

Slonecker, T., Fisher, G. B., Aiello, D. P. and Haack, B. (2010) 'Visible and Infrared Remote Imaging of Hazardous Waste: A Review', *Remote Sensing* 2 pp. 2474-2507. *Semantics Scholar* [Online]. Available at: https://pdfs.semanticscholar.org/f04c/b807d656a41acb28349189336bbe2535d539.pdf (Accessed: 25 February 2018).

Smeeckaert, J., Mallet, C., David, N., Chehata, N. and Ferraz, A. (2013) 'Large-scale Classification of Water Areas using Airborne Topographic LiDAR Data', *Remote Sensing of Environment* 138 pp. 134-148. *Science Direct* [Online]. Available at: https://www.sciencedirect.com/science/article/abs/pii/S0034425713002162 (Accessed: 10 January 2020).

Smith, M. W. (2015) 'Direct Acquisition of Elevation Data: Terrestrial Laser Scanning', *Geomorphological Techniques* 2(1.5) pp. 1-14. *Geomorphology* [Online]. Available at: https://www.geomorphology.org.uk/sites/default/files/chapters/2.1.5_TLS_0.pdf (Accessed: 16 November 2017).

Smith, M. W., Carrivick, L., and Quincey, D. (2016) 'Structure from Motion Photogrammetry in Physical Geography', *Progress in Physical Geography* 40(2) pp. 247-275. *White Rose* [Online]. Available at: http://eprints.whiterose.ac.uk/92733/3/SfM_PIPG_v2_notitle.pdf (Accessed: 15 September 2018).

Solano-Correa, Y. T., Bovolo, F. and Bruzzone, L. (2018) 'An Approach for Unsupervised Change Detection in Multitemporal VHR Images Acquired by Different Multispectral Sensors', *Remote Sensing* 10(4) pp. 1-23. *MDPI* [Online]. Available at: https://www.mdpi.com/2072-4292/10/4/533 (Accessed: 02 August 2018).

Somma, R., Matano, F., Marino, E., Caputo, T., Esposito, G., Caccavale, M., Carlino, S., Luliano, S., Mazzola, S., Molisso, F., Sacchi, M., Troise, C. and Natale, G. D. (2015) 'Application of LaserScanning for Monitoring Coastal Cliff Instability in the Pozzuoli Bay, Coroglio Site, PosillipoHill,Naples', *Engineering Geology for Society and Territory* 5 pp. 687-690. *Springer Link* [Online]. Available at: https://link.springer.com/chapter/10.1007/978-3-319-09048-1_133 (Accessed: 31 October 2017).

Spencer, T., Schuerch, M., Nicholls, R., Hinkel, J., Lincke, D., Vafeidis, A.,Reef, R., McFadden, L. and Brown, S. (2016) 'Global coastal wetland change under sea-level rise and related stresses: The DIVA Wetland Change Model', *Global and Planetary Change* 139, pp. 15-30. *ScienceDirect* [Online]. Available at: http://www.sciencedirect.com/science/article/pii/S0921818115301879 (Accessed: 14 December 2016).

Strecha, C., Zoller, R., Rutishauser, S., Brot, B., Schneider-Zapp, K., Chovancova, V., Krull, M. and Glassey, L. (2015) '*Terrestrial 3d Mapping Using Fisheye and Perspective Sensors', Pix4D Scientific White Papers[Online].Available at:https://support.pix4d.com/hc/en-us/sections/360000212943-Photogrammetry-knowledge* (Accessed: 15 November 2016).

Stuiver, C. (2013) Coastal Evolution of Soft Cliff Coasts: Headland Formation and Evolution on the Southwest Isle of Wight. University of Southampton, Engineering and the Environment, Doctoral Thesis. *University of Southampton Institutional Repository* [Online]. Available at: https://eprints.soton.ac.uk/366515/ (Accessed: 10 March 2018).

Sturdivant, E. J., Lentz, E. E., Thieler, E. R., Farris, A. S., Weber, K. M., Remsen, D. P., Miner, S. and Henderson, R. E. (2017) 'UAS-SFM for Coastal Research: Geomorphic Feature Extraction and Land Cover Classification from High-Resolution Elevation and Optical Imagery', *Remote Sensing* 9(10) pp. 1-21. *MDPI* [Online]. Available at: https://www.mdpi.com/2072-4292/9/10/1020 (Accessed: 20 July 2018).

Surfer (2014) *Contouring, Gridding and 3D Surface Mapping* Available at: https://www.goldensoftware.com/ (Accessed: 13 June 2020).

Su, L. and Gibeaut, J. (2017) 'Using UAS Hyperspatial RGB Imagery for Identifying Beach Zones Along the South Texas Coast', *Remote Sensing* 9(2) pp. 1-14. *mdpi*[Online]. Available at: http://www.mdpi.com/2072-4292/9/2/159/htm (Accessed: 02 September 2018).

Taborda, R. and Silva, A. (2012) 'COSMOS: A Lightweight Coastal Video Monitoring System', *Computers and Geosciences* 49 pp. 248-255. *ScienceDirect* [Online]. Available at: https://www.sciencedirect.com/science/article/pii/S0098300412002555 (Accessed: 14 January 2020).

Tsay, J. and Lee, M. (2012) 'SIFT for Dense Point Cloud Matching and Aero Triangulation', *XXII ISPRS Congress*, Melbourne, Australia, 25 August-01 September. International Archives of the Photogrammetry, Remote Sensing and Spatial Information Sciences Volume XXXIX-B3. [Online]. Available at: https://www.int-arch-photogramm-remote-sens-spatial-inf-sci.net/XXXIX-B3/69/2012/isprsarchives-XXXIX-B3-69-2012.pdf (Accessed: 20 June 2018).

Temiz, F. and Durduran, S. S. (2016) 'Monitoring Coastline Change Using Remote Sensing and GIS Technology: A case Study of Acigol Lake, Turkey', *IOP Conference Series: Earth and Environmental Science* 44 pp. 1-9. *IOPScience* [Online]. Available at: http://iopscience.iop.org/article/10.1088/1755-1315/44/4/042033/meta (Accessed: 01 July 2018).

Templin, T., Popielarczyk, D. and Rafal, K. (2018) 'Application of Low-Cost Fixed- Wing UAV for Inland Lakes Shoreline Investigation', *Pure and Applied Geophysics* 175(9) pp. 3263-3283. *Springer* [Online]. Available at: https://link.springer.com/article/10.1007/s00024-017-1707-7#citeas (Accessed: 23 November 2018).

Teo, T., Shih, T., Yu, S. and Tsai, F. (2016) 'The Use of UAS for Rapid 3D Mapping in Geomatics Education', *XXIII ISPRS Congress*, Prague, Czech Republic, 12-19 July. *International Archives of the Photogrammetry, Remote Sensing and Spatial Information Sciences* Volume XLI-B6. [Online]. Available at: https://www.int-arch-photogramm-remote-sens-spatial-inf-sci.net/XLI-B6/95/2016/ (Accessed:07 December 2020).

Terefenko, P., Wziatek, D. Z., Dalyot, S., Boski, T. and Lima-Filho, F. P. (2018) 'A High –Precision LiDAR-Based Methods for Surveying and Classifying Coastal Notches', *International Journal of Geo-Information* 7(8) pp. 2-16. *MDPI* [Online]. Available at: https://www.mdpi.com/2220-9964/7/8/295 (Accessed: 08 February 2019).

Tseng, Y., Jan, S., Lin, I. and Chang, Y. (2010) 'Modeled Oceanic Response and Sea Surface Cooling to Typhoon Kai-Tak', *Terrestrial Atmospheric and Oceanic Sciences* 21(1), pp. 85-98. [Online]. Available at: https://www.researchgate.net/publication/238087575(Accessed: 10th October, 2016).

Theuerkauf, E. J. and Rodriguez, A. B. (2012) 'Impacts of Transect Location and Variation in Along-Beach Morphology on Measuring Volume Change', *Journal of Coastal Research* 28(3) pp. 707-718. *JCR* [Online]. Available at: https://www.jcronline.org/doi/full/10.2112/JCOASTRES-D-11-00112.1 (Accessed: 01 March 2018).

The Vale of Glamorgan Council (2016) 'Report of the Director of Environment and Housing: Coastal Monitoring Update, Vale of Glamorgan Coastline', *Agenda Item No. 7 Scrutiny Committee (Economy and Environment): 2 February* [Online]. Available at: http://www.valeofglamorgan.gov.uk/en/our_council/Council-Structure/minutes,_agendas_and_reports/reports/scrutiny_ee/2016/16-02-02/Coastal-Monitoring-Update.aspx (Accessed: 14 January 2017).

Thomas, H. and Williams, E. (2019) 'High Resolution Terrestrial Thermography of Archaeological Sites', *Archaeological Prospection*, pp. I-10. *Wiley Library* [Online]. Available at: https://onlinelibrary.wiley.com/doi/pdf/10.1002/arp.1733 (Accessed: 01 May 2019).

Triggs, B., McLauchlan, P. F., Hartley, R. I. and Fitzgibbon, A. W. (2000) 'Bundle Adjustment-A Modern Synthesis', *International Workshop on Vision Algorithm*Berlin, Heidelberg, IWVA 1999. Vision Algorithms: Theory and Practice 1883 pp. 298-372. Springer [Online]. Available at: https://link.springer.com/chapter/10.1007/3-540-44480-7_21 (Accessed: 10 May 2018).

Tseng, Y., Jan, S., Dietrich, D. E., Lin, I. and Chang, Y. (2010) 'Modeled Oceanic Response and Sea Surface Cooling to Typhoon Kai-Tak', *Terrestrial Atmospheric and Oceanic Sciences* 21(1), pp. 85-98. [Online]. Available at: http://ntur.lib.ntu.edu.tw/bitstream/246246/178352/1/18.pdf (Accessed: 10 October 2016).

Topouzelis, K., Papakonstantinou, A. and Doukari, M. (2017) 'Coastline Change Detection Using Unmanned Aerial Vehicles and Image Processing Techniques', pp. 1-10. *Wiley Library* [Online]. Available at: https://onlinelibrary.wiley.com/doi/full/10.1002/arp.1733 (Accessed: 12 March 2019).

Tuan, N. O., Tin, H. C., Doc, L. Q. and Tuan, T. A. (2017) 'Historic Monitoring of Shoreline Changes in the Cua Dai Estuary, Central Vietnam using Multi-Temporal Remote Sensing Data', *Geosciences* 7(3) pp. 1-14. *MDPI* [Online]. Available at: https://www.mdpi.com/2076-3263/7/3/72 (Accessed: 11 November 2019).

Tunji, L. A. Q., Yusof, K. W., Hashim, A. M. and Sapari, N. (2014) 'Assessing Shoreline Response to Three Submerged Breakwater at Kerteh Bay, Terengganu, Malaysia using Landsat Imagery', *IOP Conference Series: Earth and Environmental Sciences* 20(1) pp. 1-12. *IOP Science* [Online]. Available at: https://iopscience.iop.org/article/10.1088/1755-1315/20/1/012020 (Accessed: 04 October 2017).

Turner, D., Lucieer, A. and Jong, S. M. D. (2015) 'Time Series Analysis of Landslide Dynamics Using an Unmanned Aerial Vehicle (UAV)', *Remote Sensing* 7(2) pp. 1736-1757. *MDPI* [Online]. Available at: https://www.mdpi.com/2072-4292/7/2/1736/htm (Accessed: 24 January 2019).

Turner, D., Lucieer, A. and Watson, C. (2012) 'An Automated Technique for Generating Mosaics from Ultra-High Resolution Unmanned Aerial Vehicle (UAV) Imagery, Based on Structure from Motion (SFM) Point Clouds', *Remote Sensing* 4(5) pp. 1392-1410. *MDPI* [Online]. Available at: https://www.mdpi.com/2072-4292/4/5/1392/htm (Accessed: 05 June 2020).

Turner, I. L., Harley, M. D. and Drummond, C. D. (2016) 'UAVs for Coastal Surveying', *Coastal Engineering* 111 pp. 19-24. *ScienceDirect* [Online]. Available at: https://www.sciencedirect.com/science/article/pii/S0378383916300370 (Accessed: 24 November 2016)

Tysiac, P., Wojtowicz, A. and Szulwic, J. (2016) 'Coastal Cliffs Monitoring and Prediction of Displacements Using TerrestialLaser Scanning', *Baltic Geodetic Congress* Gdansk, Poland, 22-25 June. *IEEE* [Online]. Available at: https://ieeexplore.ieee.org/abstract/document/7548006 (Accessed: 12 January 2019).

Tziavou, O., Pytharouli, S. and Souter, J. (2018) 'Unmanned Aerial Vehicle (UAV) Based Mapping in Engineering Geological Surveys: Considerations for Optimum Results', *Engineering Geology* 232() pp. 12-21. *ScienceDirect* [Online]. Available at: https://www.sciencedirect.com/science/article/abs/pii/S0013795217308670 (Accessed: 08 September 2019).

Ulvi, A., Toprak, A. S. and Yakar, M. (2017) 'The Investigation of Useability of Non-Metric Digital Cameras Mounted on Kites Platforms at the Archaeological Documentation Work', *Selcuk University Digital Archive Systems* 5(2) pp. 228-238. *Selcukedu* [Online]. Available at: http://acikerisim.selcuk.edu.tr:8080/xmlui/handle/123456789/11795 (Accessed: 15 March 2019).

Unger, J., Reich, M. and Heipke, C. (2014) 'UAV-Based Photogrammetry: Monitoring of a Building Zone', *ISPRS Technical Commission V Symposium*, Riva Del Garda, Italy 23-25 June. The International Archives of the Photogrammetry, Remote Sensing and Spatial Information Sciences [Online]. Available at: https://www.repo.uni-hannover.de/handle/123456789/916 (Accessed: 18 September 2018).

Vallet, J. Panissod, F., Strecha, C. and Tracol, M. (2011) 'Photogrammetric Performance of an Ultra-Light Weight Swinglet "UAV" ', *Unmanned Aerial Vehicle in Geomatics Conference*, Zurich, Switzerland, ISPRS ICWG I/V International Archives of the Photogrammetry, Remote Sensing and Spatial Information Sciences [Online]. Available at: https://infoscience.epfl.ch/record/169252/files/Paper-vallet_UAVg.pdf (Accessed: 23 August 2016).

Varela, M. R., Patricio, A. R., Anderson, K., Broderick, A. C., DeBell, L., Hawkes, L. A., Tilley, D., Snape, R. T. E., Westoby, M. J. and Godley, B. J. (2019) 'Assessing Climate Change Associated Sea-Level Rise Impacts on Sea Turtle Nesting Beaches Using Drones, Photogrammetry and a Novel GPS System', *Global Change Biology* 25(2) pp. 753-762. *Wiley Library* [Online]. Available at: https://onlinelibrary.wiley.com/doi/abs/10.1111/gcb.14526 (Accessed 16 April 2019).

Van, T. and Binh, T. (2009) 'Application of Remote Sensing for Shoreline Change Detection in Cuu Long Estuary', *VNU Journal of Science, Earth Sciences* 25, pp. 217-222 [Online]. Available at: https://js.vnu.edu.vn/EES/article/view/1879 (Accessed: 20 December 2012).

Vautherin, J., Rutishauser, S., Schneider-Zapp, K., Choi, H., Chovancova, V., Glass, A. and Strecha, C. (2016) 'Photogrammetric Accuracy and Modeling of Rolling Shutter Cameras', *Pix4D SA, EPFL Innovation Park Building D, CH-1015, Commission III, WG III/1*, Lausanne, [Online]. Available at: https://pix4d.com/wp-content/uploads/2016/05/pix4d-isprs-paper-rolling-shutter-final-edited.pdf (Accessed: 04 July 2016).

Vercator (2020) *The Vercator Cloud Platform*. Available at: https://vercator.com/software/ (Accessed: 13 July 2020).

Verhoeven, G., Wieser, M., Briese, C. and Doneus, M. (2013) 'Positioning in Time and Space Cost-Effective Exterior Orientation for Airborne Archaeological Photographs', *XXIV International CIPA Symposium*, Strasbourg, France, 2-6 September. *ISPRS Annals of the Photogrammetry, Remote Sensing and Spatial Information Sciences*, Volume II-5/W1, pp. 313-318. *Academic Bibliography* [Online]. Available at: https://biblio.ugent.be/publication/4125770 (Accessed: 29 November 2019).

Verhoeven, G. J. J., Loenders, J., Vermeulen, F. and Doctor, R. (2009) 'Helikite Aerial Photography-A Versatile Means of Unmanned, Radio Controlled, Low-Altitude Aerial Archaeology', *Archaeological Prospection* 16 pp. 125-138. *Wiley Library* [Online]. Available at: https://onlinelibrary.wiley.com/doi/pdf/10.1002/arp.353 (Accessed: 08 May 2019).

Vila-Concejo, A., Hughes, M. G., Short, A. D. and Ranasinghe, R. (2010) 'Estuarine Shoreline Processes in a Dynamic Low-Energy System', *Ocean Dynamics* 60(2) pp. 285-298. *Springer* [Online]. Available at: https://link.springer.com/article/10.1007/s10236-010-0273-7 (Accessed: 05 October 2010).

Visockiene, J. S., Brucas, D. and Ragauskas, U. (2014) 'Comparison of UAV Images Processing Software', Journal *of Measurements in Engineering* 2(2) pp. 111-121. *JVE Journals* [Online]. Available at: https://www.jvejournals.com/article/15152 (Accessed: 11 October 2018).

Vos, S., Lindenbergh, R. and Vries, S. (2017) 'Coastscan: Continuous Monitoring of Coastal Change using Terrestrial Laser Scanning', *Coastal Dynamics* (Paper No. 233) pp. 1518-1528. *Semantic Scholar* [Online]. Available at: https://www.semanticscholar.org/paper/Coastscan-%3A-Continuous-monitoring-of-coastal-change-Vos-Lindenbergh/9fadf0aa4e7b9b2316f2d7532018de73e377b9e5 (Accessed: 28 November 2017).

Wackrow, R., Chandler, J. H. and Bryan, P. (2007) 'Geometric Consistency and Stability of Consumer-Grade Digital Cameras for Accurate Spatial Measurement', *The Photogrammetric Record* 22(118) pp. 121-134. *Wiley Library* [Online]. Available at: https://onlinelibrary.wiley.com/doi/abs/10.1111/j.1477-9730.2007.00436.x (Accessed: 02 November 2019).

Wales Online (2014) *Watch: The moment 150 tonnes of cliff fall onto a Penarth beach* Available at: https://www.walesonline.co.uk/news/wales-news/penarth-landslide-watch-150-tonnes-6990560 (Accessed: 01 August 2015).

Wangensteen, B., Eiken, T., Odegard, R. S. and Sollid, J. L. (2007) 'Measuring Coastal Cliff Retreat in the Kongsfjorden Area, Svalbard, Using Terrestrial Photogrammetry', *Polar Research* 26(1) pp. 14-21. *TandF* [Online]. Available at: https://www.tandfonline.com/doi/abs/10.1111/j.1751-8369.2007.00002.x (Accessed: 25 August 2018).

Wang, Y., Sun, Y., Ziwei, L., Sarma, S. E., Bronstein, M. M. and Solomon, J. M. (2019) 'Dynamic Graph CNN for Learning on Point Clouds', *ACM Transactions Graphics* 38(5) pp. 1-13. *ACM Digital Library* [Online]. Available at: https://dl.acm.org/doi/pdf/10.1145/3326362?accessTab=true (Accessed: 12 July 2020).

Wang, Z., Mills, J., Xiao, W., Huang, R., Zheng, S. and Zhenhong, Li. (2017) 'A Flexible, Generic Photogrammetric Approach to Zoom Lens Calibration', *Remote Sensing* 9(3) pp. 1-15. *MDPI* [Online]. Available at: https://www.mdpi.com/2072-4292/9/3/244 (Accessed: 30 November 2019).

Warrick, J. A., Ritchie, A. C., Adelman, G., Adelman, K. and Limber, P.W. (2017) 'New Techniques to Measure Cliff Change from Historical Oblique Aerial Photographs and Structure-from-Motion Photogrammetry', *Journal of Coastal Research* 33(1) pp. 39-55. *JCR* [Online]. Available at: https://www.jcronline.org/doi/full/10.2112/JCOASTRES-D-16-00095.1 (Accessed: 25 August 2018).

Weaver, S. A., Ucar, Z., Bettinger, P. and Merry, K. (2015) 'How a GNSS Receiver is Held May Affect Static Horizontal Position Accuracy', *Plos One* 10(4) pp. 1-17. *NCBI* [Online]. Available at: https://www.ncbi.nlm.nih.gov/pmc/articles/PMC4414510/ (Accessed: 17 April 2019).

Webb, A. P. and Kench, P.S. (2010) 'The Dynamic Response of Reef Island to Sea-Level Rise: Evidence from Mylti-Decadal Analysis of Island Change in the Central Pacific', *Global and Planetary Change* 72(3) pp. 234-246. *Science Direct* [Online]. Available at: https://www.sciencedirect.com/science/article/pii/S0921818110001013 (Accessed: 16 February 2018).

Welsh Assembly Government Historic Lle A Geo-Portal for Wales http://lle.gov.wales/catalogue/item/lidarcompositedataset?lang=en (Accessed 30 June 2021).

Weinmann, M. and Jutzi, B. (2015) 'Geometric Point Quality Assessment for the Automated, Markerless and Rubust Registration of Unordered TLS Point Clouds', *ISPRS Geospatial Week 2015,* La Grande Motte, France, 28 September – 03 October. *ISPRS Annals of the Photogrammetry, Remote Sensing and Spatial Information Sciences*, Volume II-3/W5, pp. 89-96. *ISPRS* [Online]. Available at: https://www.isprs-ann-photogramm-remote-sens-spatial-inf-sci.net/II-3-W5/89/2015/ (Accessed: 15 January 2021).

Werff, H. M. A. (2019) 'Mapping Shoreline Indicators on a Sandy Beach with Supervised Edge Detection of Soil Moisture Differences', *Intl. Journal ofApplied Earth Observation and Geoinformation* 74 pp. 231-238. *Science Direct* [Online]. Available at: https://www.sciencedirect.com/science/article/pii/S0303243418304112 (Accessed: 21 January 2019).

Westoby, M. J., Brasington, J., Glasser, N. F., Hambrey, M. J. and Reynolds, J. M. (2012) 'Structure-from-motion' Photogrammetry: A Low-Cost, Effective Tool for Geosciences Application', *Geomorphology* 179 pp. 300-314. *Science Direct* [Online]. Available at: https://www.sciencedirect.com/science/article/pii/S0169555X12004217 (Accessed: 25 October 2018).

Westoby, M. J., Lim, M., Hogg, M., Pound, M. J., Dunlop, L. and Woodward, J. (2018) 'Cost-Effective Erosion Monitoring of Coastal Cliffs', *Coastal Engineering* 138 pp. 152-164. *ScienceDirect* [Online]. Available at: https://www.sciencedirect.com/science/article/pii/S0378383917303381 (Accessed: 25 August 2018).

Westoby, M. J., Dunning, S. A., Woodward, J., Hein, A. S., Marrero, S. M., Winter, K. and Sugden, D. E. (2015) 'Sedimentological Characterization of Antarctic Moraines Using UAVs and Strcture-from-Motion Photogrammetry', *Journal of Glaciology* 61(230) pp. 1088-1102. *IGS* [Online]. Available at: https://www.igsoc.org/ (Accessed: 01 September 2019).

Willis, M. D., Koenig, C. W., Black, S. L. and Castaneda, M. (2016) 'Archeological 3D Mapping: The Structure from Motion Revolution', *Journal of Texas Archeology and History* 3(1) pp. 1-36. *JTAH* [Online]. Available at: https://jtah.org/2016/06/04/vol3_article1/ (Accessed: 13 December 2018).

Wing, M. G. (2011) 'Consumer-Grade GPS Receiver Measurement Accuracy in Varying Forest Conditions', *Research Journal of Forestry* 5(2), 78-88. *Science Alert* [Online]. Available at: https://scialert.net/fulltext/?doi=rjf.2011.78.88 (Accessed: 02 December 2020).

Witjes, N. and Olbrich, P. (2017) 'A Fragile Transparency: Satellite Imagery Analysis, Non-state actors, and Visual Representations of Security', *Science and Public Policy* 44(4) pp. 524-534. *Oxford Academic* [Online]. Available at: https://academic.oup.com/spp/article-abstract/44/4/524/3778300?redirectedFrom=fulltext (Accessed: 18 June 2020).

Wolf, P.R. and Dewitt, B.A. (2000) *Elements of Photogrammetry with Applications in GIS*. 3rd Edition. United States: The McGraw-Hill.

Woodget, A. S., Austrums, R.,Maddock, I. P. and Habit, E. (2017) 'Drones and Digital Photogrammetry: From Classifications to Continous for Monitoring River Habitat and Hydromorphology', *Wires Water* 4(4) pp. 1-20. *Wiley Library* [Online]. Available at: https://onlinelibrary.wiley.com/doi/full/10.1002/wat2.1222 (Accessed: 03 April 2019).

Wu, W., Myers, E., Shi, L., Mickalski, M. and White, S. (2019) 'Modelling Tidal Datums and Spatially Varying Uncertainty in the Texas and Western Louisiane Coastal Waters', *Journal of Marine Science and Engineering* 7(2) pp. 1-24. *MDPI* [Online]. Available at: https://www.mdpi.com/2077-1312/7/2/44 (Accessed: 17 January 2020).

Xiong, L., Wang, G. and Wessel, P. (2017) 'Anti-Aliasing Filters for Deriving High-Accuracy DEMs from TLS Data: A Case Study from Freeport, Texas', *Computers and Geosciences* 100 pp. 125-134. *ScienceDirect* [Online]. Available at: https://www.sciencedirect.com/science/article/pii/S0098300416306562 (Accessed: 19 June 2020).

Xiuxiao, Y., Xueping, Z. and Jianhong, F. (2010) 'Transformation Method of Exterior Orientation Angular Elements Obtained via Position and Orientation System Under Gauss-Kruger Projection Co https://www.tandfonline.com/doi/abs/10.1007/s11806-010-0334-6 (Accessed: 29 November 2019).

Xharde, R., Long, B. F. and Forbes, D. L. (2006) 'Accuracy and Limitations of Airborne LiDAR Surveys in Coastal Environments', *IEEE International Symposium on Geoscience and Remote Sensing*, Denver, CO, USA, 31 July – 4 August. *IEEE Explore* [Online]. Available at: https://ieeexplore.ieee.org/document/4241773 (Accessed: 05 January 2018).

Xu, N. (2018) 'Detecting Coastline Change with all Available Landsat Data over 1986-2015: A case Study for the State of Texas, USA', *Atmosphere* 9(3) pp. 2-20. *MDPI* [Online]. Available at: https://www.mdpi.com/2073-4433/9/3/107 (Accessed: 19 March 2018).

Xu, G., Zheng, A., Li, X. and Su, J. (2017) 'Position and Orientation Measurement Adopting Camera Calibration by Projection Geometry of Plucker Matrices of Three-Dimensional Lines', *Scientific Reports* 7(44092) pp. 1-10. *Scientific Report* [Online]. Available at: https://www.nature.com/articles/srep44092 (Accessed: 10 September 2019).

Xu, X., Zhang, H., Han, G., Kwan, K. C., Pang, W., Fang, J. and Zhao, G. (2016) 'A Two-Phase Space Resection Model for Accurate Topographical Reconstruction from Lunar Imagery with Pushbroom Scanners', *Sensors* 16(4) pp. 1-25. *NCBI* [Online]. Available at: https://www.ncbi.nlm.nih.gov/pmc/articles/PMC4851021/ (Accessed: 30 November 2019).

Yakar, M., Yildiz, F., Metin, A., Uray, F., Ulvi, A., Karasaka, L., Mutluoglu, O. and Seker, D.Z.(2010) 'Photogrammetric Measurement of the Meke Lake and its Environment with Kite Photographs to Monitoring of Water Level to Climate Change', *XXXVIII ISPRS Commission V Symposium, Part 5*, Newcastle Upon Tyne, UK, 21-24 June. *The International Archives of the Photogrammetry, Remote Sensing and Spatial Information Sciences* [Online]. Available at: https://www.isprs.org/proceedings/XXXVIII/part5/papers/144.pdf (Accessed: 15 March 2019).

Yakar, M. and Yilmaz, M. H. (2008) 'Using in Volume Computing of Digital Close Range Photogrammetry', *ISPRS CongressCommission III,XXXVII, Part B3b* Beijing, China 3-11 July. International Society for Photogrammetry and Remote Sensing [Online]. Available at: http://www.isprs.org/congresses/beijing2008/default.aspx (Accessed: 22 December 2018).

Yan, L., Wan, J., Sun, Y., Fan, S., Yan, Y. and Chen, R. (2016) 'A Novel Absolute Orientation Method Using Local Similarities Representation', *International Journal of Geoinformation* 5(8) pp. 1-15. *MDPI* [Online]. Available at: https://www.mdpi.com/2220-9964/5/8/135 (Accessed: 25 April 2018).

Yoo, C. I. and Oh, T. S. (2016) 'Beach Volume Change Using UAV Photogrammetry Songjung Beach, Korea', *XXIII ISPRS Congress,* Prague, Czech Republic, 12-19 July. The International Archives of the Photogrammetry, Remote Sensing and Spatial Information Sciences [Online]. Available at: https://www.int-arch-photogramm-remote-sens-spatial-inf-sci.net/XLI-B8/ (Accessed: 25 November 2018).

Young, A. P. (2018) 'Decadal-Scale Coastal Cliff Retreat in Southern and Central California', *Geomorphology* 300(1) pp. 164-175. *ScienceDirect* [Online]. Available at: https://www.sciencedirect.com/science/article/pii/S0169555X17304476 (Accessed: 11 February 2018).

Young, A. P., Flick, R. E., Gutierrez, R. and Guza, R. T. (2009) 'Comparison of Short-Term Seaclii retreat Measurement Methods in Del Mar, California', *Geomorphology* 112 (3-4) pp 318-323.*ScienceDirect* [Online]. Available at: https://www.sciencedirect.com/science/article/pii/S0169555X09002566 (Accessed: 30 August 2008).

Young, A. P., Guza, R. T., O'Reilly, W. C., Burvingt, O. and Flick, R. E. (2016) 'Observations of Coastal Cliff Base Waves, Sand Levels, and Cliff Top Shaking', *Earth Surface Processes and Landforms* 41 pp. 1564-1573. *Wiley* [Online]. Available at: https://onlinelibrary.wiley.com/doi/full/10.1002/esp.3928 (Accessed: 08 February 2019).

Young, A. P., Guza, R. T., Reilly, W. C. O., Flick, R. E. and Gutierrez, R. (2011) 'Short-term Retreat Statistics of a Slowly Eroding Coastal Cliff', *Natural Hazards Earth System Science* 11 pp. 205-217. *Semantics Scholar* [Online]. Available at: https://www.semanticscholar.org/paper/Short-term-retreat-statistics-of-a-slowly-eroding-Young-Guza/68a8c64feec532bd9772b6078766b5d198ad9d37 (Accessed: 13 February 2018).

Young, A. P., Olsen, J. M., Driscoll, N., Flick, R. E., Gutierrez, R., Guza, R. T., Johnston, E. and Kuester, F. (2010) 'Comparison of Airborne and Terrestrial LiDAR Estimates of Seacliff Erosion in Southern California', *Photogrammetric Engineering and Remote Sensing* 76(4) pp. 421-427. *Ingenta Connect* [Online]. Available at: https://www.ingentaconnect.com/content/asprs/pers/2010/00000076/00000004/art00005 (Accessed: 13 February 2018).

Yousef, A. and Iftekharuddin, K. (2014) 'Shoreline Extraction from the Fusion of LiDAR DEM Data and Aerial Images Using Mutual Information and Genetic Algorithms', International Joint Conference on Neural Networks (IJCNN), Beijing, China, 6-11 July. *IEEE ExploreDigital Library* [Online]. Available at: https://ieeexplore.ieee.org/document/6889863 (Accessed: 02 February 2018).

Yuan, F., Qi, W.J. and Fang, A. P. (2014) 'Laboratory Geometric Calibration of Aerial Camera', *35th International Symposium on Remote Sensing of Environment (ISRSE35), Earth Observation and Global Environment* Change, Beijing, China, 22-26 April. *IOP Conf. Series: Earth and Environment Sciences 17(012196),IOP Science* [Online]. Available at: https://iopscience.iop.org/article/10.1088/1755-1315/17/1/012196/pdf (Accessed: 31st August 2017).

Yu, C., Zhenhong, L. and Penna, N. T. (2018) 'Interferometric Synthetic Aperture Radar Atmospheric Correction Using a GPS-Based Iterative Tropospheric Decomposition Model', *Remote Sensing of Environment*204 pp. 109-121. *Science Direct* [Online]. Available at: https://www.sciencedirect.com/science/article/pii/S0034425717305011 (Accessed: 04 April 2019).

Yu, S., Mou, Y., Xu, D., You, X., Zhou, L. and Zeng, W. (2013) 'A New Algorithm for Shoreline Extraction from Satellite Imagery with Non-Separable Wavelength and Level Set Method', *International Journal of Machine Learning and Computing* 3(1) pp. 158-163. *Semantic Scholar* [Online]. Available at: https://www.semanticscholar.org/paper/A-New-Algorithm-for-Shoreline-Extraction-from-with-Yu-Mou/77da8e7ba5ad3bd8c120bcc5785f9c1c05512875 (Accessed: 12 April 2015).

Zhang, X., Li, L. and Chen, G. (2014) 'A Photogrammetry-Based Method to Measure Total and Local Volume Changes of Unsaturated Soils During Triaxial Testing', *Acta Geotechnica* 10(1) pp. 55-82. *Springer* [Online]. Available at: https://link.springer.com/article/10.1007/s11440-014-0346-8 (Accessed: 10 October 2018).

Zhang, Y., Xiong, J. and Hao, L. (2011) 'Photogrammetric Processing of Low-Altitude Images Acquired by Unpiloted Aerial Vehicles', *The Photogrammetric Records* 26(134) pp. 190-211. *Wiley Library* [Online]. Available at: https://onlinelibrary.wiley.com/doi/abs/10.1111/j.1477-9730.2011.00641.x (Accessed: 10 October 2018).

Zhang, Z., Pan, S., Gao, C., Zhao, T. and Gao, W. (2019) 'Support Vector Machine for Regional Ionospheric Delay Modelling', *Sensors* 19(13) pp. 1-14. *MDPI* [Online]. Available at: https://www.mdpi.com/1424-8220/19/13/2947 (Accessed: 03 October 2019).

Zhao, L., Huang, S. andDissanayake, G. (2018) 'Linear SFM: A Hierarchical Approach to Solving Structure-from-Motion Problems by Decoupling the Linear and Nonlinear Components', *ISPRS Journal of Photogrammetry and Remote Sensing* 141 pp. 275-289. *ScienceDirect* [Online]. Available at: https://www.sciencedirect.com/science/article/pii/S0924271618301151 (Accessed: 27 May 2018).

Zhao, X., Carling, K. and Hakansson, J. (2017) 'An Evaluation of the Reliability of GPS-Based Transportation Data', *International Academic Conference on Transport, Logistics, Tourism and Sport Science*, Vienna, 24-25 November. *DiVA* [Online]. Available at: http://www.diva-portal.org/smash/record.jsf?pid=diva2%3A1177896&dswid=9495(Accessed: 11 April 2019).

Zhou, G. and Xie, M. (2009) 'Coastal 3-D Morphological Change Analysis Using Lidar Series Data: A Case Study of Assateague Island National Seashore', *Journal of Coastal Research* 25(2) pp. 435-447. *JCR* [Online]. Available at: https://www.jcronline.org/doi/abs/10.2112/07-0985.1 (Accessed: 30 January 2018).

Zhou, Q.Y., Park, J. and Koltun, V. (2018) 'Open3D: A Modern Library for 3D Data Processing', *Computer Vision and Pattern Processing*. *Cornell University* [Online]. Available at: https://arxiv.org/abs/1801.09847 (Accessed: 22 June 2020).

Zhou, X., Wang, G., Bao, Y. and Xiong, L. (2017) 'Delineating Beach and Dune Morphology from Massive Terrestrial Laser-Scanning Data Using Generic Mapping Tools', *Journal of Surveying Engineering* 143(4) pp. *ASCE Library* [Online]. Available at: https://ascelibrary.org/doi/abs/10.1061/(ASCE)SU.1943-5428.0000223 (Accessed: 21 January 2019).

Zhu, B., Li, J. and Tang, W. (2017) 'Correcting Insar Topographically Correlated Tropospheric Delays Using a Power Law Model Based on ERA-Interim Reanalysis', *Remote Sensing* 9(8) pp. 1-23. *MDPI* [Online]. Available at: https://www.mdpi.com/2072-4292/9/8/765 (Accessed: 04 October 2019).

Zulkifle, F. A., Hassan, R., Kasim, S. and Othman, R. M. (2017) 'A Review on Shoreline Detection Framework Using Remote Sensing Satellite Image', *International Journal of Innovative Computing* 7(2) pp. 40-51. *IJIC* [Online]. Available at: https://ijic.utm.my/index.php/ijic/article/view/149 (Accessed: 19 June 2020).

Zviely, D. and Klein, M. (2004) 'Coastal Cliff Retreat Rates at Beit-Yannay, Isreal, in the 20th Century', *Earth Surface Process Landforms* 29(2) pp. 175-184. *Wiley Library* [Online]. Available at: https://onlinelibrary.wiley.com/doi/abs/10.1002/esp.1019 (Accessed: 09 March 2018).

Appendix A

Distance Change Ratio Piechart Showing the Percentage of Change for Each Change Distance Ratio)

```
#importing libraries
import numpy as np
import open3d as o3d
import pandas as pd
import numpy as np
from scipy.spatial import ConvexHull
from matplotlib import pyplot as plt


#function 1
def read_point_cloud(pcd_file):

    return o3d.io.read_point_cloud(pcd_file)

#usage

pcd1_file = "6thwk.ply"
pcd2_file = "7thwk.ply"

sim_file_name = pcd1_file.split(".")[0] + '_' + pcd2_file.split(".")[0] + 'sim.ply'

pcd = read_point_cloud(sim_file_name)

points = np.asarray(pcd.points)
colors = np.asarray(pcd.colors)

d = {'x': points[:,0], 'y': points[:,1], 'z': points[:,2], 'r': colors[:,0], 'g': colors[:,1], 'b': colors[:,2]}
empty_d = pd.DataFrame({'x' : [], 'y': [], 'z': [], 'r': [], 'g': [], 'b': []})

dataframe = pd.DataFrame(data = d)

change = dataframe[dataframe.r < 1]
sim = dataframe[dataframe.r == 1]

grouped = sim.groupby(sim.g)

def get_group(g, key):
   if key in g.groups: return g.get_group(key)
   else: return empty_d

groupA = get_group(grouped, 0)
groupB = get_group(grouped, 0.2)
groupC = get_group(grouped, 0.4)
groupD = get_group(grouped, 0.6)
groupE = get_group(grouped, 0.8)
groupF = get_group(grouped, 1)
```

```
#funtion to convert from pandas dataframe to numpy array
def pandas_to_numpy(df):
    points_array = df[['x', 'y', 'z']].to_numpy()
    rgb_array = df[['r', 'g', 'b']].to_numpy()

    return points_array, rgb_array

#usage
sim_array = pandas_to_numpy(sim)
groupA_array = pandas_to_numpy(groupA)
groupB_array = pandas_to_numpy(groupB)
groupC_array = pandas_to_numpy(groupC)
groupD_array = pandas_to_numpy(groupD)
groupE_array = pandas_to_numpy(groupE)
groupF_array = pandas_to_numpy(groupF)


#function to get volume
def get_volume(npArray):
    if npArray.size == 0:
        return 0
    else:
        return ConvexHull(npArray).volume

#getting volume of each piece of the change array
volumeA = get_volume(groupA_array[0])
volumeB = get_volume(groupB_array[0])
volumeC = get_volume(groupC_array[0])
volumeD = get_volume(groupD_array[0])
volumeE = get_volume(groupE_array[0])
volumeF = get_volume(groupF_array[0])

dist = [0.02, 0.03, 0.04, 0.05, 0.1, 0.2]

print("distance {}, volume = {}".format(dist[0],volumeA))
print("distance {}, volume = {}".format(dist[1],volumeB))
print("distance {}, volume = {}".format(dist[2],volumeC))
print("distance {}, volume = {}".format(dist[3],volumeD))
print("distance {}, volume = {}".format(dist[4],volumeE))
print("distance {}, volume = {}".format(dist[5],volumeF))

volumes = (volumeA, volumeB, volumeC, volumeD, volumeE, volumeF)
sum_volumes = sum(volumes)

print('Sum Total:', sum_volumes)

#function that solves for percentage of the piece in the
def get_percentage(volume):

    return volume*100/sum_volumes

plt.style.use("fivethirtyeight")

slices = [get_percentage(volumeA), get_percentage(volumeB), get_percentage(volumeC),
get_percentage(volumeD), get_percentage(volumeE), get_percentage(volumeF)]
```

```
labels = ["Distance %s" % i for i in dist]

colors = [(1, 0, 0), (1, 0.2, 0), (1, 0.4, 0), (1, 0.6, 0), (1, 0.8, 0), (1, 1, 0.3)]
patches, texts = plt.pie(slices, colors=colors, startangle=90)
plt.legend(patches, labels=["{}, ({}%)".format(l, round(p, 4)) for l,p in zip(labels,slices)], loc="best")

# Set aspect ratio to be equal so that pie is drawn as a circle.
plt.axis('equal')
plt.tight_layout()
plt.show()
```

Appendix B

An Image Grid Algorithm to Sectionalize the Change Arrays into Regions

```
import matplotlib.pyplot as plt
import matplotlib.image as mpimg

img = mpimg.imread('name.jpg')

plt.imshow(img)
plt.grid(True)
plt.show()
```

Appendix C

ASSESSMENT OF THE PRECISION OF A SMART-PHONE POLE PHOTOGRAMMETRY FOR A SECOND-ORDER CLIFF SURFACE DEFORMATION STUDIES

M.A. Eboigbe[1], D. B. Kidner[2]

[1] Ph.D. Student, University of South Wales, Faculty of Engineering and Computing, UK. mitchell.eboigbe@southwalees.ac.uk
[2] Reader, University of South Wales, Faculty of Engineering and Computing, UK david.kidner@southwales.ac.uk.

KEY WORDS: Pole Photogrammetry, Coastal Cliff, Deformation Study

ABSTRACT:

Coastal cliff is almost a vertical elongated structure with a wave-cut notch and a landslip. Cliffs are geological formations with an almost unpredictable and unstoppable detachment between constitutes formations. Due to health, safety, environmental, and military restrictions, there are more regulations and restrictions on the use of drones. There are also the issues of portability and high cost for the purchase of hybrid drones and Terrestrial Laser Scanners (TLS). These negate the regular monitoring of the coastal cliff. This research develops a rapid, low-cost, and precise digital photogrammetry methodology for the continuous monitoring of the cliff by using the pole as the platform and a mobile phone as a sensor. The most practical vertical camera angle, image overlaps, survey distance to the cliff, and realistic time range for surveys are all determined from the basic surveying principles. Precise geometrically related point clouds generated are with or without the Global Navigation Satellite Systems (GNSS). The standard deviation for "alignment and surface deviation" at every point on each point cloud is ± 0.05m in the Northing and ± 0.12m on the Easting's for the self-calibrated digital camera and without the use of GNSS control points. With the GNSS controls, the maximum deviation in the XYZ coordinates is ±5 cm. Change analysis performed identifies areas of cut, fill, and the segment of threats in all point clouds. The photogrammetric technique developed is very cheap, simple, and reliable with minimum labor. The results obtained indicate the applicability of this methodology for second-order cliff Deformation study.

1. INTRODUCTION

With drones, pre-programmed flight routes are automatically set at the best angle that captures images on a regular grid pattern and flight speed (Varela et al, 2019; Colomina and Molina, 2014; Perez-Alberti and Trenhaile, 2014). To survey the cliff surface on a manual flight mission with the drone requires great experience to obtain an optimal flight mission and generate orthometric and digital models required for mapping purposes (Mancini et al, 2017). Digital images acquired arbitrarily from the ground stations to survey the cliff would be difficult to generate a complete overlapping stereo oriented model for consistent and precise 3D models and 3D maps except as a rare 'accidental success'.

The use of poles and masks as platforms would require ground-based camera locations. The distance between these ground-based stations and the cliff surface (L) is as the height (II) above the ground in aerial surveys. Like the traditional aerial surveys, camera-based stations on the ground would require very careful and systematic planning to achieve the best Ground Sampling Distance (GSD) (Huang et al, 2015), sensor stability (Roncella et al, 2014), overlap and reduce the effects of random errors and accumulation of systematic errors (Aber and Babb, 2018; James and Robson, 2014). The length between the baseline and cliff (L), the linear dimension of the pixel (px), and the camera lens' focal length (f) will determine GSD accuracies as camera pixels will be mapped to the cliff surface

Geological formations of limestone, sandstone, chalk, rock shelters, and granite characterize the cliff surface (Terefenko et al, 2018). Several crests of waves on the cliff surface depend on the formation of the sections on the cliff and such irregular spectral frequencies cause both low and high contrast across the electromagnetic spectrum (Young et al, 2016). Digital photogrammetry is more challenging when using low-quality complementary metal-oxide-semiconductor CMOS or the Charge-coupled devices CCD image sensors (Dai et al, 2014) as with this research. The best pattern of forward and side overlap and the distance between the camera's stations to the cliff surface is; therefore, determine to generate the best spatial and spectral resolutions for deformation analysis.

Due to the height of the coastal cliff and considering the very short distance between the camera location and the cliff surface, there must be careful considerations on the angle of the camera, camera calibration, stabilization, and sensor orientation to overcome yaw variation, rolls variation, altitude variation, perspective variation, barrel, and pincushion. The accuracies on the computation of the exterior orientation parameters by the BBA using the Integrated Sensor Orientation (ISO) is usually affected by both the satellite geometry and the lock on the available GNSS constellation (Rau et al, 2011). GNSS radio signals delays are mainly by the free electrons in the ionosphere and by other atmospheric conditions in the troposphere (Zhang et al, 2019). The Earth rotation induces charged particles into the magnetic field line in the ionosphere and capable of distorting the propagation of radio waves signal (Constable, 2016). Ionospheric propagation delays are of higher magnitude than the tropospheric delays and largely degrade the accuracies in single-frequency GNSS receivers' especially inbuilt GNSS sensors on smartphones and other inexpensive digital cameras (Karaim et al, 2018). Considerations are in place also to obtain the best time-lapse for satellite geometry when mapping the cliff surface using the pole photogrammetry due to drift in the GPS/INS low-quality digital camera/GPS sensor (Masiero et al, 2017).

The coastal cliff undergoes regular physical and chemical weathering processes (Earlie et al, 2017 and Sciarra et al, 2014)

as well as seawater crashing against the surface (Earlie et al, 2017). Cliff surface weathering causes an almost unpredictable and unstoppable detachment between constitutes formations and eventual collapse (Singh et al, 2016). The coastal cliffs are therefore asymmetrical with complex surface discontinuities (Letortu et al, 2018; Westoby et al, 2018; Ruzic et al, 2015; Galea et al, 2014; Somma et al, 2015 and Sciarra et al, 2014). It is difficult therefore to establish temporary/permanent control points on the cliff surface. The establishment of GNSS points close to the cliff at either the top or toe in some coastal area is practically difficult due to such high-volume sea wave and cliff surface erosion (Earlie et al, 2017). This is the situation in Penarth (study location) very peculiar with the Bristol Channel and the regular cliff face collapse. GNSS equipment is expensive to buy/ borrow and may not be available in most situations. It is imperative to develop a cost-effective and precise methodology using the Structure from Motion SFM derived point cloud for coastal cliff geotechnical and structural change detection analysis. For existing close-range digital photogrammetry techniques, consistent and accurate time-series orthomosaics and digital models for environmental monitoring are feasible on the availability of GNSS points (Ruzgiene et al, 2015 and Turner et al, 2015). The method developed is a simple and straightforward photogrammetry technique for consistent and precise evaluation of the cliff surface with or without the GNSS controls.

2. METHODOLOGY

2.1 Determine an Appropriate Vertical Camera Angle to the Cliff

The basic transformational matrixes of each grid cell relate every pixel location in the image relative to the cliff surface elevation. The digital camera self-calibration solution includes the direct computation for the interior and exterior parameters, which allows the transformation from 3D coordinate (X, Y, Z) of the ground point to a 2D coordinate (u, v) of the image in pixels. The basic perspective projection centre of the perspective lens cameras relates the scene properties as pixels where the origin is the camera centre defined by its position and orientation.

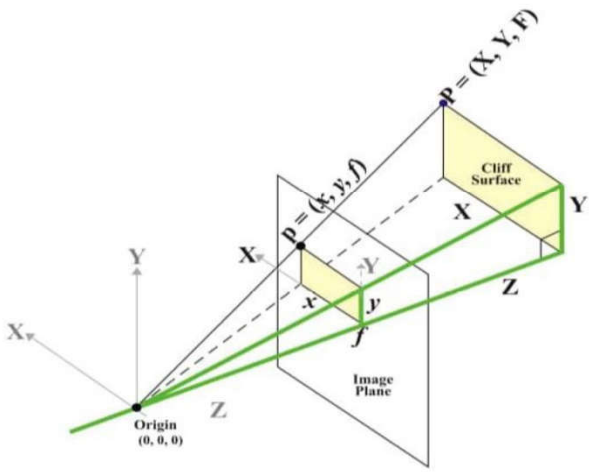

Figure 1. Perspective Projection

The origin and geometrical sequence between each grid cell determine the transformation matrix of orientation parameters that form the image of the object by relating the scene properties as pixels (Liu et al, 2016). The origin is the camera centre defined by its position and orientation (Xu et al, 2017).

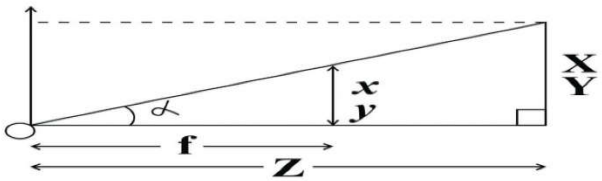

Figure 2. Central Projection

$$x = f\frac{X}{Z} \text{ and } y = f\frac{Y}{Z} \quad (1)$$

Digital photos acquired from off-nadir angle geometry will generate denser tie-points and create a better model for the cliff surface compared with photos acquired from the nadir positions (Nesbit and Hugenholtz, 2019; Juad et al, 2016; Mancini et al, 2017). The reduction of systematic errors is from the reduction of gaps between adjoining digital images on the cliff surface geometry that is vertically irregular (Nesbit and Hugenholtz, 2019). This section experiment on an appropriate vertical camera angle that would be suitable to;

a) High overlapping images that can generate a dense point cloud
b) Obtain pixel texture accuracies for cliff surfaces
c) Survey the entire height of the cliff with geometric accuracies

This practical solution is reliant on the cliff surface characteristics, the resolution of the digital camera, and the pole as a platform using the perpendicular orientation geometry as shown below.

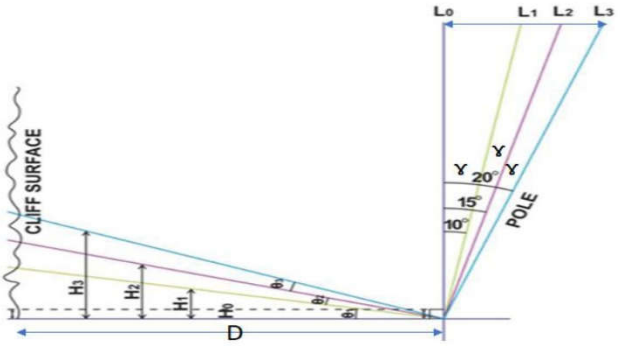

Figure 3. Viewing and Orientation Geometry to the Cliff

Θ = Observing angle
ɤ= Vertical camera angle
H = Height of the section on the cliff
D = Ground distance
Pɤ = Pixel size perpendicular to the vertical camera angle
PΘ = Angular segment on the cliff surface. $\tan \Theta = \frac{H}{D} =$ (2)

At L, the height of the cliff will be H while Pɤ is smaller provided every other photogrammetric constraint such as clouds, haze, and poor image overlap are minimal. This research experiments on the perpendicular orientation geometry using four different surveys at four different vertical cameras angle to the cliff section measuring 27 meters in length. The outcome is figure 4 below.

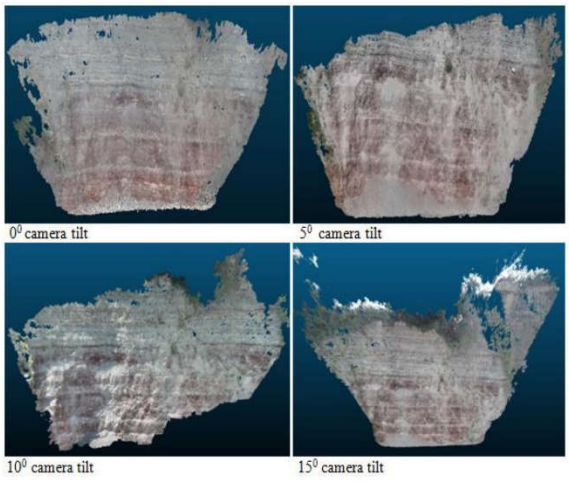

Figure 4. Dense Point Cloud obtained from Four Vertical Camera Angle

2.2 Determining the Best Distance between the Cliff Surface and the Base Line

In close-range photogrammetry, the digital camera could be as close as a few centimeters to the object being monitored which favorably improves on the image resolution (Westoby et al, 2015). However, when monitoring an unstable cliff like the Penarth, 1-2 meters could be dangerous and unfavorable to the field of view (FOV) with constraints on the orientation angle of the digital camera. The best practice would be a trade-off between the distance to the cliff surface, the FOV, and the cliff height. The camera distance to the cliff surface determines the GSD. Shorter distances between the camera and the cliff will turn out into a smaller GSD provided every other photogrammetric constraint is at minimal while larger distances could amount to greater GSD especially with the use of low/medium resolution digital cameras. Smaller GSD will have a higher spatial resolution. The GSD should be at least half of the smallest object on the ground for measurement (Tziavou et al, 2018).

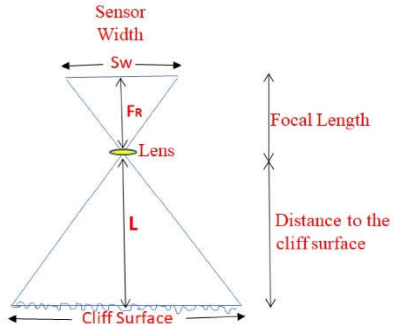

Figure 5 Sensor Width Relative to the FOV

$$GSD = \frac{L * px}{f}$$

$$L = \frac{GSD * F}{PX} \quad (3)$$

Most times the pixels, when projected onto the ground, will not be squared perfectly. The GSD would then be computed for in terms of sensor width and sensor height.

GSD = Ground Sampling Distance
L = the length between the baseline and cliff
f= the focal length of the digital camera
px = the pixel linear dimension

To determine approximately the GSD For a distance of 3 meters between the baseline and the cliff, using the Samsung (SM-G850F Camera);
The focal length of the Samsung SM-G850F camera = 1.2 mm
Pixel height = 1920
Pixel width = 1080
Approximate sensor width = 9.61923 mm
Approximate sensor height = 5.410082 mm

$$\text{Width} = \frac{3 * 5.410821}{1.2 * 1080} = \mathbf{1.25cm/px} \qquad \text{Height} = \frac{3 * 9.619238}{1.2 * 1920} = \mathbf{1.25cm/px.}$$

To derive a baseline that is photogrammetric stable between the camera position and the cliff, the cliff was surveyed three different times at three different baselines. The section of the cliff monitored is 27 meters in length. The Samsung Alpha phone SM-G850F Front Camera of 2.1 megapixels was on an 11 meters pole for these surveys. The outcome of each survey is the table I below

L (m)	No. of Photos	Average GSD (cm)	2D Key points extracted for BBA	3D Key points for BBA	Mean projection errors in pixel
3	169	1.68	3782815	1303566	0.254
5	169	0.73	3174090	786342	0.268
10	169	2.05	3958836	838557	0.309

Table 1. The outcome of three Different Surveys to determine a Practical Base Line to the Cliff

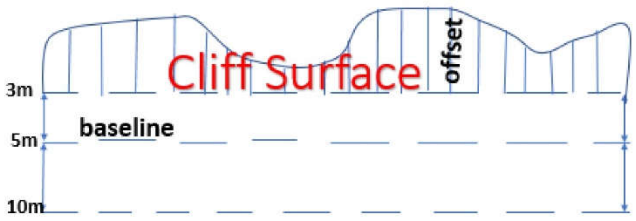

Figure 6. The Three Different Baseline Distances from the Cliff

2.3 Determine a Practicable forward and side overlap

The terrain topography and purpose of the photogrammetric project determine the choice and percentage of overlap (Pepe et al, 2018). Recommendations, however, are for a regular grid pattern (Carter et al, 2019) of 60% side overlap and 80% forward overlap (Cwiakala et al, 2018; Turner et al, 2015; Colomina and Molina, 2014). To generate tie-points with maximum density, every point in the object space should be in a minimum of 4-5 images (Ruzgiene et al, 2015).

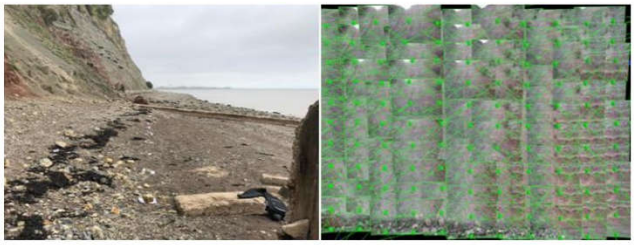

Figure 7. Degree of Overlap from Marked Points on the Ground

Poles stations were at every 1.65m marked on the ground with a white paper as shown on the Left-Hand Side LHS of fig. 4.9. The painters' pole used is 11m long and segmented at every 1m. The average percentage of overlap is 55% horizontal and 58% vertical. Figure 5 below illustrates the number of overlapping images.

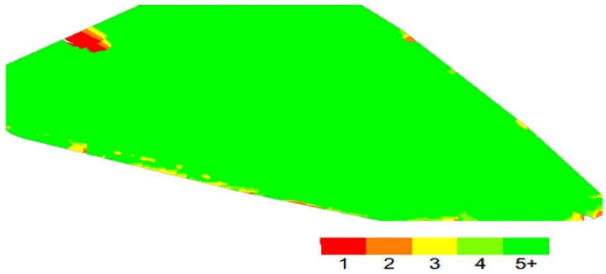

Figure 8. Number of Overlapping Images

2.4 Determine an Appropriate Time-Lapse for Surveying the Cliff with the Pole Using the Integrated Sensor Orientation (ISO)

In the ISO, the computation of the Bundle Block Adjustment BBA is by the use of the inbuilt GNSS sensors and the compact Micro-Electro-Mechanical Systems Inertial Measurement Unit (MEMS IMU) without GNSS controls and pre-defined tie points (Pepe et al, 2018 and Benassi et al, 2017). Although the ISO is straight to use, the cheap miniature sensors with cheap inbuilt GPS are downgraded easily especially in very dynamic environments (Benassi et al, 2017). The accelerometer and gyros of the MEMS-IMU are also flexible and can easily drift during use due to their microstructure compartments. The tropospheric signal delays characterized by pressure, temperature, and water vapour are relative to geographical elevation (Yu et al, 2018 and Zhu et al, 2017) with water vapour predominant in the coastal areas. The accuracies of close-range photogrammetric surveys will improve on favourable atmospheric conditions (Pepe et al, 2018) likely on lesser time durations.

Inexpensive GNSS sensors would be difficult to generate consistent and reliable dense point cloud due to inherent anomalies in the Scale Invariant Feature Transformations (SIFT) (Qu et al, 2018) which detects and extract the local features in the corresponding digital images. It would be difficult then to minimize errors from transformation and misalignments which ideally are reduced by the GNSS controls and tie points as with the Integrated Sensor Orientation (ISO) and GNSS-supported Aerial Triangulation (GNSS-AT) in digital photogrammetry (Benassi et al, 2017). To balance off systematic and random errors from the ionospheric and tropospheric delays, drifting, and downgrading of the inbuilt GPS, this research relies on the systematic field procedure(s) developed in the foregoing sections. The aim is to obtain the maximum number of images that would be calibrated for SIFT. The cliff surface was surveyed at different time-range to establish the level-of-tolerance of the inexpensive Samsung SM-G850F MEMS-IMU/inbuilt GNSS sensors on favourable atmospheric and illumination (shadow cast) conditions.

	Time Range Minutes	No. of images	% of calibrated images	Using the New field Method	Point cloud
a	00:30:03	86	100	yes	Single block mosaic
b	00:59:28	187	100	yes	Single block mosaic
c	01: 28:20	198	100	yes	Single block mosaic
d	02:16:31	490	98	80%	Multiple block mosaic
e	02:52:50	377	100	yes	Single block mosaic
f	03:05:36	517	99	yes	Single block mosaic

Table 2. Time Range to Determine the Level-of Tolerance of the Miniature Sensors

While surveys executed at lesser times will easily overcome systematic and random errors, good overlap, and a regular survey grid pattern can compensate for errors. The pattern for capturing images in **d** on table 2.was a horizontal survey grid with more images taken after the main survey to verify the effect of drifting. The dense point cloud from survey **d** in table 2. is downgraded into multiple block mosaics as shown below.

Figure 8. Multiple Block Point Cloud Showing the Effect of Drifting on the Inexpensive GNSS Sensors

3. EVALUATING THE GEOMETRIC PRECISIONS OF THE POLE SURVEY FOR CLIFF SURFACE DEFORMATION STUDIES

The different point clouds generated should be geometrically precise for evaluative purposes (Kromer et al, 2015). Comparisons were on four different point clouds obtained from four weekly surveys to determine the consistencies and reliability of the new pole mapping field sequence.

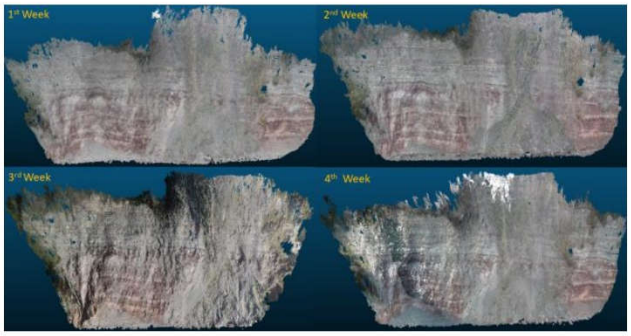

Figure 9. Dense Point Clouds from four Weekly Surveys

	1st Survey	2nd Survey	3rd Survey	4th Survey
Date of survey	02-10-18	11-10-18	22-10-18	30-10-19
N0. of images	409	461	377	496
Area covered	0.0033km^2	0.0029km^2	0.0018km^2	0.0035km^2
Average density (m^3)	12646	21118.3	25141.3	14089.7

Table 3. Procedure for the four Weekly Surveys

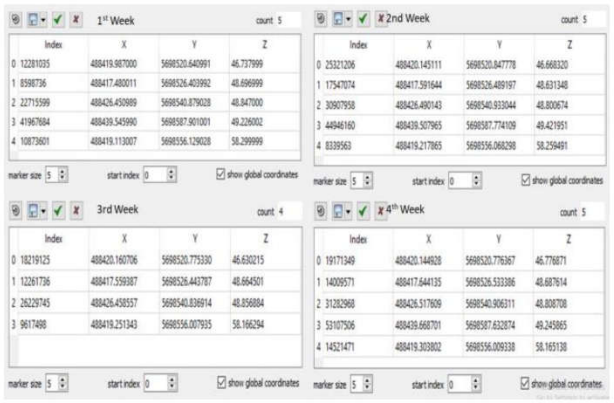

Figure 10. Geographical Coordinates of all four Weekly Surveys in CloudCompare

	Wk 1 –WK 2		Wk 1 –WK 3		Wk 1 –WK 4	
	ΔN	ΔE	ΔN	ΔE	ΔN	ΔE
Pt.1	-0.158111	-0.206787	-0.173706	-0.134339	-0.157928	-0.135376
Pt.2	-0.111633	-0.085205	-0.079376	-0.039795	-0.164124	-0.12939
Pt. 3	-0.039154	-0.054016	-0.007568	0.042114	-0.06662	-0.02728
Pt. 4	0,038025	0.126892	-0.138336	0.121093	-0.122711	0.20813
Pt. 5	-0.104858	0.06073			-0.190795	0.11969

Table 4. Accuracies of all four Weekly Surveys

The standard deviation for "alignment and surface deviation" (Westoby et al, 2018) at every point on each point cloud is ± 0.05m in the Northing and ± 0.12m on the Easting's for the self-calibrated digital camera and without the use of GNSS control points. This shows that each of the point cloud models geometrically fits into the other for a second-order cliff monitoring deformation study (Westoby et al, 2018 and Ruzic et al, 2015).

3.1 Verifying the Correctness of the CloudCompare Global Coordinates

To verify the correctness of the CloudCompare coordinates, the DSM of one of the Pole Survey Point Cloud (PSPC) was imported into ArcMap and the coordinates of the control points in CloudCompare as in Figure 10 is found to be the same as in ArcMap.

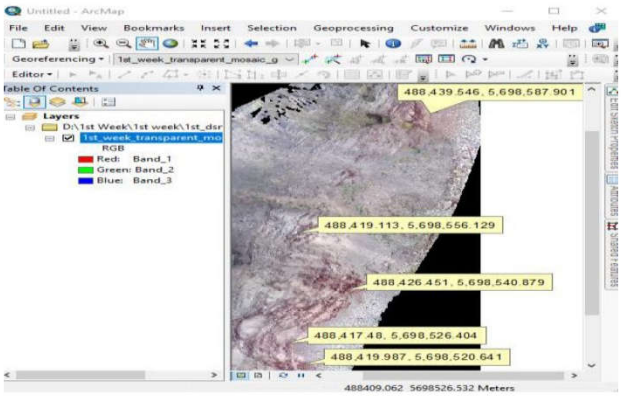

Figure 11. Verification of the CloudCompare Global Coordinates in ArcMap

The geometric accuracy defines the comparative evaluation with datasets obtained from other reliable photogrammetric techniques while the absolute accuracy is the difference of the x, y, and z coordinates of every point on the point cloud to their true geographical position on ground (Harwin and Lucieer, 2012). The 3D reconstruction process in the bundle adjustment may distort the original shape of the cliff surface alignment.

The TLS and the Pole survey were both used to survey the same stretch of the cliff surface on the 13th of March 2020. This is to be able to determine the global correctness of the digital image EXIF and structure from motion computation for bundle adjustment that optimizes the 3D location between the tie-points and the camera internal parameters (Turner et al, 2012).

The TLS survey was using the Topcon Laser scanner GLS-2000M series. The 8.9-degree telephoto camera provided the complete stereoscopic coverage of the cliff surface at 6.3 mm at 10 m resolution. Two different prism scan locations provided the precise and accurate modelling of the cliff section monitored. The fixed pole at (window scanning) enhances accuracies although it takes longer to scan but reduces the registration of the point cloud in the Topcon ScanMaster software. The height of the pole for this survey was 2 m and the prisms are 125 mm. Georeferencing was by the GEOMAX Zenith 35 series on Real-Time Kinematic (RTK) mode.

3.2 **Control Points for Georeferencing the Pole Survey**

Four markers at the bottom of the cliff with other visible points on both surveys in the middle of the inaccessible clifftop were used as manual tie-points for geolocating the pole survey in Pix4D on OSGB 1936 coordinate system as shown in figure 12 below.

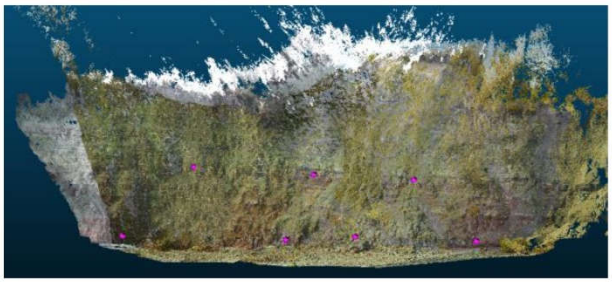

Figure 12. Control Points for Geolocating the Pole Survey

Figure 13. Pole Survey Point Cloud

The X, Y, and Z coordinates of some points at the top, sides, and at the bottom of the pole and TLS point clouds, read off, and compared in CloudCompare as shown in figure 15 and table 5 below.

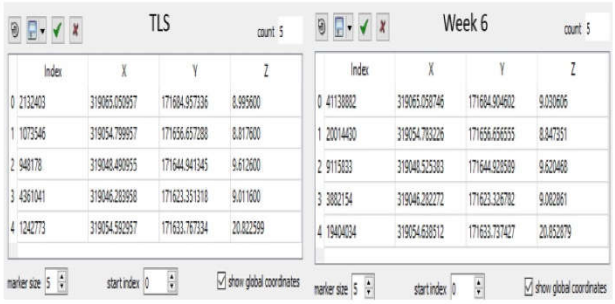

Figure 15. Example of Coordinates of TLS and Pole Survey in CloudCompare

Table 5. Differences in the Coordinates of some Points in the TLS and Pole Surveys

	TLS – Week 6		
	ΔN	**ΔE**	**ΔZ**
Point1	-0.008	0.053	-0.035
Point 2	0.017	0.001	-0.030
Point 3	-0.034	0.013	-0.008
Point 4	0.002	0.024	-0.071
Point 5	-0.045	0.030	-0.030

The maximum deviation in the XYZ coordinates of the PSPC at every point as compared with the TLSPC is 5 cm.

The accuracies of the geometry of the PSPC and the TLSPC are subject to further scrutiny by creating their contours using the triangulation and the linear interpolation gridding method in the Surfer Golden Software (Sufer, 2018). The triangulation with linear interpolation uses the anisotropy to determine its contour (Bayazit, 2019). Anisotropy is dependent on the direction irrespective of the properties of the surface materials will generate an unbiased contour interpretation (Bayazit, 2019). The choice to use the multiple refractive indexes is due to the irregular surface nature of the cliff that has the capabilities for change in direction within the shortest possible period resulting from falls and collapse.

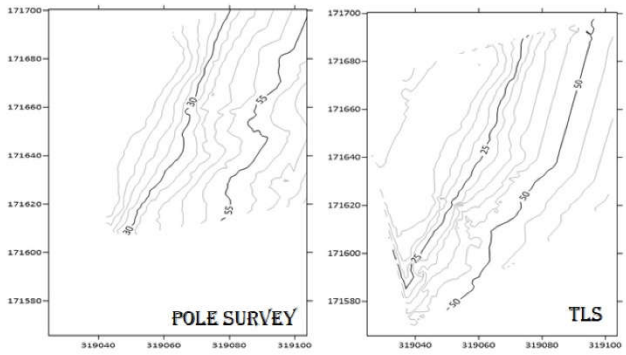

Figure 16. PSPC and TLSPC Contours generated in Suffer Golden Software

4. DISCUSSION OF RESULTS

4.1 Visual Comparison with Other Datasets

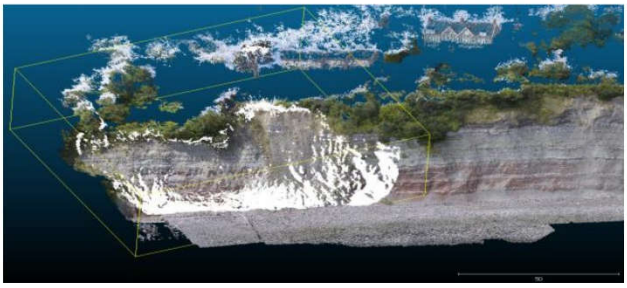

Figure 17. Pole Survey (on white) Superimposed on an Equivalength Drone Survey

Figure 18. Like-to-like Alignment (Pole Survey up and Drone Survey down)

Figure 19. 2018 Google Earth Imagery of the Study Area

Recent studies show that the M3C2 will be more effective for comparing irregular surfaces like the cliff (Lague et al, 2013). This is because the algorithm distance computation is not dependent on the spatial correlation and the dimensional orientation between the surfaces (Esposito et al, 2017).

In figure 20 below, the M3C2 in the open-source Cloudcompare is used to perform change analysis between four weekly surveys. The evaluation of the detectable surface changes is at a minimum of ±6mm. From week 1 to 2, the fuller Earth is obvious and completely erodes from week 4 to week 5. There are insignificant changes from week 2 to week 3 and complete cliff erosion at points a. b, c, d, e, f, g, h, I.

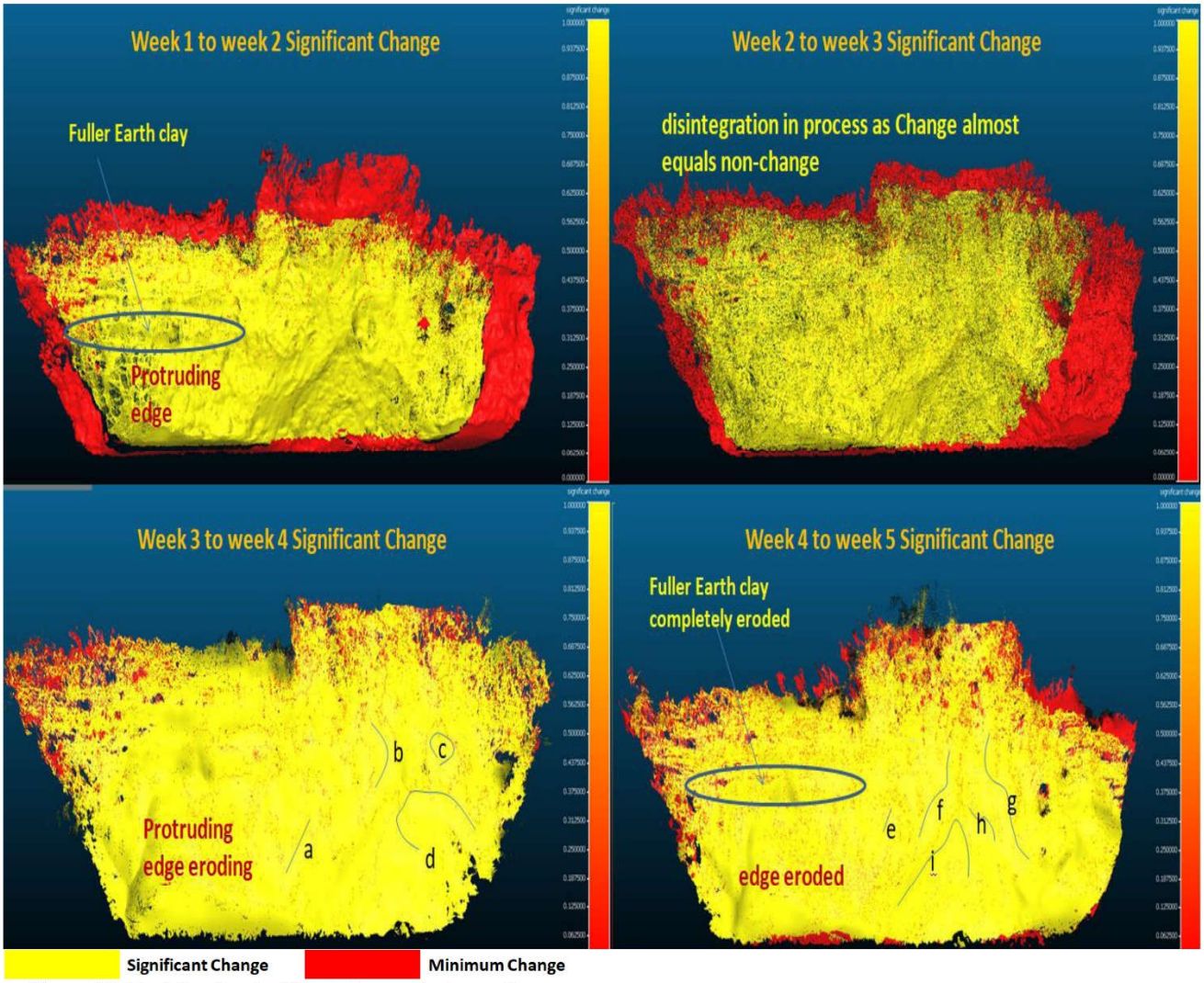

Figure 20. Explains the significant changes between four weekly surveys at 6mm detectable surface change.

5. CONCLUSION

The contribution to knowledge is a new pole digital photogrammetry methodology for coastal cliff monitoring. This research utilizes the very basic principles of photogrammetry in developing a systematic flight plan and camera orientation to able to generate precise and accurate 3D reconstructed point cloud by terrestrial pole survey for coastal cliff monitoring. The methodology developed is simple, straightforward with a regular grid network for complete stereoscopic coverage. The verification of results obtained has been by third-party software and an alternative remote sensing survey.

This methodology generates precise geometrical related point clouds with or without the GNSS controls. For use in the photogrammetry community, the most appropriate vertical camera inclination and distance to the cliff surface has been practically demonstrated and theoretically documented.

Depending on the area been mapped, surveys can be from 10 minutes to 2 hours. It is possible to attach the different digital cameras on the pole with the higher resolution cameras resulting in higher spectral accuracies. The limitation is to perform a survey in an almost equal atmospheric condition to avoid the drifting of the MEMS-IMU during the survey. Surveys performed at a very close range can detect hidden sections/crack on the cliff, but care must be not to change the viewing angle of the digital camera during use. Surveys do not require the drone licence, but care must be not to drop the pole during use.

REFERENCES

Aber, J. W. and Babb, T. A. (2018) 'The Challenges of Processing Kite Aerial Photography Imagery with Modern Photogrammetry Techniques', *International Journal of Aviation, Aeronautics, and Aerospace* 5(2) pp. 1-30. *IJAAA* [Online]. Available at: https://commons.erau.edu/ijaaa/vol5/iss2/2/ (Accessed: 25 March 2019).

Bayazit, U. (2019) 'A Greedy Region Growing Algorithm for Anisotropic Stretch Adaptive Triangulation of Geometry Images', *Graphical Models* 106(101045) pp. 1524-0703. *ScienceDirect* [Online]. Available at: https://www.sciencedirect.com/science/article/pii/S1524070319300360 (Accessed: 13 June 2020).

Benassi, F., Dall'Asta, E., Diotri, F., Forlani, G., Morra di Cella, U., Roncella, R. and Santise, M. (2017) 'Testing Accuracy and Repeatability of UAV Blocks Oriented with GNSS-Supported Aerial Triangulation', *Remote Sensing* 9(2) pp. 2-23. *MDPI* [Online]. Available at: https://www.mdpi.com/2072-4292/9/2/172 (Accessed: 11 December 2017).

Carter, N., Hashemian, A., Mckelvey, N. (2019) 'An Optimization of Small Unmanned Aerial System (sUAS) Image Based Scanning Techniques for Mapping Accident Sites', *SAE Technical Paper 2019-01-0427.SAE Mobilus* [Online]. Available at: https://saemobilus.sae.org/content/2019-01-0427/ (Accessed: 11 September 2019).

Colomina, I. and Molina, P. (2014) 'Unmanned aerial systems for photogrammetry and remote sensing: A review', *ISPRS Journal of Photogrammetry and Remote Sensing* 92, pp. 79-97. *Science Direct* [Online]. Available at: http://www.sciencedirect.com/science/article/pii/S0924271614000501(Accessed: 25 May 2016)

Constable, C. (2016) 'Earth's Electromagnetic Environment', *Surveys in Geophysics* 37(1) pp. 27-45. *Springer* [Online]. Available at: https://link.springer.com/article/10.1007/s10712-015-9351-1 (Accessed: 03 October 2019).

Cwiakala, P., Kocierz, R., Puniach, E., Nedzka, M., Mamczarz, K., Niewiem, W. and Wiacek, P. (2018) 'Assessment of the Possibility of Using Unmanned Aerial Vehicles (UAVs) for the Documentation of Hiking Trails in Alpine Areas', *Sensors* 18(1) pp. 2-28. *NCBI* [Online]. Available at: https://www.ncbi.nlm.nih.gov/pmc/articles/PMC5795845/ (Accessed: 02 July 2019).

Dai, F., Feng, Y. and Hough, R. (2014) 'Photogrammetric Error Sources and Impacts on Modelling and Surveying in Construction Engineering Applications', *Visualization in Engineering* 2(2) pp. 2-14. *Springer* [Online]. Available at: https://link.springer.com/content/pdf/10.1186%2F2213-7459-2-2.pdf (Accessed: 17 December 2018). 04017008-1 - 04017008-21.

Earlie, C., Masselink, G. and Russel, P. (2017) 'The Role of Beach Morphology on Coastal Cliff Erosion Under Extreme Waves', *Earth Surface Processes and Landforms* 43(6) pp. 1213-1228. *Wiley Library* [Online]. Available at: https://onlinelibrary.wiley.com/doi/full/10.1002/esp.4308 (Accessed: 15 February 2018).

Esposito, G., Salvini, R., Matano, F., Sacchi, M., Danzi, M., Somma, R. and Troise, C. (2017) 'Multitemporal Monitoring of a Coastal Landslide through SFM-Derieved Point Cloud Comparison', *The Photogrammetric Record* 32(160) pp. 459-479. *Ingenta Connect* [Pnline]. Available at: https://www.ingentaconnect.com/content/asprs/pers/2010/00000076/00000010/art00001;jsessionid=2b0icttstd7nn.x-ic-live-02# (Accessed 11 July 2020).

Galea, P., Amico, S. D. and Farrugia, D. (2014) 'Dynamic Characteristics of an Active Coastal Spreading Area Using Ambient Noise Measurements – Anchor Bay, Malta', *Geophysical Journal International* 199(2) pp. 1166-1175. *IEEE Xplore* [Online]. Available at: https://ieeexplore.ieee.org/document/8205841 (Accessed: 17 November 2017).

Harwin, S. and Lucieer, A. (2012) 'Assessing the Accuracy of Georeferenced Point Clouds Produced Via Multi-View Stereopsis from Unmanned Aerial Vehicle (UAV) Imagery', *Remote Sensing* 4(6) pp. 1573-1599. *MDPI* [Online]. Available at: http://www.mdpi.com/2072-4292/4/6/1573 (Accessed: 19 October 2016).

Huang, S., Zhang, Z., Ke, T., Tang, M. and Xu, X. (2015) 'Scanning Photogrammetry for Measuring Large Targets in Close Range', *Remote Sensing* 7(8) pp. 10042-10077. *MDPI* [Online]. Available at: https://www.mdpi.com/2072-4292/7/8/10042/htm (Accessed: 08 February 2019).

James, M. R. and Robson, S. (2014) 'Mitigating Systematic Error in Topographic Models Derived from UAV and Ground-Based Image Networks', *Earth Surface Processes and Landforms* 39(10) pp. 1413-1420. *Wiley Library* [Online]. Available at: https://onlinelibrary.wiley.com/doi/full/10.1002/esp.3609 (Accessed 07 February 2019).

Juad, M., Passot, S., Bivic, R. L., Delacourt, C., Grandjean, P. and Dantec, N. L. (2016) 'Assessing the Accuracy of High-Resolution Digital Surface Models Computed by PhotoSCan and MicMac in Sub-Optimal Survey Conditions', *Remote Sensing* 8(6), 465; pp. 2-18. *MDPI* [Online]. Available at: http://www.mdpi.com/2072-4292/8/6/465 (Accessed: 26 May 2018).

Karaim, M., Elsheikh, M. and Noureldin, A. (2018) '*GPS* GNSS Error Sources' inRustamov, R. B. and Hashimov, A. M. (eds), *Multifunctional Operation and Application of GPS,* IntechOpen, pp. 69-85. Available at: https://www.intechopen.com/books/multifunctional-operation-

and-application-of-gps/gnss-error-sources (Accessed: 03 October 2019).

Kromer, R. A., Abellan, A., Hutchinson, D. J., Lato, M., Edwards, T. and Jaboyedoff, M. (2015) A 4D Filtering and Calibration Techniques for Small-Scale Point Cloud Change Detection with a Terrestrial Laser Scanner, *Remote Sensing* 7(2) pp. 13029-13052. *MDPI* [Online]. Available at: https://www.mdpi.com/2072-4292/7/10/13029 (Accessed: 06July 2020).

Lague, D., Brodu, N. and Leroux, J. (2013) 'Accurate 3D Comparison of Complex Topography with Terrestrial Laser Scanner: Applications to the Rangitikei Canyon (N-Z)', *ISPRS Journal of Photogrammetry and Remote Sensing* 82 pp. 10-26. *Science Direct* [Online]. Available at: https://www.sciencedirect.com/science/article/abs/pii/S0924271613001184 (Accessed: 24 November 2017).

Letortu, P., Juad, M., Grandjean, P., Ammann, J., Costa, S., Maquaire, O., Davidson, R., Dantec, N. L. and Delacourt, C. (2018) 'Examining High-Resolution Survey Methods for Monitoring Cliff Erosion at an Operational Scale', *Behavioural Science and Public Health Titles* 55(4) pp. 457-476. *Hal. Archives* [Online]. Available at: https://hal.archives-ouvertes.fr/hal-01647588/document (Accessed: 31 August 2018).

Liu, S., Zhu, W., Zhang, C. and Sun, W. (2016) '3D Reconstruction of Indoor Scenes Using RGB-D Monocular Vision', *International Conference on Robots and Intelligent System (ICRIS),* Zhangjiajie, China, 27-28 August. *IEEE Xplore* [Online]. Available at: https://ieeexplore.ieee.org/abstract/document/7757064/authors#authors (Accessed: 10 September 2019).

Mancini, F., Castagnetti, C., Rossi, P., Dubbini, M., Fazio, N, L., Perrotti, M. and Lollino, P. (2017) 'An Integrated Procedure to Assess the Stability of Coastal Rocky Cliffs: From UAV Close-Range Photogrammetry to Geomechanical Finite Element Modelling', *Remote Sensing* (9)12 pp. 2-21. *MDPI* [Online]. Available at: https://www.mdpi.com/2072-4292/9/12/1235 (Accessed: 30 January 2019).

Masiero, A., Fissore, F. and Vettore, A. (2017) 'A Low Cost UWB Based Solutions for Direct Georeferencing UAV Photogrammetry', *Remote Sensing* 9(5) pp. 2-21. *MDPI* [Online]. Available at: https://www.mdpi.com/2072-4292/9/5/414 (Accessed: 27 March 2019).

Nesbit, P. R. and Hugenholtz, C. H. (2019) 'Enhancing UAV-SFM 3D Model Accuracy in High-Relief Landscapes by Incorporating Oblique Images', *Remote Sensing* 11(3) pp. 2-24. *MDPI*[Online]. Available at: https://www.mdpi.com/2072-4292/11/3/239/htm (Accessed: 17th June 2019).

Perez-Alberti, A. and Trenhaile, A. S. (2014) 'An Initial Evaluation of Drone-Based Monitoring of Boulder Beaches in Galicia, North-Western Spain', *Earth Surface Processes and Landforms* 40(1) pp. 105-111. *Wiley Library* [Online]. Available at: https://onlinelibrary.wiley.com/doi/full/10.1002/esp.3654 (Accessed: 27 March 2019).

Pepe, M., Fregonese, L. and Scaioni, M. (2018) 'Planning Airborne Photogrammetry and Remote- Sensing Missions with Modern Platforms and Sensors', *European Journal of Remote Sensing* 51(1) pp. 412-436. *TandF* [Online]. Available at: https://www.tandfonline.com/doi/full/10.1080/22797254.2018.1444945 (Accessed: 04 October 2019).

Qu, Y., Huang, J. and Zhang, X. (2018) 'Rapid 3D Reconstruction for Image Sequence Acquired from UAV Camera', *Sensors* 18(1):225 pp. 2-20. *NCBI* [Online]. Available at: https://www.ncbi.nlm.nih.gov/pmc/articles/PMC5795716/ (Accessed: 11 May 2018).

Rau, J. Y., Habib, A. F., Kersting, A. P., Chiang, K. W., Bang, K. I., Tseng, Y. H. and Li, Y. H. (2011),'Direct Sensor Orientation of a Land-Based Mobile Mapping System', *Sensors* 11(7) pp. 7243-7261. *NCBI* [Online]. Available at: https://www.ncbi.nlm.nih.gov/pmc/articles/PMC3231683/ (Accessed: 23 January 2019).

Roncella, R., Forlani, G., Fornari, M. and Diotri, F. F. (2014) 'Landslide Monitoring by Fixed-Based Terrestrial Stereo-Photogrammetry', *ISPRS Technical Commission V Symposium*, Riva Del Garda, Italy, 23-25 June. ISPRS Annals of the Photogrammetry, Remote Sensing and Spatial InformationSciences, Volume 11-15. *ISPRS* [Online]. Available at: https://www.isprs-ann-photogramm-remote-sens-spatial-inf-sci.net/II-5/297/2014/isprsannals-II-5-297-2014.pdf (Accessed: 08 February 2019).

Ruzic, I., Benac, C., Marovic, I. and Ilic, S. (2015) 'A Stability Assessment of Coastal Cliffs Using Digital Imagery', *Acta GeotechnicaSlovenica* 12(2) pp. 25-35. *Digital Library of University of Maribor* [Online]. Available at: https://dk.um.si/IzpisGradiva.php?id=70850&lang=eng (Accessed: 24 January 2019).

Ruzgiene, B., Berteska, T., Gecyte, S., Jakubauskiene, E. and Aksamitauskas, C. V. (2015) 'The Surface Modelling Based on UAV Photogrammetry and Qualitative Estimation', *Measurement* 73 pp. 619-627. *ScienceDirect* [Online]. Available at: https://www.sciencedirect.com/science/article/pii/S0263224115002316 (Accessed: 24 January 2019).

Sciarra, N., Marchetti, D., Avanzi, G. D. and Calista, M. (2014) 'Rock Slope Analysis on the Complex Livorno Coastal Cliff (Tuscany, Italy)', *GFDQ* 37 pp. 113-130. *GFDQ* [Online]. Available at: http://gfdq.glaciologia.it/037_2_04_2014/ (Accessed: 24 January 2019).

Singh, P. K., Kainthola, A., Panthee, S. and Singh, T. N. (2016) 'Rockfall Analysis Along Transportation Corridors in High Hill Slopes', *Environmental Earth Sciences* 75(5) pp. 1-11. *Springer Link* [Online]. Available at: https://link.springer.com/article/10.1007/s12665-016-5489-5#citeas(Accessed: 06 September 2019).

Somma, R., Matano, F., Marino, E., Caputo, T., Esposito, G., Caccavale, M., Carlino, S., Luliano, S., Mazzola, S., Molisso, F., Sacchi, M., Troise, C. and Natale, G. D. (2015) 'Application of LaserScanning for Monitoring Coastal Cliff Instability in the Pozzuoli Bay, Coroglio Site, PosillipoHill,Naples', *Engineering Geology for Society and Territory* 5 pp. 687-690. *Springer Link* [Online]. Available at: https://link.springer.com/chapter/10.1007/978-3-319-09048-1_133 (Accessed: 31 October 2017).

Surfer (2014) *Contouring, Gridding and 3D Surface Mapping* Available at: https://www.goldensoftware.com/ (Accessed: 13 June 2020).

Terefenko, P., Wziatek, D. Z., Dalyot, S., Boski, T. and Lima-Filho, F. P. (2018) 'A High –Precision LiDAR-Based Methods for Surveying and Classifying Coastal Notches', *International Journal of Geo-Information* 7(8) pp. 2-16. *MDPI* [Online]. Available at: https://www.mdpi.com/2220-9964/7/8/295 (Accessed: 08 February 2019).

Turner, D., Lucieer, A. and Jong, S. M. D. (2015) 'Time Series Analysis of Landslide Dynamics Using an Unmanned Aerial Vehicle (UAV)', *Remote Sensing* 7(2) pp. 1736-1757. *MDPI* [Online]. Available at: https://www.mdpi.com/2072-4292/7/2/1736/htm (Accessed: 24 January 2019).

Turner, D., Lucieer, A. and Watson, C. (2012) 'An Automated Technique for Generating Mosaics from Ultra-High Resolution Unmanned Aerial Vehicle (UAV) Imagery, Based on Structure from Motion (SFM) Point Clouds', *Remote Sensing* 4(5) pp. 1392-1410. *MDPI* [Online]. Available at: https://www.mdpi.com/2072-4292/4/5/1392/htm (Accessed: 05 June 2020).

Tziavou, O., Pytharouli, S. and Souter, J. (2018) 'Unmanned Aerial Vehicle (UAV) Based Mapping in Engineering Geological Surveys: Considerations for Optimum Results', *Engineering Geology* 232() pp. 12-21. *ScienceDirect* [Online]. Available at: https://www.sciencedirect.com/science/article/abs/pii/S0013795217308670 (Accessed: 08 September 2019).

Varela, M. R., Patricio, A. R., Anderson, K., Broderick, A. C., DeBell, L., Hawkes, L. A., Tilley, D., Snape, R. T. E., Westoby, M. J. and Godley, B. J. (2019) 'Assessing Climate Change Associated Sea-Level Rise Impacts on Sea Turtle Nesting Beaches Using Drones, Photogrammetry and a Novel GPS System', *Global Change Biology* 25(2) pp. 753-762. *Wiley Library* [Online]. Available at: https://onlinelibrary.wiley.com/doi/abs/10.1111/gcb.14526 (Accessed 16 April 2019).

Westoby, M. J., Dunning, S. A., Woodward, J., Hein, A. S., Marrero, S. M., Winter, K. and Sugden, D. E. (2015) 'Sedimentological Characterization of Antarctic Moraines Using UAVs and Strcture-from-Motion Photogrammetry', *Journal of Glaciology* 61(230) pp. 1088-1102. *IGS* [Online]. Available at: https://www.igsoc.org/ (Accessed: 01 September 2019).

Westoby, M. J., Lim, M., Hogg, M., Pound, M. J., Dunlop, L. and Woodward, J. (2018) 'Cost-Effective Erosion Monitoring of Coastal Cliffs', *Coastal Engineering* 138 pp. 152-164. *ScienceDirect* [Online]. Available at: https://www.sciencedirect.com/science/article/pii/S0378383917303381 (Accessed: 25 August 2018).

Xu, G., Zheng, A., Li, X. and Su, J. (2017) 'Position and Orientation Measurement Adopting Camera Calibration by Projection Geometry of Plucker Matrices of Three-Dimensional Lines', *Scientific Reports* 7(44092) pp. 1-10. *Scientific Report* [Online]. Available at: https://www.nature.com/articles/srep44092 (Accessed: 10 September 2019).

Young, A. P., Guza, R. T., O'Reilly, W. C., Burvingt, O. and Flick, R. E. (2016) 'Observations of Coastal Cliff Base Waves, Sand Levels, and Cliff Top Shaking', *Earth Surface Processes and Landforms* 41 pp. 1564-1573. *Wiley* [Online]. Available at: https://onlinelibrary.wiley.com/doi/full/10.1002/esp.3928 (Accessed: 08 February 2019).

Yu, C., Zhenhong, L. and Penna, N. T. (2018) 'Interferometric Synthetic Aperture Radar Atmospheric Correction Using a GPS-Based Iterative Tropospheric Decomposition Model', *Remote Sensing of Environment*204 pp. 109-121. *Science Direct* [Online]. Available at: https://www.sciencedirect.com/science/article/pii/S0034425717305011 (Accessed: 04 April 2019).

Zhang, Z., Pan, S., Gao, C., Zhao, T. and Gao, W. (2019) 'Support Vector Machine for Regional Ionospheric Delay Modelling', *Sensors* 19(13) pp. 1-14. *MDPI* [Online]. Available at: https://www.mdpi.com/1424-8220/19/13/2947 (Accessed: 03 October 2019).

Zhu, B., Li, J. and Tang, W. (2017) 'Correcting Insar Topographically Correlated Tropospheric Delays Using a Power Law Model Based on ERA-Interim Reanalysis', *Remote Sensing* 9(8) pp. 1-23. *MDPI* [Online]. Available at: https://www.mdpi.com/2072-4292/9/8/765 (Accessed: 04 October 2019).

Appendix D

Assessing the Respective Photogrammetric Bundle Adjustment Algorithms from Unordered Digital Images for Shoreline Monitoring

Mitchell A. Eboigbe, David Kidner, Anthony, A. Sam

Abstract— The bundle adjustment in digital photogrammetry is more than mosaicking images as in the case of the analog and analytical photogrammetry. It is a mathematical process to extract, optimize, and re-project and match points of similar intrinsic/internal parameters between overlapping images in order to create a dense geometric 3D structure of the scene. It is, therefore, a radiometric and geometric reconstruction process of bundles of light rays emanating from the object space unto the image space in order to recover exactly the X, Y and Z coordinates of the image points. Advancements in camera technology and the reduction in camera costs have made it possible to obtain low-cost ultrahigh resolution spatially accurate imagery in a static environment. With the bundle adjustment and aerial triangulation, the digital camera automatically undergoes self-calibration and resection to generate the image from the object. Independent 3D reconstruction mathematical algorithm now performs the bundle block adjustment. The reliability of the respective photogrammetric software depends on the multi-view reconstruction process by the bundle block adjustment. This study, therefore, examines the reliability of the respective bundle block adjustment algorithms in generating the tie points from the digital images and the quality of the dense point cloud for shoreline monitoring. Unlike previous studies, digital images are acquired from uncalibrated cameras on a Phantom 3 standard drone flew at multiple heights and at different sensor's orientations. The authors are desirous to understand the rigidity and evaluative the image stitching pattern of the respective bundle adjustment models for shorelines. Digital images were processed using the Pix4D, Photomodeller and the Agisoft Photoscan. Compares are made on their tie points, used/redundant images, quality of automosaics and vertical accuracies of their digital surface models. Despite the unfavorable photogrammetric conditions, the Pix4D had an average horizontal and vertical accuracies of 4 and 2 cms. Agisoft is 20cm in both the horizontal and vertical while the Photomodeler is 20cm in the horizontal and 45cm in the vertical. The number of uncalibrated images was more with the Photomodeler with two GCPs not visible on the point cloud. The graphical representation of error propagation on both axes indicates the viability of all three software although, in this preliminary investigation, the Pix4D and the Agisoft have produced better spatial and spectral accuracies with indices for accurate/precise outputs in planned photogrammetric flights along the coastline.

Keywords—Bundle Adjustment, Photogrammetric Software, Shoreline Monitoring, Unordered Digital Images

Mitchell A. Eboigbe is a Ph.D. student in the Faculty of Engineering and Computing, University of South Wales, UK. (Corresponding author: e-mail: mitchell.eboigbe@southwales.ac.uk)

Dr. David Kidner is a Reader in the Faculty of Engineering and Computing, University of South Wales, UK

Anthony A. Sam is a Lecturer in the Department of Hydrology, Maritime Academy of Nigeria, Oron.

I. INTRODUCTION

The development of robust photogrammetric software's (Ai et al, 2015; Strecha et al, 2015; Bemis et al, 2014) now provide major improvement in digital photogrammetry (Bemis et al, 2014 and Poser, 2012) and are capable of automatic image collection, reconstruction and processing into orthomosaics, and 3-dimensional models (Shahbazi et al, 2015, Remondino et al, 2011 and Poser, 2012). Improved photogrammetry sensors mounted on close range platforms with onboard GPS/GNSS receivers can generate spatially accurate, flexible and low cost high-resolution digital imageries (Colomina and Molina, 2014; Markelin et al, 2014 and Fraser, 2013). Close range digital photogrammetry is now widely used as a mapping tool for precise scientific purposes (Goncalves et al, 2018; Papakonstantinou et al, 2016; Jaud et al, 2016; Watanabe and Kawahara, 2016; Markelin et al, 2014; Ahmadabadian et al, 2013; Koutsoudis et al, 2013; Shahbazi et al, 2015; Vousdoukas et al, 2011). The rationale behind this study is that if reliable results are obtained from the very poor photogrammetric conditions, it, therefore, implies the software' evaluated are photogrammetrically stable and accurate for precise shoreline monitoring

1.1 THREE DIMENSIONAL (3D) RECONSTRUCTION PROCESS FROM THE AUTOMATIC BUNDLE BLOCK ADJUSTMENT SOLUTIONS

Advanced photogrammetric algorithms are improvements on the basic surveying principles of the pinhole camera and aerial triangulation techniques (Bemis et al, 2014 and Poser, 2012). The principles of the pinhole camera remain the process of reconstruction of bundles of light rays (Hastedt and Luhmann, 2015 and Moons et al, 2008). Orientation and calibration of camera sensors are achieved by bundle adjustment (Colomina and Molina, 2014; Kim et al, 2013; Harwin and Lucieer, 2012). With the bundle adjustment, the digital camera automatically undergoes self-calibration, resection and automatic triangulation to generate the image from the object (Damon, 2016; Pix4D Manual, 2016; Colomina and Molina 2014 and Vallet et al, 2011). The qualities of the images then formed are as a function of the inner and external parameters of the camera (Pix4D Manual, 2016 and Kim et al, 2013). These parameters constitute the mathematical relationship of points in the 3-D coordinates between the object and the image space (Strecha et al, 2015 and Kim et al, 2013). The camera inbuilt model defines its inner parameters (Vallet et al, 2011). Inner parameters are as a function of the lens type, lens distortion, transformation propensities that generates pixel coordinates from the camera frame and the focal length

(Damon, 2016 and Pix4D Manual, 2016). The external parameters determined by the bundle block adjustment from the exact camera location and orientation (PP_x, PP_y, PP_z) to the exposure points (SP_x, SP_ySP_z) with PP and SP as the pixel projection and space projection respectively. For instance, Pix4D has the option to further calibrate the camera external parameters in order to boost image quality (Pix4D Manual, 2016). Precise digital photogrammetric software's, solutions are by the BBA solution (Dominici et al, 2017; Oda et al, 2015; Strecha et al, 2015). Bundle adjustment is "stable" and "scalable" (Dominici et al, 2017 and Strecha et al 2015). The adjustment can be executed with approximate GCPs based on EXIF data and tie points (Oniga et al, 2018; Goncalves and Henriques, 2015; Vallet et al, 2011). It is also able to improve on the internal orientation (IO) parameters and refine the scene geometry (Hastedt and Luhmann, 2015; Di et al, 2014). This makes the respective model very efficient in processing a large number of digital images, unlike the space resection technique that ground control points must first be identifiable on the images (Elnima, 2015).

1.2 REVIEW OF EXISTING LITERATURE

Shorelines are predominantly homogenous surfaces (Sander et al, 2015 and Averbukh et al, 2014). Application of SFM-MVS software to process imageries of featureless surfaces like the shoreline may lead to misalignment in image matching with prevalent noises (Koutsoudis and Arnaoutoglou, 2015; Skarlatos and Kiparissi, 2012). Existing literature in the monitoring of coastlines with UAV photogrammetry has been on a planned flight pattern with pre-determined flying heights (Goncalves et al, 2018; Goncalves and Henriques, 2015). Brunier et al (2016) used a flight plan of 85% forward overlap and 50% side overlap to acquire the required overlapping photographs that would produce high contrast and textured automosaics for beach morphodynamics. Papakonstantinou et al (2016) also acquired high-resolution digital images from a fully autonomous UAV flight mission using the vertical take-off and landing. In Goncalves and Henriques (2015), a single flying height on a pre-determined flight mission was used to map out the study area. In Scarelli et al (2017), acquisition of photos was automatic while other photogrammetric principles were adhered to ensure accurate overlap of images. Photogrammetrically, automatic flight control is essential for radiometrically and geometrically precise orthomosaics (Hermandez-Lopez et al, 2013). It also helps to optimize the flight duration (Chiabrando et al, 2017). Due to the topographical nature of the coastlines, the automatic flight mission from a pre-planned flight plan is required to achieve a higher degree of overlap between images (Chiabrando et al, 2017; Harwin and Lucieer, 2012). It also helps to overcome external coastal environment influences such as wind, humidity, sea spray and other coastal area conditions that could affect UAV performance(Villa et al, 2016). In such instances where UAV were manually flown (cook, 2016), the flying heights and camera orientations were standardized to ensure maximum overlap of images. According to Turner et al (2016), a flight pattern of multiple flying heights and camera orientations are required for complex terrain. The effects of flight planning and camera orientation on the overall accuracies of UAV's products are well discussed in (Chiabrando et al, 2017 and Colomina, and Molina, 2014). None of these existing studies have discussed the accuracies obtained by manual close range photogrammetric surveys especially after coastal flooding or cliff erosion on large scales.

1.3 Aim of Study

The aim of this study is to evaluate the robustness and the analytical functionalities of the respective bundle adjustment computation in processing digital images obtained by close-range photogrammetry as part of the several assessments for an on-going research on coastline monitoring.

2.0 Study Area

The study location is at the Nigeria Maritime Academy (NMA), Oron, AkwaIbom State, Nigeria. It lies on Latitude 04^0 48^1 and Longitude 08^0 14^1. The maritime shoreline stretches approximately 3km and to the east is the Gulf of Guinea. The high tide and the low tide difference are more during the raining season (between April – August) and this could reach 15 meters. Due to fishing and other commercial activities, the high tide is marked by strand lines composed of shells, sachet water waste, plastic waste, seaweed, and other dead organisms. The maritime coastline is a safe navigation channel and the academy has some vessels on the coastline.

Fig. 1. The Study Location

3.0 MATERIALS AND METHODS

3.1 UAV SURVEYING

The UAV survey was on the 21st of July 2017 using the DJI Phantom 3 standard. The area covered is about 300m in length by 100m in breadth along the coastline of the Maritime Academy of Nigeria. The drone was flown manually using the DJI GO app at a varying flying height, not above 100m from the ground. Camera orientation was between 80^0 to 90^0. The camera sensor is 12megapixel and a 3 active bands (RGB) 0.5nm min to 0.5nm max. In all, 333 images were acquired.

3.1.1 GNSS CONTROLS

The Phantom 3 standard has an inbuilt GPS for positioning. The GPS onboard a drone is often not very accurate and could cause further errors in the 3D position, scale, and orientation (Pix4D Mapper 2.0, 2016and Wing, 2011). In order to boost the positional accuracy of our survey (Draeyer and Strecha, 2014), a GNSS survey was carried out and five ground control points established using the Promack 200 dual-frequency in the real-time kinematic mode.

3.2 PHOTOGRAMMETRIC DATA PROCESSING

There are numerous photogrammetric software's available. Examples are the VisualSFM, Photosynth, Pix4D, Python Photogrammetry, Bundler Photogrammetry, and Arc3D and lot more (Granshaw, 2016; Ai et al, 2015; Bemis et al, 2014 and Gini et al, 2013). All photogrammetric algorithms are developed by integrating the general photogrammetric theories of aerial triangulation, camera calibration parameters and bundle block adjustment (Ai et al, 2015; Lee and Rhee, 2013). Most of the open source solutions like the VisualSFM were not able to process all the images as a single solution. Some other online solutions like the DroneDeploy could process the images but without the input of the user. Not all computer vision and photogrammetric algorithms are designed for precise mapping purposes as the bundle adjustment routines and optimization differs from one software to the other (Murtiyoso et al, 2018). The PC used has the following properties: ACPI x64- Based PC on a Windows 10. More than 700GB of free hard disk space with NVIDIA GeForce GT 640. Processor Intel (R) Core (TM) i5 and 16.0GB Ram. The Agisoft PhotoScan, Photomodeler, and the Pix4D were therefore used to process the digital images. Agisoft Photoscan breaks downs all the processing into stages. Generally, the workflow of these software's commences with the initial image stitching and alignment before the building of point cloud and mesh. Texture, orthomosaic and DEM's can then be processed. In all the three software, the uncalibrated cameras were manually calibrated on their ray-cloud. This self-calibrating bundle adjustment boosts the accuracies of the image network (James et al, 2016) by manually editing the positions of the GCPs in all the images they are visible.

3.2.1 AGISOFT PHOTOSCAN

The Agisoft PhotoScan is a low-cost 3D commercial photogrammetric software (Remondino et al, 2012). The bundle block adjustment with the Agisoft PhotoScan is workable for images acquired from a different position (Jebur et al, 2018). A 30-day OpenGL Version: 4.6.0 NVIDIA 388.73trial version was used to process the images. From all the 333 images, 290 were aligned and oriented. PhotoScan is designed to perform multiple calibrations for images obtained from different spectral ranges and orientations (Bernis et al, 2014). The higher accuracy alignment parameters were used to process the images. PhotoScan also allows the placement of markers in order to optimize the camera orientations and positions (James et al, 2016). All the five ground control points were used to reconstruct the mesh, orthomosaics, and DEM.

3.2.2 PIX4D

This software uses a modified Scale Invariant Feature Transform (SIFT)or its equivalent (Tsay and Lee, 2012) that enables it to easily detect and compute the image features very accurately (Qu et al, 2018 and Strecha et al, 2012).Pix4D is a proprietary photogrammetry software, more expensive than the AgisoftPhotoScan. A 15-day Pix4D Mapper trial version 4.2.15 was used to process the images and 278 images were actually calibrated from the 333. The five GCP's improved on the relative accuracy of the model. With the Pix4D, the 3D maps option scale was used to process the images. The 3D map option is designed to produce precise 2D photomap for precise surveying and mapping purposes (Pix4D Support).

3.2.3 PHOTOMODELER UAS

Like the Agisoft PhotoScan and the Pix4D, the Photomodeler UAS is also a commercial software. The license is also cheaper when compared with Pix4D. A 30-day Photomodeler UAS 7 (64) 7.20180.1 version was used to process the images. This software is also developed from the SFM/MVS algorithms (Micheletti et al, 2015). In order to produce sufficient tie-points, Photomodeler encourages photos to be taken at the very close range and lower angles (Photomodeler, 2014). From the 333 images processed, only 197 were aligned and oriented. The five GCP's were imported as a text file and used to re-process the images. Feature detection, matching and marking and orientation are performed automatically. Ground control points are used images relative orientation and for accuracy control during block adjustment (Photomod Version 5.2.1, 2011).

4.0 RESULTS

4.1 TIE POINTS GENERATION

The times it took to create the tie points for all three points were between 45 minutes to an hour. The distribution and amount of the tie points created reduces systematic errors and improves on the overall bundle adjustment performance for quality orthomosaics and accurate DEM's (James et al, 2017 and Juad et al, 2016). The AAT (Rothermel et al, 2012) minimizes errors from misalignment and transformation between multiple images with the bundle adjustment an important phase in solving the Automatic Aerial Triangulation AAT problem (Gneeniss et al, 2015).

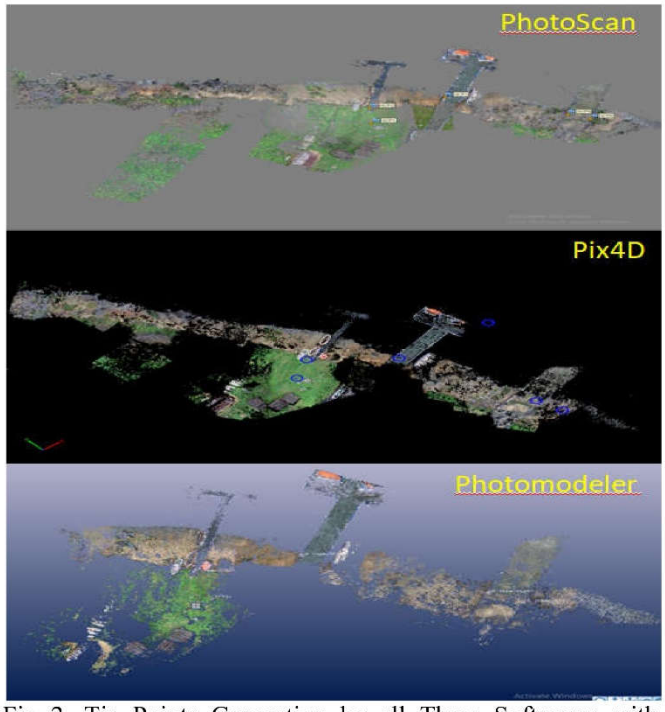

Fig 2. Tie Points Generation by all Three Softwares with GCP's

4.2 ORTHOMOSAICS

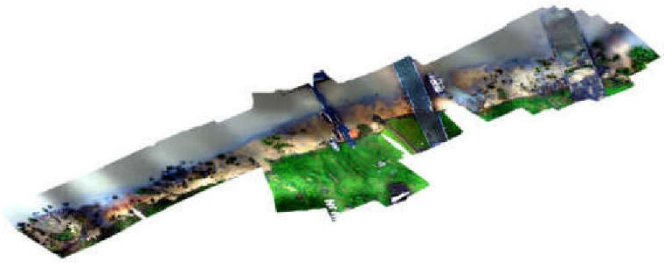

Fig. 3 Agisoft PhotoScan

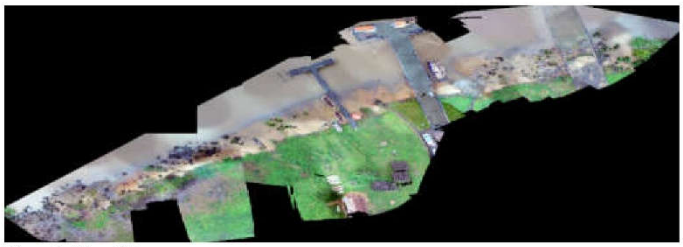

Fig. 4 Pix4D

Fig. 5. Photomodeler

TAB. 1 COORDINATE OF OBSERVED GCP'S

	X (m)	Y (m)
GCP 1	418127.6628	530929.7763
GCP2	418138.2505	530936.9992
GCP3	418164.5649	530916.1550
GCP4	418183.8616	530861.7524
GCP5	418186.8227	530850.7101

TAB. 2 COORDINATES OF GCP'S ON ORTHOMOSAIC

	AgisoftPhotoScan		Pix4D		Photomodeler	
GCP1	418127.582	530929.798	418127.677	530929.755	N/A	N/A
GCP2	418138.287	530937.012	418138.275	530936.982	418138.392	530937.087
GCP3	418164.530	530916.067	418164.566	530916.187	418164.439	530916.634
GCP4	418184.590	530862.650	418183.951	530861.697	418183.254	530861.820
GCP5	418186.950	530851.364	418186.733	530850.757	N/A	N/A

TAB. 3 DIFFERENCES BETWEEN GNSS AND COORDINATES OF GCP'S ON ORTHOMOSAIC

	AgisoftPhotoScan		Pix4D		Photomodeler	
GCP1	0.081	-0.0217	-0.014	0.0213	N/A	N/A
GCP2	-0.0365	-0.0128	-0.0245	0.0172	-0.1415	-0.0878
GCP3	0.0349	0.088	-0.0011	-0.032	0.1259	-0.479
GCP4	-0.7284	-0.8976	-0.0894	0.0554	0.6076	-0.0676
GCP5	-0.1273	-0.6539	0.0897	-0.0469	N/A	N/A

4.3 DIGITAL SURFACE MODEL AND HILLSHADE

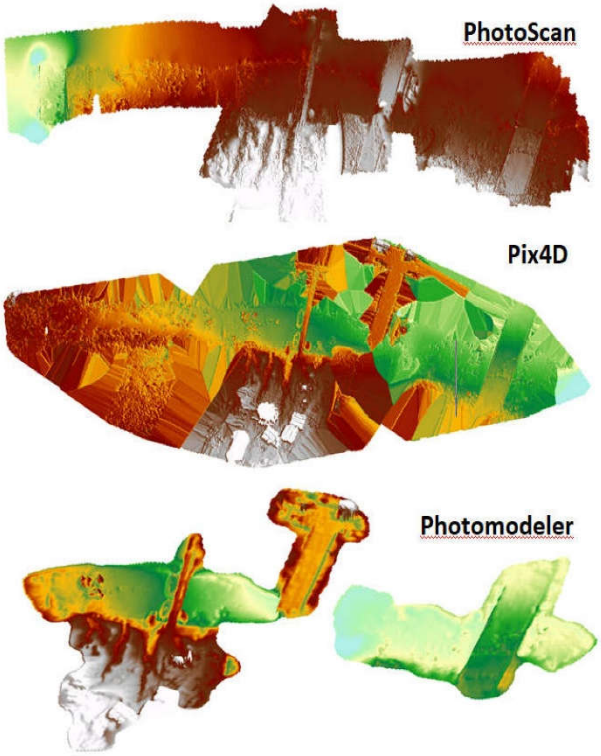

Fig. 6 Digital Surface Models

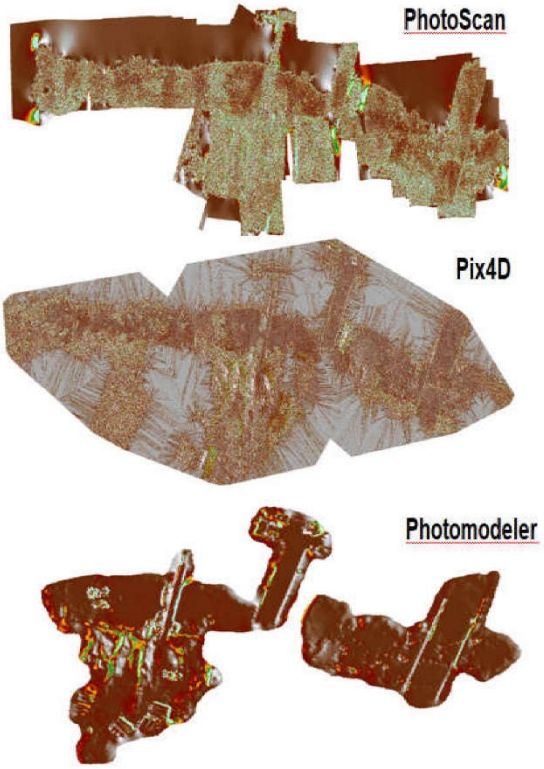

Fig.7. Hillshade

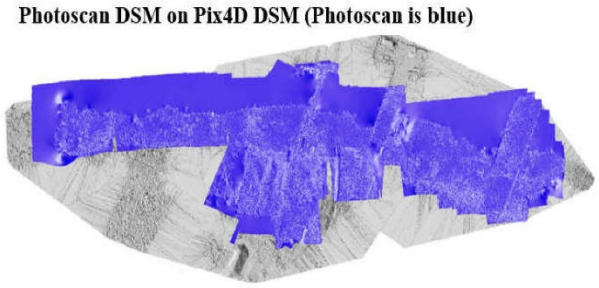

Fig. 9. DSM Overlap

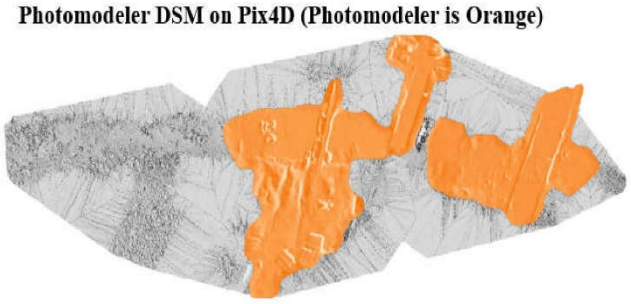

Fig. 10. DSM Overlap

4.4 VERTICAL ACCURACIES OF DSM

TABLE 4. GNSS MINUS INDIVIDUAL SOFTWARE

GNSS POINTS	PIX4D	AGISO. PHOTO	PHOTO. MDL	GNSS - PIX4D	GNSS - AGIS	GNSS - PHOT
GCP1= 24.5845	24.5756	24.6525	24.4201	0.0089	-0.068	0.1644
GCP2= 22.8505	23.2630	23.0198	23.2651	-0.4125	-0.1693	-0.4146
GCP3= 22.8075	22.7919	22.7296	22.5105	0.0156	0.0779	0.297
GCP4= 21.9665	21.9575	21.3537	21.2343	0.009	0.6128	0.7322
GCP5= 22.0805	22.0995	22.1994	21.4163	-0.019	-0.1189	0.6642

DISCUSSION

According to Ostrowski and Bakula (2016), both Pix4D and Agisoft have the capability to process nadir and oblique images simultaneously with correct image matching. The radiometric and geometric properties are reconstructed as X, Y and Z coordinates on the exact locations to become an image of the object (Massad and Omer, 2014; Neale et al, 2011). This high-level matching of points from coordinates by the predetermined matrices as algorithms differ among software. Although the general principle is by the AAT (Forlani et al, 2018; Chesley et al, 2017), the accuracies from the several photogrammetry software would always differ in both the planimetric and on the vertical (Unger et al, 2014). Unlike the analog and analytical photogrammetry, the different digital photogrammetric software's are developed specifically for some photogrammetric functions (Grussenmeyer and Al Khalil, 2008) with different accuracies and outputs (Murtiyoso et al, 2018; Smith et al, 2016; Micheletti et al, 2015; Unger et al, 2014).

In photogrammetry, the BBA is a mathematical process to extract, optimize, and re-project and match points of similar intrinsic/internal parameters between overlapping images in order to create a dense geometric 3D structure of the scene (Murtiyoso et al, 2018; Qu et al, 2018; Molg and Bolch, 2017; Wang et al, 2017; Juad et al, 2016; Triggs et al, 2000). This 3D transformation aligns and improves the geometric accuracies between tie points and control points of adjourning digital images (Murtiyoso et al, 2018). Bundle adjustment is a phase in solving the Automatic Aerial Triangulation AAT problem (Gneeniss et al, 2015). The AAT (Rothermel et al, 2012) minimizes errors from misalignment and transformation between multiple images. Poor image quality, multiple flight missions and poor overlap between successive images are causes of weak bundle adjustment (Micheletti et al, 2015). When these factors are prevalent and the outputs are geometrically and radiometrically correct, it shows the software is developed from the basic photogrammetry principles and stable for precise photogrammetry.

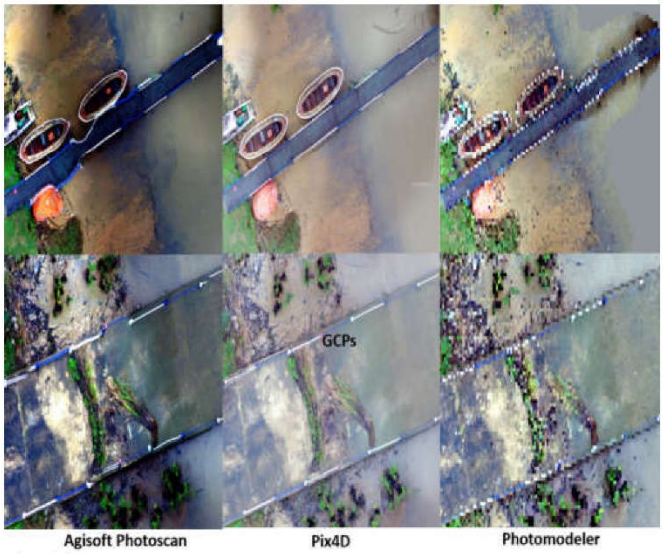

Fig. 11

A careful look_at the piers and canons explain how the tie-points on each image has been matched on each software. It also explains how effective the re-projection of the camera positions using the GCPs have been able to improve on the individual bundle adjustment. Many factors could affect the performance of the BBA. These include the quality of the overlap, reliable and well spread GCP's, the spectral resolution of the digital images, atmospheric conditions and images from different heights and orientations (Aguilar et al, 2013). To avoid bias in this comparison, the post-bundle adjustment editing was not carried out by editing or removing points (Murtiyoso et al, 2018). In the Pix4D, points have been well matched and stitched except for some small tails, which could lead to erroneous approximations especially at the outliers. This is synonymous with most non-linear least

squares gaussian problems and most photogrammetric software would prefer the Hierarchical SFM (Zhao et al, 2018). Results fromPhotomodeler is similar to the Pix4D. Images are well matched and stitched except that the orthomosaics have been segmented as the Photomodeler discarded the highest number of images. There are few mismatches in the Photoscan. A graphical representation of the horizontal and vertical accuracies of the GCPs is shown below:

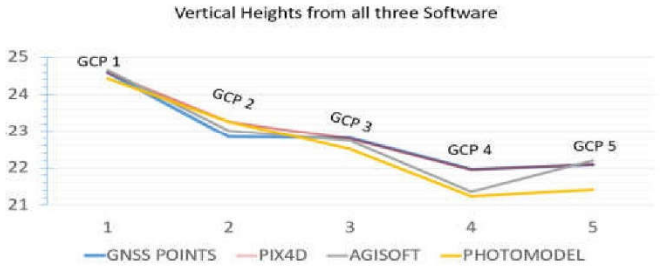

Fig. 12 Graph Showing Vertical Heights

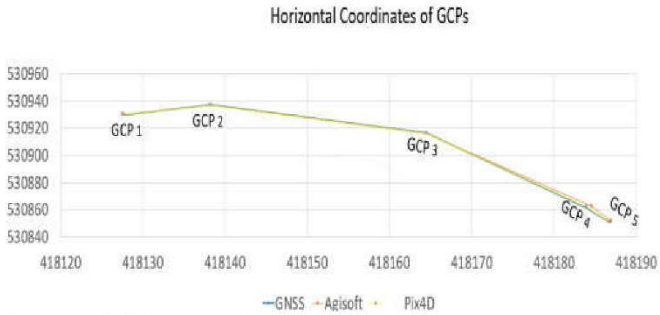

Fig 13 Graph Showing all Horizontal Coordinates

Due to the disjoint in the Photomodeler, the planimetric coordinates could not be plotted. The differences of the X, Y and Z coordinates compared with the GNSS points are in table 2, 3 and 4. From unordered digital images, the performances with all three bundle adjustments are satisfactory with potentials of improved geometric accuracies on planned photogrammetric flights.

The Agisoft Photoscanhave produced the best radiometric quality with even the wave pattern of the sea is visible. This deep reflective surface depicts more of the green vegetation, the bare earth from the sea and other features along the shoreline. A wider RGB color space with improved adjacency effects (Yeom et al, 2017; Karaimer and Brown, 2018) is advantageous in coastal zone management (Kratzer et al, 2014). On fig.11 all images are on the scale 1:100. On this scale, the Photomodeler orthomosaic is blurred. For instance, Unger et al (2014) report that the computational output with the Pix4D bundle adjustment is more robust than the Agisoft Photoscan while the latter would produce a better dense matching and texture creation. This is almost the case as with the results from this study. The tie points generated with the Pix4D is more detailed with higher geometric accuracies. On the other hand, the Agisoft Photoscan has a higher visual quality.

CONCLUSION

This preliminary investigation is to ascertain the ruggedness and functionalities of the respective bundle adjustment algorithms for close range photogrammetry in the monitoring of the coastline. An assessment of the performances of these algorithms is necessary especially for the rapid collection of field data immediately before and after the storm, by means, of close-range photogrammetry. The outcome suggests more reliability with the Pix4D and the Agisoft Photoscan. According to Murtiyoso et al (2018), improvements can be made in the computation process of the Agisoft Photoscan. As with this research, the processing time for both the Pix4D and Agisoft are almost the same (Alidoost and Arefi, 2017). The Photomodeler might not be too powerful for a homogenous surface such as the sea surface. It is also seen that the number of digital images and the quality of the images, boost the performance of the bundle adjustment process (Qu et al, 2018). All three software have had correct scaling and coordination. This survey will be repeated with more GCP's and using an automated flight mission. Compares will be on their respective MVS/SFM outputs. Flight planning and camera orientation have effects on the overall accuracies of UAV's products (Chiabrando et al, 2017). Results thereafter obtained will be compared with that of this initial investigation. On the other hand, the digital camera's internal geometry is always influenced by environmental or other systematic errors on the autopilot's aircraft position, velocity, and altitude 'tPVA' (Colomina and Molina, 2014; Blazquez and Colomina, 2012). It is imperative, also, to evaluate periodically the core metric values of non-digital cameras for stabilities and consistencies in the self-calibration leading to improved parameters (Benassi et al, 2017 and Balletti et al, 2014).

APPRECIATION

Appreciation to Dr. David Kidner for encouraging this project and special thanks to the management of the Maritime Academy of Nigeria, Oron, for allowing us to carry out this survey on their maritime base.

REFERENCES

Aguilar, M. A., Aguilar, F. J., Fernandez, I. and Mills, J. P. (2013) 'Accuracy Assessment of Commercial Self-Calibrating Bundle Adjustment Routines Applied to Archival Aerial Photography', *The Photogrammetric Record* 28(141) pp. 96-114. *Wiley* [Online]. Available at: https://onlinelibrary.wiley.com/doi/abs/10.1111/j.1477-9730.2012.00704.x (Accessed: 04 June 2018).

Ahmadabadian, A. H., Robson, S., Boehm, J., Shortis, M., Wenzel, K. and Fritsch, D. (2013) 'A Comparison of Dense Matching Algorithms for Scaled Surface Reconstruction Using Stereo Camera Rigs', *ISPRS Journal of Photogrammetry and Remote Sensing* 78 pp. 157-167. *ScienceDirect* [Online]. Available at: https://www.sciencedirect.com/science/article/pii/S0924271613000452 (Accessed: 13 October 2016).

Ai, M., Hu, Q., Li, J., Wang, M., Yuan, H. and Wang, S. (2015) 'A Robust Photogrammetric Processing Method of Low-Altitude UAV Images', *Remote Sensing*,7(3) pp. 2302-2333 *MDPI* [Online]. Available at: http://www.mdpi.com/2072-4292/7/3/2302/htm (Accessed: 29 June 2016).

Alidoost, F. and Arefi, H. (2017) 'Comparison of UAS-Based Photogrammetry Software for 3D Point Cloud Generation: A Survey over a Historic Site', *4th International GeoAdvances Workshop*, Safranbolu, Karabuk, Turkey 14-15 October. ISPRS Annals of the Photogrammetry, Remote Sensing and Spatial Information Sciences, Volume IV-4/W4, 2017 [Online]. Available at: https://www.isprs-ann-photogramm-remote-sens-spatial-inf-sci.net/IV-4-W4/55/2017/isprs-annals-IV-4-W4-55-2017.pdf (Accessed: 09 July 2018).

Balletti, C., Guerra, F., Tsioukas, V. and Vernier, P. (2014) 'Calibration of Action Cameras for Photogrammetric Purposes', *Sensors* 14(9) pp. 17471-17490. *MDPI* [Online]. Available at: https://www.mdpi.com/1424-8220/14/9/17471/htm (Accessed: 20 September 2018).

Benassi, F., Dall'Asta, E., Diotri, F., Forlani, G., Morra Di Cella, U., Roncella, R. and Santise, M. (2017) 'Testing Accuracy and Repeatability of UAV Blocks Oriented with GNSS-Supported Aerial Triangulation', *Remote sens* 9(2) pp. 1-23. *MDPI* [Online]. Available at: https://www.mdpi.com/2072-4292/9/2/172 (Accessed: 30 March 2018).

Bemis, S. P., Micklethwaite, S., Turner, D., James, M. R., Akciz, S., Thiele, S. T. and Bangash, H. A. (2014) 'Ground-Based and UAV-Based Photogrammetry: A Multi-Scale, High-Resolution Mapping Tool for Structural Geology and Paleoseismology', *Journal of Structural Geology* 69 (A) pp. 163-178. *ScienceDirect* [Online]. Available at: https://www.sciencedirect.com/science/article/pii/S0191814114002429 (Accessed: 16 June 2016).

Structure-from-Motion Photogrammetry for High-Resolution Beach Morphometric Surveys: Examples from an Embayed Rotating Beach', *Geomorphology* 261 pp. 76-88. *ScienceDirect* [Online]. Available at: https://www.sciencedirect.com/science/article/pii/S0169555X16300617# (Accessed: 18 December 2017).

Blazquez, M. and Colomina, I. (2012) 'On INS/GNSS-Based Time Synchronization in Photogrammetric and Remote Sensing Multi-SensorSystems', *PFG* 2012(2) pp. 91-104. *Ingentaconnect* [Online]. Available at: https://www.ingentaconnect.com/content/schweiz/pfg/2012/00002012/00000002/art00002 (Accessed: 20 July 2017).

Chesley, J. T., Leier, A. L., White, S. and Torres, R. (2017) 'Using Unmanned Aerial Vehicles and Structure-from-Motion Photogrammetry to Characterize Sedimentary Outcrops: An Example from the Morrison Formation, Utah, USA', *Sedimentary Geology* 354 pp. 1-7. *ScienceDirect* [Online]. Available at: https://www.sciencedirect.com/science/article/pii/S0037073817300817 (Accessed: 21 September 2018).

Chiabrando, F., Lingua, A., Maschio, P. and Lose, L. T. (2017) 'The Influence of Flight Planning and Camera Orientation in UAVs Photogrammetry. A Test in the Area of Rocca San Silvestro (LI), Tuscany', *3D Virtual Reconstruction and Visualization of Complex Architectures*, Nafplio, Greece, 1-3 March. The International Archives of the Photogrammetry, Remote Sensing and Spatial Information Sciences, Volume XLII-2/W3, [Online]. Available at: https://www.int-arch-photogramm-remote-sens-spatial-inf-sci.net/XLII-2-W3/163/2017/isprs-archives-XLII-2-W3-163-2017.pdf(Accessed: 10 August 2018).

Colomina, I. and Molina, P. (2014) 'Unmanned Aerial Systems for Photogrammetry and Remote Sensing: A Review', *ISPRS Journal of Photogrammetry and Remote Sensing* 92 pp. 79-97. *ScienceDirect* [Online]. Available at: https://www.sciencedirect.com/science/article/pii/S0924271614000501 (Accessed: 25 May 2016).

Cook, K. L. (2016) 'An Evaluation of the Effectiveness of Low-Cost UAVs and Structure from Motion for Geomorphic Change Detection', *Geomorphology* 278 pp.195-208. *ScienceDirect* [Online]. Available at: https://www.sciencedirect.com/science/article/pii/S0169555X16310686 (Accessed: 09 August 2018).

Damon, C. (2016) 'Small Unmanned Aircraft (SUA) Pilot Project. The USAID/Ghana Sustainable Fisheries Management Project (SFMP)', *Narragansett, RI: Coastal Resources Center, Graduate School of Oceanography, University of Rhode Island and Environmental Data Center. GH2014_SCI019_EDC. 29* pp. 1-29. [Online]. Available at: http://www.crc.uri.edu/download/GH2014_SCI019_EDC_FIN508.pdf (Accessed: 25 July 2016).

Di, K., Liu, Y., Liu, B., Peng, M. and Hu, W. (2014) 'A Self-Calibration Bundle Adjustment Method for Photogrammetric Processing of ChangE-2 Stereo Lunar Imagery', *IEEE Transactions on Geoscience and Remote Sensing* 52(9) pp. 5432-5442. *IEEEExplore*[Online]. Available at: https://ieeexplore.ieee.org/document/6681937/ (Accessed: 22 September 2018).

Draeyer, B. and Strecha, C. (2014) 'Pix4D White Paper: How Accurate are UAV Surveying Methods?', *Pix4D* [Online]. Available at: https://pix4d.com/wp-content/uploads/2016/11/Pix4D-White-paper_How-accurate-are-UAV-surveying-methods.pdf (Accessed: 06 July 2018).

Dominici, D. Alicandro, M. and Massimi, V. (2016) 'UAV Photogrammetry in the Post-Earthquake Scenario: Case Studies in L'Aquila', *Geomatics,Natural Hazards and Risk* 8(1) pp. 87-103. *Taylor and Francis* [Online]. Available at: https://www.tandfonline.com/toc/tgnh20/current (Accessed: 01 March 2018).

Elnima, E. E. (2015) 'A Solution for Exterior and Relative Orientation in Photogrammetry, a Genetic Evolution Approach', *Journal of King Saud University – Engineering Sciences* 27 pp. 108-113. *ScienceDirect* [Online]. Available at: https://www.sciencedirect.com/science/article/pii/S1018363913000196 (Accessed: 10 April 2018).

Forlani, G., Dall'Asta, E., Diotri, F., Morra di Cella, U., Roncella, R. and Santise, M. 'Quality Assessment of DSMs Produced from UAV Flights Georeferenced with On-Board RTK Positioning', *Remote Sensing* 10(2) pp. 1-22. *MDPI* [Online]. Available at: https://www.mdpi.com/2072-4292/10/2/311 (Accessed: 21 September 2018).

Fraser, C., S. (2013) 'Automatic Camera Calibration in Close Range Photogrammetry', *Photogrammetric Engineering and Remote Sensing* 79(4) pp. 381-388.*Ingentaconnect* [Online]. Available at: https://www.ingentaconnect.com/contentone/asprs/pers/2013/00000079/00000004/art00005?crawler=true (Accessed: 31 August 2017).

Gini, R., Pagliari, D., Passoni, D., Pinto, L., Sona, G. and Dosso, P. (2013) 'UAV Photogrammetry: Block Triangulation Comparisons', *UAV-g2013*, Rostock, Germany, 4-6 September. International Archives of the Photogrammetry, Remote Sensing and Spatial Information Sciences, Volume XL-1/W2 [Online]. Available at: https://pdfs.semanticscholar.org/89a5/0c4d6cd775c98dd3893053ad97bb5343a3fd.pdf (Accessed: 01 July 2013).

Gneeniss, A. S., Mills, J. P. and Miller, P. E. (2015) 'In-Flight Photogrammetric Camera Calibration and Validation Via Complementary Lidar', *ISPRS Journal of Photogrammetry and Remote Sensing* 100 pp. 3-13. *ScienceDirect* [Online]. Available at: https://www.sciencedirect.com/science/article/pii/S0924271614001142?via%3Dihub (Accessed: 02 March 2018).

Goncalves, J. A. and Henriques, R. (2015) 'UAV Photogrammetry for Monitoring of Coastal Areas', *ISPRS Journal of Photogrammetry and Remote Sensing* 104, pp. 101-111. *Science Direct* [Online]. Available at: http://www.sciencedirect.com/science/journal/09242716/104 (Accessed: 11 November 2016).

Goncalves, G., Duro, N., Sousa, E. and Figueiredo, I. (2015) 'Automatic Extraction of Tide-Coordinated Shoreline Using Open Source Software and Landsat Imagery', *36th International Symposium on Remote Sensing of Environment*, Berlin, Germany, 11-15 May. The International Archives of the Photogrammetry, Remote Sensing and Spatial Information Sciences, VolumeXL-7/W3 [Online]. Available at: https://www.int-arch-photogramm-remote-sens-spatial-inf-sci.net/XL-7-W3/953/2015/isprsarchives-XL-7-W3-953-2015.pdf (Accessed: 16 October 2017).

Granshaw, S. I. (2016) 'Photogrammetric Terminology: Third Edition', *The Photogrammetric Record* 31(154) pp. 210-251. *Wiley* [Online]. Available at: https://onlinelibrary.wiley.com/journal/14779730 (Accessed: 04 July 2016).

Grussenmeyer, P. and Al Khalil, O. (2008) 'A Comparison of Photogrammetry Software Packages for the Documentation of Buildings', *Halshs*-00281254, Version 1 pp. 1-9. *Halshs* [Online]. Available at: https://halshs.archives-ouvertes.fr/halshs-00281254 (Accessed: 21 September 2018).

Harwin, S. and Lucieer, A. (2012) 'Assessing the Accuracy of Georeferenced Point Clouds Produced Via Multi-View Stereopsis from Unmanned Aerial Vehicle (UAV) Imagery', *Remote Sensing* 4(6) pp. 1573-1599. *MDPI* [Online]. Available at: http://www.mdpi.com/2072-4292/4/6/1573 (Accessed: 19 October 2016).

Hastedt, H. and Luhmann, T. (2015) 'Investigations on the Quality of the Interior Orientation and its Impact in Object Space for UAV Photogrammetry', *International Conference on Unmanned Aerial Vehicles in Geomatics,* 30 August-02 September, Toronto, Canada. *International Archives on the Photogrammetry, Remote Sensing and Spatial Information Sciences*, XL-1/W4. [Online]. Available at: http://www.int-arch-photogramm-remote-sens-spatial-inf-sci.net/XL-1-W4/321/2015/isprsarchives-XL-1-W4-321-2015.pdf (Accessed: 16 June 2016)

Hernandez-Lopez, D., Felipe-Garcia, B., Gonzalez-Aguilera, D. and Arias-Perez, B. (2013) 'An Automatic Approach to UAV Flight Planning and Control for Photogrammetric Applications: A test Case in the Asturias Region (Spain)', *Photogrammetry Engineering and Remote Sensing* 79(1) pp. 87-98. *Ingentaconnect*[Online]. Available at: https://www.ingentaconnect.com/content/asprs/pers/2013/00000079/00000001/art00006?crawler=true&mimetype=application/pdf (Accessed: 06 August 2018).

James, M. R., Robson, S., Oleire-Oltmanns, S. D. and Niethammer, U. (2017) 'Optimizing UAV Topographical Surveys Processed with Structure-from-Motion: Ground Control Quality, Quantity and Bundle Adjustment', *Geomorphology* 280 pp. 51-66. *ScienceDirect* [Online]. Available at: https://www.sciencedirect.com/science/article/pii/S0169555X16311291?via%3Dihub (08 September 2018).

Jebur, A., Abed, F. and Mohammed, M. (2018) 'Assessing the Performance of Commercial AgisoftPhotoScan Software to Deliver Reliable Data for Accurate 3D Modelling', *MATEC Web of Conferences* 162 pp. 1-11. The 3rd*International Conference on Buildings, Construction and Environmental Engineering, BCEE3* [Online]. Available at: https://www.matec-conferences.org/articles/matecconf/abs/2018/21/matecconf_bcee32018_03022/matecconf_bcee32018_03022.html (Accessed 09 July 2018).

Juad, M., Passot, S., Bivic, R. L., Delacourt, C., Grandjean, P. and Dantec, N. L. (2016) 'Assessing the Accuracy of High-Resolution Digital Surface Models Computed by PhotoSCan and MicMac in Sub-Optimal Survey Conditions', *Remote Sensing* 8(6), 465; pp. 2-18. *MDPI* [Online]. Available at: http://www.mdpi.com/2072-4292/8/6/465 (Accessed: 26 May 2018).

Karaimer, H. C. and Brown, M. S. (2018) 'Improving Color Reproduction Accuracy on Cameras', *IEEE Conference on Computer Vision and Pattern Recognition (CVPR)* Salt Lake City, Utah, United States, 18-22 June. Computer Vision Foundation pp. 6440-6449 [Online]. Available at: http://openaccess.thecvf.com/content_cvpr_2018/html/Karaimer_Improving_Color_Reproduction_CVPR_2018_paper.html (Accessed: 10 September 2018).

Kim, J., Lee, S., Ahn, H., Seo, D., Seo D., Lee, J. and Choi, C. (2013) 'Accuracy Evaluation of a Smartphone-Based Technology for Coastal Monitoring', *Measurement* 46, pp. 233-248 *ScienceDirect* [Online]. Available at: https://www.sciencedirect.com/science/article/pii/S0263224112002515(Accessed: 25 July 2016).

Koutsoudis, A., Vidmar, B., Loannakis, G., Arnaoutoglou, F., Pavlidis, G. and Chamzas, C. (2013) 'Multi-Image 3D Reconstruction Data Evaluation', *Journal of Cultural Heritage* 15(1) pp. 73-79. *ScienceDirect* [Online]. Available at: https://www.sciencedirect.com/science/article/pii/S1296207412001926 (Accessed: 23 August 2016).

Kratzer, S., Harvey, E. T. and Philipson, P. 'The Use of Ocean Color Remote Sensing in Integrated Coastal Zone Management-A case study from Himmerfjarden, Sweden', *Marine Policy* 43 pp. 29-39. *ScienceDirect* [Online]. Available at: https://www.sciencedirect.com/science/article/pii/S0308597X13001036 (Accessed: 22 September 2018).

Lee, I. Wu, B. and Li, R. (2009) 'Shoreline Extraction from the Integration of LiDAR Point Cloud Data and Aerial Orthophotos Using Mean Shift Segmentation', *ASPRS Annual Conference*, 9- 13 March, Baltimore, Maryland. [Online]. Available at: https://pdfs.semanticscholar.org/c439/2edc255b392c650e2ef1e5034a574428bd54.pdf (Accessed: 05 March 2016).

Lee, H. and Rhee, H. (2013) '3-D Measurement of Structural Vibration Using Digital Close-Range Photogrammetry', *Sensors and Actuators A: Physical*196 pp. 63-69. *Science Direct* [Online]. Available at: http://www.sciencedirect.com/science/article/pii/S0924424713001258 (Accessed: 29 June 2016).

Markelin, L., Honkavaara, E., Nasi, R., Nurminen, K. and Hakala, T. (2014) 'Geometric Processing Workflow for Vertical and Oblique Hyperspectral Frame Images Collected Using UAV', *ISPRS Technical Commission III Symposium, 5 – 7 September, Zurich, Switzerland. The* International Archives of the Photogrammetry, Remote Sensing and Spatial Information Sciences, Vol *XL-3* [Online]. Available at: https://www.int-arch-photogramm-remote-sens-spatial-inf-sci.net/XL-3/205/2014/isprsarchives-XL-3-205-2014.pdf (Accessed: 13 October 2016).

Masaad, E. M. and Omer, A. H. (2014) 'Use of Scanned Aerial Images in Photogrammetric Resection and Intersection', *University of Khartoum Engineering Journal* 4(1), *pp. 38-46. UofKEJ* [Online]. *Available at: http://onlinejournals.uofk.edu/index.php/kuej/article/view/1288/1307*(Accessed: 11 June 2016).

Micheletti, N., Chandler, J. H. and Lane, S., N. (2015) 'Structure from Motion (SFM) Photogrammetry', *Geomorphological Techniques* 2(2.2) pp. 1-12. *British Society of Geomorphology* [Online]. Available at: http://geomorphology.org.uk/sites/default/files/geom_tech_chapters/2.2.2_sfm.pdf (Accessed: 11 September 2017).

Molg, N., and Bolch, T. (2017) 'Structure-from-Motion Using Historical Aerial Images to Analyse Changes in Glacier Surface Elevation', *Remote Sensing* 9(10) pp. 1-17. *MDPI* [Online]. Available at: https://www.mdpi.com/2072-4292/9/10/1021 (Accessed: 10 August 2018).

Moons, T., Gool, L. V. andVergauwen, M. (2008) '3D Reconstruction from Multiple Images Part 1: Principles', *Computer Graphics and Vision* 4(4) pp. 287-398. *SemanticsScholar*[Online]. Available at: https://pdfs.semanticscholar.org/0448/c3a1af352fc1f3819a410c43216f20d47cfa.pdf (Accessed: 17 August 2018).

Murtiyoso, A., Grussenmeyer, P., Borlin, N., Vandermeerschen, J. and Freville, T. (2018) 'Open Source and Independent Methods for Bundle Adjustment Assessment in Close-Range UAV Photogrammetry', *Drones* 2(1) pp. 2-18. *MDPI* [Online]. Available at: https://www.mdpi.com/2504-446X/2/1/3 (Accessed: 20 September 2018).

Neale, W. T., Hessel, D. and Terpstra, T. (2011) 'Photogrammetric Measurement Error Associated with LensDistortion', *SAE World Congress, Automotive,SAE Technical Paper 2011-01-0268*Detriot 12-14 April.SAE [Online]. Available at: https://saemobilus.sae.org/content/2011-01-0286 (Accessed: 01 June 2016).

Oda, K., Hattori, S., Saeki, H., Takayama, T. and Honma, R. (2015) 'Qualification of Point Clouds Measured by SFM Software', *Indoor-Outdoor Seamless Modelling, Mapping and Navigation, Tokyo*, Japan, 21-22 May. The International Archives of the Photogrammetry, Remote Sensing and Spatial Information Sciences, Volume XL-4/W5 [Online]. Available at: https://www.int-arch-photogramm-remote-sens-spatial-inf-sci.net/XL-4-W5/125/2015/isprsarchives-XL-4-W5-125-2015.pdf (Accessed: 10 November 2017).

Ostrowski, W. andBakula, K. (2016) 'Towards Efficiency of Oblique Images Orientations', *The European Calibration and Orientation Workshop*, Lausanne, Switzerland, 10-12 February. The International Archives of the Photogrammetry, Remote Sensing and Spatial Information Sciences, Volume XL-3/W4 [Online]. Available at: https://www.int-arch-photogramm-remote-sens-spatial-inf-sci.net/XL-3-W4/91/2016/isprs-archives-XL-3-W4-91-2016.pdf (Accessed: 07 September 2018).

Papakonstantinuo, A., Topouzelis, K. andPavlogeorgatos, G. (2016) 'Coastline Zones Identification and 3D Coastal Mapping Using UAV Spatial Data', *ISPRS Int. Journal of Geo-Information* 5(6),75; pp. 1-14. *MDPI* [Online]. Available at: http://www.mdpi.com/2220-9964/5/6/75 (Accessed: 30 March 2018).

Pix4D Mapper 2.0 (2016) [Online]. Available at: https://s3.amazonaws.com/mics.pix4d.com/manual_pdf/manual_2_0_January 2016.pdf (Accessed: 01 November 2016).

Poser, J. (2012) 'Comparative Imagery Analysis of Non-Metric Cameras from Unmanned Aerial Survey Aircraft', *Resource Analysis* 14 pp. 1-20. *Saint Mary's University of Minnesota Central Services Press. Winona, MN.* [Online]. Available at: http://citeseerx.ist.psu.edu/viewdoc/download?doi=10.1.1.392.4394&rep=rep1&type=pdf (Accessed: 28 June 2016).

Qu, Y., Huang, J. and Zhang, X. (2018) 'Rapid 3D Reconstruction for Image Sequence Acquired from UAV Camera', *Sensors* 18(1):225 pp. 2-20. *NCBI* [Online]. Available at: https://www.ncbi.nlm.nih.gov/pmc/articles/PMC5795716/ (Accessed: 11 May 2018).

Remondino, F., Barazzetti, L., Nex, F., Scaioni, M. and Sarazzi, D. (2011) 'UAV Photogrammetry for Mapping and 3D Modeling-Current Status and Future Perspectives', *Conference on Unmanned Aerial Vehicle in Geomatics,* Zurich, Switzerland.International Archives of the Photogrammetry, Remote Sensing and Spatial Information Sciences, Vol. XXXVIII-1/C22 UAV-g [Online]. Available at: https://is.muni.cz/el/1431/podzim2012/Z8114/um/35399132/35460312/uav_mapping_and_3D_modeling.pdf (Accessed 13 October 2016).

Remondino, F., Pizzo, S. D., Kersten, T. and Troisi, S. (2012) 'Low-Cost and Open-Source Solutions for automated Image Orientation – A critical Ovierview', *4th InternationalEuro-Mediterranean Conference* Limassol, Cyprus, October 29 – November 3. Progress in Cultural Heritage Preservation LNCS, 7616 pp. 40-54, Springer, Berlin, Heidelberg.[Online]. Available at: https://link.springer.com/book/10.1007/978-3-642-34234-9 (Accessed: 02 March 2018).

Rothermel, M., Wenzel, K., Fritsch, D. and Haala, N. (2012) 'Photogrammetric Surface Reconstruction from Imagery', *Proceedings LC3D Workshop, Berlin, 4-5 December, 1-9,* [Online]. Available at: http://www.ifp.uni-stuttgart.de/publications/2012/Rothermel_etal_lc3d.pdf (Accessed: 28 April 2018).

Scarelli, F. M., Sistilli, F., Fabbri, S., Cantelli, L., Barboza, E. G. and Gabbianelli, G. (2017) 'Seasonal Dune and Beach Monitoring Using Photogrammetry from UAV Surveys to Apply in the ICZM on the Ravenna Coast', *Remote Sensing Applications: Society and Environment* 7 pp. 27-39. *ScienceDirect* [Online]. Available at: https://www.sciencedirect.com/science/article/pii/S2352938517300666 (Accessed: 10 August 2018).

Shahbazi, M., Sohn, G., Theau, J. and Menard, P. (2015) 'Development and Evaluation of a UAV-Photogrammetry System for Precise 3D Environmental Modelling', *Sensors* 15(11). pp. 27493-27524. *MDPI* [Online]. Available at:http://www.mdpi.com/1424-8220/15/11/27493/htm(Accessed: 15 December 2016).

Strecha, C., Zoller, R., Rutishauser, S., Brot, B., Schneider-Zapp, K., Chovancova, V., Krull, M. and Glassey, L. (2015) 'Terrestrial 3d Mapping Using Fisheye and Perspective Sensors', *Pix4D Scientific White Papers*[Online].Available at: https://support.pix4d.com/hc/en-us/sections/200591029-Scientific-White-Papers#gsc.tab=0 (Accessed: 15 November 2016).

Skarlatos, D. and Kiparissi, S. (2012) 'Comparison of Laser Scanning, Photogrammetry and SFM-MVS Pipeline Applied in Structures and Artificial Surfaces', *XXII ISPRS Congress*, Melbourne, Australia, 25 August – 01 September. ISPRS Annals of the Photogrammetry, Remote Sensing and Spatial Information Sciences, Volume 1-3 [Online]. Available at: https://pdfs.semanticscholar.org/c080/841fb480f503c22e565b2a6356db2d91beca.pdf (Accessed: 16 August 2018).

Smith, M. W., Carrivick, L., and Quincey, D. (2016) 'Structure from Motion Photogrammetry in Physical Geography', *Progress in Physical Geography* 40(2) pp. 247-275. *White Rose* [Online]. Available at: http://eprints.whiterose.ac.uk/92733/3/SfM_PIPG_v2_notitle.pdf (Accessed: 15 September 2018).

Triggs, B., McLauchlan, P. F., Hartley, R. I. and Fitzgibbon, A. W. (2000) 'Bundle Adjustment-A Modern Synthesis', *International Workshop on Vision Algorithm*Berlin, Heidelberg, IWVA 1999. Vision Algorithms: Theory and Practice 1883 pp. 298-372. Springer [Online]. Available at: https://link.springer.com/chapter/10.1007/3-540-44480-7_21 (Accessed: 10 May 2018).

Turner, I. L., Harley, M. D. and Drummond, C. D. (2016) 'UAVs for Coastal Surveying', *Coastal Engineering* 111 pp. 19-24. *ScienceDirect* [Online]. Available at: https://www.sciencedirect.com/science/article/pii/S0378383916300370 (Accessed: 24 November 2016)

Unger, J., Reich, M. and Heipke, C. (2014) 'UAV-Based Photogrammetry: Monitoring of a Building Zone', *ISPRS Technical Commission V Symposium*, Riva Del Garda, Italy 23-25 June. The International Archives of the Photogrammetry, Remote Sensing and Spatial Information Sciences [Online]. Available at: https://www.repo.uni-hannover.de/handle/123456789/916 (Accessed: 18 September 2018).

Vallet, J. Panissod, F., Strecha, C. and Tracol, M. (2011) 'Photogrammetric Performance of an Ultra Light Weight Swinglet "UAV" ', *Unmanned Aerial Vehicle in Geomatics Conference*, Zurich, Switzerland, ISPRS ICWG I/V International Archives of the Photogrammetry, Remote Sensing and Spatial Information Sciences [Online]. Available at: https://infoscience.epfl.ch/record/169252/files/Paper-vallet_UAVg.pdf (Accessed: 23 August 2016).

Villa, T. F., Gonzalez, F., Miljievic, B., Ristovski, Z. D. and Morawska, L. (2016) 'An Overview of Small Unmanned Aerial Vehicles for Air Quality Measurements: Present Applications and Future Prospectives', *Sensors* 16(7) pp. 1-29. *MDPI* [Online]. Available at: http://www.mdpi.com/1424-8220/16/7/1072/html (Accessed: 10 August 2018).

Vousdoukas, M. I., Pennucci, G., Holman, R. A. and Conley, D. C. (2011) 'A Semi Automatic Technique for Rapid Environmental Assessment in the Coastal Zone Using Small Unmanned Aerial Vehicles', *Journal of Coastal Research* SI(64) pp. 1755-1759. *ProQuest* [Online]. Available at: https://search.proquest.com/openview/5c8f741c953fdf27561bdae761e74f90/1?pq-origsite=gscholar&cbl=42628 (Accessed: 20 July 2016).

Wang, Z., Mills, J., Xiao, W., Huang, R., Zheng, S. and Li, Z. (2017) 'A Flexible, Generic Photogrammetric Approach to Zoom Lens Calibration', *Remote Sens* 9(3) pp. 1-15. *MDPI* [Online]. Available at: https://www.mdpi.com/2072-4292/9/3/244/html (Accessed: 01 August 2018).

Watanabe, Y. and Kawahara, Y. (2016) 'UAV Photogrammetry for Monitoring Changes in River Topography and Vegetation', *Procedia Engineering* 154 pp. 317-325. *ScienceDirect* [Online]. Available at: https://www.sciencedirect.com/science/article/pii/S1877705816318719 (Accessed: 04 November 2017).

Wing, M. G. (2011) 'Consumer-Grade GPS Receiver Measurement Accuracy in Varying Forest Conditions', *Research Journal of Forestry* 5(2), 78-88. *Science Alert* [Online]. Available at: http://scialert.net/fulltext/?doi=rjf.2011.78.88(Accessed: 20 January 2017).

Yeom, J. M., Hwang, J., Jung, J. H., Lee, K. H. and Lee, C. S. (2017) 'Initial Radiometric Characteristics of KOMPSAT-3AMultispectral Imagery Using the 6S RadiativeTransfer Model, Well-Known Radiometric Tarps, and

MFRSR Measurements', *Remote Sens* 9(2) pp. 1-22. *MDPI* [Online]. Available at: https://www.mdpi.com/2072-4292/9/2/130 (Accessed: 22 September 2018).

Zhao, L., Huang, S. and Dissanayake, G. 'Linear SFM: A Hierarchical Approach to Solving Structure-from-Motion Problems by Decoupling the Linear and Nonlinear Components', *ISPRS Journal of Photogrammetry and Remote Sensing* 141 pp. 275-289. *ScienceDirect* [Online]. Available at: https://www.sciencedirect.com/science/article/pii/S0924271618301151 (Accessed: 27 May 2018).